M81 Galaxy

Commented by Carl H. Gibson

Editor in Chief: Rudolph E. Schild

Proceedings of Lorentz Center Workshop on New Directions in Modern Cosmology, held September 27 to October 1 in Leiden, Netherlands, 2010.

Editors: Carl H. Gibson, Rudy Schild,
N. Chandra Wickramasinghe,
Theo M. Nieuwenhuizen

Participants of the workshop were invited to submit manuscripts for publication in a Proceedings Volume of the Journal of Cosmology by Organizer Rudolph E. Schild. Manuscripts have been peer reviewed by lead Organiser Theo M. Nieuwenhuizen, the JOC Executive Editors (Gibson, Wickramasinghe) and JOC Editor-in-Chief Rudolph E. Schild. Selected public domain preprints are included to supplement the contributed JOC manuscripts. The Proceedings will be published in JOC Volume 15, the March 2011 Edition. The ordering and selection of materials presented for these Proceedings were determined by the JOC Editorial board.

Prediction for the neutrino mass in the KATRIN experiment from lensing by the galaxy cluster A1689

Theo M. Nieuwenhuizen

Center for Cosmology and Particle Physics, New York University, New York, NY 10003
On leave of: Institute for Theoretical Physics, University of Amsterdam, Science Park 904,
P.O. Box 94485, 1090 GL Amsterdam, The Netherlands

Andrea Morandi

Raymond and Beverly Sackler School of Physics and Astronomy, Tel Aviv University, Tel Aviv
69978, Israel

`t.m.nieuwenhuizen@uva.nl; andrea@wise.tau.ac.il`

ABSTRACT

The KATRIN experiment in Karlsruhe Germany will monitor the decay of tritium, which produces an electron-antineutrino. While the present upper bound for its mass is $2 \, \text{eV}/c^2$, KATRIN will search down to $0.2 \, \text{eV}/c^2$. If the dark matter of the galaxy cluster Abell 1689 is modeled as degenerate isothermal fermions, the strong and weak lensing data may be explained by degenerate neutrinos with mass of $1.5 \, \text{eV}/c^2$. Strong lensing data beyond 275 kpc put tension on the standard cold dark matter interpretation. In the most natural scenario, the electron antineutrino will have a mass of $1.5 \, \text{eV}/c^2$, a value that will be tested in KATRIN.

Subject headings: Introduction, NFW profile for cold dark matter, Isothermal neutrino mass models, Applications of the NFW and isothermal neutrino models, Fit to the most recent data sets, Conclusion

1. Introduction

The neutrino sector of the Standard Model of elementary particles is one of today's most intense research fields (Kusenko, 2010; Altarelli and Feruglio 2010; Avignone et al. 2008). While neutrino oscillations give information of differences in mass-squared values, no absolute neutrino mass is known. The masses may be of order $0.05 \, \text{eV}/c^2$ as set by the oscillations, or much larger. While a lot is known about standard (active) neutrinos (left-handed neutrinos, right-handed antineutrinos), hardly anything is known about their sterile partners (right-handed neutrinos, left-handed antineutrinos). It is even not established that the masses of active and sterile components are close to each other; in the popular seesaw mechanism, they differ by orders of magnitude (Lesgourges

– 2 –

and Pastor 2006). Still, next to WIMPs (Bertone 2010), sterile neutrinos may constitute the dark matter particles (Feng 2010). It was recently realized that lensing data allow that active plus sterile neutrinos of 1.5 eV/c^2 provide the dark matter (Nieuwenhuizen et al. 2009). Neutrinos are too light to trigger large scale structure formation (galaxy formation), and are therefore often ruled out as dark matter candidates. However, this may end up as a misconception, since structure formation can actually already be explained by the gravitational hydrodynamics of baryons alone (Nieuwenhuizen et al. 2009).

The most effective way to determine the mass of an antineutrino is tritium decay, when one of the two neutrons in its nucleus decays into a proton, an electron and an electron-antineutrino. The electron energy can be detected. Analyzing the number of events (that is, the Kurie function) near the maximal energy provides information about the antineutrino mass. Depending on statistical assumptions in the analysis of the non-detection in the Mainz and Troitsk experiments, the present upper bound is 2.2 eV/c^2 (Lobashev et al. 1999), 2.3 eV/c^2 (Kraus et al, 2005) or 2.0 eV/c^2 (Amsler et al. 2008).

The KArlsruhe TRItium Neutrino experiments (KATRIN) involve an international consortium of 16 laboratories in Europe and the USA, and are intended to search the mass down to 0.2 eV/c^2 (Otten and Weinheimer 2009). Since the square mass is tested, this means to go down to 0.04 eV^2/c^4, an improvement by two orders of magnitude with respect to Mainz-Troitsk.

Galaxy clusters are known to produce strong lensing effects. A galaxy lying behind it can be seen as an arc, ideally as a complete Einstein ring. This has been observed, see Fig. 1 which presents a double Einstein ring. The very similar phenomenon may be seen already in lensing by a glass ball, see figure 2. This so-called strong lensing is effective near the center of the cluster, say up to a radius of 300 kpc. Further out, there is still the so-called weak lensing. Indeed, since every galaxy will be slightly distorted, a statistical effect occurs for a "local group of galaxies ("local on the 2D sky, as observed by us), which then also provides information on the mass distribution of the lensing cluster. Models for structure of the cluster can be tested against these strong and weak lensing data. The clusters also have an amount of 10-15% of matter in X-ray gas, typically much more than they have galaxy mass.

The galaxy cluster Abell 1689 (A1689) is one of the most studied clusters. It is rather heavy, a few times 10^{15} solar masses, and has a large lensing arc at 150 h_{70}^{-1} kpc, which is observed at 45" from the center, the largest Einstein radius observed to date. (The Hubble constant is $H_0 = h_{70}70$ km/s Mpc, with h_{70} close to 1.0). There are good data for strong lensing (SL) and weak lensing (WL) and the X-ray gas, so it is an ideal testing ground for models. The cluster has a small intruder clump in the North East sector, which can be masked out if needed. Assuming spherical symmetry, we shall consider two models for the matter distribution in the cluster.

– 3 –
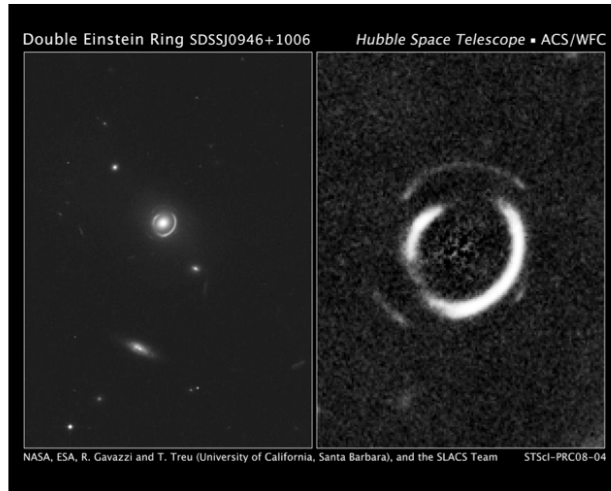
Fig. 1.— Strong lensing by a foreground galaxy photographed by the Hubble Space Telescope HST. Two background galaxies are mapped as two almost complete Einstein rings. In the enlargement on the right, the foreground galaxy is masked out.

,

Fig. 2.— Strong lensing by a glass ball at home. The central square of the background paper is distorted. Parallel lines are mapped as semi-arcs, pairs of which make up the ellipses.

2.   NFW profile for cold dark matter

Cold dark matter (CDM) is mostly thought to be related to particles heavier than the proton, like the lightest supersymmetric (SUSY) particle called neutralino. However, the assumption of CDM is subject to criticism. The so-called R-symmetry assumption implies a very long lifetime. The electron and proton have spin, are both charged and light, so they "have nowhere to go"; but if the R-symmetry is broken, the neutralino would quickly decay to electrons, protons, neutrinos and photons. In practice, the purported CDM particle has never been found, despite decades of searching. An incomplete list of acronyms of the over 60 search programs is, not mentioning updates: ADMX, AMANDA, ANAIS, ANTARES, ArDM, ATIC, BPRS, CANGAROO,

000006

<center>– 4 –</center>

CAST, CDMS, CLEAN, CMSSM, CoGeNT, COUPP, CRESST, CUORE, CYGNUS, DAMA/NaI, DAMA/LIBRA, DAMIC, DEAP, DMTPC, DRIFT, EDELWEISS, EGRET, ELEGANTS, FERMI-LAT, GENIUS, GERDA, GEDEON, HDMS, ICECUBE, IGEX, KIMS, LEP, LHC, LIBRA, LUX, MAGIC, MAJORANA, MIMAC, NAIAD, NEWAGE, ORPHEUS, PAMELA, PICASSO, ROSE-BUD, SIGN, SIMPLE, SuperCDMS, SUPER-K, TEXONO, UKDM, VERITAS, WArP, Whipple, XENON, XMASS, ZEPLIN. Upcoming are: DARWIN, DEAP-3600, EURECA, GEODM, Mini-CLEAN, SuperCDMS-SNOLab. (Notice that J, Q and Y are not covered.) Also in recent years the searching remains without detection, in particular the XENON 100 search rules out previous detection claims at DAMA, CDMS and Cogent (Aprile et al. 2010), a finding confirmed by the CDMS collaboration (Akerbib et al. 2010). While it is already acknowledged that time for supersymmetry is running out (Bertone 2010), the CMS collaboration at the Large Hadron Collider LHC reports, very recently, that within error limits it fails to detect more SUSY-like events than expected from the non-SUSY background (CMS 2011). So, though the SUSY assumption and the possibly resulting neutralino CDM are certainly not ruled out, these long trusted options are definitely on the defensive at the moment.

From the practical side in cosmology, the CDM assumption works often so well that it is presently viewed as the standard approach. This applies in particular for the cosmic microwave background. As to cosmic structures, numerical simulations have shown that the CDM density can be described fairly well by an NFW profile (Navarro, Frenk and White, 1997), which has the benefit of having a simple form. It is parametrized by a characteristic mass density ρ_0 and a length scale r_s,

$$\rho_{\mathrm{NFW}}(r) = \frac{\rho_0 \, r_s^3}{r(r+r_s)^2}. \tag{1}$$

The average density, that is, the integrated mass up to R divided by the volume, then equals

$$\bar{\rho}_{\mathrm{NFW}}(R) = \frac{3}{4\pi R^3} \, 4\pi\rho_0 r_s^3 \left(\ln\frac{R+r_s}{r_s} - \frac{R}{R+r_s} \right). \tag{2}$$

The cosmic critical density is $\rho_c = 3H_0^2/8\pi G = 9.25 \cdot 10^{-27}\mathrm{kg/m^3}$ according to the WMAP7 value for the Hubble constant, $H_0 = 70.2 \pm 1.4$ km/s/Mpc (Komatsu et al. 2010). At the redshift $z = 0.183$ of A1689 the Hubble constant reads $H_z \equiv E_z H_0$ with

$$E_z = \left[\Omega_M(1+z)^3 + (1-\Omega_M-\Omega_\Lambda)(1+z)^2 + \Omega_\Lambda \right]^{1/2} = 1.078, \tag{3}$$

(we adopt the flat cosmology $\Omega_\Lambda = 0.75$, $\Omega_M = 0.25$), so the critical density becomes $\rho_c(z) = \rho_c E_z^2$. The radius R_N where $\bar{\rho}_{\mathrm{NFW}}(R_N)$ equals $N\rho_c(z)$ is said to be the radius where the over-density

– 5 –

equals N. It defines the concentration parameter $c_N = R_N/r_s$. Customary values are $N = 200$ corresponding to c_{200} and "virial" overdensity $N = 117$ at the redshift of A1689, with its $c_{\rm vir} \equiv c_{117}$. The correspondence involved here is

$$\frac{\rho_0}{N\rho_c(z)} = \frac{\frac{1}{3}c_N^3}{\log(1+c_N) - c_N/(1+c_N)}, \tag{4}$$

with the monotonically increasing right hand side yielding a unique c_N.

3. Isothermal neutrino mass models

It is long believed that light neutrinos cannot make up the dark matter, because they cannot assist in structure formation of galaxies and clusters of galaxies. Indeed, the Jeans mechanism in hydrodynamics can only explain globular star clusters of, say, 600,000 solar masses. But gravitational hydrodynamics offers new mechanisms for cosmological structure formation, with an important role for viscosity. We shall not dwell into it here, as it is discussed at length in other papers in this volume by Gibson and Schild (2011) and Gibson (2011). This approach also answers the paradox why the ^{3}He abundance in the Galaxy is often observed at primordial level, independent of the the distance to the center and thus independent of the local amount of metallicity (Nieuwenhuizen, 2011). For the present work it suffices to notice that neutrinos need not be ruled out by arguments of structure formation and hence qualify "again" for dark matter candidates. This holds the more since the early runs of the Large Hadron Collider at the CERN did not detect supersymmetry (CMS 2011).

One may thus consider the cluster dark matter as due to degenerate fermions. The violent relaxation mechanism has explained the success of isothermal models in gravitation (Lynden Bell 1967), so it is natural to consider isothermal dark matter fermions.

The gravitational potential caused by mass elements at $\mathbf{r}' \neq \mathbf{r}$ is $\varphi(\mathbf{r}) = -G \int \mathrm{d}^3r' \rho(\mathbf{r}')/|\mathbf{r} - \mathbf{r}'|$ $+ G \int \mathrm{d}^3r' \rho(\mathbf{r}')/r'$, where we choose the zero level such that $\varphi(\mathbf{0}) = 0$. It satisfies the Poisson equation $\nabla^2\varphi(\mathbf{r}) = 4\pi G\rho(\mathbf{r})$, which in case of spherical symmetry reads

$$\varphi''(r) + \frac{2}{r}\varphi'(r) = 4\pi G\rho(r), \tag{5}$$

In the galaxy cluster there will be three relevant contributions to the matter density, $\rho = \rho_\nu + \rho_G + \rho_g$, with partial mass densities of dark matter ("ν"), Galaxies (G) and X-ray gas (g), respectively. We model the dark matter as isothermal fermions with mass m, degeneracy $\bar{g}$ and chemical potential $\mu = \alpha k_B T$. The mass density then involves a momentum integral over a Fermi-Dirac distribution,

$$\rho_\nu(r) = \bar{g}m \int \frac{\mathrm{d}^3p}{(2\pi\hbar)^3} \frac{1}{\exp\{[p^2/2m + m\varphi(r) - \mu]/k_B T\} + 1}. \tag{6}$$

– 6 –

The thermal length is $\lambda_T = \hbar\sqrt{2\pi/mk_BT}$.

Since the mass in galaxies is a few percent of the total, mainly coming from the dominant central one, we assume for the mass density from galaxies simply the isothermal distribution $\rho_G(r) = \bar{g}m\lambda_T^{-3}\exp[\alpha_G - \beta_G m\varphi(r)]$ (Nieuwenhuizen 2009). In the galaxy cluster Abell 1689 the mass density of the gas ρ_g follows from the electron density n_e as $\rho_g = 1.11\,m_N n_e$ with m_N the nucleon mass. The data for n_e densely obtained by us from X-ray observations in the interval 10 kpc $< r < 1$ Mpc, are well approximated by the exponent of a parabola in $\log r$ (Nieuwenhuizen and Morandi, 2011)

$$n_e(r) = \exp\left(-3.63 + 0.915\log\frac{r}{\text{kpc}} - 0.218\log^2\frac{r}{\text{kpc}}\right)h_{70}^{1/2}\text{cm}^{-3}. \tag{7}$$

Beyond 1 Mpc one may either continue this shape, or replace it for $r > r_{\text{iso}} = 807$ kpc by the isothermal tail (Nieuwenhuizen and Morandi, 2011)

$$\rho_g^{\text{iso}} = \frac{\sigma_{\text{iso}}^2}{2\pi Gr^2}, \qquad \sigma_{\text{iso}} = 578.5\,\frac{\text{km}}{\text{s}}. \tag{8}$$

From strong lensing data one determines the $2D$ mass density (integrated mass along the line of sight) $\Sigma(r) = \int_{-\infty}^{\infty}\mathrm{d}z\rho\left(\sqrt{r^2 + z^2}\right)$. The Poisson equation allows to express this as

$$\Sigma(r) = \frac{1}{2\pi G}\int_0^{\infty}\mathrm{d}s\frac{\cosh 2s}{\sinh^2 s}\left[\varphi'(r\cosh s) - \frac{\varphi'(r)}{\cosh^2 s}\right], \tag{9}$$

which is numerically more stable since φ' varies less than ρ. In weak lensing one determines the shear as

$$g_t(r) = \frac{\overline{\Sigma}(r) - \Sigma(r)}{\Sigma_c - \Sigma(r)}, \tag{10}$$

where the "critical projected mass density" Σ_c is a constant. The mass inside a cylinder of radius r around the cluster center, $M_{2D}(r) = 2\pi\int_0^r\mathrm{d}r'\,r'\Sigma(r')$, defines the average of Σ over a disk of radius r, $\overline{\Sigma}(r) = M_{2D}(r)/\pi r^2$. The Poisson equation allows to express this as (Nieuwenhuizen 2009)

$$\overline{\Sigma}(r) = \frac{1}{\pi G}\int_0^{\infty}\mathrm{d}s\,\varphi'(r\cosh s). \tag{11}$$

4.   Applications of the NFW and isothermal neutrino models

Cowsik and McClelland (1973) are the first to model the dark matter of the Coma cluster as an isothermal sphere of neutrinos. As for neutron stars and white dwarfs, this determines the

000009

– 7 –

neutrino mass, and yields about 2 eV/c^2. Treumann et al. (2000) considered 2 eV/c^2 neutrinos next to CDM and X-ray gas, all isothermal, and derive the density profiles for clusters such as Coma. Nieuwenhuizen (2009) applies to clusters an isothermal fermion model for a single type of dark matter, cold or not, and also isothermal for the galaxies and the X-ray gas. Fitting to weak lensing data of the Abell 1689 cluster works well and yields as the mass $(12/\bar{g})^{1/4}\,1.455\pm0.030\,h_{70}^{1/2}$ eV/c^2, where $\bar{g}$ is the fermion degeneracy. The only known candidate for such a low mass is the neutrino, for which $\bar{g} = 3 * 2 * 2 = 12$ modes are available, due to 3 families of (anti)particles with spin $\frac{1}{2}$, because helicity is not conserved in the gravitational field of the cluster. The mass lies below the experimental upper bound of 2.0 eV/c^2 but within the KATRIN window. With this mass active neutrinos constitute about 10% dark matter. Some 20% neutrino dark matter may arise provided the sterile partners have been created, too, in the early Universe. This may occur in the presence of a meV-valued Majorana mass matrix, in the time window between the freeze out of quarks and the freeze out of electrons and positrons (Nieuwenhuizen 2009).

Umetsu and Broadhurst (2008) combine weak lensing data with reddening of background galaxies out to 3 Mpc, presenting the best (extended) weak lensing data to date. Combining them with certain strong lensing data they fit an NFW profile and find a concentration parameter $c_{200} = 13.5$, well exceeding the expected value around 6-7. Nieuwenhuizen and Morandi (2011) employ the Umetsu and Broadhurst (2008) weak lensing data but use better strong lensing data of Limousin et al. (2007) and arrive at the more expected $c_{200} = 6.8$. However, they point at a systematic deviation in the weak lensing fit, related to the fact that weak lensing alone would give a value of around 7.6 (Limousin et al. 2007). They also point at a mild tendency of the strong lensing data to fall well below NFW beyond 300 kpc.

Coe et al. (2010) present improved strong lensing data by employing a non-parametirc approach. Combining these strong lensing data up to 220 kpc with the weak lensing data of Umetsu and Broadhurst (2008) beyond 220 kpc, they fit to an NFW profile and get $r_s = 338$ kpc, $c_{200} = 7.6$ (or $c_{\mathrm{vir}} = 9.6$), leading to r $M_{200} = 1.8^{+0.4}_{-0.3}10^{15}h_{70}^{-1}M_\odot$ or $M_{\mathrm{vir}} = 2.0^{+0.5}_{-0.3}10^{15}h_{70}^{-1}M_\odot$.

Nieuwenhuizen and Morandi (2011) also apply the isothermal neutrino model to their A1689 data. The approach again works well, with slightly modified parameters and neutrino mass $1.499\pm0.039\,h_{70}^{-1/2}$ eV/c^2. This theory supports a fast decay of strong lensing beyond 300 kpc. The reason is that its neutrino dark matter would be localized up to, say, 300 kpc (Nieuwenhuizen 2009), with the X-ray gas more concentrated in the outskirts. As seen in Fig 4 for a slightly different data set, in this model strong lensing decays fast beyond the region where DM is localized. Weak lensing, on the other hand, does not exhibit this, as it senses a slow decay, namely an isothermal $1/r$ decay plus an $1/r^2$ correction (Nieuwenhuizen and Morandi, 2011), see also Fig. 5 for weak lensing in the data set considered below.

The case of neutrino dark matter in clusters is also considered by Sanders (2007). While he assumes modifications of Newton gravity, we shall stay within the Newtonian scope.

– 8 –
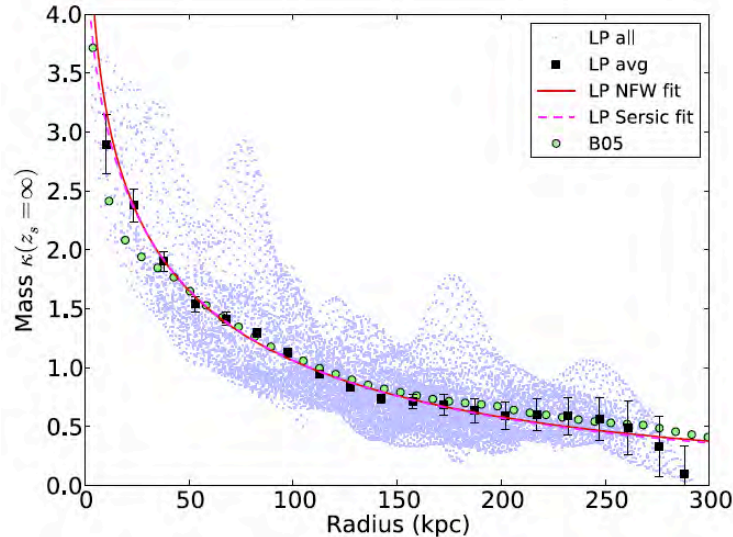
Fig. 3.— Reproduction of Figure 2 of Coe et al. (2010) by permission of the AAS. Blue: Strong lensing data of the cluster A1689 obtained with their analysis. Black: binned data. Green: data by Broahurst et al. (2005). Red: The NFW model fits well, but it does not support the fast fall off beyond 275 kpc.

5.   Fit to the most recent data sets

We now consider the best data sets to date, the strong lensing of Coe et al. (2010), combined with the weak lensing data of Umetsu and Broadhurst (2008) and the X-ray data of Nieuwenhuizen and Morandi (2011). Whereas Coe et al. (2010) used the strong lensing data up to 220 kpc and the weak lensing data beyond this, we shall now follow our 2011 work and use all strong lensing and weak lensing data, taking the gas data as input. We wish to minimize $\chi^2 = \chi^2_{\mathrm{SL}} + \chi^2_{\mathrm{WL}}$ for the 20 strong lensing data points and 11 weak lensing points.

Let us first discuss the NFW case, which involves 2 fit parameters, leaving a minimization over 20+11-2=29 non-trivial inputs. (Not having the correlation matrix between the data points of SL or WL, we perform χ^2 fits, here and further on.) The fit leads to $\chi^2_{\mathrm{SL}} = 21.4$ and $\chi^2_{\mathrm{WL}} = 14.6$. The profile parameters are $r_s = 291$ kpc and $c_{200} = 8.8$, or the virial value $c_{\mathrm{vir}} = 11.0$. With its $\chi^2/29 = 1.24$, this fit is satisfactory. But, as seen in Fig 4, the strong lensing strongly falls down beyond r_s, while the NFW profile continues gradually. So if the fall off is statistically relevant, it will pose a problem for the NFW model.

One can also make a fit to the isothermal fermion model assuming an isothermal distribution for the density of matter in galaxies, $\rho_G(r) = \bar{g}m\lambda_T^{-3}\exp[\alpha_G - \beta_G m\varphi(r)]$ (Nieuwenhuizen 2009). The fit involves five parameters, the best values being

000011

– 9 –

$$\alpha = 29.26 \pm 0.43, \quad \frac{\bar{g}m}{\lambda_T^3} = 4092 \pm 275 \frac{m_N}{\mathrm{m}^3}, \quad \sigma_\nu = 564 \pm 9 \frac{\mathrm{km}}{\mathrm{s}},$$

$$\alpha_G = 7.44 \pm 0.11, \quad \beta_G = \frac{0.745 \pm 0.03}{m\sigma_\nu^2}, \tag{12}$$

where $\sigma_\nu = \sqrt{k_B T/m}$ is a DM velocity dispersion for which $\lambda_T = \hbar\sqrt{2\pi}/m\sigma_\nu$. The result for β_G differs the most with respect to fits (Nieuwenhuizen and Morandi, 20011), but it still is close to $1/m\sigma_\nu^2$, which is the case of virial equilibrium of galaxies and DM (Nieuwenhuizen 2009). The mass comes out as

$$m = \left(\frac{12}{\bar{g}}\right)^{1/4} 1.55\,\mathrm{eV} \pm 0.04\,\mathrm{eV}/c^2. \tag{13}$$

From now on, we take $\bar{g} = 12$; in general the masses should be multiplied by the factor $(12/\bar{g})^{1/4}$.

The strong lensing fit, shown in Fig. 4, corresponds to $\chi_{\mathrm{SL}}^2 = 57.9$. Its match below 100 kpc could be improved by a different modeling of the galaxy density, which would also allow to improve the fit between 100 and 300 kpc, so this could easily bring down the present large value of χ_{SL}^2. The weak lensing fit is shown in Fig. 5. The outlying 8'th weak lensing point alone contributes an amount 10.0 to $\chi_{\mathrm{WL}}^2 = 18.1$, the 10 other points bringing 8.1, so that weak lensing is generally fit quite well. In total, the present fit thus gives the value $\chi^2/(31-5) = 2.92$, larger that for NFW. We shall not attempt to improve the fit, since this will have little impact on the value of the neutrino mass. Moreover, it is seen in Fig. 4 that the neutrino model predicts a fast decay of strong lensing beyond 275 kpc, while NFW does not. So if this decay of the Coe et al. (2010) data in Fig. 3 is statistically relevant, it supports the neutrino model and disfavors NFW. In this regard one may determine till which radius NFW predicts lensing arcs, and compare this with the observations.

6. Conclusion

The lensing data of the galaxy cluster Abell 1689 may be explained by isothermal fermions. The best case is neutrinos of nearly the same mass. Combining with previous (but less good) data sets on the same cluster we infer a mass is $m_\nu = 1.50 \pm 0.05$ (sys) ± 0.03 (stat) eV/c^2. The three species of active neutrinos have been created in thermal equilibrium and they are predicted have total mass of $M_\nu = 3m_\nu \approx 4.5$ eV/c^2. With the general relation $\Omega_\nu = M_\nu/(46h_{70}^2)$ the mass density in active neutrinos would be $\Omega_\nu^{\mathrm{act}} \approx 10\%$ of the critical mass density of the Universe. This is much more than the 1.2–3.0% allowed by the standard ΛCDM approach under various conditions and combinations with other data sets (Komatsu et al. 2010). In our philosophy neutrinos should explain most, if not all, cluster dark matter, $\Omega_\nu = 20 - 25\%$. Under reasonable conditions, another 10% can have arisen from the creation of three thermal sterile neutrinos species of 1.5 eV/c^2 (Nieuwenhuizen, 2009). If there are more sterile than active partners that would explain even more dark matter.

– 10 –
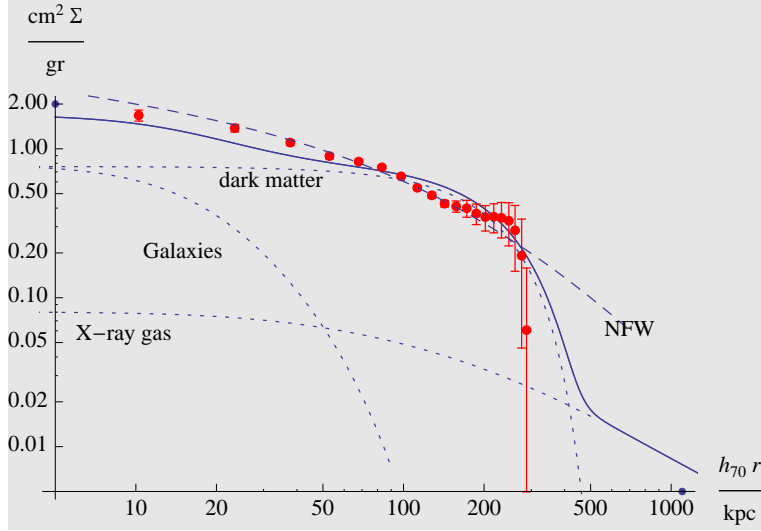
Fig. 4.— Dots: log-log plot of the binned strong lensing data of Coe et al. (2010), see Fig. 3. Dashed line: The NFW model fits well, but fails to explain the fast fall off beyond 275 kpc. Full line: Isothermal dark fermions with the measured gas and isothermal modeling of galaxies fit reasonably. Dotted lines: the separate contributions from (neutrino) dark matter, Galaxies and X-ray gas.
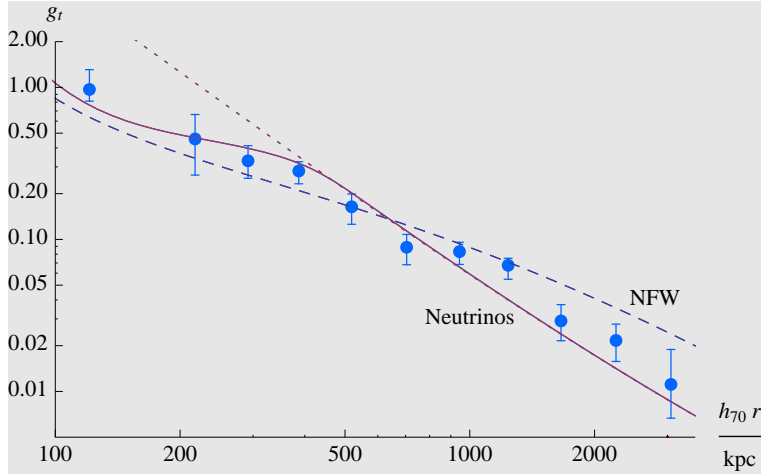
Fig. 5.— Weak lensing data of Umetsu and Broadhurst (2008). Full line: isothermal neutrinos. Dotted line: its asymptotic shape. Dashed line: NFW profile of cold dark matter.

The 1.5 eV/c^2 mass lies in the range covered by the KATRIN experiment, searching the mass of the electron antineutrino, that is expected to start taking data in 2011 (Weinheimer 2009). A discovery around 1.5 eV/c^2 would clearly prove our thesis. But non-detection would not necessarily rule out the case of nearly all non-baryonic dark matter in neutrinos. What KATRIN measures is, in leading approximation, the combination $m_{\bar{\nu}_e}^2 \equiv \sum_i |U_{ei}|^2 m_i^2$, where U_{ei} is the amplitude of the

<center>– 11 –</center>

neutrino mass eigenstate $|\nu_i\rangle$ in the electron antineutrino wavefunction, $|\bar{\nu}_e\rangle = \sum_i U_{ei}|\nu_i\rangle$, with i running from 1 to $3 + N_s$ with N_s the number of sterile neutrinos, and m_i the mass of the eigenstate $|\nu_i\rangle$ (Otten and Weinheimer, 2009). The LSDN (Aguilar et al. 2001) and MiniBoone data for short baseline neutrino oscillation experiments (Aguilar et al. 2010) can be explained by assuming one or more sterile neutrinos with mass of order 1 eV/c^2, with the solar and atmospheric neutrinos involved with much lighter masses. Therefore a conspiracy may take place, the heavier mass eigenstates having small matrix elements U_{ei}, making $m_{\bar{\nu}_e}^2$ too small to be detected at KATRIN, while dark matter may still come from neutrinos, namely the sterile ones, with masses of order of eV/c^2. A more interesting scenario is that the masses m_i are well enough separated for KATRIN to observe their effect one-by-one. (Otten and Weinheimer, 2009). Such questions and many related ones are beyond the scope of the present paper, but see Nieuwenhuizen (2011). Clearly, the (sterile) neutrino sector of the standard model of elementary particles is an exciting field of research for the near future.

As generally expected, the lensing data in A1689 can also be explained by an NFW profile. One may wonder whether there is a discriminating feature between NFW and isothermal neutrinos, that is, between CDM and νDM. There indeed is a candidate in the fast fall off of strong lensing beyond 270 kpc, first pointed at by Nieuwenhuizen and Morandi (2011) and more convincingly present in the data of Coe et al. (2010), see Figs. 3, 4. NFW would predict a smooth density profile and smooth continuation of strong lensing data. The observations conflict with this and give better support for the isothermal neutrino model, where this fall off is related to the fast fall off of neutrino density beyond, say 300 kpc. The fact that neutrinos are more localized than the X-ray gas also explains the "missing baryon paradox" for this cluster, because the X-ray gas is generally more concentrated in the outskirts, as is concluded from observations on a set of clusters (Rasheed et al 2010). One may investigate whether an NFW profile predicts beyond 300 kpc more lensing arcs than the few observed ones. The answer to this question may touch the validity of the NFW model and its assumed cold dark matter.

<center>**REFERENCES**</center>

Aguilar A. et al. (LSDN), (2001). Evidence for neutrino oscillations from the observation of $\bar{\nu}_e$ appearance in a $\bar{\nu}_\mu$ beam, Physical Review D 64, 112007 [22 pages].

Aguilar-Arevelo A. A. et al. (MiniBooNE), (2010). Event Excess in the MiniBooNE Search for $\bar{\nu}_\mu \to \bar{\nu}_e$ Oscillations, Physical Review Letters 105, 181801 [4 pages].

Akerib, D. S. et al. (CDMS Collaboration) (2010) A low-threshold analysis of CDMS shallow-site data. Physical Review D 82, 122004 [18 pages]

000014

– 12 –

Altarelli G. and Feruglio F. (2010). Discrete flavor symmetries and models of neutrino mixing, Review of Modern Physics, 82, 27012729.

Amsler C., Doser M., Antonelli M. et al. (Particle Data Group) (2008). Review of particle physics, Physics Letters B, 667, 1-1340.

Aprile E., Arisaka K., Arneodo F. et al. (Xenon 100 Collaboration) (2010). First dark matter results from the XENON100 experiment, Physical Review Letters, 105, 131302 [4 pages].

Avignone F. T., Elliott S. R. and Engel J. (2008). Double beta decay, Majorana neutrinos, and neutrino mass, Review of Modern Physics, 80, 481516.

Rasheed B., Bahcall N. and Bode P. (2010). Where are the missing baryons in clusters? arXiv:1007.1980 [10 pages].

Bertone G. (2010), The moment of truth for WIMP Dark Matter, Nature, 468, 389-393.

Cline J. M. (1992). Constraints on almost-Dirac neutrinos from neutrino-antineutrino oscillations, Physical Review Letters, 68, 3137-3140.

CMS Collaboration (2011). Search for supersymmetry in p-p collisions at 7 TeV in events with jets and missing transverse energy, arXiv:1101.1628 [30 pages].

Coe D., Narciso B., Broadhurst T. and Moustakas L. A. (2010) A high-resolution mass map of galaxy cluster substructure: LensPerfect analysis of A1689, Astrophysical Journal, 723, 1678-1702.

Cowsik, R. and McClelland, J. (1973). Gravity of neutrinos of nonzero mass in astrophysics, Astrophysical Journal, 180, 7-10.

Feng J.L. (2010). Dark Matter Candidates from Particle Physics and Methods of Detection, Annual Review of Astronomy and Astrophysics, 48, 495-545.

Gibson C. H. and Schild R. E. (2011). Primordial planet formation, Journal of Cosmology .

Gibson C. H. (2011). Why the dark matter of galaxies is clumps of micro-brown dwarfs and not Cold Dark Matter, Journal of Cosmology .

Komatsu E., Smith K. M., Dunkley J. et al. (2010). Seven-year Wilkinson anisotropy probe (WMAP) observations: Cosmological interpretation, Astrophysical Journal Supplement Series, 192, 18 [47pp].

Kraus Ch., Bornschein B. et al. (2005). Final Results from phase II of the Mainz Neutrino Mass Search in Tritium beta-Decay, EuroPhysical Journal C, 40, 447-468.

Kusenko A. (2009). Sterile neutrinos: The dark side of the light fermions, Physics Reports, 481, 1-28.

000015

– 13 –

Lesgourgues J. and Pastor S. (2006). Massive neutrinos and cosmology, Physics Reports, 429, 307-379.

Limousin M. et al. (2007). Combining Strong and Weak Gravitational Lensing in Abell 1689, Astrophysical Journal 668, 643-666.

Lobashev V. M., Aseev V. M. et al. (1999). Direct search for mass of neutrino and anomaly in the tritium beta-spectrum, Physics Letters B, 460, 227-235.

Lynden Bell D. (1967). Statistical mechanics of violent relaxation in stellar systems, Monthly Notices of the Royal Astronomical Society 136, 101-121.

Navarro, J. F., Frenk, C. S. and White, S. D. M. (1997). A universal density profile from hierarchical clustering, Astrophysical Journal 490, 493-508.

Nieuwenhuizen, T. M. (2009). Do non-relativistic neutrinos constitute the dark matter? Europhysics Letters, 86, 59001 [6 pages].

Nieuwenhuizen, T. M. (2011). Sterile neutrinos: their genesis, oscillations and role in cosmology, Journal of Cosmology .

Nieuwenhuizen, T. M., Gibson, C. H. and Schild, R. E. (2009). Gravitational hydrodynamics of large-scale structure formation, Europhysics Letters, 88, 49001 [6 pages].

Nieuwenhuizen, T. M. and Morandi M. (2011). Are observations of the galaxy cluster Abell 1689 consistent with a neutrino dark matter scenario? submitted [6 pages].

Otten, E. W. and Weinheimer C. (2008). Neutrino mass limit from tritium beta decay, Reports on Progress in Physics, 71, 086201 [81 pages].

Rasheed, B., Bahcall, N. and Bode, P. (2010). Where are the missing baryons in clusters? arXiv:1007.1980 [10 pages].

Russell, D. G., (2005a) Further Evidence for Intrinsic Redshifts in Normal Spiral Galaxies. Astrophysics and Space Science, 299, 2005, 387-403.

Sanders R. H. (2007). Neutrinos as cluster dark matter, Monthly Notices of the Royal Astronomical Society, 380, 331-338.

Umetsu, K. and Broadhurst, T. (2008). Combining lens distortion and depletion to map the mass distribution of A1689, Astrophysical Journal, 684, 177-203.

Weinheimer, C. (2009). Direct determination of Neutrino Mass from Tritium Beta Spectrum. arXiv:0912.1619 [13 pages].

000016

Do micro brown dwarf detections explain the galactic dark matter?

Theo M. Nieuwenhuizen[1], Rudolph E. Schild[2] & Carl H. Gibson[3]

Institute for Theoretical Physics, University of Amsterdam,
Science Park 904, P.O. Box 94485, 1090 GL Amsterdam, The Netherlands
[2]*Harvard-Smithsonian Center for Astrophysics, 60 Garden Street, Cambridge, MA02138, USA*
[3]*Mech. and Aerospace. Eng. & Scripps Inst. of Oceanography. Depts., UCSD, La Jolla, CA 92093, USA*
Correspondence to: Correspondence and requests for materials should
be addressed to Th. M. N. (Email: t.m.nieuwenhuizen@uva.nl).
(Dated: April 17, 2011)

The baryonic dark matter dominating the structures of galaxies is widely considered as mysterious, but hints for it have been in fact detected in several astronomical observations at optical, infrared, and radio wavelengths. We call attention to the pattern of star formation in a galaxy merger, the observed rapid microlensing of a quasar by a galaxy, the detection of "cometary knots" in planetary nebulae, and the Lyman-alpha clouds as optical phenomena revealing the compact objects to be primordial gas planets in dense clumps that merge to form stars and globular star clusters. Radio observations of "extreme scattering events" and "parabolic arcs" are found to imply the same population of compact planet mass objects in interstellar space, and measurement of the cometary knots yield mass estimates of approximately earth mass as predicted. Estimates of their total number show that they comprise enough mass to constitute the missing baryonic matter. Mysterious radio events are explained by their pair merging in the Galaxy. Latent heat of evaporated hydrogen slowly released at the 14 K freezing transition at their surface explains the thermostat setting of the "dust" temperature of cold galaxy halos. The proportionality of the central black hole mass of a galaxy and its number of globular clusters is explained.

PACS numbers: 04.70.Bw,04.20.Cv, 04.20.Jb

These authors contributed equally to the paper

I. INTRODUCTION

In 1931 Jan Oort realized that our Galaxy must contain invisible matter [1]. Fritz Zwicky soon concluded the same for clusters of galaxies, and called it dark matter (DM) [2]. The current paradigm of Cold Dark Matter (CDM, or ΛCDM including the cosmological constant) assumes it to arise from a heavy elementary particle with a small interaction cross-section. In the transition of the plasma of protons, electrons and He-ions to gas, the photons decouple and the baryons are said to condense on presumed pre-existing CDM condensations. However, despite many searches, this CDM particle has not been found [3] and this bottom-up scenario is stressed by numerous observations at its upper and lower size scales. On the largest scales, cosmic void structures are found on much larger size scales than predicted from simulations, whereas on the smallest scales, the many subhalos predicted to surround our Galaxy are not observed [4]. Moreover, the voids are emptier than simulated. And, the predicted "dark age" before the formation of stars and galaxies is coming more and more under stress with new observations of early structures arising basically every month [5, 6]. Neither does ΛCDM offer an explanation for the axis of evil [7], the dark flow [8], chain galaxies [9] or the bullet cluster [10], while correlations between galaxy parameters contradict the ΛCDM hierarchical clustering [11], as does the structure of the Local Group [12].

We shall follow an approach with two types of dark matter, "Oort" DM in galaxies, composed of baryons, and "Zwicky" DM in galaxy clusters, the true DM. Gravitational hydrodynamics or hydro-gravitational-dynamics (GHD or HGD) theory of structure formation assumes no new particle but only stresses the nonlinearity of hydrodynamics. It involves a top-down scenario starting with structure formation in the plasma at redshift z = 5100, well before the decoupling of matter and radiation at z = 1100 [13–15]. A viscous instability creates voids, which have expanded to ca 38 Mpc now, a fair estimate for the observed typical cosmic voids [16]. Just after the decoupling, all gas fragmented in Jeans clusters (JCs) of ca $6{\cdot}10^5$ solar masses, consisting of some $2 \cdot 10^{11}$ micro brown dwarfs (μBDs, muBDs) of earth mass, sometimes called MACHOs (Massive Astrophysical Compact Halo Objects). First stars occur by coagulation of μBDs, on gravitational free-fall time scales without a dark period. A fraction of Jeans clusters turned into old globular star clusters. Others got disrupted and became material for normal stars. But most of them still exist, though cold, and constitute the galactic dark matter. These dark JCs have an isothermal distribution, noticed in lensing galaxies [17, 18], which induces the flattening of rotation curves, while their baryonic nature allows to explain the Tully-Fisher and Faber-Jackson relations [15].

Nuclear synthesis attributes enough matter for the μBDs. About 4.5% of the critical density of the Universe is baryonic. At best 0.5 % is luminous, and a good 2% is observed in X-ray gas. So, the missing dark baryons may indeed be locked up in μBDs.

Questions about the nature of the baryonic dark matter (BDM) have largely been overshadowed in the past decade by even deeper questions about the non-baryonic dark matter. GHD just assumes that it is free streaming at the decoupling [15]. One of us in his modeling of the lensing properties of a galaxy cluster [19] confirmed that it should be related to cluster DM. Dark matter is described by an ideal gas of isothermal fermions, and galaxies and X-ray gas by standard isothermal models. This yields a DM mass of 1-2 eV, not the heavy mass of the hypothetical CDM particle. The best candidate is the neutrino with mass of 1.45 eV; a prediction that will be tested in the 2015 KATRIN tritium decay search. If also the right-handed (sterile) neutrinos were created in the early Universe, there should exist a 20% population of 1.45 eV neutrino hot dark matter, clumped at the scale of galaxy clusters and groups [19].

Returning to the problem of the more familiar galactic DM just consisting of baryons, it has probably been detected already in various observations but has not been considered in a single framework. The nature of the BDM seems obscure because nature places severe constraints, so it has thus far eluded detection. The BDM must be dominated by hydrogen in some form. Hydrogen can exist in its atomic form, as H_2 gas, or in ionized form, H^+. In gaseous form as H-clouds its strong signatures as radio (21 cm) and optical Lyman and Balmer alpha emission lines should have been observed in some kind of galaxy or other by now, creating a serious puzzle, that we solve here.

A second important impediment faced by the idea that the BDM is sequestered away in condensed objects is the formation question. It has long been concluded that hydrogen clouds cannot collapse to form planetary or solar mass objects because the hydrogen cannot cool quickly, and pressure forces will quickly restore the cloud. However these arguments all involve a simplifying assumption that the process can be linearized, whereas GHD starts from H condensed in μBDs. We now discuss that various types of observations support the GHD picture as the CDM theory flounders.

II.   JEANS CLUSTERS VISIBLE IN GALAXY MERGING

The GHD formation theory predicts some $3 \cdot 10^{17}$ μBDs of earth mass per galaxy grouped in some 1.7 million Jeans clusters, each with mass $6 \cdot 10^5 M_\odot$, that constitute the galactic DM halos [13]. μBD merging has led to heavier objects like planets and stars.

As exposed in Fig. 1 of the Tadpole galaxies, galaxy merging turns the dark halo JCs into young (3-10 Myr) globular clusters (YGCs) along the merging path [15, 20]. Similar behaviors are observed in e. g. the Mice and Antennae galaxy mergers. The most luminous of the "knots" in Fig. 1 has an age of 4–5 Myr and estimated mass $6.6 \cdot 10^5 M_\odot$ [21], reminiscent of a JC. Observations generally reveal that the bright blue clusters are much younger (a few Myr) than the dynamical age of the tail (ca 150 Myr), providing strong evidence that star formation occurs in situ, long after the tail was formed [21]. GHD asserts that the cold μBDs along the merging path get warmed by tidal forces, which makes them expand and coalesce at suitable moments into young stars grouped in YGCs. The ΛCDM explanation as disrupted tidal tails [22] suffers from predicted but unobserved old stars.

Estimating the amount of galactic dark matter from fig. 1, the tail begins at 420,000 lyr from the center where it exhibits the sharp boundary of the dark matter halo. If there is spherical symmetry, the enclosed mass is $2.4 \cdot 10^{12} M_\odot$, a reasonable estimate. The opening width of 1500 lyr across remains fairly constant along the trail, as expected for an induced local heating effect. From an isothermal model the number of JCs in the wake can then be estimated as 5900, which within a factor of a few coincides with the number of bright spots in Fig. 1.

From these features one can already conclude that the galactic dark matter likely has the structure predicted by GHD.

III.   QUASAR MICROLENSING BRIGHTNESS FLUCTUATIONS

Quasar micolensing has probably to date given the most compelling evidence that the BDM is contained in a network of planetary mass bodies with sufficient number to account for the entire baryonic dark matter. The first detection of this was made with brightness monitoring of the Q0957+561 A, B gravitationally lensed quasar, with two images A, B separated by 6 arcsec on the plane of the sky. 15 years of brightness monitoring revealed that a microlensing signal of amplitude 1% and time scale 1 day (observer's clock) was apparent in the data [23]. Because the signal was consistently observed for long periods of monitoring on a time scale of the monitoring frequency, 1 day, it was concluded that the microlensing originated in a population of compact objects having masses averaging $10^{-5.5} M_\odot$ and with other events up to Jupiter mass also seen.

Subsequent to this discovery, re-analysis of the quasar data [24] confirmed that the rapid fluctuations were not intrinsic to the quasar and therefore presumably microlensing. Furthermore the signal had an equal positive and negative network of peaks, as demonstrated from wavelet analysis [25]. This is understood to originate from a high optical depth and therefore is a signature that the μBD population observed in the lens galaxy must be the baryonic dark matter. This conclusion follows from a deep understanding of microlensing [26]. In general, the shear associated with gravitational lensing (macro, milli, micro, nano) causes a brightening event with a cusp-shaped profile. But in the presence of a macro-shear generated by the Q0957 lens galaxy G1, a micro-shear caused by a μBD in the lens galaxy would possibly further amplify the macro-shear or potentially de-magnify it on the micro-arcsec scale. Only in the special circumstance that the micro-shear originates in a population with unit optical depth to microlensing will the probability of micro-magnification and micro-demagnification be equal (p. 343 and Fig. 11.8 of Ref [26]) leaving a brightness profile with equal brightening and fading events on the time scale specific to the microlensing compact object, as simulated by [27]. Thus, the observed signature found to have approximately equal positive and negative events [25] uniquely indicates microlensing by a population at unit optical depth. Since the optical depth of
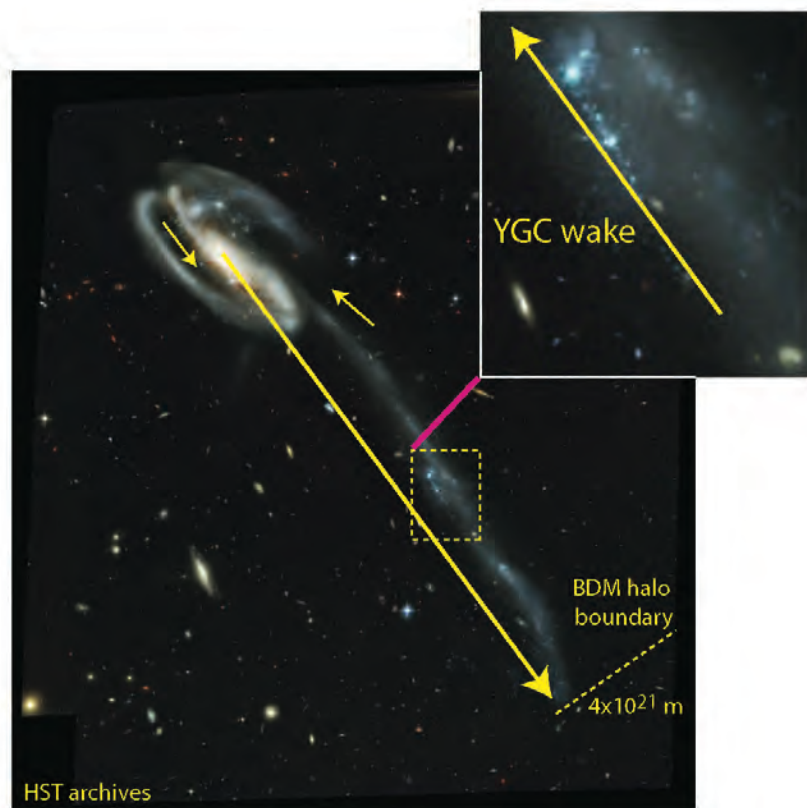
FIG. 1: As Tadpole galaxy fragments merge through the dark matter halo of the main galaxy VV29a, they exert tidal forces that trigger star formation of Jeans cluster cold micro brown dwarfs. The latter expand, coalesce and form new stars, turning the Jeans clusters into young globular clusters (YGCs). Forty-six YGCs appear as bright dots on a line pointing toward the point of merger of VV 29cdef fragments with VV29a in the insert [20]. The Tadpole tail VV29b was formed in place and not ejected by tidal forces. The diameter of the dark matter halo is eighty times the size of the central protogalaxy, and is formed by outward diffusion of Jeans clusters from the 10^{20} m protogalaxy, as their planets freeze.

image A is known to be 0.35 and of image B is 1.35, as determined by a model of the overall lensing that produces the double image, and since the lens galaxy G1 must plausibly be dominated by its baryonic dark matter, it may be concluded that the baryonic dark matter is detected as a population of μBD objects in the lens galaxy G1.

In an isothermal modeling, the average number of JCs along the quasar sightline A is 0.002 and for B 0.01. These numbers are close enough to unity to expect that along each sight line there lies exactly one JC. The estimated number of μBDs along the total light path then comes out as 18,000, confirming the observed multiple lensing events. The typical induced optical depth is 58, but the observed lower values occur if the light path traverses near the border of the JCs.

We are left with the extrapolation from theory and observation that the entire baryonic dark matter occurs in the form of a population of μBDs seen in microlensing of quasars by the grainy distribution of matter in the lens galaxy. The same population has been confirmed in several other lens systems [28–30], with microlensing mass estimates in the range $10^{-5.5}$ to $10^{-3} M_\odot$, that is, from individual μBDs to merged ones.

IV. COMETARY KNOTS IN PLANETARY NEBULAE

The μBDs are directly seen in the Helix and other planetary nebulae, see Fig. 2. Their infrared emission allows 20,000–40,000 of them to be counted in Spitzer [31]. They are found distributed in a band or shell at a central distance comparable to the Solar Oort cloud, $7 \cdot 10^{15}$ m. Because they are objects resolved at optical and infrared wavelengths, their sizes and structures

FIG. 2: Infrared observation by Spitzer of the Helix planetary nebula. The white dwarf in the center is surrounded by an Oort cavit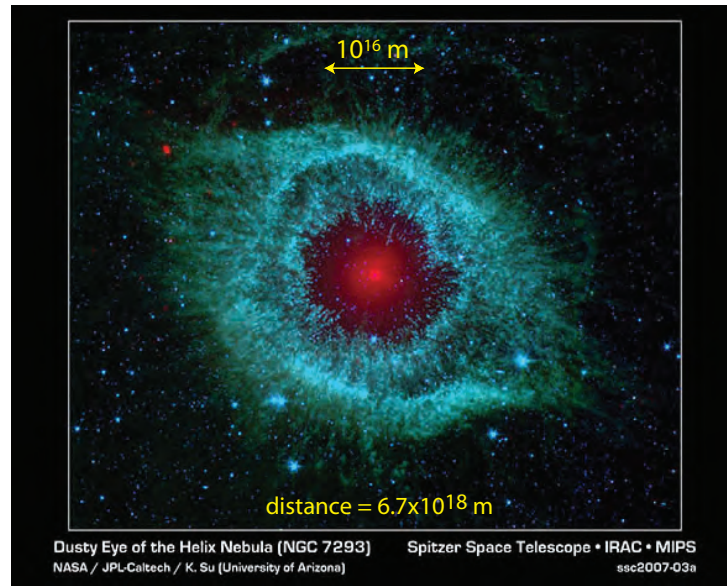y around which some 20,000–40,000 micro brown dwarfs are observed in a band perpendicular to the line-of-sight. They are visible due to heating by the plasma jet of the white dwarf.

may be estimated. Since they are radio CO emission sources, their masses may be estimated from their total CO emission and a normal CO/H emission ratio [32]. They have a cometary shape which allows their masses to also be estimated from an ablation theory applied to their outer atmospheres [33]. Both methods yield mass estimates between 10^{-6} and $10^{-5} M_\odot$. The current literature often explains them as Rayleigh-Taylor instabilities in the outflowing nebular gas. However, RT instabilities would not cause strong density contrasts in the ambient gas. Density contrasts of only 4-6 would be expected from the Rankine-Hugoniot supersonic jump condition, whereas density contrasts of 1000 are observed from direct mass estimates [33]. Attempts to measure their proper motions by comparing HST images at different epochs have been carefully done to define whether they have expanding or static distributions [34], but the results have been inconclusive. The gas outflow velocity of [35] does not refer to the proper motion measured expansion of the system of knots.

V.   ON DIRECT MACHO SEARCHES

With gas clouds apparently absent, the community turned, in the 1990s, to searches for condensed hydrogen-dominated objects and initiated microlensing searches for them. The MACHO [36–38], EROS [39–41] and OGLE [42–44] programs all found microlensing events in front of the Large and Small Magellanic Clouds (MCs) and the galactic center. Early claims that the few detections implied a population of white dwarfs were not substantiated because the population of progenitor stars could not be identified. Most observed objects are white dwarfs, Jupiters or Neptunes, probably inside the MCs and galactic center.

From GHD one expects all galactic DM of earth mass μBDs. This case is just allowed by the MACHO collaboration [36], but ruled out by EROS-1 [40]. However, for observations against the Magellanic clouds, the estimate for the radius of the μBD of $2.6 \cdot 10^{11}$ cm coincides with its typical Einstein radius, leading to the microlensing unfriendly finite-source finite-lens situation [45, 46]. Obscuration by μBDs and refraction by their atmospheres may have hindered the observation of Macho events.

For the μBDs now predicted to be grouped in JCs, blind searching is not optimal. The JCs in front of the Magellanic clouds can be identied from WMAP, Herschel or Planck imaging data. See them also in the DIRBE-COBE image of fig 3. They should be a fertile ground for MACHO searches, but the observation cadence must be greatly increased because of the low mass of the μBDs. For a terrestrial mass MACHO passing in front of a small star the total event duration is approximately 3.5 hrs. For μBD microlenses clustered with properties measured for ordinary globular clusters, some 4,100 events should be visible per year by a dedicated spacecraft that continuously monitors the stars behind any of the 3400 JCs in front of the MCs. The number would increase if a clump of clusters as described below lies in front of the LMC. There should also be multiple events on the same star.

VI.   HALO TEMPERATURES AND CIRRUS CLOUDS

If most of the baryonic dark matter is sequestered away from view in μBDs its thermal emission should still be seen as structured far-IR or sub-mm emission. The μBDs would have been warmer than ambient gas at time of μBD formation, and with their gravitationally heated cores they would be radiating heat away to the universe. Initially this would have cooled the objects significantly on time scales of 1 million years, since it has already been noticed that they are observable as T-dwarfs only in the youngest star forming regions [47]. Thereafter they would have continued to cool in the expanding and cooling universe, but with large cooling blanketing atmospheres they should then have cooled slowly.

Because hydrogen has a triple point at 13.8 K, higher than the 2.725 K cosmic microwave background, phase transitions with significant heats of condensation and fusion have the potential to act as a thermostat to set the temperature of the baryonic dark matter, thus explaining the cool galactic dust temperatures of < 20K [48] and 14–16K and 15–25K [49] as galaxy haloes. Indeed, cooling atomic hydrogen at low density and pressure passes slowly through its triple point, so the μBD population should have dominant thermal emission at or slightly above this temperature. The wavelength of peak emission would be 210 microns, or .21 mm. A detection of this thermal signature has also been made in a careful comparison of IRAF, DIRBE, BOOMERANG, and WMAP images for a Halo region of our Galaxy. These show [50] that the observed structure radiates at approximately 16K and has its peak radiation in the 220 micron DIRBE band. In fig. 3 we show one panel of fig. 2 of [50], which is now understood to be an image of the baryonic dark matter, seen in its emission peak wavelength. Although the far-IR emission of the Halo has been described as "cold dust cirrus" we find from direct imaging a clumped distribution, even with nested clumps, which suggests an interpretation of it as a clumpy distribution of JCs.

This view is supported by the amplitude of the signal. The standard Planck intensity at the DIRBE frequency of 1.25 THz caused by a thermal μBD atmosphere at 15 K is 54 GJy. With an μBD radius of $2.6 \cdot 10^9$ m and the typical distance to the next JC equal to $8.9 \cdot 10^{18}$ m, the Planck intensity is attenuated by the square of their ratio to become 0.9 kJy for the whole JC, about the highest observed value in [50]. Moreover, that nearest JC would have an angular diameter of $0.6°$, slightly less than the largest structure of Fig. 3. Next, the intensity per solid angle can be estimated as 12 MJy/sr, mildly overestimating the maximal scale of 2 MJy/sr of several objects in Fig. 3. We can also estimate the number of structures in Fig. 3. From an isothermal model we predict about 67 structures larger than $0.25°$ in diameter, which is a fair estimate.

With reasonable estimates for their intensity, angular width and number, it is likely that the concentrations in Fig. 3 arise from the JCs that constitute the full Galactic dark matter. Non-baryonic dark matter is relevant only on galaxy cluster scales.

A further aspect is the size of the μBD atmospheres. For redshift $z > 4$ the ambient temperature is above the triple point and atmospheres are large. After that, liquid drops form in the outer atmospheres which rain onto the center. This will lead to a sizable shrinking of the atmospheres, and enhanced transmissivity for radiation, an effect similar to the reionization of the inter cluster gas. The latter may be caused by neutrino condensation on the cluster [19].

VII.   RADIO EVENTS WITH FIXED SOURCES

Extreme Scattering Events were discovered as radio brightness anomalies in quasars. An event was characterized by 30% amplitude fluctuations with a cusp-profiled signature that is somewhat frequency dependent. This allowed them to be understood as a refraction event caused by a centrally condensed gaseous object passing in front of the quasar with a transverse velocity of a few hundred km s^{-1}, the radio analogue of the above quasar brightness fluctuations. A physical model was quickly developed, which included refraction by an ionized outer atmosphere acting as a negative lens that produces the observed pattern of brightness cusps [51]. The objects were described as self-gravitating clouds with approximately spherical symmetry. In the refraction model, an electron column density of 10^{20}m^{-2} is determined. The atmospheres of the objects have a size of 1 AU ($1.5 \cdot 10^{13}$ cm), and must be gravitationally bound or else confined by an ambient pressure. We notice a similarity to the properties of the μBD discovered in quasar microlensing. The ESE clouds would be self-gravitating, have mass less than $10^{-3} M_\odot$, have a size of $10^{14.5}$ cm, are a Halo population, and have typical galactic speeds. Not surprisingly, it is independently estimated that the observed objects may relate to a good part of the galactic DM [51].

A probably related phenomenon is the crescent shaped events seen in the timing data in pulsars, since like the Extreme Scattering Events in quasar brightness curves, the pulsar anomalies are attributed to a refraction phenomenon due to condensed objects along the sight lines. It is inferred that the refraction effect produces multiple images of the pulsar radio signal, and interference of the images causes the observed phenomena. The scattering medium is estimated to have structure on 1 AU for a 10^3 interstellar density enhancement [52]. This corresponds to a radio scattering atmosphere of 10^{16} kg, as expected well below the GHD prediction of an earth mass for the entire object.

VIII.   MYSTERIOUS RADIO EVENTS AS μBD MERGINGS

Recently, a mysterious class of "long duration radio transients" has been observed, lasting more than 30 minutes but less than several days, that have neither a counterpart in the near-infrared, visible or X-ray spectrum nor a quiescent radio state. The event rate is very large, $\sim 10^3 \mathrm{deg}^{-2}\mathrm{yr}^{-1}$ and they can be bright (> 1Jy). They were attributed to old galactic neutron stars [53], but this would lead to a prediction of more luminosity for distant galaxies than observed.
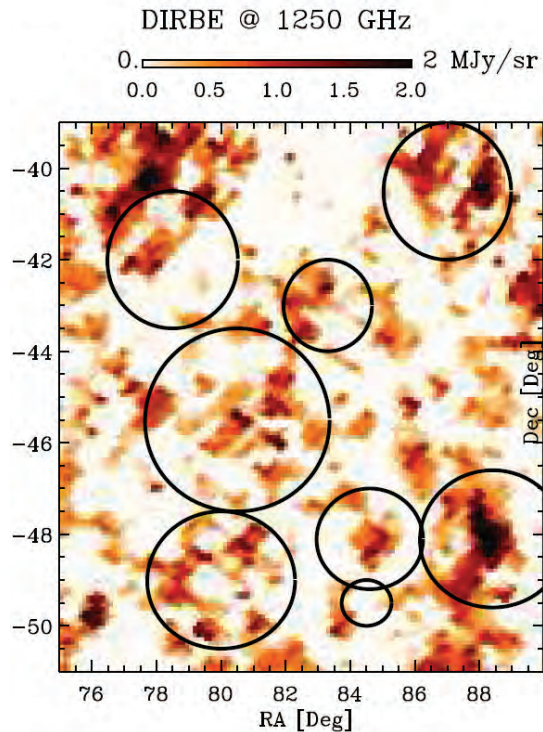
FIG. 3: The DIRBE map of a 15×12 degree region of the Halo, taken from Fig. 2 of [50], with black circles denoting regions of focus. Emission knots at the 240 micron peak of the thermal emission at the 15 K freezing-boiling point of hydrogen are here explained as a few hundred optically dark Jeans clusters at various distances aggregated in clumps.

Within GHD it is natural to connect these events to μBD mergings in the JCs that constitute the BDM halo of the Galaxy. Let us present a statistical estimate for the event frequency. For the typical duration we take $t_{ev} = 1$ day, so the effective μBD radius is estimated as $R_{bd} = v_{bd}\, t_{ev} = 2.6 \cdot 10^{11}$ cm. The typical JC has $(R_{jc}/R_{bd})^3$ cells of linear size R_{bd}. At a given moment in time the average number of μBD pairs that occupy the same cell in a given JC is 0.5. In the Galaxy the number of Jeans clusters is $1.7 \cdot 10^6$. The resulting rate of merging events is $7400/\text{deg}^2\text{yr}$, modestly overestimating the observed value.

The amount of gravitational energy available in the merging process is large, of order GM_{bd}^2/R_{bd}, which means some 10^5 J/kg. Assuming this to be emitted at distance of 3 kpc during the event time of 1 day in a frequency band of 10 GHz gives a bright radio event of 1 Jy; such events are observed, see table 2 of [53]. Ofek et al. also discuss scenarios for the emission in radio such as synchrotron radiation.

IX.   DIRECT DETECTION IN NEARBY STAR FORMING CLOUDS

Recently a 2-3 Jupiter mass object has been discovered in the ρ Ophiuchus star forming region [47]. Estimated properties were a T spectral type, a surface temperature near 1400 degrees K, and an age of one million years. At its inferred distance of 100 pc it is presumed to be a member of the ρ Ophiuchus cloud region because of its heavy visual absorption. Since active star formation in the region is underway, it is inferred that the object has formed in the standard cloud collapse scenario, and represents an object near the bottom of the stellar mass function. It cools quickly (in about a million years), so that it may represent a population of planet-mass MACHO objects. With reasonable assumptions about their luminous lifetimes and number, they have been inferred to be a cosmologically significant population [47]. In GHD one sees the Jupiters as clumps of μBDs, that may go on growing to a star. Hence this observation hints at the population of μBDs.

This discovery is discussed [47] in the context of the many similar objects found in the most active star forming regions in Orion [54, 55]. All these authors recall that such objects would not form in the framework of the standard linearized theory of star formation, and appeal to fragmentation models [56] which, however, seem incompatible with the extreme binarity seen in the statistics of double stars and our solar system's Kuiper Belt Objects.

In Table 1 we show multiple estimates of the same physical parameter where they have been independently estimated in

different research programs related to the muBDs.

Estimator	microlensing	ESE	Cometary knots	T dwarfs
Log Mass ($M_\odot$)	–5.5	< -3	–5.3 (–5.2)	–2.6
Log radius (cm)	–	14.5	15.6	9.9
Log density (cm^{-3})	–	12	6,(5.9), (5.6)	24.2
Velocity (km s^{-1})	600	500	–	–
Cosmological Signf.	yes	yes	–	yes

Table 1. Measured and inferred properties of micro brown dwarfs from various observations. ESE = Extreme Scattering Events.

X.   INFERRED SOURCE OF LYMAN-ALPHA CLOUDS

In quasar spectra a population of thousands of hydrogen-dominated clouds is seen causing weak absorption lines called the Lyman-alpha forest. Their properties have been reviewed [57]. Since they are detected as redshifts of the 1216 Å Ly-α line and are sometimes accompanied by higher level Lyman lines, their identification is secure. In a typical spectrum, one or two stronger and damped lines are also seen. In these cases there are weak metallic absorption lines at the same redshift. Because they are found along sight lines to cosmically distant quasars, much is known about their distribution from their redshifts. They are known to be relatively uniformly distributed in redshift, with, however, mild clumping at distance/size scales of 20 Mpc, showing the cosmic pattern of voids on scales of 30 - 130 Mpc. The depth of cloud absorption lines and their numbers increase with redshift z. Perhaps their most interesting property from a structural point of view is the velocity width parameter measured for each line. The average value is approximately 30 km/s, which suggests that as clouds they should dissipate on a time scales of several years. Their observed permanence was first presumed to imply that the clouds were confined by a hot inter-cluster medium, which was searched for but not found. This has left the subject with no explanation for their structure and common existence.

We propose that the clouds are in fact outer atmospheres of the μBD population in JCs detected in other observations as inferred above. JCs intersecting by the quasar sight line lie in a cylinder, so their mass can be estimated as $0.02\rho_c \cdot \pi R_{jc}^2 \cdot c/H_0$, where the factors describe the average cosmic baryon density not in X-ray gas, the JC surface area and the typical quasar distance, respectively. Though this corresponds to 0.0001 JCs only, a few thousand may actually occur because matter is clumped in filaments between voids, where the baryonic density may be 5-10 times the mean galactic mass density, i.e. about $10^7\rho_c$. In a JC located close to the quasar, about 900 μBDs will lie in front of it, which by their random motion at 30 km/s cause an absorption line of width 30 km/s. This number becomes lower for JCs closer to us, because the opening angle of the quasar covers less of their surface. At higher redshift the μBD atmosphere will be warmer and larger, which explains the increase of Ly$_\alpha$ absorption with z [57].

We attribute the broad absorption lines corresponding to b = 200 km s^{-1} to a set of JCs along the line of sight with this velocity dispersion typical for objects in galaxies, while the involved mass could then be large enough to expose the metal lines. With most JCs located in galaxies, the typical number of JCs per galaxy pierced by the light path of the quasar is 0.001, which explains that per few thousand narrow absorption lines there will typically be a few broad ones.

XI.   IRON PLANET CORES

A perplexing problem is the origin of the magnetic iron cores of the Earth, Mercury and Neptune. It is well known that most of the metallic atoms in the universe are seen in meteoritic dust as oxides of iron, silicon etc. So it is difficult to imagine how the iron was reduced to metallic form underneath an ocean of water. However, primordially formed μBDs offer a direct scenario. From their periodic mergings to form larger planets and eventually stars, they have well-mixed and massive gas and liquid-solid hydrogen layers with wide temperature ranges that gravitationally sweep up and reprocess iron and nickel oxide supernova II star dust from the interstellar medium [58]. Metal oxide dust grains meteor into the hydrogen layers where reaction kinetics and hot mixing mergers reduce iron, nickel and other oxides to metals in solid and liquid forms that sink to form dense metal core layers under oxide layers (rocks, water) with cold outer hydrogen layers. Planets near the sun lose most of their hydrogen atmospheres in their pre-stellar accretion discs and by the solar wind.

Enormous numbers of hydrogen-1 helium-4 planets are produced by the cosmological big bang according to HGD cosmology. Approximately 10^{80} planets in 10^{68} Jeans mass clumps form the baryonic dark matter of the protogalaxies before the first star. All stars form by a sequence of binary mergers of the planets from earth-mass to solar-mass, a million-fold increase in mass. The first stars after the plasma to gas transition should occur in the gravitational free fall time of the Jeans mass clumps of planets; that is, in about 30,000 years. The first supernovae and the first chemicals should be scattered among the trillion planets of the clumps in the same time interval.
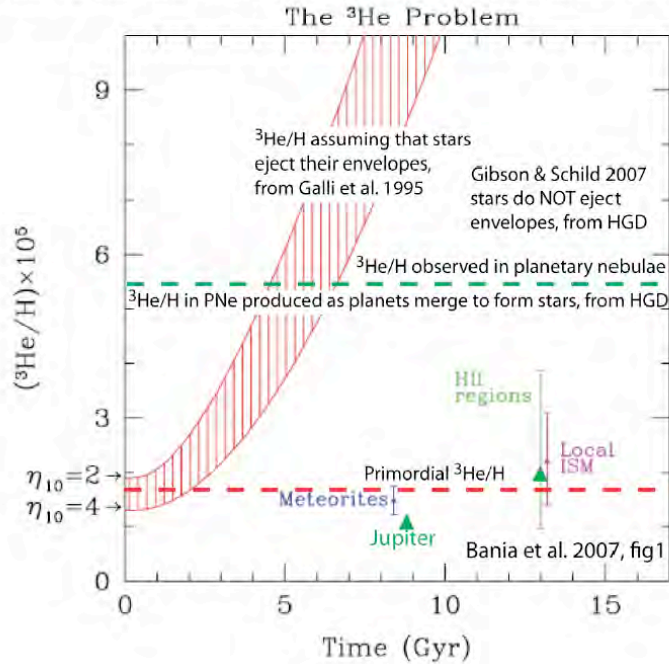
FIG. 4: Solution of the helium-3 problem [63] is provided by hydrogravitational dynamics HGD, where all stars are formed by primordial planet mergers, and do NOT eject stellar materials in massive shells as claimed by the standard models of star formation.

As the first chemicals seed the gas planets the oxides will be rapidly reduced, giving metal cores with molten rocky oceans. These cores are re-cyled periodically. As the planets merge, the metal cores become more massive, the lava oceans become deeper and the hydrogen-helium pressures become larger as the gas atmospheres also merge. Organic chemistry begins promptly in the planet atmosphere as the carbon dioxide becomes monoxide, hydrogen cyanic acid etc. in the hot, dense, moist atmospheres. Finally water oceans condense at 2 million years when the temperature of the universe cools to the critical temperature of 647 K. Only a few rare planets in close solar orbits like Mercury, Venus, Earth and Mars lose their hydrogen dominated atmospheres in favor of oxides.

Critical temperature water oceans in cometary communication provide a cosmic primordial soup for the evolution of life processes [59]. At 8 million years the temperature of the universe cools to 373 K, the freezing point of water, and the biological big bang does not cease but certainly could be expected to slow down.

XII.   BLACK HOLES, YOUNG STARS AND GLOBULAR CLUSTERS

Our conclusion that the long sought baryonic dark matter has been observed already as micro brown dwarfs of planetary mass has implications for the formation process of planets and stars. The observation of young stars (age $\sim$1 Myr) in a disk near the black hole (BH) in the center of our Galaxy known as Sag A*, is difficult to explain and termed the "paradox of youth" [60]. A new scenario is offered by GHD: in a Jeans cluster passing close by the BH the μBDs were heated by the strong tidal forces, they expanded and coagulated in situ into new stars; this JC got disrupted and its stars ended in a plane.

Tidal forces by heavy central BHs may generally have a strong impact on nearby passing JCs. Let us suppose that JCs have an appreciable chance to be transformed into a globular star cluster (gc) when their gravitational energy $GM_{BH}M_{jc}/R$ exceeds a certain bound E_c, which happens when they pass within a distance $R_* \sim M_{BH}$. In an isothermal model their number $N(R_*)$ is proportional to R_*, explaining that $N_{gc} \sim N(R_*)$ is proportional to M_{BH}, in accordance with the observation $M_{BH} \sim N_{gc}^{1.11\pm0.04}$ [61].

XIII.   HELIUM-3 IN PLANETARY NEBULAE

Nucleosynthesis following the cosmological big bang event permits formation of mostly hydrogen and helium-4, with only trace amounts of hydrogen-2, hydrogen-3 and helium-3. The primordial helium-3 to hydrogen-1 ratio is $1.4 \cdot 10^{-5}$ [62]. HGD cosmology solves a crisis in star formation theory termed the helium-3 problem, as shown in figure 4.

XIV.   CONCLUSION AND OUTLOOK

Contrary to the current opinion, the galactic dark matter (DM) is likely of baryonic origin and observed already. It may seem ironic that nature has sequestered most of the baryonic matter in nested clumps of clumps, from planet mass to cluster and then to galactic scale. The structure predicted by the theory of gravitational hydrodynamics, micro brown dwarfs (μBDs, muBDs) grouped in Jeans clusters (JCs), is supported by an impressive body of observations: quasar microlensing, planetary nebulae, 15K cold dust temperatures, "cirrus clouds", extreme scattering events, parabolic events, direct observations and long duration radio events. This picture offers an explanation for paradoxes such as the Lyman-alpha forest, iron planet cores and young stars near the black hole in the center of the Galaxy. Globular clusters seem to arise from JCs that are heated by tidal forces when passing nearby the galaxy's central black hole. Likewise, galaxy merging turns dark JCs into young globular clusters along the merging path [15], rather than producing tidal tails of old stars that have remained unobserved [22] We summarize our findings in Table 2.

The direct search by Eros-I has concluded that the case of earth mass Machos is ruled out. However, for our μBDs the Einstein radius that describes the lensing is comparable with the physical radius of the lens object, which complicates the lensing. This motivates new MACHO searches, which we plan to start in January 2011, next "LMC season", benefiting from the improvement of CCD cameras and taking into account the finite–source and finite–lens size effects. With the JCs in front of the Magellanic clouds and the Galactic bulge to be identified first by the Planck mission, or the ones detected already as "cirrus clouds" by DIRBE, BOOMERANG and WMAP, the task is reduced to searching lensing events by μBDs in their JCs, a much more direct approach than the blind searches performed till now.

The cold dark matter paradigm seems to be left with a bleak face. In our picture its purported elementary particle has no reason to exist, because large scale structure formation can progress from gravitational hydrodynamics alone [15]. Meanwhile the expected mass budget of the Galactic dark halo is well estimated by our counting of cirrus clouds and our modeling of μBD mergings as the observed radio events. For the extra-Galactic situation, these findings are in line with the optical depth in quasar micro-lensing being of order unity. In line with this, the recent Xenon 100 cold dark matter search has ruled out all previous detection claims [3]. Massive neutrinos pose an alternative DM scenario [19], which is cosmologically sound [15]. Detection of the 1.45 eV neutrino mass in Katrin 2015 would solve the notorious dark matter riddle in a dual manner, by dark baryons for the "Oort" galactic DM, clustered according to gravitational hydrodynamics, and by massive neutrinos for the "Zwicky" cluster DM.

It would also be interesting to have more cases where the JCs can be resolved into their constituent μBDs, such as it is possible in planetary nebulae. An interesting case is the star formation region in the Galaxy in the direction Crux, where individual Jeans clusters can be identified from their 14 K thermal emission in recent images [64].

Extreme reliance on linearized theories in astrophysics seems to have seriously misguided the star formation theory. When direct simulations of gravitational perturbations in a gas cloud showed collapse, the result was dismissed as unphysical and due to numerical instability [65], and eliminated by Jeans filters. However, we consider the instability as physical, producing e.g. the discussed μBDs, and the linearized theory as oversimplified. Merging and infall of μBDs then offers a new scenario for the formation of heavier objects, from super-earths to heavy stars. This work thus motivates the numerical study of the full nonlinear hydrodynamics of structure formation and the N-body dynamics of μBD merging as a precursor to star formation and galaxy merging.

Observation	Jeans cluster	micro brown dwarf	cosmol. signif.
galaxy merging	yes	inferred	yes
quasar microlensing	inferred	yes	yes
planetary nebulae	yes	yes	yes
cold halo temperatures	–	yes	–
cirrus clouds	yes	yes	yes
extreme scattering events	inferred	yes	yes
parabolic events	–	yes	–
mysterious radio events	yes	yes	yes
direct detection T-dwarf	–	inferred	–
Ly-alpha forest	inferred	yes	inferred
Iron planet cores	–	inferred	–
BH mass – # globulars	yes	inferred	–

Table 2. Observations discussed in the text, their relation to Jeans clusters and micro brown dwarfs and their cosmological significance.

[1] Oort, J. H. The force exerted by the stellar system in the direction perpendicular to the galactic plane and some related problems. *Bull. Astron. Inst. Netherl.* **6**, 249–287 (1932)

[2] Zwicky, F. Die Rotverschiebung von extragalaktischen Nebeln. *Helv. Phys. Acta* **6**, 110–127 (1933)

[3] Aprile, E. *et al.* First Dark Matter Results from the XENON100 Experiment. *arXiv:*1005.0380 (2010)

[4] Diemand, J., *et al.* Clumps and streams in the local dark matter distribution. *Nature* **454**, 735–738 (2008)

[5] Bouwens, R. J. *et al.* Constraints on the First Galaxies: $z \sim$ 10 Galaxy Candidates from HST WFC3/IR. *arXiv:*0912.4263

[6] Oesch, P. *et al.* Structure and Morphologies of $z \sim 7–8$ Galaxies from Ultra-deep WFC3/IR Imaging of the Hubble Ultra-deep Field. *Astrophys. J.* **709**, L21–L25 (2010).

[7] Schild, R. E. & Gibson, C. H. Goodness in the Axis of Evil. *arXiv:*0802.3229 (2008)

[8] Kashlinsky, A., Atrio-Barandela, F., Kocevski, D.& Ebeling, H. A measurement of large-scale peculiar velocities of clusters of galaxies: results and cosmological implications, *Astrophys. J.* **686**, L49–L52 (2008)

[9] Elmegreen, D. M. *et al.* Galaxy Morphologies in the Hubble Ultra Deep Field: Dominance of Linear Structures at the Detection Limit. *Astrophys. J.* **631**, 85–100 (2005)

[10] Lee, J. & Komatsu, E. Bullet cluster: a challenge to ΛCDM cosmology. *Astrophys. J.* **718**, 6065 (2010)

[11] Disney, M. J. *et al.* Galaxies appear simpler than expected. *Nature* **455**, 1082–1084 (2008)

[12] Kroupa, P. *et al.* Local-Group tests of dark-matter Concordance Cosmology: Towards a new paradigm for structure formation? *arXiv:*1006.1647

[13] Gibson, C. H. Turbulence in the Ocean, Atmosphere, Galaxy, and Universe. *Appl. Mech. Rev.* **49**, 299–315 (1996)

[14] Gibson, C. H. Turbulence and turbulent mixing in natural fluids. Physica Scripta, Turbulent Mixing and beyond 2009 Proceedings, T142 (2010) *arXiv:*1005.2772.

[15] Nieuwenhuizen, T. M., Gibson, C. H. & Schild, R. E. Gravitational hydrodynamics of large-scale structure formation. *Europhys. Lett.* **88**, 49001,1–6 (2009)

[16] Geller, M. J. & Huchra, J. P. Mapping the Universe. *Science* **246**, 897–903 (1989)

[17] Rusin, D. & Kochanek, C. S. The evolution and structure of early–type field galaxies: a combined statistical analysis of gravitational lenses. *Astrophys. J.* **623**, 666–682 (2005)

[18] Hubble, E. P. Distribution of luminosity in elliptical nebulae. *Astrophys. J.* **71**, 231–276 (1930)

[19] Nieuwenhuizen, T. M. Do non-relativistic neutrinos constitute the dark matter? *Europhys. Lett.* **86**, 59001, 1–6 (2009)

[20] Gibson, C. H. & Schild, R. E. Interpretation of the Tadpole VV29 merging galaxy system using Hydro-Gravitational Theory arXiv:astro-ph/0210583 (2002)

[21] Tran, H. D., Sirianni, M. *et al.* Advanced Camera for Surveys Observations of Young Star Clusters in the Interacting Galaxy UGC 10214. *Astrophys. J.* **585** 750 (2003)

[22] Bournaud, F., Duc, P. A. & Emsellem, E., High-resolution simulations of galaxy mergers: resolving globular cluster formation. *Monthl. Not. Roy. Astron. Soc.* **389**, L8–L12 (2008)

[23] Schild, R. E. Microlensing variability of the gravitationally lensed quasar Q0957+561 A,B. *Astrophys. J.* **464**, 125–130 (1996)

[24] Pelt, J., Schild, R., Refsdal, S. & Stabell, R. Microlensing on different timescales in the lightcurves of QSO 0957+561 A,B. *Astron. & Astrophys.* **336**, 829–839 (1998)

[25] Schild, R. E. A wavelet exploration of the Q0957+561 A, B brightness record. *Astrophys. J.* **514**, 598–606 (1999).

[26] Schneider, P., Ehlers, J. & Falco, E. Gravitational Lenses. (Springer, Berlin, 1992)

[27] Schild, R. E. & Vakulik, V. Microlensing of a Ring Model for Quasar Structure. *Astron. J.* **126**, 689–695 (2003).

[28] Burud, I. *et al.* An Optical Time Delay Estimate for the Double Gravitational Lens System B1600+434. *Astrophys. J.* **544**, 117–122 (2000)

[29] Burud, I. *et al.* Time delay and lens redshift for the doubly imaged BAL quasar SBS 1520+530. *Astron. & Astrophys.* **391**, 481–486 (2002)

[30] Paraficz, D. *et al.* Microlensing variability in time-delay quasars. *Astron. & Astrophys.* **455**, L1–L4 (2006)

[31] Hora, J. L., Latter, W. B., Smith, H. A. &Marengo, M. Infrared observations of the helix planetary nebula. *Astrophys. J.* **652**, 426–441 (2006); Err. - ibid. **656**, 629 (2007).

[32] Huggins, P. J., Forveille, T., Bachiller, R., Cox, P., Ageorges, N., & Walsh, J. R. High-Resolution CO and H2 Molecular Line Imaging of a Cometary Globule in the Helix Nebula. *Astrophys. J.* **573**, L55–L58 (2002)

[33] Meaburn, J. *et al.* The nature of the cometary knots in the Helix planetary nebula (NGC 7293) *Monthl. Not. Roy. Astron. Soc.* **294**, 201– 223(1998)

[34] O'Dell, C. and Handron, K. Cometary knots in the Helix nebula. *Astron. J.* **111**, 1630–1640 (1996)
Burkert A. & O'Dell, C.R. The Structure of Cometary Knots in the Helix Nebula. *Astrophys. J.* **503**, 792–797 (1998)

[35] Meaburn, J. & Boumis, P. Flows along cometary tails in the Helix planetary nebula NGC 7293. *Monthl. Not. Roy. Astron. Soc.* **402** 381–385 (2010)

[36] Alcock, C. *et al*, The MACHO Project LMC Microlensing Results from the First Two Years and the Nature of the Galactic Dark Halo. *Astrophys. J.* **486** 697–726 (1997).

[37] Alcock, C. *et al.* The MACHO Project: Microlensing Results from 5.7 Years of LMC Observations. *Astrophys. J.* **542**,

281–307 (2000)

[38] Alcock, C. *et al.* The MACHO Project: Microlensing Detection Efficiency. *Astrophys. J. Sup.* **136**, 439–462 (2001)

[39] Aubourg, E, *et al.* Evidence for gravitational microlensing by dark objects in the Galactic halo. *Nature* **365**, 623–625 (1993)

[40] Renault, C. *et al*, Search for planetary mass objects in the Galactic halo through microlensing. *Astron. & Astrophys.* **329** 522–537 (1998)

[41] Tisserand, P. *et al.*, Limits on the Macho Content of the Galactic Halo from the EROS-2 Survey of the Magellanic Clouds. *Astron. & Astrophys.* **469**, 387–404 (2007)

[42] Udalski, A. *et al.* The optical gravitational lensing experiment. Discovery of the first candidate microlensing event in the direction of the Galactic Bulge. *Acta Astron.* **43**, 289–294 (1993)

[43] Wyrzykowski, L., *et al.* The OGLE view of microlensing towards the Magellanic Clouds I. A trickle of events in the OGLE-II LMC data. *Mon. Not. R. Astron. Soc.* **397**, 1228–1242 (2009)

[44] Sumi, T. *et al.* A Cold Neptune-Mass Planet OGLE-2007-BLG-368Lb: Cold Neptunes Are Common. *Astrophys. J.* **710**, 1641–1653 (2010)

[45] Agol, E. Occultation and microlensing. *Astrophys. J.* **579** 430–436 (2002).

[46] Lee, C. H., Seitz, S., Riffeser, A. & Bender, R. Finite-source and finite-lens effects in astrometric microlensing *arXiv*:1005.3021

[47] Marsh, K., Kirkpatrick, D. & Plavchan, P. A young planetary-mass object in the ρ Oph cloud core. *Astrophys. J.* **709**, L158–L162 (2010)

[48] Radovich, M., Kahanpaa, J. & Lemke, D. Far-infrared mapping of the starburst galaxy NGC 253 with ISOPHOT. *Astron. & Astrophys.* **377**, 73–83 (2001)

[49] Liu, G., *et al.* An Investigation of the Dust Content in the Galaxy pair NGC 1512/1510 from Near-Infrared to Millimeter Wavelengths. *Astron. J.* **139**, 1190–1198 (2010)

[50] Veneziani, M. *et al.* Properties of galactic cirrus clouds observed by BOOMERanG. *Astrophys. J.* **713**, 959–969 (2010)

[51] Walker, M. & Wardle, M. Extreme scattering events and Galactic dark matter. *Astrophys. J.* **498** L125–L128 (1998)

[52] Walker, M. Extreme scattering events: insights into interstellar medium on AU-scales. *astro-ph*/0610737.

[53] Ofek, E. O. *et al.* Long-duration radio transients lacking optical counterparts are possibly galactic neutron stars. *Astrophys. J.* **711**, 517–531 (2010).

[54] Lucas, P. Weights, D. Roche, P. & Riddick, F. Spectroscopy of planetary mass brown dwarfs in Orion. *Monthl. Not. Roy. Astron. Soc.* **373**, L60–L64 (2006)

[55] Osorio, M. R. Z., Bejar, V. J. S., Martin, E. L. *et al.* Discovery of young, isolated planetary mass objects in the sigma Orionis star cluster. *Science* **290**, 103–107 (2000).

[56] Whitworth, A. P. & Stamatellos, D. The minimum mass for star formation, and the origin of binary brown dwarfs. *Astron. & Astrophys.* **458**, 817–829 (2006)

[57] Rauch, M. The Lyman Alpha Forest in the Spectra of QSOs. *Ann. Rev. Aston. & Astrophys.* **36**, 267–316 (1998)

[58] Schild, R. E. & Dekker, M. The transparency of the Universe limited by Lyman-alpha clouds. *Aston. Nachr.* **327**, 729-732 (2006)

[59] Gibson, C. H., Schild, R. E. and Wickramasinghe, N. C., The origin of life from primordial planets, *Int. J. of Astrobiology*, (2011) doi:10.1017/S147355041000352, *arXiv*:100.0504

[60] Lu, J.R., Ghez, A.M. *et al.* A disk of young stars at the Galactic center as determined by individual stellar orbits. *Astrophys. J.* **690**, 1463–1487 (2009)

[61] Burkert, A. & Tremaine, S. A correlation between central supermassive black holes and the globular cluster systems of early-type galaxies. *arXiv*:1004.0137.

[62] Fuller, G. M. and C. J. Smith, Nuclear weak interaction rates in primordial nucleosynthesis *Phys. Rev. D.*, 82:125017, *arXiv*:1009.0277v1 (2011)

[63] Gibson, C. H., Why the dark matter of galaxies is clumps of micro-brown-dwarfs and not Cold Dark Matter, *arXiv*:1102.1183 (2011)

[64] Photograph of star formation region in Crux: http://sci.esa.int/science-e/www/object/index.cfm?fobjectid=3D45626.

[65] Truelove, J. K. *et al.* The Jeans condition. A new constraint on spatial resolution in simulations of isothermal self-gravitational hydrodynamics. *Astrophys. J.* **489**, L179–L183 (1997)

ADDITIONAL MATERIAL

A. PROPERTIES OF JEANS CLUSTERS

Right after the transition of plasma to gas (decoupling of photons, recombination of electrons and protons) there appears fragmentation at the Jeans length, creating JCs, and inside them at the viscous length, creating μBDs [15]. Following Weinberg, we estimate the typical mass of a JC to be $6 \cdot 10^5 M_\odot$. Let M_{jc} denote the typical mass of the JCs and v_{jc} their velocity dispersion, and M_{bd} and v_{bd} the ones of the μBDs. We introduce the dimensionless variables $m_6 = M_{jc}/6 \cdot 10^5 M_\odot$, $v_{200} = v_{jc}/200$ km s^{-1}, $m_{bd} = M_{bd}/M_\oplus$, $v_{30} = v_{bd}/30$ km s^{-1}; these parameters are taken equal to unity in the main text, but kept free here and below.

For the distribution of μBDs in a JC we consider the isothermal model $\rho_{bd}(r) = v_{bd}^2/2\pi G r^2$ where $v_{bd} = v_{bd}^{rot}/\sqrt{2}$ is the velocity dispersion in terms of the rotation speed. The number density is $n_{bd} = \rho_{bd}/M_{bd}$. A JC has virial radius $R_{jc} =$

$GM_{jc}/2v_{bd}^2 = 4.4 \cdot 10^{16}(m_6/v_{30}^2)$ m and contains $N_{bd}^{jc} = 2.0 \cdot 10^{11}(m_6/m_{bd})$ μBDs. The time for a μBD to cross the JC is $R_{jc}/v_{bd} = 47,000\,(m_6/v_{30}^3)$ yr, short enough to induce the isothermal distribution because of Lynden Bell's "violent relaxation". The average mass density is $3M_{jc}/4\pi R_{jc}^3 = 3.3 \cdot 10^{-15}(v_{30}^3/m_6^2)$ kg/m^3.

Our galaxy with mass $m_{12}10^{12}M_\odot$ has a number $N_{jc} = 1.7 \cdot 10^6 m_{12}/m_6$ of JCs in its halo, that also form an ideal gas with an isothermal distribution $\rho_{jc} \equiv M_{jc}n_{jc} = v_{jc}^2/2\pi Gr^2$, a shape central to the explanation of the flattening of rotation curves and the Tully-Fisher and Faber-Jackson relations [15].

B.   TADPOLE GALAXY MERGING

The beginning of the wake in Fig. 1 starts at $R_{gal} = 4 \cdot 10^{21}$ m $= 420,000$ lyr from the center. Its width can be estimated at this point as $2R_{wake} = 1.5 \cdot 10^{19}$ m, and is kept fairly constant over the entire length. For spherical symmetry the mass enclosed within R_{gal} is $2v_{jc}^2 R_{gal}/G = 2.4 \cdot 10^{12}v_{200}^2 M_\odot$, a reasonable value. We estimate the number of JCs in this light path as the number in a cylinder of radius R_{wake} through the center, $N_{jc}^{wake} = \int_0^{R_{gal}} dz \int_0^{R_{wake}} dr_\perp 2\pi r_\perp n_{jc}(\sqrt{r_\perp^2 + z^2})$, yielding the estimate $N_{jc}^{wake} = 5900\, v_{200}^2/m_6$, which is correct within a factor of a few.

C.   NUMBER OF μBDs IN QUASAR MICROLENSING

Let us estimate the number of μBDs in the lens through which we observe the quasar Q0957A+B discussed in the main text. We take Hubble constant $H = 70$ km/(s Mpc). The quasar has redshift $z_Q = 1.43$ and angular distance $d_Q = 5.6 \cdot 10^{27}$ cm, the lens has $z_L = 0.355$ and $d_L = 3.2 \cdot 10^{27}$ cm. The most luminous part of the quasar is the inner ring of the accretion disk of $4 \cdot 10^{16}$ cm in diameter and 10^{14} cm wide, observed as angular diameters $1.5\,\mu$as and 3.7 nas, somewhat distorted through shear in the lens. At the position of the lens this corresponds to a luminous ring of physical diameters $d_1 = 2.3 \cdot 10^{16}$ cm and $d_2 = 5.7 \cdot 10^{13}$ cm, much less than the above JC radius, but much more than the μBD radius of $2.6 \cdot 10^{11}$ cm discussed below. The Einstein radius of an μBD in the lens is $R_E = (2/c)(GM_{bd}d_L)^{1/2} = 7.5 \cdot 10^{13}m_{bd}^{1/2}$ cm, slightly larger than d_2, so we are in the finite-source point-lens situation.

With the quasar observed in arm A under angle $\theta_A = 5''$ with respect to the center of the lensing galaxy and under $\theta_B = 1''$ in the B arm, the shortest physical distance of the light paths to the center of the lens galaxy is $r_A = \theta_A d_L = 7.8 \cdot 10^{22}$ cm and $r_B = 1.6 \cdot 10^{22}$ cm, respectively. The average number of JCs that lie along the A sight line is $N_A = n_{2D}^{jc}(r_A)\pi R_{jc}^2$, where $n_{2D}^{jc}(r) = v_{jc}^2/2GM_{jc}r$ is the projected isothermal number density. This brings $N_A = 0.002\,m_6 v_{200}^2/v_{30}^4$ and likewise $N_B = 0.01\,m_6 v_{200}^2/v_{30}^4$. Being nearly of order unity, these numbers support the fact that microlensing events are observed in both arms and put forward that each of the two sight lines of the quasar pierces through one JC.

Not having information about the distance of the sight lines to the centers of the JCs, we take for the $2D$ number density of μBDs the average value $n_{2D} = N_{bd}^{jc}/\pi R_{jc}^2$. With active area $\pi d_1 R_E$ this estimates that $18,000\,v_{30}^4/m_6\sqrt{m_{bd}}$ μBDs overlap the ring at any moment in time in either arm. The optical depth, i. e., the number of μBDs that lie inside a cylinder with radius R_E, takes the typical value $n_{2D}\,\pi R_E^2 = 58\,v_{30}^4/m_6$. (These estimates do not account for the shear). The lower values of 1.35 and 0.35 deduced from the signal analysis arise when the sight lines are near the border of the JCs, where the μBD density is lower than average. All by all, the observations are consistent with isothermal modeling of μBDs in JCs.

D.   MACHOS IN FRONT OF THE MAGELLANIC CLOUDS

The Small and Large Magellanic Clouds (MCs) are satellites of the Milky Way at distance $L = 48.5$ kpc for the LMC, having $\nu\,10^{10}$ stars in their surface of 9+84 deg^2 on the sky, with $\nu = O(1)$, per unit solid angle equivalent to $1.1\nu\,10^8/$deg^2. The angular surface of a JC at distance xL (we take the typical JC half way, $x = \frac{1}{2}$) is $\Omega_{jc} = \pi R_{jc}^2/x^2 L^2 = 3.7 \cdot 10^{-5}(m_6^2/v_{30}^4)$ deg^2, so the average number of stars of the MCs covered by a JC is $3900\,(\nu m_{jc}^2/v_{30}^4)$. The number of JCs up to distance L is $N_{jc}^L = 2v_{jc}^2 L/GM_{jc} = 1.5 \cdot 10^6(v_{200}^2/m_{jc})$, so in front of the MCs there are some $3400\,v_{200}^2/m_6$ JCs. They should be identified from direct thermal emission by the WMAP and Planck satellites, as foregrounds that have to be subtracted in order to study the cosmic microwave background.

When an μBD comes within the Einstein radius $R_E = \sqrt{4x(1-x)GM_{bd}L}/c = 2.6\,10^9\sqrt{m_{bd}}$ m to the sightline of a small star, it acts as a lens and enhances the intensity during a time $t_E = R_E/v_{jc} = 3.6\sqrt{m_{bd}}/v_{200}$ hrs. The μBDs that lens a given star within in a period Δt, lie in a strip on the sky with surface $\Delta O = 2R_E v_{jc}\Delta t$, which embodies $N_{bd}^{jc}\Delta O/\pi R_{jc}^2$ μBDs. This leads to a lensing event rate of $1.1\,(v_{200}v_{30}^4/\sqrt{m_{bd}}m_6)/$yr for each star covered by a JC and monitoring this frequency allows to estimate m_{jc}. With $3400\,m_6^2\nu/v_{30}^4$ stars of the MCs per JC, this leads $4100\,(m_6\nu v_{200}/\sqrt{m_{bd}})$ of Macho events per yr per JC and in total $1.4 \cdot 10^7\,\nu v_{200}^3/\sqrt{m_{bd}}$ events per year in front of the MCs.

In the Eros–I search some $2 \cdot 10^6$ stars were monitored, so we would expect some 2800 lensing events per year, while none was monitored. It was realized that the stellar radii are at least comparable to the Einstein radius (finite source); no lensing detection is made when the stellar radius exceeds 16 solar radii, which excludes a good part of the studied stars. However, also the deflector is extended (finite lens), because the Einstein radius of the μBD just coincides with our estimate for its physical

radius. This may lead to obscuration, and on top of this, there will be refraction effects from the atmosphere of the μBD: Lensing of earth mass μBDs towards the MCs appears to be a subtle case, that calls for more study.

Each JC has N_{bd}^{jc} μBDs with Einstein area $\Omega_E = \pi R_E^2/x^2 L^2 = 1.2\,10^{-19} m_{bd}$ deg^2. This brings a coverage fraction or "optical depth" equal to $\tau = N_{bd}^{jc}\Omega_E N_{jc}^L/4\pi = 2v_{jc}^2/c^2 = 8.9\,10^{-7}v_{200}^2$, as is well known. But JCs themselves have a much larger optical depth, $\tau = N_{bd}^{jc} R_E^2/R_{jc}^2 = 6.7\cdot 10^{-4}(v_{30}^4/m_6)$, so it is of course advantageous to identify the JCs first and search behind them.

E.   COMPOSITION OF CIRRUS CLOUDS

Fig. 3 of the cirrus clouds shows mass concentrations with kJy emission [50]. Let us assume that this DIRBE signal at $\nu = 1.25$ THz stems from thermal emission at the μBD surface with temperature 15 K, with the Planck function equal to $I_\nu = 4\pi\hbar\nu^3/[\exp(2\pi\hbar\nu/k_B T) - 1]c^2 = 54$ GJy. We first investigate whether it may arise from individual μBDs. The distance to the nearest μBD can be estimated if the Sun is inside a local Jeans cluster. The typical number density $3M_{jc}/4\pi R_{jc}^3 M_{bd}$ leads to a typical distance $d_1 = 1.2\cdot 10^{15}(m_6^{2/3} m_{bd}^{1/3}/v_{30})$ cm, or 82 AU, which is well before the Oort cloud, believed to start at 2000 AU. With the μBD radius taken from previous section, we get an intensity $J = I_\nu R_{bd}^2/d_1^2 = 2.4\,(t_d^2 v_{30}^6/m_6^{4/3} m_{bd}^{2/3})$ kJy, the observed scale. But the angular diameter of an μBD at this distance is $0.02°$, much smaller than the structures in Fig. 3.

The signal is therefore more likely arising from JCs. Their local number density is isothermal, $n = v_{jc}^2/2\pi GM_{jc}d_{SagA*}^2$, involving the distance 25,000 lyr to Sag. A*, and yields the typical distance to next JC as $d_2 = n^{-1/3} = 8.9\cdot 10^{18}(m_6^{1/3} v_{200}^{2/3})$ m or 940 lyr. The $2\cdot 10^{11}$ μBDs in next JC bring together also a kJy signal, $J = N_{bd}^{jc} I_\nu R_{bd}^2/d_2^2 = 0.92\,(t_d^2 m_6^{1/3} v_{200}^{4/3} v_{30}/m_{bd})$ kJy. At this distance the JC diameter $2R_{jc}$ appears at an angle of $2\theta = 2R_{jc}/d_2 = (m_6^{2/3} v_{200}^{2/3}/v_{30})\,0.57°$, in good agreement with the largest structures of Fig. 3. The angular surface of the JC is $\Omega = \pi\theta^2$. The intensity per unit solid angle is $dJ/d\Omega \approx J/\Omega = I_\nu N_{bd}^{jc} R_{bd}^2/\pi R_{jc}^2 \text{sr} = 11.7(t_d^2 v_{30}^2/m_6 m_{bd})$ MJy/sr. Several structures in fig. 3 have the maximal intensity of 2 MJy/sr, this is achieved for JCs for proper values of t_d and m_6.

Let us estimate the number of structures in Fig. 3. Arising from JCs with equal intensity at varying distances, they form clumped structures with diameter of $1°$ down to, say, $0.25°$, corresponding to distances $d_1 = 5.1\cdot 10^{18} m_6/v_{30}^2$ m and $d_2 = 2.0\cdot 10^{19} m_6/v_{30}^2$ m, respectively. The number of JCs in a spherical shell between them is $N_{4\pi} = 2v_{jc}^2(d_2 - d_1)/GM_{bd} = 15,000v_{200}^2/v_{30}^2$. In a DIRBE area one gets as number of JCs $N_{4\pi}15° \times 12°/4\pi\text{rad}^2 = 67v_{200}^2/v_{30}^2$, which is a fair estimate for the number of structures in Fig. 3.

We can therefore conclude that these concentrations likely arise from JCs that constitute the full Galactic dark matter.

F.   RATE OF μBD MERGING

We attribute the observed radio events to merging of μBDs in JCs that constitute the BDM of the Galaxy. Let us present a statistical estimate for its frequency. From the event duration t_{ev} the effective μBD radius is estimated as $R_{bd} = v_{bd}\,t_{ev} = 2.6\cdot 10^{11}t_d v_{30}$ cm. The typical JC has $N_{cell}^{jc} = (R_{jc}/R_{bd})^3$ cells of linear size R_{bd}. At a given moment in time its typical number of events, i. e., the number of μBD pairs that occupy the same cell, is of order unity, $\frac{1}{2}N_{bd}^{jc}(N_{bd}^{jc} - 1)/N_{cell}^{jc} = 0.50\,t_d^3 v_{30}^9/m_6 m_{bd}^2$. The rate of mergings is this number divided by t_e, viz. $3.1\cdot 10^8(m_{12}t_d^2 v_{30}^9/m_6^2 m_{bd}^2)/$yr, corresponding to $7400\,(m_{12}t_d^2 v_{30}^9/m_6^2 m_{bd}^2)/$deg^{2}yr. This estimates fairly well the observed rate $\sim 1000/$deg^{2}yr and the extraploated full sky rate $4.1\,10^7/$yr is equivalent to $6\cdot 10^{17}$ merging events in the Hubble period of 14 Gyr, which amounts to two merging events per μBD. Given that all large objects, like the Sun, arise from merged μBDs, there should still be many original μBDs, and this is observed in Fig. 2 of Helix.

The amount of energy available in the merging process is large, of order GM_{bd}^2/R_{bd}, some 10^5 J/kg. Assuming this to be emitted at distance of 3 kpc during the event time of 1 day in a frequency band of 10 GHz gives a bright radio event of 1 Jy; such events are observed, see table 2 of [53].

G.   LYMAN ALPHA FOREST

Let us consider a quasar of mass $M_q = m_9 10^9 M_\odot$ at redshift $z_q = 3$. It has a Schwarzschild radius $R_q = 2GM_q/c^2 = 3.0\cdot 10^{12} m_9$ m and angular distance $d_A(z_q) = 5.1\cdot 10^{25}$ m. A JC, at redshift z, is much larger, the number of its μBDs in front of the quasar $N_{bd}^q(z) = N_{bd}^{jc}(R_q/d_A(z_q))^2(d_A(z)/R_{jc})^2$ equals $890(m_9^2 v_{30}^4/m_6 m_{bd})d_A^2(z)/d_A^2(z_q)$.

JCs intersected by the quasar sight line lie in a cylinder of radius R_{jc}, so their mass can be estimated as $0.02\rho_c \cdot \pi R_{jc}^2 \cdot c/H_0$, where the factors describe the average cosmic baryon density not in X-ray gas, the surface area and typical quasar distance, respectively. This corresponds to 0.0001 JCs. But the typical density in filaments between cosmic voids is $5 - 10$ times the average galactic density of 0.2 $M_\odot/$pc^3, some $10^7\rho_c$, so the clumpedness of matter can explain that indeed μBDs cause a narrow absorption line per JC.

Why the dark matter of galaxies is clumps of micro-brown-dwarfs and not Cold Dark Matter

Carl H. Gibson[1,2]

[1]University of California San Diego, La Jolla, CA 92093-0411, USA

[2]cgibson@ucsd.edu, http://sdcc3.ucsd.edu/~ir118

ABSTRACT

Observations of quasar microlensing by Schild 1996 show the baryonic dark matter BDM of galaxies is micro-brown-dwarfs, primordial hydrogen-helium planets formed at the plasma to gas transition 10^{13} seconds, in trillion-planet clumps termed proto-globular-star-clusters PGCs. Large photon-viscosity ν of the plasma permits supercluster-mass gravitational fragmentation at 10^{12} seconds when the horizon scale $L_H = ct$ is matched by the Schwarz viscous scale L_{SV} of Gibson 1996. Voids begin expansion at sonic speeds $c/ 3^{1/2}$, where c is light speed and t is time, explaining 10^{25} meter size regions observed to be devoid of all matter, either BDM or non-baryonic NBDM. Most of the NBDM is weakly-collisional, strongly-diffusive, neutrino-like particles. If cold NBDM (CDM) is assumed, it must soon become warm and diffuse because it is weakly-collisional. It cannot clump and its clumps cannot clump. CDM is ruled out with 99% confidence by local–group satellite observations of Kroupa et al. 2010. The satellites are clusters of PGCs. PGCs are recaptured by the Galaxy on an accretion disk as they freeze and diffuse from its core to form its BDM halo. Stars form by viscous mergers of primordial gas planets within PGCs. Stars die by overeating mBDs, making the first chemicals, oceans and life at 2-8 Myr.

1. Introduction

Dark matter is missing mass needed to explain why rapidly rotating objects like galaxies do not fly apart due to centrifugal forces. The candidates for the dark matter are ordinary baryonic matter (protons etc.), non-baryonic matter (like neutrinos) and dark energy (a permanent anti-gravity material). According to the standard concordance model of cosmology ΛCDMHC, 70% of the missing mass is

dark energy and about 4% is baryonic. The rest is a mix of non-baryonic dark matter NBDM neutrinos (Nieuwenhuizen 2009, 2011) and a mysterious material called "cold dark matter" CDM. The collisional properties of the baryonic dark matter are crucial to and determine the gravitational structure formation of both the plasma and gas epochs (Nieuwenhuizen et al. 2009, 2010ab, 2011, Gibson & Schild 2010, Schild & Gibson 2010).   CDM is a myth that is easily dispelled by hydrogravitational dynamics HGD theory; that is, proper inclusion of basic ideas of fluid mechanics.

HGD modification of the standard model to include fluid mechanical effects of viscosity, diffusivity, fossil turbulence and turbulence (Gibson 1996, 2000, 2004, 2005) greatly simplifies the theory of gravitational structure formation and explains a large variety of observation mysteries, including the big bang itself (Gibson 2010, Gibson, Schild & Wickramasinghe 2011). Dark energy and cold dark matter are not required to explain cosmology, and are in serious conflict with a wide variety of observations. Consider the increase in the "missing mass" to luminosity ratio M/L as a function of averaging scale shown in Figure 1 (Silk 1994 p124). The missing mass M supplies gravitational attraction to prevent spinning luminous objects like galaxies and galaxy clusters from flying apart because the luminous stars have insufficient mass to overcome estimates of centrifugal forces.

Dynamical mass increases relative to luminous mass as observations extend to larger and larger scales using a variety of dynamical mass measures (Zwicky 1937). HGD analysis explains star formation, planet formation and how stars die by excessive accretion of planets till the stars exceed critical mass values and explode as supernovae. Chemicals of supernovae produce the first water oceans and a biological big bang at only 2-8 Myr when cometary panspermia of Hoyle-Wickramasinghe is merged with HGD cosmology (Gibson, Wickramasinghe and Schild 2010).
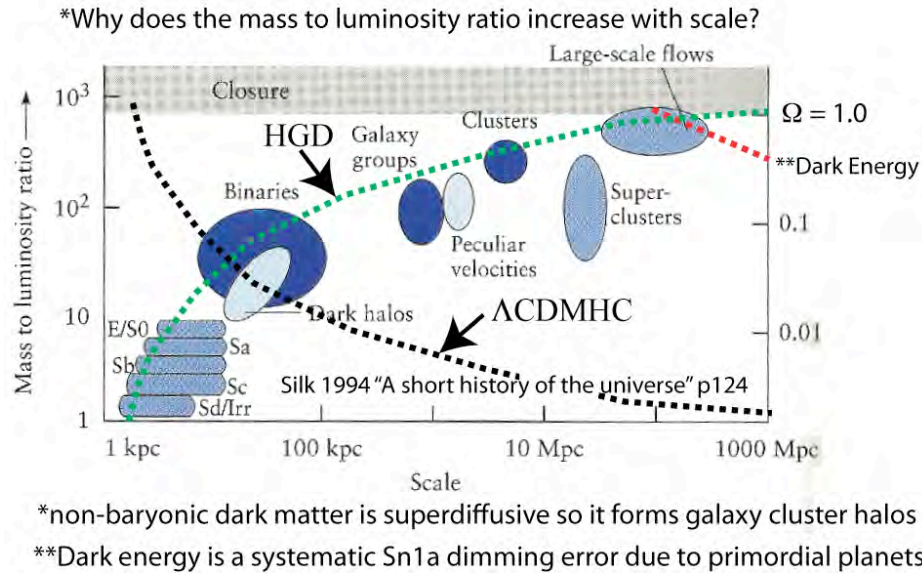
Fig. 1. Missing mass to luminosity M/L increases with scale due to the diffusivity of the dark matter, from a factor of about 30 for galaxies, to $\sim 10^3$ for superclusters of galaxies (Silk 1994). According to hydrogravitational dynamics theory HGD (Gibson 1996) the weakly collisional non-baryonic dark matter NBDM is superdiffusive. It forms halos for superclusters. Antigravitational forces of turbulence produce the big bang but they dissipate and are not permanent like Λ.

Only about a factor M/L of thirty of the mass is missing for galaxies, from their flat rotation curves that extend to about 30 kpc (10^{21} meters). However, considerably more M/L $\sim 10^3$ is needed to stabilize galaxy clusters and superclusters. If CDM clumps were really stable (they are not) and the clumps of CDM could really cluster (they cannot) then the density of the missing mass to luminosity ratio M/L should decrease with averaging length scale (not increase as usually assumed). This is shown in Fig. 1 (black dotted line), starting from infinity before the appearance of the first star where L = 0 and M is whatever quantity of CDM clumps are needed to gravitationally collect enough baryons to produce the first star, and approaching zero at large averaging scales where a few massive CDM halos become very bright as they fill with turbulent superstars and supernovae that reionize the universe.

Reionization of the universe is unnecessary according to HGD theory because the missing hydrogen of the Lyman-α forest is sequestered by primordial planets. Another unlikely standard assumption is that most of the baryons are in the intergalactic medium (Madau 2005). This follows if galaxies are formed in CDM

halos but does not if galaxies form by fragmentation of the plasma. From HGD, the mechanisms for gas to enter the sparse intergalactic medium are by AGN jets during the brief period of central black hole formation, and by supernovae, but careful observations show at least 90% of the baryons are missing from both galaxies and the intergalactic medium at small redshifts (Bregman 2007). X-ray gas at large z suggests a massive Warm-Hot Intergalactic Medium WHIM for z ~ 0 to account for the missing baryons, but fails as expected from HGD.

Predictions of HGD cosmology (green dotted) and Dark Energy (red dotted) curves are compared to the observations in Fig. 1. According to HGD, the non-baryonic dark matter cannot condense because it is weakly collisional, however cold it is assumed to be. The diffusivity of a material is proportional to the mean free path for particle collisions times the speed of the material particles, and this increases as the particle collision cross-section decreases. Therefore the reason the observed M/L ratio increases with scale in Fig. 1 is that the non-baryonic dark matter NBDM is superdiffusive because its particles are weakly collisional.   NBDM diffuses to $\sim 10^3$ larger scales than the 30 kpc observed for galaxies (10^{22} m), to the 300 Mpc size of supercluster halos (10^{25} m).

Kroupa et al. (2010) test predictions of ΛCDM models against observations of the local group of Milky Way satellites and conclude the "concordance" ΛCDMHC model is unacceptable, as shown in Figure 2. From model clustering properties assigned to CDM clumps, there should be large numbers of such clumps in the Milky Way, but these are not observed, as shown in Fig. 2A. New local group satellites termed dwarf spheroidals are detected with large M/L values $\sim 10^3$, Fig. 2C. Instead of being randomly scattered in a dark matter halo as expected from ΛCDMHC, the new faint satellites (green circles) and previously known satellites (yellow circles) are assembled in a "disk of satellites" DoS structure (predicted by HGD due to the sticky nature of PGC dark matter diffusing from the central protogalaxy core on freezing).

HGD cosmology predicts a PGC accretion disk, or "disk of structures" DoS structure, where dense plasma protogalaxies PGs are the least massive structures to form during the plasma epoch. The most massive were superclusters starting at 10^{12} seconds when plasma viscous forces first permitted fragmentation ($L_{SV} \sim L_H$, Table 1). PGs fragment into protoglobularstarcluster PGC clumps of primordial planets PFPs at the time of plasma to gas transition 10^{13} seconds, and diffuse to form the baryonic dark matter halo and the DoS accretion disk as the planets gradually freeze and the diffusivity of the PGC clumps of planets increases so the dark matter halo can form by diffusion of the baryonic dark matter BDM.
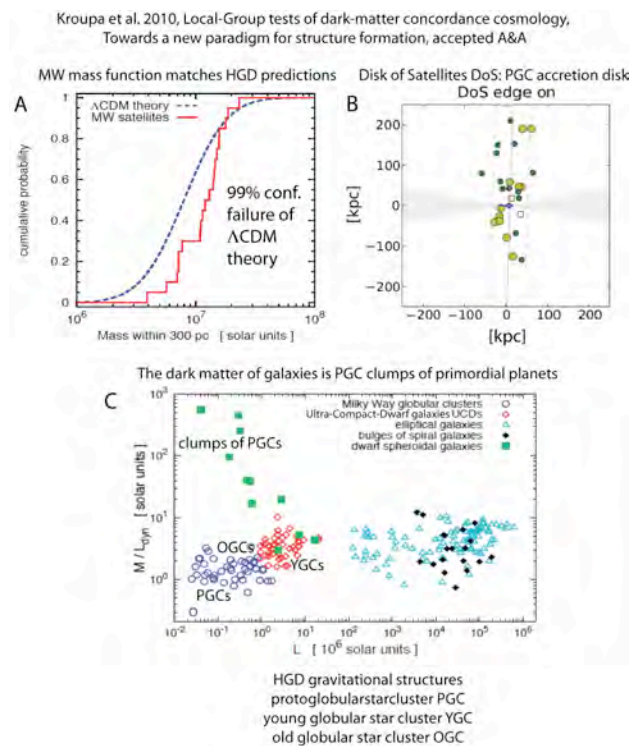
Fig. 2. Kroupa et al. (2010) evidence of ΛCDM failures to describe the local group of Milky Way satellites. A. The mass function of ΛCDM fails badly. B. The new satellites (green) are extremely dim and clustered in the known (yellow) disk of satellites (DoS). C. The M/L ratio for gravitational structures supports HGD predictions (bottom).

Cold dark matter was invented to accommodate the Jeans acoustic criterion for gravitational structure formation, where the Jeans length scale $L_J = (V_S/\rho G)^{1/2}$. Because the sound speed of the plasma is so large, its Jeans scale exceeds the scale of causal connection ct prior to decoupling. In the standard cosmological model, in

order to produce structure, it was assumed that the non-baryonic dark matter was cold to reduce its sound speed and permit condensations. We suggest this idea is physically impossible. A clump of CDM will contract by gravitational forces until its density permits collisions. It will then proceed to diffuse away as the gravitational potential energy of the CDM clump distributes itself. Clumps of CDM cannot merge to larger and larger clumps by hierarchical clustering HC. CDM clumps of all sizes are diffusively unstable.

A permanent dark energy Λ component in the universe is also unlikely and unnecessary. Such a material would cause an accelerated expansion of the universe and a decrease of density below that necessary for the universe to be closed (Fig. 1 red dotted line). According to HGD the initial big bang event is due to a turbulent instability (Gibson 2004, 2005). Because turbulence is a dissipative process, the universe must be closed (Fig. 1 green dotted line).

2. Fluid mechanics of the early universe

Figure 3 summarizes the evolution of gravitational structures in the universe according to hydrogravitational dynamics HGD theory. Table 1 summarizes the various critical length scales that enter the analysis, Gibson (1996).

Table 1. Length scales of gravitational instability

Length Scale Name	Definition	Physical Significance
Jeans Acoustic	$L_J = V_S/(\rho G)^{1/2}$	Acoustic time matches free fall time
Schwarz Viscous	$L_{SV} = (\gamma \nu/\rho G)^{1/2}$	Viscous forces match gravitational forces
Schwarz Turbulent	$L_{ST} = (\varepsilon/[\rho G]^{3/2})^{1/2}$	Turbulent forces match gravitational forces
Schwarz Diffusive	$L_{SD} = (D^2/\rho G)^{1/4}$	Diffusive speed matches free fall speed
Horizon, causal connection	$L_H = ct$	Range of possible gravitational interaction
Plummer force scale	L_{CDM}	Artificial numerical CDM halo sticking length

V_S is sound speed, ρ is density, G is Newton's constant, γ is the rate of strain, ν is the kinematic viscosity, ε is viscous dissipation rate, D is the diffusivity, c is light speed, t is time.

On the right of Fig. 3 is the turbulent big bang (Gibson 2004, 2005). When the local temperature exceeds the Planck temperature of 10^{32} K, Planck mass particles and anti-particles with mass 10^{-8} kg can spontaneously appear from the vacuum and

return to the vacuum without effect within a Planck time 10^{-43} seconds. However, rather than annihilation, the pair can merge to form the Planck equivalent of positronium, formed by electrons and positrons in supernovae. A prograde merger of an anti-Planck particle with such a Planck particle pair results in the HGD turbulent big bang universe. Further details and supporting evidence are provided by Gibson (2010) and Gibson and Schild (2010).

Strong antigravitational forces are required to power the big bang. At first these are supplied by inertial vortex forces of the big bang turbulence fireball. When the expanding, cooling fireball reaches 10^{28} K a phase change occurs. Quarks and gluons become possible. Negative pressures from gluon viscosity work against the expansion with power 10^{145} watts, producing the $\sim 10^{90}$ kg of the present universe.

The magnitude of big bang pressures is the Fortov-Planck pressure $L_{FP} = c^7 h^{-1} G^{-2}$ of $4.6 \ 10^{113}$ Pa (Keeler and Gibson 2009), where c is light speed, h is Planck's constant and G is Newton's constant (Fortov 2009). Inertial vortex forces of big bang turbulence produce negative pressures larger than L_{FP} during the initial stages of the spinning, turbulent, big bang fireball in order to extract mass-energy from the vacuum following Einstein's equations (see Peacock 2000, p. 19, section 1.5). Much larger negative stresses and mass-energy production occur during inflation once the quark-gluon plasma appears producing gluon viscosity.

The Schwarz diffusive scale L_{SD} of the non-baryonic dark matter is larger than the horizon scale L_H throughout the plasma epoch, so NBDM is taken to be a passive secondary factor in the gravitational structure formation of clusters and galaxies by the plasma according to HGD theory. Supercluster halos form at L_{SD} scales $\sim 3 \ x10^{22}$ meters at time $\sim 10^{14}$ s soon after decoupling by fragmentation at the scale of causal connection, matching observations. The indicated diffusivity of the NBDM is $\sim 10^{30}$ $m^2 \ s^{-1}$ (Gibson 2000).
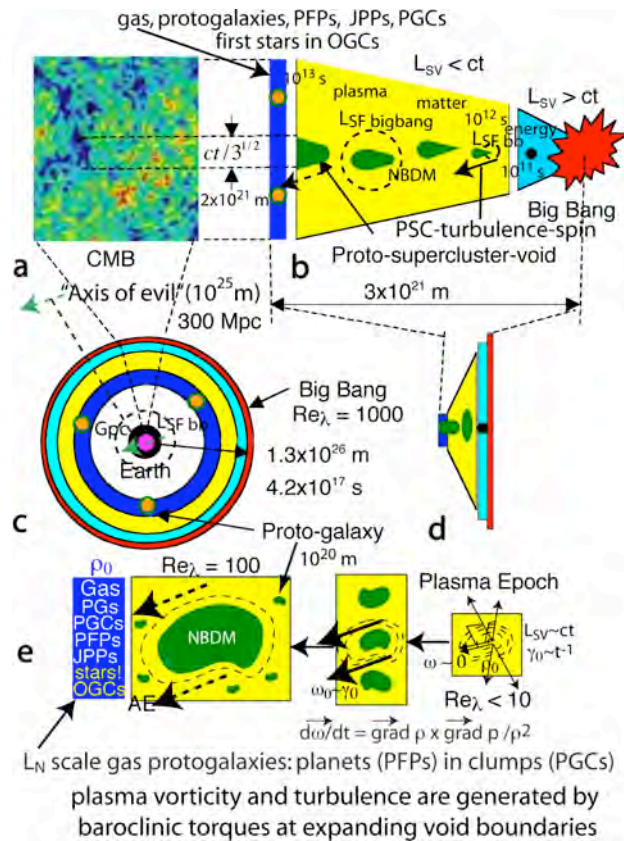
Fig. 3. Hydrogravitational dynamics HGD model for the development of structure in the universe.

Viscous forces control the first formation of gravitational structures during the plasma epoch beginning at time 10^{12} seconds (30,000 years) after the big bang. It is physically impossible for the non-baryonic dark matter to condense to form permanent clumps, as assumed by the ΛCDMHC standard model of cosmology. This is illustrated in Figure 4. In Fig. 3b we see the first structure is due to viscous-gravitational instability of the baryonic plasma at density minima, leading to fragmentation of proto-supercluster-voids that expand to scales detected in CMB temperature anomalies of Fig. 3a.

Turbulence forces and turbulence morphology develop during the plasma epoch, as shown in Fig. 3e. Our local fossil turbulence vortex line from the big bang is manifested by the "Axis of Evil", Schild and Gibson (2008). Vorticity is generated by baroclinic torques at expanding PSC-void boundaries to produce weak turbulence,

whose fossil turbulence vortex lines trigger the formation of chains of proto-galaxies at the end of the plasma epoch.
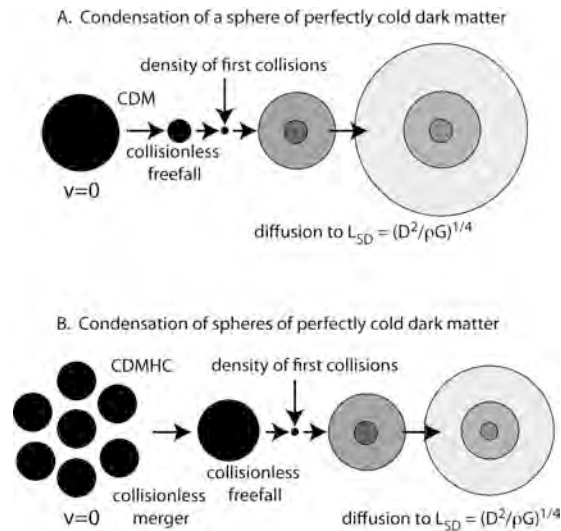
Fig. 4. Problems with the standard cosmological model of structure formation begin with the assumption that cold dark matter can remain in stable clumps. It is physically impossible for this to happen. Starting from v=0 the CDM clump in A. will experience a collisionless freefall to a smaller size and larger density where collisions will begin. The smaller the collision cross section the smaller the size and the larger the density. The material will then diffuse to scale L_{SD} (Gibson 2000). Multiple clumps in B. will evolve in a similar fashion.

As shown in Fig. 4 A, cold dark matter CDM clumps are unstable to gravitational collapse and diffusion independent of the collision cross section assumed for the non-baryonic-dark-matter NBDM particles, whatever they are. As shown in Fig. 4 B, hierarchically clustering HC clumps of CDM clumps are equally unstable to clumping and clustering and cannot possibly form the necessary "CDM halos" of concordance cosmology to collect baryons by forming deep gravitational potential wells.

The CDMHC mechanism is physically unrealistic, and should be abandoned. Numerous numerical simulations have been published that claim support for the CDMHC mechanism. They are not to be trusted because they ignore problems of diffusivity of NBDM illustrated in Fig. 4AB and assume an N body problem of gravitationally interacting objects more appropriate to proto-globular-star-cluster PGC clumps of primordial planets in hydrogravitational dynamics HGD theory than

CDM halos (green dotted curve of Fig. 1). Merging of CDM clumps to form larger stable clumps is not represented by N body gravitational simulations as assumed. A proper, logically consistent, numerical simulation of CDMHC behavior in Fig. 1 would show behavior quite orthogonal (black dotted curve of Fig. 1) to that expected for the universe where structure formation is guided by HGD theory (green dotted curve of Fig. 1).

3. Evidence that the dark matter of galaxies is primordial planets in clumps

The best evidence that the mass of galaxies is planet mass objects is the sequence of quasar microlensing studies discussed by Schild (1996), Colley and Schild (2003) and Colley et al. (2003). A foreground galaxy collects light from a background quasar on its line of sight. Light curves from mirage images are subtracted after shifting by the difference in their time delays to determine twinkling frequencies of the approximately point mass objects doing the microlensing. With the extremely precise time delay between the A and B images of 417.1 days, a small planetary quasar-crossing event time of only 12 hours was detected (Colley and Schild 2003).

For the Schild-Quasar, carefully studied for 15 years, and then followed up by the world-wide, round-the-clock, collaboration of Colley et al. (2003) giving precise 10^{-9} arc-second resolution of the background quasar, it becomes abundantly clear that the dominant galaxy-mass objects are not stars but planets. The twinkling times were not years but days and even hours. Because the mirage images differed slightly in brightness they were not uniformly distributed, but clumped (Gibson & Schild 2010, this volume). Collaborations (MACHO, EROS, etc.) that failed to detect planetary mass objects as the dark matter of galaxies have all made the fatally flawed assumption that the objects are not clumped but uniformly distributed.

Further evidence that most of the mass of galaxies is frozen hydrogen planets is given by temperatures detected by infrared and microwave space telescopes, as shown in Figure 5. Fig. 5 (top) shows the Herschel space telescope and other "dust" temperature estimates as a function of redshift back to z > 1.3. Remarkably, the

temperatures are close to what one would expect if the "dust" is not the talcum powder ceramic variety detected in comets but more likely frozen hydrogen planets in the process of star formation as predicted by HGD cosmology. The triple point of hydrogen is 13.8 K, and this is the observed lower bound. The critical point of hydrogen is 32 K, close to the upper bound of the observed temperatures. These are the thermostated temperatures one would expect for baryonic dark matter planets in clumps where the planets are merging to form stars and the stars are heating the planets to form large atmospheres of evaporated hydrogen and helium exposed to and in radiative equilibrium with the lower temperatures of outer space (green dotted line).

The ultra-luminous-infrared-galaxies (red boxes) are at temperatures above the 13.8-32 K hydrogen thermostat band. The implication is that such galaxies are particularly well supplied with planets rich in polycyclic-aromatic-hydrocarbon PAH dust. Evaporated planets and their PAH rich atmospheres are re-radiating infrared energy absorbed by such planets surrounding an active galactic nucleus that would otherwise appear in the optical frequency band (Gibson 2010, Gibson, Schild & Wickramasinghe 2010). This process will be discussed further in future work.

Dunne et al. (2011) show a rapid evolution of the "dust" of Fig. 5 over the last 5 billion years, also from the Herschel-ATLAS data. The temperature of the "dust" from nearly 2000 galaxies is binned according to temperature in figure 7 (Dunne et al. 2011 fig 7) and shows two remarkable spikes centered on 20 K and 45 K. This observation is easily explained from HGD cosmology as a reflection of the freezing-evaporation equilibrium of hydrogen dark matter planets in PGC clumps at 20K, and the expected hydrogen dark matter planet critical-boiling point temperature at 45 K near hot and exploding stars.
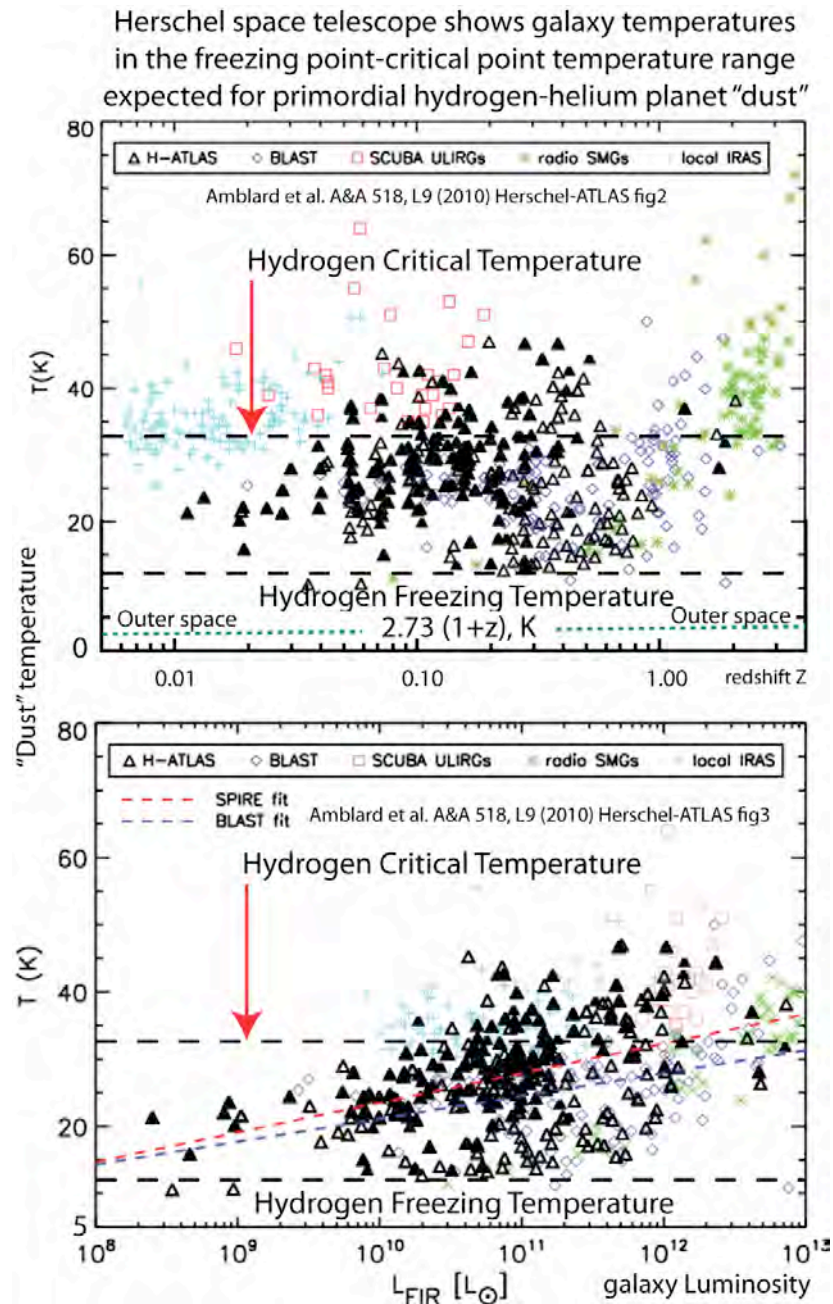
Fig. 5. Evidence from the Herschel-ATLAS temperatures that the "dust" of distant galaxies is frozen and heated primordial gas planets. The frozen hydrogen serves as a thermostat. Mergers of the planets to form stars increases the temperatures to above critical values, especially for highly luminous galaxies (bottom).

Fig. 5 (bottom) shows the temperature bounds of freezing-boiling hydrogen planets compared to the luminosity of the range of objects considered by Amblad et al. (2010) in their Herschel-ATLAS.   Objects on the right with 10^{13} solar luminosity are elliptical galaxies. Objects on the left with only 10^8 solar luminosity may be

extremely dim galaxies whose brightness is determined by rare PGC clumps of planets that have formed stars.

Evidence that the dark matter of galaxies is primordial planets in clumps is provided by space telescopes sensitive to microwave and infrared frequency bands (IRAS, DIRBE, BOOMERang, WMAP). Maps of the sky show a "cirrus cloud" morphology of "dust", where the dust is at temperatures in the triple point to critical point range 14 K to 30 K to be expected if the cloud masses were dominated not by microscopic dust but by frozen hydrogen planets that thermostat the cloud temperatures (Gibson 2010, Gibson & Schild 2010). The same clouds appear at all wavelengths (13,000 to 100 μ) and show signatures of bright PGC planet clumps with density $\sim$ 20 per squared degree. This gives a mass of 10^{42} kg for the Milky Way BDM halo assuming 10^{36} kg per PGC, confirming the HGD prediction that primordial planets in clumps dominate the mass of our Galaxy.

It is difficult to explain observations of multiple star and multiple massive planet systems using the standard models for star formation; that is, models not involving primordial planets as the source of all stars. As the resolution of the observations from space telescopes and ground telescopes increases over multiple frequency bands we see most stars are not alone but surrounded closely by large gas exo-planets and other stars. For example, the binary star system Upsilon Andromeda (http: // en.wikipedia.org / wiki / Upsilon_Andromedae) has two solar-mass stars and four confirmed (Curiel et al. 2011) 1-14 Jupiter-mass planets at distances from the stars of only 0.06 to 5 AU (10^{10} m to 10^{12} m). It is easy to understand such a gravitational pile of Jupiters and stars formed at the center of a 10^{16} m diameter Oort cavity from HGD cosmology. Rather than multiple planets and multiple stars, one expects to get only one star per cloud and no planets if the cloud is gas and microscopic dust.

The primary star of the binary Upsilon Andromeda A (u And A) is close to its supernova II death from rapidly over eating planets, with mass 1.3 solar. Most systems of exo-planets include pulsars resulting from type II supernovae, which is the likely fate of u And A, McArthur et al. (2010). The secondary star of the binary (u And B) is $\sim 10^{14}$ m distant from u And A, still deep in the Oort cavity of the PGC.

4. Summary

We find no evidence to support the standard cosmological model based on condensation of cold dark matter CDM non-baryonic dark matter NBDM. The concept of CDM is unnecessary and physically impossible, as shown in Fig. 4. All gravitational condensations during the plasma epoch and during the gas epoch are dominated by the baryonic dark matter BDM and its viscosity. Viscous forces from photon viscosity $\nu \sim 10^{26}$ m^2 s^{-1} permit gravity to fragment the plasma at mass scales decreasing from 10^{46} kg to 10^{42} kg in the time range 10^{12} s to 10^{13} s of the plasma epoch. Viscous speeds $\nu/L < V_S$ so sound speed V_S and the Jeans scale L_J are irrelevant for length scales L < ct during this epoch. Pressure gradients along with pressure forces are rapidly erased by the passage of sound. The sonic peak in the CMB temperature anisotropy spectrum reflects the expansion at the plasma sound speed $c/3^{1/2}$ of proto-supercluster-voids as rarefaction waves. The sudden decrease at plasma to gas transition to $\nu \sim 10^{13}$ m^2 s^{-1} of the 3000 K hydrogen-helium decreased the viscous fragmention mass from that of galaxies 10^{42} kg to that of Earth-mass planets 10^{25} kg.

The NBDM appears to be $\sim 97\%$ of the mass of the universe: some combination of neutrinos and possibly an additional neutrino-like weakly collisional material yet to be detected. The BDM is primordial gas planets in $\sim 10^{36}$ kg clumps with the density of globular star clusters $\sim 4\times10^{-17}$ kg m^{-3}, contrary to several microlensing consortia (MACHO, OGLE, EROS etc.) that claim to have excluded this form of BDM by finding an inadequate number of microlensing events, as shown in Figure 6 for the EROS programs (Renault et al. 1997). We suggest in Fig. 6 that these claims are

questionable based on a flawed assumption that the planetary mass objects are not

clumped and do not clump within clumps.
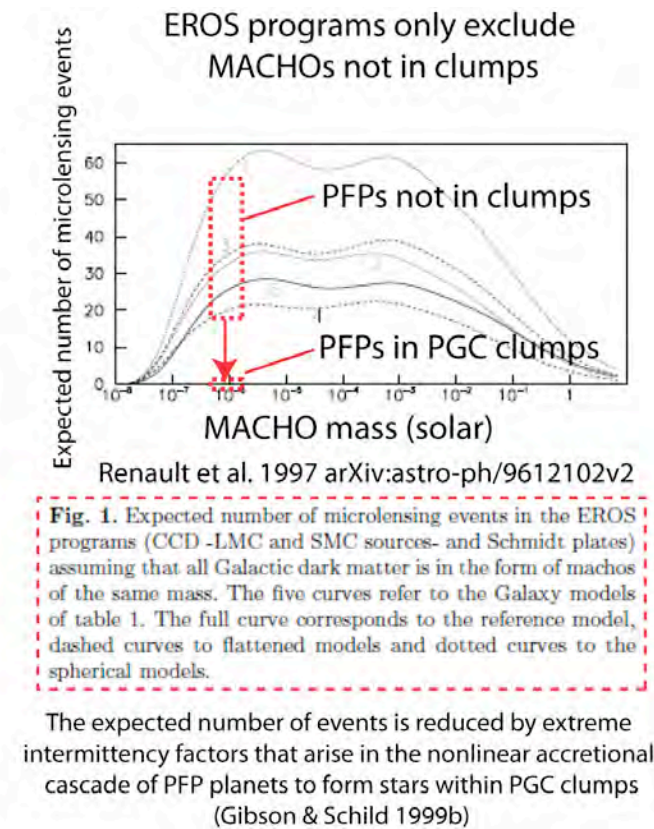
Fig. 6. EROS microlensing programs do not exclude primordial fog particle PFP planets with 10^{-6} solar mass as claimed (Renault et al. 1997 Fig. 1). A fatally flawed assumption is that such rogue planets are uniformly distributed rather than strongly clumped.

The collaborations all assume the planetary mass objects they exclude are uniformly

distributed in the Galaxy halo, which is a strange assumption since such a massive

population of planets must be frozen primordial gas planets since no other material

besides hydrogen-helium is available in sufficient quantities, and such sticky gas

planets would certainly form clumps whatever their initial conditions. As shown in

Fig. 6, the expected number of microlensing events for PFP planets in starforming

PGC clumps near the Galaxy PGC accretion disk is very small (Gibson & Schild

1999ab), but this is not considered in an EROS team review Lassere et al. (2000).

A flood of new evidence supports the HGD claim that the dark matter of galaxies is primordial planets in clumps that make all the stars. How else can hot Jupiters be explained, where Jupiter mass planets (10^{27} kg) are found orbiting stars at Mercury orbits (0.03 AU). Recent examples are provided by Deming et al. (2011) and Desert et al. (2011). Figure 7 summarizes the hydrogravitational dynamics HGD model for gravitational structure formation.
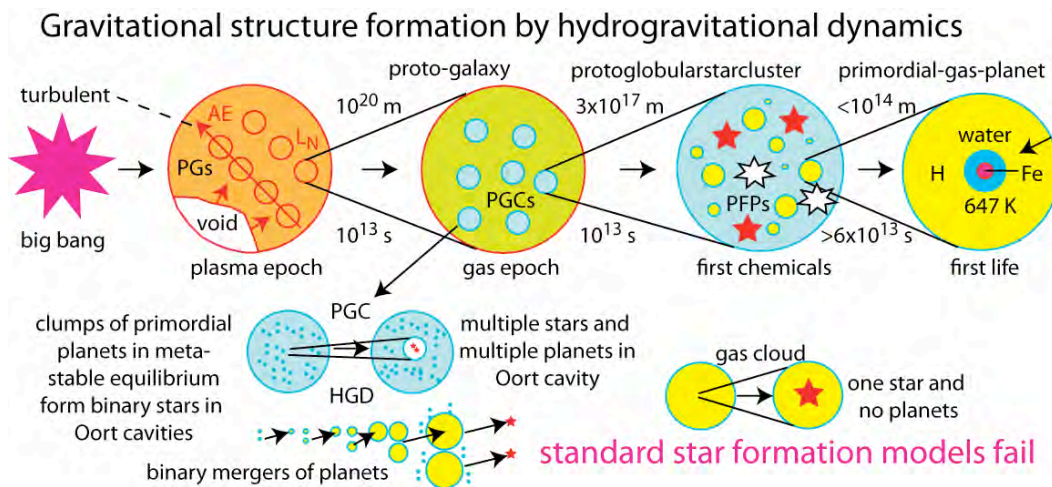
Fig. 7. HGD model for structure formation (top). HGD model for star formation compared to the standard model (bottom).

HGD length scales of Table 1 determine the various possible regimes of gravitational dynamics. Fig. 7 (top) shows plasma turbulence and superclustervoid fragmentation leading to protogalaxies in linear clusters. These fragment into Jeans scale clusters of primordial planets that form stars by binary mergers (bottom). The standard star formation models fail, and should be abandoned. Six gas planets on a flat orbit ~ 10^{10} m from a star have been recently observed by the Kepler Science Team (Lissauer et al. 2011). The system seems to be an accretion disk likely formed as gassy primordial planets merged to create the central star.

Figure 8 shows infrared and optical images of two carbon stars and the planetary nebula Helix, showing evaporated primordial planets in the process of star formation. Details about the carbon stars can be found in Olofsson et al. (2010), where the observed cometary globules are described as ejected from the star in

spherical shells or formed by the interaction of ejected spherical shells. Such models are physically unrealistic and are rendered obsolete by observations and HGD cosmology. Huge density contrasts observed (and easily explained as accreting planet-comets) cannot form in the sun or be ejected, and could not form even if they were ejected. Further discussion of planet-comets in the Helix planetary nebula is given in Gibson, Wickramasinghe and Schild (2010, Fig. 4), where primordial planets are discussed as the sites for the first oceans and first life during a biological big bang that occurred only 2-8 Myr after the cosmological event.
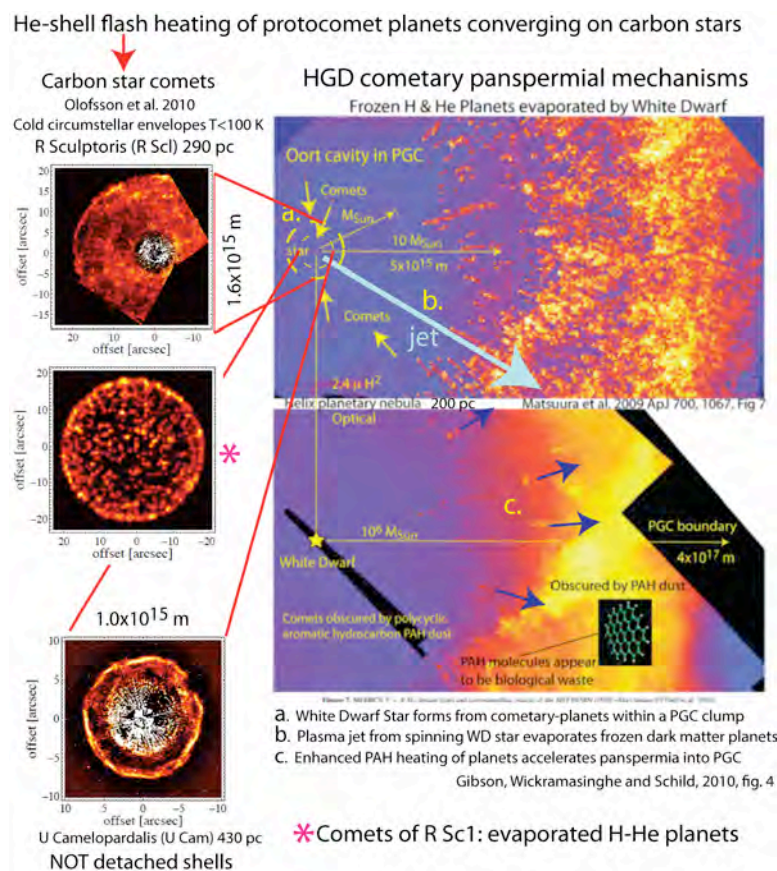
Fig. 8. Hubble space telescope images of carbon star comets (left) are interpreted as ambient primordial planets evaporated by a Helium shell flash. Sizes of the comet spheres are small compared to the Oort cavity of the Helix planetary nebula (right).

The carbon star images on the left of Fig. 8 are interpreted as examples of white dwarf and planetary nebula precursors, leading eventually to systems such as the Helix PNe, shown on the right of Fig. 8. The Helium flash of the carbon stars triggers a wave of frozen hydrogen planet evaporation that moves radially outward in a

spherical shell that is not detached from the star but is formed in place. Some of the planet-comets will continue inward to feed the growing carbon star. Some of the gas evaporated will be expelled, slowing the star growth to form a white dwarf and eventually forming an Oort cavity in the PGC clump of planets.

The Herschel space telescope has detected an enormous water spray emerging from carbon star He-flash events, with rates ($4x10^{26}$ kg/yr) up to a million earth-oceans per year in a sample of eight C-stars (Neufeld et al. 2010). Such a spray suggests and supports evaporation of large populations of ambient primordial planet-comets and their frozen water oceans by AGB He-shell thermal pulses from the carbon stars.

Figure 9 shows a collection of transiting small exoplanets detected by the Kepler Science Team (Lissauer et al. 2011). Planets very close to their star (b, c, d, e, f) have temperature ~ 647 K, the critical temperature of water, suggesting their water oceans are being evaporated as the primordial planet water oceans exceed the water critical temperature 647 K.
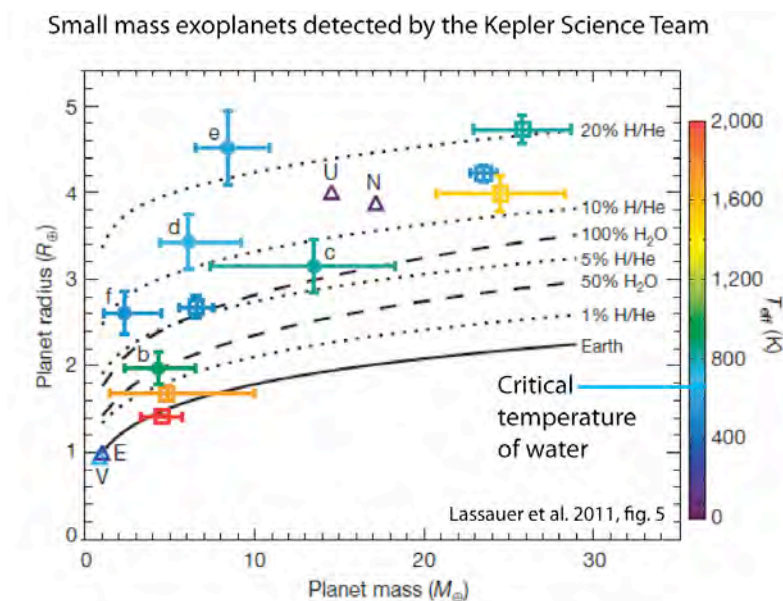
Fig. 9. Small mass exoplanets b, c, d, e detected by the Kepler Science Team are ~ 10^{10} m from star Kepler-11 on tight orbital planes within 0.5º of 89º. An accretion disk of primordial planets with evaporating water oceans is indicated. Solar planets E, V, U, and N are shown as triangles. Other small Kepler exoplanets are shown by open squares (Lassauer et al. 2011, fig. 5).

A crisis concerning mass transfer in star formation is termed the 3He (tralphium, tralpha particle) problem[1]. This isotope is produced in trace quantities by big bang nucleosynthesis (Fuller and Smith 2011), and in brown dwarfs by burning tritium. However it is also produced in stars, but is not observed in the large quantities expected if stars eject their envelopes, as shown in Figure 10.
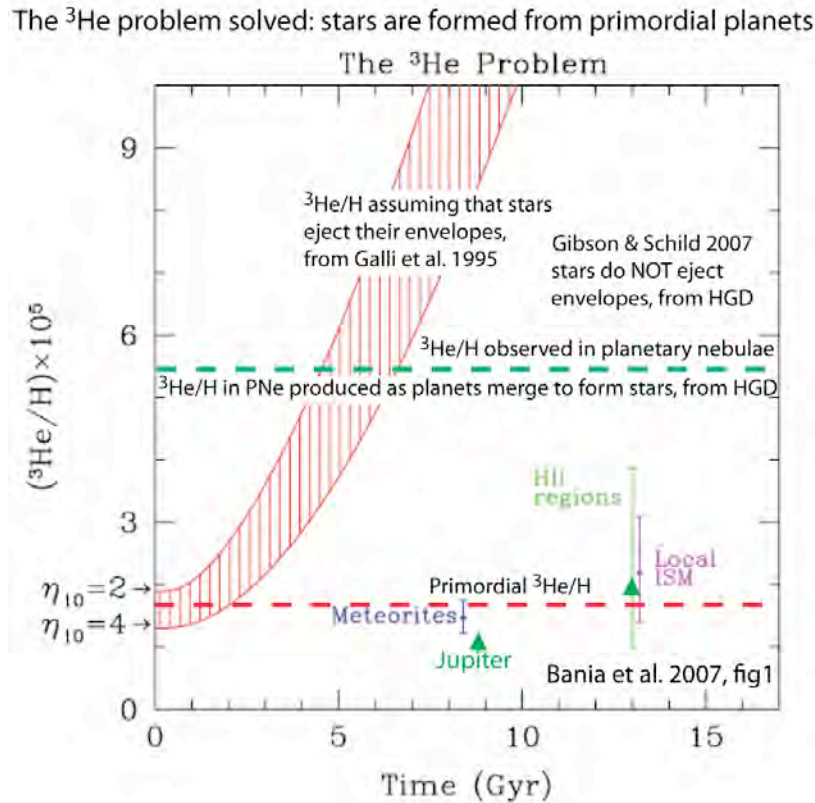
Fig. 10. Solution of the ^{3}He problem (Bania et al. 2007) is provided by hydrogravitational dynamics HGD, where all stars are formed by primordial planet mergers, and do NOT eject stellar materials in massive shells as claimed by the standard models of star formation.

Primordial values of ^{3}He/H $\sim 10^{-5}$ are observed in ionized, Oort cavity size HII regions, Leto et al. (2009). This is expected from HGD cosmology (Nieuwenhuizen 2011) because comet cores are evaporating primordial planets, with primordial gas abundances, and because it is a myth that stars eject massive envelopes by superwinds during their red giant phase, Gibson and Schild (2007). The increase in

---

[1] *And God said: "Let there be mass three." And there was mass three. And God saw tritium and tralphium, and they were good".* George Gamov about 1949.

^{3}He/H shown by the red shaded region of Fig. 10 is NOT reflected near stars, as shown by the primordial ^{3}He/H values in HII regions, Bannia et al. (2007). The large ^{3}He/H values detected in planetary nebulae PNe can be explained by plasma jet pumping by the central white dwarf. Similar large ^{3}He/H ratios are detected in old globular clusters, presumably for the same reason.

5. Conclusions

The dark matter of galaxies is mostly frozen primordial planets PFPs in proto-globular-star-cluster PGC clumps, as predicted by hydrogravitational dynamics HGD cosmology. All stars are formed within PGCs by mergers of PFPs. Increasingly precise observations by microlensing and by infrared and microwave telescopes support the predictions of HGD cosmology. Microlensing collaborations such as EROS and MACHO have not excluded planetary mass objects in clumps as the dark matter of galaxies. The observations should be repeated with much higher sampling frequencies in directions that include foreground PGC clumps of primordial planets.

The standard ΛCDMHC cosmology is physically unrealistic (Fig. 4) and increasingly in conflict with observation (Fig. 2) and basic fluid mechanical constraints. It should be abandoned. HGD cosmology corrects the standard model for many unrealistic fluid mechanical assumptions (Figs. 3) and is abundantly supported by observations (Figs. 1,2,5,8,9,10). Microlensing observations that exclude primordial planets in clumps as the galaxy dark matter (Fig. 6) must be re-interpreted. Standard models for star formation based on ΛCDMHC cosmology must be abandoned (Fig. 7). A flood of new observational evidence of exoplanets further supports the HGD claim that all stars form by mergers of primordial planets, and the more recent HGD claim that life would probably not have happened nor have been widely transmitted within and between galaxies without the millions of primordial planets per star, as predicted by HGD cosmology. HGD should be adopted as the new standard cosmological model.

As shown in Fig. 10, the primordial ^{3}He/H concentration $\sim 10^{-5}$ observed in HII regions strongly supports the HGD star formation paradigm (Niewenhuizen 2011).

6. References

Amblard, A. and 71 other authors, 2010. Herschel-ATLAS: Dust temperature and redshift distribution of SPIRE and PACS detected sources using submillimetre colours, A&A 518, L9, DOI: 10.1051/0004-6361/201014586.

Bania, T. M., Rood, R. T. and Balser, D. S. 2007. The Milky Way 3-Helium Abundance, Space Sci Rev 130: 53–62, DOI 10.1007/s11214-007-9144-z

Bregman, J. 2007. The Search for the Missing Baryons at Low Redshift, Ann. Rev. Astron. Astrophys. 45:221-259, arXiv:0706.1787v1.

Colley, W. et al, 2003. Around-the-Clock Observations of the Q0957+561A,B Gravitationally Lensed Quasar. II. Results for the Second Observing Season, ApJ, 587, 71.

Colley, W. & Schild, R. 2003. A Rapid Microlensing Event in the Q0957+561A, B Gravitational Lens System, ApJ, 594, 97.

Curiel, S. et al. 2011. A fourth planet orbiting υ Andromedae, Astronomy & Astrophysics 525: A78. doi:10.1051.

Deming, D. et al. 2011. Warm SPITZER photometry of the transiting exoplanets CoRoT-1 and CoRoT-2 at secondary eclipse, ApJ 726, 95.

Dunne L. and 40 other authors 2010. Herschel-ATLAS: Rapid evolution of dust in galaxies over the last 5 billion years, to be published in MNRAS, arXiv:1012.5186v1.

Desert, J-M et al. 2011. The atmospheres of the hot-Jupiters Kepler-5b and Kepler-6b observed during occultations with Warm-Spitzer and Kepler, arXiv:1102.0555v1.

Fortov, V. E. 2009. Extreme states of matter on Earth and in space, Physics - Uspekhi 52 (6) 615 – 647.

Fuller, G. M. and C. J. Smith 2010. Nuclear weak interaction rates in primordial nucleosynthesis, Phys.Rev.D, 82:125017, arXiv:1009.0277v1 .

Galli, D., F. Palla, F. Ferrini, U. Penco 1995. Galactic Evolution of D and ^{3}He, Astrophys. J. 443, 536–550.

Gibson, C.H. 1996. Turbulence in the ocean, atmosphere, galaxy and universe, Appl. Mech. Rev., 49, no. 5, 299–315.

Gibson, C. H. 2000. Turbulent mixing, viscosity, diffusion and gravity in the formation of cosmological structures: the fluid mechanics of dark matter, Journal of Fluids Engineering, Vol. 122, Dec. 2000, 830-835, arXiv:astro-ph/0003352.

Gibson, C. H. 2004. The first turbulence and the first fossil turbulence, Flow, Turbulence and Combustion, 72, 161–179.

Gibson, C. H. 2005. The first turbulent combustion, Combust. Sci. and Tech., 177:1049–1071, arXiv:astro-ph/0501416.

Gibson, C. H. 2010. Turbulence and turbulent mixing in natural fluids, Physica Scripta, Turbulent Mixing and beyond 2009 Proceedings, T142, arXiv:1005.2772.

Gibson, C.H. & Schild, R.E. (1999a). Quasar-microlensing versus starmicrolensing evidence of small-planetary-mass objects as the dominant inner-halo galactic dark matter, arXiv:astro-ph/9904362.

Gibson, C.H. & Schild, R.E. (1999b). Theory and observations of galactic dark matter, arXiv:astro-ph/9904366.

Gibson, C. H. and Schild, R. E. 2007. Interpretation of the Helix Planetary Nebula using Hydro-Gravitational-Dynamics: Planets and Dark Energy, arXiv:0701474v4

Gibson, C. H. and Schild, R. E. 2010. Formation of Planets by Hydrogravitational Dynamics, to be published in Journal of Cosmology Lorenz Center Workshop Proceedings, Sept. 27-Oct. 1, 2010, arXiv:1012.5522.

Gibson, C. H., Schild, R. E, and Wickramasinghe, N. C. 2011. The Origin of Life from Primordial Planets, Int. J. of Astrobiology, doi:10.1017/S1473550410000352, arXiv:1004.0504.

Gibson, C. Wickramasingh, N. & Schild, R. 2010. First life in the oceans of primordial-planets: the biological big bang, Journal of Cosmology 11, 3490-3499, arXiv:1009.1760.

Keeler, R. N. and Gibson, C. H., Matter Under Extreme Conditions: The Early Years, for Proceedings of 50th anniversary of the Joint Institute for High Temperatures, Russian Academy of Sciences (JIHT RAS), Moscow, Russia, October 19-21, 2010 arXiv:1011.3137

Kroupa, P., Famaey B., de Boer K. S., Dabringhausen J., Pawlowski M. S., Boily C. M., Jerjen H., Forbes D., Hensler G., and Metz M. 2010. Local-Group tests of dark-matter concordance cosmology, Towards a new paradigm for structure formation, A&A 523, A32, DOI: 10.1051/0004-6361/201014892.

Lasserre T., Afonso, C., etc. 2000. Not enough stellar mass Machos in the Galactic halo, Astron. Astrophys. 355, L39–L42.

Leto, P. et al. 2009. 7 mm continuum observations of ultra compact HII regions, A&A, 507, 1467–1473, DOI: 10.1051/0004-6361/200911894.

Lissauer, J. J. et al. 2011. A Closely-Packed System of Low-Mass, Low-Density Planets Transiting Kepler-11, Nature 470, 53–58, (03 February 2011), doi:10.1038/nature09760, arXiv:1102.0291.

Madau, P. 2005. The intergalactic medium, a review for the Encyclopedia of Astronomy and Astrophysics, arXiv:astro-ph/0005106v1.

McArthur, B. E., Benedict, G. F., Barnes R., Martioli E., Korzennik, S., Nelan E., and R. Paul Butler, R. P. 2010. New Observational Constraints on the υ ANDROMEDAE SYSTEM with data from the HUBBLE SPACE TELESCOPE and HOBBY-EBERLY TELESCOPE, ApJ, 715, 1203–1220.

Neufeld, D. A. et al. 2010. The widespread occurrence of water vapor in the circumstellar envelopes of carbon-rich AGB stars: first results from a survey with Herschel/HIFI, accepted for ApJL, arXiv:1012.3456.

Nieuwenhuizen, Th. M. 2009. Do non-relativistic neutrinos constitute the dark matter?, Europhys. Lett. 86, 59001, arXiv:0812.4552.

Nieuwenhuizen, Th. M. 2010. The case of 1.5 eV neutrino hot dark matter, Proceedings Marcel Grossmann XII, Paris, 2009, arXiv:1003.0459.

Nieuwenhuizen, Th. M. 2011. Primordial ^{3}He/H concentrations in HII regions prove stars are formed by mergers of primordial planets, to be published.

Nieuwenhuizen, Th. M., Gibson, C. H., Schild, R. E. 2009. Gravitational hydrodynamics of large scale structure formation, Europhys. Lett., 88, 49001, arXiv:0906.5087.

Nieuwenhuizen, Th. M., Gibson, C. H., Schild, R. E. 2010. Gravitational hydrodynamics vs observations of voids, Jeans clusters and MACHO dark matter, Proceedings Marcel Grossmann XII, Paris 2009, arXiv:1003.0453.

Nieuwenhuizen, Th. M., Schild, R. E., Gibson, C. H., 2010. Do micro brown dwarf detections explain the galactic dark matter?, arXiv:1011.2530.

Olofsson, H. et al. 2010. High-resolution HST/ACS images of detached shells around carbon stars, accepted A & A, arXiv:1003.0362v1

Peacock, J. A. 2000. Cosmological Physics, Cambridge Univ. Press, UK.

Renault, C. et al. (EROS-1 coll.) (1997). Astronom. & Astrophys. 324, L69, astro-ph/9612102v2.

Schild, R. E. (1996). Microlensing variability of the gravitationally lensed quasar Q0957+561 A,B, ApJ 464, 125.

Schild, R.E & Gibson, C.H. 2008. Lessons from the Axis of Evil, arXiv:astroph/0802.3229v2.

Schild, R. E. and Gibson, C. H. 2010. Primordial Planet Formation, to be published in Journal of Cosmology Lorenz Center Workshop Proceedings, Sept. 27-Oct. 1, 2010, arXiv:1012.5519.

Silk, J. 1994. A Short History of the Universe, Scientific American Library, New York.

Zwicky, F. 1937. On the masses of nebulae and of clusters of nebulae, ApJ 86, 217-246.

000053

ΛCDM: Triumphs, Puzzles and Remedies

L. Perivolaropoulos

Department of Physics, University of Ioannina, Greece

E-mail: `leandros@uoi.gr`

Abstract.   The consistency level of ΛCDM with geometrical data probes has been increasing with time during the last decade. Despite of these successes, there are some puzzling conflicts between ΛCDM predictions and dynamical data probes (bulk flows, alignment and magnitude of low CMB multipoles, alignment of quasar optical polarization vectors, cluster halo profiles). Most of these puzzles are related to the existence of preferred anisotropy axes which appear to be unlikely close to each other. A few models that predict the existence of preferred cosmological axes are briefly discussed.

000055

ΛCDM: Triumphs, Puzzles and Remedies

A wide range of precise cosmological observations (Hicken *et al.*, 2009; Astier *et al.*, 2006; Kowalski *et al.*, 2008; Komatsu *et al.*, 2009; Reid *et al.*, 2010) that developed during the past two decades are well described by a class of cosmological models that rely on a set of simple assumptions:

- The universe is homogeneous and isotropic on scales larger than a few hundred Mpc.
- General Relativity is the correct theory that describes gravity on all macroscopic scales.
- The universe consists of radiation (photons), matter (dark matter, baryons and leptons) and dark energy (a substance with repulsive gravitational properties which dominates at recent cosmological times and leads to accelerating cosmic expansion (Copeland, Sami & Tsujikawa, 2006)).
- Primordial fluctuations that gave rise to structure formation were created as quantum fluctuations in an approximately scale invariant process that took place during inflation.

The simplest representative of the above class of models is the ΛCDM model (Sahni, 2002; Padmanabhan, 2003). In this model the role of dark energy is played by the *cosmological constant*, a homogeneous form of energy whose density remains constant even in an expanding background. This is the current *standard cosmological model* and it is consistent with the vast majority of cosmological observations. Such observations involve geometric probes (Hicken *et al.*, 2009; Astier *et al.* 2006; Kowalski *et al.*, 2008; Komatsu *et al.*, 2009; Reid *et al.*, 2010) (direct probes of the large scale cosmic metric) and dynamical probes (Bertschinger, 2006; Nesseris & Perivolaropoulos, 2008) of the large scale cosmic structure that probe simultaneously the large scale cosmic metric and the gravitational growth of perturbations, namely the theory of gravity on large scales.

Geometric probes of the cosmic expansion include the following:

- Type Ia supernovae (SnIa) standard candles (Hicken *et al.*, 2009; Astier *et al.*, 2006; Kowalski *et al.*, 2008).
- The angular location of the first peak in the CMB perturbations angular power spectrum(Komatsu *et al.*, 2009). This peak probes the integrated cosmic expansion rate using the last scattering horizon as a standard ruler.
- Baryon acoustic oscillations of the matter density power spectrum. These oscillations also probe the integrated cosmic expansion rate on more recent redshifts using the last scattering horizon as a standard ruler (Reid *et al.*, 2010).
- Other less accurate standard candles (Gamma Ray Bursts (Basilakos & Perivolaropoulos, 2008), HII starburst galaxies (Plionis *et. al.*, 2009)) and standard rulers (cluster gas mass fraction (Allen *et. al.*, 2004) as well as probes of the age of the universe (Krauss & Chaboyer, 2003).

Dynamical probes of the cosmic expansion and the gravitational law on cosmological scales include:

- X-Ray cluster growth data (Rapetti *et. al.*, 2008).
- Power spectrum of Ly-α forest at various redshift slices (McDonald *et al.*, 2005; Nesseris & Perivolaropoulos, 2008).
- Redshift distortion observed through the anisotropic pattern of galactic redshifts on cluster scales (Hawkins *et al.*, 2003)
- Weak lensing surveys (Benjamin *et al.*, 2007; Amendola, Kunz & Sapone, 2008)

000056

These cosmological observations converge on the fact that the simplest model describing well the cosmic expansion rate is the one corresponding to a cosmological constant (Padmanabhan, 2003) in a flat space namely

$$H(z)^2 = H_0^2 \left[\Omega_{0\mathrm{m}}(1+z)^3 + \Omega_\Lambda\right] \tag{1}$$

where $H(z)$ is the Hubble expansion rate at redshift z, $H_0 = H(z=0)$, $\Omega_{0\mathrm{m}}$ the present matter density normalized to the present critical density for flatness and $\Omega_\Lambda = 1 - \Omega_{0\mathrm{m}}$ is the normalized dark energy density which is time independent in the simplest case of the cosmological constant (ΛCDM).

In view of the wide range of successful predictions of ΛCDM , three possible approaches develop for cosmological research:

- **Mainstream Observers Approach:** Supporters of this approach focus on the majority of cosmological data that are consistent with ΛCDM . Thus, one assumes validity of ΛCDM and uses cosmological observations to impose constraints on the model parameters (such as $\Omega_{0\mathrm{m}}$) with the best possible accuracy. The advantage of this approach is that given the present status of cosmological observations, it is the most likely to lead to accurate physical results. On the other hand, this approach is unlikely to reveal any new physics beyond ΛCDM if such physics is hidden in the data.

- **Theorist's Approach:** This approach focuses on theoretical motivation and uses intuition and theoretical appeal to construct models more general than ΛCDM which usually include the standard model as a special point in parameter space. In this approach, the parameter space of the theory is initially enlarged in directions motivated by theoretical arguments. Subsequently, cosmological observations are used to constrain this parameter space in a region which is usually around the point corresponding to ΛCDM . The advantage of this approach is that it can produce beautiful and exciting theoretical results and predictions. On the other hand, it is unlikely to lead to the discovery of new physics because the simplicity of ΛCDM makes it a preferable model -in the context of a Bayesian approach- compared to any more complicated theoretical model.

- **Outlier Data Approach:** This approach focuses on the minority of data (outliers) that are inconsistent with ΛCDM at a level of more than $2-3\sigma$. Then one identifies common features of these data and constructs theoretical models consistent with these features. These models are used to make non-trivial predictions for upcoming cosmological observations. The construction of these models is not guided by theoretical motivation but by existing data which however may be affected by systematic or large statistical fluctuations. The disadvantage of this approach is that there is a relatively high probability that these 'outlier' data may be infected by large systematic or statistical fluctuations. As a result, the corresponding theoretical models may turn out to be unrealistic by future observations. On the other hand, if the 'outlier' data turn out to be representative of the real world, this approach is the most likely to reveal the existence of new physics. Historically, it may be verified that indeed this approach has led to the discovery of new models that constitute better descriptions of Nature than previous 'standard models'. For example, in the early '90s preliminary 'outlier' data (Efstathiou, Sutherland & Maddox, 1990) had challenged the sCDM model (flat $\Omega_{0\mathrm{m}} = 1$) which was at the time the 'standard' cosmological model. Such data had provided early hints that $\Omega_{0\mathrm{m}} < 1$ but at the time they were considered systematic or statistical fluctuations. Only after the SnIa data (Perlmutter *et al.*, 1999), it was realized that the sCDM model needs to be abandoned in favor of ΛCDM .

Therefore, the question that needs to be addressed is the following: *Are there currently similar data that challenge the current standard model (ΛCDM) and what are their common features?*

The answer to this question is positive. Indeed, these challenging to ΛCDM data may be summarized as follows (Perivolaropoulos, 2008):

(i) **Large Scale Velocity Flows:** ΛCDM predicts significantly smaller amplitude and scale of flows than what observations indicate. It has been found that the dipole moment (bulk flow) of a combined peculiar velocity sample extends on scales up to $100h^{-1}Mpc$ ($z \leq 0.03$) with amplitude larger than $400km/sec$ (Watkins, Feldman & Hudson 2009). The direction of the flow has been found consistently to be approximately in the direction $l \simeq 282°$, $b \simeq 6°$. Other independent studies have also found large bulk velocity flows on similar directions on scales of about $100h^{-1}Mpc$ (Lavaux $et.$ $al.$, 2010) or larger (Kashlinsky $et.$ $al.$, 2009). The expected rms bulk flow in the context of ΛCDM normalized with WMAP5 $(\Omega_{0m}, \sigma_8) = (0.258, 0.796)$ on scales larger than $50h^{-1}Mpc$ is approximately $110km/sec$. The probability that a flow of magnitude larger than $400km/sec$ is realized in the context of the above ΛCDM normalization (on scales larger than $50h^{-1}Mpc$) is less than 1%. A possible connection of such large scale velocity flows and cosmic acceleration is discussed by Tsagas (2010).

(ii) **Alignment of low multipoles in the CMB angular power spectrum:** The normals to the octopole and quadrupole planes are aligned with the direction of the cosmological dipole at a level inconsistent with Gaussian random, statistically isotropic skies at 99.7% (Copi $et.$ $al.$, 2010). The corresponding directions are: octopole plane normal $(l, b) = (308°, 63°)$, quadrupole plane normal $(l, b) = (240°, 63°)$ (Tegmark, de Oliveira-Costa & Hamilton 2003), CMB dipole moment $(l, b) = (264°, 48°)$ (Lineweaver $et.$ $al.$, 1996). A related effect has also been recently observed by considering the temperature profile of 'rings' in the WMAP temperature fluctuation maps (Kovetz, Ben-David & Itzhaki, 2010). It was found that there is a ring with anomalously low mean temperature fluctuation with axis in the direction $(l, b) = (276°, -1°)$ which is relatively close to the above directions (particularly that corresponding to the bulk velocity flows).

(iii) **Large scale alignment in the QSO optical polarization data:** Quasar polarization vectors are not randomly oriented over the sky with a probability often in excess of 99.9%. The alignment effect seems to be prominent along a particular axis in the direction $(l, b) = (267°, 69°)$ (Hutsemekers $et.$ $al.$, 2005).

(iv) **Profiles of Cluster Haloes:** ΛCDM predicts shallow low concentration and density profiles in contrast to observations which indicate denser high concentration cluster haloes (Broadhurst $et.$ $al.$, 2005; Umetsu & Broadhurst, 2008).

(v) **Missing power on the low l multipoles of the CMB angular power spectrum** which leads to a vanishing correlation function $C(\theta)$ on angular scales larger than $60°$ (Copi $et.$ $al.$ 2007; Copi $et.$ $al.$, 2010)

In addition to the above large scale effects there are issues on galactic scales (missing satellites problem (Klypin $et.$ $al.$, 1999) and the cusp/core nature of the central density profiles of dwarf galaxies (Gentile $et.$ $al.$, 2004)).

Three of the above five large scale puzzles are large scale effects related to preferred cosmological directions (CMB multipole alignments, QSO polarization alignment and large scale bulk flows) which appear to be not far from each other (Antoniou & Perivolaropoulos, 2010). Their direction is approximately normal to the axis of the ecliptic poles $(l, b) = (96°, 30°)$ and lies close to the ecliptic plane and the equinoxes. This coincidence has triggered investigations for possible systematic effects related to the CMB preferred axis but no significant such effects have been found (Copi $et.$ $al.$, 2010).

In addition, it has been shown recently (Antoniou & Perivolaropoulos, 2010) that the Union2 SnIa data hint towards a direction of maximum accelerating expansion that is abnormally close to the directions of the above preferred axes. In Table 1, I show the directions of the

Table 1. Directions of Preferred axes from different cosmological observations.

Cosmological Obs.	l	b	Reference
SnIa Union2	309°	18°	(Antoniou & Perivolaropoulos, 2010)
CMB Dipole	264°	48°	(Lineweaver *et. al.*, 1996)
Velocity Flows	282°	6°	(Watkins, Feldman & Hudson 2009)
Quasar Alignment	267°	69°	(Hutsemekers *et. al.*, 2005)
CMB Octopole	308°	63°	(Bielewicz, Gorski & Banday, 2004)
CMB Quadrupole	240°	63°	(Bielewicz, Gorski & Banday, 2004)
Mean	278° ± 26°	45° ± 27°	-

preferred axes from different cosmological observations along with the corresponding references.

These directions are also shown in Figure 1 in galactic coordinates. It is straightforward to show (Antoniou & Perivolaropoulos, 2010) that the probability of such proximity among axes directions that should be independent of each other is less than 1%. Thus, unless there is a hidden common systematic (Peiris & Smith, 2010), the existence of a cosmological preferred axis may be attributed to physical effects. An incomplete list of these effects is the following:

- An anisotropic dark energy equation of state (Zumalacarregui *et. al.*, 2010; Koivisto & Mota, 2006; Battye & Moss, 2009) due perhaps to the existence of vector fields (Armendariz-Picon, 2004; Esposito-Farese, Pitrou & Uzan, 2010).

- Dark Energy and/or Dark matter perturbations on scales comparable to the horizon scale

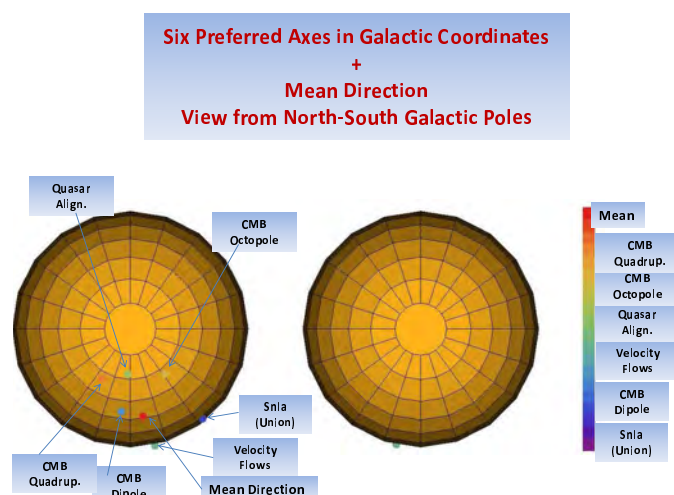**Figure 1.** The coordinates of the preferred axes of Table 1 are all located in a region less than a quarter of the North Galactic Hemisphere (left). The south galactic hemisphere (right) is also shown for completeness. The bulk flow direction is also visible in the south galactic hemisphere because it is close to the equator. The mean direction obtained in Table 1 with coordinates $(l, b) = (278°, 45°)$ is also shown.

000059

(Rodrigues, 2008; Jimenez & Maroto, 2009). For example an off center observer in a 1Gpc void would experience the existence of a preferred cosmological axis through the Lemaitre-Tolman-Bondi metric (Alexander *et. al.*, 2009; Garcia-Bellido & Haugboelle, 2008; Dunsby *et. al.*, 2010; Garfinkle, 2010).

- Turbulent structure formation could also lead to large scale non-Gaussian features which would lead to the existence of a preferred axis (Schild & Gibson, 2008).

- Deviations from the isotropic cosmic expansion rate induced by a fundamental violation of the cosmological principle eg through a multiply connected non-trivial cosmic topology (Luminet, 2008), rotating universe coupled to an anisotropic scalar field (Carneiro & Mena Marugan, 2001), non-commutative geometry (Akofor *et. al.*, 2008) or simply a fundamental anisotropic curvature (Koivisto *et. al.*, 2011).

- Statistically anisotropic primordial perturbations (Armendariz-Picon, 2007; Pullen & Kamionkowski, 2007; Ackerman, Carroll & Wise 2007). For example, inflationary perturbations induced by vector fields (Dimopoulos *et. al.*, 2009; Bartolo *et. al.*, 2009). Note however that inflationary models with vector fields usually suffer from instabilities due to the existence of ghosts (Himmetoglu, Contaldi & Peloso, 2009).

- The existence of a large scale primordial magnetic field (Kahniashvili, Lavrelashvili & Ratra, 2008; Barrow, Ferreira & Silk, 1997; Campanelli, 2009). Evidence for such a magnetic field has recently been found in CMB maps (Kim & Naselsky, 2009).

The confirmation of the existence of a cosmological preferred axis would constitute a breakthrough in cosmological research. Given the present status of cosmological observations such a confirmation is one of the most probable directions from which new physics may emerge.

Given the preliminary evidence for anisotropy discussed above, it is important to extend and intensify efforts for the possible confirmation of this evidence. Such confirmation may be achieved by extending the SnIa compilations towards larger datasets and deeper redshifts that span as uniformly as possible all directions in the sky. This is important in view of the fact that the Union2 compilation is less uniform and detailed in the south galactic hemisphere. In addition it is important to extend other cosmological data related to CMB low multipole moments, bulk velocity flows and quasar polarization to confirm the present existing evidence for preferred axes in these datasets. Finally, alternative probes of cosmological anisotropies may be considered like higher CMB multipole moments, non-gaussian features and polarization in the CMB maps, alignments of geometric features of various structures on large scales (there is already some preliminary evidence for alignment of handedness of spiral galaxies (Longo, 2009) along an axis not far from the directions of the other preferred axes of Table 1), alignment of optical polarization from various cosmological sources or studies based on cosmic parallax (Quartin & Amendola, 2010). It is also important to derive observational signatures that can clearly distinguish between the various different origins of the preferred axes.

References

Ackerman, L., Carroll, S. M. and Wise, M. B. (2007). Imprints of a Primordial Preferred Direction on the Microwave Background. Phys. Rev. D **75**, 083502 [Erratum-ibid. D **80**, 069901 (2009)].

Akofor, E., Balachandran, A. P., Jo, S. G., Joseph, A. and Qureshi, B. A. (2008). Direction-Dependent CMB Power Spectrum and Statistical Anisotropy from Noncommutative Geometry. JHEP **0805**, 092.

Alexander, S., Biswas, T., Notari A. and Vaid, D. (2009). Local Void vs Dark Energy: Confrontation with WMAP and Type Ia Supernovae. JCAP **0909**, 025.

000060

Allen, S. W., Schmidt, R. W., Ebeling, H., Fabian A. C. and van Speybroeck, L. (2004). Constraints on dark energy from Chandra observations of the largest relaxed galaxy clusters. Mon. Not. Roy. Astron. Soc. **353**, 457.

Amendola, L., Kunz M. and Sapone D. (2008). Measuring the dark side (with weak lensing). JCAP **0804**, 013.

Antoniou, I. and Perivolaropoulos, L. (2010). Searching for a Cosmological Preferred Axis: Union2 Data Analysis and Comparison with Other Probes. JCAP **1012**, 012.

Armendariz-Picon, C. (2004). Could dark energy be vector-like? JCAP **0407**, 007.

Armendariz-Picon, C. (2007). Creating Statistically Anisotropic and Inhomogeneous Perturbations. JCAP **0709**, 014.

Astier, P. *et al.* [The SNLS Collaboration] (2006). The Supernova Legacy Survey: Measurement of $Omega_M, Omega_Lambda$ and from the First Year Data Set. *Astron. Astrophys.* **447**, 31.

Barrow, J. D., Ferreira P. G. and Silk, J. (1997). Constraints on a Primordial Magnetic Field. Phys. Rev. Lett. **78**, 3610.

Bartolo, N., Dimastrogiovanni, E., Matarrese S. and Riotto, A. (2009). Anisotropic bispectrum of curvature perturbations from primordial non-Abelian vector fields. JCAP **0910**, 015.

Basilakos S. and Perivolaropoulos L. (2008). Testing GRBs as Standard Candles. Mon. Not. Roy. Astron. Soc. **391**, 411.

Battye, R. and Moss, A. (2009). Anisotropic dark energy and CMB anomalies. Phys. Rev. D **80**, 023531.

Benjamin, J. *et al.* (2007). Cosmological Constraints From the 100 Square Degree Weak Lensing Survey. Mon. Not. Roy. Astron. Soc. **381**, 702.

Bertschinger, E. (2006). On the Growth of Perturbations as a Test of Dark Energy. Astrophys. J. **648**, 797.

Bielewicz, P., Gorski K. M. and Banday, A. J. (2004). Low order multipole maps of CMB anisotropy derived from WMAP. Mon. Not. Roy. Astron. Soc. **355**, 1283.

Broadhurst, T. J., Takada, M., Umetsu, K., Kong, X., Arimoto, N., Chiba, M. and Futamase, T. (2005). The Surprisingly Steep Mass Profile of Abell 1689, from a Lensing Analysis of Subaru Images. Astrophys. J. **619**, L143.

Campanelli, L. (2009). A Model of Universe Anisotropization. Phys. Rev. D **80**, 063006.

Carneiro S. and Mena Marugan, G. A. (2001). Anisotropic cosmologies containing isotropic background radiation. Phys. Rev. D **64**, 083502.

Copeland E. J., Sami M. and Tsujikawa S. (2006). Dynamics of dark energy. *Int. J. Mod. Phys. D* **15**, 1753.

Copi, C. J., Huterer, D., Schwarz, D. J. and Starkman G. D. (2006). On the large-angle anomalies of the microwave sky. Mon. Not. Roy. Astron. Soc. **367**, 79.

Copi, C., Huterer, D., Schwarz D. and Starkman, G. (2007). The Uncorrelated Universe: Statistical Anisotropy and the Vanishing Angular Correlation Function in WMAP Years 1-3. Phys. Rev. D **75**, 023507.

Copi, C. J., Huterer, D., Schwarz D. J. and Starkman, G. D. (2010). Large-angle anomalies in the CMB. Adv. Astron. **2010**, 847541.

Dimopoulos, K., Karciauskas, M., Lyth D. H. and Rodriguez, Y. (2009). Statistical anisotropy of the curvature perturbation from vector field perturbations. JCAP **0905**, 013.

Dunsby, P., Goheer, N., Osano, B. and Uzan, J. P. (2010). How close can an Inhomogeneous Universe mimic the Concordance Model? JCAP **1006**, 017.

Efstathiou, G., Sutherland, W. J. and Maddox, S. J. (1990). The cosmological constant and cold dark matter. Nature **348**, 705.

Esposito-Farese, G., Pitrou C. and Uzan, J. P. (2010). Vector theories in cosmology. Phys. Rev. D **81**, 063519.

Garcia-Bellido J. and Haugboelle, T. (2008). Confronting Lemaitre-Tolman-Bondi models with Observational Cosmology. JCAP **0804**, 003.

Garfinkle, D. (2010). The motion of galaxy clusters in inhomogeneous cosmologies. Class. Quant. Grav. **27** 065002.

Gentile, G., Salucci, P., Klein, U., Vergani, D. and Kalberla, P. (2004). The cored distribution of dark matter in spiral galaxies. Mon. Not. Roy. Astron. Soc. **351**, 903.

Gorski K. M., Hansen F. K. and Lilje, P. B. (2007). Hemispherical power asymmetry in the three-year Wilkinson Microwave Anisotropy Probe sky maps. Astrophys. J. **660**, L81.

Hawkins, E. *et al.* (2003). The 2dF Galaxy Redshift Survey: correlation functions, peculiar velocities and the matter density of the Universe. Mon. Not. Roy. Astron. Soc. **346**, 78.

Hicken, M. *et al.* (2009). Improved Dark Energy Constraints from 100 New CfA Supernova Type Ia Light Curves. Astrophys. J. **700**, 1097.

Himmetoglu, B., Contaldi C. R., and Peloso, M. (2009). Instability of anisotropic cosmological solutions supported by vector fields. Phys. Rev. Lett. **102**, 111301.

Hutsemekers, D., Cabanac, R., Lamy, H. and Sluse, D. (2005). Mapping extreme-scale alignments of quasar polarization vectors. Astron. Astrophys. **441**, 915.

Jimenez J. B., and Maroto, A. L. (2009). Large-scale cosmic flows and moving dark energy. JCAP **0903**, 015.

Kahniashvili, T., Lavrelashvili G. and Ratra, B. (2008). CMB Temperature Anisotropy from Broken Spatial Isotropy due to an Homogeneous Cosmological Magnetic Field. Phys. Rev. D **78**, 063012.

Kashlinsky A., Atrio-Barandela, F., Kocevski, D., and Ebeling H. (2009). A measurement of large-scale peculiar velocities of clusters of galaxies: results and cosmological implications. Astrophys. J. **686**, L49.

Kim J. and Naselsky, P. (2009). Alfven turbulence in the WMAP 5 year data and a forecast for the PLANCK. JCAP **0907**, 041.

Klypin, A. A., Kravtsov, A. V., Valenzuela, O. and Prada, F. (1999). Where are the missing galactic satellites? Astrophys. J. **522**, 82.

Koivisto T. and Mota, D. F. (2006). Dark Energy Anisotropic Stress and Large Scale Structure Formation. Phys. Rev. D **73**, 083502.

Koivisto, T. S., Mota, D. F., Quartin M. and Zlosnik, T. G. (2011). On the Possibility of Anisotropic Curvature in Cosmology. Phys. Rev. D **83**, 023509.

Komatsu E. *et al.* [WMAP Collaboration] (2009). Seven-Year Wilkinson Microwave Anisotropy Probe (WMAP) Observations: Cosmological Interpretation. *Ap.J. Suppl.* **180**, 330.

Kovetz, E. D., Ben-David, A. and Itzhaki, N. (2010). Giant Rings in the CMB Sky. Astrophys. J. **724**, 374.

Kowalski, M. *et al.* (2008). Improved Cosmological Constraints from New, Old and Combined Supernova Datasets. Astrophys. J. **686**, 749.

Krauss, L. M. and Chaboyer, B. (2003). Age Estimates of Globular Clusters in the Milky Way: Constraints on Cosmology. Science **299**, 65.

Land, K. and Magueijo, J. (2005). The axis of evil. Phys. Rev. Lett. **95**, 071301 (2005).

Lavaux, G. Tully, R. B., Mohayaee, R. and Colombi, S. (2010). Cosmic flow from 2MASS redshift survey: The origin of CMB dipole and implications for LCDM cosmology. Astrophys. J. **709**, 483.

Lineweaver, C. H., Tenorio, L., Smoot, G. F., Keegstra, P., Banday, A. J. and Lubin, P. (1996). The Dipole Observed in the COBE DMR Four-Year Data. Astrophys. J. **470**, 38.

Longo, M. J. (2009). Evidence for a Preferred Handedness of Spiral Galaxies. arXiv:0904.2529.

Luminet, J. P. (2008). The Shape and Topology of the Universe. arXiv:0802.2236 [astro-ph].

McDonald, P. *et al.* [SDSS Collaboration] (2005). The Linear Theory Power Spectrum from the Lyman-alpha Forest in the Sloan Digital Sky Survey. Astrophys. J. **635**, 761.

Nesseris, S. and Perivolaropoulos, L. (2008). Testing LCDM with the Growth Function $\delta(a)$: Current Constraints. Phys. Rev. D **77**, 023504.

Padmanabhan, T (2003). Cosmological constant: The weight of the vacuum. Phys. Rept. **380**, 235.

Peiris H. V. and Smith, T. L. (2010). CMB Isotropy Anomalies and the Local Kinetic Sunyaev-Zel'dovich Effect. Phys. Rev. D **81**, 123517.

Perivolaropoulos, L. (2008). Six Puzzles for LCDM Cosmology. Invited article to the TSPU anniversary volume "The Problems of Modern Cosmology" on the occasion of the 50th birthday of Prof. S. D. Odintsov. arXiv:0811.4684.

Perlmutter S. *et al.* [Supernova Cosmology Project Collaboration] (1999). Measurements of Omega and Lambda from 42 High-Redshift Supernovae. Astrophys. J. **517**, 565.

Plionis, M., Terlevich, R., Basilakos, S., Bresolin, F., Terlevich, E., Melnick, J. and Georgantopoulos, I. (2009). Alternative High-z Cosmic Tracers and the Dark Energy Equation of State. J. Phys. Conf. Ser. **189**, 012032.

Pullen A. R. and Kamionkowski, M. (2007). Cosmic Microwave Background Statistics for a Direction-Dependent Primordial Power Spectrum. Phys. Rev. D **76**, 103529.

Quartin M. and Amendola, L. (2010). Distinguishing Between Void Models and Dark Energy with Cosmic Parallax and Redshift Drift. Phys. Rev. D **81**, 043522.

Rapetti, D., Allen, S. W., Mantz A. and Ebeling, H. (2008). Constraints on modified gravity from the observed X-ray luminosity function of galaxy clusters. arXiv:0812.2259 [astro-ph].

Reid B. A. *et al.* [SDSS Collaboration] (2010). Baryon Acoustic Oscillations in the Sloan Digital Sky Survey Data Release 7 Galaxy Sample. Mon. Not. Roy. Astron. Soc. **401**, 2148.

Rodrigues, D. C. (2008). Anisotropic Cosmological Constant and the CMB Quadrupole Anomaly. Phys. Rev. D **77**, 023534.

Sahni, V. (2002). The cosmological constant problem and quintessence.Class. Quant. Grav. **19**,

3435.

Schild R. E. and Gibson C. H. (2008). Goodness in the Axis of Evil. arXiv:0802.3229 [astro-ph].

Tegmark, M., de Oliveira-Costa, A. and Hamilton A. (2003). A high resolution foreground cleaned CMB map from WMAP. Phys. Rev. D **68**, 123523.

Tsagas, C. G. (2010). Large-scale peculiar motions and cosmic acceleration. Mon. Not. Roy. Astron. Soc. **405**, 503.

Umetsu, K. and Broadhurst, T. (2008). Combining Lens Distortion and Depletion to Map the Mass Distribution of A1689. Astrophys. J. **684**, 177.

Watkins, R., Feldman, H. A. and Hudson, M. J. (2009). Consistently Large Cosmic Flows on Scales of 100 Mpc/h: a Challenge for the Standard LCDM Cosmology. Mon. Not. Roy. Astron. Soc. **392**, 743.

Zumalacarregui, M., Koivisto, T. S., Mota, D. F. and Ruiz-Lapuente, P. (2010). Disformal Scalar Fields and the Dark Sector of the Universe. JCAP **1005**, 038.

arXiv:1103.5331v1 [astro-ph.CO] 28 Mar 2011

What do we really know about Dark Energy?

Ruth Durrer[*]

CEA, SPhT, URA 2306, F-91191 Gif-sur-Yvette, France

March 29, 2011

Abstract

In this paper we discuss what we truly know about dark energy. I shall argue that up to date our single indication for the existence of dark energy comes from distance measurements and their relation to redshift. Supernovae, CMB anisotropies and observations of baryon acoustic oscillations, they all simply tell us that the observed distance to a given redshift z is larger than the one expected from a Friedmann Lemître universe with matter only and the locally measured Hubble parameter.

1 Introduction

Nearly thirteen years ago, measurements of the luminosity of type Ia supernovae (SN1a) as function of their redshift [1] have led to the interpretation that the expansion our Universe is presently accelerated and therefore the energy density of the Universe is presently dominated by a component with strongly negative pressure, $P < -\rho/3$, like during inflation. This was an entirely unexpected result but it has been confirmed with many more observations from SN1a data [2], from observations of CMB anisotropies and polarization [3], from weak lensing [4], from baryon acoustic oscillations [5], from galaxy surveys [7] and from cluster data [6]. All this data is consistent with the so called concordance model, a Friedmann Lemaître (FL) universe with a nearly scale invariant spectrum of Gaussian initial fluctuations as predicted by inflation.

In the concordance model, the energy content of the Universe is dominated by a cosmological constant $\Lambda \simeq 1.7 \times 10^{-66} (\text{eV})^2$ such that $\Omega_\Lambda = \Lambda/(3H_0^2) \simeq 0.73$. Here H_0 denotes the Hubble constant which we parameterize as $H_0 = 100h\,\text{km s}^{-1}\text{Mpc}^{-1} = 2.1332h \times 10^{-33}\text{eV}$. The second component of the concordance model is pressure-less matter with $\Omega_m = \rho_m/\rho_c = \rho_m/(3H_0^2/8\pi G) \simeq 0.13/h^2$. Here G is Newton's constant. About 83% of this matter is 'dark matter', i.e. an unknown non-baryonic component and only about 17% is in the form of baryons (mainly hydrogen and helium), $\Omega_b h^2 \simeq 0.022$. The energy densities of photons and neutrinos are subdominant, $\Omega_\gamma h^2 = 2.48 \times 10^{-5}$, $0.002 < \Omega_\nu h^2 < 0.01$, and curvature is compatible with zero.

This situation is disturbing for two main reasons:

---

[*]On leave from Geneva University

1. The two most abundant components of the Universe have only been inferred
    by their gravitational interaction on cosmological scales.
    Dark matter: on the scale of galaxies, clusters and the Hubble scale.
    Dark energy: only on the Hubble scale.

2. Including particle physics into the picture, we realize that the cosmological
    constant is in no way distinguishable from vacuum energy. The latter has
    not only also the form $T_{\mu\nu}^{\mathrm{vac}} = \rho^{\mathrm{vac}} g_{\mu\nu}$, but it also couples only to gravity.
    Hence there is no experiment that can ever distinguish between a cosmological
    constant Λ and a vacuum energy density[1] $\rho_{\mathrm{vac}} = \Lambda/(8\pi G)$. My conclusion
    is, that we therefore should not distinguish between the two. We then find
    that cosmology determines the present vacuum energy density to be $\rho_{\mathrm{vac}} \simeq$
    $(2.7 \times 10^{-3} \mathrm{eV})^4 h^2$. On the other hand, 'natural values' for the vacuum energy
    are, e.g. the supersymmetry breaking scale which must be larger than about
    1TeV or, if there is no supersymmetry at this scale, the string scale or the
    Planck scale. The resulting estimates for ρ_{vac} are by 60 respectively 120
    orders of magnitude too large. Probably the worst estimate ever in physics!
    Of course, we can introduce a counter term to compensate the 'bare vacuum
    energy' in order to obtain the true, observed value. But, unlike, e.g. the
    electric charge, vacuum energy density is not protected in quantum theory.
    Corrections to it run like E_{max}^4 where E_{max} is the cutoff of the theory. Hence
    the tiny value of ρ_{vac} has to be readjusted at each order in perturbation
    theory by a corresponding, much larger counter term. A truly unsatisfactory
    situation. Even if we are ready to accept this and say that this is an UV
    problem with quantum field theory which should not be mixed up with the IR
    problem of the cosmological constant, in principle, we also have to introduce
    a time dependent IR cutoff to the vacuum energy we expect to run like $H(t)^4$,
    where $H(t)$ is the Hubble parameter at time t. Such a contribution which at
    present has to be of the order of $3H_0^2/(8\pi G)$ was much larger in the past and
    is clearly in contradiction with cosmological observations.
    See [8] for the opposite point of view on the dark energy problem.

Dark matter cannot be any particle of the standard model since all stable standard
model particles except the neutrino and the graviton, either emit photons or would
have left their imprint on nucleosynthesis (baryons). Neutrinos, on the other hand,
have too small masses, too large free-streaming scales, to account for the dark
matter seen e.g. in dwarf galaxies [9] and for other aspects of clustering on small
scales (e.g Ly-α [10]). This is even more true for the graviton which is massless. But
we know from particle physics that there have to be modifications to the standard
model at energies not much larger than 1TeV. Most of the popular proposals of such
modifications, like e.g. supersymmetry, do predict massive stable particles with
weak interaction cross sections and the correct abundance so that they could play
the role of dark matter. Hence there is no shortage of very reasonable candidates
which we have not been able to detect so far. Furthermore, if e.g. the simplest
supersymmetric models are realized, and the dark matter particle is the neutralino,
there is justified hope to detect it soon, either at HLC [11] or via direct dark matter
detection experiments [12].

---

[1]Differences of vacuum energies are of course very well measurable e.g. via the Casimir force
or the Lamb shift in atomic spectra.

2

The second point above, however, is very disturbing. On the one hand, the fact that such an unexpected result has been found by observations shows that present cosmology is truly data driven and not dominated by ideas which can be made to fit sparse observations. Present cosmological data are too good to be brought into agreement with vague ideas. On the other hand, a small cosmological constant is so unexpected and so difficult to bring into agreement with our ideas about fundamental physics, that people have started to look into other possibilities.

One idea is that the cosmological constant should be replaced by some other form of 'dark energy', maybe an ordinary or a tachyonic scalar field [13]. Another possibility is to modify the left hand side of Einstein's equation, i.e. to modify gravity. For a review see [14]. Models where the Einstein-Hilbert action is modified by $R \to f(R)$ have been investigated [15], but also theories with extra dimensions (for reviews/introductions see e.g. [16]) which, when reduced to four dimensions contain terms which deviate from Einstein gravity, the simplest and best studied example is the DGP model [17].

All these models are quite speculative and one has to test in each case that they do not contain dangerous 'ghosts' or other instabilities, which are expected from generic higher derivative terms [18, 19]. Furthermore, even if one of these models is realized in nature, the question, why we do *not* measure a cosmological constant gravitationally remains. However, there may by more satisfactory ways to address this question like de-gravitation [20] or emerging gravity [21, 22].

Another, more conservative possibility is to take into account the fact that the true Universe is inhomogeneous at least on small scales. The question then is wether the clumpiness could mimic the presence of a cosmological constant [23, 24, 25]. Another, more extreme attempt is to assume that the background universe is not homogeneous but only isotropic, a Lemaître-Tolman-Bondi model [26]. Interestingly, these questions are still open. I shall come back to this point later.

In the present paper I do not want to discuss or judge these possibilities, but I want to investigate what present data really has measured. As always when our interpretation of the data leads us to a very unexpected, unnatural 'corner' in the space of physical theories, it may be useful to take a step back and reflect on what the measurements really tell us and how much of what we conclude is actually interpretation of the data which might be doubted.

In the next section I shall go over the main physical observations one by one and address this question. In section 3 we discuss what this means for dark energy and in section 4 I conclude.

Notation: We use t as conformal time such that $ds^2 = a^2(t)(-dt^2 + \gamma_{ij}dx^i dx^j)$. The scale factor is normalized to one today, $a_0 = a(t_0) = 1$ but spatial curvature K is arbitrary. $\Omega_X = \rho_X(t_0)/\rho_c(t_0) = 8\pi G\rho_X(t_0)/(3H_0)^2$ is the (present) density parameter of the component X.

2   What do we really measure?

2.1   Supernovae Ia

Let us start with the first data which gave strong indication of an accelerating universe, the supernovae type Ia observations. SN1a observations measure the light

curve and the spectrum of supernovae. The latter is not only used to determine the redshift, but also indicative for the type of the supernovae while the light curve can be translated into a luminosity distance, $D_L(z)$ to the supernova. For this, correlations between the light curve maximum and its width are used to reduce the scatter and derive the intrinsic luminosity. SN1a are so called modified standard candles [2]. By this correction, the intrinsic scatter of SNIa luminosities of about 1.5mag can be reduced to 0.2mag [27]. It is very likely that in the near future this error can be reduced by at least a factor of two [28]. Astronomical magnitudes are related to the luminosity distance by

$$m(z_1) - m(z_2) = 5\log_{10}\left(D_L(z_1)/D_L(z_2)\right).\qquad(1)$$

Hence an error in the magnitude translates to an error in the luminosity distance via

$$\frac{\delta D_L(z)}{D_L(z)} = \frac{\log(10)}{5}\delta m(z) = 0.46\delta m(z).\qquad(2)$$

Or, an error of 0.2 in the magnitude corresponds to an error of nearly 10% in the luminosity distance. This is the optical precision we can reach at this time, not including systematic errors like e.g. evolution.

If we now *assume* that the geometry of the Universe is Friedmann Lemaître (FL), we can relate the luminosity to the energy content of the universe via the standard formula

$$
\begin{aligned}
D_L(z) &= (1+z)\chi_K\left(\int_0^z \frac{dz'}{H(z')}\right) \quad \text{where} \;\; \chi_K(r) = \frac{1}{\sqrt{K}}\sin(r\sqrt{K}), \;\; \text{and}\\
H(z) &= H_0\sqrt{\Omega_m(1+z)^3 + \Omega_K(1+z)^2 + \Omega_r(1+z)^4 + \Omega_{DE}(z)}.\qquad(3)
\end{aligned}
$$

Here K is spatial curvature and $\chi_K(r) \to r$ for $K \to 0$. For negative values of K the square roots become imaginary and $\sin(r\sqrt{K})/\sqrt{K} = \sinh(r\sqrt{|K|})/\sqrt{|K|}$. $\Omega_K = -K/H_0^2$ and $\Omega_{m,r}$ are the matter respectively radiation density parameter. $\Omega_{DE}(z) = \rho_{DE}(z)/\rho_c(z = 0)$ is the contribution from dark energy. For a cosmological constant $\Omega_{DE}(z) = \Lambda/(3H_0^2)$ is constant.

In Fig. 1 we show the relative difference in the luminosity distance of a Universe with the density parameters $(\Omega_\Lambda, \Omega_m, \Omega_K) = (0.7, 0.3, 0)$ between one with $(\Omega_\Lambda, \Omega_m, \Omega_K) = (0, 1, 0)$ and $(\Omega_\Lambda, \Omega_m, \Omega_K) = (0.7, 0.3, 0)$ between $(\Omega_\Lambda, \Omega_m, \Omega_K) = (0, 0, 1)$. The first difference is larger than 10% already for redshifts $z > 0.1$ and should therefore easily be visible in present supernova data. The second never gets larger than 0.15, but observations of many supernovae should still easily distinguish a Λ-dominated universe from a negative curvature dominated one. This is what SN1a observers claim they can do. Most of the data comes from redshifts below and up to $z \simeq 1$. In this regime, observers therefore detect a luminosity distance which is significantly larger than the one of a flat matter dominated or a curvature dominated Universe with the same Hubble constant.

Hence, if the error estimates of SN1a observers can be trusted, these data indicate either that the geometry of the Universe be not Friedmann, or that the luminosity distance is dominated at low redshift by an accelerating component which behaves similar to a cosmological constant.
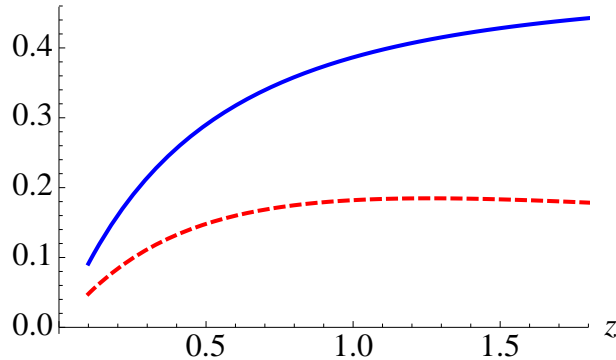
Figure 1: The relative differences $(D_L - D_L(0,1,0))/D_L)$ (blue, solid) and $(D_L - D_L(0,0,1))/D_L)$ (red, dashed)are shown as function of the redshift z, where D_L is the luminosity distance for the concordance model $(\Omega_\Lambda, \Omega_m, \Omega_K) = (0.7, 0.3, 0)$.

2.2 Baryon acoustic oscillations

Another way to measure distances is to compare angles subtended by objects of a given size when placing them at different redshifts. For any metric theory, this angular diameter distance is simply related to the luminosity distance by

$$D_A = D_L/(1+z)^2 \,.$$

Baryon acoustic oscillations are the relics in the matter power spectrum of the oscillations in the baryon-photon plasma prior to decoupling. Once hydrogen recombines and the photons decouple from the electrons, the baryon perturbations evolve like the pressure-less dark matter. Matching this evolution to the oscillations prior to decoupling, one obtains for the positions of the peaks and troughs in the baryon spectrum

$$k_{n\text{through}} = (n + 1/2)\,\pi/s \quad \text{and} \quad k_{n\text{peak}} = (n + 3/2)\,\pi/s \,, \tag{4}$$

where s is the comoving sound horizon at decoupling,

$$s = \int_0^{t_{\text{dec}}} c_s dt \,. \tag{5}$$

More precise values are obtained by numerical codes like CAMBcode [29] and by analytical fits [30, 31]. The angular diameter distance measures a scale subtended at a right angle to the line of sight. If we can measure the difference in redshift Δz between the 'point' and the 'tail' of an object aligned with the line of sight, the corresponding comoving distance is given by

$$\Delta t(z) = \frac{\Delta z}{H} = \frac{\Delta z}{1+z} D_H(z) \,, \quad D_H = \frac{z+1}{H(z)} \,. \tag{6}$$

With present data on large scale structure we have just measured the 3-dimensional power spectrum in different redshift bins. We cannot yet distinguish between transverse and longitudinal directions. This measures a (comoving) geometrical mean
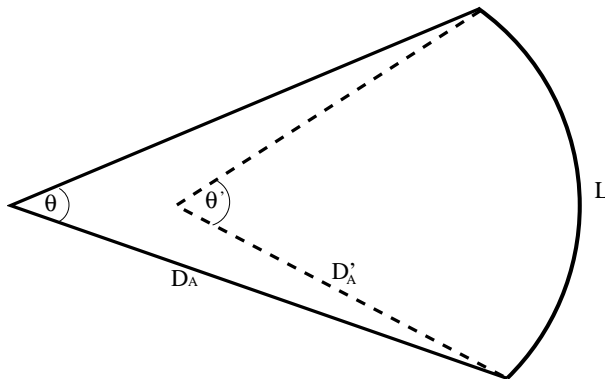
Figure 2: The change of the angle subtended by the CMB acoustic peaks when changing only the distance to the last scattering surface.

$D_V(z) = (D_H(z)D_A(z)^2)^{1/3}$. Results for this scale at redshifts z=0.275 and the ratio $D_V(z_2)/D_V(z_1)$ for $z_2 = 0.3$ and $z_1 = 0.2$ have been published [5].

The observational results from the luminous red galaxy sample of the SDSS catalog [5] are in good agreement with the cosmological concordance model ΛCDM cosmology with $\Omega_\Lambda \simeq 0.7$, $\Omega_m \simeq 0.3$ and no appreciable curvature. Of course, this experiment measures in principle the same quantity as SN1a observations since for all metric theories of gravity $D_A = D_L/(1 + z)^2$, but BAO observations have very different systematics and the fact that they agree well with SN1a is highly non-trivial. There are however objections to the significance of the BAO measurements, see e.g. Refs [32, 33].

Again, these data support a measurement of distance which is significantly larger than the distance to the same redshift with the same Hubble parameter in a $\Omega_m = 1$ Universe.

2.3   CMB

Our most precise cosmological measurements are the CMB observations which have determined the CMB anisotropies and polarization to high precision [3]. These measurements will even be improved substantially by the Planck satellite presently taking data [34]. The CMB data is doubly precious since it is not only very accurate but also relatively simple to calculate in a perturbed FL universe which allows for very precise parameter estimation. For an overview of the physics of the CMB, see [35]. The positions of the acoustic peaks, the relics of the baryon-photon oscillations in the CMB power spectrum, allow for a very precise determination of the angular diameter distance to the last scattering surface. If this distance is changed, keeping all other cosmological parameters fixed, the CMB power spectrum, changes in a very simple way, as shown in Fig. 2.

The angle θ subtended by a given scale L simply changes to $\theta' = \theta \cdot (D_A/D'_A)$. Assuming that the signal comes entirely from the last scattering surface and is not influenced otherwise by the change of its distance from us (this neglects the integrated Sachs Wolfe effect relevant for low harmonics ℓ), we can assume that the

correlation function of the CMB sky at distance D'_A at angle θ' is equal to that of the CMB sky at distance D_A at angle θ, $C'(\theta') = C(\theta)$. Translating this to the power spectrum one obtains for $\ell \gtrsim 20$, see Ref. [36],

$$C_\ell = \left(\frac{D'_A}{D_A}\right)^2 C'_{\frac{D'_A}{D_A}\ell}. \tag{7}$$

In addition to this distance which is very well measured by CMB experiments, also the matter and baryon density at the last scattering surface as well as the spectral index n and the fluctuation amplitude A are well determined by the CMB. Assuming that dark matter and baryons are neither destroyed nor generated between the time of last scattering and today, this leads to the well known value of their present density parameters.

Present CMB data can be fit equally well by the concordance ΛCDMmodel as by a flat matter dominated model with nearly the same values for $\Omega_m h^2$, $\Omega_b h^2$, and n where the angular diameter distance is scaled to a value which is in good agreement with D_A from the concordance model, $D_A(z_*) \simeq 12.9$Mpc. (Note that this is the distance as measured at decoupling, today its value is $(z_* + 1)D_A(z_*)$.) More details on these results can be found in Ref. [36].

We have discussed this here not because with think that the true model is actually the CDM model with $\Omega_m = 1$, but to make clear what aspect of dark energy the CMB data really measure: it is again a distance, the distance to the last scattering surface, i.e. to $z_* \simeq 1090$.

2.4 Weak lensing

Weak lensing measurements determine the weak distortion of galaxy shapes by gravitational lensing from the matter distribution in the foreground of the imaged galaxies. The advantage is that this signal is sensitive only to the total clustered mass in front of the galaxy. The disadvantage is that the signal is small, the ellipticity due to lensing is only about 1% of the typical intrinsic ellipticity of galaxies, and only statistical results can be obtained. For a review see [4]. So far, because of limitations on the knowledge of the redshift distribution of foreground galaxies and other statistical problems, weak lensing has mainly been used to determine the combination $\sigma_8\sqrt{\Omega_m} \simeq 0.6$, which leads to 'bananas' in the $\sigma_8 - \Omega_m$ plane. But future surveys like DES or Euclid are expected to lead to significant improvements, see Ref. [38] for forecasts. Here σ_8 is the amplitude of matter fluctuations in spheres of radius $8h^{-1}$Mpc. It is determined by the amplitude A of CMB anisotropies and the spectral index n.

This measurement by itself may not be so interesting for dark energy, but in combination with CMB anisotropies it is consistent with the same amplitude, spectral index and, especially matter density as the CMB and therefore can be regarded as independent support of the CMB result. It is also interesting that this provides a measurement of $\Omega_m h^2$ at low redshift, $z < 1$ which is consistent with the CMB result at $z = z_* \simeq 1090$.

2.5   Large scale structure

One of the oldest cosmological measurements are determinations of the correlation function and the power spectrum of the galaxy distribution. At present, the biggest galaxy survey is the Sloan Digital Sky Survey, SDSS [7] which has mapped the galaxy distribution on the northern hemisphere out to redshift $z \simeq 0.2$ and the luminous red galaxies to $z \simeq 0.5$. This led to a determination of the galaxy power spectrum down to $k \simeq 0.02h/\mathrm{Mpc}$ [37].

The main problem here is that we compare this measured galaxy power spectrum with the calculated matter power spectrum. The latter can be calculated very accurately on large scales by relativistic cosmological perturbation theory and quite accurately on small scales by Newtonian N-body simulation. However, the relation between this matter distribution and the distribution of galaxies is still to some extend an unsolved debate which goes under the name of 'biasing'. On small scales, it is clear that the galaxy formation process is highly non-linear and may depend on other parameters than the matter density alone (e.g. the metallicity which would favor the formation of galaxies in the vicinity of already existing galaxies).

On large scales, most workers in the field assume that bias is linear and close to one, however, simple investigations of a toy model biasing scheme show that contrary to the matter distribution, the galaxy distribution may very well acquire a white noise component which would dominate on very large scales [39, 40].

If we disregard these problems and assume that in the measured range, or at least where linear perturbation theory applies, bias is linear, we can also use the galaxy power spectrum to get a handle on σ_8, n and $\Omega_m h^2$, with different systematics than from other probes. Interestingly, the power spectrum bends from $\propto k$ behavior to $\propto k^{-3} \ln^2(kt_{\mathrm{eq}})$ behavior at the equality scale, $k_{\mathrm{eq}} \simeq \pi/t_{\mathrm{eq}}$. Since $t_{\mathrm{eq}} \propto 1/(\Omega_m h)$ the position of this turnover (which is very badly constrained with present data), together with the amplitude which is proportional to $\Omega_m h^2$ would allow us to infer both, the Hubble parameter and the matter density parameter from the matter power spectrum.

Features in the galaxy power spectrum, like the BAO's or redshift space distortions might actually be less affected by biasing and therefore provide more promising cosmological probes. However, since they contain less information than the full power spectrum, measuring the latter will always have an advantage.

Finally, in future surveys which go out to very large scales, $z \simeq 2$, it will be very important to clearly relate the observed galaxy distribution to relativistic linear perturbation variables, i.e. to take into account relativistic effects in the matter power spectrum [41, 42, 43]. This actually does not only represent an additional difficulty but even more a new opportunity.

2.6   Cluster abundance and evolution

The earliest data favoring a low density Universe probably comes from the observation of cluster abundance and evolution [44]. Clusters are the largest bound structures in the Universe and as such very sensitive the amplitude of density fluctuations on large scales $\propto \sigma_8 \Omega_m$. Actually, clusters usually form at fixed velocity dispersion. Therefore, the cluster density strongly constrains the velocity power spectrum, $P_V \propto \Omega_m^{1.2} \sigma_8^2$ (see, e.g. [35]). Comparing observations with numerical

simulations gives [45]

$$\Omega_m^{0.6}\sigma_8 = 0.495 \pm \begin{array}{c} 0.034 \\ 0.037 \end{array} .$$

If we insert $\sigma_8 \simeq 0.8$, this is in rough agreement with $\Omega_m \simeq 0.3$, but certainly requires $\Omega_m < 1$.

3   What do we know about 'dark energy'?

What do these observations really tell us about dark energy? I think it is clear, even though I did not enter into any details about observational problems, that each observation taken by itself is not conclusive. There are always many things that can go wrong for any one cosmological probe. We have assumed that systematics are reasonably well under control and we can trust our results. This is supported by the fact that many different probes with independent systematics give the same result: A value of $\Omega_m h^2 \sim 0.13$ and a distance to redshift $z \overset{<}{\sim} 1$ which is not in agreement with flat matter dominated universe but with a ΛCDM universe.

However, we do not measure Λ with any cosmological probe. We only infer it from distance measurements by assuming that the formula (3) can be applied which only holds for homogeneous and isotropic FL models. On the other hand, we know that the true Universe is at least perturbed. Naively, one may argue that the gravitational potential is small $\Psi \sim 10^{-5}$ and therefore corrections coming from clustering will be small. But even if Ψ is small, we know that curvature perturbations which are second derivatives, $\partial_i\partial_j\Psi \sim 4\pi G\delta\rho \overset{>}{\sim} 4\pi G\rho$ are not small. On galactic scales they are many orders of magnitude larger than the background term, $|\partial_i\partial_j\Psi| \gg H^2$. Since such terms may well enter into the perturbed expansion law $H(z)$, it is not clear that they cannot affect the distance for redshifts where clustering has become relevant. This is the point of view of workers on back reaction and clearly, before we have not examined it in detail, we cannot exclude this possibility. Unfortunately, this is a relativistic effect of non linear clustering and our understanding of these effects is still rather poor.

Dyer & Roeder, '72 [46] have argued that the photons which end up in our telescope go preferentially through empty or at least under-dense space and therefore the distance formula should be corrected to the one of an open universe. But as we have seen, this is not sufficient and actually Weinberg, '76 [47] has shown that the shear term which is present if matter is clustered in the case of simple 'Schwarzschild clumps' exactly corrects for the missing Ricci term and reproduces the FL universe formula. In a generic, clumpy spacetime the Sachs equation yields

$$\frac{d^2 D_A}{dv^2} = -\frac{1}{2}(|\sigma|^2 + R_{\mu\nu}k^\mu k^\nu)D_A$$

Hence the presence of shear always leads to deceleration, like matter density. But the measured quantity is not $D_A(v)$ but $D_A(z)$ so we have to study how the redshift is affected by clumping due to the motion of observers.

$$\frac{dz}{dv} = u_{a;b}k^a k^b$$

9

If the expansion of matter (observers) is substantially reduced in a clumping universe this can reduce the redshift at fixed v and therefore lead to seemingly larger distance. Similar ideas have been put forward by Wiltshire [48], but of course we need to study this quantitatively.

Another possibility may be that the Universe is also statistically not homogeneous. From CMB observations we infer that it is very isotropic and this leaves us with spherically symmetric Lemaître-Tolman-Bondi (LTB) models. Clearly, this possibility which violates the cosmological principle is not very attractive. It is therefore important to investigate whether we can test it observationally, and the answer is fortunately affirmative: The relation between the speed of expansion, $H(z)$, and the distance $D_L(z)$ in an FL universe is given by Eq. (3). In an LTB model this relation no longer holds. Therefore independent measurements of both $H(z)$ and $D_L(z)$ (or $D_A(z)$) which test relation (3), can check whether distances are really given by the FL expressions. This at the same time also checks whether clustering modifies distances in an important way. At present we do have relatively good distance measures out to $z \sim 0.5$ but no independent measurements of $H(z)$. These may be obtained in the future from large galaxy surveys like DES or Euclid, which will allow us to measure separately the radial and the transverse matter power spectrum.

Other tests whether 'dark energy' is truly a new component in the stress energy tensor or simply a misinterpretation of the observed distance can come from measurements of the growth factor of linear perturbations which we can determine with future weak lensing surveys like Euclid or via correlations of large scale structure and the integrated Sachs Wolfe effect. In a Λ-dominated universe the linear growth of clustering is modified in a very specific way and we would not expect a simple misinterpretation of observed distances to mimic also this behavior.

4   Conclusions

In this work I have pointed out that all *present* claims about the existence of dark energy have not measured Ω_Λ or even less Ω_{DE} and w directly, but just the distance redshift relation $D_L(z)$. They then have inferred the existence of dark energy by assuming the form (3) for this relation, which holds in a FL universe. Even though many of you (especially the observers, I guess) may regard this point as trivial, I find it important to be aware of it before one is ready to postulate unobserved scalar fields with most unusual properties, or violations of General Relativity on large scales.

I have not discussed the many possible pitfalls of the observations, which weaken any one observation, but my confidence relies on the fact that independent observations with different systematics find the same result. I hope they are not too strongly influenced by 'sociology', i.e.: if your finding disagrees with the results of others it must be wrong and therefore you do not publish it, however, if it agrees well it must be right and therefore you do not have to investigate every possible systematics which would increase your error bars and make your result less "competitive".

The beauty of research in cosmology is that data come in fast and there is justified hope that the question whether relation (3) holds for the real Universe,

will be answered in the not very far future.

References

[1] A.G. Riess et al. 1998 *Observational Evidence from Supernovae for an Accelerating Universe and a Cosmological Constant.* Astron. J. **116**, 1009-1038 [arXiv:astro-ph/9805201];
S. Perlmutter et al. 1999 *Measurements of Omega and Lambda from 42 High-Redshift Supernovae.* Astrophys. J. **517**, 565-586 [arXiv:astro-ph/9812133].

[2] R. Kessler et al. 2009 *First-year Sloan Digital Sky Survey-II (SDSS-II) Supernova Results: Hubble Diagram and Cosmological Parameters.* Astrophys. J. Suppl. **185**, 32 [arXiv:0908.4274].

[3] D. Larson et al. 2011 *Seven-Year Wilkinson Microwave Anisotropy Probe (WMAP) Observations: Power Spectra and WMAP-Derived Parameters.* Astrophys. J. Suppl. **192**, 16 [arXiv:1001.4635] (and references therein).

[4] P. Schneider 2007 *Weak Gravitational Lensing,* in *Gravitational Lensing: Strong, Weak & Micro.* Lecture Notes of the 33rd Saas-Fee Advanced Course, G. Meylan, P. Jetzer & P. North (eds.), Springer-Verlag: Berlin, 273 [arXiv:astro-ph/0509252].

[5] W. Percival et al. 2010 *Baryon Acoustic Oscillations in the Sloan Digital Sky Survey Data Release 7 Galaxy Sample.* MNRAS **401**, 2148-2168 (and references therein).

[6] R. Bielby 2010 *The VLT LBG Redshift Survey I: Clustering and Dynamics of ~ 1000 Galaxies at $z \sim 3$.* [arXiv:1005.3028],
Heng Yu, Zong-Hong Zhu 2010 *Combining Optical and X-ray Observations of Galaxy Clusters to Constrain Cosmological Parameters.* [arXiv:1011.6060].

[7] K. Abazajian et al. 2009 *The Seventh Data Release of the Sloan Digital Sky Survey.* Astrophys. J. Suppl., **182**, 543 [arXiv:0812.0649].

[8] E. Bianchi and C. Rovelli 2010 *Why all these prejudices against a constant?* [arXiv:1002.3966]

[9] A. Boyarsky, O. Ruchayskiy and D. Iakubovskyi, 2009 *A lower bound on the mass of Dark Matter particles.* JCAP **0903**, 005 [arXiv:0808.3902].

[10] M. Viel, M. G. Haehnelt and V. Springel 2010 *The effect of neutrinos on the matter distribution as probed by the Intergalactic Medium.* JCAP06(2010)015 [arXiv:1003.2422].

[11] J. Ellis 2010 *New Light on Dark Matter from the LHC.* [arXiv:1011.0077].

11

[12] J. Billard, F. Mayet, J. F. Macias-Perez, D. Santos, C. Grignon and O. Guil-laudin 2010 *Directional detection of Dark Matter.* Proc. of the 45th Rencontres De Moriond: Electroweak Interactions And Unified Theories, 6-13 Mar 2010, La Thuile, Italy [arXiv:1004.2365]
R. Foot 2010 *A comprehensive analysis of the dark matter direct detection experiments in the mirror dark matter framework.* Phys. Rev. **D82**, 095001 [arXiv:1008.0685].

[13] E. Linder 2008 *The Dynamics of Quintessence, The Quintessence of Dynamics.* Gen. Rel. Grav. **40**, 329-356

[14] R. Durrer and R. Maartens 2008 *Dark Energy and Modified Gravity.* Gen. Rel. Grav. **40**, 301-328;
R. Maartens and R. Durrer, 2010, *Dark Energy and Modified Gravity*, in "Dark Energy: Observational & Theoretical Approaches", ed. Ruiz-Lapuente, P., Cambrige University Press, pp48-91.

[15] S. Capozziello and M. Francaviglia 2008 *Extended Theories of Gravity and their Cosmological and Astrophysical Applications.* Gen. Rel. Grav. **40**, 357-420.

[16] R. Maartens 2004 *Brane-world gravity.* Living Rev. Rel. **7**, 7 [arXiv:gr-qc/0312059];
V. Sahni, 2005 *Cosmological surprises from braneworld models of dark energy.* [arXiv:astro-ph/0502032];
R. Durrer, 2005 *Braneworlds.* AIP Conf. Proc. **782**, 202 [arXiv:hep-th/0507006].

[17] G. R. Dvali, G. Gabadadze and M. Porrati 2000 *Metastable gravitons and infinite volume extra dimensions.* Phys. Lett. B **484**, 112
G. R. Dvali, G. Gabadadze and M. Porrati, 2000 *4D gravity on a brane in 5D Minkowski space.*, Phys. Lett. B **485**, 208.

[18] M. Ostrogradski 1850 *Memoire de l'Academie St. Petersbourg.* Ser. VI **4**, 385.

[19] R. P. Woodard 2006 *Avoiding Dark Energy with 1/R Modifications of Gravity.* [arXiv:astro-ph/0601672].

[20] C. de Rham 2009 *An Introduction to Cascading Gravity and Degravitation.* Can. J. Phys. **87**, 201-220 [arXiv:0810.0269].

[21] T. Jacobson 1995 *Thermodynamics of Spacetime: The Einstein Equation of State.* Phys. Rev. Lett. **75**, 1260 [arXiv:astro-ph/9504004].

[22] T. Padmanabhan 2010 *Thermodynamical Aspects of Gravity: New insights.* Rep. Prog. Phys. **73**, 046901 [arXiv:0911.5004].

[23] M. Bucher 2008 *Dark Energy from structure: a status report.* Gen. Rel. Grav. **40**, 467-527.

[24] S. Räsänen 2008 *The effect of structure formation on the expansion of the universe,* Int. J. Mod. Phys. **D17**, 2543-2548 [arXiv:0805.2670].

[25] C. Clarkson and R. Maartens 2010 *Inhomogeneity and the foundations of concordance cosmology.* Class. Quantum Grav. **27**, 124008 [arXiv:1005.2165].

[26] K. Enqvist 2008 *Lemaitre-Tolman-Bondi model and accelerating expansion .* Gen. Rel. Grav. **40**, 451-466.

[27] A. Kim et al. 1997 *Implications For The Hubble Constant from the First Seven Supernovae at $z \geq 0.35$.* Astrophys. J. **476**, L63-L67 [astro-ph/9701188].

[28] B. Nicols 2011, *private communication.*

[29] A. Lewis, A. Challinor, and A. Lasenby 2000 *Efficient computation of CMB anisotropies in closed FRW models.* Astrophys. J. **538**, 473-476 [arXiv:astro-ph/9911177].

[30] D. Eisenstein and W. Hu 1998 *Baryonic features in the matter transfer function.* Astrophys. J. **496**, 605 [arXiv:astro-ph/9709112].

[31] F. Montanari 2010 *The Baryonic Acoustic Oscillations and the Large-Scale Structure of the Universe.* Tesi di Laurea, Padua.

[32] F. Sylos Labini 2010 *Breaking of self-averaging properties and selection effects in the Luminous Red Galaxies sample.* [arXiv:1011.4855].

[33] A. Cabre, E. Gaztanaga 2010 *Have Baryonic Acoustic Oscillations in the galaxy distribution really been measured?* [arXiv:1011.2729].

[34] see website `http://www.esa.int/esaSC/120398_index_0_m.html`.

[35] R. Durrer 2008 *The Cosmic Microwave Background.* 401p, Cambridge University Press.

[36] M. Vonlanthen, S. Räsänen and R. Durrer 2010 *Model-independent cosmological constraints from the CMB.* JCAP **08**, 023
(DOI: 10.1088/1475-7516/2010/08/023).

[37] B.A. Reid et al. 2010 *Cosmological Constraints from the Clustering of the Sloan Digital Sky Survey DR7 Luminous Red Galaxies.* Mon. Not. Roy. Astron.Soc. **404**, 60-85 (DOI: 10.1111/j.1365-2966.2010.16276.x) [arXiv:0907.1659v2].

[38] B. Joachimi and S.L. Bridle 2010 *Simultaneous measurement of cosmology and intrinsic alignments using joint cosmic shear and galaxy number density correlations.* Astron. Astrophys. **523**, A1.

[39] R. Durrer, A. Gabrielli, M. Joyce and F. Sylos Labini 2003 *Bias and the power spectrum beyond the turn-over.* Astrophys.J. **585**, L1-L4

[40] J. Béltran and R. Durrer 2010 *Effects of biasing on the matter power spectrum at large scales.* [arXiv:1006.2343].

[41] J. Yoo, M. Zaldarriaga, and L. Hernquist 2009 *New Perspective on Galaxy Clustering as a Cosmological Probe: General Relativistic Effects.* Phys. Rev. **D80**, 083514.

[42] J. Yoo 2010 *General Relativistic Description of the Observed Galaxy Power Spectrum: Do We Understand What We Measure?*, Phys. Rev. **D82**, 083508.

[43] C. Bonvin and R. Durrer 2011 *What galaxy surveys really measure.* in preparation.

[44] N. Bahcall and R. Cen 1992 *Galaxy clusters and cold dark matter - A low-density unbiased universe?* Astrophys. J. **398**, L81-L84.

[45] Pierpaoli, E., Scott, D. and White, M. 2001 *Power spectrum normalization from the local abundance of rich clusters of galaxies.* Mon. Not. Roy. Astron. Soc. **325**, 77.

[46] C. Dyer and R. Roeder 1972 *The Distance-Redshift Relation for Universes with no Intergalactic Medium.* Astrophys. J. Lett. **174**, L115.

[47] S. Weinberg 1976 *Apparent luminosities in a locally inhomogeneous universe.* Astrophys. J. **208**, L1.

[48] D. Wiltshire 2007 *Exact solution to the averaging problem in cosmology.* Phys. Rev. Lett. **99**, 251101 [arXiv:0709.0732];
D. Wiltshire 2008 *Dark energy without dark energy.* In "Dark Matter in Astroparticle and Particle Physics: Proceedings of the 6th International Heidelberg Conference", eds H.V. Klapdor-Kleingrothaus and G.F. Lewis, (World Scientific, Singapore), 565-596 [arXiv:0712.3984],
D. Wiltshire 2008 *Cosmological equivalence principle and the weak-field limit.* Phys. Rev. **D78**, 084032 [arXiv:0809.1183].

Natural observer fields and redshift

ROBERT MACKAY
COLIN ROURKE

We sketch the construction of a space-time with an observer field which has redshift satisfying Hubble's law but no big bang.

1   Introduction

This paper is part of a program whose aim is to establish a new paradigm for the universe in which there is no big bang. There are three pieces of primary evidence for the big bang: the distribution of light elements, the cosmic microwave background, and redshift. This paper concentrates on redshift. Alternative explanations for the other pieces of primary evidence are given in other papers in the program.

The context for our investigation of redshift is the concept of an *observer field* by which we mean a future-pointing time-like vector field. An observer field is *natural* if the integral curves (field lines) are geodesic and the perpendicular 3–plane field is integrable (giving normal space slices). It then follows that the field determines a local coherent notion of time: a time coordinate that is constant on the perpendicular space slices and whose difference between two space slices is the proper time along any field line. This is proved in [6, Section 5].

In a natural observer field, red or blueshift can be measured locally and corresponds precisely to expansion or contraction of space measured in the direction of the null geodesic being considered (this is proved in Section 2 of this paper). Therefore, if you assume the existence of a global natural observer field, an assumption made implicitly in current conventional cosmology, then redshift leads directly to global expansion and the big bang. But there is no reason to assume any such thing and many good reasons not to do so. It is commonplace observation that the universe is filled with heavy bodies (galaxies) and it is now widely believed that the centres of galaxies harbour supermassive objects (normally called black holes). The neighbourhood of a black hole is not covered by a natural observer field. You do not need to assume that there is a

2   *Robert MacKay and Colin Rourke*

singularity at the centre to prove this. The fact that a natural observer field admits a coherent time contradicts well known behaviour of space-time near an event horizon.

In this paper we shall sketch the construction of a universe in which there are many heavy objects and such that, outside a neighbourhood of these objects, space-time admits natural observer fields which are roughly expansive. This means that redshift builds up along null geodesics to fit Hubble's law. However there is no global observer field or coherent time or big bang. The expansive fields are all balanced by dual contractive fields and there is in no sense a global expansion. Indeed, as far as this makes sense, our model is roughly homogeneous in both space and time (space-time changes dramatically near a heavy body, but at similar distances from these bodies space-time is much the same everywhere).

A good analogy of the difference between our model and the conventional one is given by imagining an observer of the surface of the earth on a hill. He sees what appears to be a flat surface bounded by a horizon. His flat map is like one natural observer field bounded by a cosmological horizon. If our hill dweller had no knowledge of the earth outside what he can see, he might decide that the earth originates at his horizon and this belief would be corroborated by the strange curvature effects that he observes in objects coming over his horizon. This belief is analogous to the belief in a big bang at the limit of our visible universe.

This analogy makes it clear that our model is very much bigger (and longer lived) than the conventional model. Indeed it could be indefinitely long-lived and of infinite size. However, as we shall see, there is evidence that the universe is bounded, at least as far as boundedness makes sense within a space-time without universal space slices or coherent time.

This paper is organised as follows. Section 2 contains basic definitions and the proof of the precise interrelation between redshift and expansion in a natural observer field. In Section 3 we cover the basic properties of de Sitter space on which our model is based and in Section 4 we prove that the time-like unit tangent flow on de Sitter space is Anosov. This use of de Sitter space is for convenience of description and is probably not essential. In Section 5 we cover rigorously the case of introducing one heavy body into de Sitter space and in Section 6 we discuss the general case. Here we cannot give a rigorous proof that a suitable metric exists, but we give instead two plausibility arguments that it does. Finally in Section 7 we make various remarks.

For more detail on the full program see the second author's web site at:
http://msp.warwick.ac.uk/~cpr/paradigm/
but please bear in mind that many parts of the program are still in very preliminary form.

Natural observer fields and redshift   **3**

We shall use the overall idea of this program namely that galaxies have supermassive centres which control the dynamic, and that stars in the spiral arms are moving outwards along the arms at near escape velocity. (It is this movement that maintains the shape of the arms and the long-term appearance of a galaxy.) However this paper is primarily intended to illustrate the possibility of a universe satisfying Hubble's law without overall expansion and not to describe our universe in detail.

2   Observer fields

A pseudo-Riemannian manifold L is a manifold equipped with non-degenerate quadratic form g on its tangent bundle called the *metric*. A *space-time* is a pseudo-Riemannian 4–manifold equipped with a metric of signature $(-, +, +, +)$. The metric is often written as ds^2, a symmetric quadratic expression in differential 1–forms. A tangent vector v is *time-like* if $g(v) < 0$, *space-like* if $g(v) > 0$ and *null* if $g(v) = 0$. The set of null vectors at a point form the *light-cone* at that point and this is a cone on two copies of S^2. A choice of one of these determines the *future* at that point and we assume *time orientability*, ie a global choice of future pointing light cones. An *observer field* on a region U in a space-time L is a smooth future-oriented time-like unit vector field on U. It is *natural* if the integral curves (field lines) are geodesic and the perpendicular 3–plane field is integrable (giving normal space slices). It then follows that the field determines a coherent notion of time: a time coordinate that is constant on the perpendicular space slices and whose difference between two space slices is the proper time along any field line; this is proved in [6, Section 5].

A natural observer field is *flat* if the normal space slices are metrically flat. In [6] we found a dual pair of spherically-symmetric natural flat observer fields for a large family of spherically-symmetric space-times including Schwarzschild and Schwarzschild-de-Sitter space-time, namely space-times which admit metrics of the form:

$$(1) \qquad\qquad ds^2 = -Q\,dt^2 + \frac{1}{Q}\,dr^2 + r^2\,d\Omega^2$$

where Q is a positive function of r. Here t is thought of as time, r as radius and $d\Omega^2$, the standard metric on the 2–sphere, is an abbreviation for $d\theta^2 + \sin^2\theta\,d\phi^2$ (or more symmetrically for $\sum_{j=1}^{3} dz_j^2$ restricted to $\sum_{j=1}^{3} z_j^2 = 1$). The Schwarzschild metric is defined by $Q = 1 - 2M/r$, the de Sitter metric by $Q = 1 - (r/a)^2$ and the combined Schwarzschild de Sitter metric by $Q = 1 - 2M/r - (r/a)^2$ (for $M/a < 1/\sqrt{27}$). Here M is mass (half the Schwarzschild radius) and a is the "radius of the visible universe". In these cases one of these observer fields is expanding and the other contracting and it

4   *Robert MacKay and Colin Rourke*

is natural to describe the expanding field as the "escape" field and the dual contracting field as the "capture" field. The expansive field for Schwarzschild-de-Sitter space-time is the main ingredient in our redshifted observer field.

Redshift

Natural observer fields are ideally suited for a study of redshift. It is easy to define a local coefficient of expansion or contraction of space. Choose a direction in a space slice and a small interval in that direction. Use the observer field to carry this to a nearby space slice. The interval now has a possibly different length and comparing the two we read a coefficient of expansion. Intuitively we expect this to coincide with the instantaneous red or blue shift along a null geodesic in the same direction and for total red/blue shift to coincide with expansion/contraction integrated along the null geodesic. As this is a key point for the paper we give a formal proof of this fact.

The metric has the form

$$(2) \qquad\qquad ds^2 = -dt^2 + g_{ij}(x,t)dx^i dx^j$$

where g is positive definite. The observer field is given by $\dot{x} = 0, \dot{t} = 1$. It has trajectories $x = \text{const}$ with proper time t along them.

The redshift z of an emitter trajectory $x = x_e$ of the observer field as seen by a receiver trajectory $x = x_r$ is given by

$$(3) \qquad\qquad 1 + z = \frac{dt_r}{dt_e}$$

for the 1-parameter family of null geodesics connecting the emitter to the receiver in the forward direction.

The rate ρ of expansion of space in spatial direction ξ, along the observer field, is given by

$$\rho(\xi) = \frac{\partial}{\partial t} \log \sqrt{g_{ij}\xi^i\xi^j} = \frac{1}{2}\frac{\partial g_{ij}}{\partial t}\xi^i\xi^j / (g_{ij}\xi^i\xi^j).$$

We claim that $\log(1 + z)$ can be written as $\int \rho(v)\, dt$ where $v(t)$ is the spatial direction of the velocity of the null geodesic at time t.

We prove this first for one spatial dimension. Then the null geodesics are specified by $g(\frac{dx}{dt})^2 = 1$. Without loss of generality, take $x_e < x_r$, thus $\frac{dt}{dx} = \sqrt{g}$. Differentiating with respect to initial time t_e, we obtain

$$\frac{d}{dx}\frac{dt}{dt_e} = \frac{1}{2}\frac{\partial g}{\partial t}g^{-1/2}\frac{dt}{dt_e}$$

Natural observer fields and redshift **5**

Thus

$$\log (1 + z) = \int_{x_e}^{x_r} \frac{1}{2} \frac{\partial g}{\partial t} g^{-1/2} \, dx.$$

Use $\frac{dt}{dx} = \sqrt{g}$ to change variable of integration to t:

$$\log (1 + z) = \int_{t_e}^{t_r} \frac{1}{2} \frac{\partial g}{\partial t} g^{-1} \, dt$$

But $\rho(v) = \frac{1}{2} \frac{\partial g}{\partial t} g^{-1}$. So

$$\log (1 + z) = \int_{t_e}^{t_r} \rho(v) \, dt.$$

To tackle the case of n spatial dimensions, geodesics of a metric G on space-time (t, x) are determined by stationarity of

$$E = \int \frac{1}{2} G_{\alpha\beta} \frac{dx^\alpha}{d\lambda} \frac{dx^\beta}{d\lambda} d\lambda$$

over paths connecting initial to final position in space-time. This includes determination of an affine parametrisation λ. The null geodesics are those for which $E = 0$. Consider a null geodesic connecting the trajectory x_e to the trajectory x_r. Generically, it lies in a smooth 2-parameter family of geodesics connecting x_e to x_r, parametrised by the initial and final times t_e, t_r. A 1-parameter subfamily of these are null geodesics, namely those for which $E = 0$. Differentiating with respect to a change in (t_e, t_r), and using stationarity of E with respect to fixed endpoints, we obtain

$$\delta E = p_0(t_r)\delta t_r - p_0(t_e)\delta t_e,$$

where

$$p_0 = G_{0\beta} \frac{dx^\beta}{d\lambda}$$

(0 denoting the t-component). So the subfamily for which $E = 0$ satisfies

$$\frac{dt_r}{dt_e} = \frac{p_0(t_e)}{p_0(t_r)}.$$

Thus

$$\log (1 + z) = \log |p_0(t_e)| - \log |p_0(t_r)|,$$

which is minus the change in $\log |p_0|$ from emitter to receiver (note that $p_0 < 0$).

Now

$$\frac{d}{dt} \log |p_0| = \frac{dp_0}{dt} p_0^{-1}.$$

6   *Robert MacKay and Colin Rourke*

Hamilton's equations for geodesics with Hamiltonian $\frac{1}{2}G^{\alpha\beta}p_\alpha p_\beta$ give

$$\frac{dp_0}{d\lambda} = -\frac{1}{2}\frac{\partial G^{\alpha\beta}}{\partial t}p_\alpha p_\beta, \ \ \frac{dt}{d\lambda} = G^{0\beta}p_\beta.$$

So

$$\frac{d}{dt}\log|p_0| = \frac{-\frac{1}{2}\frac{\partial G^{\alpha\beta}}{\partial t}p_\alpha p_\beta}{p_0 G^{0\beta}p_\beta}.$$

Now $G^{\alpha\beta}G_{\beta\gamma} = \delta^\alpha_\gamma$ implies that

$$\frac{\partial G^{\alpha\beta}}{\partial t} = -G^{\alpha\gamma}\frac{\partial G_{\gamma\delta}}{\partial t}G^{\delta\beta}$$

and $G^{\delta\beta}p_\beta = \frac{dx^\delta}{d\lambda}$ which we denote by v^δ, so

$$\frac{d}{dt}\log|p_0| = \frac{\frac{1}{2}\frac{\partial G_{\alpha\beta}}{\partial t}v^\alpha v^\beta}{p_0 v^0}$$

For a null geodesic, $p_0 v^0 = -p_i v^i$ (where the implied sum is over only spatial components). For our form of metric (2), $-p_i v^i = -g_{ij}v^i v^j$ and the numerator also simplifies to only spatial components, so we obtain

$$\frac{d}{dt}\log|p_0| = -\frac{\frac{1}{2}\frac{\partial g_{ij}}{\partial t}v^i v^j}{g_{ij}v^i v^j} = -\rho(v).$$

So

$$\log(1+z) = \int_{t_e}^{t_r}\rho(v)\,dt$$

as desired.

Uniform expansion and the Schwarzschild-de-Sitter case

An important special case of the metric is when g is of the form $\lambda(t)h$ where λ is a positive function and h is independent of t. Locally this defines the warped product of a 3–manifold with time. This is the class of metrics used in conventional cosmology (the Friedman-Lemaître-Robertson-Walker or FLRW–metrics). The further special case where h is the standard quadratic form for Euclidean space $\mathbb{R}^3$ and $\lambda(t) = \exp(t/a)$ is the unique fully homogeneous FLRW–metric. This metric is uniformly expanding, has non-zero cosmological constant (CC) namely $3/a^2$ and is the most natural choice of metric for an expanding universe.

As remarked above, the Schwarzschild-de-Sitter and Schwarzschild metrics admit flat natural observer fields. In [6, Section 6] we calculated the space expansion/contraction in the three principal directions. The average is always expansive and, as we shall see later, of a size appropriate for Hubble's law.

Natural observer fields and redshift   **7**

3   de Sitter space

We give here a summary of the properties of de Sitter space that we shall need. Full proofs can be found in [3].

Definitions

Minkowski n–space $\mathbb{M}^n$ is $\mathbb{R}^n = \mathbb{R} \times \mathbb{R}^{n-1}$ (time cross space) equipped with the standard $(-, +, \dots, +)$ metric. The time coordinate is x_0 and the space coordinates are $x_1, \dots, x_{n-1}$. The *Lorentz n–group* is the group of isometries of Minkowski space fixing $\mathbf{0}$ and preserving the time direction. This implies that a Lorentz transformation is an (affine) linear isomorphism of $\mathbb{R}^n$. If, in addition to preserving the time direction, we also preserve space orientation then the group can be denoted $\mathrm{SO}(1, n-1)$. Notice that a Lorentz transformation which preserves the x_0–axis is an orthogonal transformation of the perpendicular $(n-1)$–space, thus $\mathrm{SO}(n-1)$ is a subgroup of $\mathrm{SO}(1, n-1)$ and we refer to elements of this subgroup as (Euclidean) rotations about the x_0–axis.

Minkowski 4–space $\mathbb{M}$ is just called *Minkowski space* and the Lorentz 4–group is called the *Lorentz group*.

Now go up one dimension. *Hyperbolic* 4–*space* is the subset of $\mathbb{M}^5$

$$\mathbb{H}^4 = \{\|\mathbf{x}\|^2 = -a^2, \ x_0 > 0 \mid \mathbf{x} \in \mathbb{M}^5\}$$

and *de Sitter space* is the subset of $\mathbb{M}^5$

$$\mathrm{deS} = \{\|\mathbf{x}\|^2 = a^2 \mid \mathbf{x} \in \mathbb{M}^5\}.$$

There is an isometric copy $\mathbb{H}^4_-$ of hyperbolic space with $x_0 < 0$. The induced metric on hyperbolic space is Riemannian and on de Sitter space is Lorentzian. Thus de Sitter space is a space-time. The *light cone* is the subset

$$L = \{\|\mathbf{x}\| = 0 \mid \mathbf{x} \in \mathbb{M}^5\}$$

and is the cone on two 3–spheres with natural conformal structures (see below). These are S^3 and S^3_- where S^3 is in the positive time direction and S^3_- negative.

The constant a plays the role of (hyperbolic) radius and we refer to it (with tongue in cheek) as the "radius of the universe". This is not intended to have any cosmological meaning.

Points of

$$S^3 \cup S^3_- \cup \mathrm{deS} \cup \mathbb{H}^4 \cup \mathbb{H}^4_-$$

8   *Robert MacKay and Colin Rourke*

are in natural bijection with the set of half-rays from the origin and we call this *half-ray space*. SO(1, 4) acts on half-ray space preserving this decomposition and is easily seen to act transitively on each piece. Planes through the origin meet half-ray space in *lines* which come in three types: *time-like* (meeting $\mathbb{H}^4$) *light-like* (tangent to light-cone) and *space-like* (disjoint from the light cone). Symmetry considerations show that lines meet $\mathbb{H}^4$ and deS in geodesics (and all geodesics are of this form). Figure 1 is a projective picture illustrating these types.
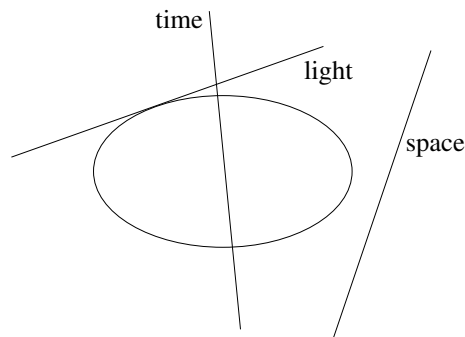
Figure 1: Types of lines (geodesics)

$\mathbb{H}^4$ with the action of SO(1, 4) is the *Klein model* of hyperbolic 4–space. S^3 is then the sphere at infinity and SO(1, 4) acts by conformal transformations of S^3 and indeed is isomorphic to the group of such transformations.

SO(1, 4) also acts as the group of time and space orientation preserving isometries of deS and should perhaps be called the *de Sitter group* as a result.

A simple combination of elementary motions of deS proves that SO(1, 4) acts transitively on lines/geodesics of the same type in half-ray space and indeed acts transitively on *pointed lines*. In other words:

Proposition 1   *Given geodesics l, m of the same type and points $P \in l$, $Q \in m$, there is an isometry carrying l to m and P to Q.*

It is worth remarking that topologically deS is $\mathbb{R} \times S^3$. Geometrically it is a hyperboloid of one sheet ruled by lines and each tangent plane to the light cone meets deS in two ruling lines. These lines are light-lines in $\mathbb{M}^5$ and hence in deS. (See Figure 2, which is taken from Moschella [7].)

Natural observer fields and redshift   **9**
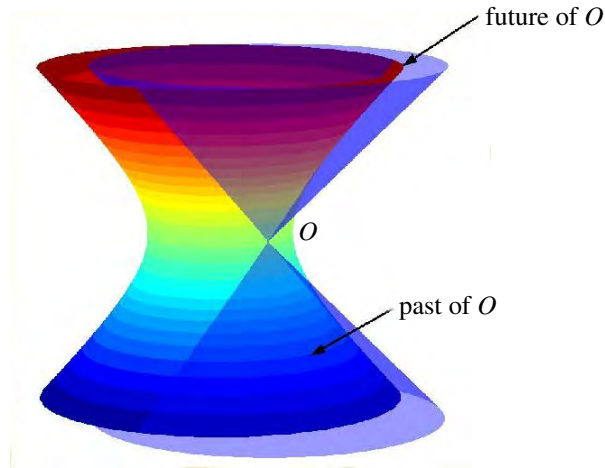
Figure 2: Light-cones: the light-cone in deS is the cone on a 0–sphere (two points) in the dimension illustrated, in fact it is the cone on a 2–sphere. The figure is reproduced from [7].

The expansive metric

Let Π be the 4–dimensional hyperplane $x_0 + x_4 = 0$. This cuts deS into two identical regions. Concentrate on the upper complemetary region Exp defined by $x_0 + x_4 > 0$. Π is tangent to both spheres at infinity S^3 and S^3_-. Name the points of tangency as P on S^3 and P_- on S^3_-. The hyperplanes parallel to Π, given by $x_0 + x_4 = k$ for $k > 0$, are also all tangent to S^3 and S^3_- at P, P_- and foliate Exp by paraboloids. Denote this foliation by $\mathcal{F}$. We shall see that each leaf of $\mathcal{F}$ is in fact isometric to $\mathbb{R}^3$. There is a transverse foliation $\mathcal{T}$ by the time-like geodesics passing through P and P_-.

These foliations are illustrated in Figures 3 and 4. Figure 3 is the slice by the (x_0, x_4)–coordinate plane and Figure 4 (the left-hand figure) shows the view from the x_4–axis in 3–dimensional Minkowski space (2–dimensional de Sitter space). This figure and its companion are again taken from Moschella [7].

Let G be the subgroup of the Lorentz group which fixes P (and hence P_- and Π). G acts on Exp. It preserves both foliations: for the second foliation this is obvious, but all Lorentz transformations are affine and hence carry parallel hyperplanes to parallel hyperplanes; this proves that it preserves the first foliation. Furthermore affine considerations also imply that it acts on the set of leaves of $\mathcal{F}$ by scaling from the origin. Compare this action with the conformal action of G on S^3 (the light sphere at infinity). Here G acts by conformal isomorphisms fixing P which are similarity transformations of $S^3 - P \cong \mathbb{R}^3$. The action on the set of leaves of $\mathcal{F}$ corresponds to

10   *Robert MacKay and Colin Rourke*
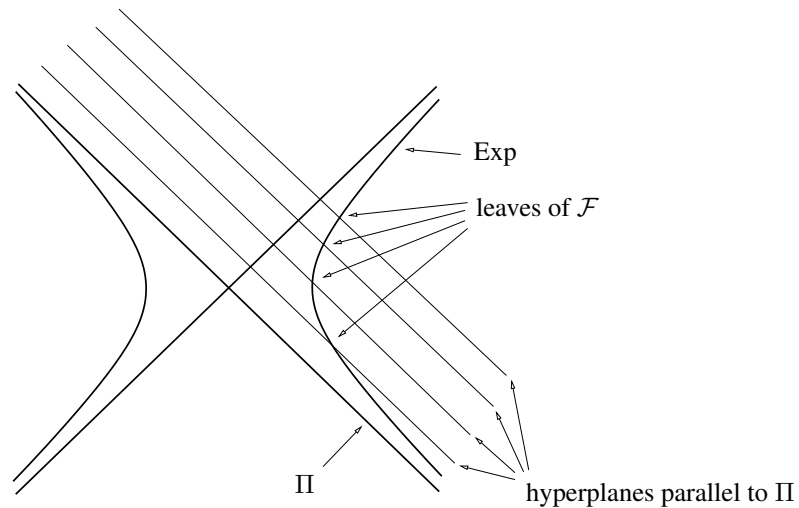
Figure 3: The foliation $\mathcal{F}$ in the (x_0, x_4)–plane
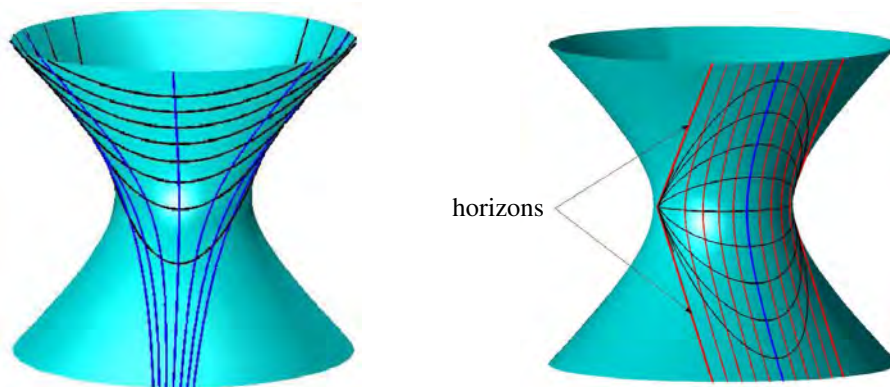
Figure 4: Two figures reproduced from [7]. The left-hand figure shows the foliation $\mathcal{F}$ (black lines) and the transverse foliation $\mathcal{T}$ by geodesics (blue lines). The righthand figure shows the de Sitter metric as a subset of deS.

dilations of $\mathbb{R}^3$ and the action on a particular leaf corresponds to isometries of $\mathbb{R}^3$. By dimension considerations this gives the full group of isometries of each leaf. It follows that each leaf has a flat Euclidean metric.

We can now see that the metric on Exp is the same as the FLRW metric for a uniformly expanding infinite universe described in Section 2 above. The transverse foliation by time-like geodesics determines the standard observer field and the distance between hyperplanes defining $\mathcal{F}$ gives a logarithmic measure of time. Explicit coordinates are

Natural observer fields and redshift   **11**

given in [3]. Notice that we have proved that every isometry of Exp is induced by an isometry of deS.

It is worth remarking that exactly the same analysis can be carried out for $\mathbb{H}^4$ where the leaves of the foliation given by the same set of hyperplanes are again Euclidean. This gives the usual "half-space" model for hyperbolic geometry with Euclidean horizontal sections and vertical dilation.

Time-like geodesics in Exp

We have a family of time-like geodesics built in to Exp namely the observer field mentioned above. These geodesics are all *stationary*. They are all equivalent by a symmetry of Exp because we can use a Euclidean motion to move any point of one leaf into any other point. Other time-like geodesics are *non-stationary*. Here is a perhaps surprising fact:

Proposition 2 *Let l, m be any two non-stationary geodesics in* Exp. *Then there is an element of $G = $* Isom(Exp) *carrying l to m.*

Thus there in no concept of conserved velocity of a geodesic with respect to the standard observer field in the expansive metric. This fact is important for the analysis of black holes in de Sitter space, see below.

The proof is easy if you think in terms of hyperbolic geometry. Time-like geodesics in Exp are in bijection with geodesics in $\mathbb{H}^4$ since both correspond to 2–planes through the origin which meet $\mathbb{H}^4$. But if we use the upper half-space picture for $\mathbb{H}^4$ stationary means vertical and two non-stationary geodesics are represented by semi-circles perpendicular to the boundary. Then there is a conformal map of this boundary (ie a similarity transformation) carrying any two points to any two others: translate to make one point coincide and then dilate and rotate to get the other ones to coincide.

The de Sitter metric

There is another standard metric inside de Sitter space which is the metric which de Sitter himself used. In standard coordinates for de Sitter space, this metric takes the form given in (1) with $Q = 1 - (r/a)^2$. The metric is illustrated in Figure 4 on the right. This metric is static, in other words there is a time-like Killing vector field (one whose

12   *Robert MacKay and Colin Rourke*

associated flow is an isometry). The region where it is defined is the intersection of $x_0 + x_4 > 0$ defining Exp with $x_0 - x_4 < 0$ (defining the reflection of Exp in Ξ, the (x_1, x_2, x_3, x_4)–coordinate hyperplane). The observer field, given by the Killing vector field, has exactly one geodesic leaf, namely the central (blue) geodesic. The other leaves (red) are intersections with parallel planes not passing through the origin. There are two families of symmetries of this subset: an SO(3)–family of rotations about the central geodesic and shear along this geodesic (in the (x_0, x_1)–plane). Both are induced by isometries of deS.

This metric accurately describes the middle distance neighbourhood of a black hole in empty space with a non-zero CC. The embedding in deS is determined by the choice of central time-like geodesic. Proposition 2 then implies that there are precisely two types of black hole in a standard uniformly expanding universe. There are stationary black holes which, looking backwards in time, all originate from the same point. Since nothing real is ever completely at rest, this type of black hole is not physically meaningful. The second class are black holes with non-zero velocity. Looking backwards in time these all come from "outside the universe" with infinite velocity (infinite blueshift) and gradually slow down to asymptotically zero velocity. If this description has any relation to the real universe then this phenomenon might give an explanation for observed gamma ray bursts. In any case it underlines clearly the unreality of assuming the existence a standard uniformly expanding universe containing black holes.

In the next section we consider a metric which accurately describes the immediate neighbourhood of the black hole as well as its surroundings.

The contractive metric

Reflecting in Ξ (the (x_1, x_2, x_3, x_4)–coordinate hyperplane) carries Exp to the subset Cont defined by $x_0 - x_4 < 0$. Exactly the same analysis shows that Cont has an FLRW-metric with constant warping function $\exp(-t/a)$, which corresponds to a uniformly *contracting* universe with *blueshift* growing linearly with distance. Since the subsets Exp and Cont overlap (in the region where the de Sitter metric is defined), by homogeneity, any small open set in deS can be given two coordinate systems, one of which corresponds to the uniformly expanding FLRW-metric and the other to the uniformly contracting FLRW-metric. These overlapping coordinate systems can be used to prove that the time-like geodesic flow is Anosov.

Natural observer fields and redshift **13**

4 The Anosov property

A C^1 flow ϕ on a manifold M is equivalent to a vector field v by $d\phi_\tau(x) = v(\phi_\tau(x))$ where ϕ_τ is the diffeomorphism given by flowing for time τ. The flow is *Anosov* if there is a splitting of the tangent bundle TM as a direct sum of invariant subbundles $E^- \oplus E^+ \oplus \mathbb{R}v$ such that, with respect to a norm on tangent vectors, there are real numbers $C, \lambda > 0$ such that $u \in E^-$ respectively E^+ implies $|u_t| \le C \exp(-\lambda|t|) |u|$ for all $t > 0$ respectively $t < 0$ where u_t is $d\phi_t(u)$. If M is compact then different norms do not affect the Anosov property, only the value of C, but if M is non-compact one must specify a norm.

The *time-like geodesic flow* on a space-time is the flow on the negative unit tangent bundle $T_{-1}(M) = \{v \in TM \mid g(v) = -1\}$ induced by flowing along geodesics. More geometrically we can think of $W = T_{-1}(M)$ as the space of germs of time-like geodesics. Thus a point in W is a pair (X, x) where $X \in M$ and x is an equivalence class of oriented time-like geodesics through X, where two are equivalent if they agree near X; this is obviously the same as specfiying a time-like tangent vector at X up to a positive scale factor. The geodesic flow ψ is defined by $\psi_\tau(X, x) = x(\tau)$ where $x()$ is the geodesic determined by x parametrised by distance from X.

Proposition 3 $T_{-1}(\mathrm{deS})$ *is a Riemannian manifold and* ψ *is Anosov.*

To prove the proposition we need to specify the norm on the tangent bundle of $W = T_{-1}(\mathrm{deS})$ and prove the Anosov property. Using Proposition 1 we need only do this at one particular point (X, x) in W and then carry the norm (and the Anosov parameters) around W using isometries of deS. We choose to do this at (Q, g) where $Q = (0, 0, 0, a)$ and g is determined by the (x_0, x_4)–plane. These are the central point and vertical geodesic in Figure 4. Recall that Ξ is the hyperplane orthogonal to g at Q (orthogonal in either Minkowski or Euclidean metric is the same here!) and let Ξ' be a nearby parallel hyperplane. A geodesic near to g at Q can be specified by choosing points T, T' in Ξ, Ξ' near to Q and to specify a point of W near to (Q, g) we also need a point on one of these geodesics and we can parametrize such points by hyperplanes parallel and close to Ξ. We can identify the tangent space to W at (Q, g) with these nearby points of W in the usual way and for coordinates we have Euclidean coordinates in Ξ and Ξ' and the distance between hyperplanes. This gives us a positive definitive norm on this tangent space.

Now recall that we have a foliation $\mathcal{T}$ of deS near Q by time-like geodesics passing through P and P_- (the time curves in the expanding metric) and dually (reflecting in

Ξ) another foliation $\mathcal{T}'$ which are the time curves in the contracting metric ie geodesics passing through P' and P'_- the reflected points. Let E^+ be the subspace determined by $\mathcal{T}$ at points of Ξ near Q and let E^- be determined similarly by $\mathcal{T}'$. These meet at (Q, g) and span a subspace of codimension 1. The remaining 1–dimensional space is defined by (Q_ϵ, g) where Q_ϵ varies through points of g near Q. The Anosov property holds with $\lambda = a$ and $C = 1$ by the expanding and contracting properties of the two metrics which we saw above.

Alternatively, one can study the Jacobi equation $v'' = Mv = -R(u, v, u)$ for linearised perpendicular displacement v to a time-like geodesic with tangent u (without loss of generality, unit length). Now $\mathrm{Tr}M = -\mathrm{Ric}(u, u) = -\Lambda g(u, u) = \Lambda$. But de Sitter space has rotational symmetry about any time-like vector, in particular u, so M is a multiple of the identity, hence $\frac{\Lambda}{3}$. Thus $v'' = \frac{\Lambda}{3}v$ and $v(t) = v^+ e^{-t/a} + v^- e^{t/a}$, demonstrating the splitting into vectors which contract exponentially in forwards and backwards time respectively.

5   The Schwarzschild de Sitter metric

In this section we look at the effect of introducing a black hole into de Sitter space. There is an explicit metric which modifies the standard Schwarzschild metric to be valid in space-time with a CC (see eg Giblin–Marolf–Garvey [4, Equation 3.2]) given by:

(4) $$ds^2 = -Q(r)\,dt^2 + Q(r)^{-1}\,dr^2 + r^2\,d\Omega^2$$

Here $Q(r) = 1 - 2M/r - (r/a)^2$ where M is mass (half the Schwarzschild radius) and the CC is $3/a^2$ as usual.

There are several comments that need to be made about this metric.

(A)   It is singular where $Q = 0$ ie when $r = 2M$ approx and when $r = a$ approx (we are assuming that a is large). The singularity at $r = 2M$ is at (roughly) the usual Schwarzschild radius. It is well known to be removable eg by using Eddington–Finkelstein coordinates. The singularity at $r = a$ is a "cosmological horizon" in these coordinates and is again removable. This is proved in Giblin–Marolf–Garvey (op cit) and more detail is given below.

(B)   The metric is static in the sense that the time coordinate corresponds to a time-like Killing vector field. But like the de Sitter metric described above, the time field is completely unnatural so this stasis has no physical meaning. Indeed for these coordinates *no* time curve is a geodesic.

Natural observer fields and redshift   **15**

(C) Comparing equations (1) in the de Sitter case ($Q = 1 - (r/a)^2$) and (4) we see that the former is precisely the same as the latter if the Schwarzschild term $-2M/r$ is removed. In other words if the central mass (the black hole) is removed the Schwarzschild metric (modified for CC) becomes the de Sitter metric. This is why we call this the Schwarzschild de Sitter metric. Physically what this means is that as r increases (and the Schwarzschild term tends to zero) the metric approximates the de Sitter metric closely. Thus the metric embeds the black hole metric with CC into de Sitter space and in particular we can extend the metric past the cosmological horizon at $r = a$ which can now be seen as a removable singularity. This will be proved rigorously below.

(D) We can picture the metric inside deS by using Figure 4 (right). Imagine that the central geodesic (blue) is a thick black line. This is the black hole. The other vertical (red) lines are the unnatural observer field given by the time lines. The horizontal black curved lines are the unnatural space slices corresponding to the unnatural observer field. The thick red lines marked "horizon" are the "cosmological horizon" which is removable and we now establish this fact rigorously.

Extending the expansive field to infinity

We shall use the ideas of Giblin et al [4] to extend the metric (4) beyond the horizon at $r = a$ to the whole of Exp. In [6] we proved that there is a unique pair of flat space slices for a spherically-symmetric space-time which admits such slices. Since this is true for both the Schwarzschild-de-Sitter metric and Exp it follows that the expansive observer field (the escape field) found in [6] for the Schwarzschild-de-Sitter metric merges into the standard expansive field on Exp. We shall need to make a small change to de Sitter space to achieve the extension but we shall not disturb the fact that the space satisfies Einstein's equation $\mathrm{Ric} = \Lambda g$ with CC $\Lambda = 3/a^2$. Recall that $Q(r) = 1 - 2M/r - (r/a)^2$.

A *horizon* is an r_0 for which $Q(r_0) = 0$. Q has an inner horizon r_b and an outer horizon r_c. It is convenient to treat r_b, r_c as the parameters instead of a, M. Thus

$$Q(r) = -\frac{1}{a^2 r}(r - r_b)(r - r_c)(r + r_b + r_c),$$

and then a, M become functions of r_b, r_c, as

$$a^2 = r_b^2 + r_c^2 + r_b r_c, M = r_b r_c (r_b + r_c)/2a^2.$$

16   *Robert MacKay and Colin Rourke*

Suppose $\kappa := \frac{1}{2}Q'(r_0) \neq 0$ and $Q''(r_0) < 0$. This is true at both horizons, but we shall just extend beyond r_c.

$$Q'(r) = \frac{2}{a^2 r^2}(a^2 M - r^3)$$

so $\kappa = (a^2 M - r_c^3)/a^2 r_c^2$.

We will achieve the goal as a submanifold of $\mathbb{R}^5$ with coordinates (X, T, y_1, y_2, y_3):

$$X^2 - T^2 = Q(r)/\kappa^2$$

The submanifold is given the metric

$$ds^2 = -dT^2 + dX^2 + \beta(r)dr^2 + r^2 d\Omega^2$$

with

$$\beta(r) = \frac{4\kappa^2 - Q'(r)^2}{4\kappa^2 Q(r)}.$$

The numerator of β contains a factor $(r - r_c)$ which cancels the factor $(r - r_c)$ of Q, and $\beta(r) \in (0, \infty)$ for all $r \in (r_b, \infty)$.

The above submanifold and metric are obtained using the coordinate change

$$X(r, t) = \frac{1}{\kappa}\sqrt{Q(r)}\cosh(\kappa t),$$

$$T(r, t) = \frac{1}{\kappa}\sqrt{Q(r)}\sinh(\kappa t).$$

The metric satisfies Ric $= \Lambda g$ because the original metric does in the region $Q(r) > 0$, so the new one does for $r \in (r_b, r_c)$, but the submanifold and the coefficients of the metric are given by rational expressions in r, so $Ric = \Lambda g$ wherever g is regular.

Asymptotic form for large r

$$\beta(r) = \frac{a^2((r^3 - a^2 M)^2 r_c^4 - (r_c^3 - a^2 M)^2 r^4)}{(r_c^3 - a^2 M)^2 r^3(r^3 - a^2 r + 2Ma^2)}$$

It is convenient to use $r_c^3 - a^2 M = \frac{1}{2}r_c(3r_c^2 - a^2)$. Then:

$$\beta(r) = \frac{4a^2 r_c^2}{(3r_c^2 - a^2)^2} \frac{1 - \frac{(3r_c^2 - a^2)^2}{4r_c^2}r^{-2} - 2a^2 M r^{-3} + a^4 M^2 r^{-6}}{1 - a^2 r^{-2} + 2Ma^2 r^{-3}}$$

The factor at the front can be written $(\kappa a)^{-2}$, and is close to 1 for M small, so we write $\beta(r) = (\kappa a)^{-2}\tilde{\beta}(r)$. Now $(3r_c^2 - a^2)/2r_c$ is close to a for small M, so it is sensible to extract the leading correction $-a^2 r^{-2}$ in the numerator, writing

$$4a^2 r_c^2 - (3r_c^2 - a^2)^2 = r_b(8r_c^3 + 7r_b r_c^2 - 2r_b^2 r_c - r_b^3).$$

Natural observer fields and redshift   **17**

Thus:

$$\tilde{\beta}(r) = \frac{1 - a^2r^{-2} + \frac{r_b}{4r_c^2}(8r_c^3 + 7r_br_c^2 - 2r_b^2r_c - r_b^3)r^{-2} - 2a^2Mr^{-3} + a^4M^2r^{-6}}{1 - a^2r^{-2} + 2Ma^2r^{-3}}$$

$$\sim \left(1 + \frac{r_b(8r_c^3 + 7r_br_c^2 - 2r_b^2r_c - r_b^3)}{4r_c^2(r^2 - a^2)} - \frac{4Ma^2}{r(r^2 - a^2)} + O(M^2a^3r^{-5})\right)$$

An an alternative we can scale X, T to $X' = \kappa aX, T' = \kappa aT$ so that the submanifold is

$$X'^2 - T'^2 = a^2Q(r) = a^2 - r^2 - 2Ma^2/r$$

which is an $O(Ma^2/r^3)$ perturbation of the standard hyperboloid for large r. The metric then is

$$ds^2 = (\kappa a)^{-2}(-dT'^2 + dX'^2 + \tilde{\beta}(r)dr^2) + r^2d\Omega^2.$$

Interestingly, this is not asymptotic to the de Sitter metric as $r \to \infty$ because of the factor $(\kappa a)^{-2}$, although it does tend to 1 as $M \to 0$. Scaling the metric by this factor does not help because then the last term becomes $(\kappa a)^2r^2d\Omega^2$.

6   The model

Recall that we are assuming that most galaxies have supermassive centres and that most stars in those galaxies are travelling on near escape orbits. This implies that most of the sources of light from distant galaxies is from stars fitting into an escape field. We also fit into the escape field from our own galaxy. In [6] we proved that these fields are expansive, see Section 2, and as we saw above, they each individually merge into the standard expansive field on de Sitter space. We shall give two plausibility arguments to show that this extension works with many black holes and therefore for many black holes in de Sitter space there is locally a (roughly uniformly) expansive field outside the black holes which we call the *dominant* observer field. Our model is de Sitter space with many black holes, one for each galaxy in the universe, and anywhere in the model there is a dominant observer field which locally contains all the information from which expansion (and incorrectly, the big bang) are deduced. Thus any observer in any of these fields observes a pattern of uniform redshift and Hubble's law.

There are dual contractive fields and the two are in balance, so that this universe "in the large" is not expanding. Indeed the expansive field only covers the visible parts of the universe. Most of the matter in the universe is contained in the supermassive black holes at the centres of galaxies and this matter is not in any sense in an expanding

18   *Robert MacKay and Colin Rourke*

universe. The space slices in De Sitter space are infinite but there is no need to assume this for the real universe (merely that they are rather large) for a description along these lines to make sense; cf final remark (2).

The first plausibility argument: Anosov property

We saw that de Sitter space has an Anosov property. Anosov dynamical systems have stability. Changes made locally die out exponentially fast. Therefore we can introduce the black holes one at a time and modify the metric successively to accomodate them. This argument would be fully rigorous if it was possible to give estimates that prove that the disturbances do not build up. Unfortunately, although the changes do die out exponentially, the coefficient is roughly $1/a$ which is very small. Thus this argument only proves what we want for galaxies which are of the order of the "radius of the universe" apart.

Nevertheless it does strongly suggest that the result we want is correct.

The second plausibility argument: the charged case

Kastor and Traschen [5] give an explicit solution for the metric appropriate to many charged black holes in de Sitter space. Again this proof does not apply to the real universe because the assumption made is that the charge cancels out gravitational attraction and well known observations (eg Zwicky [10]) clearly show that gravity is alive and well for galaxies in the real universe.

Nevertheless it does again strongly suggest that the result we want is correct.

7   Final remarks

(1)   Evidence from the Hubble ultra deep field

Note that the expansion from a heavy centre is not uniform. Near the centre the radial coordinate contracts and the tangential coordinates expand, with the nett effect that is still expansive on average. This is described in detail in [6, Section 6]. When these expansive fields are fitted together to form the global expansive field for the universe, because of the non-uniformity in each piece, the result is highly non-uniform in other

Natural observer fields and redshift **19**

words is filled with gravitational waves. There are also very probably many other sources of gravitational waves which add to the non-uniformity.

There is strong direct evidence for gravitational waves in deep observations made by the Hubble telescope, see [8]. It is also worth commenting that may also be indirect evidence provided by gamma ray bursts which may well be caustics in the developing observer field caused by the same non-uniformity, but see also the comments about black holes entering an expanding universe made in Section 3 above.

(2) Bounded space slices

The model we constructed above has infinite space slices for the dominant observer field, based as it is on the flat slicing of de Sitter space. There is however a nearby model where the slicing is titled a little so that the space slices are bounded. This has the effect of causing the expansion to drop off over very long distances and we cannot resist pointing out that this is exactly what is observed [1, 2] and conventionally ascribed to dark energy.

(3) Cosmological constant

We used de Sitter space as a substrate for our model because of the wealth of structure and results associated with this space. It has the consequence that we are assuming a non-zero CC. However it is quite plausible that one could splice together many copies of Schwarzschild space, which has zero CC, and obtain a similar model but here there is no hint at any rigorous proof.

(4) Estimates

Our attitude throughout this paper has been the construction of a model which demonstrates that redshift and expansion do not have to be associated with a big bang and therefore we have avoided direct estimates of the size of the expansion that we have considered. But we finish with just this. The estimate of linear expansion for the natural flat observer field near a black hole is $T/2$ where $T = \sqrt{2M}r^{-3/2}$, [6, Section 5]. Further out the rate tends towards an expansion rate of $1/a$ corresponding to the CC. Galaxies are typically spaced about 10^7 light years apart. So we expect an expansion of about $\sqrt{M} \times 10^{-10.5}$ and if this is the observed Hubble expansion of $10^{-10.5}$ then we find M is of the order of one light year. In solar masses this is $10^{12.5}$ solar masses.

20   *Robert MacKay and Colin Rourke*

This is within the expected range for a galactic centre though we should point out that it is 2.5 orders of magnitude smaller than the estimate of 10^{15} solar masses obtained in the main paper in this program [9]. This discrepancy is probably due to ignoring angular momentum, see the next remark.

(5)   Health warning

This paper has used a fully relativistic treatment throughout. However the main paper in the program [9] uses a combination of Newtonian dynamics and relativistic effects especially in the derivation of the rotation curve of a galaxy and the full dynamic. It needs rewriting in a fully relativistic form using the Kerr metric because non-zero angular momentum is crucial to the treatment. This probably means that the analysis in this paper will need to be changed.

References

[1]   *The supernova cosmology project*, Lawrence Berkeley Laboratory, see
      http://panisse.lbl.gov

[2]   *The high-Z supernova search*, see
      http://cfa-www.harvard.edu/cfa/oir/Research/supernova/

[3]   *Notes on de Sitter space*, http://msp.warwick.ac.uk/~cpr/paradigm/notes.pdf

[4]   **J T Giblin**, **D Marolf**, **R Garvey**, *Spacetime embedding diagrams for spherically symmetric black holes*, General Relativity and Gravitation 36 (2004) 83–99

[5]   **D Kastor**, **J Traschen**, *Cosmological multi-black-hole solutions*, Phys Rev D 47 (1993) 5370–5

[6]   **R MacKay**, **C Rourke**, *Natural flat observer fields in spherically-symmetric spacetimes*, submitted for publication, available at
      http://msp.warwick.ac.uk/~cpr/paradigm/escape-submit.pdf

[7]   **U Moschella**, The de Sitter and anti-de Sitter sightseeing tour, Séminaire Poincaé 1 (2005) 1–12, available at http://www.bourbaphy.fr/moschella.pdf

[8]   **C Rourke**, *Optical distortion in the Hubble Ultra-Deep Field*, available at
      http://msp.warwick.ac.uk/~cpr/paradigm/HUDF-2.pdf

[9]   **C Rourke**, *A new paradigm for the structure of galaxies*, available at
      http://msp.warwick.ac.uk/~cpr/paradigm/struc-gal.pdf

[10] **F Zwicky**, *Die Rotverschiebung von extragalaktischen Nebeln*, Helvetica Physica Acta 6 (1933) 110–127. See also Zwicky, F. (1937). *On the Masses of Nebulae and of Clusters of Nebulae*, Astrophysical J 86 (1937) 217 DOI:10.1086/143864

Natural observer fields and redshift **21**

Mathematics Institute, University of Warwick, Coventry CV4 7AL, UK

R.S.MacKay@warwick.ac.uk, cpr@msp.warwick.ac.uk

http://www.warwick.ac.uk/~mackay/, http://msp.warwick.ac.uk/~cpr

Multiscale approach to inhomogeneous cosmologies

Alexander Wiegand

Fakultät für Physik, Universität Bielefeld,

Universitätsstraße 25,

D--33615 Bielefeld, Germany

Email: wiegand@physik.uni-bielefeld.de

Abstract

The backreaction of inhomogeneities onto the global expansion of the universe suggests a possible link of the formation of structures to the recent accelerated expansion. In this paper, the origin of this conjecture is illustrated and a model that allows a more explicit investigation is discussed. Additionally to this conceptually interesting feature, the model leads to a ΛCDM like distance-redshift relation that is consistent with supernova data.

Averaged Equations For The Expansion Of The Universe

The averaging problem

The evolution of our universe is described by Einstein's equations of General Relativity. These are ten coupled differential equations for the coefficients of the metric that describes our spacetime. In the cosmological case, where we are only interested in the overall evolution and not in the detailed local form of the inhomogeneous metric, cosmologists widely work with the assumption that the global evolution is described by the single homogeneous and isotropic solution of the Einstein Equations: They use a homogeneous isotropic fluid as the content of the universe that sources the evolution of the homogeneous and isotropic Robertson Walker (RW) metric and therefore determines the lapse of the expansion. This latter is thereby condensed into the evolution of a single quantity, the scale factor $a(t)$. The fundamental question, dating back to Shirokov and Fisher (1963) and most prominently raised by George Ellis in 1983 (Ellis (1983)), is then, if this procedure leads to the correct description of the global behaviour of our spacetime. Are the Einstein equations the correct effective equations that describe the average evolution, even if they are local equations?

To address this question, one has to find a way to explicitly average the equations. This is necessary, because if one performs an average of an inhomogeneous metric whose time evolution has been determined by the use of the ten Einstein equations, one finds a result that differs from the classical case above. This is already evident from the fact that Einsteins equations are nonlinear. But already at the linear level, as soon as the volume element of the domain of averaging is time dependent, this non commutation is present. This is easy to see from a derivation of the definition of the average of a scalar quantity f, $\langle f \rangle_D(t) := \int_D f(t,X) \sqrt{^{(3)}g(t,X)}\, d^3 X / V_D(t)$ with respect to time which provides $\partial_t \langle f \rangle_D - \langle \partial_t f \rangle_D = \langle f\theta \rangle_D - \langle f \rangle_D \langle \theta \rangle_D \neq 0$, θ being the local expansion rate. So, if we take an implicitly averaged metric, i.e. the RW metric, and the effective homogeneous matter source, and then calculate its time evolution with the standard Friedmann equation, this will not give the average of the time evolved quantity. Or to put it short, time evolution and averaging do not commute, often strikingly written as $G_{\mu\nu}(\langle g_{\mu\nu} \rangle) \neq \langle G_{\mu\nu}(g_{\mu\nu}) \rangle$ and depicted in Fig. 1.
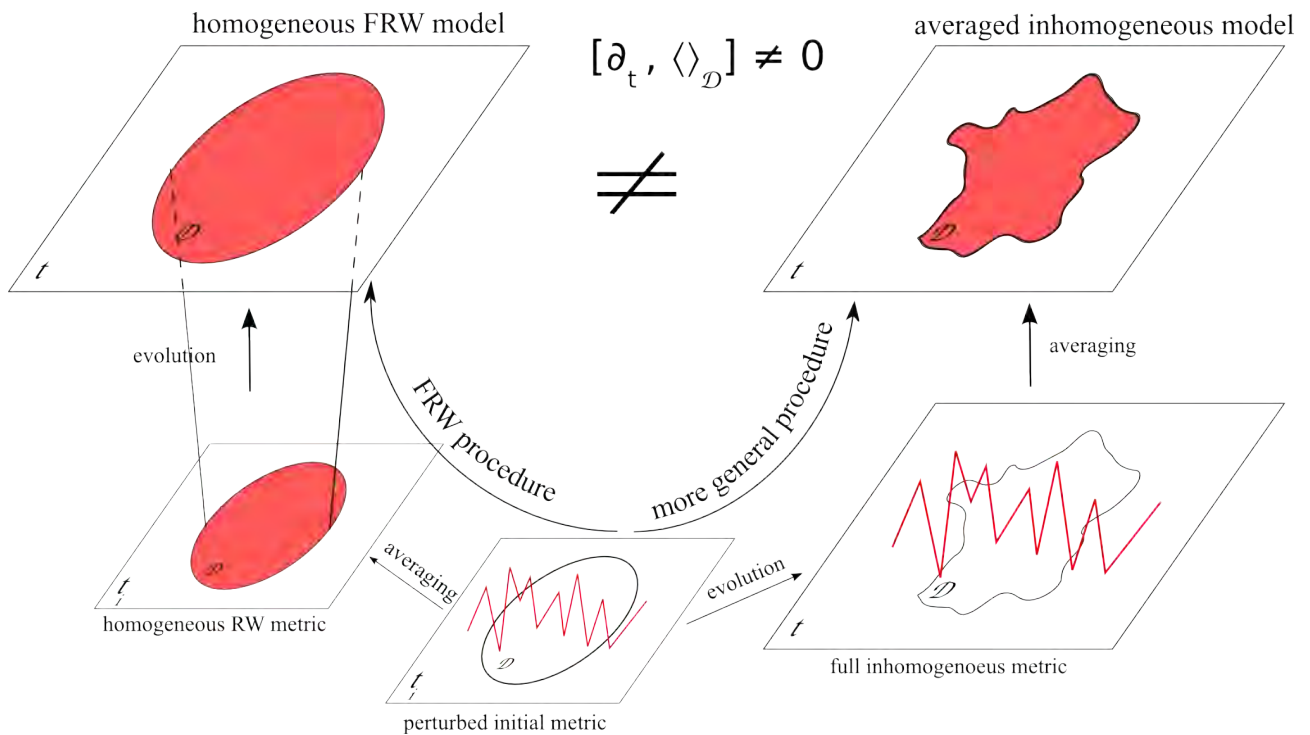
Figure 1: *Illustration of the cause of the departure of the average evolution from the standard Friedmann solutions: The noncommutativity of spatial averaging and time evolution. The standard Friedmannian picture is the left branch, where you first average the inhomogeneous matter distribution and calculate the evolution of this homogeneous soup by the Einstein equations. In contrast to that, in the averaged model shown by the right branch, the perturbation evolution is still performed with the full metric and only then, the average is taken. The two approaches give different results. But the main question remains: How big is this difference?*

000101

Provenance of the averaged equations

In the recent literature, the question of how big the difference between these two approaches is, has received growing interest, mainly due to attempts to relate it to the dark energy problem (Räsänen (2004), Kolb *et al.* (2005)). Since then, there have been many calculations trying to quantify the impact of this noncommutativity of time evolution and averaging. The direct way of trying to average the Einstein equations in their tensorial form turned out to be very difficult, because it is not clear how to define a meaningful average of tensors. Therefore the most popular scheme to work with is still the one by Buchert (Buchert (2000) and Buchert (2001)). In this approach, one uses the ADM equations to perform a 3+1 split of the spacetime into spatial hypersurfaces orthogonal to the fluid flow. The source is also in this case often taken to be a perfect fluid and the equations take their simplest form in the frame of an observer comoving with the fluid. After this split one can identify scalar, vector and tensor parts of the resulting equations. For the scalar sector there is then a straightforward definition of an average quantity as the integral of the scalar function over a comoving domain of the spatial hypersurface, divided by the volume of this domain. The use of this definition astonishingly provides a set of two differential equations for the average scale factor of the averaging domain, that resembles closely the Friedmann equations in the homogeneous case:

$$3 H_D^2 = 8 \pi G \langle \rho \rangle_D - \frac{1}{2} \langle R \rangle_D - \frac{1}{2} Q_D + \Lambda \tag{1}$$

$$\frac{\ddot{a}_D}{a_D} = -4 \pi G \langle \rho \rangle_D + Q_D + \Lambda \tag{2}$$

This is surprising, because in this approach it is not necessary to constrain the matter source to a completely homogeneous one, but one can have arbitrarily large spatial variations in the density. There are, however, two important differences between the general averaged evolution equations (1) and (2) for the volume scale factor and the Friedmann equations. First of all, there is one extra term Q_D, which is called the kinematical backreaction term. It encodes the departure of the matter distribution in the spatial hypersurface from a homogeneous distribution. This is because it is defined as the variance of the local expansion rate of the spacetime minus the variance of the shear inside the domain $\mathcal{D}$. Therefore, if the expansion fluctuations are bigger than the shear fluctuations, Q_D is positive and contributes to the acceleration of the spatial domain (c.f. Eq. (2)). For dominating shear fluctuations, Q_D is negative, and decelerates the domain's expansion. This effective term Q_D that emerges from the explicit averaging procedure, induces the second difference to the standard Friedmann equations. By the integrability condition of the equations for the average scale factor (Eqs. (1) and (2)), Q_D is connected to the average internal curvature of the domain $\mathcal{D}$. Unlike in the

Friedmann case, where the curvature scales as a_D^{-2}, the dependence of the average curvature $\langle R \rangle_D$ on a_D, has not necessarily the form of a simple power law. In fact it can be shown that the curvature picks up an integrated contribution of the variation of $\mathcal{Q}_D$ and evolves in this way generically away from the flat initial conditions, expected to emerge from inflation.

Uncommon properties of the averaged model

These two changes to the standard Friedmann equations may alter the expansion history considerably. Regarding Eq. (2), it is easy to see, that for $Q_D > 4\pi G \langle \varrho \rangle_D$ there may even be an accelerated epoch of expansion without the presence of a cosmological constant. It may seem surprising that even in a universe only filled with a perfect fluid of ordinary (or dark) matter, there may be an effective acceleration of a spatial domain $\mathcal{D}$. This occurs, because in the calculation of the average expansion rate of $\mathcal{D}$, the local expansion is weighted with its corresponding volume. Therefore, faster expanding subregions of $\mathcal{D}$, which will by their faster growth occupy a larger and larger volume fraction of $\mathcal{D}$, will

Figure 2: *Phase space of the solutions to the averaged equations Eqs. (1) and (2). The deceleration parameter $q^D = 1/2\,\Omega_m^D + 2\Omega_Q^D$ is in the present case of $\Lambda = 0$ effectively a measure of Ω_Q^D and Ω_m^D is the matter parameter on $\mathcal{D}$. The point in the middle is the EdS model and the line r=0 encompasses the Friedmann models i.e. $\Omega_Q^D = 0$.*

eventually dominate its expansion. Subregions that slow down their expansion, will finally only occupy a negligible fraction of the volume of $\mathcal{D}$. This means that a volume weighted average of the expansion rate will start with a value between the one of the slow and fast expanding regions, when they have still a comparable size, but will be driven towards the value of the fastest expanding domain in the late time limit. This growth in the average expansion rate corresponds to an acceleration of the growth of the volume scale factor.
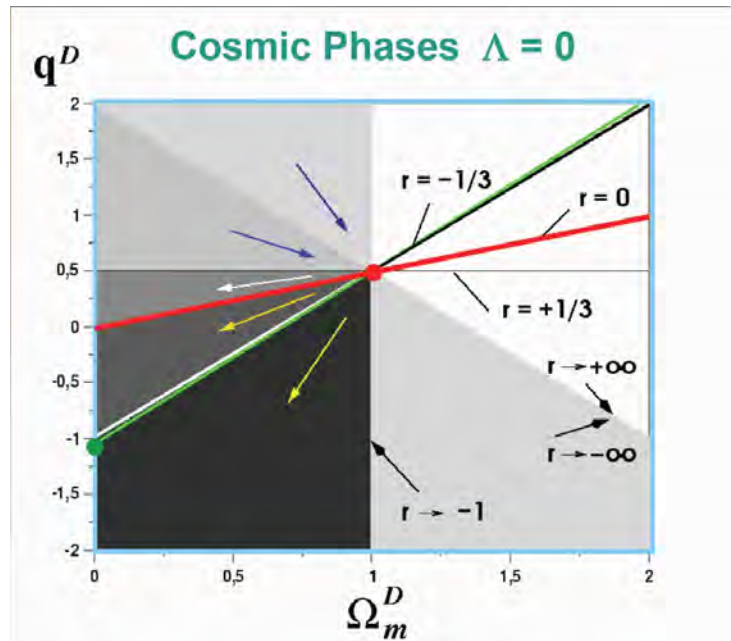
A convenient way to illustrate the possible departure of the solutions of the equations for the average scale factor, from the Friedmann solution, is the phase space diagram in Fig. 2. For a universe without cosmological constant every path in this two dimensional plane, corresponds to a solution of the averaged equations. Scaling solutions for which the a_D-dependence of the kinematical backreaction Q_D is given by a single power law a_D^n , show up as straight lines. The Friedmann solutions lie on the line $r=0$. A first phase space analysis of this parameter space in Buchert *et al.* (2006) has shown, that the EdS model in the middle is an unstable saddle point. Perturbations of the homogeneous state in the matter dominated era, will therefore drive the universe away from it in the direction indicated by the arrows. This is also the region in which the Q_D term is positive. Therefore the instability of the Friedmann model leads naturally to accelerated expansion, if the phase space is traversed rapidly enough. A more elaborated phase space analysis may soon be found in Roy and Buchert (2011).

The important changes to the Friedmann model that emerge when passing to explicit averages, may be summarized in the following generalized concepts:

1. The single homogeneous and isotropic solution of Einstein's equations is replaced by explicit averages of the equations of general relativity.
2. The background is now generically interacting with the structure in the spatial hypersurfaces.
3. The inhomogeneities do no longer average out on the background.
4. The full Riemannian curvature degree of freedom is restored and the equations no longer are restricted to a constant curvature space.

A more detailed review of our current understanding of the description of the average evolution may be found in Buchert (2008) and Räsänen (2006).

Partitioning Models

To build a specific model using the above framework there have been several attempts. As the equations for $a_D(t)$ are not closed, one has to impose, like in the Friedmann case, an equation of state for the fluid. The problem is here, that the fluid composed of backreaction Q_D and average curvature $\langle R \rangle_D$ is only an effective one. Therefore it is not clear which equation of state one should choose. In Roy and Buchert (2009) for example, the equation of state of a Chaplygin gas has

been used. Another approach in Buchert *et al.* (2006) has been to take a constant equation of state which leads to simple scaling solutions for the $a_\mathcal{D}$-dependence of $\mathcal{Q}_\mathcal{D}$ and $\langle R \rangle_D$. Those will be generalized here by the partitioning model, described in detail in Wiegand and Buchert (2010).

Model construction

As the name suggests, this is done by a partitioning of the background domain $\mathcal{D}$ into subdomains. To have a physical intuition about the evolution of the subdomains, a reasonable choice is to partition $\mathcal{D}$ into overdense $\mathcal{M}$- and underdense $\mathcal{E}$-regions. $\mathcal{M}$ and $\mathcal{E}$ regions will also obey the average equations (1) and (2) and there are consistency conditions, resulting from the split of the $\mathcal{D}$ equations into $\mathcal{M}$ and $\mathcal{E}$ equations, that link the evolution of $\mathcal{D}$, $\mathcal{M}$ and $\mathcal{E}$. The reason for the split is that it offers the possibility to replace the unintuitive backreaction parameter $\mathcal{Q}_\mathcal{D}$ by a quantity that illustrates more directly the departure from homogeneity, namely the volume fraction of the overdense regions $\lambda_\mathcal{M}$. As explained above, $\lambda_\mathcal{M}$ is expected to decrease during the evolution and it is this decrease that drives the acceleration. The physical motivation to split into over and underdense regions is, that from the structure of the cosmic web, one may expect $\mathcal{E}$ regions, which are mainly composed of voids, to be more spherical than $\mathcal{M}$ regions. On $\mathcal{E}$, the expansion fluctuations should therefore be larger than the shear fluctuations and so $\mathcal{Q}_\mathcal{E}$ should be positive. The shear fluctuation dominated $\mathcal{M}$ regions should have a negative $\mathcal{Q}_\mathcal{M}$. This increases the difference between the faster expanding $\mathcal{E}$ and the decelerating $\mathcal{M}$ regions even further and therefore magnifies the expansion fluctuations on $\mathcal{D}$ that drive acceleration via a positive $\mathcal{Q}_\mathcal{D}$. The fact that $\mathcal{Q}_\mathcal{M}$ and $\mathcal{Q}_\mathcal{E}$ are nonzero is the main difference to a similar model of Wiltshire (Wiltshire (2007a), Wiltshire (2007b)).

The generalization of the single scaling laws mentioned above, is achieved by imposing the scaling on $\mathcal{M}$ and on $\mathcal{E}$. In Li and Schwarz (2008) the authors showed that $\mathcal{Q}_\mathcal{D}$ and $\langle R \rangle_D$ may be expressed in a Laurent series starting at a_D^{-1} and a_D^{-2} respectively. This behaviour breaks down if the fluctuations with respect to the mean density become of order one. This happens later on $\mathcal{M}$ and on $\mathcal{E}$ because on these regions the mean values lie above, resp. below, the global mean and

therefore the fluctuations on $\mathcal{M}$ with respect to this overdense mean are smaller than the variation between the peaks on $\mathcal{M}$ and the troughs on $\mathcal{E}$. Therefore the a_D^{-1} scaling for $\mathcal{Q}_D$ on $\mathcal{M}$ and $\mathcal{E}$ is expected to hold true even if the $\mathcal{D}$ regions already depart from this perturbatively determined behaviour. The partitioning model is therefore the first step of a generalization to an arbitrary nonlinear behaviour of $\mathcal{Q}_D$ and $\langle R \rangle_D$ on the global domain $\mathcal{D}$.

Using this Ansatz for the $\mathcal{Q}_D$-evolution on $\mathcal{M}$ and $\mathcal{E}$, and exploiting the consistency conditions for the partitioning, it is possible to arrive at a model that depends only on three parameters: The Hubble rate today H_{D_0}, the matter density today $\Omega_m^{D_0}$ and the volume fraction of the overdense regions today $\lambda_{\mathcal{M}_0}$. In this parametrization H_{D_0} sets only the time scale, so we may fix the evolution with $\Omega_m^{D_0}$ and $\lambda_{\mathcal{M}_0}$. Assuming for $\Omega_m^{D_0}$ the concordance value of 0.27, the model shows that the more structure there is, indicated by a low value of $\lambda_{\mathcal{M}_0}$, the higher the acceleration on the domain $\mathcal{D}$ will be.

To analyze what the order of magnitude of $\lambda_{\mathcal{M}}$ is today, an N-body simulation was studied. Smoothing the point distribution on 5h^{-1}Mpc and applying a simple number count for the determination of $\lambda_{\mathcal{M}_0}$, a value of 0.09 was obtained. An analysis by a Voronoi tessellation gave about 0.02. To obtain a definite value, this analysis clearly has to be improved. One would have to use a proper SPH smoothing and trace the overdense regions, that are fixed in the initial conditions, until today. But in any case, $\lambda_{\mathcal{M}_0}$ seems to be in the region below 0.1. Interestingly

Figure 3: *Evolution of the backreaction parameter $\mathcal{Q}_D$ in course of cosmic time. From a value of Ω_Q^D of around 10^{-7} at a redshift of $z \approx 1000$ $\mathcal{Q}_D$ first decreases like a_D^{-1} and becomes approximately constant for a long period of the evolution when $\dot{\lambda}_{\mathcal{M}_0}$ gets important.*

enough, this is the region for $\lambda_{\mathcal{M}_0}$ which leads to a nearly constant $\mathcal{Q}_D$ on $\mathcal{D}$, shown in Fig. 3. So for low values of $\lambda_{\mathcal{M}_0}$, $\mathcal{Q}_D$ acts like a cosmological constant.
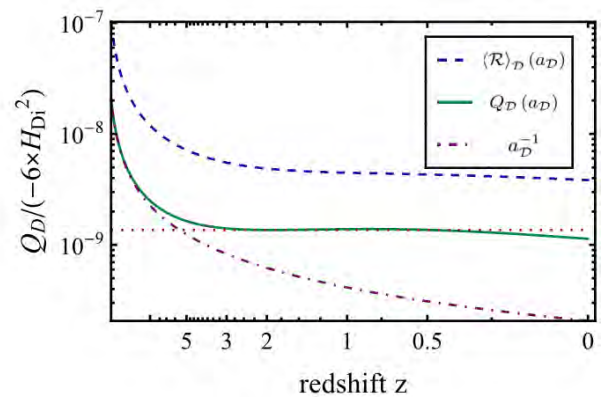
Observational strategies

This may also be seen by a fit of the model to luminosity distances of supernovae (SN). To convert the evolution of the average scale factor $a_\mathcal{D}$ into luminosity distances, we use the result of Räsänen (2009), who investigated the propagation of light in inhomogeneous universes and provided a formula linking the observed luminosity distance to the volume scale factor $a_\mathcal{D}$. The resulting probability contours in the parameter space $\Omega_m^{D_0}$ - $\lambda_{\mathcal{M}_0}$ in Fig. 4 show, that indeed the region around an $\Omega_m^{D_0}$ of 0.3 and a $\lambda_{\mathcal{M}_0}$ below 0.1 is favoured by the data.
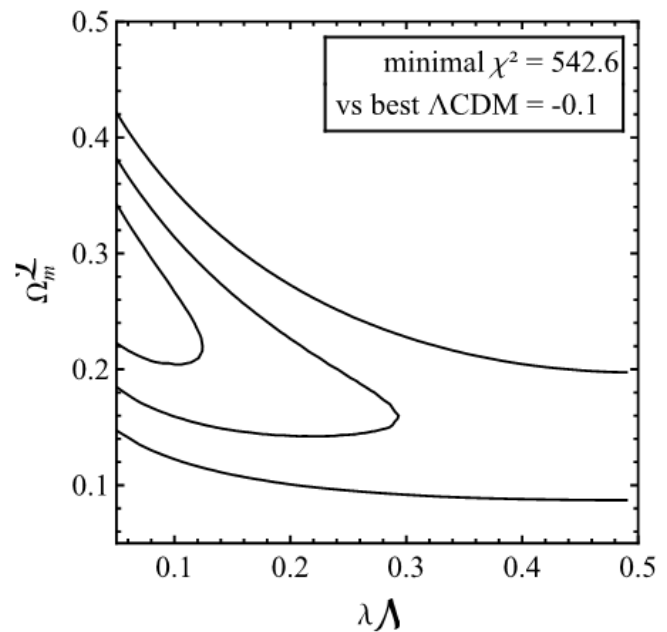
Figure 4: *Probability contours of a fit of the partitioning model to the Union2 SN data set. The model gives a comparably reasonable fit as a simple ΛCDM model.*

To further test the viability of the model, it will soon be compared with more observational data. But as it is probably possible to fit also this, as indicated by the success of Larena *et al.* (2009), we need a quantity that will definitively allow to find out whether this model or one with a real cosmological constant fits better. To decide that, one may use a quantity introduced by Clarkson *et al.* (2008), namely the C-function

$$C(z) = 1 + H^2 \left(D\,D'' - D'^2 \right) + H\,H'\,D\,D'$$

It consists of derivatives of the Hubble rate H(z) and the angular diameter distance D(z), and is constructed such that for every FRW model it is exactly 0 for any z. For the partitioning model this is generically not the case and for several choices of parameters the difference is shown in Fig. 5. Unfortunately, the function C(z) is too complicated to evaluate it using present day data, but as shown in Larena *et. al* (2009), Euclid may be able to derive its values.
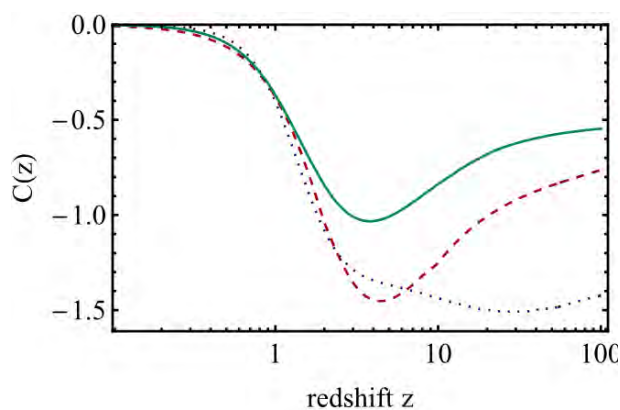
Figure 5: *Plot of Clarkson's C-function for several models discussed in Wiegand (2010). The model presented here is shown as the dotted line. The dashed line is its nonperturbative generalization and the solid line is a single scaling model. For every Friedmann model C(z)=0 which allows one to distinguish averaged models from FRW models.*

000107

Conclusion

Routing the accelerated expansion back to inhomogeneities would be an interesting possibility to avoid problems with a cosmological constant, such as the coincidence problem and would give the sources of acceleration a physical meaning. Perturbatively analyzed it is clear that the effect is way to small to give rise to an acceleration on the scale of the Hubble volume (Brown *et al.* (2009a), Brown *et al.* (2009b)). There are however semirealistic nonperturbative models like Räsänen (2008) that show that a considerable effect is not excluded. Furthermore it has been shown why perturbative models are not able to give a definite answer on the magnitude of the effect Räsänen (2010). So it seems that the question of how the growth of structure influences the overall expansion of the universe is still an open issue. The presented partitioning model has shown, that a ΛCDM like expansion is possible in the context of these models, without the prior assumption of $Q_{\mathcal{D}}$=const., which emerges here more naturally. Furthermore it has been shown how this is related to the formation of structure described by the parameter $\lambda_{\mathcal{M}}$. Finally, using the Clarkson's C-function, we will have, at the latest with the data from the Euclid satellite, a handle on how to distinguish acceleration due to inhomogeneities from the presence of a strange fluid. All in all, these are promising prospects for the future...

Acknowledgments

References

Brown, I. A., Behrend, J. and Malik, K. A. (2009). Gauges and Cosmological Backreaction. JCAP, **11,** 027

Brown, I. A., Robbers, G. and Behrend, J. (2009). Averaging Robertson-Walker cosmologies. JCAP, **4**, 016

Buchert, T. (2000). On average properties of inhomogeneous fluids in general relativity: 1. dust cosmologies. Gen. Rel. Grav. **32**, 105

Buchert, T. (2001). On average properties of inhomogeneous fluids in general relativity: 2. perfect fluid cosmologies. Gen. Rel. Grav. **33**, 1381

Buchert, T., Larena, J. and Alimi, J.-M. (2006). Correspondence between kinematical backreaction and scalar field cosmologies -- the 'morphon field'. Class. Quant. Grav. **23**, 6379

Buchert, T. (2008). Dark Energy from structure -- a status report. Gen. Rel. Grav. **40**, 467

Clarkson, C., Bassett, B. A., Hui-Ching Lu, T. (2008). A general test of the Copernican Principle. Phys. Rev. Lett. **101** 011301

Ellis G.F.R. (1983): Relativistic cosmology: its nature, aims and problems. In General Relativity and Gravitation (D. Reidel Publishing Company, Dordrecht, 1984), pp. 215--288

Kolb, E.W., Matarrese, S., Notari, A. and Riotto, A. (2005). Effect of inhomogeneities on the expansion rate of the Universe. Phys. Rev. D **71**, 023524

Larena, J., Alimi, J.-M., Buchert, T., Kunz, M. and Corasaniti, P.-S. (2009). Testing backreaction effects with observations. Phys. Rev. D **79**, 083011

Li, N. and Schwarz, D. J. (2008). Scale dependence of cosmological backreaction. Phys. Rev. D **78**, 083531

Räsänen, S. (2004). Dark energy from back-reaction. JCAP **2**, 003

Räsänen, S. (2006). Accelerated expansion from structure formation. JCAP **11**, 003

Räsänen, S. (2008). Evaluating backreaction with the peak model of structure formation. JCAP **4**, 026

Räsänen, S. (2009). Light propagation in statistically homogeneous and isotropic dust universes. JCAP **2**, 011

Räsänen, S. (2010). Applicability of the linearly perturbed FRW metric and Newtonian cosmology. Phys.Rev. D **81** 103512

Roy, X. and Buchert, T. (2010). Chaplygin gas and effective description of inhomogeneous universe models in general relativity. Class. Quant. Grav. **27** 175013

Roy, X. and Buchert, T. (2011). Global gravitational instability of FLRWbackgrounds: dynamical system analysis of the dark sectors. In preparation.

Shirokov, M.F. and Fisher, I.Z. (1963). Sov. Astron. J. 6, 699; reprinted in Gen. Rel. Grav. **30**, 1411 (1998).

Wiegand, A. and Buchert, T. (2010). Multiscale cosmology and structure-emerging Dark Energy: A plausibility analysis. Phys. Rev. D **82** 023523

Wiltshire, D. L. (2007). Cosmic clocks, cosmic variance and cosmic averages. NJP **9**, 377

Wiltshire, D. L. (2007). Exact Solution to the Averaging Problem in Cosmology. Phys. Rev. Let. **25**, 251101

000109

arXiv:1103.5974v1 [astro-ph.CO] 30 Mar 2011

Inhomogeneities in the universe

Francesco Sylos Labini

Centro Enrico Fermi, Piazza del Viminale 1, 00184 Rome, Italy and
Istituto dei Sistemi Complessi CNR, Via dei Taurini 19, 00185 Rome, Italy

E-mail: `sylos@centrofermi.it`

Abstract. Galaxy structures represent one of the most challenging observations in cosmology. Whether or not these structures are found to be compatible with the standard model of galaxy formation crucially depends on the a-priori and assumptions encoded in the statistical methods employed to characterize the data and on the a-posteriori hypotheses made to interpret the results. We present strategies to test the most common assumptions, i.e. spatial homogeneity and statistical homogeneity and isotropy. These tests provide evidences that, in the available samples, galaxy distribution is spatially inhomogeneous but statistically homogeneous and isotropic. Different conclusions are obtained through statistical tools based on a-priori assumptions that not verified in the data when directly tested. Thus we find that the observed galaxy structures are not compatible with the standard model of galaxy formation, e.g. LCDM, that predicts spatial homogeneity at small scales (i.e., $r < 10$ Mpc/h), structures of relatively limited size (i.e. $r < 100$ Mpc/h) and anti-correlations at large scales (i.e. $r > 150$ Mpc/h). While the observed inhomogeneities pose a fundamental challenge to the standard picture of cosmology they also represent an important opportunity which may open new directions for many cosmological puzzles.

PACS numbers: 98.65.-r,98.65.Dx,98.80.-k

Inhomogeneities in the universe   2

1. Introduction

One of cornerstone of modern cosmology is obtained by the observations of the three dimensional distribution of galaxies [1, 2]. In recent years there has been a fast growth of data which has allowed a detailed characterization of galaxy structures at low redshift (i.e., $z < 0.3$) and small scales (i.e., $r < 150$ Mpc/h) . While many authors (see e.g., [3, 4, 5, 6, 7, 8, 9]) have claimed that the data are compatible with the theoretical expectations, and thus they are currently used to estimate a number of cosmological parameters, there are some critical issues which have not received the due attention (see e.g., [10, 11, 12, 14, 15, 16]). The critical points concern the a-priori assumptions which are usually used, without being tested, in the statistical analysis of the data and the a-posteriori hypotheses that are used to interpret the results. Among the former, there are the assumptions of spatial homogeneity and of translational and rotational invariance (i.e., statistical homogeneity) which are built in the standard estimators of galaxy correlations [17]. While these estimators are certainly the correct ones to use when these properties are verified, it is an open question of whether the data satisfy these assumptions. It is indeed well known that galaxies are organized into large scale structures, like clusters, filaments and voids, with large fluctuations [18, 19, 20, 21, 22] and it is not obvious a-priori that spatial or statistical homogeneity are satisfied in a sample of any size. Indeed the critical point is that the assumptions of spatial and statistical homogeneity are encoded in the statistical methods and thus these properties are supposed to be satisfied inside (i.e., not at larger scales) any considered sample where these methods are employed [17].

While it is possible that at large enough scales galaxy distribution becomes spatially uniform, this is certainly not the case at small enough scales. Thus it comes the question of the determination of the scale beyond which spatial homogeneity is satisfied. To investigate this problem it is necessary to use statistical methods which are able to directly test spatial homogeneity, and that thus do not assume it a-priori. This is precisely the reason to introduce statistical methods which more general than the usual ones [17]. However when facing the question of testing spatial homogeneity, one has to consider a number of subtle possibilities which may affect the determinations of statistical quantities via volume averages [11]. In brief the central problem is the stability of finite sample determinations: when a statistical quantity depends on the finite size of the sample then this is not a meaningful and useful estimator of an ensemble average property. A critical analysis of finite-sample volume averages is thus necessary to identify the subtle effects induced by spatial inhomogeneities.

As mentioned above, there is then a second kind of ad-hoc hypotheses which are often used in the interpretation of the statistical analysis. There are some results which are a-priori unexpected but that, a-posteriori, are interpreted as due to some intervening effects in the data, as for example galaxy evolution or selection effects. While it is very well possible that such effects are present in the data, it is however necessary not to parameterize their influence simply through the introduction of ad-hoc functions and

Inhomogeneities in the universe   3

parameters (see e.g. [23, 24, 4] and discussion in [11]), rather to develop focussed tests to understand whether the additional hypotheses are supported by the actual data.

To frame the problem of the comparison of theoretical predictions with data we focus the attention on the real space correlation properties of standard models. The Friedmann-Robertson-Walker (FRW) geometry is derived under the assumptions that matter distribution is exactly translational and rotational invariant [25]. This implies that the matter density is assumed to be constant in a spatial hyper-surface. The FRW metric describes the geometry of the universe in terms of a single function, the scale factor, which obeys to the Friedmann equations [25]. On the top of the mean field one can consider statistically homogeneous and isotropic small-amplitude fluctuations. These furnish the seeds of gravitational clustering which eventually give rise to the structures we observe in the present universe. The growth of fluctuations into non-linear structures is considered to have a negligible effect on the space-time dynamics, which is instead driven by the uniform mean field [26]. The statistical properties of matter density fluctuations have to satisfy an important condition in order to be compatible with the FRW geometry [27, 28]. In its essence, the condition is that fluctuations in the gravitational potential induced by density fluctuations do not diverge at large scales [29, 17]. This situation requires that the matter density field fluctuations decay in the fastest possible way with scale [30]. Correspondingly the two-point correlation function becomes negative at larger scales (i.e., $r > 150$) Mpc/h which imply the absence of larger structures of tiny density fluctuations. Are the large scale structures and fluctuations compatible with such a scenario [31] ?

This paper is organized as follows. In Sect.2 we briefly review the main properties of both spatially homogeneous and inhomogeneous stochastic density fields. All definitions are given in the ensemble sense, and for ergodic processes, in the infinite volume limit. The main features of density fields in standard cosmological models are presented in Sect.3, focusing the attention to real space correlation properties. In the case of a real point distribution (Sect.4) the information that can be exacted from the data is thorough a statistical analysis in a finite sample, and hence through the computation of volume averages. We discuss how to set up a strategy to analyze a point distribution in a finite volume, stressing the sequence of steps that should be considered in order to reduce as much as possible the role of a-priori assumptions encoded in the statistical analysis. The analysis of the galaxy data is presented in Sect.5. We discuss that galaxy distribution, at relatively low redshifts (i.e., $z < 0.3$) and small scales (i.e., $r < 150$ Mpc/h) is characterized by large density fluctuations which correspond to large-scale correlations. We emphasize that by using the standard statistical tools one reaches a different conclusion. This occurs because these methods are based on several important assumptions: some of them, when directly tested are not verified, while others are very strong ad-hoc hypotheses which require a detailed investigation. Finally in Sect.6 we draw our main conclusions.

000112

Inhomogeneities in the universe   4

2. A brief review of the main statistical properties

In this section we review the main probabilistic properties of mass density fields. This means that we consider ensemble averages or, for ergodic cases, volume averages in the infinite volume limit. The probabilistic properties of a distribution are useful to be studied in view of its statistical characterization in finite samples (see Sec.4).

A mass density field can be represented as stationary stochastic process that consists in extracting the value of the microscopic density function $\rho(\vec{r})$‡ at any point of the space. This is completely characterized by its probability density functional $\mathcal{P}[\rho(\vec{r})]$. This functional can be interpreted as the joint probability density function (PDF) of the random variables $\rho(\vec{r})$ at every point $\vec{r}$. If the functional $\mathcal{P}[\rho(\vec{r})]$ is invariant under spatial translations then the stochastic process is *statistically homogeneous* or translational invariant (stationary) [17]. When $\mathcal{P}[\rho(\vec{r})]$ is also invariant under spatial rotation then the density field is *statistically isotropic* [17].

A crucial assumption usually used, when comparing theoretical prediction to data, is that stochastic fields are required to satisfy spatial *ergodicity*. Let us take a generic observable $\mathcal{F} = \mathcal{F}(\rho(\vec{r}_1), \rho(\vec{r}_2), ...)$ function of the mass distribution $\rho(\vec{r})$ at different points in space $\vec{r}_1, \vec{r}_2, ...$. Ergodicity implies that $\langle \mathcal{F} \rangle = \overline{\mathcal{F}} = \lim_{V \to \infty} \overline{\mathcal{F}}_V$, where the symbol $\langle ... \rangle$ is for the (ensemble) average over different realizations of the stochastic process, and $\overline{\mathcal{F}}_V = \frac{1}{V} \int_V \mathcal{F} dV$ is the spatial average in a finite volume V [17].

2.1. Spatially homogeneous distributions

The condition of *spatial homogeneity* (*uniformity*) is satisfied if the ensemble average density of the field $\rho_0 = \langle \rho \rangle$ is strictly positive, i.e. for an ergodic stochastic field,

$$\langle \rho \rangle = \lim_{R \to \infty} \frac{1}{V(R; \vec{x_0})} \int_{V(R; \vec{x_0})} \rho(r) d^3 r > 0 \quad \forall \vec{x_0} , \tag{1}$$

where R is the linear size of a volume V with center in $\vec{x_0}$. It is necessary to carefully test spatial homogeneity before applying the definitions given in this section to a finite sample distribution (see Sect.4). Indeed, for inhomogeneous distributions the *estimation* of the average density substantially differs from its asymptotic value and thus the sample estimation of ρ_0 is biased by finite size effects. Unbiased tests of spatial homogeneity can be achieved by measuring conditional properties (see below).

A distribution is spatially inhomogeneous up to a scale λ_0 if

$$\left| \frac{1}{V(R; \vec{x_0})} \int_{V(R; \vec{x_0})} d^3 x \rho(\vec{x}) - \rho_0 \right| < \rho_0 \quad \forall R > \lambda_0 \ , \forall \vec{x_0} . \tag{2}$$

This equation defines the homogeneity scale λ_0 which separates the strongly fluctuating regime $r < \lambda_0$ from the regime where fluctuations have small amplitude relative to the asymptotic average.

‡ We use the symbol $\rho(r)$ for the microscopic mass density and $n(r)$ for the microscopic number density. However in the following sections we consider only the number density, as it is usually done in studies of galaxy distributions. In that case we can simply replace the symbol $\rho(r)$ with $n(r)$ and all the definitions given in this section remain unchanged.

Inhomogeneities in the universe   5

The quantity $\langle \rho(\vec{r_1})\rho(\vec{r_2})\rangle dV_1 dV_2$ gives, in a single realization of a stochastic process, the a-priori probability to find two particles simultaneously placed in the infinitesimal volumes dV_1, dV_2 respectively around $\vec{r_1}, \vec{r_2}$. The quantity

$$\langle \rho(r_{12})\rangle_p dV_1 dV_2 = \frac{\langle \rho(\vec{r_1})\rho(\vec{r_2})\rangle}{\rho_0} dV_1 dV_2 \tag{3}$$

gives the a-priori probability of finding two particles placed in the infinitesimal volumes dV_1, dV_2 around $\vec{r_1}$ and $\vec{r_2}$ with the condition that the origin of the coordinates is occupied by a particle (Eq.3 is the ratio of unconditional quantities, and thus, for the roles of probabilities, it defines a conditional quantity) [17].

For a stationary and spatially homogeneous distribution (i.e., $\rho_0 > 0$), we may define the reduced two-point correlation function as

$$\xi(r_{12}) = \frac{\langle \rho(r_{12})\rangle_p}{\rho_0} - 1 = \frac{\langle \rho(r_{12})\rangle}{\rho_0^2} - 1 \ . \tag{4}$$

This function characterizes correlation properties of density fluctuations with small amplitude with respect to the (ensemble) average density.

Let us now discuss the information that can be extracted from $\xi(r)$, when spatial homogeneity has been already proved. Suppose that correlations have a finite range so that in this case we have

$$\xi(r) = A \exp(-r/r_c) \ , \tag{5}$$

where r_c is the *correlation length* of the distribution and A is a constant. Structures of fluctuations have a size determined by r_c. This length scale depends only on the rate of decay of the correlation function. Another characteristic length scale can be defined as $\xi(r_0) = 1$; from Eq.5 we find

$$r_0 = r_c \cdot \log(A) \ , \tag{6}$$

i.e., it depends on the amplitude A of the correlation function §. The two scales r_0 and r_c have a completely distinct meaning: the former marks the crossover from large to small fluctuations while the latter quantifies the typical size of clusters of *small amplitude* fluctuations. When $\xi(r)$ is a power-law function of separation (i.e. $\xi(r) \sim r^{-\gamma}$ with $0 < \gamma < 3$) then the correlation length r_c is infinite and there are clusters of all sizes [17]. (In cosmology the term correlation length is very often used to mean the scale r_0 instead of r_c. This is in our opinion a confusing terminology, and we use the standard one in statistical physics defined in Eqs.5-6.)

The two-point correlation function defined by Eq.4 is simply related to the normalized mass variance in a volume $V(R)$ of linear size R [17]

$$\sigma^2(R) = \frac{\langle M(R)^2\rangle - \langle M(R)\rangle^2}{\langle M(R)\rangle^2} = \frac{1}{V^2(R)}\int_{V(R)} d^3r_1 \int_{V(R)} d^3r_2 \xi(r_{12}) \ . \tag{7}$$

§ When $\xi(r)$ has a more complex behavior than Eq.5, the scale r_0 is different from Eq.6 but simple to computed from its definition, i.e. $\xi(r_0) = 1$. However the finite range of positive correlations generally corresponds to an exponential decay of the type of Eq.5.

000114

Inhomogeneities in the universe   6

The scale r_* at which fluctuations are of the order of the mean, i.e. $\sigma(r_*) = 1$, is proportional to the scale r_0 at which $\xi(r_0) = 1$ and to the scale λ_0 defined in Eq.2.

For spatially uniform systems, when the volume V in Eq.7 is a real space sphere‖, it is possible to proceed to the following classification for the scaling behavior of the normalized mass variance at large enough scales [29, 17]:

$$\sigma^2(R) \sim \begin{cases} R^{-(3+n)} & \text{for } -3 < n < 1 \\ R^{-(3+1)}\log R & \text{for } n = 1 \\ R^{-(3+1)} & \text{for } n > 1 \end{cases} . \tag{8}$$

For $-3 < n < 0$ (which corresponds to $\xi(r) \sim r^{-\gamma}$ with $0 < \gamma = 3 + n < 3$), mass fluctuations are *"super-Poisson"*, typical of systems at the critical point of a second order phase transition [17]: there are long-range correlations and the correlation length r_c is infinite. For $n = 0$ fluctuations are Poisson-like and the system is called *substantially Poisson*: there are no correlations (i.e., a purely Poisson distribution) or correlations limited to small scales of the type described by Eq.5, i.e. a finite correlation length. This behavior is typical of many common physical systems, e.g., a homogeneous gas at thermodynamic equilibrium at sufficiently high temperature. Finally for $n \geq 1$ fluctuations are *"sub-Poisson"* or *super-homogeneous* [29, 17] (or hyper-uniform [30]). In this case $\sigma^2(R)$ presents the fastest possible decay for discrete or continuous distributions [29] and the two-point correlation function has to satisfy a global constraint (see Sect.3). Examples are provided, for instance, by the one component plasma, a well-known system in statistical physics [32], and by a randomly shuffled lattice of particles [17, 33].

Note that any *uniform* stochastic process has to satisfy the following condition

$$\lim_{R \to \infty} \sigma^2(R) = \lim_{R \to \infty} = \frac{1}{V^2(R)} \int_{V(R)} d^3r_1 \int_{V(R)} d^3r_2 \xi(r_{12}) = 0 \tag{9}$$

which implies that the average density ρ_0, in the infinite volume limit, is a well defined concept, i.e. $\rho_0 > 0$ [17].

2.2. Spatially inhomogeneous distributions

A distribution is spatially inhomogeneous in the ensemble (or in the infinite volume limit) sense if $\lambda_0 \to \infty$. For statistically homogeneous distributions, from Eq.2, we get that the ensemble average density is $\rho_0 = 0$. Thus unconditional properties are not well defined: if we randomly take a finite volume in an infinite inhomogeneous distribution, it typically contains no points. Therefore only conditional properties are well defined, as for instance the average conditional density defined in Eq.3.

For fractal object the average conditional mass included in a spherical volume grows as $\langle M(r) \rangle_p \sim r^D$: for $D < 3$, the average conditional density presents a scaling behavior of the type

$$\langle \rho(r) \rangle_p = \frac{\langle M(r) \rangle_p}{V(r)} \sim r^{D-3} , \tag{10}$$

‖ The case in which the volume is a Gaussian sphere can be misleading, see e.g. [29]

Inhomogeneities in the universe 7

so that $\lim_{r\to\infty}\langle\rho(r)\rangle_p = 0$. The hypotheses underlying the derivation of the Central Limit Theorem are violated by the long-range character of spatial correlations, resulting in a PDF of fluctuations that does not follow the Gaussian function [17, 34]. Actually it typically displays "long tails" [35] which can be associated with the divergence of some moments of the distribution.

It is possible to introduce more complex inhomogeneous distributions than Eq.10, for instance the multi-fractal distributions for which the scaling properties are not described by a single exponent, but they change in different spatial locations being characterized by a spectrum of exponents [17]. Another simple (and different !) example is given by a distribution in which the scaling exponent in Eq.10 depends on distance, i.e. $D = D(r) < 3$.

3. Statistical properties of the standard model

As discussed in the introduction, an important constraint must be valid for any kind of initial matter density fluctuation field in the framework of FRW models. This is represented by the condition of super-homogeneity, corresponding in cosmology to the so-called condition of "scale-invariance" of the primordial fluctuations power spectrum (PS)¶ [29]. To avoid confusion, note that in statistical physics the term "scale invariance" is used to describe the class of distributions which are invariant with respect to scale transformations. For instance, a magnetic system at the critical point of transition between the paramagnetic and ferromagnetic phase, shows a two-point correlation function which decays as a non-integrable power law, i.e. $\xi(r) \sim r^{-\gamma}$ with $0 < \gamma < 3$ (super-Poisson distribution in Eq.8). The meaning of "scale-invariance" in the cosmological context is therefore completely different, referring to the property that the mass variance at the horizon scale be constant (see below) [29].

3.1. Basic Properties

Matter distribution in cosmology is assumed to be a realization of a *stationary* stochastic point process that is also spatially uniform. In the early universe the homogeneity scale λ_0 is of the order of the inter-particle distance, and thus negligible, while it grows during the process of structure formation driven by gravitational clustering. The main property of primordial density fields in the early universe is that they are super-homogeneous, satisfying Eq.8 with $n = 1$. This latter property was firstly hypothesized in the seventies [27, 28] and it subsequently gained in importance with the advent of inflationary models in the eighties [29].

In order to discuss this property, let us recall that the initial fluctuations are taken to have Gaussian statistics and a certain PS. Since fluctuations are Gaussian, the knowledge of the PS gives a complete statistical description of the fluctuation field. In a FRW

¶ The PS of density fluctuations is $P(\vec{k}) = \left\langle |\delta_\rho(\vec{k})|^2 \right\rangle$, where $\delta_\rho(\vec{k})$ is the Fourier Transform of the normalized fluctuation field $(\rho(\vec{r}) - \rho_0)/\rho_0$ [29].

000116

Inhomogeneities in the universe   8

cosmology there is a fundamental characteristic length scale, the horizon scale $R_H(t)$ that is simply the distance light can travel from the Big Bang singularity $t = 0$ until any given time t in the evolution of the Universe, and it grows linearly with time. Harrison [27] and Zeldovich [28] introduced the criterion that matter fluctuations have to satisfy on large enough scales. This is named the Harrison-Zeldovich criterion (H-Z); it can be written as

$$\sigma^2(R = R_H(t)) = \text{constant}. \tag{11}$$

This condition states that the mass variance at the horizon scale is constant: it can be expressed more conveniently in terms of the PS for which Eq.11 is equivalent to assume $P(k) \sim k$ (the H-Z PS) and that in a spatial hyper-surface $\sigma^2(R) \sim R^{-4}$ [29, 17].

3.2. Physical implications of super-homogeneity

In order to illustrate the physical implications of the H-Z condition, one may consider the gravitational potential fluctuations $\delta\phi(\vec{r})$, which are linked to the density fluctuations $\delta\rho(\vec{r})$ via the gravitational Poisson equation: $\nabla^2\delta\phi(\vec{r}) = 4\pi G\delta\rho(\vec{r})$. From this, transformed to Fourier space, it follows that the PS of the potential $P_\phi(k) = \left\langle |\delta\hat{\phi}(\vec{k})|^2 \right\rangle$ is related to the density PS $P(k)$ through the equation $P_\phi(k) \sim \frac{P(k)}{k^4}$. The H-Z condition, $P(k) \sim k$, corresponds therefore to $P_\phi(k) \propto k^{-3}$, so that the variance of the gravitational potential fluctuations, $\sigma_\phi^2(R) \approx \frac{1}{2}P_\phi(k)k^3|_{k=R^{-1}}$, is constant with k [29].

The H-Z condition is a *consistency constraint* in the framework of FRW cosmology. Indeed, the FRW is a cosmological solution for a perfectly homogeneous Universe, about which fluctuations represent inhomogeneous perturbations. If density fluctuations obey to a different condition than Eq.11, and thus $n < 1$ in Eq.8, then the FRW description *will always break down* in the past or future, as the amplitude of the perturbations become arbitrarily large or small. Thus the super-homogeneous nature of primordial density field is a fundamental property independently on the nature of dark matter. This is a very strong condition to impose, and it excludes even Poisson processes ($n = 0$ in Eq.8) [29] for which the fluctuations in gravitational potential diverge at large scales.

3.3. The small scales behavior

Various models of primordial density fields differ for the behavior of the PS at large wavelengths depending on the specific properties hypothesized of the dark matter component. For example, in the Cold Dark Matter (CDM) scenario, where elementary non-baryonic dark matter particles have a small velocity dispersion, the PS decays as a power law $P(k) \sim k^{-2}$ at large k. For Hot Dark Matter (HDM) models, where the velocity dispersion is large, the PS presents an exponential decay at large k. However at small k they both exhibit the H-Z tail $P(k) \sim k$ which is indeed the common feature of all density fluctuations compatible with FRW models. The scale $r_c \approx k_c^{-1}$ at which the PS shows the turnover from the linear to the decaying behavior is fixed to be the size of the horizon at the time of equality between matter and radiation [41].

000117

Inhomogeneities in the universe   9

3.4. The two-point correlation function and super-homogeneity

The super-homogeneity (or H-Z) condition corresponds to the following limit condition

$$\int_0^\infty d^3r\xi(r) = 0 \,, \tag{12}$$

which is another way to reformulate the condition that $\lim_{k\to 0} P(k) = 0$. This means that there is a fine tuned balance between small-scale positive correlations and large-scale negative anti-correlations [29, 17]. Note that Eq.12 is different, and much stronger, from the requirement that any *uniform* stochastic process has to satisfy, i.e. Eq.9 [17]. In terms of correlation function $\xi(r)$ CDM/HDM models present the following behavior: it is positive at small scales (decaying as $\xi(r) \sim r^{-1}$ for CDM and being almost flat for HDM), it crosses zero at r_c and then it is negative approaching zero with a tail which goes as $-r^{-4}$ (in the region corresponding to $P(k) \sim k$) [17].

3.5. Baryonic acoustic oscillations

To conclude let us mention the baryon acoustic oscillations (BAO) scale [36]. The physical description which gives rise to these oscillations is based on fluid mechanics and gravity: when the temperature of the plasma was hotter than $\sim 10^3$ K, photons were hot enough to ionize hydrogen so that baryons and photons can be described as a single fluid. Gravity attracts and compresses this fluid into the potential wells associated with the local density fluctuations. Photon pressure resists this compression and sets up acoustic oscillations in the fluid. Regions that have reached maximal compression by recombination become hotter and hence are now visible as local positive anisotropies in the cosmic microwave background radiation (CMBR), if the different $k-$modes are assumed to have the same phase.

For our discussion, the principal point to note is that while $k-$oscillations are delocalized, in real space the correlation function shows a characteristic feature: $\xi(r)$ has a localized feature at the scale r_{bao} corresponding to the frequency of oscillations in k space. This simply reflects that the Fourier Transform of a regularly oscillating function is a localized function. Formally the scale r_{bao} corresponds to a scale where a derivative of $\xi(r)$ is not continuous [17, 37].

3.6. Size of structures and characteristic scales

There are thus three characteristic scales in the LCDM-type models (see Fig.1). The first is the homogeneity scale which depends on time $\lambda_0 = \lambda_0(t)$, the second is the scale r_c where $\xi(r_c) = 0$ (that roughly corresponds to the scale defined in Eq.5) which is fixed by the initial properties of the matter density field as well as the third scale r_{bao}. As long as the homogeneity scale is smaller than r_{bao}, r_c, these two scales are substantially unchanged by gravitational dynamics: at those scales this is in the linear regime as fluctuations have a small enough amplitude, and it linearly amplifies the initial fluctuations spectrum. The rate of growth of the homogeneity scale can be simply
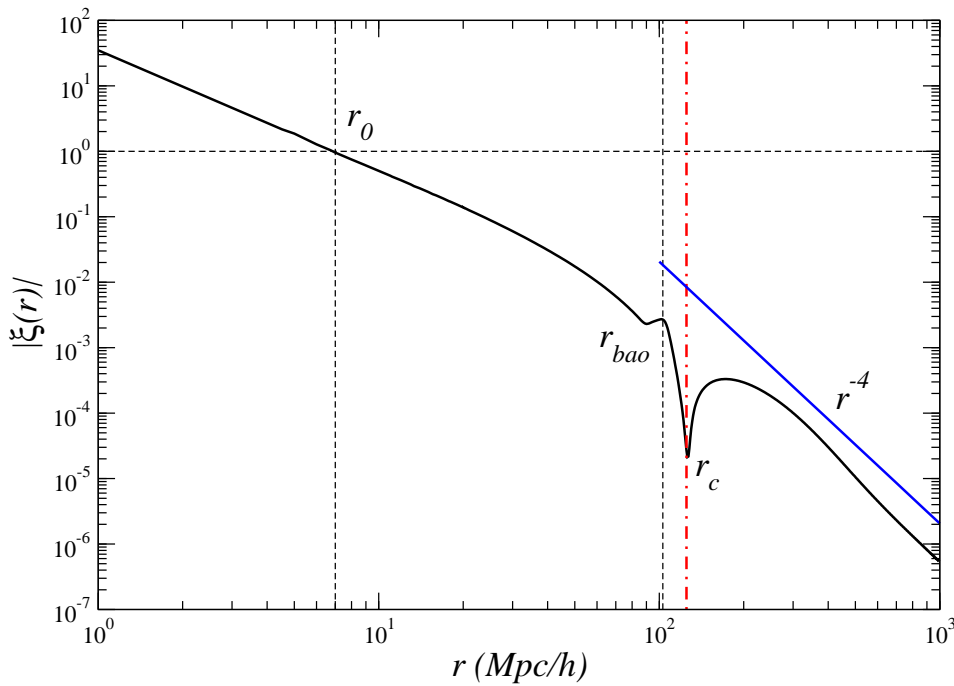
Figure 1. Schematic behavior of the two-point correlation function for the LCDM case. At small scales $r < r_0 \approx 10$ Mpc/h (where $\xi(r_0) = 1$) non-linear gravitational clustering has changed the initial shape of $\xi(r)$. At larger scales $\xi(r)$ has been only amplified by gravitational clustering in the linear regime. For $10 < r < r_c \approx 120$ Mpc/h the correlation is positive and with small amplitude. At larger scales it is negative and characterized by the $\xi(r) \sim -r^{-4}$ behavior. The location of r_{bao} is fixed by cosmological parameters: in the example shown $r_{bao} < r_c$ as predicted by the "concordance model" [3].

computed by using the linear perturbation analysis of a self-gravitating fluid in an expanding universe [26]. Given the initial amplitude of fluctuations and the assumed initial PS of matter density fluctuations, it results that $\lambda_0(t_{now}) \approx 10$ Mpc/h [38].

From the characterization of the two-point correlation function of galaxy distribution we can identify three fundamental tests of standard models [+]:

- If the homogeneity scale λ_0 is much larger (i.e., a factor 5-10) than ~ 10 Mpc/h, then there is not enough time to form non-linear structures in LCDM models [11].

- If the correlation length r_c (i.e., the zero point of $\xi(r)$) is much larger than ~ 100 Mpc/h then there is a problem in the description of the early universe physics.

- The clear test of inflationary models is given by the detection of the negative part of the correlation function, i.e. the range of scales it behaves as $\xi(r) \sim -r^{-4}$: all models necessarily predict such a behavior [*].

[+] For the power-spectrum there are additional complications, related how galaxies are biased with respect to the underlying density field: see [39, 31, 40] for further details.

[*] In the same range of scales the PS is expected to be linear with the wave-number, i.e. $P(k) \sim k$. However selection effects may change the behavior of the PS to constant but not the functional behavior

000119

4. Testing assumptions in the statistical methods

A number of different statistics, determined by making a volume average in a finite sample, can be used to characterize a given distribution. In addition, each statistical quantity can be measured by using different estimators. For this reason we have to set up a strategy to attack the problem if we do not know a-priori which are the properties of the given finite sample distribution. To approach the problem we have to reduce as much as possible the number of a-priori assumptions used the statistical methods, to get the correct information from the data.

We limit our discussion to the case of interest, i.e. a set of N point particles (i.e. galaxies) in a volume V. The microscopic number density can be simply written as $n(\vec{r}) = \sum_i^N \delta^3(\vec{r} - \vec{r_i})$, where $\delta^3(\vec{r})$ is the Dirac delta function. The statistical quantities defined in Sect.2 can be rewritten in terms of the stochastic variable

$$N_i(V) = \int_{V(\vec{y_i})} d^3x\, n(\vec{x}) \,, \tag{13}$$

where $\vec{y_i}$ identifies the coordinates of the center of the volume V. If the center $\vec{y_i}$ coincides with a point particle position $\vec{r_i}$, then Eq.13 is a conditional quantity. Instead, if the center $\vec{y_i}$ can be any point of space (occupied or not by a particle) then the statistics in Eq.13 is unconditional and it is useful to compute, for instance, the mass variance defined in Eq.7.

For inhomogeneous distributions, unconditional properties are ill-defined (Sect.2) and thus we firstly analyze conditional quantities to then pass, only when in which spatial homogeneity has been detected inside the given sample, to unconditional ones. Therefore, in what follows we take in Eq.13 as volume V a sphere of radius r with center in a distribution point particle, i.e. we consider the stochastic variable defined by the number of points in a sphere $\sharp$ of radius r centered on the ith point of the given set, i.e. $V = V(r; \vec{r_i})$. The PDF $P(N(r)) = P(N; r)$ of the variable $N_i(r)$ (at fixed r) contains, in principle, information about moments of any order [42]. The first moment is the average conditional density and the second moment is the conditional variance [11].

However before considering the moments of the PDF we should study whether they represent statistically meaningful estimates. Indeed, in the determination of statistical properties through volume averages, one implicitly assumes that statistical quantities measured in different regions of the sample are stable, i.e., that fluctuations in different sub-regions are described by the same PDF. Instead, it may occur that measurements in different sub-regions show systematic (i.e., not statistical) differences, which depend, for instance, on the spatial position of the specific sub-regions. In this case the considered statistic is not statistically stationary in space and its whole-sample average value (i.e., any finite-sample estimation of the PDF moments) is not a meaningful descriptor.

of $\xi(r)$ [39, 31, 40].

$\sharp$ When we take a spherical shell instead of a sphere, then we define a differential quantity instead of an integral one.

Inhomogeneities in the universe 12

4.1. Self-averaging

A simple test to determine whether there are systematic finite size effects affecting the statistical analysis in a given sample of linear size L consists in studying the PDF of $N_i(r)$ in sub-samples of linear size $\ell < L$ placed in different spatial regions of the sample (i.e., $S_1, S_2, ..., S_N$). When, at a given scale $r < \ell$, $P(N(r), \ell; S_i)$ is the same, modulo statistical fluctuations, in the different sub-samples, i.e.,

$$P(N(r); \ell; S_i) \approx P(N(r); \ell; S_j) \, \forall i \neq j \,, \tag{14}$$

it is possible to consider whole sample average quantities. When determinations of $P(N(r); \ell; S_i)$ in different regions S_i show *systematic* differences, then whole sample average quantities are ill defined. In general, this situation may occur because: (i) the lack of the property of translational invariance or (ii) the breaking of the property of self-averaging due to finite-size effects induced by large-scale structures/voids (i.e., long-range correlated fluctuations).

While the breaking of translational invariance imply the lack of self-averaging property the reverse is not true. For instance suppose that the distribution is spherically symmetric, with origin at r_* and characterized by a smooth density profile, function of the distance from r_* [15]. The average density in a certain volume V, depends on the distance of it from r_*: there is thus a systematic effect and Eq.14 is not satisfied. On the other hand when a finite sample distribution is dominated by a single or by a few structures then, even though it is translational invariant in the infinite volume limit, a statistical quantity characterizing its properties in a finite sample can be substantially affected by finite size fluctuations. For instance, a systematic effect is present when the average (conditional) density largely differs when it is measured into two disjointed volumes placed at different distances from the relevant structures (i.e., fluctuations) in the sample. In a finite sample, if structures are large enough, the measurements may differ much more than a statistical scattering ††. That systematic effect sometimes is refereed to as cosmic variance [22] but that is more appropriately defined as breaking of self-averaging properties [11], as the concept of variance (which involves already the computation of an average quantity) maybe without statistical meaning in the circumstances described above [11]. In general, in the range of scales in which statistical quantities give sample-dependent results, then they do not represent fair estimations of asymptotic properties of the given distribution [11].

4.2. Spatial homogeneity

The self-averaging test (Eq.14) is the first one to understand whether a distribution is spatially homogeneous or not inside a given sample. As long as the PDF $P(N, r)$ does not satisfy Eq.14 then the distribution is not only spatially inhomogeneous, but the moments of the PDF are not useful estimators of the underlying statistical properties.

†† The determination of statistical errors in a finite volume is also biased by finite size effects [31, 16]

Inhomogeneities in the universe   13

Suppose that Eq.14 is found to be satisfied up to given scale $r < L$. Now we can ask the question: is spatial homogeneity reached for $r < L$?

As mentioned in Sect.2, to this aim it is necessary to employ statistical quantities that do not require the assumption of spatial homogeneity such as conditional ones [17, 11]. Particularly the first moment of $P(N, r)$ provides an estimation of the average conditional density defined in Eq.3, which can be simply written as

$$\overline{n(r)_p} = \frac{1}{M(r)} \sum_{i=1}^{M(r)} \frac{N_i(r)}{V(r)} = \frac{1}{M(r)} \sum_{i=1}^{M(r)} n_i(r) . \tag{15}$$

We recall that $N_i(r)$ gives the number of points in a sphere of radius r centered on the ith point and the sum is extended to the all $M(r)$ points contained in the sample for which the sphere of radius r is fully enclosed in the sample volume (this quantity is r dependent because of geometrical constraints, see, e.g., [11]). Analogously to Eq.15 the estimator of the conditional variance can be written as

$$\overline{\sigma_p^2(r)} = \frac{1}{M(r)} \sum_{i=1}^{M(r)} n_i^2(r) - \overline{n(r)_p}^2 . \tag{16}$$

When, at the scales $< r$, self-averaging properties are satisfied, one may study the scaling properties of $\overline{n(r)_p}$ and of $\overline{\sigma_p^2(r)}$. As long as $\overline{n(r)_p}$ presents a scaling behavior as a function of spatial separation r, as in Eq.10 with $D < 3$, the distribution is spatially inhomogeneous. When $\overline{n(r)_p} \approx$ const. then this constant provides an estimation of the ensemble average density and the scale λ_0 where the transition to a constant behavior occurs, marks the homogeneity scale. Only in this latter situation it is possible to study the correlation properties of weak amplitude fluctuations. This can be achieved by considering the function $\xi(r)$ defined in Eq.4.

4.3. The two-point correlation function

Before proceeding, let us clarify some general properties of a generic statistical estimator which are particularly relevant for the two-point correlation function $\xi(r)$. As mentioned above, in a finite sample of volume V we are only able to compute a statistical estimator $\overline{X_V}$ of an ensemble average quantity $\langle X \rangle$. The estimator is valid if

$$\lim_{V \to \infty} \overline{X_V} = \langle X \rangle . \tag{17}$$

If the ensemble average of the finite volume estimator satisfies

$$\langle \overline{X_V} \rangle = \langle X \rangle \tag{18}$$

the estimator is unbiased. When Eq.18 is not satisfied then there is a systematic offset which has to be carefully considered. Note that the violation of Eq.14 implies that Eq.18 is not valid as well. Finally the variance of an estimator is $\sigma_V^X = \langle \overline{X_V}^2 \rangle - \langle \overline{X_V} \rangle^2$. The results given by an estimator must be discussed carefully considering its bias and its variance in any finite sample. A strategy to understand what is the effect of these features consists in changing the sample volume V and study finite size effects [17, 31, 11]. This is crucially important for the two-point correlation function $\xi(r)$ as

Inhomogeneities in the universe 14

any estimator $\overline{\xi(r)}$ of it is generally biased, i.e. it does not satisfy Eq.18 [31, 43]. This is because the estimation of the sample mean density is biased when correlations extend over the whole sample size. Indeed, the most common estimator of the average density is

$$\overline{n} = \frac{N}{V} \,, \tag{19}$$

where N is the number of points in a sample of volume V. It is simple to show that its ensemble average value can be written as [31]

$$\langle \overline{n} \rangle = \langle n \rangle \left(1 + \frac{1}{V} \int_V d^3r \xi(r) \right) \,. \tag{20}$$

Therefore only when $\xi(r) = 0$ (i.e., for a Poisson distribution), Eq.19 is an unbiased estimator of the ensemble average density: otherwise the bias is determined by the integral of the ensemble average correlation function over the volume V.

The most simple estimator of $\xi(r)$ is the Full-Shell (FS) estimator [31] that can be simply written, by following the definition given in Eq.4, as

$$\overline{\xi(r)} = \frac{\overline{(n(r))_p}}{\overline{n}} - 1 \,, \tag{21}$$

where $\overline{(n(r))_p}$ is the estimator of the conditional density in spherical shells rather than in spheres as for the case of Eq.15. Suppose that in a spherical sample of radius R_s, to estimate the sample density, instead of Eq.19, we use the estimator

$$\overline{n} = \frac{3}{4\pi R_s^3} \int_0^{R_s} \overline{(n(r))_p} 4\pi r^2 dr \,. \tag{22}$$

Then, the estimator defined by Eq.21 must satisfies the following integral constraint

$$\int_0^{R_s} \overline{\xi(r)} r^2 dr = 0 \,. \tag{23}$$

This condition is *satisfied independently of the functional shape of the underlying correlation function* $\xi(r)$. Thus the integral constraint for the FS estimator does not simply introduce an offset, but it causes a change in the shape of $\overline{\xi(r)}$ for $r \to R_s$. Other choices of the sample density estimator [31, 43] and/or of the correlation function introduce distortions similar to that in Eq.23.

In order to clarify the effect of the integral constraint for the FS estimator, let us rewrite the ensemble average value of the FS estimator (i.e., Eq.21) in terms of the ensemble average two-point correlation function

$$\langle \overline{\xi(r)} \rangle = \frac{1 + \xi(r)}{1 + \frac{3}{R_s^3} \int_0^{R_s} \xi(r) r^2 dr} - 1 \,. \tag{24}$$

By writing Eq.24 we assume that the stochastic noise is negligible, which of course is not a good approximation at any scale. However in this way we may be able to single out the effect of the integral constraint for the FS estimator. From Eq.24 it is clear that this estimator is biased, as it does not satisfy Eq.18 but only Eq.17.

As an illustrative example, let us now consider the case in which the theoretical $\xi(r)$ is a given by LCDM model. The (ensemble average) estimator given by Eq.24,
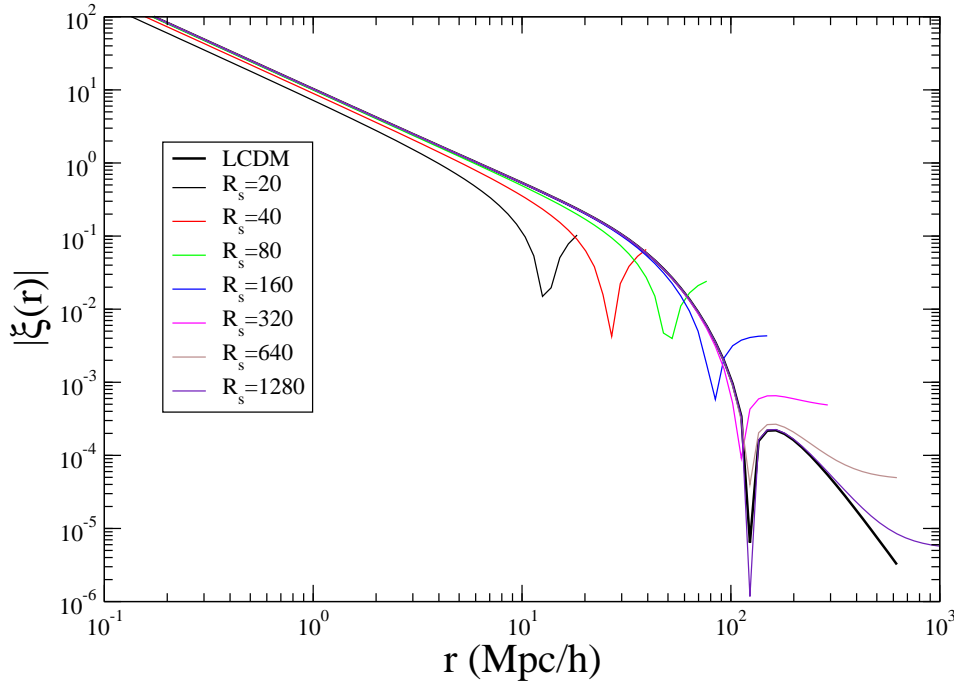
Inhomogeneities in the universe   15

Figure 2. Absolute value of the estimation of the correlation function of the LCDM model with the integral constraint described by Eq.24. The tick solid line represents the theoretical model (From [31]). The zero crossing scale correspond to the cusp.

in spherical samples of different radius R_s, is shown in Fig.2. One may notice that for $R_s > r_c$ the zero point of $\overline{\xi(r)}$ remains stable, while when $R_s < r_c$ it is linearly dependent on R_s. The negative tail continues to be non-linearly distorted even when $R_s > r_c$. For instance, when $R_s \approx 600$ Mpc/h we are not able to detect the $\xi(r) \sim -r^{-4}$ tail that becomes marginally visible only when $R_s > 1000$ Mpc/h. Thus the stability of the zero-point crossing scale should be the first problem to be considered in the analysis of $\overline{\xi(r)}$.

5. Results in the data

We briefly review the main results obtained by analyzing several samples of the Sloan Digital Sky Survey (SDSS) [10, 12, 11, 34, 15] and of the Two degree field Galaxy Redshift Survey (2dFGRS) [44, 13, 14]. For the different catalogs we selected, in the angular coordinates, a sky region such that (i) it does not overlap with the irregular edges of the survey mask and (ii) it covers a contiguous sky area. We computed the metric distance $R(z; \Omega_m, \Omega_\Lambda)$ from the redshift z by using the cosmological parameters $\Omega_m = 0.25$ and $\Omega_\Lambda = 0.75$.

The SDSS catalog includes two different galaxy samples constructing by using different selection criteria: the main-galaxy (MG) sample and the Luminous Red Galaxy (LRG) sample. In particular, the MG sample is a flux limited catalog with apparent magnitude $m_r < 17.77$ [45], while the LRG sample was constructed to be volume-limited

Inhomogeneities in the universe   16

(VL) [46]. A sample is flux limited when it contains all galaxies brighter than a certain apparent flux f_{min}. There is an obvious selection effect in that it contains intrinsically faint objects only when these are located relatively close to the observer, while it contains intrinsically bright galaxies located in wide range of distances [6]. For this reason one constructs a volume limited (VL) sample by imposing a cut in absolute luminosity L_{min} and by computing the corresponding cut in distance $r_{max} \approx \sqrt{L_{min}/(4\pi f_{min})}$, so that all galaxies with $L > L_{min}$, located at distances $r < r_{max}$, have flux $f > f_{min}$, and are thus included in the sample. By choosing different cuts in absolute luminosity one obtains several VL samples (with different L_{min}, r_{max}). Note that we use magnitudes instead of luminosities and that the absolute magnitude must be computed from the redshift by taking into account both the assumptions on the cosmology (i.e. the cosmological parameters, which very weakly perturb the final results given that the redshifts are low, i.e. $z < 0.2$) and the K-corrections (which are measured in the SDSS case).

For the MG sample we used standard K-corrections from the VAGC data [47]: we have tested that our main results do not depend significantly on K-corrections and/or evolutionary corrections [11]. The MG sample angular region we consider is limited, in the SDSS internal angular coordinates, by $-33.5° \le \eta \le 36.0°$ and $-48.0° \le \lambda \le 51.5°$: the resulting solid angle is $\Omega = 1.85$ sr. For the LRG sample, we exclude redshifts $z > 0.36$ and $z < 0.16$ (where the catalog is known to be not complete [45, 4]), so that the distance limits are: $R_{min} = 465$ Mpc/h and $R_{max} = 1002$ Mpc/h. The limits in R.A α and Dec. δ considered are: $\alpha \in [130°, 240°]$ and $\delta \in [0°, 50°]$. The absolute magnitude is constrained in the range $M \in [-23.2, -21.2]$. With these limits we find $N = 41833$ galaxies covering a solid angle $\Omega = 1.471$ sr [48]. Finally for 2dFGRS, to avoid the effect of the irregular edges of the survey we selected two rectangular regions whose limits are [14]: in southern galactic cap (SGC) ($-33° < \delta < -24°$, $-32° < \alpha < 52°$), and in northern galactic cap (NGC) ($-4° < \delta < 2°$, $150° < \alpha < 210°$); we determined absolute magnitudes M using K-corrections from [49, 14].

5.1. Redshift selection function

In order to have a simple picture of the redshift distribution in a magnitude limited sample, we report Fig.3 galaxy counts as a function of the radial distance, in bins of thickness 10 Mpc/h, in the northern and southern part of the 2dFGRS [14, 13]. One may notice that a sequence of structures and voids is clearly visible, but there is an overall trend (a rise, a peak and then a decrease of the density) which is determined by a luminosity selection effect. Indeed, $n(R)$ in a flux limited sample is usually called redshift selection function, as it is determined by both the redshift distribution and by the luminosity selection criteria of the survey. It is thus not easy, by this kind of analysis, to determine, even at a first approximation, the main properties of the galaxy distributions in the samples. Nevertheless, one may readily compute that there is a $\sim 30\%$ of difference in the sample density between the northern and the southern part of the catalog: one needs to refine the analysis to clarify its significance. Note that
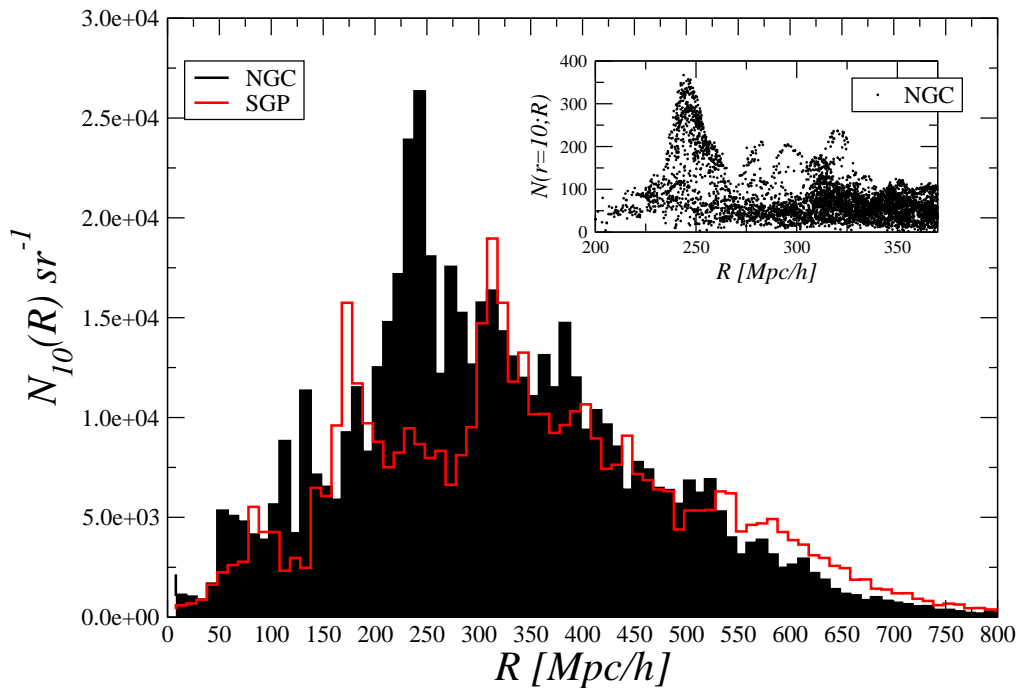
Inhomogeneities in the universe 17

Figure 3. Radial density in bins of thickness 10 Mpc/h in the northern (NGC) and souther (SGC) part of the 2dFGRS magnitude limited sample. There is a large structure at ~ 240 Mpc/h. In the inset panel it is shown the distribution of $N_i(r; R)$ for $r = 10$Mpc/h in a VL sample in the NGC. (Adapted from [14]).

large scale $\sim 30\%$ fluctuations are not uncommon. For instance, fluctuations have been found in galaxy redshift and magnitude counts that are close to 50% occurring on ~ 100 Mpc/h scales [18, 19, 20, 21].

5.2. Radial counts

A more direct information about the value of the density in a VL sample, is provided by the number counts of galaxies as a function of radial distance $n(R)$ in a VL sample. For a spatially homogeneous distribution $n(R)$ should be constant while, for a fractal distribution it should exhibit a power-law decay, even though large fluctuations are expected to occur given that this not an average quantity [50].

In the SDSS MG VL samples, at small enough scales, $n(R)$ (see Fig.4) shows a fluctuating behavior with peaks corresponding to the main structures in the galaxy distribution [11]. At larger scales $n(R)$ increases by a factor 3 from $R \approx 300$ Mpc/h to $R \approx 600$ Mpc/h. Thus there is no range of scales where one may approximate $n(R)$ with a constant behavior. The open question is whether the growth of $n(R)$ for $R > 300$ Mpc/h is induced by structures or it is caused by a selection effect in data. Both are possible but both must be very detailed discussed. For instance in [24] it is argued that a substantial evolution causes that growth, while in [11] it is discussed, by making a more complete analysis (see next section), that structures certainly contribute to such
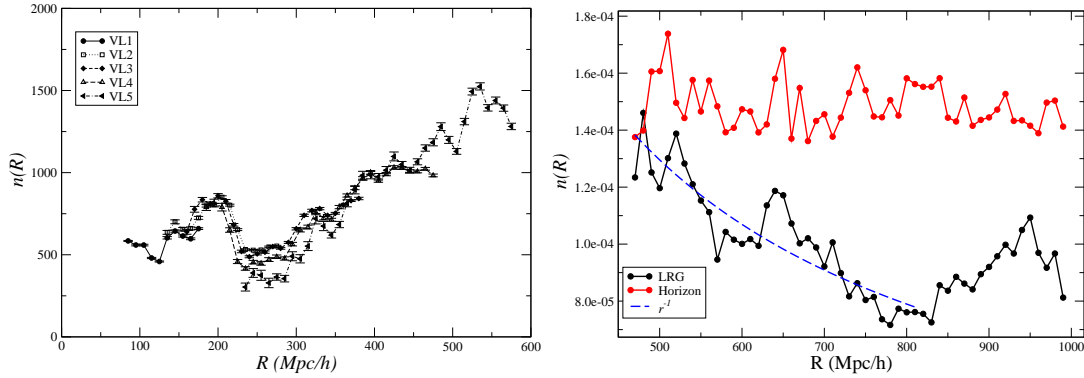
Inhomogeneities in the universe   18

Figure 4. *Left panel*: Radial density in the volume limited samples of the MG catalog. Note the amplitude of $n(R)$ for the MG VL samples has been normalized by taking into account the different selection in luminosity in the different samples (From [11]). *Right Panel*: The same for the LRG sample and for a mock sample extracted from the Horizon simulations [51] (units are in $(Mpc/h)^{-3}$). The blue dashed line decays as r^{-1} and it is plotted as reference. (From [48]).

a behavior. (Note that in mock catalogs drawn from cosmological N-body simulations one measures an almost constant density [11, 14]).

Given that, by construction, also the LRG sample should be VL [52, 7, 4] the behavior of $n(R)$ is expected to be constant if galaxy distribution is close to uniform (up to Poisson noise and radial clustering). It is instead observed that the LRG sample $n(R)$ shows an irregular and not constant behavior (see the right panel of Fig.4) rather different from that seen in the MG sample. Indeed, there are two main features: (i) a negative slope between 400 Mpc/h < r < 800 Mpc/h (i.e., $0.16 < z < 0.28$) and (ii) a positive slope up to a local peak at $r \sim 950$ Mpc/h (i.e., $z \sim 0.34$). Note that if $n(R)$ were constant we would expect a behavior similar to the one shown by the mock sample extracted from the Horizon simulation [51] with the same geometry of the real LRG sample (see Fig.4) [48].

An explanation that it is usually given for this result [7, 4], is that the LRG sample is "quasi" VL, in that it does not show a constant $n(R)$. Thus, the features in $n(R)$ are absorbed in the properties of a selection function, which is unknown *a priori*, but that it is defined *a posteriori* as the difference between an almost constant $n(R)$ and the behavior observed. This explanation is unsatisfactory as it is given *a posteriori* and no independent tests have been provided to corroborate the hypothesis that an important observational selection effect occurs in the data, other than the behavior of $n(R)$ itself. A different possibility is that the behavior of $n(R)$ is determined, at least partially, by intrinsic fluctuations in the distribution of galaxies and not by selection effects.

By addressing the behavior of $n(R)$ to unknown selection effects, it is implicitly assumed that more than the 20% of the total galaxies have not be measured for observational problems [48]. This looks improbable [52] although a more careful investigation of the problem must be addressed. Note also that the deficit of galaxies

Inhomogeneities in the universe   19

would not be explained by a smooth redshift-dependent effect, rather the selection must be strongly redshift dependent as the behavior of $n(R)$ is not monotonic. These facts point, but do not proof, toward an origin of the $n(R)$ behavior due to the intrinsic fluctuations in the galaxy distribution.

5.3. Test on self-averaging properties

Galaxy counts provide only a rough analysis of fluctuations, especially because one is unable to average it and because it samples different scales differently as the volume in the different redshift bins is not the same. The analysis of the stochastic variable represented by the number of points in spheres $N_i(r)$ an help to overcome these problems, as it is possible to construct volume averages and because it is computed in a simple real sphere sphere. (See an example in the inset panel of Fig.3).

Let us thus pass to the self-averaging test described in Sect.4.1. To this aim we divide the sample into two non-overlapping regions of equal volume, one at low (L) and the other at high (H) redshifts. We then measure the PDF $P_L(N;r)$ and $P_H(N;r)$ in the two volumes. Given that the number of independent points is not very large at large scales (i.e., $M(r)$ in Eq.15 not very larger than $\sim 10^4$), in order to improve the statistics especially for large sphere radii, we allow a partial overlapping between the two sub-samples, so that galaxies in the L (H) sub-sample count also galaxies in the H (L) sub-sample. This overlapping clearly can only smooth out differences between $P_L(N;r)$ and $P_H(N;r)$.

We first consider two SDSS MG VL samples from the data release 6 (DR6) [11] and then from the DR7 [15]. In a first case (upper - left panels of Fig.5), at small scales ($r = 10$ Mpc/h), the distribution is self-averaging (i.e., the PDF is statistically the same) both in the DR6 sample (that covers a solid angle $\Omega_{DR6} = 0.94$ sr) than in the DR7 sample ($\Omega_{DR7} = 1.85$ sr $\approx 2 \times \Omega_{DR6}$ sr). Instead, for larger sphere radii i.e., $r = 80$ Mpc/h, (bottom - right panels of Fig.5) in the DR6 sample, the two PDF show clearly a systematic difference. Not only the peaks do not coincide, but the overall shape of the PDF is not smooth displaying a different shape. Instead, for the sample extracted from DR7, the two determinations of the PDF are in good agreement (within statistical fluctuations). We conclude that in DR6 for $r = 80$ Mpc/h there are large density fluctuations which are not self-averaging because of the limited sample volume [11, 15]. They are instead self-averaging in DR7 because the volume is increased by a factor two.

For the other sample we consider, which include mainly bright galaxies, the breaking of self-averaging properties does not occur as well for small r but it is found for large r. Other radial distance-dependent selections, like galaxy evolution [24], could in principle give an effect in the same direction if they increase the number density with redshift. However this would not affect the conclusion that, on large enough scales, self-averaging is broken. Note that in the SDSS samples for small values of r the PDF is found to be statistically stable in different sub-regions of a given sample. For this reason we do not

Inhomogeneities in the universe 20

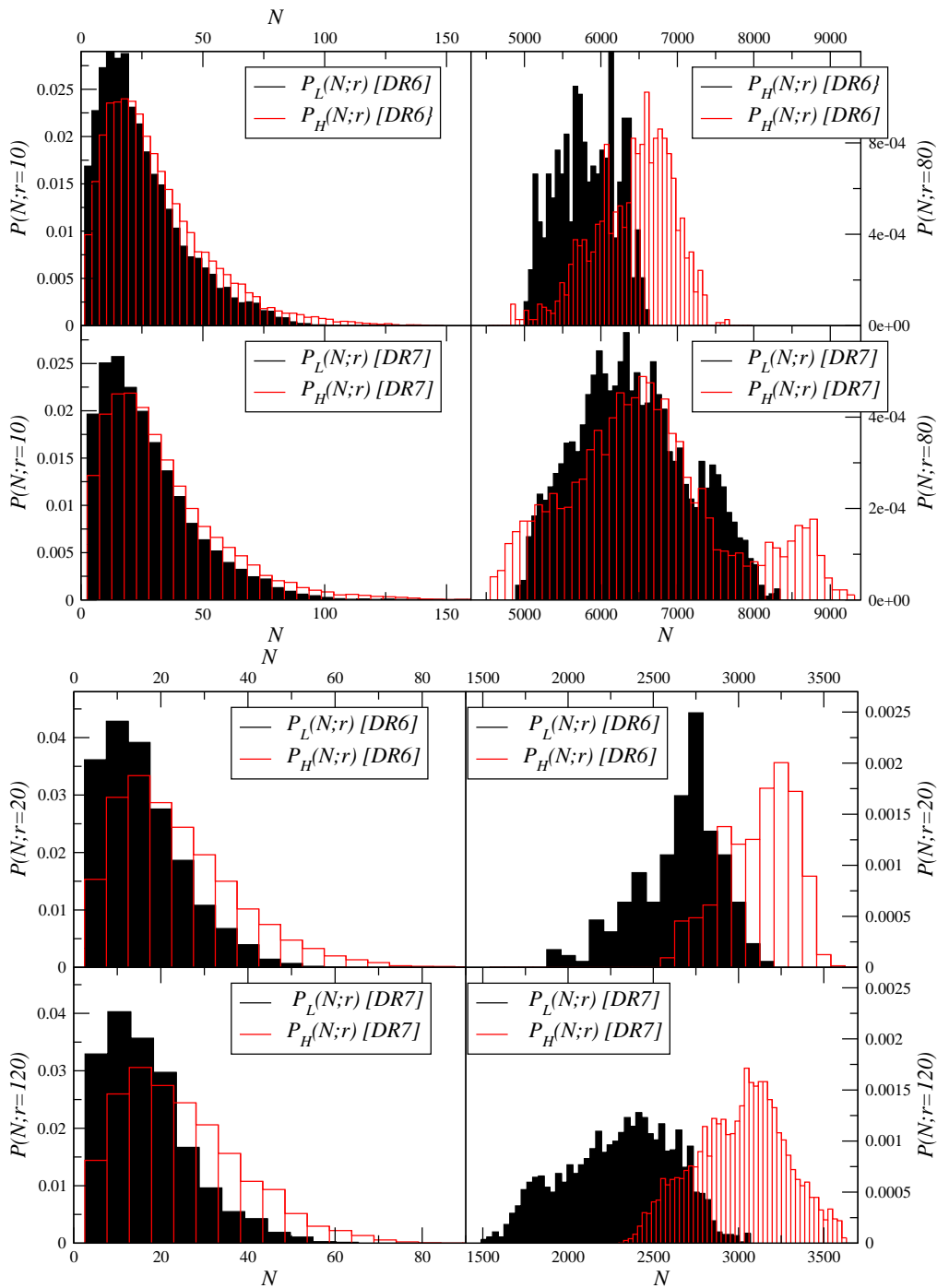**Figure 5.** *Upper Panels:* PDF of the counts in spheres in the sample defined by $R \in [125, 400]$ Mpc/h and $M \in [-20.5, -22.2]$ in the DR6 and DR7 data, for two different values of the sphere radii $r = 10$ Mpc/h and $r = 80$ Mpc/h. *Lower Panels:* The same but for the sample defined by $R \in [200, 600]$ Mpc/h and $M \in [-21.6, -22.8]$ and for $r = 20, 120$ Mpc/h. (Adapted from [15]).
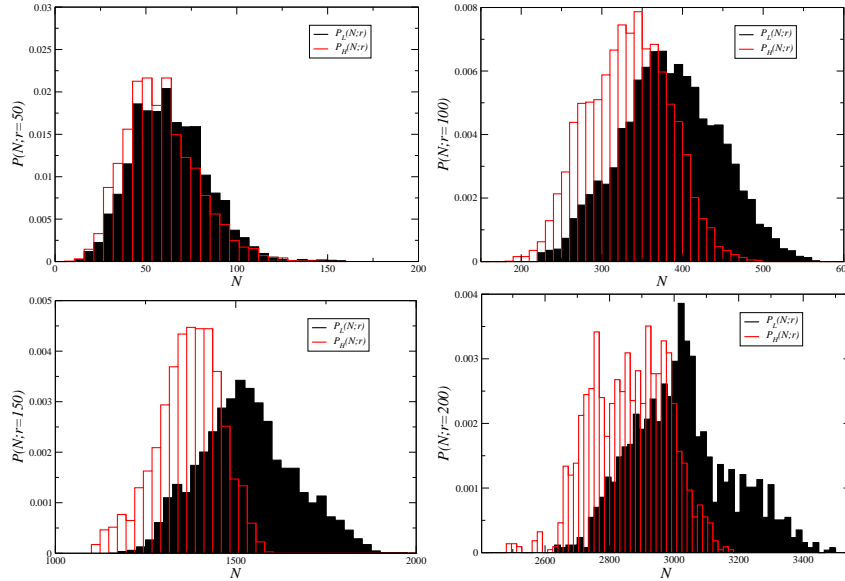
000129

Inhomogeneities in the universe   21

Figure 6. *Upper Left Panel:* PDF for $r = 50$ Mpc/h in the LRG sample (From [48]). The number of points contributing to the histogram is respectively for L and H $M(r) = 13277, 13099$. *Upper Right Panel:* The same for $r = 100$ Mpc/h. Here $M(r) = 7929, 7690$. *Bottom Left Panel:* The same for $r = 150$ Mpc/h. Here $M(r) = 3495, 3150$. *Bottom Right Panel:* The same for $r = 200$ Mpc/h. Here $M(r) = 1465, 1354$.

interpret the lack of self-averaging properties as due to a "local hole" around us: this would affect all samples and all scales, which is indeed not the case [15]. Because of these large fluctuations in the galaxy density field, self-averaging properties are well-defined only in a limited range of scales where it is then statistically meaningful to measure whole-sample average quantities [11, 34, 15].

For the LRG sample (see Fig.6) one may note that for $r = 50$ Mpc/h the two determinations are much closer than for lager sphere radii for which there is actually a noticeable difference in the whole shape of the PDF. The fact that $P_H(N; r)$ is shifted toward smaller values than $P_L(N; r)$ is related to the decaying behavior of the redshift counts (see Fig.4): most of the galaxies at low redshifts see a relatively larger local density than the galaxies at higher redshift.

Due the breaking of self-averaging properties in the different samples for $r < 150$ Mpc/h we conclude that there is no evidence for a crossover to spatial uniformity. In the next section we refine the analysis for smaller scales by characterizing the shape of the PDF and the scaling of its moments.

5.4. Probability density function and its moments

In the range of scales in which self-averaging properties are found to hold, we can further characterize the shape of the PDF and the scaling of its moments. We first computed the average conditional density (Eq.15) finding a pronounced r dependence, as can be seen
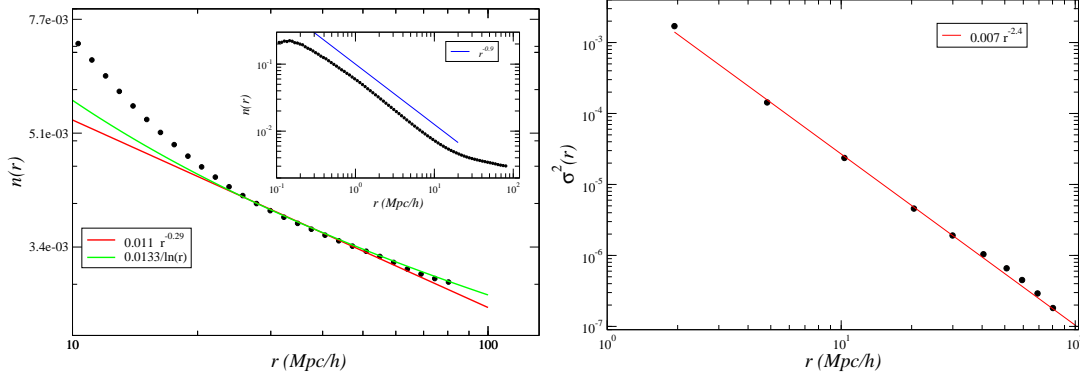
Inhomogeneities in the universe   22

Figure 7. *Left Panel:* Conditional average density $\overline{n}(r)$ of galaxies as a function of radius. In the inset panel it is shown the behavior of in the full range of scales. Note the change of slope at ≈ 20 Mpc/h and note also that there is no flattening up to ≈ 80 Mpc/h. The statistical significance of the last few points at the largest scales is weaker (see text). Our conjecture is that we have a logarithmic correction to the constant behavior, although we cannot exclude the possibility that it is power law with an exponent ≈ -0.3 *Right Panel:* Variance σ^2 of the conditional density $n_i(r)$ as a function of radius. Conversely, the variance for a Poisson point process would display a $1/r^3$ decay.

in Fig.7. We detect a change of slope in the conditional average density in terms of the radius r at about ≈ 20 Mpc/h. At this point the decay of the density changes from an inverse linear decay to a slow logarithmic one. Our best fit is $\overline{n(r)} \approx \frac{0.0133}{\log r}$, that is the average density depends only weakly on r. Alternatively, an almost indistinguishable power-law fit is provided by $\overline{n(r)} \approx 0.011 \times r^{-0.29}$. Moreover, the density $\overline{n(r)}$ does not saturate to a constant up to ~ 80 Mpc/h, i.e., up to the largest scales probed in this sample where self-averaging properties have been tested to hold. Our best fit for the variance is ($\sigma^2(r) \approx 0.007 \times r^{-2.4}$ see right panel of Fig.7). Given the scaling behavior of the conditional density and variance, we conclude that galaxy structures are characterized by non-trivial correlations for scales up to $r \approx 80$ Mpc/h.

To probe the whole distribution of the conditional density $n_i(r)$, we fitted the measured PDF with Gumbel distribution via its two parameters α and β [34]. The Gumbel distribution is one of the three extreme value distribution [53, 54]. It describes the distribution of the largest values of a random variable from a density function with faster than algebraic (say exponential) decay. The Gumbel distribution's PDF is given by

$$P(y) = \frac{1}{\beta} \exp\left[-\frac{y - \alpha}{\beta} - \exp\left(-\frac{y - \alpha}{\beta} \right) \right] . \tag{25}$$

With the scaling variable

$$x = \frac{y - \alpha}{\beta} \tag{26}$$

the density function (Eq.25) simplifies to the parameter-free Gumbel
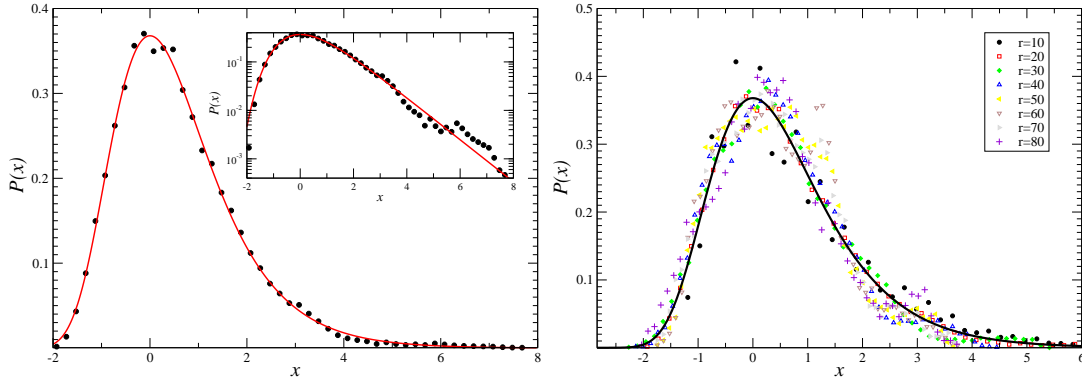
$$P(x) = e^{-x - e^{-x}} . \tag{27}$$

Inhomogeneities in the universe   23

Figure 8. *Left Panel:* One of the best fits is obtained for $r = 20$ Mpc/h. The data is rescaled by the fitted parameters α and β. The solid line corresponds to the parameter-less Gumbel distribution Eq.27. The inset depicts the same on log-linear scale. *Right Panel:* Data curves of different r scaled together by fitting parameters α and β for each curves. The solid line is the parameter-free Gumbel distribution Eq.27.

The mean and the variance of the Gumbel distribution (Eq.25) is $\mu = \alpha + \gamma\beta$, $\quad \sigma^2 = (\beta\pi)^2/6$ where $\gamma = 0.5772\ldots$ is the Euler constant.

One of our best fit for the PDF is obtained for $r = 20$ Mpc/h (see left panel Fig. 8). The data, moreover, convincingly collapses to the parameter-less Gumbel distribution (Eq.27) for all values of $r \in [10, 80]$ Mpc/h, with the use of the scaling variable x from Eq.26 (see right panel Fig. 8). Note that for a Poisson point process the number $N(r)$ fluctuations are distributed exactly according to a Poisson distribution, which in turn converges to a Gaussian distribution for large average number of points $\overline{N(r)}$ per sphere. In our samples, $\overline{N(r)}$ was always larger than 20 galaxies, where the Poisson and the Gaussian PDFs differ less than the uncertainty in our data. Note also that due to the Central Limit Theorem, all homogeneous point distributions (not just the Poisson process) lead to Gaussian fluctuations [17]. Hence the appearance of the Gumbel distribution is a clear sign of inhomogeneity and large scale structures in our samples.

We have thus established scaling and data collapse over a wide range of radius (volume) in galaxy data. Scaling in the data indicates criticality [17, 34]. The average galaxy density depends only logarithmically on the radius, which suggests a Gumbel scaling function. Indeed, it was recently conjectured [55] that only three types of distributions appear to describe fluctuations of global observables at criticality. In particular, when the global observable depends logarithmically on the system size, the corresponding distribution should be a (generalized) Gumbel [34].

5.5. Two-point correlation analysis

When one determines the standard two-point correlation function one makes implicitly the assumptions that, inside a given sample the distribution is: (i) self-averaging and (ii) spatially uniform. The first assumption is used when one computes whole sample average quantities. The second is employed when supposing that the estimation of the

Inhomogeneities in the universe   24

sample average gives a fairly good estimation of the ensemble average density. When one of these assumptions, or both, is not verified then the interpretation of the results given by the determinations of the standard two-point correlation function must be reconsidered with great care.

To show how non self-averaging fluctuations inside a given sample bias the $\xi(r)$ analysis, we consider the estimator

$$\overline{\xi(r)} + 1 = \overline{\xi(r; R, \Delta R)} + 1 = \overline{n(r, \Delta r)_p} \cdot \frac{V(r^*)}{N(r^*; R, \Delta R)}, \tag{28}$$

where the second ratio on the r.h.s. is now the density of points in spheres of radius r^* averaged over the galaxies lying in a shell of thickness ΔR around the radial distance R. If the distribution is homogeneous, i.e., $r^* > \lambda_0$, and statistically stationary, Eq.28 should be (statistically) independent on the range of radial distances $(R, \Delta R)$ chosen. The two-point correlation function is defined as a ratio between the average conditional density and the sample average density: if both vary in the same way when the radial distance is changed, then its amplitude remains nearly constant. This however does not imply that the amplitude of $\overline{\xi(r)}$ is meaningful, as it can happen that the density estimated in sub-volumes of size r^* show large fluctuations and so the average conditional density, and this occurring with a radial-distance dependence. To show that the $\overline{\xi(r)}$ analysis gives a meaningful estimate of the amplitude of fluctuations, *one has to test that this amplitude remains stable by changing the relative position of the sub-volumes of size r^* used to estimate the average conditional density and the sample average density.* This is achieved by using the estimator in Eq.28. While standard estimators [56, 43, 31] are not able to test for such an effect, as the main contributions for both the conditional density and the sample average density come from the same part of the sample (typically the far-away part where the volume is larger). We find large variations in the amplitude of $\overline{\xi(r)}$ in the SDSS MG VL samples (see the left panel of Fig.9). This is simply an artifact generated by the large density fluctuations on scales of the order of the sample sizes. The results that the estimator of $\xi(r)$ has nearly the same amplitude in different samples, e.g., [57, 58, 59, 60, 7, 8, 9], despite the large fluctuations of $N_i(r; R)$, are simply explained by the fact that $\overline{\xi(r)}$ is a ratio between the average conditional density and the sample average density: both vary in the same way when the radial distance is changed and thus the amplitude is nearly constant. To summarize the fact that by using different normalizations, which however are all in principle equally valid if the distribution has a well-defined average density inside the sample, we have shown that the amplitude of the estimated correlation function varies in the SDSS samples. This is due to the fact that both the assumptions on which the determination of the standard to point correlation function is based on, are not verified in these samples and that λ_0 is certainly larger than the samples size.

The right panel of Fig.9 clearly show that there is a finite-size dependence of both the amplitude of the correlation function and of the zero-crossing scale: this situations looks like the one shown in Fig.2. Thus prior to the characterization of a fine feature as the BAO scale, it is necessary to test that the correlation function remains stable
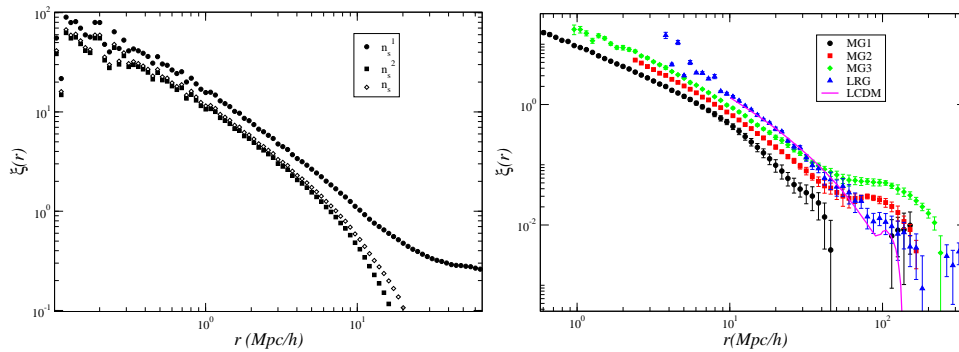
Inhomogeneities in the universe   25

Figure 9.   *Left panel:* The two-point correlation function in a MG-VL sample estimated by Eq.28: the sample average density is computed in spheres of radius $r^* = 60$ Mpc/h and considering all center-points lying in a bin of thickness $\Delta R = 50$ Mpc/h centered at different radial distance R: $R_1 = 250$ Mpc/h (n_s^1) and $R_2 = 350$ Mpc/h (n_s^2). The case in which we have used the estimation of the sample average N/V (n_s) is also shown and it agrees with the FS estimator (adapted from [11]). *Right Panel:* The Landy and Szalay [56] estimator of $\xi(r)$ in various MG-VL sample and in a LRG sample of the SDSS. The most evident feature is the finite-size dependence of both the amplitude and the zero-crossing (adapted from [16]). The solid line is a LCDM model.

as a function of the sample size. This shows that estimator of $\xi(r)$ in the LRG sample is indeed biased by volume-dependent systematic effects that make the detection of correlations only an estimate of a lower limit of their amplitude [16]. A similar conclusion was reached by [61], i.e. that when corrections for possible systematics are taken into account the correlation function may not be consistent with as high amplitude a peak as claimed by [3]. To clarify this issue, as discussed above, it is necessary to consider the set of tests for statistical and spatial homogeneity discussed above.

Instead of investigating the origin of the fluctuating behavior of $n(R)$, some authors [4] focused their attention on the effect of the radial counts on the determination of the two-point correlation function $\xi(r)$. In particular, they proposed mainly two different tests to study what is the effect of $n(R)$ on the determination of $\xi(r)$. The first test consists in taking a mock LRG sample, constructed from a cosmological N-body simulation of the LCDM model, and by applying a redshift selection which randomly excludes points in such a way that the resulting distribution has the same $n(R)$ of the real sample. Then one can compare $\xi(r)$ obtained in the original mock and in redshift-sampled mock. [4] find that there is a good agreement between the two. This shows that the particular kind of redshift-dependent random sampling considered for the given distribution, does not alter the determination of the correlation function. Alternatively we may conclude that, under the assumption that the observed LRG sample is a realization of a mock LCDM simulation, the $n(R)$ does not affect the result. However, if we want to test whether the LRG sample has the same statistical properties of the mock catalog, we cannot clearly proof (or disproof) this hypothesis by assuming a priori that this is true.

In other words, standard analyses ask directly the question of whether the data are compatible with a given model, by considering only a few statistical measurements. As it was shown by [5] the LRG correlation function does not pass the null hypothesis, i.e. it are compatible with zero signal, implying that the volume of current galaxy samples is not large enough to claim that the BAO scale is detected. In addition, by *assuming* that the galaxy correlations are modeled by a LCDM model, one may find that the data allow to constrain the position of the BAO scale. In our view this approach is too narrow: in evaluating whether a model is consistent with the data, one should show that *at least the main* statistical properties of the model are indeed consistent with the data. As discussed above, a number of different properties can be considered, which are useful to test the assumptions of (i) self-averaging (ii) spatial homogeneity. When, inside the given sample, the assumption (i) and/or (ii) are/is violated then the compatibility test of the data with a LCDM model is not consistent with the properties of the data themselves.

6. Conclusion

The statistical characterization of galaxy structures presents a number of subtle problems. These are associated both with the a-priori assumptions which are encoded in the statistical methods used in the measurements and in the a-posteriori hypotheses that are invoked to explain certain measured behaviors. By increasing the number of the former, as for example, bias, luminosity evolution, selection effects, one may find that the data are compatible with a certain model. However it is possible to introduce direct tests to understand both whether the a-priori assumptions are compatible with the data and whether it is necessary to introduce a-posteriori untested, but plausible, hypotheses to interpret the results of the data analysis. For instance, the analysis of the simple counts as a function of distance, in the SDSS samples, shows clearly that the observed behavior is incompatible with model predictions. As mentioned above, one may assume that the differences between the model and the observations are due to selection effects. Then this becomes clearly the most important assumption in the data analysis that must be stressed clearly and explicitly. In addition, one may consider whether there is an independent way to study whether there are such strong selection effects in the data.

On the basis of the series of test we have presented, aiming to directly test whether spatial and statistical homogeneity are verified inside the available samples, extracted both from the SDSS and 2dFGRS catalogs, we conclude that galaxy distribution is characterized by structures of large spatial extension. Given that we are unable to find a crossover toward homogeneity, the amplitude of these structures remain undetermined and their main characteristic is represented by the scaling behavior of their relevant statistical properties. In particular, we discussed that the average conditional density presents a scaling behavior of the type $\sim r^{-\gamma}$ with $\gamma \approx -1$ up to ~ 20 Mpc/h followed by a $\gamma \approx -0.3$ behavior up to ~ 100 Mpc/h. Correspondingly the probability density

Inhomogeneities in the universe   27

function (PDF) of galaxy (conditional) counts in spheres show a relatively long tail: it is well fitted by the Gumbel function instead than by the Gaussian function, as it is generally expected for spatially homogeneous density fields.

Our statistical tests can thus provide direct observational tests of the basic assumptions used in the derivation of the FRW models, i.e. spatial and statistical homogeneity. In this respect it is worthing to clarify in more details the subtle difference between these two concepts [15]. A widespread idea in cosmology is that the so-called concordance model of the universe combines *two* fundamental assumptions. The first is that the dynamics of space-time is determined by Einstein's field equations. The second is that the universe is homogeneous and isotropic. This hypothesis, usually called the Cosmological Principle, is though to be a *generalization* of the Copernican Principle that "the Earth is not in a central, specially favored position" [63, 64]. The FRW model is derived under these two assumptions and it describes the geometry of the universe in terms of a single function, the scale factor, which obeys to the Friedmann equation [25]. There is a subtlety in the relation between the Copernican Principle (all observes are equivalent and there are no special points and directions) and the Cosmological Principle (the universe is homogeneous and isotropic). Indeed, the fact that the universe looks the same, at least in a statistical sense, in all directions and that all observers are alike does not imply spatial homogeneity of matter distribution. It is however this latter condition that allows us to treat, above a certain scale, the density field as a smooth function, a fundamental hypothesis used in the derivation of the FRW metric. Thus there are distributions which satisfy the Copernican Principle and which do not satisfy the Cosmological Principle [17]. These are statistically homogeneous and isotropic distributions which are also spatially inhomogeneous. Therefore the Cosmological Principle represents a specific case, holding for spatially homogeneous distributions, of the Copernican Principle which is, instead, much more general. Statistical and spatial homogeneity refer to two different properties of a given density field. The problem of whether a fluctuations field is compatible with the conditions of the absence of special points and direction can be reformulated in terms of the properties of the PDF which generates the stochastic field.

By analyzing the PDF in the available galaxy samples we can make tests on both the Copernican and Cosmological Principles at low redshift, where we can neglect the important complications of evolving observations onto a spatial surface for which we need a specific cosmological model. We have discussed, however, that the statistical properties of the matter density field up to a few hundreds Mpc is crucially important for the theoretical modeling. We have shown that galaxy distribution in different samples of the SDSS is compatible with the assumptions that this is transitionally invariant, i.e. it satisfies the requirement of the Copernican Principle that there are no spacial points or directions. On the other hand, we found that there are no clear evidences of spatial homogeneity up to scales of the order of the samples sizes, i.e. ~ 100 Mpc/h. This implies that galaxy distribution is not compatible with the stronger assumption of spatial homogeneity, encoded in the Cosmological Principle. In addition, at the largest

Inhomogeneities in the universe   28

scales probed by these samples (i.e., $r \approx 150$ Mpc/h) we found evidences for the breaking of self-averaging properties, i.e. that the distribution is not statistically homogeneous. Forthcoming redshift surveys will allow us to clarify whether on such large scales galaxy distribution is still inhomogeneous but statistically stationary, or whether the evidences for the breaking of spatial translational invariance found in the SDSS samples were due to selection effects in the data.

We note an interesting connection between spatial inhomogeneities and large scale flows which can be hypothesized by assuming that the gravitational fluctuations in the galaxy distribution reflect those in the whole matter distribution, and that peculiar velocities and accelerations are simply correlated. Peculiar velocities provide an important dynamical information as they are related to the large scale matter distribution. By studying their local amplitudes and directions, these velocities allow us, in principle, to probe deeper, or hidden part, of the Universe. The peculiar velocities are indeed directly sensitive to the total matter content, through its gravitational effects, and not only to the luminous matter distribution. However, their direct observation through distance measurements remains a difficult task. Recently, there have been published a growing number of observations of large-scale galaxy coherent motions which are at odds with standard cosmological models [67, 66, 68, 69].

It is possible to consider the PDF of gravitational force fluctuations generated by source field represented by galaxies, and test whether it converges to an asymptotic shape within sample volumes. In several SDSS sample we find that density fluctuations at the largest scales probed, i.e. $r \approx 100$ Mpc/h, still significantly contribute to the amplitude of the gravitational force [65]. Under the hypotheses mentioned above we may conclude that that large-scale fluctuations in the galaxy density field can be the source of the large scale flows recently observed.

As a final remark we mention the growing work to understand the effect of inhomogeneities on the large scale dynamics of the universe [70, 71, 72, 64, 73, 74, 75, 76]. As long as structures are limited to small sizes, and fluctuations have low amplitude, one can just treat fluctuations as small-amplitude perturbations to the leading order FRW approximation. However if structures have "large enough" sizes and "high enough" amplitudes, a perturbation approach may loose its validity and a more general treatment of inhomogeneities needs to be developed. From the theoretical point of view, it is then necessary to understand how to treat inhomogeneities in the framework of General Relativity. To this aim one needs to carefully consider the information that can be obtained from the data. At the moment it is not possible to get some statistical information for large redshifts ($z \approx 1$), but the characterization of relatively small scales properties (i.e., $r < 200$ Mpc/h) is getting more and more accurate. According to FRW models the linearity of Hubble law is a consequence of the homogeneity of the matter distribution. Modern data show a good linear Hubble law even for nearby galaxies ($r < 10$ Mpc/h). This raises the question of why the linear Hubble law is linear at scales where the visible matter is distributed in-homogeneously. Several solution to this apparent paradox have been proposed [72, 77, 78]: this situation shows that already

Inhomogeneities in the universe   29

the small scale properties of galaxy distribution have a lot to say on the theoretical interpretation of their properties. Indeed, while observations of galaxy structures have given an impulse to the search for more general solution of Einstein's equations than the Friedmann one, it is now a fascinating question whether such a more general framework may provide a different explanation to the various effects that, within the standard FRW model, have been *interpreted* as Dark Energy and Dark Matter.

[1] York D et al 2000 *Astronom.J.* **120** 1579
[2] Colless M et al 2001 *Mon.Not.R.Acad.Soc.* **328** 1039
[3] Eisenstein D J et al 2005 *Astrophys.J.* **633** 560
[4] Kazin I et al 2010 *Astrophys.J.* **710** 1444
[5] Cabrè A and Gaztanaga E `arXiv:1011.2729`
[6] Zehavi I et al 2002 *Astrophys.J.* **571** 172
[7] Zehavi I et al 2005, *Astrophys.J.* **630** 1
[8] Norberg E et al 2001 *Mon.Not.R.Acad.Soc.* **328** 64
[9] Norberg E et al 2002 *Mon.Not.R.Acad.Soc.* **332** 827
[10] Sylos Labini F Vasilyev N L and Baryshev Yu V 2007, *Astron.Astrophys.* **465** 23
[11] Sylos Labini F Vasilyev N L Baryshev Y V 2009 *Astron.Astrophys* **508** 17
[12] Sylos Labini F et al 2009 *Europhys.Lett.* **86** 49001
[13] Sylos Labini F Vasilyev N L Baryshev Y V 2009 *Europhys.Lett.* **85** 29002
[14] Sylos Labini F Vasilyev N L Baryshev Y V 2009 *Astron.Astrophys.* **496** 7
[15] Sylos Labini F and Baryshev Y V 2010 *J.Cosmol.Astropart.Phys.* **JCAP06** 021
[16] Sylos Labini F Vasilyev N L Baryshev Yu V López-Corredoira M 2009 *Astron.Astrophys.* **505** 981
[17] Gabrielli A Sylos Labini F Joyce M and Pietronero L 2005 *Statistical Physics for Cosmic Structures* (Springer Verlag, Berlin)
[18] Ratcliffe A Shanks T Parker Q A and Fong R 1998, *Mon.Not.R.Acad.Soc.* **293** 197
[19] Busswell G S et al 2004 *Mon.Not.R.Acad.Soc.* **354** 991
[20] Frith W J et al 2003 *Mon.Not.R.Acad.Soc.* **345** 1049
[21] Frith W J Metcalfe N and Shanks T 2006 *Mon.Not.R.Acad.Soc.* **371** 1601
[22] Yang A and Saslaw W C `arXiv:1009.0013v1`
[23] Blanton M R et al 2003 *Astrophys.J.* **592** 819
[24] Loveday J 2004 *Mon.Not.R.Acad.Soc.* **347** 601
[25] Weinberg S 2008 *Cosmology* (Oxford University Press, Oxford)
[26] Peebles, P J E *Large Scale Structure of the Universe*, (Princeton University Press, Princeton 1980)
[27] Harrison E R 1970 *Phys.Rev.D* **1** 2726
[28] Zeldovich Ya B 1972 *Mon.Not.R.Acad.Soc.* **160** 1
[29] Gabrielli A Joyce M and Sylos Labini F 2002 *Phys.Rev.* **D65** 083523
[30] Torquato S and Stillinger F H 2003 *Phys. Rev.* **E 68** 041113
[31] Sylos Labini F and Vasilyev N L 2008 *Astron.Astrophys* **477** 381
[32] Gabrielli A et al 2003 *Phys.Rev.* **D67** 043406

Inhomogeneities in the universe   30

[33] Gabrielli A Joyce M and Torquato S 2008 *Phys.Rev.* **E77** 031125
[34] Antal T Sylos Labini F Vasilyev N L and Baryshev Y V 2009 *Europhys.Lett.* **88** 59001
[35] Bouchaud J-P and Potters M 1999 *Theory of Financial Risks* (Cambridge University Press, Cambridge) `cond-mat/9905413`
[36] Eiseinstein D J and Hu W 1998 *Astrophys.J.* **496** 605
[37] Bashinsky S and Bertshinger E 2002 *Phys. Rev. Lett.* **87** 1301
[38] Springel V et al 2005 *Nature* **435** 629
[39] Durrer R Gabrielli A Joyce M and Sylos Labini F 2003 *Astrophys.J.* **585** L1
[40] Jiménez J B and Durrer R 2010 `arXiv:1006.2343v1`
[41] Peacock J A 1999 *"Cosmological physics"* (Cambridge University Press, Cambridge)
[42] Saslaw W C 2000 *"The Distribution of the Galaxies"* (Cambridge University Press)
[43] Kerscher M 1999 *Astron.Astrophys.* **343** 333
[44] Vasilyev N L Baryshev Yu V and Sylos Labini F 2006 *Astron.Astrophys.* **447** 431
[45] Strauss M A et al 2002 *Astrophys.J.* **124** 1810
[46] Eisenstein D J et al 2001 *Astrophys.J.* **12** 2267
[47] Blanton M R and Roweis S 2007 *Astron.J.* **133** 734
[48] Sylos Labini F 2010 `arXiv:1011.4855v1`
[49] Madgwick D S et al 2002 *Mon.Not.R.Acad.Soc* **333** 133
[50] Gabrielli A and Sylos Labini F 2001 *Europhys.Lett.* **54** 1
[51] Kim J Park C Gott J R and Dubinski J 2009 *Astrophys.J.* **701** 1547
[52] Eisenstein D J et al 2001 *Astronom.J.* **12** 2267
[53] Fisher R A and Tippett L H C 1928 *Cambridge Phil. Soc.* **28** 180
[54] Gumbel E J 1958 *Statistics of Extremes* (Columbia University Press)
[55] Bramwell S T 2009 *Nature Physics* **5** 444
[56] Landy S D and Szalay A 1993 *Astrophys.J.* **412** 64
[57] Davis M and Peebles P J E 1983 *Astrophys.J.* **267** 465
[58] Park C Vogeley M S Geller M J and Huchra J P 1994 *Astrophys.J.* **431** 569
[59] Benoist C Maurogordato S da Costa L N Cappi A and Schaeffer R 1996 *Astrophys.J.* **472** 452
[60] Zehavi I et al 2002 *Astrophys.J.* **571** 172
[61] Sawangwit U et al 2009 `arXiv:0912.0511v1`
[62] Martínez V J et al 2009 *Astrophys.J.* **696** L93
[63] Bondi H 1952 *Cosmology* (Cambridge University Press, Cambridge)
[64] Clifton T and Ferreira P G 2009 *Phys.Rev.* **D80** 103503
[65] Sylos Labini F 2010 *Astron.Astrophys.* **523** A68
[66] Lavaux G Tully R B Mohayaee R and Colombi S 2010 *Astrophys.J.* **709** 483
[67] Watkins R Feldman H A and Hudson M J 2009 *Mon.Not.R.Acad.Soc.* **392** 743
[68] Kashlinsky A Atrio-Barandela F Kocevski D and Ebeling, H 2008 *Astrophys.J.* **686** L49
[69] Kashlinsky A Atrio-Barandela F Ebeling H Edge A and Kocevski D. 2010 *Astrophys.J.* **712** L81
[70] Ellis G 2008 *Nature* **452** 158
[71] Buchert T 2008 *Gen.Rel.Grav.* **40** 467
[72] Wiltshire D L 2007 *Phys.Rev.Lett.* **99** 251101
[73] Clarkson C and Maartens R 2010 *Class. Quantum Grav.* **27** 124008
[74] Rasanen S 2008 *Int.J.Mod.Phys* **D17** 2543
[75] Kolb E W Marra V and Matarrese S 2010 *Gen.Rel.Grav.* **42** 1399
[76] Célérier M N Bolejko K and Krasiński A 2010 *Astron. Astrophys.* **518** A21
[77] Baryshev Y V 2006 *AIP Conf.Proc.* **822** 23
[78] Joyce M et al 2000 *Europhys.Lett.* **50** 416

Systematical effects in WMAP data

Hao Liu[1] and Ti-Pei Li[1,2,3]

`liuhao@ihep.ac.cn`

`litp@tsinghua.edu.cn`

Received ⎯⎯⎯⎯⎯⎯⎯⎯⎯; accepted ⎯⎯⎯⎯⎯⎯⎯⎯⎯

---

[1]Key Laboratory of Particle Astrophysics, Institute of High Energy Physics, Chinese Academy of Sciences, Beijing, China

[2]Department of Physics and Center for Astrophysics, Tsinghua University, Beijing, China

[3]Department of Engineering Physics and Center for Astrophysics, Tsinghua University, Beijing, China

– 2 –

ABSTRACT

Previously, by re-analyzing the Wilkinson Microwave Anisotropy Probe (WMAP) raw data, we have seen significantly different cosmic microwave background (CMB) results to the WMAP official release, especially at the largest-scale structure detectable for the CMB anisotropy - the $l = 2$ component, which is also called the CMB quadrupole. In this article, we first introduce the discovered differences, and then explain why the WMAP official release should be questioned. Since the differences are caused by complex systematical effects, we also manage to organize the involved systematical effects to show their inter relations, so that we can see clearly what we are doing in each work, and what we need to do in future works.

Subject headings: cosmic microwave background – cosmology: observations – methods: data analysis

– 3 –

1.   INTRODUCTION

The CMB anisotropy map detected by the WMAP mission is of great importance in understanding the birth and evolution of the Universe (Bennett et al. 2003). In order to detect the CMB anisotropy, the WMAP spacecraft works on the L2 point of the Sun-Earth system in the shade of the Earth, receiving the CMB signal with two antennas A and B separated by $141°$. The spacecraft is designed to provide full-sky image of the CMB anisotropy, thus the way it scans the sky is rather complex: The spacecraft spins while it moves around the Sun synchronously with the Earth, the spin axis is close to the Sun-to-Earth axis, but they don't overlap: The spin axis continuously moves around the Sun-to-Earth axis, otherwise the area near the north and south poles of the ecliptic system won't be observed. Although the scan pattern is complex, the recorded datum is simply the difference between the signals received by the two antennas, which looks like $D^i = T_A^i - T_B^i + etc$ (See Equ. 1 for details) The raw data are accumulation of D^is in time order, thus it's called the time-order data (TOD) (Limon et al. 2008). The TOD is transformed into a CMB anisotropy map by map-making processes (Hinshaw et al. 2003a), and it's right here that the difference between us and WMAP begins.

The spacecraft works in differential mode, thus detection to the CMB isotropy component, the 2.73 K blackbody emission, is made impossible. This component is the largest-scale structure of CMB, also called the monopole, or $l = 0$ spherical harmonic component, because we often use spherical harmonics to decompose the CMB anisotropy map. The $l = 1$ spherical harmonic component is called the dipole component, representing a smaller-scale structure than $l = 0$. This component is also undeterminable because it's impossible to distinguish the real CMB dipole from the Doppler dipole signal caused by the solar system's motion towards the CMB rest frame. Therefore the largest-scale structure determinable is the $l = 2$ component, called the CMB quadrupole. However, it has been discovered by the WMAP mission ever since the first data release (WMAP1) that the detected CMB quadrupole is only $1/5 \sim 1/10$ of the expected

– 4 –

value by the ΛCDM model - the standard cosmology theory (Hinshaw et al. 2003b; Bennett et al. 2003). This is called the low-l anomaly. Considering the uncertainty due to cosmic variance, the detected quadrupole value is roughly within $1 \sim 2\sigma$, which looks not very abnormal; however, this is a common misconception, because the quadrupole power can never be negative. In ordinary cases, when we get a value that is right 1σ lower than the expected value E, the convention is to use the probability for the value being in range $-\infty \sim E - \sigma$ as the probability of "nothing is abnormal"; however, for the CMB quadrupole, all values below zero are forbidden, thus the range for the probability estimation is $0 \sim E - \sigma$, not $-\infty \sim E - \sigma$, which gives a substantially lower probability. Especially, if the true CMB quadrupole is $1/10$ as we believe now, then the probability for the claim "nothing abnormal for the CMB quadrupole" will also be roughly 10% as before. Therefore, the lower is the true quadrupole, the more attention should be paid to the possibility that either the WMAP data or the standard cosmology is in trouble.

It seems that the WMAP team choose to preserve both, and they have changed their CMB power spectrum estimation method for low-l in their later releases from WMAP3 to WMAP7, so that they can obtain a litter bit higher quadrupole estimation. (Hinshaw et al. 2007; Nolta et al. 2009; Jarosik et al. 2010) Although this only slightly mitigates the low-l anomaly, the advantage is that they don't have to introduce substantial modification to their CMB anisotropy maps. However, we have found out that there could be a potential error in processing the WMAP TOD. If the error does exist, then the true CMB quadrupole component in the CMB anisotropy map could be not higher but even lower than released by WMAP. As explained above, a even lower quadrupole value is a strong implication for another way out for the problem: We should be careful in claiming success of the standard cosmology.

In map-making, the first and most important thing is to determine the antenna pointing vectors. This is easy to understand: If we don't know the antenna pointing vectors accurately, then we don't know where are we actually observing. We have found out that, with a difference

– 5 –

as small as $7'$ in the antenna pointing vectors (about half pixel), the derived CMB product could be significantly different (Liu & Li 2009b), and the new map seem to be better consistent to the TOD than the released WMAP CMB anisotropy map (Liu & Li 2010a). With these results, it's necessary to study further to find out more evidences about which is correct. In later work (Liu et al. 2010), we have discovered that, given the $\sim 7'$ pointing vector difference, estimation of the true Doppler dipole signal d will be consequently different. Since the true Doppler dipole signal d must be removed from the original time-order data before using them to make a CMB temperature map, difference in estimating d will certainly leave something on the final CMB temperature map: Let the estimated Doppler dipole signal be $d' = d - \Delta d$, then after removing d' from the TOD, Δd will be left in the TOD as an unwanted contamination. Since mapmaking from TOD is very well linear, we can make an output map from Δd to get the unwanted component on the final CMB temperature aroused by Δd (which looks very similar to Fig. 2 left). It's amazing that the unwanted component aroused by Δd closely resembles the CMB quadrupole component claimed by WMAP (Fig. 2 right); however, there is definitely no CMB signal in Δd! Thus it's quite reasonable to believe that the WMAP CMB quadrupole is largely artificial, and by this way the WMAP CMB results are strongly questioned. The above fact is also confirmed by Moss et al. (2010); Roukema (2010a). In Liu et al. (2010), we have also found out that the WMAP spacecraft attitude information (which determines the antenna pointing vectors) is not recorded synchronously with the signal difference D^i, which casts doubt on the antenna pointing estimation in WMAP mission. Such asynchronism can be seen directly by checking the TOD files, and it has also been confirmed by independent authors with different methods (Roukema 2010b; Liu & Li 2010c). Moreover, we have discovered that, even if the antenna pointing vectors are correctly calculated, there are other effects that can create an "equivalent" pointing error, which can work together with real pointing error to amplify the overall effect. In fact, the equivalent pointing error has a very high upper limit, thus it can also produce the entire WMAP CMB quadrupole alone (Liu & Li 2010b).

– 6 –

Since there are several inducements involved in the problem of the difference between our result and WMAP, and each inducement can affect several different aspects of the data processing, we manage to organize the involved systematical effects in this article, and put them into a clear uniform frame, by which we will be able to see clearly what has been solved in each old work, and what is still unknown and need to be done in future work, so as to bring a possible solution to the problem.

2. THE DIFFERENCE BETWEEN OUR RESULTS AND WMAP

The most often seen results of the WMAP mission are the CMB anisotropy map and the CMB power spectrum, as shown in Fig. 1. The CMB anisotropy map produced in our work looks very similar to the one in the WMAP release, but we can find out the difference between them by subtracting our map from the WMAP one, and smooth the difference to a lower resolution (Fig. 2, left). It's interesting that, by doing so, we will obtain a map that is almost same to the quadrupole plot of the released WMAP CMB quadrupole (Fig. 2, right). Since all spherical harmonics are linearly independent, this indicates that for the quadrupole components Q_w of WMAP and Q_{ll} of us, we have $Q_w - Q_{ll} \sim Q_w$, with which we immediately get $Q_{ll} \sim 0$ without having to compute the CMB power spectrum. By computing the CMB power spectrum from our new maps, this has been confirmed and Q_{ll} is only about 20% of Q_w (Liu & Li 2009b). With later works, it's discovered that Q_{ll} could be as low as 8% of Q_w.

Not only the large scacle, but also the small scale CMB power spectrum has been computed for our new CMB anisotropy maps, which is also lower than WMAP, as shown in Fig. 3, In this figure, the power spectrum estimating process has also been validated by the good consistency between the CMB power spectra derived by us and by the WMAP team from the same WMAP released maps (solid and dotted lines).
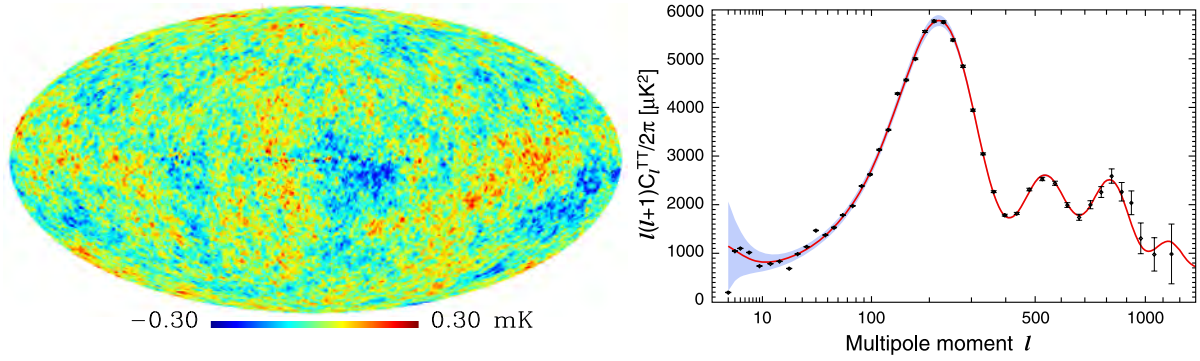
– 7 –

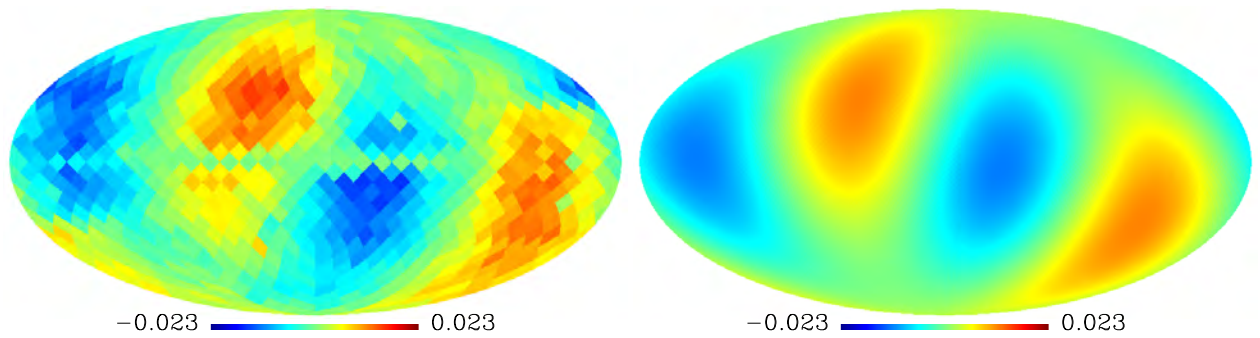Fig. 1.— The CMB anisotropy map and power spectrum obtained by WMAP.

Fig. 2.— *Left panel:* The difference in CMB anisotropy maps, WMAP minus ours, smoothed to $N_{side} = 8$. *Right panel:* The quadrupole component of the WMAP CMB anisotropy map. Both in Galactic coordinate and units of mK.

– 8 –

With the new CMB power spectrum, we have derived new best-fit cosmological parameters, as shown in Table. 1. For example, the dark matter density Ω_c is about 20% higher, and the dark energy density Ω_Λ is about 10% lower.

3.   WHY THE WMAP CMB RESULT SHOULD BE QUESTIONED

We have enough reason to question the WMAP result: Firstly, as presented in Fig. 2 of Liu et al. (2010) (looks very similar to Fig. 2 here), the released WMAP CMB quadrupole can be well reproduced without using any CMB data, which is very surprising. The correctness of this result has been confirmed by several authors (Roukema 2010a; Moss et al. 2010), and we have released the source code we used to accept worldwide verifications[1]. Moreover, in the same article, we have found evidence for an existing timing error by reading the WMAP TOD directly, which has later been independently confirmed (Roukema 2010b; Liu & Li 2010c). Another team from UK has also questioned the reliability of the WMAP beam profile, which can significantly affect the small scale CMB power spectrum (Sawangwit & Shanks 2010a,b). They have also provided a nice review about questioning our knowledge of the Universe (Sawangwit & Shanks 2010c). It's also suggested by Cover (2009) that the WMAP data calibration course should be more carefully checked in order to provide reliable CMB result: He tried to recalibrate the WMAP TOD and found out that, if the calibration parameters are allowed to change, then we can get a better fit even if there is no CMB anisotropy. In other words, the CMB anisotropy is too weak that it can

---

[1]The source code is available at the web site of Tsinghua Center for Astrophysics:

http://dpc.aire.org.cn/data/wmap/09072731/release_v1/source_code/v1/,

and the CosmoCoffee forum: http://cosmocoffee.info/viewtopic.php?p=4525#4525

– 9 –

Table 1: The best-fit cosmological parameters

| Description	Symbol	Value		
		WMAP5-only [1]	WMAP5+BAO+SN [1]	This work
Hubble constant (km/s/Mpc)	H_0	$71.9^{+2.6}_{-2.7}$	70.1 ± 1.3	71.0 ± 2.7
Baryon density	Ω_b	0.0441 ± 0.0030	0.0462 ± 0.0015	0.053 ± 0.0030
Dark matter density	Ω_c	0.214 ± 0.027	0.233 ± 0.013	0.270 ± 0.027
Dark energy density	Ω_Λ	0.742 ± 0.030	0.721 ± 0.015	0.677 ± 0.030
Fluc. Ampl. at $8h^{-1}$ Mpc	σ_8	0.796 ± 0.036	0.817 ± 0.026	0.921 ± 0.036
Scalar spectral index	n_s	$0.963^{+0.014}_{-0.015}$	$0.960^{+0.014}_{-0.013}$	0.955 ± 0.015
Reionization optical depth	τ	0.087 ± 0.017	0.084 ± 0.016	0.109 ± 0.017

[1] from Hinshaw et al. (2009)
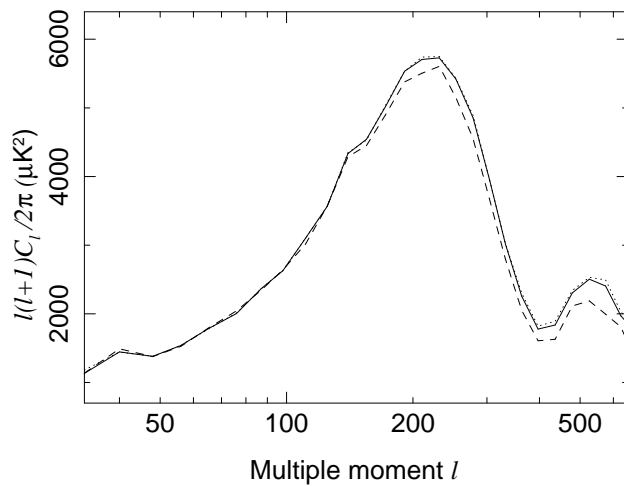
Fig. 3.— The CMB power spectra derived with our software from our new map (*dash line*), with our software but from the WMAP official maps (*dotted line*), and directly released by the WMAP team (*solid line*).

– 10 –

possibly be twisted by potential calibration uncertainties. This is probably the only publicly available 3rd-party work that has reached the very difficult WMAP data calibration course.

4.   ORGANIZING THE INVOLVED SYSTEMATICAL EFFECTS

As a preparation, let's introduce some basic things about the TOD. The TOD consists of the CMB signal, the Doppler dipole signal d, the foreground F, the 1/f noise, the observation noise n, and possible systematical deviation δ, as shown here in sequence:

$$D = T_A - T_B + d + F + f^{-1} + n + \delta \tag{1}$$

The TOD are derived from uncalibrated TOD by a calibration process, in which the system gain G and baseline B are determined:

$$D_{uncal} = B + G \times D \tag{2}$$

Most work mentioned in this article is related to the antenna pointing error. What makes things confusing is that there are several inducements of the pointing error and several impacts produced by the pointing error. It's easy to confuse them three, thus we should keep in mind the logical relationship:

$$Inducements \rightarrow PointingError \rightarrow Impacts \tag{3}$$

There are at least three kinds of inducements: direct pointing error, something like, e.g., the antenna has been misplaced; pointing error caused by timing error (Liu et al. 2010); equivalent pointing error caused by the side-lobe response uncertainty (Liu & Li 2010b). As for the impacts, there are at least four: the Doppler dipole signal d and the map-making from TOD to sky map are both affected by pointing error, and both can occur in either calibration processes or post-calibration processes, thus the combinations are four. Although there are

– 11 –

several inducements and impacts, the connecting point is uniform: the pointing error. Thus we call the combination of each inducement with each impact an individual systematical effect: $3(Inducements) \times 4(Impacts) = 12(Sys.Err)$, thus there are 12 different combinations. With each work, some of the combinations can be confirmed, whereas some of the combinations may be rejected. We give a list of the inducements and impacts in Table. 2, so as to refer to them by numbers hereafter.

5.   OVERVIEW OF PREVIOUS WORKS

With the organized systematical effects, we can now start to summarize previous works and see what we have actually done in each work.

First of all, in Liu & Li (2009b), we have obtained different CMB results to the WMAP release in both large-scale and small-scale; however, the large-scale difference is determined by the systematical effect combination 1, 2, 3 with 1, 2, 3 (inducements first, then impacts, same henceforth), and the small-scale difference is determined by the combination 1, 2 with 1, 2, 4. However, in later work by Roukema (2010a), the combination 1, 2 with 4 for small-scale difference has been rejected. The combination 1, 2 with 1, 2 for the small scale difference is still possible, which need to be checked in the future.

Table 2: List of the inducements and impacts of the pointing error

	Inducements	Impacts
1	Direct	Doppler, in calibration
2	Timing	Mapmaking, in calibration
3	Equivalent	Doppler, post-calibration
4	–	Mapmaking, post-calibration

– 12 –

Several months later, in Liu et al. (2010), the inducement 2 is discovered with a suggested timing error amplitude of 25.6 ms, and this was soon confirmed by the following works of Roukema (2010b) and Liu & Li (2010c). Also in Liu et al. (2010), we have discovered that the WMAP CMB quadrupole can be reproduced without using any CMB data, which strongly suggests something wrong in the data processing, especially when the fact has later been confirmed by Roukema (2010b) and Moss et al. (2010). In other words, given this fact, at least one of the 12 combinations should be true, and the true CMB quadrupole is likely to be nearly zero. As explained in § 1, this strongly implicates that the standard cosmology is violated.

Then, in Liu & Li (2010b), we have discovered inducement 3, and this is the first time for us to realize that, even if the antenna pointing vectors are absolutely accurate, there is still effect that can produce equivalent pointing error, which can even produce the entire WMAP quadrupole component alone. Thus we have developed a method of model fitting, trying to ignore the sources and remove all similar effects together on the large-scale.

Recently, the existence of the timing error has been confirmed by Roukema (2010b) in temperature map space and by Liu & Li (2010c) in TOD space. The most important difference between these two works is that, they are done in the TOD and CMB map respectively, which are two different spaces: The mapping from TOD to CMB map is multi-to-one[2], but the inverse mapping is one-to-one. By working purely in the TOD space, we can completely ignore the mapping attribute between the two spaces and obtain a straightforward evidence. Although the two works are essentially different, they have come to very well consistent results: the WMAP TOD timing is rejected at $> 8\sigma$ by both, and both found out that the suggested 25.6 ms timing error is within 1.7σ. Thus inducement 2 stands a good chance to be true, as well as the possibility

---

[2]Theoretically speaking, this mapping is one-to-multi, because the monopole in the CMB map can be any value. However, in practice, significantly different TOD can bring to nearly same CMB map, especially for the large-scale, thus it's more useful to regard the mapping as multi-to-one.

– 13 –

of combination 1, 2, 3 with 1, 2, 3: As mentioned above, the large scale difference between WMAP and us is determined by such a combination.

6.   DISCUSSION

As discussed in Sec. 3, we have enough reason to question the current WMAP result for the quadrupole of the CMB anisotropy, especially with the discovered fact that the WMAP quadrupole can be reproduced without using any CMB data. As for the small scale, some of the systematical effect combinations responsible for the CMB small-scale power spectrum difference has been rejected, but not all, thus we should still be careful, especially when there are works suggesting extra uncertainty for the small-scale coming from the beam profile issue (Sawangwit & Shanks 2010a,b,c).

An apparent advantage of our new map is that the axis-of-evil will disappear. It has been discovered since the first WMAP release that the WMAP CMB quadrupole and Octupole are aligned (de Oliveira-Costa et al. 2004; Eriksen et al. 2004; Jaffe et al. 2005; Schwarz et al. 2004), which is called the axis-of-evil problem; however, in our work, the quadrupole has almost disappeared, thus they are no longer aligned (Liu & Li 2009b) and the problem of axis-of-evil has been softened.

However, even with our new maps, there are still unexplained anomalies. In previous works, we have discovered that the pixels that are $141°$ away from hot galactic pixels are systematically cooled (Liu & Li 2009a), which is called a $141°$ ring cooling effect. This work has been independently confirmed by Aurich et al. (2009) and they have also discovered that, by removing the pixels affected by the cooling effect, the large-scale CMB two-point correlation function seem to be better consistent to the ΛCDM expectation (their Fig. 6). In another work (Li et al. 2009), we have discovered that the WMAP CMB temperatures are correlated with the number of

– 14 –

observations, which is apparently abnormal. In our new maps, it's true that these two anomalies become weaker, but they still exist, remind us that there might be even more undiscovered imperfections in the WMAP data.

There are several works involving the pointing error in the calibrated TOD, but few work has been done to the uncalibrated TOD like Cover (2009). Study in this area could possibly give an answer, or at least more helpful evidences to the problem.

– 15 –

REFERENCES

Aurich, R., Lustig, S. & Steiner, F., 2009, Class. Quantum Grav., 27, 095009

Bennett, C. L. et al., 2003, ApJ, 583, 1

Cover, K. S. 2009, Europhysics Letters, 87, 69003

Gorski, K. M. et al., 2005, ApJ, 622, 759

Hinshaw, G. et al., 2003a, ApJS, 148, 63

Hinshaw, G. et al., 2003b, ApJS, 148, 135

Hinshaw, G. et al., 2007, ApJS, 170, 288

Hinshaw, G. et al., 2009, ApJS, 180, 225

Jarosik, N. et al., 2010, arxiv:1001.4744

Li, T.P., Liu H., Song L.M., Xiong S.L., & Nie J.Y. 2009, MNRAS, 398, 47

Liu, H. & Li, T.P. 2009a, Sci China G-Phy Mech Astron, 52, 804; arXiv:0809.4160v2

Liu, H. & Li, T. P. 2009b, arXiv:0907.2731

Liu, H. & Li, T. P. 2010a, Chin. Sci. Bull., 55, 907

Liu, H. & Li, T. P. 2010b, arXiv:1005.2352

Liu, H. & Li, T. P. 2010c, arXiv:1009.2701

Liu, H., Xiong, S. L. & Li, T. P. 2010, arXiv:1003.1073

Limon, M. et al. 2008, Available in electronic form at http://lambda.gsfc.nasa.gov; *Wilkinson Microwave Anisotropy Probe (WMAP) : The Five-Year Explanatory Supplement*, Greenbelt, MD: NASA/GSFC (2008)

– 16 –

Moss A., Scott D. & Sigurdson K. 2010, arxiv:1004.3995

Nolta, M. et al., 2009, ApJS, 180, 296

Roukema, B. F. 2010a, A&A, 518, A34

Roukema, B. F. 2010b, arxiv:1007.5307

Sawangwit, U., & Shanks, T. 2010, arXiv:1006.1270

Sawangwit, U., & Shanks, T. 2010, MNRAS, 407, L16

Sawangwit, U., & Shanks, T. 2010, Astronomy and Geophysics, 51, 050000

de Oliveira-Costa, A., Tegmark, M., Zaldarriaga, M. & Hamilton, A. 2004, Phys. Rev. D, 69, 063516

Eriksen, H.K., Hansen, F.K, Banday, A.J., Grski, K.M. & Lilje, P.B. 2004, ApJ, 605, 14

Schwarz, D.J., Starkman, G.D., Huterer, D. & Copi, C.J. 2004, Phys. Rev. Lett., 93, 221301

Jaffe, T.R. et al. 2005, ApJ, 629, L1

This manuscript was prepared with the AAS LATEX macros v5.2.

Primordial Planet Formation

Rudolph E. Schild[1,2]

[1]Center for Astrophysics, 60 Garden Street, Cambridge, MA 02138, USA

[2]rschild@cfa.harvard.edu

and

Carl H. Gibson[3,4]

[3]University of California San Diego, La Jolla, CA 92093-0411, USA

[4]cgibson@ucsd.edu, http://sdcc3.ucsd.edu/~ir118

ABSTRACT

Recent spacecraft observations exploring solar system properties impact standard paradigms of the formation of stars, planets and comets. We stress the unexpected cloud of microscopic dust resulting from the DEEP IMPACT mission, and the existence of molten nodules in STARDUST samples. And the theory of star formation does not explain the common occurrence of binary and multiple star systems in the standard gas fragmentation scenario. No current theory of planet formation can explain the iron core of the earth, under oceans of water.

These difficulties are avoided in a scenario where the planet mass objects form primordially and are today the baryonic dark matter. They have been detected in quasar microlensing and anomalous quasar radio brightening bursts. The primordial planets often concentrate together to form a star, with residual matter seen in pre-stellar accretion discs around the youngest stars.

These primordial planet mass bodies were formed of hydrogen-helium, aggregated in dense clumps of a trillion at the time of plasma neutralization 380,000 years after the big bang. Most have been frozen and invisible, but are now manifesting themselves in numerous ways as sensitive modern space telescopes become operational. Their key detection signature is their thermal emission spectrum,

pegged at the 13.8 degrees Kelvin triple point of hydrogen, the baryonic dark matter (Staplefeldt et al. 1999).

Keywords: Dark Matter; Planet Formation: Cosmic structure

1. Introduction

Recent discoveries of numerous planets seen orbiting ordinary stars in the local universe caught some, but not all, astronomers by surprise. The common view among professionals, shared with the general public, was that all such planets were formed in dust discs of the star as it formed and were caused by the star formation. Planets were seen orbiting in flat discs around the several stars with near-perfect edge-wise orientation to the human observer, many large and close to the star. An alternative view (Gibson, 1996) claimed all the hot, primordial, H-^{4}He gas emerging from the plasma epoch transition to gas would fragment under viscous-gravitational control to form planetary-mass gas clouds in dense clumps of a trillion. Rather than planets forming from stars, all stars should form from these primordial gas planets within their protostarcluster clumps.

It has been long recognized that most of the ordinary matter - protons, neutrons, and electrons as well as the atoms they constitute, are unseen and therefore were called baryonic dark matter. But although dark to most observations, the material had a gravitational signature from which it was understood to be present in large amounts in the Halo of our Milky Way Galaxy. So it was concluded that if it has a gravitational signature it should be possible to use the light bending properties of mass to detect the dark matter as gravitational lenses.

This idea received a strong boost when studies of the gravity associated with lensing galaxies seen along the paths to multiply imaged quasars gave a direct detection of the grainy texture of the lensing gravity, demonstrating that the mass of the lensing galaxy is dominated by objects with approximately the mass of the Earth, with stars

making only a minor contribution (Schild, 1996). The mass could be estimated because the duration of events was quite short, approximately a day. The most extreme event found had an observed duration of only 12 hours, which, because of the cosmological expansion of time, corresponded to a time of only 5 hours referenced to the clock of an observer at the luminous quasar (Colley and Schild, 2003). Events caused by a microlensing star should have 30-year duration (Schild and Vakulik, 2005) and the frequently observed microlensing signal in Q0957+561 must be caused by a planetary object with a millionth of a solar mass.

Such rapid events represented a remarkable feat of nature. Recall that a quasar has 100 times the luminosity of an ordinary galaxy like our own Milky Way, and the observed 5-hour brightening and fading event seen as a 1% brightness change thus represents somebody effectively throwing a switch and all the luminosity equivalent to the billions of stars in a distant galaxy being switched on and off in 2 1/2 hours.

This is not really what happens, of course. It is a trick of nature operating through the Einstein General Theory of Relativity, whereby the gravitational field of a planet mass body comes perfectly into the line of sight to the distant quasar, and the gravitational field deflects the quasar brightness to a different direction, producing a brightness fading to some other observers at some other places. So although it was understood that the observation of a 5-hour microlensing event evidenced a multitude of free-roaming planets in the lensing galaxy at a redshift of 0.37, called rogue planets, they were in a cosmologically remote galaxy and not amenable to close study by direct observation. Rather than eight planets per star observed in the solar system the quasar microlensing result requires an average of many millions.

It was desirable to find such objects closer to home where they could be studied individually, and searches closer to home, in the Halo of our Galaxy where they had already been seen in aggregate stabilizing the rotation structure, but unfortunately most searches organized assumed a stellar mass, and the gravitational signature was therefore not found. (Alcock, C. et al. 1998). Even as the rapid brightness

fluctuations corresponding to light bending from planet mass objects were being recognized in more lensed quasars, the Halo searches continued to disappoint. This was largely because it was being assumed that the dark matter would be uniformly distributed in space, contrary to the common observation that stars tend to cluster on all size scales, from double stars to star clusters to galaxies and their clusters.

The decisive observational clue came with a technological development, when detectors capable of measuring the feeble radiation of any object even slightly above that absolute zero of temperature were fitted to balloon-borne and orbiting telescopes. Already in 1985 the IRAS spacecraft had detected a feeble signature understood to be coming from all directions but unfortunately called "cirrus dust" clouds because of the way the radiation seemed to be a mottled distribution above and below the galaxy's disc (Low et al, 1984). Only when more recent generations of infrared and sub-millimeter detectors had been developed could the true nature of the feeble signature be understood.

This happened suddenly when maps of the sky taken by different spacecraft (COBE, IRAS, Boomerang, WMAP) operating in the same direction toward the Halo were intercompared (Veniziana et al. 2010) and the same structures seen. Because the different spacecraft detected different wavelengths, the inter-comparison allowed the temperature of the feeble structures to be measured, though at first still thought to be the infrared radiating dust clouds. Only when it was recognized that the temperature was being consistently found to be the same for all directions could the nature of the "infrared cirrus" be correctly inferred (Nieuwenhuizen et al. 2010). Figure 1 (Gibson 2010 Fig. 1) shows some of the Veniziani et al. (2010) evidence, compared to our interpretation that the "dust" of the "cirrus clouds" is actually primordial planets in their protoglobularstarcluster PGC clumps. The size of the observed clumps 4×10^{17} meters closely matches the size of a globular star cluster.
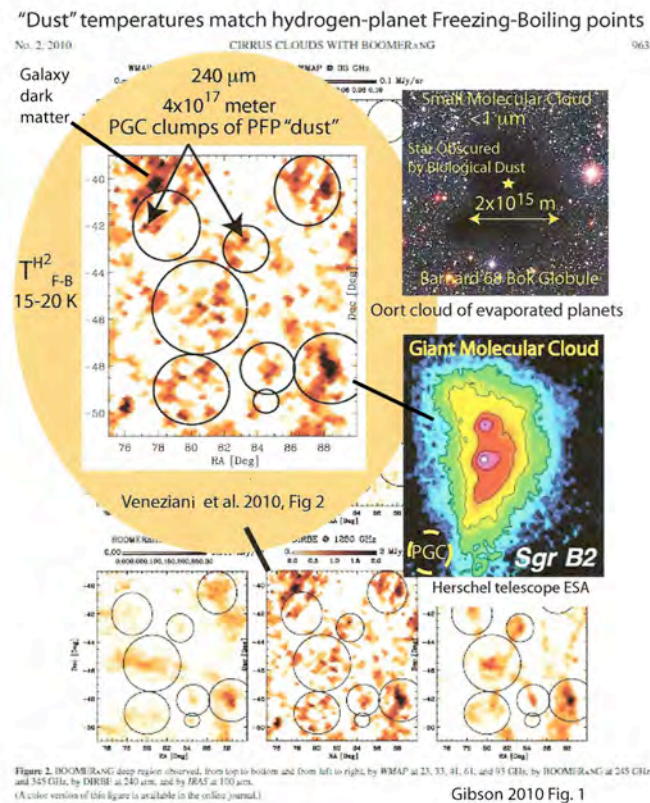
Fig. 1. Oval at left top is an image of so-called cirrus "dust" clouds of the Milky Way Galaxy (Veniziani et al. 2010, Fig. 2) at DIRBE microwave wavelength 240 µ compared to three other microwave images at the bottom showing the same features. The "dust" temperatures match the freezing to boiling point thermostat range of ~ 15-20 K for hydrogen planets, therefore indicated as the "dust". Thus cirrus "dust" clouds are "Giant Molecular Clouds" (right center), presently interpreted as clumps of planet clump PGCs representing the Galaxy dark matter. The dark matter is obscured for optical wavelengths < 1 µ as shown (right top) for a star or stars obscured by an Oort cloud of microscopic PAH dust produced as planets are accreted and evaporated.

It is easy to see from Fig. 1 that the cirrus dust clouds are the Galaxy dark matter simply by estimating the number of PGC clumps of primordial planets from the images, realizing that each protoglobularstarcluster PGC clump represents a dark matter mass of more than a million stars. Comparing the DIRBE 240 µm image with the Herschel Sgr B2 image of a dense molecular cloud, we infer an average PGC density on the sky of about 20 PGCs per square degree. Since there are 38,800 square degrees on the sky, and since each PGC has mass ~ 10^{36} kg, we estimate the "cirrus cloud" mass to be ~ 10^{42} kg, as expected if the "dust" of the clouds is primordial planets and the "clouds" are PGC clumps.

Detection of μBD planetary objects from temperature happened because the temperature found was an important one in the physical chemistry of hydrogen, the most common element in the universe and the most probable candidate for the ordinary dark matter. Hydrogen is a gas that condenses to liquid and then forms solid ice at low temperatures.   It has large latent heats of evaporation and fusion, so a thermostat temperature range between the triple point temperature and critical temperature is the signature of a cloud of gas planets cooled by outer space and heated by adjacent stars and friction. A range of cloud temperatures between the triple point and critical point matches a range of planetary masses in dark matter planet clouds either cooled by outer space or heated by adjacent stars. Thus if we imagine a primordial planetary atmosphere slowly cooling by radiating into space, it will remain at its triple point temperature for a long time as the hydrogen gas condenses to hydrogen snow and the heat of condensation slowly radiates away, producing a thermal signature pegged at the triple point temperature as observed.

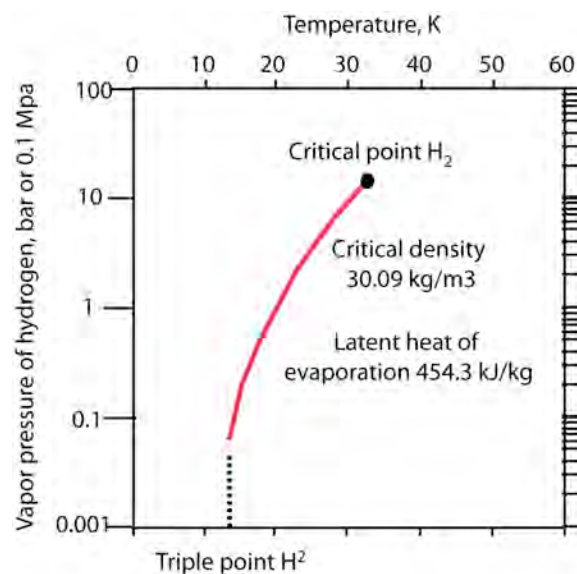Fig. 2. Vapor pressure of gas-liquid H_2 between its gas-liquid-solid triple point and gas-liquid critical point. The large latent heat of H_2 evaporation thermostats PGC dark matter planet clouds to a 14-30 K triple point-critical point temperature range.

The hydrogen gas triple point temperature is 13.8 degrees Kelvin. The temperature inferred from the intercomparison of spacecraft observations (Veneziani et al,

2010) was inferred to be 15-20 K with small variation between the observed structures, about as expected. Thus the radiating mass in the halo of our galaxy can be inferred to be predominantly clouds of frozen hydrogen planets, particularly because nobody had ever predicted that "infrared cirrus" composed of interstellar dust grains would have this universally measured temperature. From Fig. 2, frozen hydrogen on microscopic dust grains in a vacuum would rapidly evaporate.

When this was realized, it was immediately obvious why temperatures measured for halos of other galaxies (going back to Price, Duric, & Duncan, 1994 with many similar determinations since) also were approximately 15 degrees Kelvin. Thus it is now apparent that a way exists to detect the ordinary dark matter anywhere it aggregates in the cold vastness of space, and this will provide an important tool to study the dark matter structures formed in galaxy collisions and in galaxy clumps, from its thermal emission. These temperature determinations are now common from PLANCK and HERSCHEL spacecraft data.

It is important to ask this question. If these hydrogen clouds are in fact the outer atmospheres of primordial planets that are the universal ordinary dark matter, at what time after the Big Bang (at what redshift) did they cool below the hydrogen triple point temperature? Recall that when the primordial planet clump structures seen today formed at the time when the universe had a temperature near 4000 K so that the expanding plasma had an important viscosity decrease 380,000 years after the big bang, freeing the gas to fragment into the planet-mass structures that would have been cooling ever since. Contraction would have re-heated their centers, whence monotonic cooling must have occurred, even as the background of remnant big Bang radiation would itself have been monotonically cooling, and is measured today to be 2.73 K. At some point the background temperature must have passed through the 13.8 degree hydrogen triple point, and the primordial planetary objects would have begun to freeze out hydrogen to become hydrogen ice which would have then snowed down through the atmospheres to the planetary surfaces. We will consider below how this produced dramatic weather effects on the primordial

planets, but we wish here to discuss what the effects of the shrinking snowing atmospheres would have had on the UV-optical light transmission of the universe.

Given the present temperature of the universe and the rate the temperature falls with redshift, we easily calculate that the remnant Big Bang radiation and hence the temperature of the universe fell below the 13.8 degree hydrogen triple point temperature at redshift z = 6.0. It has already been noticed that distant quasars evidence a dramatic change in the transparency of the universe to hydrogen sensitive wavelengths at redshifts of approximately 6.3 (Fan et al, 2006). Presently this is attributed to a "re-ionization" of the hydrogen gas of the observable universe at this redshift, but with no explanation of exactly why at the particular observed redshift of 6.3. In particular, there had been no prediction that the transmission of the universe would have dramatically increased at z = 6.3. The possibility that the transparency of the universe should be significantly affected by the atmospheres of a population of primordial planet clouds has already been considered by Schild and Dekker (2006).

We predict that if the hydrogen transparency increase of the universe is due to shrinking primordial planet atmospheres, other observational manifestations should be discovered. For example, the shrunken planets would have lower cross sections for collisions with implications for changes in their collisional dynamics, increasing diffusion of the PGC planet clouds from the galaxy central core to form the galaxy dark matter halo. With suddenly smaller atmospheres there would be fewer planet collisions and Ofek et al. (2010) events as the star formation rate decreases. In some ways it can be seen that the cooling of the universe below the hydrogen triple point represents a phase change, which will have implications for the rate of aggregation into stars and in their collisional interaction signatures (Nieuwenhuizen et al. 2010).

2. Detection of Primordial Planets

As the population of primordial planets has been evolving throughout the history of the universe, their detection will be complicated according to the redshift being probed. In the local universe, we see the objects in experiments related to microlensing of quasars, where a distant quasar at a redshift of approximately 2 is seen aligned with a foreground galaxy at a typical redshift below 1. As the global gravitational field of the lensing foreground galaxy creates multiple images of the distant quasar, the individual objects within the lensing galaxy in line with the background quasar can modify the quasar light further. This created signatures of any mass bodies in the lensing galaxy, and signatures of stars (Schild & Smith, 1991). Planets (Schild 1996), and star clusters (Mao and Schneider, 1998) have been recognized.

Here we are particularly interested in the planet signatures. Because of the small brief structures caused by quasar-planetary alignments, the planet signatures are discussed under the topic of microlensing, or even nanolensing, and the first demonstration of the phenomenon operating at planetary scale by Schild (1996) in quasar Q0957+561 was quickly followed by discoveries in other gravitational lens quasar systems.   In Q2237 (Vakulik et al. 2007), a microlensing event from a 0.001 M_{Sun} free-roaming (Jupiter mass) planet was found. Systems 0B1600+43, (90 day microlensing, 0.0001 M_{Sun} (Burud et al, 2000), RXJ 0911.4, 90 days, 0.0001 M_{Sun} (Hjorth et al, 2002), FBQ 0951 (Jakobsson, et al, 2005, SBS1520 and FBQ 0951 (90 day, 0.0001 to 0.0001 M_{Sun} (Paraficz et al, 2006) produced similar detections.

By far the best brightness monitoring data revealing the microlensing signature is from the first discovered and longest monitored system, Q0957+561. This is because it has the best-determined time delay, accurate to 0.1 day (Colley et al, 2003). Recall that the quasar microlensing is revealed by comparing two images of a multiply imaged quasar and correcting for the delay between arrival of the multiple images. The only quasar with delay measured to such 0.1 day precision is

Q0957+561, following an intense monitoring effort by an international consortium (Colley et al. 2003). This allowed Colley and Schild (2003) to securely detect an event with a 12-hour total duration, the most rapid ever detected. A wavelet analysis of the longer brightness record in this quasar lens system demonstrated several hundred microlensing events (Schild 1999).

But because these were all planet mass bodies seen in remote galaxies, it was desirable to detect the objects in the Halo of our own Galaxy. Unfortunately the results of 2 research consortia that sought the primordial planet signal failed in spite of monitoring 7 million stars in the Large Magellanic Cloud for the microlensing signature. While published accounts make the claim that the objects do not exist and ignore the many detections in the quasar lens systems, it is easy to understand that the local failures result from systematic errors of assumptions, like the assumption that the hydrogen atmosphere would be too small to cause refraction, or the assumptions about the sizes of the stars monitored. Microlensing consortia (MACHO, EROS, OGLE etc.) have made the fatal assumption that the planetary objects they claim to exclude are uniformly distributed: not clumped and clustered as observed in Fig. 1. Thus, they have excluded nothing. New observations are planned focusing on stars with foreground planet clouds.

3. Weather on Heating and Cooling Primordial Planets

Although halo searches could not find the free-roaming planet mass bodies, many have since been found in star formation regions in the vicinity of the sun (Lucas et al, 2006; Marsh et al, 2010, Zapatero Osario, 2002). They would only be found in young star-forming regions because after their compressional heating they quickly cool and become no longer visible. Their present properties of temperature, spectrum, color, and luminosity have been measured and masses inferred to be planetary from model fitting. Objects so recently formed have normal solar metal compositions, unlike the primordial objects in general.

11

Many of the weather effects expected on the primordial planets would be related to weather phenomena known on earth and on other solar system planets. On Earth, latent heats of fusion and evaporization of water rather than hydrogen are important weather drivers, causing local heating of gas masses (clouds) and strong vertical motions. Freezing point temperatures of water ice are clear in clouds where rain and hail are formed. Horizontal winds are produced when atmospheric gases replace the vertical convective elements. The convecting elements are internally heated by latent heat of fusion and vaporization, and become driven out of local thermal equilibrium, further driving weather phenomena.

Images of primordial planet atmospheres formed by star heating are available from space telescopes. Figure 3 shows images of primordial planets evaporated near a white dwarf star in our nearest planetary nebula Helix.

Oort cavities are formed within PGC clumps of planets by the star formation process of accreting planets. As shown in Fig. 3, the Oort cavity size is $(M_{star}/\rho_{PGC})^{1/3} \sim 3 \times 10^{15}$ m, where $M_{star} \sim 1.5 \times 10^{30}$ kg is the mass of the star formed and ρ_{PGC} is the density of PGC planet clumps $\sim 4 \times 10^{-17}$ kg/m^3. Biological PAH dust from the evaporated planets fills the cavity, as seen by the Spitzer infrared space telescope image (bottom right). Smaller solar system scales are shown for comparison (bottom left). Matsuura et al. (2009) show hydrogen resonant images that reveal primordial planets and their wakes as well as planet proto-comets on their way to accretion that are invisible in the optical band Hubble space telescope image. The planets ejected by the plasma jet must refreeze when they reach distances of $\sim 10^{16}$ m from the central star and begin radiation to outer space.

Journal of Cosmology, Lorentz Center Workshop Proceedings, Sept. 27-Oct. 1, 2010   12
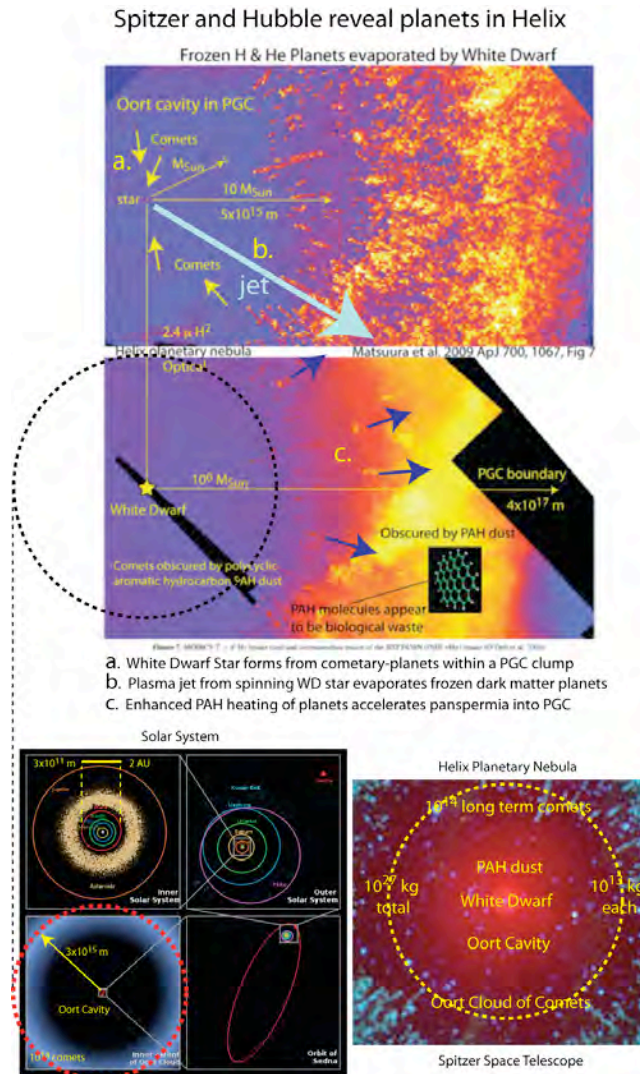

Fig. 3. Primordial planets heated and cooled in nearby planetary nebula Helix. A central white dwarf star is overfed by accreting primordial planets so that it contracts to high density $\sim 10^{10}$ kg/m^3 and its spin rate increases. A powerful plasma jet (blue arrow top) is produced that evaporates and radially expels some planets bounding the Oort Cavity. Some continue to fall into the cavity as comets (top image for a 2.4 µ infrared H$_2$ resonance).

New classes of weather are expected for the heated and cooled primordial planets of Fig. 3. Terrestrial weather is largely driven by direct heating of the Earth atmosphere and surface due to the absorption of sunlight, and the earth core is being heated from tidal forces. The primordial planets, in contrast, monotonically cool over the history of the universe, with external heating when stars are formed nearby. Furthermore the hydrogen atmospheres will initially extend far beyond the solid cores, where the Earth has lost most of its atmospheric gases, particularly

hydrogen, and the present earth atmosphere extends only a small fraction above its solid-core radius.

This will create the potential for much larger velocities and more violent atmospheric effects. We recall that the escape velocity on earth is 11 km/sec. Thus infalling meteors and meteorites will have this velocity plus an "inter-solar system orbital velocity" of order 50 km/sec. Dissipation of the kinetic energy of these interlopers will cause local heating effects in the atmosphere and produce locally high winds.

Terrestrial falling snow is limited to terminal velocity speed dominated by atmospheric friction. For the primordial planets there would presumably be a strong radial center-to-edge temperature and density gradient, and hydrogen ice would ordinarily form at the top of the large atmosphere. Falling hydrogen ice should accumulate and create snowballs of unknown size and density contrast over their long journey to the surface, perhaps even becoming crystalline and comparable to hail stones, with potential for larger velocities limited to the escape velocity, but perhaps limited to the local sound speed.

Recall that observations of solar system comets seem to show surfaces of compressed icy solids and powdery dust (Kearsley et al. 2008). Mean densities of comets are approximately a quarter of terrestrial crystalline rock densities, suggesting a powdery consistency throughout. This suggests that the surfaces of Oort Cloud comets were formed at the time of formation of the sun, in hydrogen ice snowstorms.

Modern observations of Kuiper belt and Oort cloud objects allow sizes to be measured, and mean densities to be inferred in cases of binary objects. With the understanding that these outer solar system objects had a primordial origin, where a contracting hydrogen cloud developed a heated center that was hotter for larger objects, it is possible to make a prediction about measured densities as a function of

total mass. In this picture the most massive objects had the hottest core and the largest hydrogen envelope, so they remained longest with elevated temperatures and attracted the most dust which would melt at the central core. Subsequent slow evaporation of hydrogen would have left relatively more time to add to the central core of molten stratified dust. And since the present day cool object has a relatively larger fraction of metals in solidified crystalline material, the heavy remnants will have a higher mean density than the lighter remnants, which accumulated more dust on the surface where it remained a more porous dust layer.

These speculations are only intended to remind that strong weather forces would be expected where the primordial planets have potentially larger atmospheres and a potentially large overall temperature gradient. With strong forces potentially in play, stratified turbulence is also likely, as will be discussed in a companion report focused upon the analysis of atmospheric forces and universal similarities. A variety of stratified turbulence and turbulent mixing signatures within the planet cluster containing the sun have been identified from radio telescope signals (Gibson 2010).

4. When and how did planets form?

The traditional view of the formation of the Earth and all planets seen orbiting stars is that formation began in pre-stellar discs around newly forming stars. The only ingredients presumed available are microscopic interstellar dust particles, plus primordial gases dominated by hydrogen. This is supposed to occur within "cores" of large gas clouds having sufficient mass to make hundreds or thousands of stars.

However there is presently no theory of where the gas clouds came from in the first place, and the process by which cores form is not understood, since it is believed that the predominantly hydrogen gas cannot cool rapidly enough to prevent compressional heating generating pressure that would re-expand the cloud core.

Recent developments in understanding of hydrodynamical forces on the expanding Big Bang gas with dissipative viscous forces produce a very different picture

(Gibson, C. & Schild, R. 2003). Within low 10^{-5} density enhancements structure formed by the condensation-void separation process on mass scales of galaxies to galaxy clusters before recombination. At plasma neutralization, 380,000 years after the Big Bang, the entire baryonic matter content of the universe underwent a very large decrease in viscosity, freeing up the gas to further condense on mass scales of planets (primordial-fog-particles, PFPs, in the discovery reference Gibson 1996) and of cluster mass aggregates with 10^6 M_{Sun}. Notice that this produces a hierarchical clumping of mass on scales of planets within clusters within galaxies within clusters of galaxies. But in particular, no stars formed primordially within this framework.

In this picture, the newly formed structures in quiescent universal expansion would develop small random motions, and as the process of separation and condensation was underway locally, some of the cluster scale perturbations would have interacted, jostling the contained primordial planets and causing some to collide and stick together, initiating pairing of pairs of pairs etc. for a bottoms-up aggregation that resulted finally in a structure massive enough that central temperatures climbed above the fusion temperature and density, and a star began to shine. Statistics describing the ubiquity of presently observed orbiting double/multiple stars and binary Kuiper belt objects result from this pairwise aggregating process. The ubiquity of dynamically double and multiple gravitating systems (Kern & Elliot, 2006) defy the simplistic gas fragmentation hypothesis of star and planet formation.

At the time of formation, 380,000 years after the big bang, the primordial planets would have been predominantly hydrogen gas spheres, with a radius comparable to the separation distance of 10^{14} m. Since then they would have gradually cooled and shrunk. Where these objects are seen near white dwarfs in planetary nebulae of the local universe like the central star of Helix (Fig. 3) they are called "cometary knots". The planet atmospheres are of size 10^{13} m (Meaburn et al, 1992), which is 100 A.U. Recall that a million of these had to aggregate to form the sun, which is compatible with the known diameter and volume of the Oort cloud. Such large objects would have swept up the interstellar medium of the Galaxy disc and Halo (Schild 2007) so

Journal of Cosmology, Lorentz Center Workshop Proceedings, Sept. 27-Oct. 1, 2010   16

the initial hydrogen composition would evolve to higher metal richness in parallel with the stellar population of the Galaxy.

The collection of interstellar dust by this mechanism can solve several problems in the planet formation scenario. Recall that the standard picture requires dust grains to collide and stick together, whence the larger grains also collide and eventually aggregate as planet mass bodies. The problem is that this process of colliding and sticking must be highly efficient for all mass scales, dust to pebbles to boulders to mountains to planets, since if it fails for any mass scale, the entire process breaks down. But colliding rocks together always produces simple recoil or fracturing. In the history of our civilization, nobody has reported two rocks colliding together and sticking. This point will be further discussed in the following section.

5. Iron cores of Planets

The theory of the formation of the planets is confounded by two observational facts. The widely accepted theory considers that planets were formed in pre-stellar discs that can be seen as the equatorial plane of several nearby stars with favorable orientation. Such discs can be found from infrared signatures in young star forming regions, and are known to dissipate and disappear on time scales of 5 million years (Currie et al. 2010).

However the mechanism by which the planets form within the disc is problematic. It is postulated that dust grains of oxides of iron and silicon etc found in interstellar space collide and stick together, producing larger grains that collide and stick, in an accretional cascade that eventually produces planets.

There is a serious problem with this scenario. The experiment has been done billions of times in our civilization, and rocks colliding with rocks have never been observed to stick together; they always recoil or break up. But the process must work efficiently for all sizes of colliding rocks from interstellar dust grains to stones

to rocks and mountains, or the process breaks down. Such an accretional cascade seems impossible.

Attempts to create the process in a laboratory have failed, as expected. These experiments have been summarized by Blum and Wurm (2008). It takes a careful reading to understand that the "Porosity index" quoted, consistently shows that the marginally sticking fragments are not held together by crystalline forces, but rather by much weaker van der Waals forces, and in a reference cited as "Schraepler and Wurm, unpublished data" it is noted that a single ballistic inbound particle breaks up the weakly bound chains and clumps, and the process breaks down.

This problem is sidestepped if the planets are formed in a two-step process, with the first step occurring after plasma neutralization and the second in the pre-stellar accretion discs around young forming stars. In the first step, which occurred in the long history following plasma neutralization at $z = 1000$ until approximately $z = 1$ when the sun formed, the primordial rogue planets roamed the Halo of the Galaxy and their large hydrogen atmospheres swept up all the interstellar dust distributed by supernovae and by carbon stars (Schild, 2007). The dust grains meteored into the hydrogen atmospheres and collected at the centers because of their metallic densities. Later, in the prestellar disc phase, strong interactions caused them to shed their hydrogen atmospheres to create the sun, and further collisions among them modified the population further, including removal of the residual hydrogen by evaporation.

A second important problem of planet formation is the iron core of the Earth. Anyone seeing rusting hulks of junked automobiles knows that iron has a strong propensity to oxidize, and every steel-maker knows how difficult it is to reduce iron oxide to base metal; it is done in high temperature blast furnaces in the presence of hot reducing carbon monoxide.

The metallic ions in interstellar dust are always found as oxides, so when and where in the universe was this processed to become iron cores of planets surmounted by oceans of water? This would naturally have happened when the mBD population of planet mass objects with very large hydrogen atmospheres roamed the universe and swept clean the interstellar medium. Interstellar dust grains would have meteored into the extended cooling hydrogen atmospheres and vaporized. The hydrogen is known to reduce any metal to form water which precipitates out, and the dense metallic vapors settled to the mBD center to stratify with all other metallic ions according to density, beneath an ocean of water.

These events would have been most common in the early universe, before z = 6 when cooling of the universe below the hydrogen triple point caused the atmospheres to freeze out hydrogen as snow and reduce the sizes of the atmospheres. At higher redshifts, $6 < z < 1000$, the planets would have had frequent collisions and mergers in their accretional cascades that sometimes produced stars. Release of gravitational binding energy would have re-heated the primordial planets, particularly their metallic cores, and the initially stratified reduced metals would have been smeared somewhat to become the ore deposits mined today.

Over the duration of the universe, the nature of planets would have evolved. At initial formation, such primordial planets would have had large sticky atmospheres but negligible relative motion in a quiescent expanding universe. This would have resulted in some collisional accretion even before the universe had created metals, and locally violent interactions would have produced further accumulations, generating a mass spectrum with a long tail toward higher sub-stellar masses but ultimately also stellar masses.

In this way, the first generation Pop III stars formed gently and early from hot large atmosphere gas planets of almost pure hydrogen. Their first generation of supernovae, plus the collapsing galaxy-central objects soon to become black holes after passing through a temperature realm sufficiently high to fuse hydrogen, would

have been the first luminosity in the universe, which at z = 1000 had cooled below 4000 K. With further expansion and cooling of the Universe, but also with accumulating larger relative motions, interactions of the primordial planets and their stars gradually increased.

In the hydrogravitational dynamics HGD picture of global structure formation, the above local scenario of star formation would have increasingly been affected by the events that shaped the formation and structures of galaxies. Over time, such events would have impressed larger relative velocities onto primordial planets and stars, increasing interactions and further accelerating accretional cascade from planets to stars. In addition, matter was also clumping from a redshift 1000 onwards on scales of Jeans Clusters, and just as the initial interactions of the quiescent expansion were few, there would have been some at first. The result would have been that a few such cluster mass objects would have interacted and the violent velocities generated would have triggered extensive star formation in globular clusters. With matter initially clumped as mBDs in Jeans Clusters, the initial interaction of two clusters would have strongly increased the process of collisional cascade, and the first luminosity of the universe would have been dominated by these collisionally interacting proto-globular-star-clusters. This would explain why the primordial globular clusters have profoundly different star formation histories and dynamics than the more recently forming open clusters. Without the primordial formation picture of Jeans mass structures, the origin of globular clusters has never been understood.

Subsequent star formation in the universe would have been predominantly in the Jeans cluster mass clouds fragmented into mBDs and their primordial sub-stellar cascade products, which are principally objects of less than Jupiter mass. This is inferred from the fact that the recently discovered planets found orbiting stars in the solar vicinity have a sharp upper mass limit of $\sim 10^{28}$ kg ~ 18 M$_{Jupiter}$ (Watson et al, 2010). But without the initial strong interactions of the HGD structure formation

picture, the difference between the presently forming open clusters and the ancient globulars has never been explained.

In the present day star formation in open clusters, stars are seen commonly forming as double and multiple stars, where the gas fragmentation picture does not generate such multiple systems. In the HGD scenario with primordial mBD formation, the multiple star seeds formed long before a recent jolt triggered star formation.

6. The HGD universal spectrum of mass fragmentation

A surprising result of the hydrogravitational dynamics HGD scenario of structure formation is the way the universe develops a fragmenting hierarchy of structure, with its key elements arranged in a top down sequence of structures of decreasing mass between voids expanding at the plasma sonic velocity near light speeds. It reflects the common observation that galaxies are usually found in clusters of galaxies, globular star clusters are in galaxies, and stars are found in clusters. It is clear that this should be true for the HGD fragmentational schenario since the instability of density minima is enhanced by the expansion of space but condensations on maxima is inhibited. The opposite is expected for the standard (but false) ΛCDM scenario where gravitational structures build up from small masses to large controlled by (impossible) cold dark matter CDM condensations and superclusters are the last rather than first structures to form.

We show in Figure 4 the predicted viscous fragmentation mass scales of the plasma and gas epochs (Gibson 1996). The length scale of fragmentation is determined by a balance between viscous and gravitational forces at the Schwarz viscous scale $L_{SV} = (\nu\gamma/\rho G)^{1/2}$, where ν is the kinematic viscosity, γ is the rate-of-strain of the fluid, ρ is the density and G is Newton's gravitational constant. For the first plasma gravitational structures to form, L_{SV} must become smaller than the scale of causal connection $L_H = ct$, where c is the speed of light and t is the time since the cosmological big bang. This occurs at time $t \sim 10^{12}$ seconds (about 30,000 years).

Momentum is transported in the plasma by photons that collide with free electrons, that in turn drag along their associated ions (protons and alph-particles). The kinematic viscosity ν is estimated (Gibson 2000) to be $\sim 10^{26}$ m^2 s^{-1}, γ is $\sim 10^{-12}$ s^{-1} and $\rho \sim 4 \times 10^{-17}$ kg m^{-3}. so $L_{SV} \sim 2 \times 10^{20}$ m $\sim L_H = 3 \times 10^{20}$ m. The mass scale is $\sim 10^{45}$ kg; that is, the mass of a supercluster of $\sim 10^3$ galaxies. The density ρ remains constant in the fragments with time but the masses of the subsequent fragments decrease because both ν and γ decrease as the universe cools and expands. The smallest plasma fragments are galaxies as shown in Fig. 4 on the right.

Notice, however, that the HGD structure formation scenario also has important consequences for the microlensing detection of its component objects. A concentric hierarchical structure boosts and increase on several scales at the same time. Insofar as the studies appear smaller than their projected Einstein rings, each consecutive structure increases magnification. The compounding of images behind a network of rogue planets behind a microlensing star has already been simulated by Schild and Vakulik (2003), but in principle the further lensing by a star cluster and galaxy need to be considered.
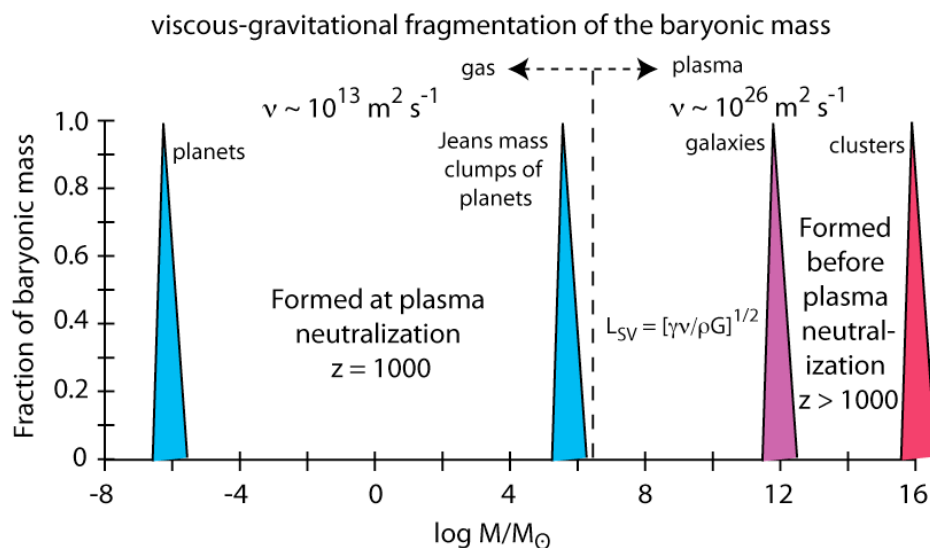

Fig. 4. Fragmentation of the baryonic mass under viscous-gravitational control. The first structures to fragment were at super-galaxy-cluster mass, when the horizon scale of causal connection ct exceeded the viscous-gravitational scale L_{SV} in the plasma epoch (right). At later times in the plasma epoch, lower mass concentrations down to galaxy

mass would form (Gibson 1996). A dramatic decrease in kinematic viscosity at plasma neutralization accounts for the decrease in fragmentation mass from that of galaxies to that of planets in clusters.

In the plasma epoch, galaxy super-clusters formed first, and subsequent structure formation decreased at plasma neutralization to a minimum mass scale of galaxies (10^{42} kg) within clusters, and with characteristic $\delta T/T$ amplitude of 10^{-5}. With the severe viscosity drop to $\nu \sim 10^{13}$ m^2 s^{-1} at the time of plasma neutralization 10^{13} seconds, internal structure formed on scales of Jeans clusters and planets, but not stars. The latter would be formed in an accretional cascade of planet mass hydrogen spheres, as mathematically simulated by Truelove (1997) who, however, treated them as "numerical instabilities" in his calculation. With a turbulent hydrodynamical formation scenario, it would be unsurprising if the scales of structure formation in the universe, from galaxy super-clusters, galaxies, star clusters, to planets, follow a self-similar mathematics (Oldershaw, 2010).

The remainder of this section describes how to reasonably understand the broad range of Solar System objects found in the local universe: planets, KBO's, asteroids, comets, and meteorites.

At the time of plasma neutralization, the temperature of the universe was ~ 4000 K and no metals existed. As the universe cooled, a first generation of massive stars resulted in supernova enhancement of the interstellar medium, and the hydrogen gradually became contaminated with metals. This would have happened on a time scale of 10 million years (Gibson, 1996; Gibson and Schild, 2010).

From the known objects studied within our Solar System, we infer that the lowest mass objects had cooled sufficiently at their centers that any inbound dust collected at the center without melting. Some transitional objects would have a small molten core which cooled sufficiently quickly that its outer layers never melted in a hot core. The still more massive objects would have retained a molten core longer and developed density stratified layers of minerals from later generations of

supernovae. Collisions of the mBD would have re-heated the cores and redistributed the stratified layers to form ores of the elements and primary compounds. The objects probably retained their extensive hydrogen envelopes, until interactions in the pre-solar accretion disc stripped away the hydrogen. Since the most massive mBD objects in this pre-solar processing would have been hotter if more massive, The HGD formation picture makes the qualitative prediction that the presently observable mean density should be highest for the most massive mBDs.

At the time of the Sun's formation, a million of these objects would have aggregated as the solar mass, leaving only nine planets in a pre-solar nebula with an accretion disc. Violent collisional events would have dumped most of the objects into the forming sun, ultimately stripping most bodies of their hydrogen and leaving the cores in the orbital plane.

In the pre-solar nebula, also called the accretion disc plane, a second period of structural modification took place. Collisions between pre-planetary bodies created meteoritic material, and re-heated and smeared the planetary interiors, mixing the metallic ores, and ejecting some of the bodies entirely. In this phase higher local densities and velocities would have stripped all bodies of their residual hydrogen outer atmospheres, and left nine planets, small meteoritic rocks, larger asteroid fragments, and unprocessed material in the distant Kuiper Belt and Oort cloud.

7. Surprises from the NASA's space missions STARDUST and DEEP IMPACT

An important confirmation of the 2-epoch planet formation scenario is seen in the quite unexpected results of the 2004 STARDUST space mission, in which dust grains released by Comet Temple I were collected in a jell that flew by the astronomical body (Brownlee, 2009). Two surprising aspects of the returned samples point to the same unexpected physics. The chemical composition of the samples, rich in Calcium Aluminum Inclusions, indicated that the chemistry of their formation occurred in a very high temperature environment, so they could not have formed where the comet has been stored for millenia in the outer solar system. A second

surprise was that the captured cometary material was rich in molten chondrules that again indicated formation in a hot environment, not the outer Solar system where comets hibernate. Today planetary scientists ponder how the solar system turned itself inside-out, but in the primordial formation scenario, more probably these materials formed when the primordial planets were still hot before losing hydrogen, and before the Solar System formation had begun.

Another NASA space mission with surprising results was the Deep Impact mission to Comet Temple 1 to propel a 700 lb mass into the surface and examine the resulting dust cloud (A'Hearn, 2009). Instead of finding the rocks expected in the debris cloud, only a fine powder was found in the subsurface ejecta. This demonstrated that the ancient comet had collected dust throughout the history of the universe, but the dust grains had not collided and stuck together as predicted in the standard dust collision models. The powdery dust was so fine that its cloud saturated the detectors in the spacecraft.

8. Conclusions.

Recent Solar System spacecraft missions have produced results that have taken the community by surprise. Chemical composition and molten chondrules have forced the conclusion that the system has been turned inside out, with no previous evidence of this. And the existence of fine dust with no rocks in outer solar system bodies defies the theory that dust grains easily collide and stick together to form crystalline rocks. And the long-standing problem of how does the Earth come to have an iron core surmounted by an ocean of water has heretofore been unexplained.

While these sweeping statements describe reasonably the state of knowledge of solar system structure, they leave many unfinished details. The key point here is that planet formation was a 2-step process, with primordial rogue planets creating solid and semi-solid cores, and pre-solar disc evolution creating the presently observed structures near the sun (fig. 3 lower left). What has not been taken into

account is the existence of not just the inner nine planets of the sun, but the many millions of primordial planets per star.

In this way, planetary formation does not need to begin with rocky particles colliding and sticking together on all mass scales from dust to moons. The key ingredient is the existence of primordial gas rogue planets with extensive hydrogen atmospheres that collect interstellar material and stratify it by density at molten centers, so that when hydrogen-stripped in the pre-solar disc, their modified remnants supply all the ingredients of the observed solar system.

9. References

A'Hearn, M. 2009. Deep Impact and the Origin and Evolution of Cometary Nuclei, Springer, ISBN 978-0-387-85454-0.

Alcock, C. et al, 1998. EROS and MACHO Combined Limits on Planetary-Mass Dark Matter in the Galactic Halo, ApJ,499, L9.

Blum, J. & Wurm, Gerhard, 2008. The Growth Mechanisms of Macroscopic Bodies in Protoplanetary Disks, ARA&A, 46, 21.

Brownlee, D. 2009. Comet Samples Returned by Stardust, Insight into the Origin of Comets and Crystalline Silicates in Disks, in Cosmic Dust - Near and Far: ASP Conference Series, Vol. 414, proceedings of a conference held 8-12 September 2008 in Heidelberg, Germany. Edited by Thomas Henning, Eberhard Grün, and Jürgen Steinacker. San Francisco: Astromomical Society of the Pacific, p.157.

Burud, L. et al, 2000. An Optical Time Delay Estimate for the Double Gravitational Lens System B1600+434, ApJ, 544, 117.

Burud, L. et al, 2002. A&A, Time delay and lens redshift for the doubly imaged BAL quasar SBS 1520+530, 391, 481

Colley, W. et al, 2003. Around-the-Clock Observations of the Q0957+561A,B Gravitationally Lensed Quasar. II. Results for the Second Observing Season, ApJ, 587, 71.

Colley, W. & Schild, R. 2003, A Rapid Microlensing Event in the Q0957+561A, B Gravitational Lens System, ApJ, 594, 97

Currie, T. et al, 2010. The Morphologies and Lifetimes of Transitional Protoplanetary Disks, arXiv:1002.1715.

Fan, X. et al, 2006. Observational Constraints on Cosmic Reionization, Ann Rev Ay & Ap, 44, 415.

Gibson, C. H. 1996. Turbulence in the ocean, atmosphere, galaxy and universe, Appl. Mech. Rev., 49, no. 5, 299–315.

Gibson, C. H. 2010. Turbulence and turbulent mixing in natural fluids, Physica Scripta, Turbulent Mixing and beyond 2009 Proceedings, T142, arXiv:1005.2772.

Gibson, C. Wickramasingh, N. & Schild, R. 2010. First life in primordial-planet oceans: the biological big bang, arXiv:1009.1760

Gibson, C. H., Schild, R. E, and Wickramasinghe, N. C. 2010. The Origin of Life from Primordial Planets, Int. J. of Astrobiology, doi:10.1017/S1473550410000352, arXiv:1004.0504.

Gibson, C. & Schild, R. 2003. Evidence for Hydro-Gravitational Structure Formation Theory versus Cold-Dark-Matter, Hierarchical-Clustering, and Jeans 1902, astro-ph/0304483

Hjorth, J. 2002, The Time Delay of the Quadruple Quasar RX J0911.4+0551, ApJ, 572, L11.

Jakobsson, P. 2005. An optical time delay for the double gravitational lens system FBQ 0951+2635, A&A, 431, 103.

Kearsley, A. et al, 2008. Dust from comet Wild 2: Interpreting particle size, shape, structure, and composition from impact features on the Stardust aluminum foils, Meteoritics and Planetary Sciences, 43, 41.

Kern, S. & Elliot, J. 2006. The Frequency of Binary Kuiper Belt Objects, ApJ, 643, L57.

Low, F.J. 1984. Infrared cirrus - New components of the extended infrared emission, ApJ, 278, L19.

Lucas, P. Weights, D. Roche, P. Riddick, F. 2006. Spectroscopy of planetary mass brown dwarfs in Orion, MNRAS Letters, 373, L60.

Marsh, K. Kirkpatrick, D. and Plavchan, P. 2010. A Young Planetary-Mass Object in the ρ Oph Cloud Core, ApJ, 709, L158.

Mao, S. & Schneider, P. 1998. Evidence for substructure in lens galaxies? MNRAS, 295, 587.

Meaburn, J. et al, 1992. Dust in the neutral globules of the Helix nebula, NGC 7293, MNRAS, 255, 177.

Meaburn, J. 1998. The nature of the cometary knots in the Helix planetary nebula (NGC 7293), MNRAS, 294, 201.

Meyers, P.C. 2008. Protostellar Masses due to Infall and Dispersal, ApJ, 687, 340.

Meyers, P.C. 2009. On the Distribution of Proto-Star Masses, ApJ, 706, 1341.

Meyers, P.C. 2010. Star Forming Gas in Young Clusters, ApJ, 714, 1280.

Nieuwenhuizen, T. M., Schild, R. E., Gibson, C. H., 2010. Do micro brown dwarf detections explain the galactic dark matter?, arXiv:1011.2530.

O'Dell, C. and Handron, K. 1996. Cometary Knots in the Helix Nebula, ApJ, 111, 1630.

Ofek, E. 2010. Long-duration Radio Transients Lacking Optical Counterparts are Possibly Galactic Neutron Stars, ApJ, 711, 517.

Oldershaw, R. 2010. An Infinite Fractal Cosmos, JCos, 4, 674.

Paraficz, D. et al. 2006. Microlensing variability in time-delay quasars, Astron & Astrophys, 455 L1-L4.

Price, R. Duric, N. & Duncan, W. 1994. Cool Dust in Spiral Galaxy NGC 3079, in A.S.P. Conference Series, 58, 211.

Schild, R. 1996.   Microlensing Variability of the Gravitationally Lensed Quasar Q0957+561 A,B, ApJ, 464, 125.

Schild, R. 1999. A Wavelet Exploration of the Q0957+561A,B Brightness Record, ApJ, 514, 598.

Schild, R. 2007. The Evolution of the Chemical elements of the Universe, astro-ph/0701474.

Schild, R. & Dekker, M. 2006. The transparency of the Universe limited by Lyα clouds, AN, 327, 729.

Schild, R. and Smith, R.C. 1992. Microlensing in the Q0957 + 561 gravitational mirage, AJ, 101, 813.

Schild, R. & Vakulik, V. 2003. Microlensing of a Ring Model for Quasar Structure, Astron. J., 126, 689, arXiv:astro-ph/0303356.

Stapelfeldt, K. et al, 1999, ApJ, 516, L95.

Truelove, J. et al, 1997. The Jeans Condition: A New Constraint on Spatial Resolution in Simulations of Isothermal Self-gravitational Hydrodynamics, ApJ, 489, L179.

Vakulik, V. et al. 2003. Q2237+0305 source structure and dimensions from light-curve simulation, MNRAS, 382, 819.

Veneziani et al. 2010. Properties of Galactic cirrus clouds observed by Boomerang, ApJ, 713, 959-969.

Watson, C. et al. 2010. Estimating the masses of extra-solar planets, arXiv: 1006.2069.

Zapatero Osario, M. 2002. Science, 290, 103.

Formation of Planets by Hydrogravitational Dynamics

Carl H. Gibson [1,2]

[1] University of California San Diego, La Jolla, CA 92093-0411, USA
[2] cgibson@ucsd.edu, http://sdcc3.ucsd.edu/~ir118

and

Rudolph E. Schild[3,4]

[3] Center for Astrophysics, 60 Garden Street, Cambridge, MA 02138, USA
[4] rschild@cfa.harvard.edu

ABSTRACT

From hydro-gravitational cosmology, hydrogen-^{4}helium gas planets in million-star-mass clumps fragment at the plasma to gas transition 300,000 years after the big bang. Binary planet mergers form larger planets and stars: globular star clusters in the limit. Star-less frozen-planet clumps persist as the dark matter of galaxies as observed by Schild in 1996, and predicted by Gibson in 1996.   Plasma structures with protogalaxysupercluster-mass appear at 30,000 years when photon-viscous forces match gravitational fragmentation forces at the horizon scale ct of the expanding universe, where c is the speed of light and t is the time. Protosuperclustervoid and protogalaxyvoid boundaries expand at sound speeds $c/3^{1/2}$ producing weak turbulence and linear clusters of gas protogalaxies that are fossils of turbulent-plasma vortex-lines. Continued primordial planet accretion by stars leads to supernovae, with early life formation in critical temperature water oceans seeded by the resulting C, N, O, etc. first chemicals. Information about evolving life chemistry in $>10^{80}$ hot water oceans is communicated by merger fragments between the growing hydrogen planets: a cosmic primordial soup with Hoyle/Wickramasinghe cometary panspermia.

1. Introduction

The standard (concordance) cold dark matter model of cosmology is based on the Jeans 1902 theory of gravitational instability of a gas nebula, where numerous

unwarranted assumptions are made to simplify the conservation laws of fluid mechanics (Jeans 1902). Jeans assumed inviscid Euler momentum equations with linear perturbation stability analysis, thus neglecting crucially important viscous forces and turbulence forces. He also neglected any effects of diffusivity on gravitational structure formation, unaware of a massive population of super-diffusive neutrinos.   The resulting linear acoustics equations were then solved by neglecting density (the Jeans swindle) giving the Jeans length scale $L_J=V_S/(\rho G)^{1/2}$ as the single criterion for gravitational instability, where V_S is the speed of sound, ρ is density and G is Newton's gravitational constant.

Density wavelengths smaller than the Jeans scale were incorrectly assumed by Jeans 1902 to be stabilized by pressure forces. This is also a fatal error of the concordance model. Those density wavelengths larger than L_J are incorrectly taken to be unstable linear modes that may grow in amplitude without limit. Large errors result from the Jeans 1902 criterion, which fails to predict the formation of primordial-gas planets at the plasma-gas transition (Gibson 1996), and fails to predict fragmentation of supercluster, cluster, and galaxy mass objects in the plasma. Significant errors result from a lack of understanding of turbulence and fossil turbulence, since the big bang is a result of a turbulence instability (Gibson 2005) and the boundary conditions of the evolving universe are set by the fossils of big bang turbulence (Gibson 2004). Numerous manifestations of big bang fossil vorticity turbulence have been documented (Schild and Gibson 2008, Gibson 2010ab). The existence of an "axis of evil" preferred direction on the sky clearly shows a first order departure from the standard cosmological model.

Because the Jeans scale is larger than the horizon scale $L_H = ct$ during the plasma epoch, no plasma structures should form during this period 3,000 to 300,000 years (10^{11} to 10^{13} seconds) after the big bang event by the Jeans 1902 acoustic criterion. The baryonic material (H and He plasma) is necessarily a small fraction, ~4%, of the total mass required for a "flat" (neither open nor closed) universe (Peebles 1993).

According to "cold-dark-matter" CDM theories, the non-baryonic dark matter component with its unknown weakly-collisional particles is arbitrarily assumed to be cold to reduce the CDM Jeans scale L_{JCDM} below the horizon L_H during the plasma epoch, permitting condensation as "seeds", or cold-dark-matter CDM halos. Observational tests of the CDM model fail badly in the local group of galaxies (Kroupa et al. 2010).

Such CDM halos were imagined to "hierarchically cluster" HC to much larger masses over time, producing massive gravitational potential wells into which the baryonic-dark-matter BDM could fall and form the first stars in a few hundred million years of dark ages. The resulting CDMHC model is standard in present day astronomy, astrophysics and cosmology.

Is the standard CDMHC model true? Can viscosity be neglected in the plasma epoch? Can turbulence[1] be neglected? Can fossil turbulence[2] be neglected? If the non-baryonic-dark-matter NBDM is nearly collisionless, can its diffusivity be neglected? No, clearly not. Whatever it is, NBDM is super-diffusive and cannot condense, as assumed by CDMHC, to guide the structure formation of the BDM. The reverse is true (Gibson 1996). Even though its mass is smaller, the sticky, collisional, baryonic matter forms galaxy and galaxy cluster structures that gravitationally guide the non-baryonic material to form large cluster and supercluster halos. When fluid mechanical constraints are imposed an entirely different cosmology emerges, termed hydrogravitational dynamics HGD.

As a natural part of the discussion of the two theories of cosmology, the question of a permanent form of anti-gravity arises. Anti-gravity is needed in any big bang theory beginning at Planck densities. This is why Einstein was forced to include a

---

[1] Turbulence is defined as an eddy-like state of fluid motion where the inertial-vortex forces of the eddies are larger than any other forces that tend to damp the eddies out. By this definition, turbulence always cascades from small scales to large.

[2] Fossil turbulence is defined as a perturbation in any hydrophysical field produced by turbulence that persists after the fluid is no longer turbulent at the scale of the perturbation.

cosmological constant Λ in his general relativity equations (Peacock 2000, p15). Anti-gravitational forces occur naturally in the turbulent HGD big bang model due to turbulence stresses and gluon viscosity, and vanish at the end of the inflation epoch.

Thus a permanent "dark energy" cosmological constant Λ is unnecessary. A much more plausible candidate for the NBDM is provided by neutrinos (Nieuwenhuizen 2009). Nieuwenhuizen estimates a neutrino mass sufficient to exceed the baryonic matter by a factor of six, and possibly the factor of thirty needed to flatten the universe. Because turbulence creates entropy, HGD cosmology predicts a closed universe with non-baryonic dark matter mass in this 6-30 times baryonic range.

In the following, we first summarize the hydrogravitational dynamics theory that leads to the formation of primordial planets as the dark matter of galaxies. We contrast HGD predictions with those of standard CDMHC cosmologies, and provide discussion of results and conclusions. Remarkably, the presence of complex life forms on Earth is powerful evidence against CDMHC cosmology where life formation faces formation of stars with a handful of planets beginning in the hydrogen freezing temperatures of 300 Myr. Extraterrestrial life comes easily and naturally from HGD cosmology, which has cometary panspermia built into its star formation mechanism of hydrogen planet mergers (Gibson et al. 2010ab).

2. Comparison of HGD cosmology with ΛCDMHC cosmology

Figure 1abcde summarizes HGD cosmology. Turbulence dominates the big bang event shown at the right of Fig. 1a until the kinematic viscosity increases from Planck values of order $\nu_P = L_P \times c \sim 10^{-27}$ m^2 s^{-2}, to gluon-viscous values that are much larger, where L_P is the Planck length scale and c is the speed of light. Reynolds numbers of the turbulent combustion process monotonically increase drawing energy from the vacuum by negative turbulence stresses (Gibson 2010).

Much larger negative viscous stress occur when the spinning turbulent fireball cools from 10^{32} K to 10^{28} K, so the quark-gluon plasma can form. Gluons transfer momentum over larger collision distances than the Planck scale, increasing the viscosity and negative stresses proportionately. An exponential inflationary event is triggered, with displacement velocities up to $\sim 10^{25}$ c, increasing the mass-energy of the universe to values $\sim 10^{97}$ kg, compared to $\sim 10^{53}$ kg visible in our present horizon $L_H = ct$. Because the turbulent temperature fluctuations of the big bang are stretched far beyond the horizon scales L_H, they become the first fossil temperature turbulence (Gibson 2004). Vortex lines produced at Planck scales persist throughout the inflationary expansion to become the first fossil vorticity turbulence.

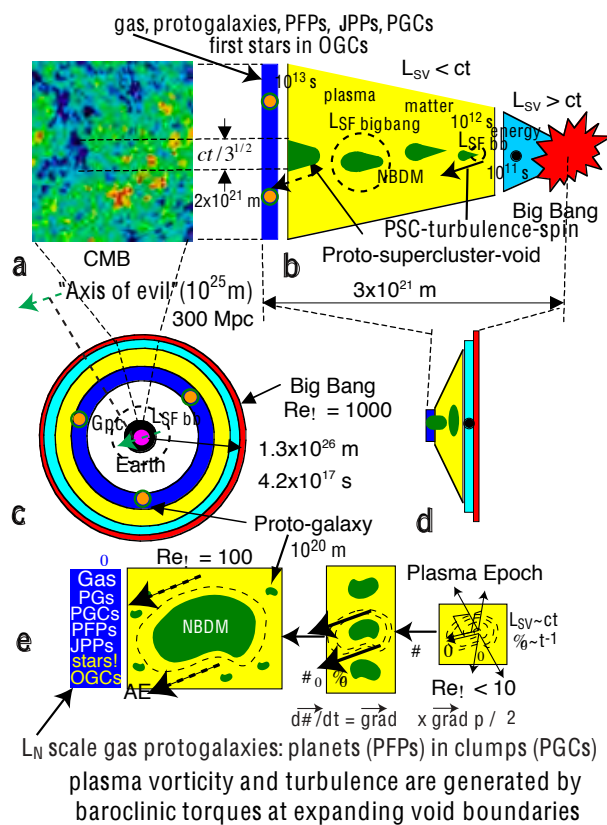Fig. 1. Hydrogravitational dynamics cosmology (Gibson, 2010). In **a.** CMB temperature anomaly patterns reflect protosupercluster (PSC) and protosuperclustervoid patterns at the sonic scale $ct/3^{1/2}$ of the voids formed at 10^{12} seconds when the viscous-gravitational scale L_{SV} first matched the increasing horizon scale L_H. Vorticity **e.** produced at void boundaries determines the

morphology of plasma protogalaxies, which fragment into proto-globulular-star-clusters PGC clumps of primordial-fog-particle PFP planets at transition to gas.

A mass of $\sim 10^{16}$ kg is produced by the big bang event in $\sim 10^{-27}$ sec, giving a power of 10^{60} watts. A mass of $\sim 10^{97}$ kg is produce by inflation in $\sim 10^{-33}$ sec, giving a power of 10^{147} watts. Nucleosynthesis gives H, ^{4}He and electrons in $\sim 10^3$ sec. Mass exceeds energy at $\sim 10^{11}$ sec. Gravitational structure formation cannot occur until the plasma epoch, when the horizon scale L_H exceeds the viscous Schwarz scale L_{SV} at time $\sim 10^{12}$ sec. As shown in Fig. 1e, the first gravitational structures were protosuperclustervoids due to fragmentation at density minima. Mass scales of the fragments $\sim 10^{46}$ kg match supercluster masses. Weak turbulence produced by torques at spinning void boundaries has been detected by Sreenivasan and Bershadskii from the statistics of CMB temperature anisotropies (Gibson 2010).

The standard ΛCDMHC cosmology attempts to make gravitational structures in the plasma epoch as shown in Figure 2 (top). The non-baryonic dark matter is assumed to be cold to reduce the Jeans scale to less than the scale of causal connection L_H. Cold dark matter CDM seeds are assumed to condense and hierarchically cluster HC to from gravitational potential wells to collect the baryonic plasma. Accoustic oscillations of the plasma within such potential wells accounts for the prominent acoustic peak observed in CMB temperature anisotropies.
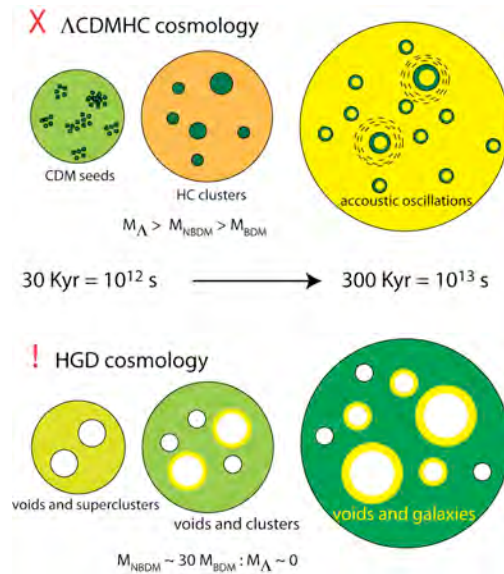
Fig. 2. Contrast between ΛCDMHC and HGD models of structure formation during the plasma epoch. At the top, cold dark matter CDM seeds condense at the Jeans scale and then hierarchically cluster HC to form potential wells that collect acoustically oscillating plasma. At the bottom, hydrogravitational dynamics HG predicts a sequence of fragmentations from supercluster to galaxy scales, controlled by viscous and turbulence forces (Gibson 2010).

Figure 2 (bottom) shows the HGD structure formation scenario. Even though the NBDM mass greatly exceeds that of the baryonic plasma, it cannot condense or cluster until after the plasma epoch because it is so weakly collisional (Gibson 2000). Fossils of the turbulent rate-of-strain, density, and spin at the $t_0 = 10^{12}$ sec time of first structure persist to this day.

Figure 3 (top) contrasts ΛCDMHC cosmologies with the HGD cosmology Figure 3 (bottom) during the early years of the gas epoch between 10^{13} sec and 10^{16} sec.
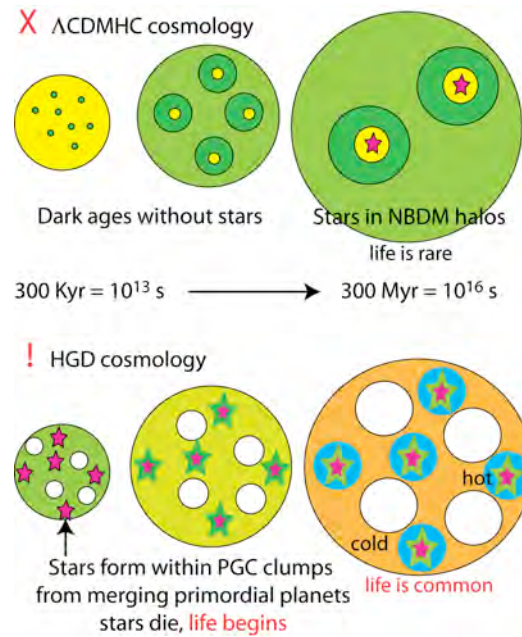
Fig. 3. Contrast between ΛCDMHC and HGD models of structure formation during the early years of the gas epoch beginning at 10^{13} sec. The first stars appear after 10^{16} sec according to ΛCDMHC (top), ending 300 Myr of dark ages. The first stars and first chemicals occur quite promptly according to HGD cosmology (bottom), within the fossil freefall time $t_0 = 10^{12}$ sec. Jeans mass protoglobularstarcluster PGC clumps of primordial-fog-particle PFP planets form at the transition time 10^{13} sec., setting the stage for the biological big bang (Gibson, Schild and Wickramasinghe 2010) beginning at 6×10^{13} sec when planetary oceans first condense.

All stars form within PGC clumps of PFP planets by a sequence of mergers of the hydrogen-helium gas planets. Old globular star clusters OGC have the baryonic density $\rho_0 = 4\times10^{-17}$ kg m^{-3} of the time of first structure t_0. This is also the density of protogalaxies formed with Nomura scale 10^{20} meters and the Nomura morphology determined by numerical simulations of weak turbulence, as shown in Figure 4.

Journal of Cosmology, Lorentz Center Workshop Proceedings, Sept. 27-Oct. 1, 2010   9
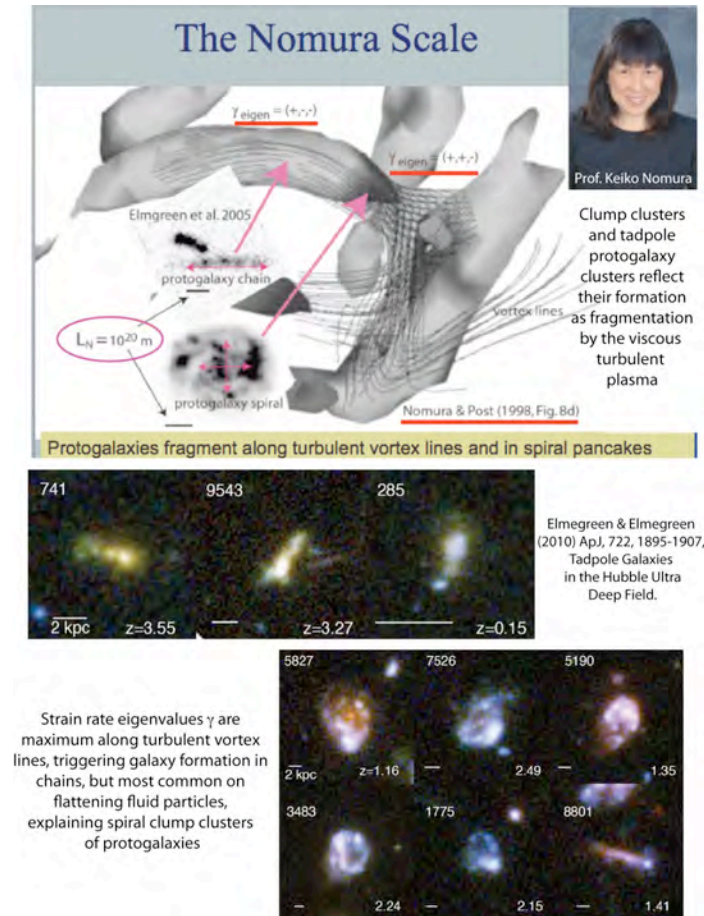
Fig. 4. Tadpole and clump cluster protogalaxies observed by Elmegreen & Elmegreen (2010) compared to the morphology of weak turbulence simulated by Nomura & Post (1998).

Direct numerical simulations of weak turbulence (Nomura & Post 1998) confirm the mathematical expectation that most spherical turbulent fluid particles flatten into pancakes with rate-of-strain eigenvalues γ_{eigen} (+,+,-). The unanticipated morphology is that these form spiral structures at the base of vortex lines with γ_{eigen} (+,-,-), as shown at the top of Fig. 4. Protogalaxies fragmenting at the end of the plasma epoch maintain this Nomura morphology, as shown by the linear and spiral clusters of galaxies detected in the Hubble Space Telescope Ultra Deep Field images. Horizontal bars of scale 2 kpc are shown showing the bright clumps are close to the Nomura viscous length scale of the late plasma epoch, at $L_N = 10^{20}$ meters.

This high density $\rho_0 = 4 \times 10^{-17}$ kg m^{-3} of globular clusters and protogalaxies exceeds the average galaxy density by four orders of magnitude. Stars in OGCs are typically small and long lived, supporting the HGD scenario that the transition from plasma to gas was extremely gentle. First stars formed in the standard cosmology scenario of Fig. 3 (top) are claimed to be such massive superstars that when they condense from the turbulent gas clouds collected by the massive assembled CDM halos Fig. 3 (top right) they immediately detonate to re-ionize the universe. The re-ionization hypothesis is unnecessary to explain the lack of hydrogen observed in distant quasar spectra. It is unsupported by observations intended to detect the enormous radiation events of the superstar supernovae. It never happened. According to the HGD cosmology of Fig. 3 (bottom) the hydrogen planets in their PGC clumps have become the dark matter of galaxies by freezing. Figure 5 shows the HGD model of spiral galaxy formation. The non-baryonic dark matter diffuses to larger scales than the baryonic dark matter halos, and provides a small fraction of the density within the PGC baryonic dark matter halo.

As shown in Fig. 5 (top) the plasma protogalaxies promptly fragment at the PGC Jeans mass of a million solar masses, each containing a trillion primordial gas fog particle PFPs with Earth mass. The time of fragmentation is determined by the large density ρ_0 of the protogalaxies, so the PGC/PFP formation time τ_g is significantly smaller than t. The same rapid time of formation applies to mergers of PFPs to make larger planets and finally stars. Thus the first star of HPD cosmology should appear in a PGC near the core of a protogalaxy at a time not much different than the plasma to gas transition time 10^{13} seconds, as shown in Fig. 5 (top right). Strong viscous forces of the gas planets requires the mergers of planets to be gentle, so the first stars formed will be small and long lived, as observed in old globular star clusters OGCs. Such mergers should be mostly binary, leading to binary planets and binary stars, as observed. Numerous planet fragments are collected gravitationally as comets and meteors by the larger objects, including biochemical information

produced as living organisms form when the first oceans are seeded with the first chemicals (Gibson, Schild and Wickramasinghe 2010).
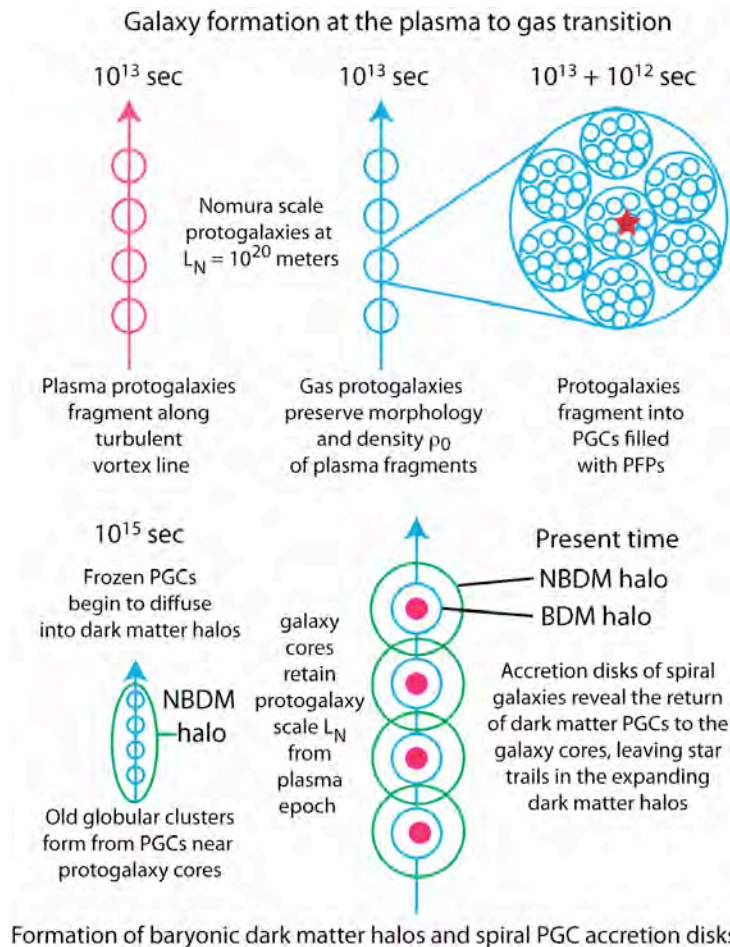
Fig. 5. Galaxy formation at the plasma to gas transition (top) at time 10^{13} sec. Formation of baryonic dark matter halos by diffusion of freezing baryonic dark matter PGCs out of the L_N scale galaxy cores (bottom).

The model of spiral galaxy formation of Fig. 5 is supported by the compound image of nearby galaxy M81, shown in Figure 6. The central core of old stars matches the L_N scale of the original protogalaxy from which PGCs diffused to form the 10^{22} meter diameter dark matter halo. Those clumps of PGCs that escaped from the core have small direct collision probability for their frozen planets, which makes them strongly diffusive, but large collision probability for tidal interactions, which tiggers star formation and friction. Infrared images of protostars forming in the wake of

PGC centers of gravity can be seen in release images of the Milky Way disk from the Planck space telescope and the Herschel space telescope (Gibson, Schild & Wickramasinghe 2010, figs. 11 & 12).
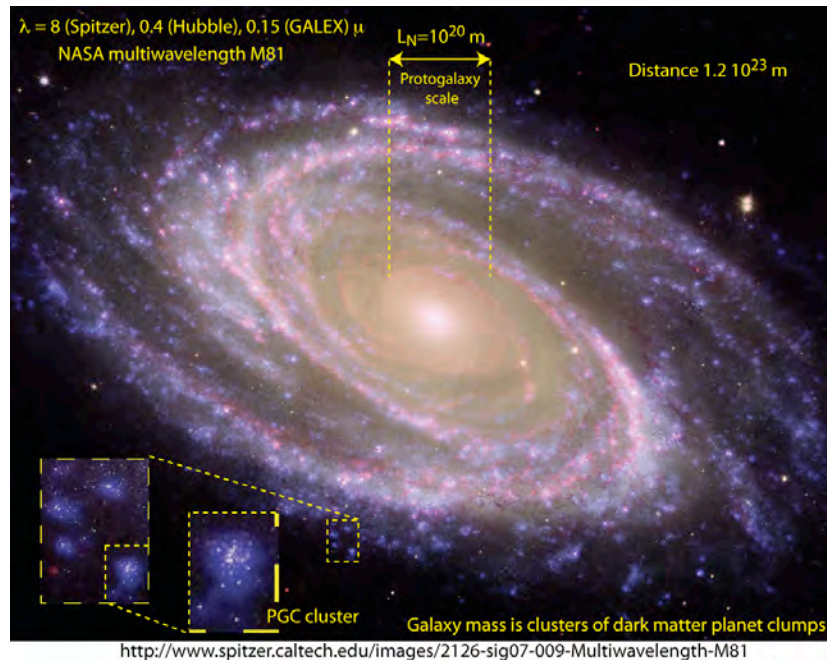
Fig. 6. A multiwavelength image of nearby galaxy M81 (1.2×10^{23} m) is shown from the infrared telescope Spitzer at 8 microns, the Hubble space telescope at 0.4 microns, and the ultraviolet 0.15 micron telescope GALEX. Star trails of the merging objects are revealed in the frictional PGC accretion disk of M81. The baryonic dark matter of the spiral galaxy accretion disk is revealed to be clusters of PGCs (lower left). Individual PGCs appear as bright dots, probably turbulent O-B star complexes triggered into formation by tidal forces.

Temperatures detected by the infrared telescopes Planck and Herschel match triple point and critical temperatures expected for boiling and freezing hydrogen planets as they merge, collide and re-freeze as expected in the HGD scenario for star formation by accretional cascades from PFP mass to star mass within PGC clumps.

3. Discussion

The standard model ΛCDMHC is physically untenable and observationally unsupported. As shown in Fig. 2 (top) the scenario requires gravitational

condensation of a nearly collisionless fluid: cold dark matter CDM. How can a nearly collisionless fluid condense, and how can its condensates merge to form stable CDM halos? No matter how cold and motionless the CDM particles are initially, they will not be cold for long, and even if they are merged somehow, they cannot hierarchically cluster HC to form larger mass halos.

Imagine a sphere of perfectly cold dark matter, where its particles are initially completely motionless, as shown in Figure 7.
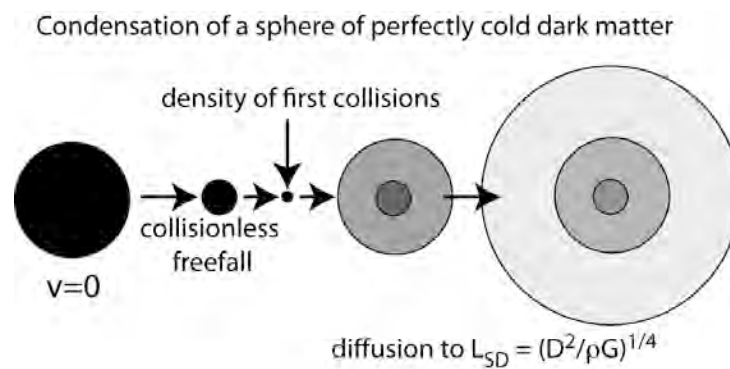
Fig. 7. Instability of weakly collisional cold dark matter to diffusion. A sphere of motionless cold dark matter particles would collapse to a density where collisions occur, so the particle motions must randomize and thermalize. The sphere will grow to the Schwarz diffusive scale, where the diffusion velocity matches the gravitational velocity (Gibson 2000).

As shown in the Fig. 7 counterexample, CDM condensations are physically impossible. So are mergers of CDM condensates by hierarchical clustering HC.

Gluon viscous forces terminate the big bang, fossilizing turbulent big bang temperature fluctuations by inflation beyond the scale of causal connection ct. Gravitational structure begins in the plasma epoch when the Schwarz viscous scale L_{ST} matches ct at time 10^{12} sec. L_{ST} is $(\gamma\nu/\rho G)^{1/2}$, where γ is the rate-of-strain $\sim t^{-1}$, ν is the kinematic viscosity, ρ is the density and G is Newton's constant. The viscosity during the plasma epoch occurs by photon collisions with free electrons. The collision cross section for such events is well known as well as the density of

electrons as a function of time (Peebles 1993), giving $\nu \sim 4\times10^{26}$ m^2 s^{-1} (Gibson 1996). The initial fragmentation mass scale of the plasma is easily calculated to be that of superclusters.

Clusters and galaxies form as the plasma cools. Voids grow at sonic speeds $c/3^{1/2}$ creating weak turbulence at void boundaries (Gibson 2010). Because Reynolds numbers of the turbulence is small, the Schwarz turbulence scale $L_{ST} = \varepsilon^{1/2}/(\rho G)^{3/4}$ is not much larger than L_{SV}, where ε is the viscous dissipation rate of the turbulence. Thus the Kolmogorov scale $L_K = (\nu^3/\varepsilon)^{1/4}$ of the weak plasma turbulence fixes the size and mass of the protogalaxies emerging from the plasma epoch with the Nomura weak turbulence morphology, where all quantities are known. The kinematic viscosity of the gas is much smaller than that of the plasma at transition, so the viscous Schwarz scale is decreased and the mass scale is that of the Earth. Fragmentation also occurs at the Jeans scale because heat is transferred at light speeds but pressure is transferred at sound speeds. This mismatch makes it impossible to maintain constant temperature as primordial gas fog particles PFPs fragment.

4. Conclusions

Gravitational structure formation after the turbulent big bang occurs in the plasma epoch by a viscous fragmentation process beginning at 30,000 years, or 10^{12} seconds. Protosuperclustervoids expand at near light speeds starting at this time to form the 10^{25} meter completely empty regions observed at present, contradicting the standard ΛCDMHC cosmology that suggests voids are the last features to form as the universe evolves rather than the first.

Weak turbulence results from the plasma void expansions that determines the morphology and scales of the protogalaxies, as shown in Figs. 4-6. The kinematic viscosity of the primordial gas $\gamma \sim 10^{13}$ m^2 s^{-1} at the transition temperature ~ 3000

Journal of Cosmology, Lorentz Center Workshop Proceedings, Sept. 27-Oct. 1, 2010   15

K. Protogalaxies promptly fragment at Jeans mass to form PGCs and Earth mass to form PFPs, as shown in Fig. 5 (top).

All stars form by PFP mergers within PGC clumps. Most of the PFPs remain as frozen hydrogen gas planets. Clumps of PGC clumps comprise the dark matter of galaxies. The non-baryonic dark matter diffuses to form galaxy cluster halos, as shown by Fig. 7. We see that rather than ∼ 10 planets per star there are 30,000,000. It is easy to understand Jupiter mass planets observed orbiting stars at distances matching the orbit of planet Mercury using hydrogravitational dynamics HGD cosmology. It is easy to understand overfeeding stars to form supernovae by continued planet accretion. Gravitational collection of the chemicals produced by the hydrogen gas planets reduces iron and nickel to metals, produces rock layers, oceans and the complex chemistry of life.

It seems clear that the ΛCDMHC cosmological model should be abandoned.

REFERENCES

Elmegreen, B. G. and Elmegreen, D. M. 2010. Tadpole Galaxies in the Hubble Ultra Deep Field, Ap. J, 722, 1895-1907.

Gibson, C. H. 2000. Turbulent mixing, viscosity, diffusion and gravity in the formation of cosmological structures: the fluid mechanics of dark matter, Journal of Fluids Engineering, Vol. 122, Dec. 2000, 830-835, arXiv:astro-ph/0003352.

Gibson, C. H. 2004. The first turbulence and the first fossil turbulence, Flow, Turbulence and Combustion, 72, 161–179.

Gibson, C. H. 2005. The first turbulent combustion, Combust. Sci. and Tech., 177:1049–1071, arXiv:astro-ph/0501416.

Gibson, C. H. 2010. Turbulence and turbulent mixing in natural fluids, Physica Scripta, PSTOP/366248/SPE, T140, Turbulent Mixing and Beyond 2009, Trieste, ICTP conference proceedings, arXiv:1005.2772.

Gibson, C. H., Schild, R. A., and Wickramasinghe 2010a. The origin of life from primordial planets, Int. J. of Astrobiol., doi:10.1017/S1473550410000352, 1-16.

Gibson, C., Wickramasingh, N. & Schild, R. 2010b. First life in the oceans of primordial-planets: the biological big bang, Journal of Cosmology 11, 3490-3499, arXiv:1009.1760.

Jeans, J. H. 1902. The stability of spherical nebula, Phil. Trans., 199A, 0-49.

Kroupa, P., Famaey, B., de Boer, K. S. et al. 2010. Local-Group tests of dark-matter concordance cosmology: Towards a new paradigm for structure formation, accepted A&A, http://dx.doi.org/10.1051/0004-6361/201014892.

Nieuwenhuizen, T. M. 2009. Do non-relativistic neutrinos constitute the dark matter? Europhys. Lett. 86, 59001, 1–6.

Nieuwenhuizen, T. M. 2008. Supermassive black holes as giant Bose-Einstein condensates, Europhys. Lett. 83, 10008, 1–6, doi:10.1209/0295-5075/83/10008.

Nomura, K. K. & Post, G. K. 1998. The structure and dynamics of vorticity and rate of strain in incompressible homogeneous turbulence, J. Fluid Mech. 377, 65–97.

Peebles, P. J. E. 1993. Principles of Physical Cosmology, Princeton University Press, Princeton, NJ.

Peacock, J. A. 2000. Cosmological Physics, Cambridge Univ. Press, UK.

Schild, R. 1996. Microlensing variability of the gravitationally lensed quasar Q0957+561 A,B, ApJ, 464, 125.

Schild, R.E & Gibson, C.H. 2008. Lessons from the Axis of Evil, arXiv:astroph/0802.3229v2.

000199

Explanation of the Helium-3 problem

Theo M. Nieuwenhuizen[1,2]⋆
[1] *Center for Cosmology and Particle Physics, New York University, 4 Washington Place, New York, NY 10003, USA*
[2] *Institute for Theoretical Physics, University of Amsterdam, Science Park 904, P.O. Box 94485, 1090 GL Amsterdam, The Netherlands*

22 April 2011

ABSTRACT

One of the tests of nucleosynthesis theory is the ^{3}He abundance in the Galaxy. ^{3}He$^+$ is observed through its 3.46 cm hyperfine level in HII regions and the ^{3}He/H ratio compares well with theory. Since ^{3}He can be created or destroyed in nuclear reactions, one would expect that its abundance shows a trend with the amount of such reactions, so with distance to the Center of the Galaxy and with metallicity. Such trends are lacking in observations. This is explained by assuming that the HII clouds are recently formed out of the primordial micro brown dwarfs of earth mass predicted by gravitational hydrodynamics. If indeed existing, they would preserve their primordial ^{3}He/H ratio and spread this when evaporating into HII clouds, independent of the location in the Galaxy.

In the development of the argument, it is also explained that wide binaries do not rule out the MACHO dark matter predicted by gravitational hydrodynamics, but are rather immersed as visible partners in Jeans clusters of dark micro brown dwarfs.

1 INTRODUCTION

Nucleosynthesis in the WMAP era is said to be a parameter-free theory, see e. g. Steigman (2007). With cosmology described by the Friedman-Lemaitre-Robertson-Walker metric and the number of neutrino species known, accurate predictions can be made, ready for comparison with observations. We will discuss one of these tests, the one for ^{3}He, that is in agreement with theory, but has a puzzling aspect.

2 THE HELIUM-3 PROBLEM

^{3}He is produced in nucleosynthesis and the observed abundance ^{3}He/H$\approx 1.0 \cdot 10^{-5}$ agrees with theory. But not all is well, so let us explain the way to observe it. The ^{3}He nucleus consists of two protons and a neutron, so it has spin $\frac{3}{2}$ or $\frac{1}{2}$. The singly ionized ^{3}He$^+$ contains one electron, thus the singlet spin-$\frac{1}{2}$ state brings an analogy with the neutral H-atom. Indeed, there is an analog of the 21-cm spin-flip transition, which occurs roughly at $21/Z^2$=21/4 cm, more precisely at 3.46 cm. The emission by this transition line provides an observational signature of singly ionized ^{3}He located in regions of ionized H gas (so-called HII regions) and in planetary nebulae that also contain ionized H and ^{3}He.

HII regions have been created rather recently in the cosmic history (Rood et al. 1984, 2002; Bania et al. 2007), and are thus expected to reflect the chemical history of the surroundings. ^{3}He can be created or destroyed in nuclear reactions. One would thus expect its local concentration in the Galaxy to depend on the amount of reactions that have taken place, a measure for which is the local metallicity. Since near the Center more reactions took place, there is a clear gradient in the metallicity, so one also expects a significantly higher ^{3}He concentration near the Center than in the outskirts. But though observations show fluctuating concentrations, there is no statistical trend with distance or with metallicity. Specifically, low values of ^{3}He/H$\approx 1.0 \cdot 10^{-5}$ are observed at 4, 9, 10, 12 and 16 kpc from the Center, while up to two-three times higher values are observed in between (Rood et al. 2002).

The important point for the present paper is that the HII regions show no evidence for stellar ^{3}He enrichment during the last 4.5 Gyr; the low values thus being found at any distance from the Center is called *the* ^{3}He *problem* (Bania et al. 2007). This situation creates a paradox, since it calls for a delicate balance between creation and destruction *independent of the amount of reactions* (the metallicity). The relevant data indicate that the extra-mixing occurs in 90 to 95% of the low-mass stars (Charbonnel and Do Nascimento 1998; Charbonnel 1998). This is the best current solution to the "^{3}He Problem". To

2   *T.M. Nieuwenhuizen*

be compatible with this result, Galactic chemical evolution models (Tosi 2000) require that $\sim 90\%$ of solar analog stars are non-producers of ^{3}He. But the two best observed planetary nebulae do have higher concentration (Rood et al. 2002), and consequently should then both be members of the 10% class of stars that do produce ^{3}He – which seems unlikely and actually looks to be an ad-hoc fix of the standard model. For a review of the current status of ^{3}He evolution, see Romano et al. (2003).

3   MICRO BROWN DWARFS FROM GRAVITATIONAL HYDRODYNAMICS

Gravitational hydrodynamics is an approach that stresses the role of turbulence in cases of small viscosity (more precisely, large Reynolds number) and the possibility of viscous structure formation of turbulent flows on scales where the Reynolds number is low. It is well understood that at the transition from plasma to neutral gas (decoupling or recombination), the newly formed gas breaks up at the Jeans scale, forming Jeans clumps of some 600,000 $M_\odot$. It was put forward by Gibson (1996) that the Jeans clumps themselves fragment at the viscous scale into objects of earth mass, turning the Jeans gas clumps into Jeans clusters of some $2 \cdot 10^{11}$ micro brown dwarfs (μBDs) of earth mass. The Galaxy is predicted to contain about two million Jeans clusters in its halo that make up the full Galactic dark matter (Nieuwenhuizen et al. 2010, Gibson 2011).

These objects are belong to the class called MACHOs (Massive Astrophysical Compact Halo Objects). They have been detected in quasar micro lensing (Schild 1996) and the observed signature has approximately equal positive and negative events (Schild 1999), uniquely indicating microlensing by a population at unit optical depth. However, in direct searches in front of the Magellanic clouds they have not been detected. Inspection of the literature in this field reveals that this low mass scale was covered only in one paper (Renault et al. 1998). This reports observations carried out in the early and mid nineties using a telescope of 40 cm in diameter. Later MACHO searches did not cover this mass range, so the controversy between the Schild detection and the Renault et al. non-detection was never resolved. It is planned to redo the MACHO search in front of the Magellanic clouds using a much larger telescope (Schild 2011). They will be searched in what is normally called cirrus dust clouds, but what could just be an agglomeration of dark Jeans clusters. One further indication for this bold assumption is that the temperature of "cirrus dust" is about 15 K (Veneziani et al. 2010), i. .e., near the H triple point of 13.8 K. While cold dust theories have no explanation why the dust should minimally have this temperature, the required release of latent heat of these compact hydrogen clouds would then keep them long at this temperature, before finally freezing.

Analysis of wide binaries in the Galaxy halo has ruled out any MACHO dark matter component more heavy than 43 $M_\odot$ (Yoo et al. 2004). That this conclusion is somewhat too strong (Longhitano & Binggeli 2010), will be of little help in our situation. For a typical wide separation of the components, the major axis is of the order $a = 18,000$ AU $= 0.09$ pc. In our case the relevant MACHO objects for this application are the individual Jeans clusters of 600,000 $M_\odot$ and radius of 1.4 pc, so they would completely disrupt the binaries – if they were on their own. However, we now point out that these halo wide binaries - being much smaller than the Jeans clusters - must lie inside Jeans clusters themselves, as a result of which they must be much more stable than commonly expected. So we predict that these wide binaries have a center of mass motion of ca 200 km/s, a mutual speed of ca 20 km/s and are embedded in a baryonic dark matter matrix of ca 600,000 $M_\odot$. These features can be tested. Clearly, stabilized inside Jeans clusters, wide binaries do not rule out the MACHO dark matter.

One would expect that the fragmentation of the Jeans cloud has been seen in numerics. When Truelove et al. (1997) noticed instabilities in their simulations, they dismissed them as unphysical and built in Jeans filters to remove them. Recently instabilities at the $10^{-3} - 10^{-4} M_\odot$ level were observed in the simulation of the first stars in turbulent gas clouds (Clark et al. 2011): the gas first fragments and then the fragments aggregate to form the stars. The authors carefully explain how the gas can cool, namely grace to the formation of molecular hydrogen (H_2) with help of a small fraction of free electrons still present, so that heat can be radiated away through H_2 levels. This allows the gas to cool locally after which it can fragment. Though the authors did not carefully sort out what would be the minimal fragmentation scale, their fragmentation at the $10^{-3} - 10^{-4} M_\odot$ level is a already strong support for the gravitational hydrodynamics picture and indeed points towards its predicted earth mass MACHOs.

Nuclear synthesis attributes enough matter for the μBDs. About 4.5% of the critical density of the Universe is baryonic. At best 0.5 % is luminous, and some 2–3% is observed in X-ray gas. The *missing baryon problem* refers to the fact that most of the baryons are unaccounted for, about 60% is missing at cosmic scales; an inventory of baryons in and around the Milky Way reveals at best 25% of the expected baryons. Though they are believed to be located in unobserved relatively cool X-ray clouds, this need not be the full or the only explanation. Indeed, the missing dark baryons may be locked up in μBDs. Radiation from what is commonly called "cold cirrus clouds" or "cold cirrus dust" is observed to have a temperature of 15 K (Veneziani et al. 2010), or, more generally, temperatures between 40 K and 15 K (Amblard et al. 2010). Dust models have no explanation for the minimum of 15 K. But the radiation may actually arise from the thermal atmospheres of μBDs (Nieuwenhuizen et al. 2010). The fact that H has a critical point at 33 K and a triple point at 13.8 K coincides with many observations of "cold dust" temperatures by the Herschel telescope between 15 and 40 K, with the lower values condensing near 15 K, see Figures 2 and 3 of Amblard et al. (2010).

The picture of baryonic dark matter locked up in μBDs grouped in – mostly – dark Jeans clusters (JCs) explains another,

000201

not often mentioned problem: *the missing Jeans clusters problem*. Indeed, it is agreed that after the decoupling all gas fragments in Jeans clumps, but where are they now? Gravitational hydrodynamics asserts that they just constitute the halo dark matter of galaxies.

From the point of view of galactic structures there is a lot of support for the picture of Jeans clouds consisting of micro brown dwarfs. Galactic rotation curves flatten when the ca $2 \cdot 10^6$ JCs of the Galaxy have an isothermal distribution $\rho(r) \approx v^2/2\pi G r^2$, where v is the velocity dispersion, about 200 km/s for Jeans clusters in the Galaxy and 20 km/s for μBDs inside a Jeans cluster. The Tully-Fisher and and Faber-Jackson relations follow if one assumes that star formation arises when JCs heat each others mBDs by tidal forces when they come within a certain radius of each other, which brings the proportionality $Luminosity \sim \#\,\text{stars} \sim \int \mathrm{d}^3 r\, \rho^2(r) \sim v^4/R_*$ for some characteristic radius R_* (Nieuwenhuizen et al. 2009).

In galaxy merging the observed young globular clusters may not or not only appear due to tidal disruption, and its unknown star formation process, but also due to tidal heating of the mBDs, which expand and can form stars millions of years after the merging process has taken place (Nieuwenhuizen et al. 2010). Thus the galaxy merging process can transform, along the merging path, dark Jeans clusters in situ in the observed bright young globular clusters.

Mysterious radio events were reported by Ofek et al. (2010). They are frequent (1000/square degree/year), radio loud (> 1Jy), and have neither a precursor nor a follow up, and have no detectable counterparts in the infrared, visible or X-ray spectrum. Within isothermal modeling, they have been connected to merging of μBDs inside Jeans clusters, and the event duration of more than half an hour to several days allowed to estimate their radius as $3 \times$ (the duration in days) $\times$ (the solar radius) (Nieuwenhuizen et al. 2010).

The theory of star formation that has always been inconclusive, strongly benefits from the principle that star (and larger planet) formation arises from aggregations of μBDs (Gibson and Schild 2011). The *iron planet core problem* acknowledges that metalic iron planet cores, like in the earth, are difficult to explain, since iron is mostly observed in oxides, both on earth and in intergalactic space. But primordial μBDs with hot H atmospheres as massive as the Earth, can collect intergalactic chemicals C, N, O, S, P, Si etc. of the first supernovae as well as nickel and iron oxides as gravitational "vacuum cleaners", while the initially hot, moist, H atmospheres are all too eager to reduce the oxides for making molten iron-nickel cores under molten rock oceans until the water oceans condense at 2 million years at critical temperature 647 K (Gibson, Schild & Wickramasinghe 2011). Iron cores are then explained from repeatedly merging iron cores with molten rock layers in the frictional accretions of the μBDs to form larger and larger planets and finally stars (Nieuwenhuizen et al. 2010).

A relation between globular clusters and black holes was discussed (Nieuwenhuizen et al. 2010) and will be expanded elsewhere, in particular in connection with role of Jeans clusters in solving the so-called last parsec problem in black hole merging processes.

Nowadays galaxies are observed at redshifts basically up to $z = 10$. This being considered before the reionization era, they should not be visible but immersed in H clouds, so that many unobserved weak galaxies are invoked, which should ionize the gas and create a "pencil of visibility" in our direction. The galaxy UDFy-38135539 was established to have redshift $z = 8.55$, so we see light that it emitted 600 million years after the big bang (Lehnert et al. 2010). The authors say in the abstract that a significant contribution from other, probably fainter galaxies nearby, is needed to explain its visibility. This is a deus ex machina, an ad hoc argument to save the standard theory. μBDs, on the other hand, offer a more obvious explanation: the hydrogen is locked up in condensed objects, so most of the space is empty and transparent (Nieuwenhuizen et al. 2010, Gibson 2011).

One observes that the amount of dust and the rate of star formation had a peak at redshift $z \sim 2$ and are smaller in recent times. This higher amount of dust content in massive galaxies at higher redshift is difficult to explain in standard dust evolution models (Dunne et al. 2010). But it finds an easy explanation if one accepts that the "dust" radiation is produced by the atmospheres of μBDs. In the course of time, they are more and more used up because they coagulate to form heavier objects and stars. Consequently, less fuel for star formation is ultimately available and less μBD outer surface exists to emit "dust" radiation.

4   THE ANSWER TO THE HELIUM-3 PROBLEM

Within gravitational hydrodynamics it is natural to identify the HII clouds with partly or fully evaporated Jeans clusters, in which a large fraction of the μBDs, if not all, evaporated by heating in a strong star forming region. In such a case the μBDs of a Jeans cluster can expand into a gas cloud. Though they would have swept up metals produced by super novae, there would have been little ^{3}He in the interstellar medium, so they would have kept the primordial ^{3}He content up to then. Thus it would not change when they evaporated into HII clouds, so the primordial value would appear independent of their location in the Galaxy and independent of the local metallicity, which explains the ^{3}He problem.

The most massive and largest HII region in the Local Group is the region 30 Doradus in the Large Magellanic Cloud. It has been carefully studied recently (Lopez et al 2008). In addition to a large ionized gas mass $\sim 8 \cdot 10^5 M_\odot$ (Kennicutt 1984), the 30 Doradus nebula also has $\sim 10^6 M_\odot$ of CO (Johansson et al. 1998). This HII mass is approximately the mass of

000202

4   *T.M. Nieuwenhuizen*

a single Jeans cluster, supporting the just mentioned gravitational hydrodynamics picture, while the CO content exhibits a large metallicity.

In conclusion, in gravitational hydrodynamics many problems, like the 15 K cold dust temperature, the visibility of early galaxies and the ^{3}He problem, find a simple explanation.

Acknowledgment

It is a pleasure to thank David Hogg for pointing us at the wide binary problem.

REFERENCES

Amblard, A., Cooray, P. et al. (2010).   Herschel-ATLAS: Dust temperature and redshift distribution of SPIRE and PACS detected sources using submillimetre colours. Astronomy and Astrophysics, 518, L9

Bania, T. M., Rood, R. T., Balser, D. S. (2007). The Milky Way 3-Helium Abundance. Space Science Reviews, 130, 53-62.

Charbonnel, C. (1998), Mixing in stars and the evolution of the He-3 abundance. Space Science Review 84, 199-206

Charbonnel, C., Do Nascimento, J. D. (1998). How many low-mass stars do destroy He-3? Astronomy and Astrophysics 336, 915-919

Clark, P. C., Glover, S. O. C., Klessen, R. S., Bromm, V. (2011). Gravitational fragmentation in turbulent primordial gas and the initial mass function of population III stars. The Astrophysical Journal, 727, 110 (18pp)

Dunne, L., Gomez, H. et al. (2010). Herschel-ATLAS: Rapid evolution of dust in galaxies in the last 5 billion years. arXiv:1012.5186

Gibson, C. H., (1996). Turbulence in the Ocean, Atmosphere, Galaxy, and Universe. Applied Mechanics Reviews 49, 299–315

Gibson, C. H. (2011). Why the dark matter of galaxies is clumps of micro-brown-dwarfs and not Cold Dark Matter, Journal of Cosmology, Lorentz Center workshop Proceedings: New Directions in Modern Cosmology, Sept. 27 - Oct. 1, 2010, arXiv:1102.1183.

Gibson, C. H. and Schild R. E. (2011). Formation of Planets by Hydrogravitational Dynamics, Journal of Cosmology, Lorentz Center workshop Proceedings: New Directions in Modern Cosmology, Sept. 27 - Oct. 1, 2010, arXiv:1012.5522.

Gibson, C. H., Schild R. E. and Wickramasinghe, N. C. (2011). The Origin of Life from Primordial Planets, Int. J. of Astrobiology, doi:10.1017/S1473550410000352, arXiv:1004.0504.

Johansson, L. E. B. , Greve A. et al. (1998). Results of the SEST key programme: CO in the magellanic clouds - VII. 30 Doradus and its southern HII regions. Astronomy and Astrophysics 331, 857-872

Kennicutt, Jr., R. C. (1984). Do giant HII regions preferentially form in the outer disks of galaxies? Astrophysical Journal 287, 116-130

Lehnert, M. D., Nesvadba, et al. (2010). Spectroscopic confirmation of a galaxy at redshift z = 8.6. Nature, 467, 940-942

Longhitano, M., Binggeli, B. (2010). The stellar correlation function from SDSS - A statistical search for wide binary stars. Astronomy and Astrophysics 509, A46

Lopez, M. R., Krumholz, A. D. et al. (2008). What Drives the Expansion of Giant HII Regions?: A Study of Stellar Feedback in 30 Doradus. arXiv:1008.2383.

Nieuwenhuizen, T. M., Gibson, C. H., Schild, R. E. (2009). Gravitational hydrodynamics of large-scale structure formation. Europhysics Letters, 88, 49001,1–6

Nieuwenhuizen, T. M., Schild, R. E., Gibson, C. H. (2011). Do micro brown dwarf detections explain the galactic dark matter? Journal of Cosmology, Lorentz Center workshop Proceedings: New Directions in Modern Cosmology,

Ofek, E. O. et al. (2010). Long-duration radio transients lacking optical counterparts are possibly galactic neutron stars. Astrophysical Journal, 711, 517–531

Renault, C. et al. (1998). Search for planetary mass objects in the Galactic halo through microlensing. Astronomy and Astrophysics, 329, 522–537

Romano D, Tosi M, Matteucci F, Chiappini C. et al. (2003). Light element evolution resulting from WMAP data Monthly Notices of the Royal Astronomical Society 346, 295-303

Rood, R.T., Bania, T.M., Wilson, T.L. (1984). The 8.7-Ghz hyperfine line of He-3+ in galactic H-II regions. Astrophysical Journal, 280, 629-647

Rood, R. T.; Bania, T. M., Balser, D.S., (2002). The Saga of 3He. Science, 295, 804-805

Schild, R. E. (1996). Microlensing variability of the gravitationally lensed quasar Q0957+561 A,B. Astrophysical Journal, 464, 125–130

Schild, R. E. (1999). A wavelet exploration of the Q0957+561 A, B brightness record. Astrophysical Journal, 514, 598606.

Schild, R. E. (2011). Private communication

Steigman, G. (2007). Primordial Nucleosynthesis in the Precision Cosmology Era. Annual Review of Nuclear and Particle Science 57, 463-491.

Truelove, J. K., Klein, R. I., McKee, C. F., Holliman, J. H., Howell, L. H., Greenough, J. A. (1997). The Jeans condition. A new constraint on spatial resolution in simulations of isothermal self-gravitational hydrodynamics. Astrophysical Journal, 489, L179-L183

M. Tosi (2000). In: The Light Elements and Their Evolution, Proceedings of IAU Symposium 198, ed. by L. da Silva, M. Spite, J.R. de Medeiros (ASP, San Francisco, 2000), pp. 525-532

Veneziani, M., Ade, P. A. R. et al. (2010). Properties of galactic cirrus clouds observed by BOOMERanG, Astrophysical Journal, 713, 959–969

Yoo, J., Chanamé, J. and Gould, A. (2004). The end of the MACHO era: limits on halo dark matter from stellar halo wide binaries, Astrophysical Journal 601, 311-318.

000203

Local-Group tests of dark-matter concordance cosmology

Towards a new paradigm for structure formation

P. Kroupa[1], B. Famaey[1,2]⋆, K. S. de Boer[1], J. Dabringhausen[1], M.S. Pawlowski[1], C.M. Boily[2], H. Jerjen[3],
D. Forbes[4], G. Hensler[5], and M. Metz[1]⋆⋆

[1] Argelander Institute for Astronomy, University of Bonn, Auf dem Hügel 71,D-53121 Bonn, Germany
   e-mail: `pavel|deboer|joedab|mpawlow@astro.uni-bonn.de, manuel.metz@dlr.de`
[2] Observatoire Astronomique, Université de Strasbourg, CNRS UMR 7550, F-67000 Strasbourg, France
   e-mail: `benoit.famaey|christian.boily@astro.unistra.fr`
[3] Research School of Astronomy and Astrophysics, ANU, Mt. Stromlo Observatory, Weston ACT2611, Australia
   e-mail: `jerjen@mso.anu.edu.au`
[4] Centre for Astrophysics & Supercomputing, Swinburne University, Hawthorn VIC 3122, Australia
   e-mail: `dforbes@swin.edu.au`
[5] Institute of Astronomy, University of Vienna, Türkenschanzstr. 17, A-1180 Vienna, Austria
   e-mail: `hensler@astro.univie.ac.at`

accepted for publication

Abstract. Predictions of the concordance cosmological model (CCM) of the structures in the environment of large spiral galaxies are compared with observed properties of Local Group galaxies. Five new possibly irreconcilable problems are uncovered: 1) A great variety of published CCM models consistently predict some form of relation between dark-matter-mass and luminosity for the Milky Way (MW) satellite galaxies, but none is observed. 2) The mass function of luminous sub-halos predicted by the CCM contains too few satellites with dark matter (DM) mass $\approx 10^7\ M_\odot$ within their innermost 300 pc than in the case of the MW satellites. 3) The Local Group galaxies and data from extragalactic surveys indicate there is a correlation between bulge-mass and the number of luminous satellites that is not predicted by the CCM. 4) The 13 new ultra-faint MW satellites define a disc-of-satellites (DoS) that is virtually identical to the DoS previously found for the 11 classical MW satellites, implying that most of the 24 MW satellites are correlated in phase-space. 5) The occurrence of two MW-type DM halo masses hosting MW-like galaxies is unlikely in the CCM. However, the properties of the Local Group galaxies provide information leading to a solution of the above problems. The DoS and bulge–satellite correlation suggest that dissipational events forming bulges are related to the processes forming phase-space correlated satellite populations. These events are well known to occur since in galaxy encounters energy and angular momentum are expelled in the form of tidal tails, which can fragment to form populations of tidal-dwarf galaxies (TDGs) and associated star clusters. If Local Group satellite galaxies are to be interpreted as TDGs then the substructure predictions of the CCM are internally in conflict. All findings thus suggest that the CCM does not account for the Local Group observations and that therefore existing as well as new viable alternatives have to be further explored. These are discussed and natural solutions for the above problems emerge.

Key words. galaxies: dwarf – galaxies: evolution – gravitation – Local Group – dark matter – cosmology: theory

1. Introduction

Our understanding of the cosmological world relies on two fundamental assumptions: 1) The validity of General Relativity, and 2) conservation of matter since the Big Bang. Both assumptions yield the concordance cosmological model (CCM), according to which an initial inflationary period is followed by (exotic, i.e., non-baryonic) dark-matter (DM) structures forming and then accreting baryonic matter, which fuels star for-

mation in the emerging galaxies, and according to which dark energy (represented by a cosmological constant Λ) drives the acceleration of the Universe at a later epoch. One important way to test assumption (1) is to compare the phase-space properties of the nearest galaxies with the expectations of the CCM. These tests are the focus of the present contribution.

The possibility of the existence of DM was considered more than 85 years ago (Einstein 1921; Oort 1932; Zwicky 1933), and has been under heavy theoretical and experimental scrutiny (Bertone et al. 2005) since the discovery of non-Keplerian galactic rotation curves by Rubin & Ford (1970) and

---

⋆ Alexander von Humboldt Fellow
⋆⋆ now at the Deutsches Zentrum für Luft- und Raumfahrt, Königswinterer Str. 522-524, 53227 Bonn, Germany

000204

their verification and full establishment by Bosma (1981). The existence of DM is popularly assumed because it complies with the General Theory of Relativity, and therefore Newtonian dynamics, in the weak-field limits. Newtonian dynamics is the simplest form of gravitational dynamics given that the equations of motion are linear in the potential, and is thus readily accessible to numerical simulations of cosmic evolution, upon which the concordance scenario of structure formation is based (Blumenthal et al. 1984).

The concordance bottom-up scenario of structure formation involving the repeated accretion of clumps of cold dark matter (CDM) is assumed to operate throughout the Universe on all scales. CDM particles with masses of order of about 100 GeV are the preferred candidates to account for constraints placed on the matter density, Ω_M, of thermal relics with realistic cross-sections (see, e.g., eq. 28 of Bertone et al. 2005). For lighter particle candidates, the damping scale becomes too large: for instance, a hot DM (HDM) particle candidate ($m_{HDM} \approx$ few eV) would have a free-streaming length of ≈ 100 Mpc leading to too little power at the small-scale end of the matter power spectrum. The existence of galaxies at redshift $z \approx 6$ implies that the coherence scale should have been smaller than 100 kpc or so, meaning that warm DM (WDM) particles with mass $m_{WDM} \approx 1 - 10$ keV are close to being ruled out (Peacock 2003).

CDM is a concept that, together with the cosmological constant (Λ), has been motivated primarily by large-scale observations of, e.g., the cosmic microwave background (CMB) radiation (WMAP, Spergel et al. 2007; Komatsu et al. 2009), the accelerating universe (Riess et al. 1998; Perlmutter et al. 1999), or the power spectrum of density perturbations from the SDSS (Tegmark et al. 2004) and the 2dF galaxy redshift survey (Cole et al. 2005), all of which serve as empirical benchmarks for calibrating and constraining theoretical scenarios and cosmological models. This concordance ΛCDM model is consistent with observations on the Gpc to Mpc scales (Reyes et al. 2010), but it implies that the Universe evolves towards an infinite energy content[1] due to the creation of vacuum energy from dark-energy-driven accelerated expansion (e.g. Peacock 1999)[2]. Less problematically perhaps, but nevertheless noteworthy, the DM particle cannot be contained in the Standard Model of particle physics without implying a significant revision of particle physics (e.g. Peacock 1999). Strong evidence for the existence of DM has been suggested by the observations of the interacting galaxy-cluster pair 1E0657-56 (the "Bullet cluster", Clowe et al. 2006). The velocity of the sub-cluster relative to the large cluster has since been calculated to be about 3000 km s^{-1} so that the observed morphology can arise (Mastropietro & Burkert 2008). But according to Angus &

McGaugh (2008) and Lee & Komatsu (2010), such high velocities between a sub-cluster and a main galaxy cluster are virtually excluded in the CCM. Near the centre of lens-galaxies, the observed delay times between the multiple images of strongly lensed background sources cannot be understood if the galaxy has a standard (NFW or isothermal) DM content and if, at the same time, the Hubble constant has a classical value of 70 km s^{-1} Mpc^{-1}: the solution is either to decrease the Hubble constant (in disagreement with other observations), or to consider the known baryonic matter (with constant mass-to-light ratio) as the one and only source of the lensing (Kochanek & Schechter 2004). On Local Volume scales (within about 8 Mpc), it has been pointed out that the Local Void contains far fewer dwarf galaxies than expected if the CCM were true. At the same time, there are too many large galaxies in the less crowded parts such that the arrangement of massive galaxies in the Local Volume is less than 1 per cent likely in the CCM (Peebles & Nusser 2010).

This discussion highlights that there are important unsolved issues in the CCM. This clearly means that substantial effort is required to understand the problems, to perhaps distill additional clues from the data that can provide solutions, and to improve the theory.

Galaxy formation and evolution is a process that happens on scales much smaller than 1 Mpc. Ironically, a major limitation of our ability to develop a physically consistent model of how galaxies evolved out of the dark comes from incomplete knowledge of the Local Group, in particular from the lack of understanding of the structure and distribution of dwarf satellite galaxies. But, over the past few years, a steady flow of new results from nearby galaxies including the Milky Way (MW) and the significantly higher numerical resolution of computational studies of galaxy formation have allowed ever more rigorous tests of the CCM.

According to the DM hypothesis, galaxies must have assembled by means of accretion and numerous mergers of smaller DM halos. Therefore, galaxies such as the MW should be swarmed by hundreds to thousands of these halos (Moore et al. 1999a; Diemand et al. 2008), whereby the number of sub-halos is smaller in WDM than in CDM models (Knebe et al. 2008). Furthermore, the triaxial nature of the flow of matter at formation would make it impossible to destroy halo substructure by violent relaxation (Boily et al. 2004). These sub-halos should be distributed approximately isotropically about their host, and have a mass function such that the number of sub-halos in the mass interval $M_{vir}, M_{vir} + dM_{vir}$ is approximately $dN \propto M_{vir}^{-1.9} dM_{vir}$ (Gao et al. 2004).

In contrast to this expectation, only a few dozen shining satellites have been found around both the MW and Andromeda (M31), while the next largest disc galaxy in the Local Group, M33, has no known satellites. The MW hosts the 11 "classical" (brightest) satellites, while 13 additional "new" and mostly ultra-faint satellite galaxies have been discovered in the past 15 years primarily by the Sloan Digital Sky Survey (SDSS)[3]. While the MW satellites are distributed

---

[1] One may refer to this issue as the "cosmological energy catastrophy" in allusion to the black body UV catastrophy, which led Max Planck to heuristically introduce an auxiliary (= _Hilfsgröße_ in German) number h, to reproduce the black body spectrum.

[2] Energy conservation is a problematical issue in General Relativity (GR). The stress-momentum-energy tensor is a pseudo tensor and so is not invariant under a transformation to a different coordinate system and back. This may perhaps be considered to indicate that GR may not be complete.

[3] For convenience, the 11 brightest satellite galaxies are here referred to as the "classical" satellites because these were known before

highly anisotropically (e.g. Klimentowski et al. 2010), observations of the internal kinematics (velocity dispersion) of the satellites suggest they are the most DM dominated galaxies known (e.g. fig. 15 in Simon & Geha 2007). That is, the velocity dispersions of their stars seem to be defined by an unseen mass component: the stars are moving faster than can be accounted for by their luminous matter. The known satellites may therefore be the luminous "tip of the iceberg" of the vast number of dark sub-halos orbiting major galaxies such as the MW.

Much theoretical effort has been invested in solving the problem that the number of luminous satellites is so much smaller than the number of DM-halos predicted by the currently favoured concordance ΛCDM hypothesis: stellar feedback and heating processes limit baryonic growth, re-ionisation stops low-mass DM halos from accreting sufficient gas to form stars, and tidal forces from the host halo limit growth of the DM sub-halos and lead to truncation of DM sub-halos (Dekel & Silk 1986; Dekel & Woo 2003; Macciò et al. 2009; Koposov et al. 2009; Okamoto & Frenk 2009; Kirby et al. 2009; Shaya et al. 2009; Busha et al. 2010; Macciò et al. 2010). This impressive and important theoretical effort has led to a detailed quantification of the DM-mass–luminosity relation of MW satellite galaxies. Moreover, the discovery of new (ultra-faint) dSph satellites around the MW suggests the validity of the "tip of the iceberg" notion. These lines of reasoning have generally led to the understanding that within the ΛCDM cosmology, no serious small-scale issues are apparent (e.g. Tollerud et al. 2008; Primack 2009).

In this contribution we test whether the CCM can be viewed as a correct description of the Universe by studying generic properties of the Local Group[4], which is a typical environment for galaxies – the Local Group properties *must* conform to the CCM if it is to be valid universally. To test this hypothesis, we critically examine state-of-the art models calculated within the CDM and WDM framework by a number of independent research groups developed to explain the properties of the faint satellite galaxies, by comparing them with the following observations: the mass-luminosity relation for dSph satellites of the Milky Way (Sect. 2); the mass-distribution of luminous-satellite halo-masses (Sect. 3); and the observed relation between the bulge mass of the host galaxy and the number of satellites (Sect. 4). The question of whether the Disc-of-Satellites (DoS) exists, and if in fact the latest MW satellite discoveries follow the DoS, or whether the existence of the DoS is challenged by them, is addressed in Sect. 5. In Sect. 5, the observed invariance of late-type baryonic galaxies is also discussed in the context of the Local Group. In these sections it emerges that the CCM has problems relating to the observed data. In Sect. 6 the problems are interpreted as clues to a possible solution of the origin of the satellite galaxies. The implications of testing the CCM on the Local Group for gravitational theories are also discussed. Conclusions regarding the consequences of this are drawn in Sect. 7.

2. The satellite mass – luminosity relation (problem 1)

Our understanding of the physical world relies on some fundamental physical principles. Among them is the conservation of energy. This concept implies that it is increasingly more difficult to unbind sub-components from a host system with increasing host binding energy.

Within the DM hypothesis, the principle of energy conservation therefore governs how DM potentials fill-up with matter. There are two broadly different physical models exploring the consequences of this, namely models of DM halos based on internal energy sources (mostly stellar feedback), and models based on external energy input (mostly ionisation radiation). In the following, the observational mass–luminosity data for the known satellite galaxies are discussed, and the data are then compared to the theoretical results that are calculated within the CCM.

2.1. The observational data

Based on high quality measurements of individual stellar line-of-sight velocities in the satellite galaxies, Strigari et al. (2008) (hereinafter S08) calculate dynamical masses, $M_{0.3kpc}$, within the inner 0.3 kpc of 18 MW dSph satellite galaxies over a wide range of luminosities ($10^3 \lesssim L/L_\odot \lesssim 10^7$). The LMC and SMC are excluded, as is Sagittarius because it is currently experiencing significant tidal disturbance. S08 significantly improve the previous works by using larger stellar data sets and more than double the number of dwarf galaxies, and by applying more detailed mass modelling. Their results confirm the earlier suggestion by Mateo et al. (1993), Mateo (1998), Gilmore et al. (2007), and Peñarrubia et al. (2008) that the satellites share a common DM mass scale of about $10^7 M_\odot$, "and conclusively establish" (S08) this common mass scale.

The finding of S08 can be quantified by writing

$$\log_{10} M_{0.3kpc} = \log_{10} M_0 + \kappa \log_{10} L, \qquad (1)$$

and by evaluating the slope, κ, and the scaling, M_0. S08 derive $\kappa = 0.03 \pm 0.03$ and $M_0 \approx 10^7 M_\odot$. Using the Dexter Java application of Demleitner et al. (2001), a nonlinear, asymmetric error weighted least squares fit to the S08 measurements reproduces the common mass and slope found by S08, as can be seen from the parameters listed in Table 1. By excluding the least luminous dSph data point, one obtains the same result (Table 1).

It follows from Eq. 1 that

$$(M_{0.3kpc})^{1/\kappa} = M_0^{1/\kappa} L \quad (\kappa \neq 0),$$
$$M_{0.3kpc} = M_0 \qquad (\kappa = 0). \qquad (2)$$

This central mass of the DM halo can be tied by means of high-resolution CDM simulations to the total halo virial mass before its fall into the host halo (S08, see also Sect. 3),

$$M_{vir} = (M_{0.3kpc})^{1/0.35} \times 10^{-11} M_\odot, \qquad (3)$$

---

the SDSS era. These include the LMC and the SMC with the others being dwarf spheroidals. The other, more recently discovered satellites are fainter than the faintest "classical" satellites (UMi and Draco), and these are called the "new" or the "ultra-faint" satellites or dwarfs (see Table 2).

[4] Useful reviews of the Local Group are provided by Mateo (1998) and van den Bergh (1999).

000206

4 Kroupa et al.: Local Group tests of cosmology

yielding $M_{\mathrm{vir}} = 10^9 \, M_\odot$ for $M_{0.3\mathrm{kpc}} = 10^7 \, M_\odot$ (the common-mass scale for $\kappa = 0$). Thus, substituting $M_{0.3\mathrm{kpc}}$ into Eq. 3 using Eq. 2, leads to

$$(M_{\mathrm{vir}})^{0.35/\kappa} = M_0^{1/\kappa} \times 10^{-(11\times0.35)/\kappa} \, L. \qquad (4)$$

This value of the halo mass near $10^9 \, M_\odot$ for the satellites in the S08 sample is confirmed by a new analysis, in which Wolf et al. (2010) show that the mass can be derived from a velocity dispersion profile within the deprojected 3D half light profile with minimal assumptions about the velocity anisotropy. In this way they obtain a robust mass estimator.

The observed 5σ lower value for $0.35/\kappa \equiv \eta$ is thus $\eta = 2.06$ (with $\kappa = 0.02 + 5 \times 0.03$ from Table 1).

2.2. Model type A: Internal energy sources

Dekel & Silk (1986) and Dekel & Woo (2003) studied models according to which star formation in DM halos below a total halo mass of $M_{\mathrm{vir}} \approx 10^{12} M_\odot$ is governed by the thermal properties of the inflowing gas, which is regulated primarily by supernova feedback. These models demonstrate that the mass-to-light ratio of sub-halos follows $M_{\mathrm{vir}}/L \propto L^{-2/5}$ (eq. 24 of Dekel & Woo 2003; see also eq. 33 of Dekel & Silk 1986). This approximately fits the observed trend for dSph satellite galaxies (Mateo 1998).

These models thus imply that

$$(M_{\mathrm{vir}})^{\eta_{\mathrm{th}}} = \zeta \, L, \qquad (5)$$

where L is the total luminosity, M_{vir} is the virial DM halo mass, $\eta_{\mathrm{th}} = 5/3$, and ζ is a proportionality factor. In essence, this relation states that more-massive halos have a larger binding energy such that it becomes more difficult to remove matter from them than from less massive halos.

Comparing with Eq. 4 and with its resulting η value as given at the end of Sect. 2.1, it follows that the observed 5σ lower value for $\eta = 0.35/\kappa = 2.06$ is in conflict with Eq. 5 where $\eta_{\mathrm{th}} = 5/3 = 1.67$.

2.3. Model type B1, B2: External energy source

Busha et al. (2010) follow a different line of argument to explain the dSph satellite population by employing the DM halo distribution from the *via Lactea* simulation. Here the notion is that re-ionisation would have affected DM halos variably, because of an inhomogeneous matter distribution. A given DM halo must grow above a critical mass before re-ionisation to form stars or accrete baryons. Thus the inhomogeneous re-ionisation model (Busha et al. 2010, their fig. 6) implies, upon extraction of the theoretical data and using the same fitting method as above, theoretical κ-values of 0.15–0.17. These disagree however, with the observational value of 0.02 with a significance of more than $4\,\sigma$, i.e. the hypothesis that the observational data are consistent with the models can be discarded with a confidence of 99.99 per cent (Table 1).

Busha et al. (2010) suggest that adding scatter into the theoretical description of how DM halos are filled with luminous baryons would reduce the discrepancy, but it is difficult to see

Table 1. The slope of the DM-mass–luminosity relation of dSph satellite galaxies. Fitted parameters for Eq. 1.

data	κ	radius [pc]	M_0 [$10^7 \, M_\odot$]
Observational:			
1	$+0.02 \pm 0.03$	300	1.02 ± 0.39
2	$+0.02 \pm 0.03$	300	1.01 ± 0.40
3	$+0.01 \pm 0.03$	300	1.09 ± 0.44
*4	-0.03 ± 0.05	600	6.9 ± 4.9
DM Models:			
A: feedback	0.21	300	—
B1: re-ionisation, SPS	0.15 ± 0.02	300	0.24 ± 0.06
B2: re-ionisation	0.17 ± 0.01	300	0.18 ± 0.02
C: SAM	0.42 ± 0.02	300	2.0 ± 0.9
*D: Aq-D-HR	0.17 ± 0.02	600	0.41 ± 0.14
E1: 1keV(WDM)	0.23 ± 0.04	300	0.069 ± 0.045
E2: 5keV(WDM)	0.12 ± 0.02	300	0.43 ± 0.081
F: Aq-infall	0.13 ± 0.01	300	0.32 ± 0.022

Notes to the table: Fits to $\kappa = 0.35/\eta$: data 1–4 are observational values, data A–F are models (see Sect. 2). Notes: 1: our fit to S08 (who give central 300 pc masses, 18 satellites, their fig. 1). 2: our fit to S08 without Seg.1 (faintest satellite, i.e. 17 satellites, their fig. 1). 3: our fit to S08 without Seg.1 and without Hercules (i.e. 16 satellites, their fig. 1). 4: our fit to the observational data plotted by Okamoto & Frenk (2009) (who give central 600 pc masses, only 8 satellites, their fig. 1). A: Dekel & Silk (1986); Dekel & Woo (2003), stellar feedback (Eq. 5). B1: our fit to Busha et al. (2010), their SPS model. B2: our fit to Busha et al. (2010), inhomogeneous re-ionisation model. C: our fit to Macciò et al. (2010), semi-analytical modelling (SAM), fit is for $L_V > 3 \times 10^5 \, L_{V,\odot}$. D: our fit to Okamoto & Frenk (2009) (Aq-D-HR). E1: our fit to the 1 keV WDM model of Macciò & Fontanot (2010). E2: our fit to the 5 keV WDM model of Macciò & Fontanot (2010). F: our fit to the Aquarius sub-halo-infall models of Cooper et al. (2010). *: the entries with an asterisk are for the central 600 pc radius region.

how this can be done without violating the actual scatter in the observed $M_{0.3\mathrm{kpc}} - L$ relation.

2.4. Model type C: Semi-analytical modelling (SAM)

Filling the multitude of DM halos with baryons given the above combined processes was investigated by Macciò et al. (2010). They semi-analytically modelled (SAM) DM sub-halos based on N−body merger tree calculations and high-resolution re-computations. The authors state "We conclude that the number and luminosity of Milky Way satellites can be naturally accounted for within the (Λ)Cold Dark Matter paradigm, and this should no longer be considered a problem."

Their theoretical mass–luminosity data are plotted in their fig. 5, and a fit to the redshift $z = 0$ data for $L_V > 3 \times 10^5 \, L_{V,\odot}$ satellites is listed in Table 1. The theoretical SAM data set shows a steep behaviour, $\kappa = 0.42$. Given the observational data, this model is ruled out with a confidence of more than ten σ.

2.5. Model type D: High-resolution baryonic physics simulations (Aq-D-HR)

The satellite population formed in a high-resolution N-body ΛCDM re-simulation with baryonic physics of one of the MW-type "Aquarius" halos is studied by Okamoto & Frenk (2009). The treatment of baryonic processes include time-evolving photoionisation, metallicity-dependent gas cooling and photo-heating, supernova (SN) feedback, and chemical enrichment by means of SN Ia and II and AGB stars. Re-ionisation is included and the galactic winds driven by stellar feedback are assumed to have velocities proportional to the local velocity dispersion of the dark-matter halo. In these models 100 per cent of the SNII energy is deposited as thermal energy. Galactic winds are thus produced even for the least-massive dwarf galaxies. Winds are observed in strong starbursts induced through interactions rather than in self-regulated dwarf galaxies, which may pose a problem for this ansatz (Ott et al. 2005). The details of the simulations are provided by Okamoto et al. (2010). The resultant sub-halo population with stars can, as claimed by the authors, reproduce the S08 common-mass scale.

Following the same procedure as for the above models, this claim is tested by obtaining κ from their fig. 1 (upper panel, red asterisks) and comparing it to the observational data also plotted in their fig. 1 (note that Okamoto & Frenk 2009 plot the masses within 600 pc rather than 300 pc as used above). From their plot of the observational data, which only includes central-600 pc masses for the eight most luminous satellites, it follows that $\kappa_{obs,OF} = -0.03 \pm 0.05$. This is nicely consistent with the full S08 sample (18 satellites) discussed above. However, for their model data one finds that $\kappa = 0.17 \pm 0.02$, i.e. the model can be discarded with a confidence of 3σ or 99.7 per cent.

2.6. Model type E1, E2: WDM

Macciò & Fontanot (2010) present theoretical distributions of satellite galaxies around a MW-type host halo for different cosmological models, namely ΛCDM and WDM with three possible DM-particle masses of $m_{WDM} = 1$, 2, and 5 keV. They perform numerical structure formation simulations and apply semi-analytic modelling to associate the DM sub-halos with luminous satellites. They suggest the luminosity function and mass–luminosity data of observed satellites is reproduced by the WDM models implying a possible lower limit to the WDM particle of $m_{WDM} \approx 1$ keV.

The model and observational mass–luminosity data are compared in their fig. 5 for $m_{WDM} = 1$ and 5 keV. The slopes of these model data are listed in Table 1. From Table 1 it follows that the WDM model with $m_{WDM} \approx 1$ keV is ruled out with very high confidence (4σ or 99.99 per cent), and also has too few satellites fainter than $M_V \approx -8$ (their fig. 4). WDM models with $m_{WDM} \approx 5$ keV are excluded at least with a 3σ or 99.7 per cent confidence, and, as is evident from their fig. 4, the models contain significantly too few satellites brighter than $M_V = -11$.

2.7. Model type F: Infalling and disrupting dark-matter satellite galaxies

Cooper et al. (2010) study CDM model satellites in individual numerical models of dark matter halos computed within the Aquarius project. Semi-analytical modelling is employed to fill the sub-halos with visible matter, and the orbits of the infalling satellites are followed. General agreement with the observed satellites is claimed.

Much as the other models above, in this numerical CDM model of substructure and satellite formation in a MW type host halo, the MW sub-halos fall-in stochastically and therefore do not agree with the observed phase-space correlated satellites, i.e. with the existence of a rotating DoS (Sect. 5 below). Furthermore, the presented model mass-luminosity data (their fig. 5) lead to a too steep slope (Table 1) compared to the observations and the DM-based model is excluded with a confidence of at least 99.7 per cent. In addition, fig. 5 of Cooper et al. (2010) shows a significant increase in the number of model satellites with a similar brightness as the faintest known satellite (Segue 1, hereinafter Seg. 1). This is in contradiction with the failure to find any additional satellites of this luminosity in the most recent data mining of the existing northern SDSS data, as discussed in Sect. 6.2 below. Indeed, observations suggest that Seg. 1 is a star cluster rather than a satellite galaxy (Niederste-Ostholt et al. 2009), worsening this problem.

2.8. Discussion

In Fig. 1, the latest theoretical ansatzes A–F to solve the cosmological substructure problem are compared with the latest observational limit on the slope κ of the DM-mass–luminosity relation of dSph satellite galaxies (Eq. 1).

The theoretical results always lead to a trend of luminosity with halo mass as a result of energy conservation. But the observed satellites do not show an increasing trend of luminosity with DM mass, according to Mateo (1998), Peñarrubia et al. (2008), and Strigari et al. (2008). From Fig. 1 we note that seven ΛCDM models of the satellites deviate 4σ or more from the data, while only one (the WDM model E2 with $m_{WDM} = 5$ keV, Table 1) deviates more than 3σ from the data. The likelihood [5] that any of the DM models describes the data is thus less than 0.3 per cent.

As a caveat, the observed absence of a DM-mass-luminosity relation partially depends on the data for the ultra-faint dwarfs: indeed, for the classical (most luminous) dSphs, Serra et al. (2009) argue that there may be a trend, $\kappa > 0$, essentially because of their proposed increase in the mass of the Fornax dSph satellite. It is on the other hand plausible that the ultra-faint dwarfs do not possess any dark halo (see Sect. 6), and that the enclosed mass derived is due to observational artifacts. In that case they should not be used as a possible improvement for the missing satellite problem. This, however, would pose a problem for the DM hypothesis.

---

[5] The *likelihood* = 1−(confidence in per cent)/100 gives an indication of how well the data can be accounted for by a given model. The *confidence*, as used throughout this text, is the probability level at which a model can be discarded.
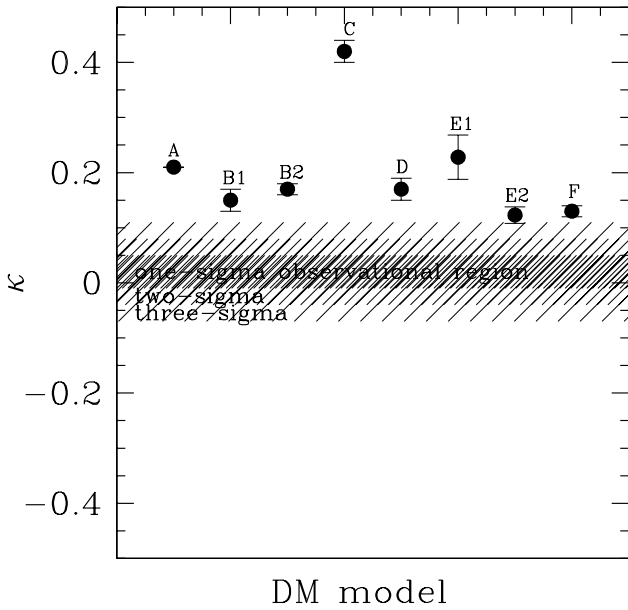
6   Kroupa et al.: Local Group tests of cosmology

Fig. 1. The slope of the mass–luminosity relation, κ (Eq. 1), for the models listed in Table 1. The observational constraints with confidence intervals are depicted as hatched regions (1, 2, and 3σ region). Satellites with a larger dark-matter mass are on average more luminous such that the mass–luminosity relation has $\kappa > 0$. However, the observational constraints lie in the region $\kappa \approx 0$ (see Table 1). The hypothesis that the data are consistent with any one of the models can be discarded with very high (at least 3σ, or more than 99.7 per cent) confidence.

Adén et al. (2009b) suggest that for the Hercules dSph satellite inter-loper stars need to be removed from the observational sample, which would require a revision of the mass within 300 pc to the value $M_{0.3\mathrm{kpc}} = 1.9^{+1.1}_{-1.6} \times 10^6 \, M_\odot$ (instead of the value $M_{0.3\mathrm{kpc}} = 7.2^{+0.51}_{-0.21} \times 10^6 \, M_\odot$ derived by S08). This new mass measurement, however, now lies more than $4\,\sigma$ away from all ΛCDM-models considered above (Table 1). Hercules can thus not be understood in terms of a DM-dominated model. Adén et al. (2009b) do state that DM-free models cannot be excluded (note also Fig. 6 below), or that Hercules may be experiencing tidal disturbances in its outer parts. Tidal disturbance, however, would have to be very significant for its inner structure to be affected, because if one would require conformity with the theoretical DM-models its $M_{0.3\mathrm{kpc}}$ mass would have to have been much higher and similar to the value derived by S08 ($\approx 10^7 \, M_\odot$). Given the current Galactocentric distance of Hercules of 130 kpc and the result that the inner region of a satellite is only affected by tides after significant tidal destruction of its outer parts (Kazantzidis et al. 2004), this scenario is physically implausible. There are therefore three possibilities: (i) Hercules is a DM-dominated satellite. This, however, then implies that no logically consistent solution within the CDM framework is possible because its mass–luminosity datum would lie well away from the theoretical expectation. (ii) Hercules has no DM. This implies that it cannot be used in the mass-luminosity data analysis above and would also imply there to exist an additional type of DM-free satellites, which, however, share virtually all observable physical characteristics with the putatively DM filled satellites. (iii) Hercules

has been significantly affected by tides. This case is physically implausible because of its large distance, but it would imply that Hercules cannot be used in the mass-luminosity analysis above (just as Sagittarius is excluded because of the significant tidal effects it is experiencing). Omitting Hercules from the data leads to a revised observational slope $\kappa = 0.01 \pm 0.03$ such that none of the conclusions reached above about the performance of the DM-models are affected.

A point of contention for DM models of dSph satellite galaxies is that the DM halos grow at various rates and are also truncated variously due to tidal influence. The highly complex interplay between dark-matter accretion and orbit-induced accretion truncation leads to the power-law mass function of DM halos, and at the same time would imply that the outcome in which all luminous DM sub-halos end up having the same DM mass were incompatible with the DM-theoretical expectations (see Sect. 3).

Summarirising Sect. 2, while the theoretical results always lead to a trend of luminosity with halo mass, the observed satellites do not show this trend. The hypothesis that the CCM accounts for the data can be discarded with more than 99.7 per cent significance.

3. The mass function of CDM halo masses (problem 2)

One of the predictions of the ΛCDM hypothesis is the self-similarity of DM-halos down to (at least) the mass range of dwarf galaxies, i.e. that massive halos contain sub-halos of lower mass, with the same structure in a statistical sense (Moore et al. 1999a; for a major review see Del Popolo & Yesilyurt 2007). The mass function of these sub-halos is, up to a critical mass M_{crit}, well approximated by

$$\xi_{\mathrm{sub}}(M_{\mathrm{vir}}) = \frac{dN}{dM_{\mathrm{vir}}} \propto M_{\mathrm{vir}}^{-1.9}, \tag{6}$$

where dN is the number of sub-halos in the mass interval $M_{\mathrm{vir}}, M_{\mathrm{vir}} + dM_{\mathrm{vir}}$ (Gao et al. 2004), M_{crit} is given by $M_{\mathrm{vir}} \approx 0.01 M_{\mathrm{h}}$ with M_{h} is the virial mass of the hosting CDM-halo. The virial mass, M_{vir}, is defined by

$$M_{\mathrm{vir}} = \frac{4\pi}{3} \Delta_{\mathrm{vir}} \rho_0 r_{\mathrm{vir}}^3, \tag{7}$$

where ρ_0 is the critical density of the Universe and Δ_{vir} is a factor such that $\Delta_{\mathrm{vir}}\rho_0$ is the critical density at which matter collapses into a virialised halo, despite the overall expansion of the Universe. The virial radius r_{vir} is thereby determined by the density profile of the collapsed CDM-halo. For $M_{\mathrm{vir}} > 0.01 \, M_{\mathrm{h}}$, the mass function steepens (Gao et al. 2004), so that it is effectively cut off at a mass M_{max} (see Eq. 8 below). It is reasonable to identify M_{max} with the mass of the most massive sub-halo, which must be higher than M_{crit}, where the mass function begins to deviate from Eq. 6 and lower than M_h, the mass of the host-halo. Therefore, $M_{\mathrm{crit}} < M_{\mathrm{max}} < M_h$.

Thus, a halo with $M_{\mathrm{vir}} \approx 10^{12} \, M_\odot$, like the one that is thought to be the host of the MW, should have a population of sub-halos spanning several orders of magnitude in mass. It is well known that, in consequence, a steep sub-halo mass

function such as Eq. 6 predicts many more low-mass sub-halos than the number of observed faint MW satellites (Moore et al. 1999a; Klypin et al. 1999), a finding commonly referred to as the *missing satellite problem*. Efforts to solve this problem rely on physical processes that can either clear CDM-halos of all baryons or inhibit their gathering in the first place, which would affect low-mass halos preferentially (e.g. Moore et al. 2006; Li et al. 2010; Sect. 2). More specifically, Li et al. (2010) find that the mass function of luminous halos, $\xi_{\text{lum}}(M_{\text{vir}})$, would essentially be flat for $10^7 M_\odot \leq M_{\text{vir}} < 10^9 M_\odot$. All sub-halos with $M_{\text{vir}} \geq 10^9 M_\odot$ would keep baryons and therefore $\xi_{\text{lum}}(M_{\text{vir}}) = \xi_{\text{sub}}(M_{\text{vir}})$ in this mass range. Thus, the mass function of *luminous sub-halos* can be written as

$$\xi_{\text{lum}}(M_{\text{vir}}) = k k_i M_{\text{vir}}^{-\alpha_i}, \tag{8}$$

with

$$\alpha_1 = 0, \quad k_1 = 1, \qquad\qquad 10^7 \leq \tfrac{M_{\text{vir}}}{M_\odot} < 10^9,$$
$$\alpha_2 = 1.9, \quad k_2 = k_1 (10^9)^{\alpha_2 - \alpha_1}, \quad 10^9 \leq \tfrac{M_{\text{vir}}}{M_\odot} \leq M_{\text{max}},$$

where the factors k_i ensure that $\xi_{\text{vir}}(M_{\text{vir}})$ is continuous where the power changes and k is a normalisation constant chosen such that

$$\int_{10^7}^{M_{\text{max}}} \xi_{\text{vir}}(M_{\text{vir}}) \, dM_{\text{vir}} = 1. \tag{9}$$

From a mathematical point of view, Eq. 8 is the probability distribution of luminous sub-halos. We note that the luminous sub-halo mass function proposed in Moore et al. (2006) is similar to the one in Li et al. (2010). In the high-mass part, it has the same slope as the mass function for all sub-halos and flattens in the low-mass part (cf. fig. 3 in Moore et al. 2006). The lower mass limit for luminous halos is however suggested to be $M_{\text{vir}} \approx 10^8 \, M_\odot$ in Moore et al. (2006). The mass function of *all sub-halos* has $\alpha_1 \approx \alpha_2 \approx 1.9$ (Gao et al. 2004).

3.1. NFW halos

It is well established that the theoretical density profiles of galaxy-sized CDM-halos are similar to a universal law, as proposed by Navarro et al. (1997). The NFW profile is given by

$$\rho_{\text{NFW}}(r) = \frac{\delta_c \rho_0}{r/r_s \, (1 + r/r_s)^2}, \tag{10}$$

where r is the distance from the centre of the halo and ρ_0 is the critical density of the Universe, while the characteristic radius r_s and δ_c are mass-dependent parameters.

By integrating $\rho_{\text{NFW}}(r)$ over a volume, the total mass of CDM within this volume is obtained. Thus,

$$M(r) = \int_0^r \rho(r') 4\pi r'^2 \, dr' \tag{11}$$

is the mass of CDM contained within a sphere of radius r around the centre of the CDM-halo, and $M(r) = M_{\text{vir}}$ for $r = r_{\text{vir}}$. Performing the integration on the right-hand side of Eq. 11 and introducing the concentration parameter $c = r_{\text{vir}}/r_s$ leads to

$$M(r) = \frac{4\pi \rho_0 \delta_c r_{\text{vir}}^3}{c^3} \left[\frac{r_{\text{vir}}}{r_{\text{vir}} + c\,r} + \ln\left(1 + \frac{c\,r}{r_{\text{vir}}}\right) - 1 \right]. \tag{12}$$

The parameter δ_c can be expressed in terms of c,

$$\delta_c = \frac{\Delta_{\text{vir}}}{3} \frac{c^3}{\ln(1+c) - c/(1+c)}, \tag{13}$$

as can be verified by setting $r = r_{\text{vir}}$ in Eq. 12 and substituting $M(r_{\text{vir}}) = M_{\text{vir}}$ by Eq. 7.

If the halo is luminous, it is evident that $M(r)$ is smaller than the total mass included within r, M_r. However, assuming that the MW satellites are in virial equilibrium and that their dynamics is Newtonian in the weak-field limit, the mass-to-light ratios calculated for them are generally high and imply that they are DM-dominated and thus, $M(r) = M_r$ would be a good approximation. This relation is therefore adopted for the present discussion. In this approximation $M(r = 0.3\text{kpc}) = M_{0.3\text{kpc}}$.

In principle, the parameters ρ_0 (Navarro et al. 1997), c (Bullock et al. 2001), and Δ_{vir} (Mainini et al. 2003) depend on the redshift z but for the purpose of the present paper only $z = 0$ needs to be considered, as this is valid for the local Universe. Thus,

$$\rho_0 = \frac{3H_0^2}{8\pi G}, \tag{14}$$

where the Hubble constant $H_0 = 71 \, \text{km s}^{-1} \, \text{Mpc}^{-1}$ (Spergel et al. 2007), $\Delta_{\text{vir}} \simeq 98$ for ΛCDM-cosmology (Mainini et al. 2003), and

$$\log_{10}(\bar{c}) = 2.31 - 0.109 \log_{10}\left(\frac{M_{\text{vir}}}{M_\odot}\right), \tag{15}$$

where $\bar{c}$ is the expectation value of c as a function of M_{vir}. Thus, $\bar{c}$ decreases slowly with M_{vir}, while the scatter in the actual c is rather large, being

$$\sigma_{\log_{10} c} = 0.174 \tag{16}$$

(Macciò et al. 2007). The only caveat here is that the NFW profile is used to integrate the mass, while the now-preferred Einasto profile (Navarro et al. 2010, Sect. 1) makes only a small difference in the central parts.

3.2. Probing the ΛCDM hypothesis with $M_{0.3\text{kpc}}$

S08 use the stellar motions in 18 MW satellites to calculate their mass within the central 300 pc, $M_{0.3\text{kpc}}$. They assume the satellites to be in virial equilibrium and that Newtonian dynamics can be applied to them. The sample from S08 can be enlarged to 20 satellites by including the Large Magellanic Cloud (LMC) and the Small Magellanic Cloud (SMC), since van der Marel et al. (2002) estimated the mass of the LMC within the innermost 8.9 kpc, M_{LMC}, using the same assumptions as S08. This implies that $M_{\text{LMC}} = (8.7 \pm 4.3) \times 10^9 \, M_\odot$, of which the major part would have to be DM. Equations. 7, 12, 13 and 15 have been used to create tabulated expectation values of $M(r)$ for NFW-halos with different M_{vir} and it can thereby be seen that for a typical NFW-halo with $M(r = 8.9 \, \text{kpc}) = 8.7 \times 10^9 \, M_\odot$, $M(r = 0.3 \, \text{kpc}) = 2.13 \times 10^7 \, M_\odot = M_{0.3\text{kpc}}$, and $M_{\text{vir}} = 1.2 \times 10^{11} \, M_\odot$. We note that the SMC has about 1/10th of the mass of the LMC (Kallivayalil et al. 2006), hence the virial mass of its halo
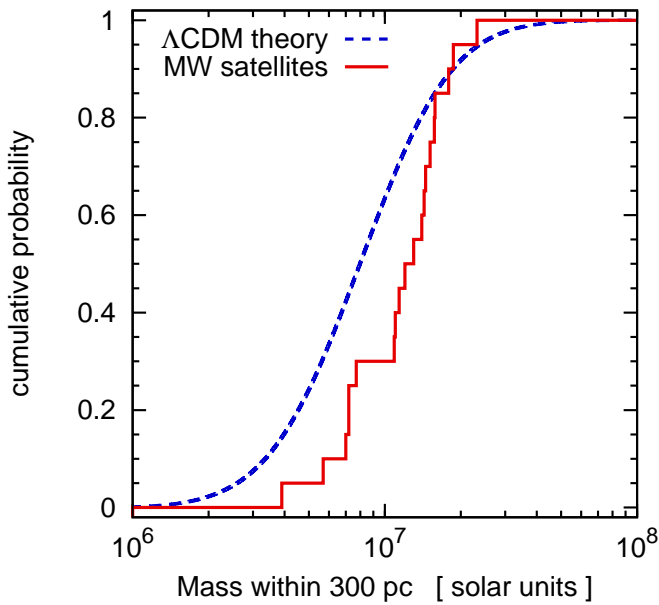
8   Kroupa et al.: Local Group tests of cosmology

Fig. 2. The *mass function of luminous satellite problem.* The cumulative distribution function for the mass within the central 300 pc, $M_{0.3\text{kpc}}$, of the MW satellites (solid line) and the cumulative distribution function for $M_{0.3\text{kpc}}$ of a sample of 10^6 CDM-halos picked from the parent distribution of luminous sub-halos (Eq. 8, dashed line). The null hypothesis is that the MW satellite $M_{0.3\text{kpc}}$ masses are drawn from this parent distribution. The maximum distance between the two curves is 0.333 so that the null hypothesis can be discarded with 98.9 per cent confidence.

can be estimated as $M_{\text{vir}} = 1.2 \times 10^{10}\ M_\odot$, corresponding to $M_{0.3\text{kpc}} = 1.51 \times 10^7\ M_\odot$.

To test the shape of the MW satellite distribution function against the shape of the distribution of the $M_{0.3\text{kpc}}$ values of the MW-satellites, artificial samples of 10^6 $M_{0.3\text{kpc}}$ masses are generated in concordance with the ΛCDM hypothesis, using Monte Carlo simulations. As noted in Sect. 3.1, $M_{0.3\text{kpc}}$ is well approximated by $M(r = 0.3\text{kpc})$ in a CDM-dominated galaxy. $M(r = 0.3\text{kpc})$ can be calculated if M_{vir} and c are given, and the expectation value for c is a function of M_{vir}. The first step is therefore to choose a value for M_{vir} using uniform random deviates and the probability distribution of luminous halos given in Eq. 8 (see e.g. chapter 7.2 in Press et al. 1992 for details). The next step is to attribute a value for $\log_{10}(c)$ to the chosen M_{vir}. This is done by multiplying Eq. 16 with a Gaussian random deviate and adding the result to the value for $\log_{10}(\bar{c})$, which is calculated from Eq. 15. After transforming $\log_{10}(c)$ to c, $M_{0.3\text{kpc}} = M(r = 0.3\text{kpc})$ of the given halo can be calculated from Eq. 12, using Eqs. 7 and 13. These steps are repeated, until a sample of 10^6 $M_{0.3\text{kpc}}$ values is generated.

If two samples are given, the maximum distance between their cumulative distribution functions, D, can be calculated. Performing the KS-test, this quantity D allows an estimate of how likely it is that they are drawn from the same distribution function. The null hypothesis is that the observed satellite galaxies are drawn from the theoretically calculated mass function of luminous halos; the parent distribution is thus as-

sumed to be the mass function of $M(0.3\text{kpc})$ values of luminous sub-halos according to the ΛCDM hypothesis. Assuming in Eq. 8 that $M_{\text{max}} = 10^{11}\ M_\odot$, which is approximately the mass estimated for the CDM halo of the LMC, and taking $M_{\text{min}} = 10^7\ M_\odot$, leads to $D = 0.333$. According to the KS-test, given the parent distribution the probability of an even larger distance is 0.011. This means that the null hypothesis can be excluded with 98.9 per cent confidence. Both cumulative distributions are shown in Fig. 2[6].

Omitting the LMC and SMC from the observational sample but keeping $M_{\text{min}} = 10^7\ M_\odot$ and $M_{\text{max}} = 10^{11}\ M_\odot$ in the theoretical sample yields $D = 0.294$, leading to the exclusion of the null hypothesis with a confidence of 95.5 per cent. In addition setting $M_{\text{max}} = 4 \times 10^{10}\ M_\odot$, which is the M_{vir} that corresponds to the most massive $M_{0.3\text{kpc}}$ in the S08 sample (i.e. the most massive remaining sub-halo), yields $D = 0.301$ leading to exclusion of the null hypothesis with a confidence of 96.3 per cent. The latter two tests comprise a homogeneous mass-sample of observed satellites as compiled by S08.

That the mass function is expected to steepen at $M_{\text{crit}} = 0.01\ M_{\text{h}}$ even increases the discrepancy between the ΛCDM hypothesis and the observations. Reinstating the LMC and SMC back into the observational sample and cutting off $\xi_{\text{sub}}(M_{\text{vir}})$ at $M_{\text{max}} = 10^{10}\ M_\odot$ (with $M_{\text{min}} = 10^7\ M_\odot$), which would be close to M_{crit} for the CDM-halo of the MW (see Sect. 3), and one order of magnitude below the estimated mass of the CDM-halo of the LMC, implies that $D = 0.359$ and an exclusion with 99.5 per cent confidence.

On the other hand, setting $M_{\text{max}} = 10^{12}\ M_\odot$ (with $M_{\text{min}} = 10^7\ M_\odot$) leads to $D = 0.329$ and an exclusion with 98.8 per cent confidence. Any reasonable uncertainty in the actual value of M_{max} can therefore be excluded as an explanation of the discrepancy between the observed sample of $M_{0.3\text{kpc}}$ and a sample generated based on the ΛCDM hypothesis. As a consequence, the same is true for the uncertainty in the actual mass of the halo of the MW, M_{h}, since M_{max} is linked to M_{h} (see Sect. 3).

Thus M_{max} is kept at $10^{11}\ M_\odot$ in the following. Adjusting the lower limit of $\xi_{\text{lum}}(M_{\text{vir}})$ from $10^7\ M_\odot$ to $10^8\ M_\odot$ then leads to $D = 0.319$ and an exclusion of the null-hypothesis with a confidence of 98.4 per cent. The mass of $10^8\ M_\odot$ is the M_{vir} suggested by the lowest $M_{0.3\text{kpc}}$ in the sample from S08. We note that the likelihood decreases with decreasing M_{max}, because of the overabundance of $M_{0.3\text{kpc}} \approx 10^7\ M_\odot$ halos becoming more prominent in the observational sample.

S08 suggest that $\xi_{\text{lum}}(M_{\text{vir}})$ might even be cut off below a mass of $\approx 10^9 M_\odot$, either because halos below that mass do not contain baryons or do not form at all. Indeed, modifying $\xi_{\text{lum}}(M_{\text{vir}})$ given by Eq. 8 accordingly, results in an agreement between the theoretical distribution and the data ($D = 0.188$ with an exclusion confidence of only 70 per cent). A $\xi_{\text{lum}}(M_{\text{vir}})$

---

[6] Monte Carlo experiments are used to quantify the confidence values for the KS-tests: Drawing the corresponding number of sub-halo masses (e.g. 20 as in this case) from Eq. 8, D' is calculated. This is repeated 10^5 times. Counting of D' values gives the fraction of cases when $D' > D$, where D is the actually obtained D' value from the data (e.g. $D = 0.333$ in this case). These fractions are reported here as likelihood values, and are about half as large as the probability values obtained using approximate methods, as, e.g., by Press et al. (1992).

with a lower mass limit of $10^9 \, M_\odot$ is however in disagreement with the ΛCDM hypothesis, since the limiting mass below which all CDM-halos are dark ought to be two orders of magnitude lower according to Li et al. (2010).

As a final note, the newly derived reduced mass of Hercules (see end of Sect. 2.8) affects neither the calculated likelihoods nor the conclusions reached here.

Summarising Sect. 3, the mass distribution of the predicted DM halos of observed satellites is consistent with the ΛCDM hypothesis with at most 4.5 per cent likelihood. Assuming the dSph satellites are in virial equilibrium, the observationally deduced DM halo masses of the MW satellites show a significant overabundance of $M_{0.3\mathrm{kpc}} \approx 10^7 \, M_\odot$ halos and a lack of less-massive values compared to the theoretically calculated distribution for luminous sub-halos, despite much effort to solve the *common-mass-scale problem* (Sect. 2).

4. The bulge mass versus satellite number relation (problem 3)

According to a straight forward interpretation of the CCM, more massive DM host halos have a larger number of luminous satellites because the number of sub-halos above a low-mass threshold increases with host halo mass, given the host halo mass waxes by accreting sub-halos. The sub-halos are accreted mostly individually without a physical link to the processes occurring at the centre of the host halo. There indeed does not appear to be an observed relation between the halo mass and the bulge mass, since pairs of galaxies with and without a bulge (such as M31, Rubin & Ford 1970, and M101, Bosma et al. 1981, respectively) but with the same rotation velocity can be found. It would be useful to return to models A–F (Sect. 2) and to include the formation of the host galaxy in the modelling to quantify the degree of correlation between the bulge mass and number of luminous satellites actually expected in the CCM. When doing so, the same type of models will also have to account for the presence of bulge-less galaxies having the same DM-halo mass, as pointed out above. That is, it would *not* suffice to merely demonstrate that some sort of bulge-mass–satellite number correlation emerges in the CCM. The case $M_{\mathrm{bulge}} = 0$ must emerge naturally within the model, since two-thirds of all bright disk galaxies have no bulge or only a small one (Combes 2009b).

On the basis of extragalactic observational data, Karachentsev et al. (2005) note, but do not quantify, the existence of a correlation between the bulge luminosity and the number of associated satellite galaxies such that galaxies without a bulge have no known dSph companions, such as M101. Karachentsev et al. (2005) also point out that the number of known dSph satellites increases with the tidal environment.

The existence of this correlation can be tested in the Local Group, where good estimates of the number of satellites within the nominal virial radii of the respective hosts and of the stellar bulge masses of the three major galaxies (MW, M31, and M33) exist. Only the satellites brighter than $L_V = 0.2 \times 10^6 \, L_\odot$ ($M_V < -8.44$) are considered, given that the census of fainter satellites is incomplete for the MW (notably in the southern

hemisphere), and also for M31 and M33 given their distances. By restricting this analysis to satellites with $L_V > 0.2 \times 10^6 \, L_\odot$, the result becomes robust against the discovery of additional satellites since these would typically be fainter. The result is displayed in Fig. 3: a linear correlation between the bulge mass and the number of early-type satellites is suggested. An error-weighted least squares linear fit to the data yields

$$N_{\mathrm{dSph}} = (4.03 \pm 0.04) \times M_{\mathrm{bulge}}/(10^{10} \, M_\odot). \qquad (17)$$

In terms of the present-day stellar mass fraction, the dSph satellites of the MW add-up to at most a few times $10^7 \, M_\odot$, so that they amount to about 0.15 per cent of the mass of the bulge. Given that Eq. 17 is a linear fit to three data points only, it will be important to check the reality of this correlation by surveying disc galaxies in the Local Volume with different bulge masses for a deep and exhaustive sampling of satellite galaxies.

Given the small number of observational data points underlying Eq. 17, one should not over-interpret this result, but it is legitimate to inquire how significant the empirical correlation between bulge mass and the number of satellites is. In view of the observation by Karachentsev et al. (2005) noted above, it may be indicative of a physical correlation.

The significance of the Local Group bulge–satellite correlation is evaluated by performing a Monte Carlo experiment, the null hypothesis of which is that there is no correlation. This hypothesis would appear to be plausible in the CCM because the number of satellites depends mostly on the host DM halo mass, while the bulge is produced by baryonic processes taking place near the center of the host DM halo. Three pairs of M_{bulge} and N_{dSph} values are chosen randomly from uniform distributions such that $M_{\mathrm{bulge}} \in [0, 4.6 \times 10^{10} \, M_\odot]$ and $N_{\mathrm{dSph}} \in [0, 28]$[7]. For each three-point data set, a linear regression yields a measure of the degree of correlation. This is performed 10^6 times. The following incidences are counted: 1) the resulting linear relation passes the $(M_{\mathrm{bulge}}, N_{\mathrm{dSph}}) = (0, 0)$ point[8] *and* the slope of the linear relation has a relative uncertainty smaller than a given value; and the second test is 2) the slope of the linear relation has a relative uncertainty smaller than a given value. The relative uncertainty in the slope used here is based on the uncertainties in the data. Applying this relative uncertainty to Eq. 17 leads to $N_{\mathrm{dSph}} \approx (4 \pm 1) \times M_{\mathrm{bulge}}/(10^{10} \, M_\odot)$. Taking the upper and the lower 1σ limit of the slope, this equation thereby passes the lower and the upper 1σ values of the data (Fig. 3)[9].

---

[7] The upper bounds of the intervals are the 3σ upper values of M_{bulge} and N_{dSph} of M31. The scaling of the axes is, however, irrelevant for the results of the Monte Carlo experiments, because the aim is to test how likely a correlation results, given the null hypothesis.

[8] The precise condition here is as follows: Let there be three Monte Carlo pairs $(M_{\mathrm{bulge}}, N_{\mathrm{dSph}})_i$, $i = 1...3$. A linear regression yields a slope and an axis intersection, both with uncertainties expressed as σ values. If the axis intersection lies within 5σ of the $(0, 0)$ point, then this particular set of bulge–satellite pairs is counted. Note that the test does not require the slope to be the same as the observed value.

[9] The uncertainty in the slope given by Eq. 17 is a measure for how close the data lie to the straight line fitted to them, i.e. very close in the given case. However, the uncertainties on the data suggests that the observed case is rather improbable (although obviously not impossible), even if the correlation between N_{dSph} and M_{bulge} is real. The
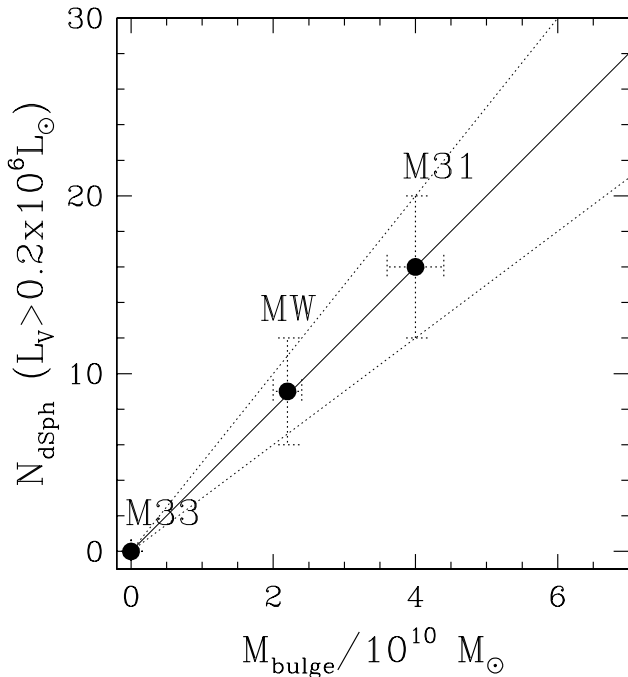
Fig. 3. The number of dSph and dE satellite galaxies more luminous than $0.2 \times 10^6 \, L_\odot$ is plotted versus the bulge mass of the host galaxy (MW: Zhao 1996, M31: Kent 1989, M33: Gebhardt et al. 2001). Only satellites within a distance of 270 kpc of the MW and M31 are used. The solid line (slope= 4.03) is Eq. 17. The upper (slope= 5.03) and the lower (slope= 3.03) dotted lines illustrate the relative uncertainty assumed in the Monte Carlo experiment (see Sect. 4).

The Monte Carlo result is that case 1) occurs 44 000 times, while case 2) occurs 157 000 times. Thus, if the correlation evident in Fig. 3 were unphysical, then observing it would have a likelihood of 0.044 and 0.157, respectively. Given the data on the Local Group, the above hypothesis that the bulge mass and number of satellites are not correlated can therefore be discarded with a confidence of 95.6 per cent and 84.3 per cent in case 1) and case 2), respectively.

Summarising Sect. 4, the null hypothesis that the bulge mass and the number of satellites are independent quantities and that bulgeless galaxies have no dSph satellites is rejected, based on the Local Group data, with a confidence of more than 95.6 per cent. With the absence of a DM-mass–luminosity relation for the observed satellites (Sect. 2), this suggests that our present understanding of how satellite dwarf galaxies form and evolve may need revision. In the formation modelling of satellite galaxies within the CCM it will therefore be necessary to include also the formation of the host galaxy, to quantify the correlation between bulge mass and the number of satellites within the CCM. It will also be essential to refine this correlation using deep observational extra galactic surveys.

---

uncertainty on the slope stated in Eq. 17 would therefore not be a good basis for the test performed here.

5. The disc of satellites (DoS) and invariant baryonic galaxies (problems 4 and 5)

The DoS is now addressed in view of the new satellite galaxies, and in Sect. 5.5 the issue that the two major DM halos of the Local Group, which happen to be similar, are occupied by similar disk galaxies is addressed within the context of the CCM.

An important constraint for understanding the origin and nature of the observed satellite galaxies comes from them being significantly anisotropically distributed about the MW, and possibly also about Andromeda. The problem of the MW system for the CCM was emphasised by Kroupa et al. (2005). They pointed out that the observed satellite system of the MW was incompatible at the 99.5 per cent confidence level with the theoretical distribution expected if the satellites were DM sub-halos tracing an isotropic DM host halo. Until then, the prediction within the DM hypothesis was that the distribution of sub-halos ought to be nearly spherical and tracing the shape of the host DM halo. For example, Aubert et al. (2004) show a MW-type DM halo to have an infall asymmetry of only about 15 per cent. The sub-halos enter the host halo along filaments and then phase-mix and virialise within the growing host DM halo. Similar sub-halo distributions are obtained in CDM and WDM models (Knebe et al. 2008).

The DoS is a pronounced feature of the MW satellite system (Metz et al. 2009b), and a similar structure was reported for the Andromeda system (Koch & Grebel 2006) for which, however, the distance uncertainties are larger and the satellite population is richer and more complex including dSph, dE, and dIrr galaxies. In the case of the well-studied MW, the DoS is very pronounced for the classical (11 brightest) satellites including the LMC and SMC. But how are the new satellites, the ultra-faint ones, distributed? Much hope for the CCM rests on the new discoveries being able perhaps to alleviate the DoS problem.

Watkins et al. (2009) and Belokurov et al. (2010) reported the discovery of two new MW satellite galaxies, Pisces I and II, respectively, enlarging the total MW satellite system to 24 satellites. Pisces I and II were found in the southern part of the SDSS survey area, making them the two first non-classical satellite galaxies found in the southern Galactic hemisphere. Furthermore, distances to a number of the already known satellite galaxies have been updated in recent years, most notably the new distance estimate for Boo II by Walsh et al. (2008), which changes the distance from 60 to 42 kpc. An updated list of all currently known satellites is provided in Table. 2 upon which the following analysis is based.

Metz et al. (2007) and Metz et al. (2009a) employed a sophisticated fitting routine to find the DoS. Here, an intuitive plane-fitting algorithm and a new disc-test are introduced. The plane-fitting algorithm leads to perfect agreement with the results obtained by Metz et al., and the new test allows an assessment of how discy the satellite distribution is.

5.1. Parameters of the DoS

A simple and straightforward method is described to calculate the DoS parameters $l_{\rm MW}$, $b_{\rm MW}$, $D_{\rm p}$, and Δ, which are, respec-

Table 2. Data for the currently known MW satellites.

Name	α_{2000} [h m s]	δ_{2000} [° m s]	$r_{\rm helio}$ [kpc]	$l_{\rm MW}$ [°]	$b_{\rm MW}$ [°]	$r_{\rm MW}$ [kpc]	Ref.	$v_{\rm GSR}^{220}$ [kms^{-1}]	$v_{\rm GSR}^{250}$ [kms^{-1}]	Δv [kms^{-1}]	Ref.	L_V [$L_\odot$]	Ref.
New:													
Boo	14 00 05	+14 30 21	64 ± 2	357.9	76.5	61	2; 10; 28; 8	94.4	94.2	±3.4	21	$(2.6 \pm 0.5) \times 10^4$	2; 18
Boo II	13 58 05	+12 51 36	45 ± 2	348.6	78.9	43	30; 31; 14					$(9.2 \pm 5.4) \times 10^2$	30; 18; 31
CVn	13 28 04	+33 33 27	214 ± 9	84.2	80.0	213	36; 8; 16; 17	64.8	69,7	±0.6	13; 29	$(2.0 \pm 0.3) \times 10^5$	36; 18
CVn II	12 57 10	+34 19 20	154 ± 5	129.4	81.3	155	25; 3; 12; 8	-97.5	-93,2	±1.2	29	$(7.5 \pm 3.1) \times 10^3$	25; 3; 18
CBe	12 26 59	+23 54 37	43 ± 2	202.2	75.5	44	3; 8; 23	47.4	40.4	±0.9	29	$(3.1 \pm 1.1) \times 10^3$	3; 18; 22
Her	16 31 04	+12 47 24	135 ± 4	31.2	38.2	129	3; 7; 8; 1; 26	128.6	140,0	±1.1	29; 1	$(2.9 \pm 0.7) \times 10^4$	3; 18; 26
Leo IV	11 32 58	-00 32 09	156 ± 5	261.1	56.3	156	3; 20	10.6	-6,0	±1.4	29	$(1.3 \pm 0.3) \times 10^4$	3; 18; 27; 9
Leo V	11 31 09	+02 13 05	176 ± 10	257.9	58.3	176	4; 9	58.5	42,8	±3.1	4	$(6.4 \pm 2.4) \times 10^3$	4; 9
Pis I	23 40 00	-00 18 00	80 ± 14	100.2	-57.8	80	32; 15	42.1	58,0		15		
Pis II	22 58 31	+05 57 09	182 ± 36*	84.1	-47.6	181	6					$\sim 8.6 \times 10^3$	6
Seg I	10 07 04	+16 04 40	23 ± 2	206.2	39.5	28	3	94.5	79,3	±1.3	11	$(3.4 \pm 2.7) \times 10^2$	3; 18
Seg II	02 19 16	+20 10 31	35 ± 2	157.0	-31.1	41	5	54.8	67,6	±2.5	5	$(8.6 \pm 2.7) \times 10^2$	5
UMa	10 34 49	+51 55 48	100 ± 4	162.0	51.3	105	34; 29; 24	-6.9	-0,3	±1.4	29	$(1.4 \pm 0.4) \times 10^4$	18
UMa II	08 51 30	+63 08 22	30 ± 5	159.7	30.4	37	35	-29.0	-17,1	±1.9	29	$(3.3 \pm 1.0) \times 10^3$	35; 18; 22
Wil1	10 49 22	+51 03 10	41 ± 6	164.4	48.8	46	33; 8					$(1.1 \pm 0.6) \times 10^3$	33; 18
Classical:													
Car†	06 41 37	-50 58 00	101 ± 5	255.2	-21.7	103	19	22.5	-4,9	±3	19	4.5×10^4	19
Dra†	17 20 19	+57 54 48	82 ± 6	93.5	34.6	82	19	-112.3	-87,7	±2	19	2.8×10^5	19
For†	02 39 59	-34 27 00	138 ± 8	230.0	-63.4	140	19	-29.2	-40,4	±3	19	1.6×10^7	19
Leo I	10 08 27	+12 18 30	250 ± 30	224.7	48.6	254	19	179.9	165,4	±2	19	4.9×10^6	19
Leo II	11 13 29	+22 09 12	205 ± 12	217.5	66.1	208	19	17.0	9,0	±2	19	5.9×10^5	19
LMC†	05 23 34	-69 45 24	49 ± 2	268.5	-33.4	48	19	143.3	118,6		19	2.1×10^9	37
SMC†	00 52 44	-72 49 42	58 ± 2	291.6	-47.4	55	19	49.6	32,5		19	5.7×10^8	37
Sgr†	18 55 03	-30 28 42	24 ± 2	9.4	-22.4	16	19	161.1	164,0	±5	19	2.0×10^7	19
Scu†	01 00 09	-33 42 30	79 ± 4	234.6	-81.9	79	19	77.9	73,8	±3	19	2.4×10^6	19
Sex	10 13 03	-01 36 54	86 ± 4	237.8	40.8	89	19	76.9	56,4	±3	19	5.4×10^5	19
UMi†	15 09 11	+67 12 54	66 ± 3	114.2	43.2	68	19	-92,9	-71,7	±2	19	3.1×10^5	19

Notes to the table: Data for the MW satellites used for fitting the DoS. Seg 1 and 2 (marked in *italics*) are included in this list for reference, but they have not been included in the fitting because they appear to be diffuse star clusters (Niederste-Ostholt et al. 2009). The positions are given both in Heliocentric coordinates (right ascension α_{2000}, declination δ_{2000}, and Heliocentric distance $r_{\rm helio}$ for epoch J2000.0) and in Galactocentric coordinates assuming the Sun to have a distance of 8.5 kpc from the MW centre. $l_{\rm MW}$ gives the Galactic longitude with 0° pointing from the Galactic centre to the Sun. $b_{\rm MW}$ is the latitude as seen from the Galactic centre and $r_{\rm MW}$ the radial distance from the centre of the MW. The coordinates were obtained using data from the references listed in the column labelled Ref., where more than one source is given, the distances to the satellites were obtained by error-weighted averaging over the available measurements. The satellite's line-of-sight velocities with respect to the Galactic standard of rest (GSR) are calculated assuming the Sun to move into the direction $l = 90°$, $b = 0°$ (in Heliocentric, Galactic coordinates) with a velocity of either 220 kms^{-1} ($v_{\rm GSR}^{220}$) or 250 km^{-1} ($v_{\rm GSR}^{250}$). The measurement-uncertainties for the radial velocities reported in the respective papers (referred to in column Ref.) are reproduced in the column labelled Δv. Finally, L_V gives the satellite luminosities in the photometric V-band; again uncertainty-weighted averages are quoted when more than one reference is given in column Ref. Data marked with † have measured proper motions, listed in table 1 of Metz et al. (2008). *: As no distance uncertainties for Pisces II are available in the literature, the error is estimated to be 20 percent of the distance. *References:* 1: Adén et al. (2009a), 2: Belokurov et al. (2006), 3: Belokurov et al. (2007), 4: Belokurov et al. (2008), 5: Belokurov et al. (2009), 6: Belokurov et al. (2010), 7: Coleman et al. (2007b), 8: de Jong et al. (2008), 9: de Jong et al. (2010), 10: Dall'Ora et al. (2006), 11: Geha et al. (2009), 12: Greco et al. (2008), 13: Ibata et al. (2006), 14: Koch et al. (2009), 15: Kollmeier et al. (2009), 16: Kuehn et al. (2008), 17: Martin et al. (2008a), 18: Martin et al. (2008b), 19: Mateo (1998), 20: Moretti et al. (2009), 21: Muñoz et al. (2006), 22: Muñoz et al. (2010), 23: Musella et al. (2009), 24: Okamoto et al. (2008), 25: Sakamoto & Hasegawa (2006), 26: Sand et al. (2009), 27: Sand et al. (2010), 28: Siegel (2006), 29: Simon & Geha (2007), 30: Walsh et al. (2007), 31: Walsh et al. (2008), 32: Watkins et al. (2009), 33: Willman et al. (2005a), 34: Willman et al. (2005b), 35: Zucker et al. (2006a), 36: Zucker et al. (2006b), 37: van den Bergh (1999).

12   Kroupa et al.: Local Group tests of cosmology

tively, the direction of the DoS-normal vector in Galactic lon-
gitude and latitude, the smallest distance of the DoS plane to
the Galactic centre, and the thickness (twice the height) of the
DoS.

The positions of satellites on the sky and their radial dis-
tances (compiled for convenience in Table 2) are transformed
into a Galactocentric, cartesian coordinate system assuming the
distance of the Sun to the centre of the MW to be 8.5 kpc. The
z-coordinate points into the direction of the Galactic north pole
and the Sun lies in the MW disk plane.

The 3D coordinates are projected into two dimensions,
plotting z against a projection onto a plane defined by the
Galactic longitude l_{MW}. This resembles a view of the MW
satellite system as seen from infinity and from within the MW
disc plane. The view of the satellite system is rotated in steps
of $1°$. For each step, a linear fit is made to the projected satellite
distribution. The linear fit is determined using the least squares
method, demanding the satellite-distances, as measured per-
pendicularly to the fitted line, to become minimal. This line
constitutes a plane seen edge-on in the current projection. The
two free parameters of the fit are the closest distance from the
MW centre, D_P, and the inclination b_{MW} of the normal vector
to the z-axis (a polar plane has $b_{MW} = 0°$). The plane-normal-
vector's longitude is l_{MW}, given by the projection. The fits are
performed for each angle l_{MW} between $0°$ and $360°$. After half
of a rotation, the view is identical to the one of $180°$ before,
mirrored along the z-axis.

For each angle l_{MW}, the root mean square (RMS) thick-
ness, Δ, of the satellite distribution around the fitted line is de-
termined. The normal vector to the best-fit disc solution (the
DoS) to the full 3-dimensional distribution of the MW satel-
lites is then given by those l_{MW} and b_{MW} that give the smallest
RMS thickness Δ_{min}.

To account for the uncertainties in the distance of the satel-
lites, the major source of error, the procedure is repeated 1000
times. Each time, the radial position of each satellite is ran-
domly chosen from a normal distribution centered on the satel-
lite's radial distance. It has a standard deviation given by the
distance uncertainties to the satellite galaxies. Once a realisa-
tion with varied radial distances is set up, the coordinate trans-
formation into the Galactic coordinate system is performed.
The parameters of the best fits are determined for each realisa-
tion. Their final values are determined by averaging the results
of all realisations, the standard deviations of their values are
adopted as the uncertainties in the fits.

Fitting all 24 currently known satellite galaxies within a
distance of 254 kpc from the MW, the minimum disc thickness
is found to be $\Delta_{min} = 28.9 \pm 0.6$ kpc. This is more than 14σ
away from the maximum thickness of $\Delta_{max} = 55.7 \pm 1.3$ kpc
obtained at a $90°$ projection of the data. *Thus, the DoS is highly
significant.* The position of the minimum thickness gives the
best-fit disc, the DoS. The normal vector defining the DoS
points to $l_{MW} = 156°.4 \pm 1°.8$ and has an inclination of $b_{MW} =
-2°.2 \pm 0°.6$, i.e. is nearly perfectly polar. D_P, the closest dis-
tance of the DoS from the MW centre, is 8.2 ± 1.0 kpc $\ll \Delta_{min}$.
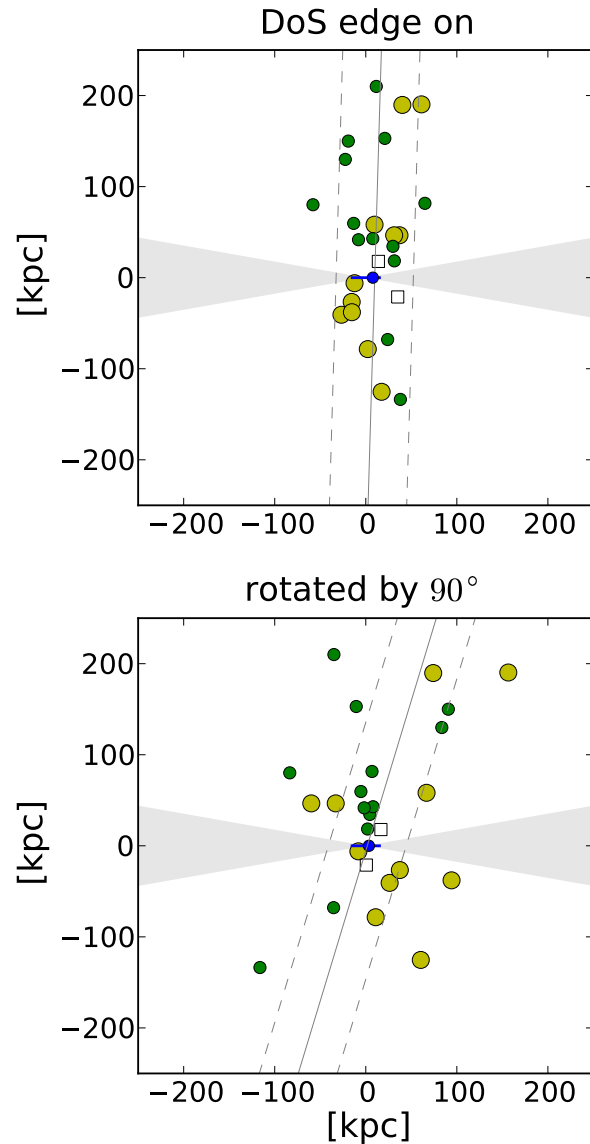

Fig. 4. Parameters of the MW DoS: the 3-D distribution of the MW
satellite galaxies. The 11 classical satellites are shown as large (yel-
low) cirlces, the 13 new satellites are represented by the smaller
(green) dots, whereby Pisces I and II are the two southern dots. The
two open squares near the MW are Seg 1 and 2; they are not included
in the fit because they appear to be diffuse star clusters nearby the
MW, but they do lie well in the DoS. The obscuration-region of $\pm10°$
from the MW disc is given by the horizontal gray areas. In the cen-
tre, the MW disc orientation is shown by a short horizontal line, on
which the position of the Sun is given as a blue dot. The near-vertical
solid line shows the best fit (seen edge-on) to the satellite distribution
at the given projection, the dashed lines define the region $\pm 1.5 \times \Delta_{min}$,
Δ_{min} being the RMS-thickness of the thinnest DoS ($\Delta_{min} = 28.9$ kpc
in both panels). *Upper panel*: an edge-on view of the DoS. Only three
of the 24 satellites are outside of the dashed lines, giving $N_{in} = 21$,
$N_{out} = 3$ and thus a ratio of $\mathcal{R} = N_{in}/N_{out} = 7.0$. Note the absence of
satellites *in large regions of the SDSS survey volume* (upper left and
right regions of the upper panel, see also fig. 1 in Metz et al. 2009a
for the SDSS survey regions). *Lower panel*: a view rotated by $90°$, the
DoS is seen face-on. Now, only 13 satellites are close to the best-fit
line, 11 are outside, resulting in $\mathcal{R} = 1.2$. Note that by symmetry the
Southern Galactic hemisphere ought to contain about the same num-
ber of satellites as the Northern hemisphere. Thus, *The Stromlo Milky
Way Satellite Survey* is expected to find about eight additional satel-
lites in the Southern hemisphere.

000215

5.2. A novel disc test

Another test to determine whether the satellite galaxies are distributed in a disc can be performed by comparing the number of satellites near the plane to the number further away: Let N_{in} be the number of all satellites that have a perpendicular distance of less than 1.5 times the minimal disc thickness Δ_{min} from the line-fit. Accordingly, N_{out} represents all satellites further away. Both N_{in} and N_{out} are determined for each rotation angle, measuring distances from the line (i.e. plane viewed edge-on in the given projection) that fits the distribution in the given projection best. This is illustrated in Fig. 4. It shows an edge-on view of the best-fit plane, along with a view rotated by 90°. Both views see the disc of the MW edge-on.

Figure 5 shows the ratio of galaxies found within the DoS to those outside (solid black line), $\mathcal{R} = N_{in}/N_{out}$. The situation is shown for the unvaried distances. If the MW satellites were distributed in a disc, $\mathcal{R}$ would approach a maximum when looking edge-on, while it will rapidly decrease once the projection is rotated out of the disc plane. It is a good test to discriminate a disc-like distribution from a spheroidal one. The latter would not lead to much variation in the ratio.

It can be seen that $\mathcal{R}$ approaches a maximum close to the best-fit l_{MW}. At the maximum, only two of the 24 satellite galaxies are found outside of the required distance from the disc. The maximum $\mathcal{R}$ is thus 11.0, situated only a few degrees away from the l_{MW} that gives the smallest thickness. This has to be compared to the broad minimum of $\mathcal{R} \approx 1$. The disc-signature is obvious, proving the existence of a DoS that incorporates the new satellites found in the SDSS.

5.3. Classical versus new satellites: is there a DoS in both cases?

In addition to the above analysis of all 24 known MW satellites, the analysis is also carried out separately for two distinct subsamples: the 11 classical, most-luminous satellite galaxies and the 13 new satellites discovered mostly in the SDSS. Each of them uses an own minimal thickness, given by the subsample distribution, in determining $\mathcal{R}$. If all satellite galaxies follow the same distribution, given by the DoS, a separate fitting should lead to similar parameters. If, on the other hand, the new (mostly ultra-faint) satellites follow a different distribution, then this would challenge the existence of a DoS. *It is worth emphasising that while the brightest satellites in a ΛCDM model of a MW-type halo may exceptionally form a weak disc-like structure (Libeskind et al. 2009), none of the existing CCM-based theoretical satellite distributions predict the whole satellite population to be disc-like.*

Furthermore, comparing the results for the classical 11 satellites with the ones obtained by the more sophisticated fitting technique used by Metz et al. (2007) is a good test to check whether the present technique gives reliable results.

The graphs for both subsamples are included in Fig. 5, the results for classical satellites are represented by the dashed yellow, the new (SDSS) satellite galaxies by the dashed green line. Both are in good agreement not only with the combined sample, but also with each other. They peak at their best-fit l_{MW},
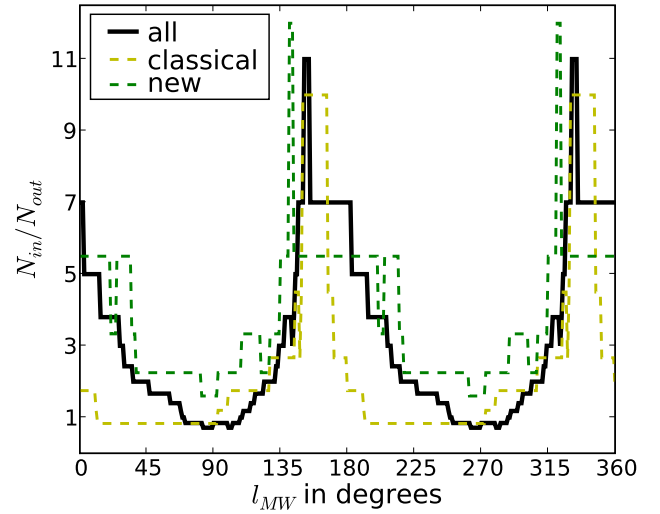

Fig. 5. Testing for the existence of the DoS. The behaviour of $\mathcal{R}$ for each view of the MW, given by the Galactic longitude of the normal vector for each plane-fit. $\mathcal{R} = N_{in}/N_{out}$ is the ratio of the number of satellites within $1.5 \times \Delta_{min}$ (Δ_{min} = 28.9 kpc), N_{in}, to those further away from the best-fit line, N_{out}, calculated for all 24 known satellites, as well as for the fits to the 11 classical and the 13 new satellites separately (taking their respective RMS thicknesses as the relevant Δ_{min}). The disc-like distribution can be clearly seen as a strong peak close to $l_{MW} = 150°$. Note that the position of the peaks are close to each other for both subsamples separately. This shows that the new satellite galaxies independently define the same DoS as the classical satellite galaxies.

with each of them having an N_{out} of only one galaxy at the peak.

Applying the technique presented in Sect. 5.1 to calculate the DoS parameters, the new satellites have a best-fit disc with a normal vector pointing to $l_{MW} = 151°.4 \pm 2°.0$, only five degrees away from the direction that was obtained by considering all known MW satellites. The inclination is $b_{MW} = 9°.1 \pm 1°.0$, again an almost perpendicular orientation of the DoS relative to the MW disc, being only 11 degrees away from the value determined before. The derived RMS thickness is $\Delta_{min} = 28.6 \pm 0.5$ kpc, essentially identical to the one given by all satellite galaxies. The minimum distance from the MW centre is $D_P = 18.3 \pm 1.3$ kpc.

The fitting to the 11 classical satellites leads to results that are in very good agreement, too. The best-fit position for the 11 classical satellites is $l_{MW} = 157°.6 \pm 1°.1$ and $b_{MW} = -12°.0 \pm 0°.5$, the thickness is found to be $\Delta = 18.3 \pm 0.6$ kpc, and the closest distance to the MW centre is $D_P = 8.4 \pm 0.6$ kpc. This is in excellent agreement with the results of Metz et al. (2007). In that paper, the authors reported that $l_{MW} = 157°.3$, $b_{MW} = -12°.7$, $\Delta_{min} = 18.5$ kpc, and $D_P = 8.3$ kpc. This illustrates that the results are extremely accurate despite employing a more simple disc-finding technique.

The agreement of the fit parameters for the two subsamples *separately* is impressive. Two populations of MW satellite galaxies (classical versus ultra-faint) with different discovery histories and methods define the same DoS. This shows

that the new, faint satellites fall close to the known, classical, DoS ($\equiv$DoS$_{cl}$). Even without considering the classical satellite galaxies, the new satellites define a disc, DoS$_{new}$, that has essentially the same parameters. This confirms the existence of a common DoS$\approx$DoS$_{new}$ $\approx$DoS$_{cl}$.

5.4. The DoS – Discussion

A pronounced DoS is therefore a physical feature of the MW system. But what is its origin? Is the existence of both the classical-satellite DoS$_{cl}$ and the new-satellite DoS$_{new}$, such that DoS$_{new}$ $\approx$ DoS$_{cl}$, consistent with the CCM?

It has been suggested that the highly anisotropic spatial satellite distribution maps a highly prolate DM halo of the MW that would need to have its principal axis oriented nearly perpendicularly to the MW disc (Hartwick 2000). However, there is still much uncertainty and disagreement as to the shape and orientation of the MW DM halo: Fellhauer et al. (2006) used the bifurcation of the Sagittarius stream to constrain the shape of the MW DM halo to within about 60 kpc, finding it to be close to spherical. The measurement of the shape of the DM halo of the MW within 60 kpc by Law et al. (2009), also based on the Sagittarius stream, suggests that the DM halo is triaxial, but with major and minor axes lying within the plane of the MW disc. The DM halo of the MW would therefore not trace a similar three-dimensional structure as the satellites, unless the major axis of the MW halo changes its orientation by about 90 degrees beyond 60 kpc and becomes essentially disc-like (i.e. highly oblate). Law & Majewski (2010) find a new slightly oblate solution to the MW DM halo shape at distances from 20 to 60 kpc. In this solution, the minor axis points along the line Sun–MW-centre suggesting a similar orientation of this extra potential as the DoS. The authors emphasise that this model is not strongly motivated within the current CDM paradigm, it merely serving as a "numerical crutch". Given this disagreement about the shape and orientation of the MW DM halo, a significant future observational and theoretical effort to clarify the situation is needed.

An additional issue for the CCM is that the normal to the DoS is defined mostly by the outermost satellites, while the direction of the average orbital angular momentum vector is defined by the innermost satellites for which proper motions have been measured. Both, the normal and the average orbital angular momentum vector are nearly co-aligned implying a strong degree of *phase-space correlation* between the satellites such that the DoS is rotating (Metz et al. 2008). This rotational DoS is not expected if the satellites merely trace the MW DM halo, because they would have independent infall histories and would therefore not be correlated in phase space.

This phase-space feature has been addressed by Libeskind et al. (2009). In a thorough analysis of structure formation on MW-galaxy scales, they show that the MW constitutes an improbable but possible constellation of CDM-dominated satellites about a MW-type disk galaxy, the satellites having (of course) independent infall and accretion histories. They analyse an N-body sample of 30946 MW-mass DM host halos with mass in the range $2 \times 10^{11}\,M_\odot$ to $2 \times 10^{12}\,M_\odot$

for the properties of their substructure distribution. They first select from this sample only those halos that host a galaxy of similar luminosity as the MW (specifically, galaxies more luminous in the V-band than $M_V = -20$). From this remaining sample of 3201 (10 per cent) hosts, they select those that contain at least 11 luminous satellites, leaving 436 (1.4 per cent) host halos. In this sample of 436 systems, about 30 per cent have 6 luminous satellites with orbital angular momenta aligned to a degree similar to that of the MW system. Thus, only 0.4 per cent of all existing MW-mass CDM halos would host a MW-type galaxy with the right satellite spatial distribution. As the authors point out, this probability of 4×10^{-3} that the DM model accounts for the observed MW-type satellite system would be lower still if proper motion measurements of additional satellites affirm the orbital angular momentum correlation highlighted by Metz et al. (2008), or if the satellites that may be discovered in the southern hemisphere by the *Stromlo Milky Way Satellite Survey* (Jerjen 2010)[10] also lie within the DoS. All 13 new satellites define the same DoS as the 11 classical ones, and furthermore, the latest additions in the southern Galactic hemisphere also lie in the DoS (Sect. 5.3), *suggesting that the DM hypothesis is much less likely than 0.4 per cent to be able to account for the MW satellite system in MW-type DM halos.*

Li & Helmi (2008) and D'Onghia & Lake (2008) propose an interesting alternative solution to the *satellite phase-space correlation problem*: they suggest that the correlation is caused by the infall of groups of DM-dominated dwarf galaxies. Unfortunately, this proposition is challenged by all known nearby groups of dwarf galaxies being spatially far too extended to account for the thinness of the DoS (Metz et al. 2009b). It may be thought that the groups that have fallen in correspond to compact dwarf groups that do not exist any longer because they have subsequently merged. But this is compromised by the observation that their putative merged counterparts in the field do not seem to exist (Metz et al. 2009b). Indeed, Klimentowski et al. (2010) model a MW-type system and deduce "... that such a disc is probably not an effect of a group infall unless it happened very recently" (their section 4.2.2). Furthermore, this notion would seem to imply that dwarf galaxy groups are full of dSph galaxies, while the pristine (before group infall) MW halo would have formed none, in conflict with the observed morphology-density relation (e.g. Okazaki & Taniguchi 2000).

It needs to be emphasised that the DM-based models have so far not addressed the issue that the DoS lies nearly perpendicularly to the MW disc; DM-based models need to *postulate* that this occurs, and it may indeed simply be chance. The combined probability that a DM-based model accounts for the observed MW-type system, which has the properties that the satellites have correlated angular momenta and form a DoS highly inclined to the baryonic disc of the host galaxy, cannot currently be assessed but is, by logical implication, smaller than 4×10^{-3}.

But perhaps the MW is a very special system, an outlier within the DM-based framework? This possibility can be as-

---

[10] http://www.mso.anu.edu.au/~jerjen/SMS_Survey.html

sessed by considering the nearest MW-similar DM halo. It hosts a similar disc galaxy, Andromeda, which has a similar satellite system to the MW but is however richer and more complex, and has a larger bulge mass than the MW (Fig. 3). Andromeda may also have a DoS (Koch & Grebel 2006, see also fig. 4 in Metz et al. 2009a)[11] suggesting that these satellite distributions may not be uncommon among MW-type DM halos.

Thus, a Local Group consisting of two dominant DM halos of similar (MW-type) mass would have a likelihood of 0.4 per cent times 1.4 per cent, i.e. 5.6×10^{-5}, to appear with two MW-type disc galaxies, one of them having a pronounced rotating DoS with 11 or more luminous satellites, and the other having at least 11 luminous satellites.

5.5. Invariant baryonic galaxies

The Libeskind et al. (2009) analysis, described in Sect. 5.4, also shows that about 10 per cent of MW-type DM halos would host a MW-luminous galaxy, the 90 per cent of others would presumably host galaxies with lower luminosities suggesting a large variation between DM halo and luminous galaxy properties. This however, appears to be a problem considering the properties of observed disc galaxies. By using a principal component analysis on hundreds of disc galaxies, Disney et al. (2008) demonstrate that observed disc galaxies are simple systems defined by one underlying parameter, rather than about six if the galaxies were immersed in DM halos. Citing additional similar results, van den Bergh (2008) and Gavazzi (2009) reach the same conclusion, as well as Gentile et al. (2009) and Milgrom (2009a). This is further supported by an entirely independent study of star-forming galaxies, which again shows a remarkably small variation of behaviour (Pflamm-Altenburg & Kroupa 2009b). The discovery that the ratio of DM mass to baryonic mass within the DM core radius is constant for galaxies (Sect. 6.4.1 below) is another statement of the same effect.

The small amount of variation for disc galaxies thus appears to be very difficult to reconcile with the large variation inherent in the DM model, as quantified by the Libeskind et al. (2009) analysis: 90 per cent of MW-mass DM halos would have disc galaxies that differ substantially in luminosity from the MW in the CCM, and yet the closest neighbour, Andromeda, is similar to the MW. This is the *invariant-baryonic-galaxy problem*.

Summarising Sect. 5, the CCM is highly significantly challenged by the spatial distribution of MW satellite galaxies and by the similarity of rotationally supported galaxies. The *phase-space correlation problem* of the classical satellites is enhanced significantly after the inclusion of the new ultra-faint satellites, and the Local Group enhances the *invariant baryonic galaxy problem*.

---

[11] Note that the rich satellite system of M31 may have a sub-population of satellites in a disc-like structure (Metz et al. 2009a).

6. The origin of dSph and dE galaxies: an alternative proposition and deeper implications

What has been learned so far? The DM-mass–luminosity data of MW dSph satellite galaxies appear to conflict with the CCM results, and the mass function of DM masses of the dSph satellites is not in good agreement with the mass function of luminous sub-halos calculated within the CCM. The correlation bulge-mass versus satellite-number is tentative (for having only three points) but will very likely pass the test of time because the error bars allow for a conclusive significance test. The two quantities appear to be physically related as indicated strongly by the Local Group data and also extragalacitc surveys, but clearly much more work needs to be done both observationally and theoretically to refine the implied correlation. The highly pronounced phase-space correlation of the MW satellites means that any formation mechanism must have involved correlated orbital angular momenta of the satellites.

Given that the formation of a bulge involves highly dissipative processes, it emerges that a highly dissipative process seems to have formed the bulge and the correlated orbital angular momenta of the satellites. This leads to the real possibility that the origin of both the MW bulge and its satellite population is related to a galaxy–galaxy encounter. Indeed, it is well known and documented that galaxy encounters lead to the formation of bulges *and* tidal arms that can host the formation of tidal-dwarf galaxies (TDGs). These are then naturally correlated in phase space. Since the bulge and the satellites of the MW are about 11 Gyr old, we are led to the scenario that the proto-Galaxy may have had a major encounter or merger about 11 Gyr ago during which the bulge and the satellites formed (Pawlowski et al. 2010). Wetzstein et al. (2007) demonstrated in a series of numerical models that the number of TDGs increases indeed with the gas fraction of the pre-collision galaxy. This is relevant to galaxy encounters at a high redshift, where galaxy encounters are expected to have been frequent.

Noteworthy is that a scenario for the origin of dSph satellite galaxies along the above lines had been suggested already before the DM hypothesis was widely accepted, namely that they may be ancient TDGs (Lynden-Bell 1976, 1983; Kunkel 1979). This proposition can naturally account for their correlated phase-space distribution in the form of a rotating disc-like distribution (Sect. 5), and would lend a new viewpoint on the difficulty of understanding the properties of the MW dSph satellites as DM sub-halos documented above.

6.1. The evolution of TDGs

A natural way to explain the satellite phase-space correlation as well as the bulge-satellite relation is thus to identify the dSph satellite galaxies of the MW with a population of ancient TDGs that probably formed during a gas-rich encounter between the early MW and another galaxy. But if they all formed at the same time, how can the different chemical properties and star-formation histories of the different dwarf galaxies then be explained within this scenario? If the DM hypothesis is not viable for the MW satellite population, how can the high mass-to-light ratios of the satellites be explained?

It is known that the satellite galaxies all have ancient populations of an indistinguishable age (Grebel 2008), perhaps being created when the TDGs were born. Or, the ancient population comes from the precursor host galaxy. TDGs may also form with globular clusters as long as the star-formation rate surpasses a few $M_\odot$/yr for 10 Myr (Weidner et al. 2004). The chemo-dynamical modelling by Recchi et al. (2007) has shown that once a TDG (without DM) forms it is not natural for it to blow out the gas rapidly. Rather, the rotationally-supported small gas-rich discs of young TDGs begin to evolve through self-regulated star formation either until their gas is consumed or removed through ram-pressure stripping. Consequently, their internal evolution through star formation can be slow and individual, such that TDGs that formed during one encounter event can exhibit different chemical properties many Gyr after their formation. Removal of the interstellar medium from the TDG through ram-pressure takes about half to a few orbital times, which is typically one to a few Gyr after formation. This time scale is consistent with the observed cessation of star formation in most MW dSph satellites (Grebel 1999). The TDGs that have remained at large distances from their hosts retain their gas and appear as dIrr galaxies (Hunter et al. 2000). Once formed, TDGs cannot fall back onto their hosts and merge since dynamical friction is insignificant for them. A TDG may be dispersed (but not accreted) if it happens to be on a near radial orbit, which, however, is unlikely given the torques acting on the tidally expelled material from which the TDG forms during the encounter.

If the dSph satellites are ancient TDGs then understanding their internal kinematics remains a challenge though because TDGs do not contain significant amounts of DM (Barnes & Hernquist 1992; Wetzstein et al. 2007; Bournaud et al. 2007; Gentile et al. 2007; Milgrom 2007). However, the inferred large M/L ratios of dSph satellites (and especially of the ultra-faints) may not be physical values but may be a misinterpretation of the stellar phase-space distribution within the satellite. If this were to be the case then the absence of a "DM-mass"-luminosity relation (Sect. 2) for dSph satellites would be naturally understood.

The following gedanken-experiment illustrates that this could be the case. An unbound population of stars on similar orbits, each slightly inclined relative to the other orbits, will reconfigure at apogalacticon and an observer would see a stellar phase-space density enhancement and would also observe a velocity dispersion. The M/L ratio calculated from the observed velocity dispersion would not be a true physical M/L ratio. Models related to this idea have been studied by Kuhn (1993). Moreover, resonant orbital coupling can periodically inflate kinematically measured M/L values (Kuhn & Miller 1989; Kuhn et al. 1996). Fully self-consistent Newtonian N-body models have demonstrated that unphysically high M/L ratios arise indeed if TDGs are allowed to orbit a host galaxy sufficiently long such that the remaining stellar population within the ancient TDG adopts a highly non-isotropic phase-space distribution function (Kroupa 1997; Klessen & Kroupa 1998; Metz & Kroupa 2007). These models suggest that it may be wrong to use an observed velocity dispersion to calculate a mass for a dSph satellite. Thus, tidal shaping of TDGs over
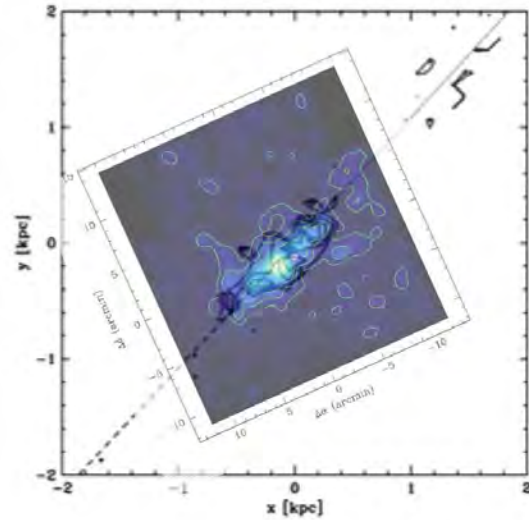

Fig. 6. Model RS1-5 from Kroupa (1997) (on the kpc grid) is plotted over the surface brightness contours of Hercules by Coleman et al. (2007a) (celestial coordinate grid). The dashed and dotted curve are, respectively, the past and future orbit of RS1-5.

a Hubble time can produce remnant objects that have internal highly-anisotropic stellar phase-space distributions that would be falsely interpreted by an observer as corresponding to a high M/L ratio, as explicitly shown by Kroupa (1997). Intriguingly, these models reproduce the gross physical parameters of dSph satellites well (Metz & Kroupa 2007), and thus constitute the simplest available stellar dynamical solutions of dSph satellites constructed without fine-tuning.

It is indeed remarkable how model RS1-5 of Kroupa (1997), shown here as a snapshot (Fig. 6), is an essentially perfect match to the dSph satellite Hercules (see fig. 2 in Coleman et al. 2007a) discovered 10 years later by Belokurov et al. (2007). The half-light radius is 180 pc in the model and 168 pc for Hercules, RS1-5 has a velocity dispersion of about $2.8\ \mathrm{km\,s^{-1}}$ (table 2 in Kroupa 1997), while Hercules has a measured velocity dispersion of $3.72 \pm 0.91\ \mathrm{km\,s^{-1}}$ (Adén et al. 2009a), and the inferred mass-to-light ratio that one would deduce from velocity dispersion measurements based on the assumption of equilibrium is about 200 in both cases. Both RS1-5 and Hercules have luminosities agreeing within one order of magnitude (the model being the brighter one), yet RS1-5 has no DM.

The TDG models for dSph satellites proposed by Lynden-Bell (1976, 1983) and Kunkel (1979) and calculated by Kroupa (1997) and Klessen & Kroupa (1998), which are based on observed properties of TDGs, thus lead to a population of ancient TDGs that are in reasonable agreement with the observed luminosities, dimensions, and M/L ratios of dSph satellites (Metz & Kroupa 2007). These model-dSph satellites require no fine tuning of parameters but only assume the formation about 10 Gyr ago of about $10^7\ M_\odot$ heavy TDGs composed purely of baryonic matter. This theoretical framework of satellite galaxies does not imply any relation between luminosity and (wrongly inferred) "dynamical mass", in agreement with the lack of this relation

(Sect. 2). And it would naturally explain why the mass function of luminous DM sub-halos cannot account for the observations (Sect. 3). Within Newtonian dynamics, this dynamical modelling over many orbits around the MW DM halo has demonstrated that even low-mass satellites do not easily disrupt unless they are on virtually radial orbits (Kroupa 1997; Metz & Kroupa 2007).

Summarising Subsect. 6.1, the physics of TDG formation and evolution is sufficiently well understood to conclude that 1) *once formed at a sufficient distance from the host, TDGs will take an extremely long time to dissolve, if at all*; and 2) the TDGs formed will naturally lead to a population of ancient TDGs that resemble dSph satellites. A bulge-mass–number of satellite correlation and a DoS arise naturally in this scenario.

6.2. On the substructure problem

The MW dSph satellites can therefore be understood as ancient TDGs that formed within a DM universe. But on the other hand, the extensive modelling within the CCM strictly implies, if DM is cold or warm (but not hot), that MW-luminous galaxies must be accompanied by hundreds (with a slight dependence on the cold or warm nature of DM) of shining albeit faint satellites, which are not of tidal origin (Knebe et al. 2008; Macciò et al. 2010; Busha et al. 2010; Koposov et al. 2009). For example, Tollerud et al. (2008) conjecture that "there should be between 300 and 600 satellites within $D = 400$ kpc of the Sun that are brighter than the faintest known dwarf galaxies and that there may be as many as 1000, depending on assumptions." Deep follow-up observations of the low S/N ultra-low-luminosity satellite candidates introduced by Walsh et al. (2009) show that these are not dSphs as a population. These results show that there is not a significant number of missing, ultra-low-luminosity satellites ($M_V > -2, D < 40$ kpc) in the SDSS footprint, i.e. an area covering half of the Northern hemisphere (Jerjen et al., in prep.). This may be a problem because of the ΛCDM prediction that there should be a dozen additional satellites ($M_V < 0, D < 40$ kpc) in a quarter celestial sphere (e.g. fig. 4 in Koposov et al. 2009; see also Cooper et al. 2010).

If the dSph satellites are ancient TDGs stemming from an early gas-rich encounter involving the proto-MW and probably contributing a collision product to the MW bulge (see Sect. 4), then this would mean that the MW would have a severe substructure problem as there would not be any satellites with DM halos less massive than about $10^{10} M_\odot$ with stars, in conflict with DM predictions provided by, e.g., Knebe et al. (2008), Diemand et al. (2008), Busha et al. (2010), Macciò et al. (2010), and Koposov et al. (2009). Perhaps a few dSph satellites are ancient TDGs, such as the classical or nine brightest satellites, and the remainder are the DM dominated sub-halos? This possibility is unlikely, because the new satellites span the same DoS (Sect. 5.3) and because they do not form a population with physical properties that differ distinctly from those of the classical satellites (e.g. Strigari et al. 2008).

Summarising Subsect. 6.2, based purely on the existence of the satellite phase-space correlation and the formation and survival of TDGs in a hierarchical structure formation framework, the validity of the DM hypothesis must be questioned, because the dSph satellites cannot be two types of object at the same time, namely DM-dominated sub-structures and ancient DM-free TDGs.

6.3. Early-type galaxies

But if TDGs account for the dSph satellites of the MW, would they then not also be an important population in other environments? The production of TDGs in the CCM has been calculated by Okazaki & Taniguchi (2000). Intriguingly, they find that TDGs naturally match the observed number of dE galaxies in various environments. The result of Okazaki & Taniguchi (2000) is rather striking, since they find that within the CCM framework only one to two long-lived (i.e., bright) TDGs need to be produced on average per gas-dissipational encounter to cater for the population of dwarf elliptical (dE) galaxies and for the density–morphology relation in the field, in galaxy groups and in clusters[12].

Viewing dE galaxies as old TDGs would be consistent with them deviating from the mass-radius, $M(r)$, relation of pressure-supported (early-type) stellar systems. The dE and dSph galaxies follow a $r \propto M^{1/3}$ sequence reminiscent of tidal-field-dominated formation. *All* other pressure-supported galactic systems (elliptical galaxies, bulges, and ultra-compact dwarf galaxies) with stellar mass $M > 10^6 M_\odot$ follow instead the relation $r \propto M^{0.60 \pm 0.01}$ (see fig. 2 in Dabringhausen et al. 2008, see also fig. 7 in Forbes et al. 2008 and fig. 11 in Graham & Worley 2008), which may result from opacity-limited monolithic collapse (Murray 2009). Viewing dE galaxies as TDGs would also be consistent with the observation that they have essentially stellar mass-to-light ratios similar to globular clusters (Bender et al. 1992; Geha et al. 2003; Dabringhausen et al. 2008; Forbes et al. 2008). If dE (baryonic mass $> 10^8 M_\odot$) and dSph (baryonic mass $< 10^8 M_\odot$) galaxies are old TDGs, why do they appear as different objects? That the dE and dSph galaxies differ in terms of their baryonic-matter density may be a result of the finding that below $10^8 M_\odot$ spheroidal objects on the $r \propto M^{1/3}$ relation cannot hold their warm gas and consequently they must expand (Pflamm-Altenburg & Kroupa 2009a), becoming more susceptible to tides from their host.

dE galaxies are pressure-supported stellar systems, while young TDGs are rotationally supported (Bournaud et al. 2008). With a mass of less than typically $10^9 M_\odot$, the velocity dispersion of their stellar populations becomes comparable to their rotational velocity (of the order of 30 km s^{-1}). That a sizeable fraction of dE galaxies show rotation, some even with spiral

---

[12] Note that Okazaki & Taniguchi (2000) write: "Adopting the galaxy interaction scenario proposed by Silk & Norman, we find that if only a few dwarf galaxies are formed in each galaxy collision, we are able to explain the observed morphology-density relations for both dwarf and giant galaxies in the field, groups of galaxies, and clusters of galaxies." They also state "The formation rate of TDGs is estimated to be $\sim 1 - 2$ in each galaxy interaction." and proceed to compare this number with the actually observed number of TDGs born in galaxy encounters. This statement is at odds with the quotation in Bournaud (2010).

structure (Jerjen et al. 2000; Barazza et al. 2002; Geha et al. 2003; Ferrarese et al. 2006; Chilingarian 2009; Beasley et al. 2009), is thus also consistent with their origin as TDGs. For an excellent review on dE galaxies the reader is referred to Lisker (2009).

One is thus led to the following seemingly logical impasse. In the CCM, TDGs are formed and their number and distribution is calculated to match the number and distribution of observed dE galaxies in the different environments. Within the CCM, the observed luminous dwarf sub-structures are thus naturally accounted for by TDGs. But the dE galaxies cannot be both, DM sub-halos *and* TDGs at the same time.

Summarising Subsect. 6.3, the physical processes at play during structure formation in the CCM imply that dE galaxies ought to be identified as ancient TDGs. Thus, there would be no room for shining DM substructures.

6.4. Deeper implications: gravitational dynamics

In Sects. 6.2 and 6.3 it has been shown that the DM hypothesis leads to a problem when accounting for the number of satellite and dE galaxies because the formation of TDGs is an intrinsic outcome of structure formation. In Sects. 2 to 5 it has also been shown that the CCM seems to have a rather major problem accounting for the observed Galactic satellites and their internal properties. This situation suggests that alternative ideas should be considered to help us understand the origin of these problems, and indeed repeat the steps that had led to a full-fledged DM framework of structure formation but with a different outlook. Since structure formation in the DM framework relies on Newtonian gravitation in the weak-field limit, one is naturally led to relax insistence on Newtonian dynamics in the weak-field limit and to consider modified gravitation theories, which remain compatible with General Relativity in the strong field regime and with the observed large-scale structure. We note that adopting non-Newtonian dynamics in the weak-field limit would *not* necessarily rule out the existence of DM: on the scale of galaxy clusters DM might still be needed, but instead of being warm or cold, it would be *hot* (Angus et al. 2009).

6.4.1. Non-Newtonian weak-field gravity

Alternatives to Newtonian dynamics in the weak-field limit have been studied in great detail. The increasingly popular modified-Newtonian-dynamics (MOND) approach rests on a modification of the Newtonian acceleration in the weak-field limit, i.e. when the Newtonian acceleration a is smaller than a threshold a_0 (Milgrom 1983; Bekenstein & Milgrom 1984; Sanders & McGaugh 2002; Bekenstein 2004; Famaey & Binney 2005; Famaey et al. 2007; Sanders 2007, 2008; McGaugh 2008; Nipoti et al. 2008; Tiret & Combes 2008; Bruneton et al. 2009). A modified-gravity (MOG) adding a Yukawa-like force in the weak-field limit has also been under investigation (Moffat & Toth 2009a; Moffat & Toth 2009b, and references therein). In addition, an extension of the General Theory of Relativity to a class of alternative theories of gravity without DM and based on generic functions $f(R)$ of the

Ricci scalar curvature R have been developed and successfully applied to the problem of galactic rotation curves (e.g. Capozziello et al. 2009). For a brief review of MOND and MOG and Milgrom's proposition on the possible physical origin for the existence of a_0, the reader is directed to the Appendix.

Both the MOND and MOG approaches have been applied to the satellite galaxy problem with appreciable success (Milgrom 1995; Brada & Milgrom 2000; Angus 2008; Moffat & Toth 2008; McGaugh & Wolf 2010). It has already been conclusively demonstrated that spiral galaxy rotation curves are well recovered in MOND purely by the baryon distribution without any parameter adjustments (Sanders & McGaugh 2002; McGaugh 2004, 2005a; Sanders & Noordermeer 2007), and MOG is reported to also do well on this account (Brownstein & Moffat 2006). In contrast, the DM approach can only poorly reproduce the vast variety of rotation curves, and cannot explain the amazing regularities found in them (McGaugh 2004; McGaugh et al. 2007; Gentile et al. 2009; Milgrom 2009a). Notably, the realisation (Gentile et al. 2009; Milgrom 2009a) that the ratio of DM mass to baryonic mass within the DM core radius is constant despite the large variation in the DM–to–baryonic-matter ratio globally within galaxies cannot be understood within the DM hypothesis. A constant ratio within that radius implies that the distribution of baryonic matter is indistinguishable from that of the supposedly present DM (as already found by Bosma 1981). This implies a hitherto not predicted near-exact coupling between DM and baryonic matter that does not arise naturally in the CCM, while outside that radius the effects of DM should become noticeable McGaugh (2010). The only way to physically couple DM and baryons with each other to this degree would be by postulating the existence of an unknown dark force that acts only between DM particles and baryons. The modified DM cosmology would then comprise inflation, dark matter, a dark force, and dark energy.

In MOND models, this behaviour of gravity comes naturally. That the rotation curves would be purely defined by the baryonic matter distribution in non-DM models indeed would naturally explain the later finding based on a large sample of galaxies by Disney et al. (2008), Gentile et al. (2009), and Milgrom (2009a) that disc galaxies appear to be governed by a single parameter. Furthermore, the high galaxy-cluster–galaxy-cluster velocities required to obtain the features of the Bullet cluster have been shown to be extremely unlikely in the CCM (Sect. 1), but these velocities are found to naturally occur in MOND (Angus & McGaugh 2008). Last but not least, the *time-delay problem* of the CCM mentioned in Sect. 1 would disappear naturally.

6.4.2. A consistency check

If it were true that the physical Universe is non-Newtonian in the weak-field limit, then a simple test would provide a consistency check: high dynamical mass-to-light ratios, $(M/L)_{dyn}$, (derived assuming Newtonian dynamics) would not be due to DM but due to the dynamics being non-Newtonian in the

weak-field limit and/or be due to objects being unbound non-equilibrium systems (Sect. 6.1). Thus, taking MOND to be a proxy for non-Newtonian dynamics in the weak-field limit (MOND is, arguably, the currently available simplest alternative to Newtonian dynamics in the weak-field limit), all systems with non-stellar $(M/L)_{dyn}$ values (as derived in Newtonian gravity) would have to have internal accelerations roughly below the MONDian value[13] $a_o = 3.9$ pc/Myr^2. That is, all pressure-supported (spheroidal) stellar systems that appear to be dominated dynamically by DM would need to have an internal acceleration $a < a_o$. Note that the emphasis here is on pressure-supported systems since rotationally supported systems have been extensively and successfully studied in non-Newtonian gravitational theories and because dSph and dE galaxies are mostly pressure-supported objects.

Figure 7 shows the acceleration,

$$a(r_e) = G \frac{M}{r_e^2} = G \frac{0.5 \Upsilon \cdot L_V}{r_e^2}, \tag{18}$$

that a star inside a pressure-supported system experiences at the effective radius, r_e, of its host system with luminosity spanning 10^4 to $10^{12} L_\odot$. Here $M = 0.5 \Upsilon L_V$ is the stellar mass within r_e and L_V is the absolute V-band luminosity in solar units. The stellar mass-to-light ratio in the V-band is $\Upsilon \approx 3$ for collisionless systems (two-body relaxation time longer than a Hubble time), while $\Upsilon \approx 1.5$ for collisional systems, i.e. for systems that have evaporated a significant fraction of their faint low-mass stars by means of energy equipartition (Kruijssen & Lamers 2008; Kruijssen & Mieske 2009). Values of $(M/L)_{dyn}$ as high as 10 can be expected for purely baryonic systems if these retain their stellar remnants and hot gas. For example, the mass of an E galaxy may be comprised of only 30 per cent or less of stars, the rest consisting of stellar remnants and gas that cannot cool to form new stars (Parriott & Bregman 2008; Dabringhausen et al. 2009), meaning that $\Upsilon = 5$ would be an underestimate in that case. Ultra-compact dwarf galaxies, UCDs (sometimes also understood as extremely massive star clusters), have high stellar M/L values perhaps due to a bottom-heavy IMF (Mieske & Kroupa 2008) or a top-heavy IMF (Dabringhausen et al. 2009).

By comparing the two panels in Fig. 7, it is indeed evident that only those systems with $a < a_o$ show non-baryonic $(M/L)_{dyn}$ values. This is more clearly shown in Fig. 8 where the MOND prediction for the range of dynamical mass-to-light ratios measured by a Newtonist living in a MONDian universe is plotted as a function of Newtonian acceleration. For this figure, the MOND expectation for the mass-to-light ratio, which an observer who thinks to live in a Newtonian world would deduce, was calculated as follows. Adopting a conservative value of the baryonic mass-to-light ratio Υ_{bar} between 0.7 (for a globular cluster with an old metal-poor population depleted in low-mass stars) and 5 (for an old metal-rich population), the predic-
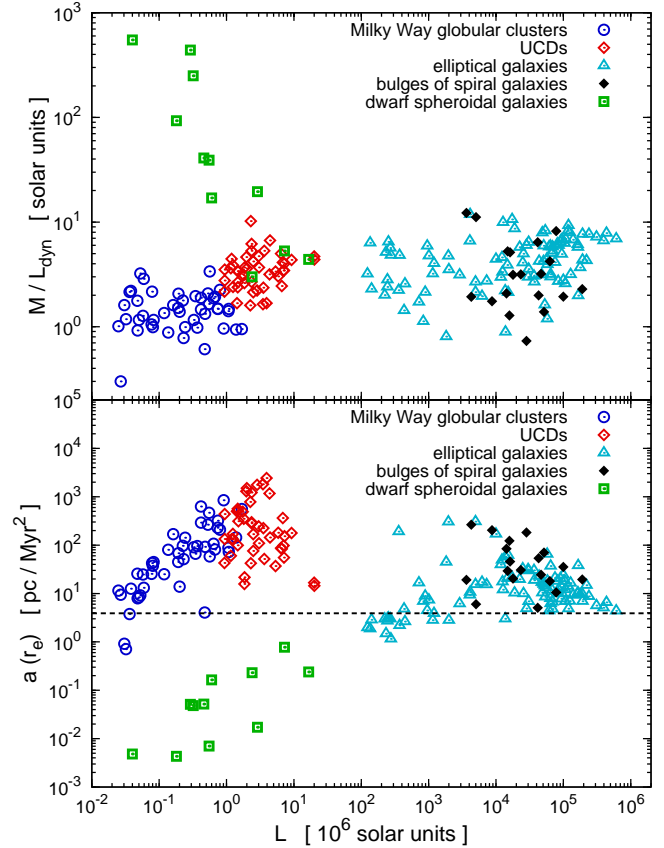

Fig. 7. *Upper panel*: The dynamical $(M/L)_{dyn}$ ratio (calculated assuming Newtonian dynamics to be valid in the weak-field limit) in dependence of the luminosity, L_V, for pressure-supported stellar systems following Dabringhausen et al. (2008). Note that here dE ($< 10^{10} L_\odot$) and E ($> 10^{10} L_\odot$) galaxies are both plotted with the same symbol. *Lower panel*: The Newtonian acceleration (Eq. 18) of a star located at the effective radius within the host system in dependence of the host luminosity. The dashed line is a_0. Note that M/L_{dyn} is high in pressure-supported stellar systems only when $a < a_0$. In both panels: UCD=ultra compact dwarf galaxy. Comparing the upper and lower panels shows that evidence of DM ($M/L_{dyn} > 10$) appears only when $a < a_0$.

tion of MOND inside the effective radius is (Famaey & Binney 2005; Angus et al. 2009)

$$(M/L)_{dyn\,mond} = 0.5 \times \Upsilon_{bar} \times \left(1 + \sqrt{1 + 4a_o/a}\right). \tag{19}$$

We note that, writing customarily $x = g/a_o$, where g is the actual full acceleration experienced by a ballistic particle (in MOND)[14], Eq. 19 follows from the form of the transition MOND function (Milgrom 1983)

$$\mu(x) = x/(1 + x), \tag{20}$$

which is valid up to $x \approx 10$. The theoretical transition derived by Milgrom (1999) and mentioned in the Appendix would yield virtually the same result.

---

[13] Note that this statement is approximately true for all non-Newtonian gravitational theories since they must account for the same non-Newtonian phenomena in the weak-field limit.

[14] In the notation applied here, the MOND formula becomes $a = \mu(x)\, g$, where the Newtonian acceleration a is given by Eq. 18.
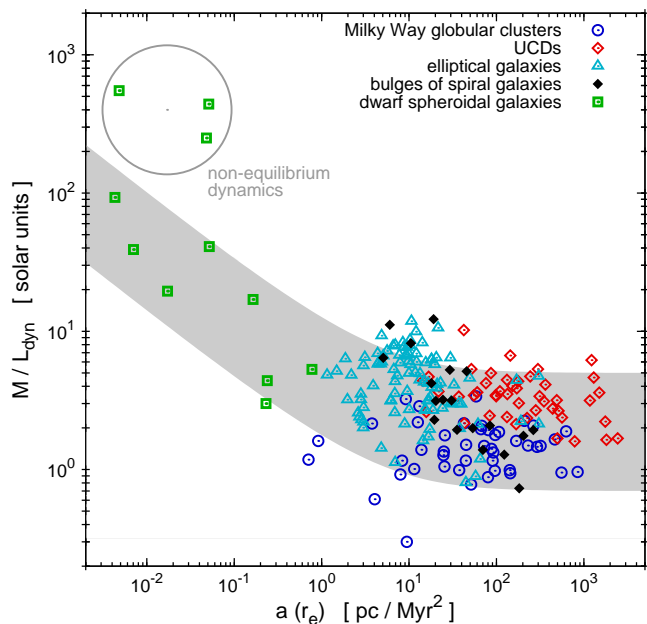
Fig. 8. The correlation between the acceleration $a(r_e)$ and the dynamical mass-luminosity ratio $(M/L)_{dyn}$ derived assuming Newtonian dynamics is shown for the same objects as in Fig. 7. The shaded region indicates the range in $(M/L)_{dyn}$ as it follows directly from MOND models (without any parameter adjustments) using Eq. 19. The graph shows the consistency of the data in a MONDian universe for an observer who interprets observations with Newtonian dynamics. Encircled dwarf spheroidals outside this range (UMa, Dra, and UMi) may indicate non-equilibrium dynamics, either because the whole system is unbound, or because of unbound interloper stars among the member stars (see Sect. 6.4.2). That virtually all pressure-supported stellar systems fall in the shaded MOND region suggests a successful consistency check. That is, stellar dynamics is MONDian rather than Newtonian on galactic scales.

The three classical dwarfs that lie outside the predicted MOND range for $(M/L)_{dyn}$ in Fig. 8 are UMa, Draco, and UMi. UMa may have an anisotropic velocity dispersion (Angus 2008); Draco is known to be a long-standing problem for MOND, but the technique of interloper removal developed by Serra et al. (2009) could probably solve the problem, although this particular case remains open to debate; UMi is a typical example of a possibly out-of-equilibrium system, as it is elongated with substructure and shows evidence of tidal tails (D. Martinez-Delgado, priv. communication). Ultra-faint dwarf spheroidals are expected to be increasingly affected by this kind of non-equilibrium dynamics, as shown to be true even for Newtonian weak-field dynamics (Kroupa 1997, Sect. 6.1), and even more strongly so in MOND (McGaugh & Wolf 2010).

Summarising Subsect. 6.4, well-developed non-Newtonian weak-field approaches exist and have been shown to account for galaxy properties more succesfully than the CCM, which would need to be extended by a dark force to account for the observed strong coupling between DM and baryons. All known pressure-supported stellar systems ranging from elliptical to dwarf satellite galaxies behave dynamically as expected in a MONDian universe. In DM cosmology, the association of

highly non-stellar $(M/L)_{dyn}$ values with $a < a_o$ would be coincidental as it is not built into the theory. It is, however, natural in a MONDian universe for observers who interpret weak-field observations with Newtonian dynamics.

7. Conclusions and perspectives

We inhabit a Universe for which physicists seek mathematical formulations. A successful formulation of gravitational physics, the General Theory of Relativity (GR), requires the existence of non-baryonic dark matter (DM) in order to account for the observed rotation curves of galaxies and other dynamical effects in this theory, which has Newtonian dynamics as its weak-field limit. On the other hand, non-Newtonian weak-field gravitational theories have also been formulated to account for the "DM-effects" observed in galaxies.

Finding a definitive test that distinguishes between these two different solutions to the problem of galactic dynamics and cosmological structure formation is difficult. Both DM and modified gravity are designed to solve similar problems, so the test must rely on subtle differences between the models and the observational data. Thus far, GR+DM+Λ+inflation (the CCM) accounts for the emergence of structure on large scales, and Reyes et al. (2010) were able to exclude certain versions of alternative gravitational theories that had already been known by the respective community to be unstable (Contaldi et al. 2008). But, as shown here, the CCM appears to have insurmountable problems on galaxy scales such that other alternative approaches need to be studied. A speculative ansatz to perhaps solve the observed near-exact DM–baryon coupling in galaxies within a DM-Newtonian cosmology would be to extend the CCM by postulating the existence of a *dark force* (DF) leading to a GR+DM+DF+Λ+inflation cosmology that should perhaps be investigated in more detail in the future. The greatest differences between the two competing approaches (CCM versus non-Newtonian dynamics in the weak-field limit) are expected in the weak gravitational regime where the subtleties of non-Newtonian weak-field dynamics are most pronounced, which is why the constituents of the outer edges of galaxies allow the most stringent tests.

This contribution has statistically assessed whether the observed properties of satellite galaxies in the Local Group, which are the result of structure formation in the weak-field limit, are consistent with the CCM. Given that a substantial number of independent research groups working in the traditional CDM and WDM approaches have by now made firm statements about the dwarf satellite galaxies of the MW and Andromeda, the CCM can be tested sensitively on these scales within the Local Group.

Five new problems for the CCM on the scale of the Local Group and dwarf galaxies have been uncovered: (i) the observed absence of a mass-luminosity relation (Sect. 2, the *DM-mass–luminosity problem*); (ii) the mass function of luminous galactic satellites (Sect. 3, the *mass function of luminous satellite problem*); (iii) the observed relation between the bulge mass and the number of satellites (Sect. 4, the *bulge-satellite correlation problem*); (iv) the accordance with the Milky Way's disc-of-satellites of the recently detected ultra-faint dwarfs

(Sect. 5, the *phase-space correlation problem*); and (v) the low probability that two neighbouring MW-type DM halos contain similar MW-type disk galaxies (Sect. 5.5, the *invariant-baryonic-galaxy problem*).

It is found that the CCM is consistent with the Local Group data with a combined probability[15] $p \ll 3 \times 10^{-3}$. The five problems thus appear to rather strongly challenge the notion that the CCM successfully accounts for galactic structure in conflict with a vast volume of reported research (compare with Fanelli 2010). All these challenges constitute a strong motivation for numerous future observational and theoretical investigations. For instance, the disk of satellites will have to be confirmed by surveys such as Pan-Starrs (Burgett & Kaiser 2009) and the Stromlo Milky Way Satellite Survey (SMS) (Jerjen 2010). Given the existence of the DoS and by symmetry, the southern hemisphere ought to also contain about 16 satellites, such that the SMS survey is expected to discover about 8 new southern satellites (Fig. 4). It will also be essential to refine the correlation between bulge-mass and satellite-number with extragalactic surveys. On the theoretical side, more inclusive modelling is needed to address these challenges within the CCM while, at the same time, existing viable alternatives should be further explored.

With this contribution, the following clues have emerged suggesting the need for a new scenario for the origin and nature of dSph satellite galaxies. The observed correlation between bulge mass and number of satellites suggests that a link between these two quantities may exist. The phase-space correlation of the classical and ultra-faint satellite galaxies implies that angular momentum conservation played an important role in establishing the satellite distribution. Given that bulges form in dissipational encounters, during which angular-momentum conservation rearranges matter on Galactic scales to be in highly correlated phase-space structures (tidal arms), a natural path thus opens to understand the likely origin of satellite galaxies. Already in the 1970's a tidal origin for dwarf spheroidal galaxies was suggested, based on their arrangement around the Milky Way (Sect. 6). This solution does imply, however, that the dSph galaxies are ancient TDGs and not DM sub-haloes. Furthermore, by logical implication, dE galaxies would also be TDGs (Sect. 6.3). This would imply that the vast majority of $\lesssim 10^{10}\,M_\odot$ DM sub-halos are unable to make stars. This, however, would be in conflict with all the CCM computations available to date *to the extend that the CCM would have to be discarded in favour of a universe without cold or warm DM.* In this case, the non-Keplerian rotation curves of galaxies and other DM effects additionally suggest that we live in a non-Newtonian weak-field framework within which galaxies would be pure baryonic objects[16].

This scenario would naturally solve problems (iii) and (iv), while it would not imply a "dynamical mass"-luminosity relation if the dwarfs are out of equilibrium, so could possibly solve problem (i). For purely baryonic galaxies, problem (ii) would not exist anymore by definition. Problem (v) would also vanish naturally. What is more, while in the CCM the association of highly non-stellar $(M/L)_{dyn}$ values with $a < a_o$ would be coincidental because it is not built into the theory, it is natural in a non-Newtonian universe for weak-field observers who interpret observations with Newtonian dynamics. Noteworthy is that the same statement can be made for the Tully-Fisher scaling relation for rotationally-supported galaxies (Tully & Fisher 1977; McGaugh 2005b; Combes 2009a) as well as the newly found scaling relation of Gentile et al. (2009) and Milgrom (2009a). The supposed mass-deficit seen in young rotating and gaseous TDGs (such as those of NGC 5291) constitutes independent empirical evidence towards this same statement. Young tidal dwarf galaxies (TDG), which should be devoid of collisionless DM, appear to nevertheless exhibit a mass-discrepancy in Newtonian dynamics. This is a significant problem for the DM hypothesis, but it is naturally explained by MOND (Gentile et al. 2007; Milgrom 2007). Also, while the high Bullet-cluster velocity is hard to account for in the CCM, it is natural in MOND (Sect. 1, 6.4 and 6.4.1). And, it has already been noted by Sanders (1999) that the dynamical-mass – baryon-mass discrepancy observed in galaxy clusters is nearly removed in MONDian dynamics.

It would thus appear that within the non-Newtonian weak-field framework a much more complete, self-consistent, and indeed simpler understanding of the Galaxy's satellites as well as of major galaxies may be attained, than within the CCM.

However, to affirm this statement, this alternative cosmological scenario will have to be investigated in as much detail as is now available for the CCM in order to perform equivalent tests as presented here for the DM hypothesis and to ascertain which of the non-Newtonian weak-field dynamics theories (and which versions of the theories) can most successfully account for the physical world. Models of merging gas-rich disc galaxies need to be computed in MOND, for example, to study how the formation of TDGs proceeds and how the number of satellites thus formed correlates with the bulge that forms as a result of the encounter. These populations of satellites associated with globular clusters that formed along with them would naturally appear in (more than one) closely related planes explaining the Lynden-Bell & Lynden-Bell (1995) streams, because a gas-rich galaxy pair undergoes many close encounters in MOND, each spawning some TDGs and globular clusters, before perhaps finally merging.

Figure 9 schematically depicts the structure formation scenario in this non-Newtonian weak-field framework: while

---

[15] Summarising the likelihoods, p, that the CCM accounts for the observed data in the Local Group are in the individual tests: (1) mass–luminosity data: $p_1 < 0.3$ per cent (Sec. 2); (2) mass function of luminous sub-halos: $p_2 < 4.5$ per cent (Sect. 3); (3) bulge–satellite number: $p_3 \approx 4.4$ per cent (Sect. 4); (4) a MW-type galaxy with at least 11 satellites in a DoS: $p_4 = 0.4$ per cent; (5) a M31-type galaxy with at least 11 satellites: $p_5 = 1.4$ per cent (Sect. 5.4). Thus, the combined probability that the general CCM framework accounts for the Local Group is $p \ll 3 \times 10^{-3}$.

[16] Given that Newton derived the gravitational $1/r^2$ law over a very limited physical range (Solar System), while with the Local Group gravitational physics is probed on a length scale nearly eight orders of magnitude larger and in a much weaker field regime, it need not be surprising that an adjusted gravitational law is needed.

22   Kroupa et al.: Local Group tests of cosmology

Fig. 9. A new cosmological structure formation framework: the mangrove merger tree. In a modified-Newtonian weak-field framework, purely baryonic galaxies merge thereby spawning new dwarf galaxies giving rise to the morphology-density relation (adapted from Metz 2008).

purely baryonic galaxies would merge, these events would spawn dwarf galaxies such that a density–morphology relation would be established (more dE galaxies in denser environments, Okazaki & Taniguchi 2000).

The MONDian modelling by Tiret & Combes (2008) and Combes & Tiret (2009) has already shown that TDGs are produced during gas-dissipational galaxy mergers, and that the interaction times between galaxies are much longer, while the number of mergers is smaller than in a DM universe. Hence, the number of observed galaxy encounters would be given foremost by the long time scale of merging and thus by more close galaxy-galaxy encounters per merging event rather than on a high number of mergers.

This would imply that compact galaxy groups do not evolve statistically over more than a crossing time. In contrast, assuming DM-Newtonian dynamics to hold, the merging time scale would be about one crossing time because of dynamical friction in the DM halos such that compact galaxy groups ought to undergo significant merging over a crossing time. The lack of significant evolution of compact groups, if verified observationally, would appear not to be explainable if DM dominates galaxy dynamics. Analyses of well-studied compact groups indeed indicate this to be the case (Presotto et al. 2010).

Thus, many observational problems may be solved uncontrived by adopting non-Newtonian weak-field dynamics, and perhaps this was, in the end, the most self evident explanation to the discovery of non-Keplerian rotation curves by Rubin & Ford (1970)[17].

---

[17] On 19 June 2009, the final day of the conference "Unveiling the Mass: Extracting and Interpreting Galaxy Masses" in Kingston, Ontario, in honour of the career of Vera Rubin, PK asked her whether she would be very dismayed if her discovery that galaxies have non-

References

Adén, D., Feltzing, S., Koch, A., et al. 2009a, A&A, 506, 1147

Adén, D., Wilkinson, M. I., Read, J. I., Feltzing, S., Koch, A., Gilmore, G. F., Grebel, E. K., & Lundström, I. 2009b, ApJ, 706, L150

Angus, G. W. 2008, MNRAS, 387, 1481

Angus, G. W., Famaey, B., & Diaferio, A. 2009, MNRAS, 1871

Angus, G. W., & McGaugh, S. S. 2008, MNRAS, 383, 417

Aubert, D., Pichon, C., & Colombi, S. 2004, MNRAS, 352, 376

Barazza, F. D., Binggeli, B., & Jerjen, H. 2002, A&A, 391, 823

Barnes, J. E., & Hernquist, L. 1992, Nature, 360, 715

Beasley, M. A., Cenarro, A. J., Strader, J., & Brodie, J. P. 2009, AJ, 137, 5146

Bekenstein, J., & Milgrom, M. 1984, ApJ, 286, 7

Bekenstein, J. D. 2004, Phys. Rev. D, 70, 083509

Belokurov, V., Zucker, D. B., Evans, N. W., et al. 2006, ApJ, 647, L111

Belokurov, V., Zucker, D. B., Evans, N. W., et al. 2007, ApJ, 654, 897

Belokurov, V., Walker, M. G., Evans, N. W., et al. 2008, ApJ, 686, L83

Belokurov, V., Walker, M. G., Evans, N. W. et al. 2009, MNRAS, 397, 1748

Belokurov, V., Walker, M. G., Evans, N. W., Gilmore, G., Irwin, M. J., Just, D., Koposov, S., Mateo, M., Olszewski, E., Watkins, L. & Wyrzykowski, L. 2010, ApJ, 712, L103

Bender, R., Burstein, D., & Faber, S. M. 1992, ApJ, 399, 462

Bertone, G., Hooper, D., & Silk, J. 2005, Physics Reports, 405, 279

Blanchet, L., & Le Tiec, A. 2009, Phys. Rev. D, 80, 023524

Blumenthal, G. R., Faber, S. M., Primack, J. R., & Rees, M. J. 1984, Nature, 311, 517

Boily, C. M., Nakasato, N., Spurzem, R., & Tsuchiya, T. 2004, ApJ, 614, 26

Bosma, A. 1981, AJ, 86, 1791

Bosma, A., Goss, W. M., & Allen, R. J. 1981, A&A, 93, 106

Bournaud, F. 2010, Advances in Astronomy, 2010, 1

Bournaud, F., Duc, P.-A., Brinks, E., et al. 2007, Science, 316, 1166

Bournaud, F., Duc, P.-A., & Emsellem, E. 2008, MNRAS, 389, L8

Brada, R., & Milgrom, M. 2000, ApJ, 541, 556

Brownstein, J. R., & Moffat, J. W. 2006, ApJ, 636, 721

Bruneton, J.-P., & Esposito-Farèse, G. 2008, Phys. Rev. D, 76, 124012

Bruneton, J.-P., Liberati, S., Sindoni, L., & Famaey, B. 2009, Journal of Cosmology and Astro-Particle Physics, 3, 21

Bullock, J. S., Kolatt, T. S., Sigad, Y., et al. 2001, MNRAS, 321, 559

Burgett, W., & Kaiser, N. 2009, Proceedings of the Advanced Maui Optical and Space Surveillance Technologies Conference, held in Wailea, Maui, Hawaii, September 1-4, 2009, Ed.: S. Ryan, The Maui Economic Development Board., p.E39

Keplerian rotation curves would not be due to dark mater but rather non-Newtonian weak-field dynamics. Prof. Rubin replied that she would in fact be delighted, since the non-Keplerian rotation curves are an empirical observation of hitherto not understood physics, and one needs to keep an open mind in seeking solutions.

Busha, M. T., Alvarez, M. A., Wechsler, R. H., Abel, T., & Strigari, L. E. 2010, ApJ, 710, 408

Capozziello, S., Piedipalumbo, E., Rubano, C., & Scudellaro, P. 2009, A&A, 505, 21

Chilingarian, I. V. 2009, MNRAS, 394, 1229

Cole, S., Percival, W. J., Peacock, J. A., et al. 2005, MNRAS, 362, 505

Coleman, M. G., de Jong, J. T. A., Martin, N. F., et al. 2007a, ApJ, 668, L43

Coleman, M. G., Jordi, K., Rix, H.-W., Grebel, E. K., & Koch, A. 2007b, AJ, 134, 1938

Combes, F. 2009a, A&A, 500, 119

Combes, F. 2009b, 4 pages, Concluding remarks in "Galaxies in isolation: exploring Nature vs Nurture", (May 2009, Granada, Spain), arXiv:0909.2752

Combes, F., & Tiret, O. 2009, in The Invisible Universe, ed. J-M. Alimi, A. Fuzfa, P-S. Corasaniti, AIP pub, eprint arXiv:0908.3289

Contaldi, C. R., Wiseman, T., & Withers, B. 2008, Phys. Rev. D, 78, 044034

Cooper, A. P., Cole, S., Frenk, C.S., White, S.D.M., et al. 2010, MNRAS, 756, xxx

Clowe, D., Bradač, M., Gonzalez, A. H., Markevitch, M., Randall, S. W., Jones, C., & Zaritsky, D. 2006, ApJ, 648, L109

Dabringhausen, J., Hilker, M., & Kroupa, P. 2008, MNRAS, 386, 864

Dabringhausen, J., Kroupa, P., & Baumgardt, H. 2009, MNRAS, 394, 1529

Dall'Ora, M., Clementini, G., Kinemuchi, K., et al. 2006, ApJ, 653, L109

de Jong, J. T. A., Rix, H.-W., Martin, N. F., Zucker, D. B., Dolphin, A. E., Bell, E. F., Belokurov, V., & Evans, N. W. 2008, AJ, 135, 1361

de Jong, J. T. A., Martin, N. F., Rix, H.-W., Smith, K. W., Jin, S., & Macciò, A. V. 2010, ApJ, 710, 1664

Dekel, A., & Silk, J. 1986, ApJ, 303, 39

Dekel, A., & Woo, J. 2003, MNRAS, 344, 1131

Del Popolo, A., & Yesilyurt, I. S. 2007, Astronomy Reports, 51, 709

Demleitner, M., Accomazzi, A., Eichhorn, G., Grant, C. S., Kurtz, M. J., & Murray, S. S. 2001, Astronomical Data Analysis Software and Systems X, in ASP Conference Proceedings, Vol. 238. Edited by F. R. Harnden, Jr., Francis A. Primini, and Harry E. Payne. San Francisco: Astronomical Society of the Pacific, p. 321

Diemand, J., Kuhlen, M., Madau, P., et al. 2008, Nature, 454, 735

Disney, M. J., Romano, J. D., Garcia-Appadoo, D. A., et al. 2008, Nature, 455, 1082

D'Onghia, E., & Lake, G. 2008, ApJ, 686, L61

Einstein, A. 1921, Festschrift der Kaiser-Wilhelm Gesellschaft zur Föderung der Wissenschaften zu ihrem zehnjährigen Jubiläum dargebracht von ihren Instituten, Springer, Berlin, p. 50

Esposito-Farèse, G. 2009, lecture given at the "School on Mass" (Orleans, France, June 2008), eprint arXiv:0905.2575

Fanelli, D. 2010, PLoS ONE 5(4): e10271. doi:10.1371/journal.pone.0010271

Famaey, B., & Binney, J. 2005, MNRAS, 363, 603

Famaey, B., Gentile, G., Bruneton, J.-P., & Zhao, H. S. 2007, Phys. Rev. D, 75, 063002

Fellhauer, M., et al. 2006, ApJ, 651, 167

Ferrarese, L., Cote, P., Jordan, A., et al. 2006, ApJS, 164, 334

Forbes, D. A., Lasky, P., Graham, A. W., & Spitler, L. 2008, MNRAS, 389, 1924

Gao, L., White, S. D. M., Jenkins, A., Stoehr, F., & Springel, V. 2004, MNRAS, 355, 819

Gavazzi, G. 2009, Revista Mexicana de Astronomia y Astrofisica Conference Series, 37, 72

Gebhardt, K., Lauer, T. R., Kormendy, J., et al. 2001, AJ, 122, 2469

Geha, M., Guhathakurta, P., & van der Marel, R. P. 2003, AJ, 126, 1794

Geha, M., Willman, B., Simon, J. D., Strigari, L. E., Kirby, E. N., Law, D. R., & Strader, J. 2009, ApJ, 692, 1464

Gentile, G., Famaey, B., Combes, F., Kroupa, P., Zhao, H. S., & Tiret, O. 2007, A&A, 472, L25

Gentile, G., Famaey, B., Zhao, H., & Salucci, P. 2009, Nature, 461, 627

Gibbons, G. W., & Hawking, S. W. 1977, Phys. Rev. D, 15, 2738

Gilmore, G., Wilkinson, M. I., Wyse, R. F. G., et al. 2007, ApJ, 663, 948

Graham, A. W., & Worley, C. C. 2008, MNRAS, 388, 1708

Grebel, E. K. 1999, in IAU Symposium, Vol. 192, The Stellar Content of Local Group Galaxies, ed. P. Whitelock & R. Cannon, p.17

Grebel, E. K. 2008, Baryonic Properties of the Darkest Galaxies, in Dark Galaxies and Lost Baryons, IAU Symposium, 244, 300

Greco, C., Dall'Ora, M., Clementini, G., et al. 2008, ApJ, 675, L73

Hartwick, F. D. A. 2000, AJ, 119, 2248

Hunter, D. A., Hunsberger, S. D., & Roye, E. W. 2000, ApJ, 542, 137

Ibata, R., Chapman, S., Irwin, M., Lewis, G., & Martin, N. 2006, MNRAS, 373, L70

Jerjen, H. 2010, Advances in Astronomy, 2010, 1

Jerjen, H., Kalnajs, A., & Binggeli, B. 2000, A&A, 358, 845

Kallivayalil, N., van der Marel, R. P., & Alcock, C. 2006, ApJ, 652, 1213

Karachentsev, I. D., Karachentseva, V. E., & Sharina, M. E. 2005, in IAU Colloq. 198: Near-fields cosmology with dwarf elliptical galaxies, ed. H. Jerjen & B. Binggeli, 295–302

Kazantzidis, S., Mayer, L., Mastropietro, C., Diemand, J., Stadel, J., & Moore, B. 2004, ApJ, 608, 663

Kent, S. M. 1989, AJ, 97, 1614

Kirby, E. N., Guhathakurta, P., Bullock, J. S., et al. 2009, Astro2010: The Astronomy and Astrophysics Decadal Survey, Science White Papers, no. 156

Klessen, R. S., & Kroupa, P. 1998, ApJ, 498, 143

Klimentowski, J., Lokas, E. L., Knebe, A., Gottloeber, S., Martinez-Vaquero, L. A., Yepes, G., & Hoffman, Y. 2010, MNRAS, 402, 1899

Klypin, A., Kravtsov, A. V., Valenzuela, O., & Prada, F. 1999, ApJ, 522, 82

Koch, A., & Grebel, E. K. 2006, AJ, 131, 1405

Koch, A., Wilkinson, M. I., Kleyna, J. T., et al. 2009, ApJ, 690, 453

Kochanek, C. S., & Schechter, P. L. 2004, Measuring and Modeling the Universe, 117

Kollmeier, J. A., Gould, A., Shectman, S., et al. 2009, ApJ, 705, L158

Komatsu, E., Dunkley, J, Nolta, M. R., et al. 2009, ApJS, 180, 330

Koposov, S. E., Yoo, J., Rix, H.-W., et al. 2009, ApJ, 696, 2179

Knebe, A., Arnold, B., Power, C., & Gibson, B. K. 2008, MNRAS, 386, 1029

Kroupa, P. 1997, New Astronomy, 2, 139

Kroupa, P., Theis, C., & Boily, C. M. 2005, A&A, 431, 517

Kruijssen, J. M. D., & Lamers, H. J. G. L. M. 2008, A&A, 490, 151

Kruijssen, J. M. D., & Mieske, S. 2009, A&A, 500, 785

Kuehn, C., Kinemuchi, K., Ripepi, V., et al. 2008, ApJ, 674, L81

Kuhn, J. R. 1993, ApJ, 409, L13

Kuhn, J. R., & Miller, R. H. 1989, ApJ, 341, L41

Kuhn, J. R., Smith, H. A., & Hawley, S. L. 1996, ApJ, 469, L93

Kunkel, W. E. 1979, ApJ, 228, 718

Law, D. R., & Majewski, S. R. 2010, ApJ, 714, 229

Law, D. R., Majewski, S. R., & Johnston, K. V. 2009, ApJ, 703, L67

Lee, J., & Komatsu, E. 2010, ApJ, 718, 60

Li, Y.-S., & Helmi, A. 2008, MNRAS, 385, 1365

Li, Y.-S., De Lucia, G., & Helmi, A. 2010, MNRAS, 401, 2036

24   Kroupa et al.: Local Group tests of cosmology

Libeskind, N. I., Frenk, C. S., Cole, S., Jenkins, A., & Helly, J. C. 2009, MNRAS, 399, 550

Lisker, T. 2009, Astronomische Nachrichten, 330, 1043 (arXiv:0910.1594)

Lynden-Bell, D. 1976, MNRAS, 174, 695

Lynden-Bell, D. 1983, in IAU Symposium, Vol. 100, Internal Kinematics and Dynamics of Galaxies, ed. E. Athanassoula, 89–91

Lynden-Bell, D., & Lynden-Bell, R. M. 1995, MNRAS, 275, 429

Macciò, A. V., & Fontanot, F. 2010, MNRAS, 404, L16

Macciò, A. V., Kang, X., & Moore, B. 2009, ApJ, 692, L109

Macciò, A. V., Dutton, A. A., van den Bosch, F. C., Moore, B., Potter, D., & Stadel, J. 2007, MNRAS, 378, 55

Macciò, A. V., Kang, X., Fontanot, F., Somerville, R. S., Koposov, S., & Monaco, P. 2010, MNRAS, 402, 1995

Mainini, R., Macciò, A. V., Bonometto, S. A., & Klypin, A. 2003, ApJ, 599, 24

Martin, N. F., Coleman, M. G., De Jong, J. T. A., et al. 2008, ApJ, 672, L13

Martin, N. F., de Jong, J. T. A., & Rix, H.-W. 2008, ApJ, 684, 1075

Mastropietro, C., & Burkert, A. 2008, MNRAS, 389, 967

Mateo, M. L. 1998, ARA&A, 36, 435

Mateo, M., Olszewski, E.W., Pryor, C., et al. 1993, AJ, 105, 510

McGaugh, S. S. 2004, ApJ, 609, 652

McGaugh, S. S. 2005a, Physical Review Letters, 95, 171302

McGaugh, S. S. 2005b, ApJ, 632, 859

McGaugh, S. S., de Blok, W. J. G., Schombert, J. M., Kuzio de Naray, R., & Kim, J. H. 2007, ApJ, 659, 149

McGaugh, S. S. 2008, ApJ, 683, 137

McGaugh, S. 2010, American Institute of Physics Conference Series, 1240, 13 (arXiv:0912.3943)

McGaugh, S. S., & Wolf, J. 2010, arXiv:1003.3448

Metz, M. 2008, PhD thesis, University of Bonn

Metz, M., & Kroupa, P. 2007, MNRAS, 376, 387

Metz, M., Kroupa, P., & Jerjen, H. 2007, MNRAS, 374, 1125

Metz, M., Kroupa, P., & Libeskind, N. I. 2008, ApJ, 680, 287

Metz, M., Kroupa, P., & Jerjen, H. 2009a MNRAS, 394, 2223

Metz, M., Kroupa, P., Theis, C., Hensler, G., & Jerjen, H. 2009b, ApJ, 697, 269

Mieske, S., & Kroupa, P. 2008, ApJ, 677, 276

Milgrom, M. 1983, ApJ, 270, 365

Milgrom, M. 1995, ApJ, 455, 439

Milgrom, M. 1999, Phys. Lett. A, 253, 273

Milgrom, M. 2007, ApJ, 667, L45

Milgrom, M. 2009a, MNRAS, 398, 1023

Milgrom, M. 2009b, Phys. Rev. D, 80, 123536

Milgrom, M. 2010, MNRAS, 403, 886

Moffat, J. W. 2006, Journal of Cosmology and Astro-Particle Physics, 3, 4

Moffat, J. W., & Toth, V. T. 2008, ApJ, 680, 1158

Moffat, J. W., & Toth, V. T. 2009a, MNRAS, L203+

Moffat, J. W., & Toth, V. T. 2009b, Classical and Quantum Gravity, 26, 085002

Moore, B., Ghigna, S., Governato, F., et al. 1999a, ApJ, 524, L19

Moore, B., Diemand, J., Madau, P., Zemp, M., & Stadel, J. 2006, MNRAS, 368, 563

Moretti, M. I., Dall'Ora, M., Ripepi, V., et al. 2009, ApJ, 699, L125

Muñoz, R. R., Carlin, J. L., Frinchaboy, P. M., Nidever, D. L., Majewski, S. R., & Patterson, R. J. 2006, ApJ, 650, L51

Muñoz, R. R., Geha, M., & Willman, B. 2010, AJ, 140, 138

Murray, N. 2009, ApJ, 691, 946

Musella, I., Ripepi, V. and Clementini, G., et al. 2009, ApJ, 695, L83

Navarro, J. F., Frenk, C. S., & White, S. D. M. 1997, ApJ, 490, 493

Navarro, J. F., Ludlow A., Springel, V., et al. 2010, MNRAS, 402, 21

Niederste-Ostholt, M., Belokurov, V., Evans, N. W., Gilmore, G., Wyse, R. F. G., & Norris, J. E. 2009, MNRAS, 398, 1771

Nipoti, C., Ciotti, L., Binney, J., & Londrillo, P. 2008, MNRAS, 386, 2194

Okamoto, S., Arimoto, N., Yamada, Y., & Onodera, M. 2008, A&A, 487, 103

Okamoto, T., & Frenk, C. S. 2009, MNRAS, 399, L174

Okamoto, T., Frenk, C. S., Jenkins, A., & Theuns, T. 2010, MNRAS, 658

Okazaki, T., & Taniguchi, Y. 2000, ApJ, 543, 149

Oort, J. H. 1932, Bull. Astr. Inst. Neth. VI, 249

Ott, J., Walter, F., & Brinks, E. 2005, MNRAS, 358, 1453

Parriott, J. R., & Bregman, J. N. 2008, ApJ, 681, 1215

Pawlowski, M., Kroupa, P., Metz, M., de Boer, K.S. 2010, A&A, submitted

Peacock, J. A. 2003, Royal Society of London Transactions Series A, vol. 361, Issue 1812, p.2479-2495

Peacock, J. A. 1999, Cosmological Physics, by John A. Peacock, pp. 704. ISBN 052141072X. Cambridge, UK: Cambridge University Press, January 1999

Peebles, P. J. E., & Nusser, A. 2010, Nature, 465, 565

Peñarrubia, J., McConnachie, A. W., & Navarro, J. F. 2008, ApJ, 672, 904

Perlmutter, S., Aldering, G., Goldhaber, G., et al. 1999, ApJ, 517, 565

Pflamm-Altenburg, J., & Kroupa, P. 2009, MNRAS, 397, 488

Pflamm-Altenburg, J., & Kroupa, P. 2009b, ApJ, 706, 516

Press, W. H., Teukolsky, S. A., Vetterling, W. T., & Flannery, B. P. 1992, Numerical recipes in C. The art of scientific computing, 2nd ed, Cambridge University Press, Cambridge

Primack, J. R. 2009, American Institute of Physics Conference Series, 1166, 3 (arXiv:0902.2506)

Presotto, V., Iovino, A., Pompei, E., & Temporin, S. 2010, A&A, 510, A31

Recchi, S., Theis, C., Kroupa, P., & Hensler, G. 2007, A&A, 470, L5

Reyes, R., Mandelbaum, R., Seljak, U., Baldauf, T., Gunn, J. E., Lombriser, L., & Smith, R. E. 2010, Nature, 464, 256

Riess, A. G., Filippenko, A. V., Challis, P., et al. 1998, AJ, 116, 1009

Rubin, V. C., & Ford, W. K. Jr 1970, ApJ, 159, 379

Sakamoto, T., & Hasegawa, T. 2006, ApJ, 653, L29

Sand, D. J., Olszewski, E. W., Willman, B., Zaritsky, D., Seth, A., Harris, J., Piatek, S., & Saha, A. 2009, ApJ, 704, 898

Sand, D. J., Seth, A., Olszewski, E. W., Willman, B., Zaritsky, D., & Kallivayalil, N. 2010, ApJ, 718, 530

Sanders, R. H. 1999, ApJ, 512, L23

Sanders, R. H. 2005, MNRAS, 363, 459

Sanders, R. H. 2007, MNRAS, 386, 1588

Sanders, R. H. 2008, talk presented at XX Rencontres de Blois, Astroparticle physics, eprint arXiv:0806.2585

Sanders, R. H., & McGaugh, S. S. 2002, ARA&A, 40, 263

Sanders, R. H., & Noordermeer, E. 2007, MNRAS, 379, 702

Serra, A. L., Angus, G. W., & Diaferio, A. 2009, eprint arXiv:0907.3691

Shaya, E., Olling, R., Ricotti, M., et al. 2009, Astro2010: The Astronomy and Astrophysics Decadal Survey, Science White Papers, no. 274

Siegel, M. H. 2006, ApJ, 649, L83

Simon, J. D., & Geha, M. 2007, ApJ, 670, 313

Skordis, C. 2009, Classical and Quantum Gravity, 26, 143001

Spergel, D. N., Bean, R., Dore, O., et al. 2007, ApJS, 170, 377

Strigari, L. E., Bullock, J. S., Kaplinghat, M., et al. 2008, Nature, 454, 1096 (S08)

Tegmark, M., Blanton, M. R., Strauss, M. A., et al. 2004, ApJ, 606, 702

Tiret, O., & Combes, F. 2007, A&A, 464, 517

Tiret, O., & Combes, F. 2008, in Astronomical Society of the Pacific Conference Series, Vol. 396, ed. J. G. Funes & E. M. Corsini, 259

Tollerud, E. J., Bullock, J. S., Strigari, L. E., & Willman, B. 2008, ApJ, 688, 277

Tully, R. B., & Fisher, J. R. 1977, A&A, 54, 661

Unruh, W. G. 1975, Phys. Rev. D, 14, 870

van den Bergh, S. 1999, A&A Rev., 9, 273

van den Bergh, S. 2008, Nature, 455, 1049

van der Marel, R. P., Alves, D. R., Hardy, E., & Suntzeff, N. B. 2002, AJ, 124, 2639

Walsh, S. M., Jerjen, H., & Willman, B. 2007, ApJ, 662, L83

Walsh, S. M., Willman, B., Sand, D., Harris, J., Seth, A., Zaritsky, D., & Jerjen, H. 2008, ApJ, 688, 245

Walsh, S. M., Willman, B., & Jerjen, H. 2009, AJ, 137, 450

Watkins, L. L., Evans, N. W., Belokurov, V., Smith, M. C., Hewett, P. C., Bramich, D. M., Gilmore, G. F., Irwin, M. J., Vidrih, S., Wyrzykowski, Ł. & Zucker, D. B. 2009, MNRAS, 398, 1757

Weidner, C., Kroupa, P., & Larsen, S. S. 2004, MNRAS, 350, 1503

Weil, M. L., Eke, V. R., & Efstathiou, G. 1998, MNRAS, 300, 773

Wetzstein, M., Naab, T., & Burkert, A. 2007, MNRAS, 375, 805

Willman, B., Blanton, M. R., West, A. A., et al. 2005, AJ, 129, 2692

Willman, B., Dalcanton, J. J., Martinez-Delgado, D., et al. 2005, ApJ, 626, L85

Wolf, J., Martinez, G. D., Bullock, J. S., Kaplinghat, M., Geha, M., Muñoz, R. R., Simon, J. D., & Avedo, F. F. 2010, MNRAS, 778

Zhao, H. S. 1996, MNRAS, 283, 149

Zhao, H. S. 2008, Journal of Physics Conference Series, 140, 012002

Zhao, H., & Famaey, B. 2010, Phys. Rev. D, 81, 087304

Zlosnik, T., Ferreira, P., & Starkman, G. 2007, Phys. Rev. D, 75, 044017

Zucker, D. B., Belokurov, V., Evans, N. W., et al. 2006, ApJ, 643, L103

Zucker, D. B., Belokurov, V., Evans, N. W., et al. 2006, ApJ, 650, L41

Zwicky, F. 1933, Helvetica Physica Acta, 6, 110

Appendix: A brief review of MOND and MOG and Milgrom's proposition on the possible physical origin and value of a_0

Theoretical approaches trying to embed MOND within a Lorentz-covariant framework (Bekenstein 2004; Sanders 2005; Zlosnik et al. 2007; Zhao 2008; Bruneton & Esposito-Farèse 2008; Blanchet & Le Tiec 2009; Esposito-Farèse 2009; Skordis 2009; Milgrom 2009b) are currently under intense scrutiny, and a quasi-linear formulation of MOND has been discovered only recently (Milgrom 2010; Zhao & Famaey 2010), which appears to allow easier access to N-body calculations.

However, none of these theories is (yet) fully satisfactory from a fundamental point of view (see e.g. Contaldi et al. 2008; Bruneton & Esposito-Farèse 2008; Reyes et al. 2010) and moreover none of them explains (yet) why the acceleration threshold, a_0, which is the single parameter of MOND (adjusted by fitting to one single system), is about $c \sqrt{\Lambda/3}$ (where Λ is the cosmological constant and c the speed of light), or that $a_0 \approx cH_0/2\pi$, where H_0 is the current Hubble constant. They also require a transition function, $\mu(x)$ (e.g. Eq. 20), from the Newtonian to the modified regime, a function not (yet) rooted in the theory.

A possible explanation of the coincidence $a_0 \approx c \sqrt{\Lambda/3}$ and a theoretically-based transition function are suggested by Milgrom (1999). In Minkowski (flat) space-time, an accelerated observer sees the vacuum as a thermal bath with a temperature proportional to the observer's acceleration (Unruh 1975). This means that the inertial force in Newton's second law can be defined to be proportional to the Unruh temperature. On the other hand, an accelerated observer in a de Sitter universe (curved with a positive cosmological constant Λ) sees a non-linear combination of the Unruh (1975) vacuum radiation and of the Gibbons & Hawking (1977) radiation due to the cosmological horizon in the presence of a positive Λ. Milgrom (1999) then defines inertia as a force driving such an observer back to equilibrium as regards the vacuum radiation (i.e. experiencing only the Gibbons-Hawking radiation seen by a non-accelerated observer). Observers experiencing a very small acceleration would thus see an Unruh radiation with a low temperature close to the Gibbons-Hawking one, meaning that the inertial resistance defined by the difference between the two radiation temperatures would be smaller than in Newtonian dynamics, and thus the corresponding acceleration would be larger. This is given precisely by the MOND formula of Milgrom (1983) with a well-defined transition-function $\mu(x)$, and $a_o = c\,(\Lambda/3)^{1/2}$. Unfortunately, no covariant version (if at all possible) of this approach has been developed yet.

The theoretical basis of the MOG approach relies on chosen values of integration constants in solving the equations of the theory. This approach seems to work well from an observational point of view, but it's fundamental basis needs further research, as is also the case for MOND. It is noteworthy that a formulation of MOG in terms of scalar, vector, and tensor fields (Moffat 2006) may possibly hint at a convergence with the Bekenstein (2004) tensor-vector-scalar theory of gravity.

EXTRATERRESTRIAL LIFE AND CENSORSHIP

N. Chandra Wickramasinghe

Cardiff Centre for Astrobiology, Llwynypia Road, Cardiff CF14 0SY, UK

E mail: ncwick@gmail.com

Abstract

In this article I chronicle a series of landmark events, with which I was personally involved, that relate to the development of the theory of cosmic life. The interpretation of events offered here might invite a sense of incredulity on the part of the reader, but the facts themselves are unimpeachable in regard to their authenticity. Of particular interest are accounts of interactions between key players in an unfolding drama connected with the origins of life. Attempts to censor evidence incompatible with the cosmic life theory are beginning to look futile and a long-overdue paradigm shift may have to be conceded.

Keywords: Dark Matter; Planet Formation: Cosmic structure; Astrobiology

1.   **Introduction**

The ingress of alien microbial life onto our planet, whether dead or alive should not by any rational argument be perceived as a cause for concern. This is particularly so if, as appears likely, a similar process of microbial injection has continued throughout geological time. Unlike the prospect of discovering alien intelligence which might be justifiably viewed with apprehension, the humblest of microbial life-forms occurring extraterrestrially would not constitute a threat. Neither would the discovery of alien microbes impinge on any issues of national sovereignty or defence, nor challenge our cherished position as the dominant life-form in our corner of the Universe.

Over the past three decades we have witnessed a rapid growth of evidence for extraterrestrial microbial life. Along with it has grown a tendency on the part of scientific establishments to deny or denounce the data or even denigrate the advocates of alien life. My own personal involvement in this matter dates back to the 1970's when, together with the late Fred Hoyle, I was investigating the nature of interstellar dust. At this time evidence for organic molecules in interstellar clouds was accumulating at a rapid pace, and the interstellar dust grains that were hitherto believed to be comprised of inorganic ices were shown by us to contain complex organic polymers of possible biological provenance (Wickramasinghe, 1974; Wickramasinghe, et al, 1977; Hoyle and Wickramasinghe, 1977a,b). These discoveries came as a surprise to astronomers, and for a long time the conclusion was resisted that such molecules might have a relevance to life on the Earth (Hoyle and Wickramasinghe, 1986a,b).

Biologists in the 1960's and 1970's had no inkling of the intimate connection of their subject with astronomy. The holy grail of biology was the hypothesis that life emerged from a primordial soup generated *in situ* from inorganic molecules on the primitive Earth (Oparin, 1953).   The primordial soup theory gained empirical support from the classic studies of Miller (1953) and Miller and Urey (1959) that showed the production of minute quantities of amino acids and sugars by sparking mixtures of inorganic gases. Ponnamperuma and Mack (1965) later demonstrated the production of nucleotides (components of DNA) under similar conditions in the laboratory. Finally the experiments of Sagan and Khare (1971) showed the production of amino acids from gases exposed to ultraviolet light (1971). All such experimental triumphs were greeted as crucial steps towards understanding the origin of life

on the Earth, although it was never clear that the experimental conditions used in the laboratory had any relevance to the primitive Earth. The early terrestrial atmosphere that is now believed to have been oxidising would have inhibited any synthesis of organics of the type demonstrated by Miller, Sagan and Ponnamperuma.

The hypothesis of the terrestrial origin of the chemical building blocks of life might have been thought plausible before it was discovered that vast quantities of biogenic organic molecules existed within the interstellar clouds (Hoyle et al, 1978; Kwok, 2009). Having first argued for a complex biochemical composition of interstellar dust, Hoyle and I were among the first to make a connection between complex organic molecules in interstellar clouds and life on Earth (Hoyle and Wickramasinghe, 1976, 1978, 1981).   The total amount of organic material in the galaxy in the form of organic dust and PAH's accounts for about a third of all the carbon present in interstellar space – a truly vast quantity amounting to some billion or so solar masses (see review by Kwok, 2009).

2. **Censorship Dawns**

My first inkling of any censorship relating to extraterrestrial life came when we made the intellectual leap from prebiology in space to fully-fledged biology outside the Earth (Hoyle and Wickramasinghe, 1976, 1982; Hoyle et al, 1984). In setting out to explore the hypothesis that interstellar grains were not just abiotic organic polymers but bacterial cells in various stages of degradation, we made a prediction that interstellar dust in the infrared spectral region must have the signature of bacteria (Hoyle et al, 1982). Infrared sources near the galactic centre were a prime target for this investigation and on our instigation approaches were made to the Anglo-Australian telescope committees to provide time on the AAT to test our seemingly wild hypothesis. An application for observing time for this project made by my brother Dayal T. Wickramasinghe at ANU and David Allen was duly refused as "having no scientific value" (Wickramasinghe, 2005). In the event, Dayal, who was allocated time on the AAT for a totally different project, found a reason to illicitly study the spectrum of the Galactic Centre source GC-IRS7. When he did so he discovered an amazingly close fit to our predicted absorption curve for bacteria – a prediction that was made a full 3 months ahead of the serendipitous observations being made (Hoyle et al, 1982). See Fig. 1.
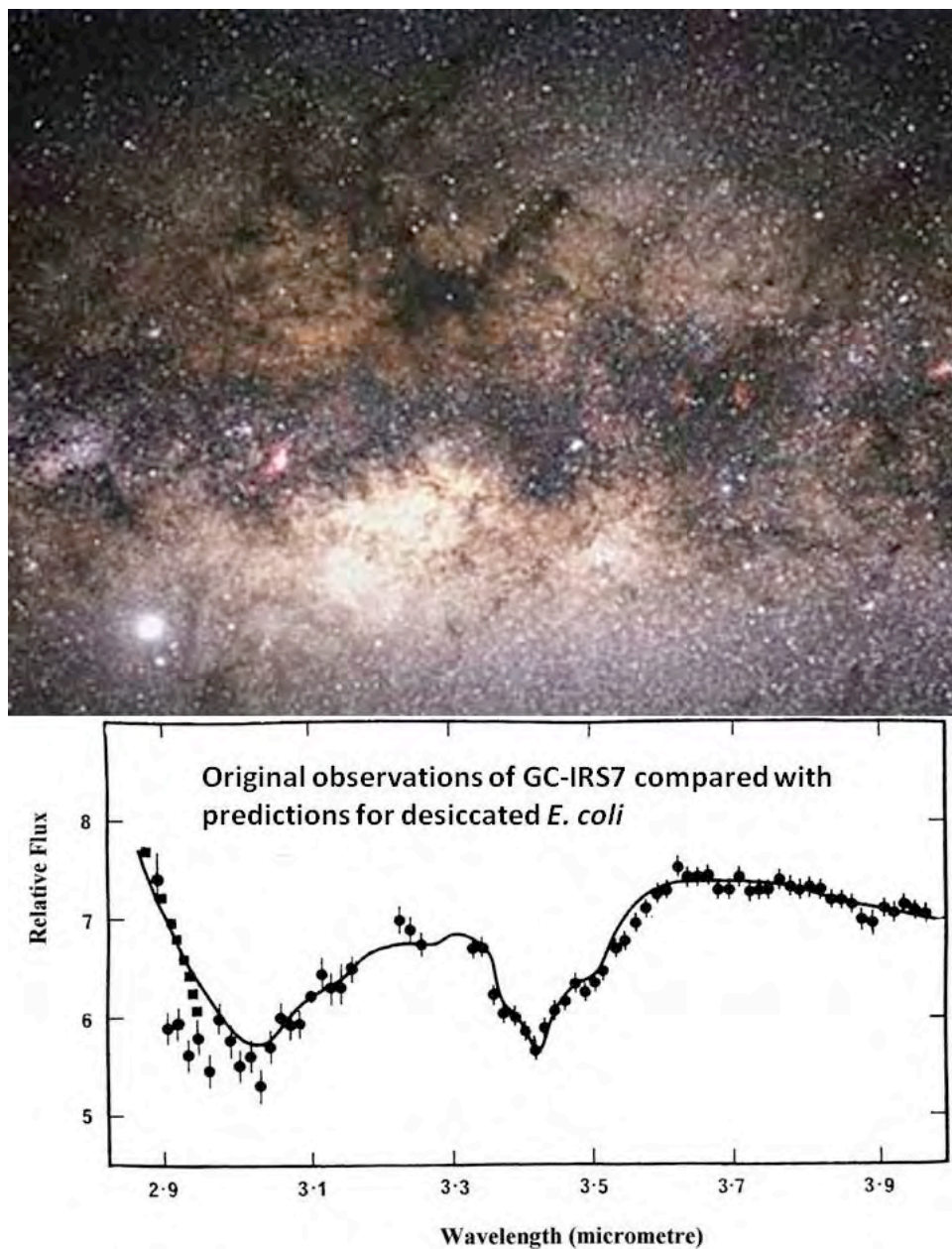
Fig. 1. The first observations by D.T. Wickramasinghe and D.A. Allen of the Galactic Centre source GC-IRS7 compared with the predictions for desiccated *E. Coli* (Hoyle, Wickramasinghe and Al-Mufti, 1984).

From 1982 to the present day astronomical observations of interstellar dust and molecules ranging in wavelength from the far ultraviolet to the infrared have continued to support the biological origin. It would appear that a large fraction of interstellar grains and molecules must have a biological provenance, implying that microbial life exists on a grand galactic or even cosmological scale (Wickramasinghe, 1994, 2010; Hoyle and Wickramasinghe, 2000,

J.Wickramasinghe et al, 2010; Gibson and Wickramasinghe, 2010; Gibson, Schild and Wickramasinghe, 2010).

After 1982, when evidence for cosmic life and panspermia acquired a status close to irrefutable, publication avenues that were hitherto readily available became suddenly closed. With the unexpected discovery that comets had an organic composition, with comet dust possessing infrared spectra consistent with biomaterial (Hoover et al, 1986; Hoyle and Wickramasinghe, 1986a,b) attitudes hardened to a point that panspermia and related issues were decreed taboo by all respectable journals and institutions.

The peer review system that was operated served not only to exclude poor quality research but also to deliberately filter publication of any work that challenged the standard theory of life's origins.

Even though the general public revelled in ideas of extraterrestrial life, science was expected to shun this subject no matter how strong the evidence, albeit through a conspiracy of silence. It was an unwritten doctrine of science that extraterrestrial life could not exist in our immediate vicinity, or, that if such life did exist, it could not have a connection with Earth.

3.   The Meteorite Microfossil Saga

This campaign of explicit denials and censorship may have started between 1962 and 1965 when microorganisms were actually recovered from the stratosphere using balloons flown to heights between 20 and 43km. Although the lower heights in this range were not great enough to exclude terrestrial contamination, the density dependence with height of the recovered particles was consistent with an *infall* rate of 10^{19} cells per year (Greene et al, 1962-65). This important pioneering work, carried out by NASA at the dawn of the Space Age, probably rang alarm bells to which the authorities had to react, and react they surely did. I was told by Leslie Hale, an atmospheric scientist at Penn State University that this exciting programme of work was suddenly halted by funds being withdrawn. Nothing more was said.

Journals like *Nature* and *Science* had for a long time served as staunch guardians of reigning paradigms across the whole of science, straddling cosmology and biology, acting in a sense as the secular "protectors of the faith". Notwithstanding the constraints imposed by such a role these journals did in fact occasionally publish ground-breaking research that contradicted

reigning paradigms. Sometimes they published highly controversial work and invited debate and refutation.

The first reports of the detection of microbial fossils in meteorites were published in the columns of *Nature* by Claus, Nagy and others (Claus and Nagy, 1961; Nagy et al, 1962, 1963). No sooner than these publications appeared a vigorous campaign of refutation and denial was mounted by Anders and others, also in the columns of *Nature* (Anders, 1962; Anders and Fitch. 1962; Fitch et al, 1962). With a ruthless and forceful denigration of these claims on grounds of alleged contamination, the microfossil saga faded from view for a full 20 years. And with a veritable army of nay-sayers braying so stridently the world became convinced that this was a quagmire to which one should never return.

The early pioneers of microfossil discovery were thus silenced and had little choice but to recant. I was told by a reliable witness that Claus was ruthlessly bullied into capitulation, and Nagy also retreated somewhat whilst continuing to hint in his writings that it might be so, rather in the manner of Galileo Galilei's whispered "*E pur si mouve*" – and yet it moves.

Whilst such rumblings continued the earlier work of Claus and Nagy came to be superseded in quality by investigations carried out by Hans Dieter Pflug in 1981. Twenty years on, with improved techniques of sample preparation, electron microscopy and laser ion probe spectroscopy, the signal-to-noise ratio for microfossil detection was improved by at least an order of magnitude. In 1980 Hans Pflug corresponded with Fred Hoyle and myself to inform us that his new studies corroborate our own by now well-publicised claims of extraterrestrial microbial life. In his investigation of the Murchison meteorite ultra-thin slices of the meteorite were placed on a perfectly clean membrane and the mineral matrix leached out with hydrofluoric acid, thus leaving any included organic structures intact. Pflug discovered a wide range of organic structures uncannily similar to terrestrial microorganisms; and with laser ion probe studies and EDAX analysis he found their chemical compositions and forms to be consistent with microbial fossils.

I invited Hans Pflug to visit us in Cardiff and on the 26th of November 1981 he delivered a lecture, introduced by Fred Hoyle, that left the audience speechless. The poster for the lecture and some of his key images are shown in Fig. 2. The response to Pflug's discoveries differed markedly from the earlier attitudes to Claus and Nagy. Pflug was not attacked on grounds of contamination or artifacts, but he was given what could be described as the "silent treatment". This was the same manner in which my own collaborations with Hoyle at the

time were received. There were muffled whisperings in University common rooms, but nothing in the way of a well-formulated technical criticism ever appeared in print.
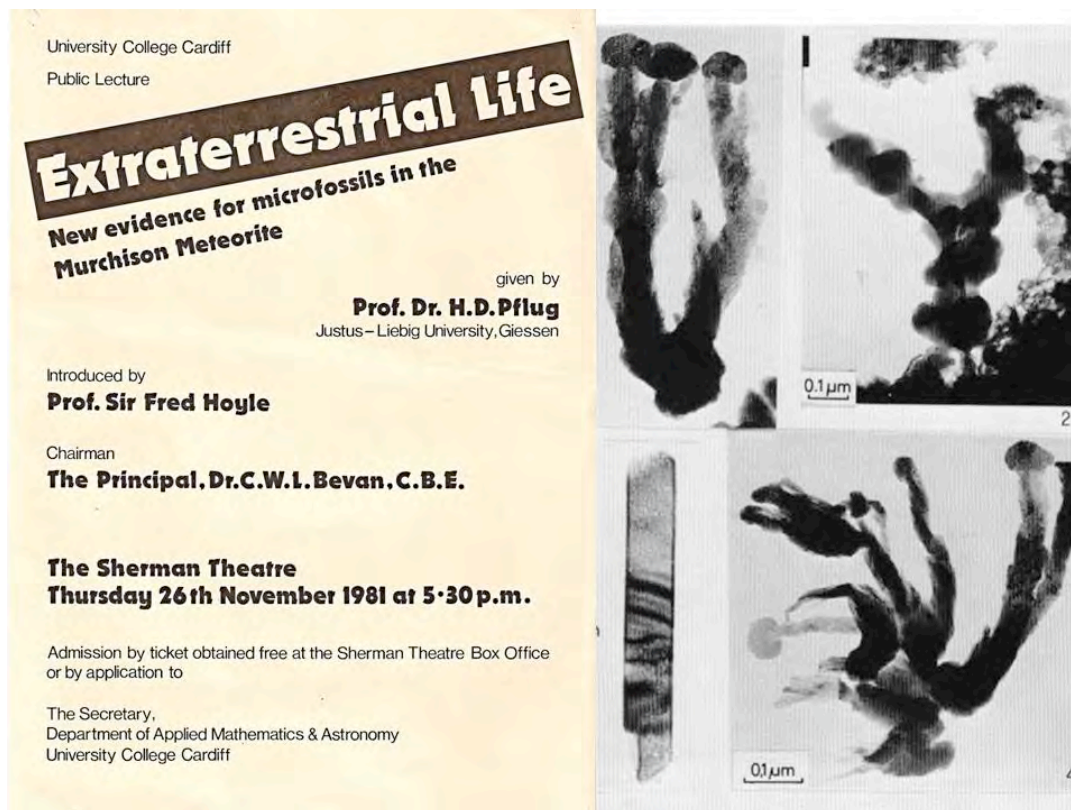

Fig. 2 Pflug's lecture poster and an example of a microfossil of *pedomicrobium* in the Murchison Meteorite.

4.   **A Conference in Sri Lanka**

With a confluence of observations and data from many directions pointing to a cosmic origin of life a rare opportunity came along for me to organise an international conference between 1st and 11th December 1982 in Colombo, Sri Lanka. The conference had the title "Fundamental Studies and the Future of Science" and was convened by the Institute of Fundamental Studies (IFS) and the office of His Excellency the President of Sri Lanka. The participants included Fred Hoyle and several key players in the unfolding drama of cosmic life. Fred Hoyle gave the first talk entitled "From Virus to Man" and Hans Pflug followed this with a breath-taking presentation of his work on meteorite microfossils. His Excellency President Junius Jayawardene (incidentally a fan of Fred Hoyle) sat speechless in the front row of the audience.

Fig. 3. The Bandaranaike Memorial Conference Hall in Colombo. Venue for the conference in December 1982 presided over by His Excellency the President of Sri Lanka, and including amongst others: Sir Fred Hoyle, Hans Pflug, Bart Nagy, Gustaf Arrhenius, Cyril Ponnamperuma, Phil Solomon, Sir Arnold Wolfendale and Chandra Wickramasinghe.

Just as one felt that the game was up for Earth-centred life, Gustaf Arrhenius, the grandson of Svante Arrhenius, slated Pflug mercilessly for reviving the ignominious microfossil saga of the 1960's. One is enjoined, he argued, not to pay any attention to morphology. All that was permitted to take place in meteorite formation processes are catalysis, chemistry and mineralogy. What Hans Pflug showed us in Colombo were artifacts! Life look-alikes, not life!

After much heated arguments about microfossils, Sri Lankan-born Cyril Ponnamperuma's lecture trawled through extensions of the Miller-Urey synthesis adding little to the debate. The question that reverberated through the lofty spaces of the Chinese-built BMICH auditorium was stark and simple: "Was the evidence we saw for extraterrestrial life real or illusory?" Heated arguments continued late into the night in the hotel bar of the Oberoi – the luxury hotel where the participants stayed. It was amusing to hear pontification by Gustav Arrhenius denouncing his grandfather Svante for ever raising the spectre of panspermia. It was obvious that there could be no consensus. Bartholamew Nagy, who was due to speak on the next day, was seen scampering between rival cliques like a rabbit scared out of its wits.

Nagy had been billed to give a talk in support of Pflug, but in the event he delivered a talk with the unimposing title: "Search for potential biochemical fossils less than 3.5×10^9 years old", concentrating on the safe option of microfossils in terrestrial sediments. The irony was that whilst microfossils in terrestrial sedimentary rocks were considered valid observations, similar or even identical structures in extraterrestrial rocks were necessarily all contaminants!

Atmospheric physicist E.K. Bigg next showed images of the very earliest microscopic particles collected at great heights in the stratosphere, some of which may be identified with microbial particles entering the Earth from outside. Bigg was understandably guarded in his conclusions, however, so he did not attract the hostility that Hoyle, Pflug or Nagy had received. It is ironical that weak evidence often goes unchallenged; the stronger the evidence that challenges a reigning paradigm, the more vehement the protestations and rebuttals tend to be.

Phil Solomon (SUNY), the pioneer of interstellar CO observations, summed up the session with a brilliant talk on "Molecular Clouds in the Galaxy", which after all was where the modern revival of panspermia began in the 1970's.

Throughout this historic meeting, whether in hotel bars, or as we toured the magnificent beaches and historical monuments of Sri Lanka, the arguments about alien life never ceased. With all the relevant people assembled at the same place at the same time it felt as though a momentous paradigm shift was in the air. But that was not to be. Conceding anything at all seemed difficult. There was a great hesitancy to admit anything at all that might "rock the boat" – a boat that now seemed to be sailing in stormy tropical waters of the Indian Ocean, at any rate from the vantage point of conservative science.

Sir Arnold Wolfendale, former Astronomer Royal, had friends in Sri Lanka and felt very much at home there, but not so with the portents of a paradigm shift that appeared ominously on the horizon. He proposed that the matters discussed in Colombo be *properly* resolved at a discussion meeting of the Royal Astronomical Society, a meeting that he as President of the RAS was able to convene. Thus ended a conference in tropical Sri Lanka with what seemed to be a disappointingly indecisive result. Despite the weight of facts and evidence presented, and the good humour that prevailed, few admitted to have changed their mind. As Julius Caesar said "People willingly believe what they want to believe..." (*The Gallic War*, 3.18)

9

5.   Meeting of the Royal Astronomical Society

As promised by Wolfendale a discussion meeting of the Royal Astronomical Society with the title "Are interstellar grains bacteria?" took place at the Scientific Societies Lecture Theatre in Savile Row London on 11th November 1983. Fred Hoyle and I presented arguments for our thesis of cosmic life and several others including Nobel Laureate Harry Kroto followed on with what amounted to no more than polemical retorts. Phil Solomon summarised the turbulent proceedings thus:

"A strong case for identification of grains with bacteria has been made and nothing yet presented appears to destroy the case. The issue is one which in spite of its dramatic implications can be settled in the near future by further observations....."

Summaries of the papers presented at this meeting are published in *The Observatory*, Vol 104, No.1060, pp129-139, June 1984.

6.   Further Developments

Further studies and more extensive observations of interstellar dust, comets, cometary debris and meteorites have added to the evidence in quick succession (J.Wickramasinghe et al, 2010; Smith et al, 2007). Astronomical observations deploying new telescopes and instruments yielded spectroscopic data that confirms the dominance of complex organic molecules similar to biological degradation products in interstellar clouds and even in distant galaxies at high redshifts (Wickramasinghe et al 2004; Wickramasinghe, 2010; Gibson and Wickramasinghe, 2010). Hydrogravitational dynamics HGD theory supports cometary panspermia and the early formation of complex life, in 705 F hot water oceans of primordial hydrogen planets that formed the first stars and chemicals (Gibson, Schild and Wickramasinghe 2010; Gibson, Wickramasinghe and Schild, 2011). A cosmological primordial soup (Miller and Urey 1959) existed on 10^{80} merging primordial gas planets and their comets, all tracking progress in organic chemistry among the planets at time 2 Myr when the density of the cosmos was larger than the density at present by a factor of 10^{8}. Thirty million frozen primordial gas planets per star in protoglobularstarclusters make up the dark matter of galaxies according to HGD cosmology.

Extensive studies of comets after the 1986 perihelion passage of Comet Halley and the *Giotto Mission* showed to the consternation of most astronomers that cometary dust did indeed contain a large fraction of complex organics with spectra resembling biomaterial. Whipple's

dirty snowball model of comets was seriously challenged. Cometary dust collections in the *Stardust Mission* to Comet Wildt 2 also confirmed the presence of either degradation products of life or the building blocks of life, in the destruction trails left by high-speed dust particles as they were slowed in blocks of aerogel. Unfortunately, however, because the aerogel was not sterilized, no biological inferences could be drawn. The Deep Impact Mission to comet Tempel 1 in 2004 once again confirmed the organic composition of comets but also showed evidence of clay minerals, consistent with the presence of liquid water at an early stage in the comet's history (A'Hearn et al, 2005; Lisse et al, 2006). This is important because it would show that comets could provide habitats for the replication of cosmic bacteria – thus making these celestial bodies viable homes for life.

The 2001-2009 ISRO-Cardiff studies of dust recovered using balloons flown to heights of 41km in the stratosphere showed not only the presence of viable cultures of UV resistant microorganisms, but also evidence for larger 15-20 micron-sized clumps of dormant microorganisms (Narlikar et al, 2003; Wainwright et al, 2003). The latter were detected with the use of fluorescent dyes showing the presence of viable but not culturable microorganisms. The possibility of terrestrial contamination was virtually excluded, the height of 41km being too high for lofting large clumps of terrestrial material from the surface; and so we were led to conclude that here is evidence of a continuing incidence of microorganisms from space. From our collection statistics we estimated a daily input of viable biomaterial of about 0.1 tonne averaged over the whole Earth.

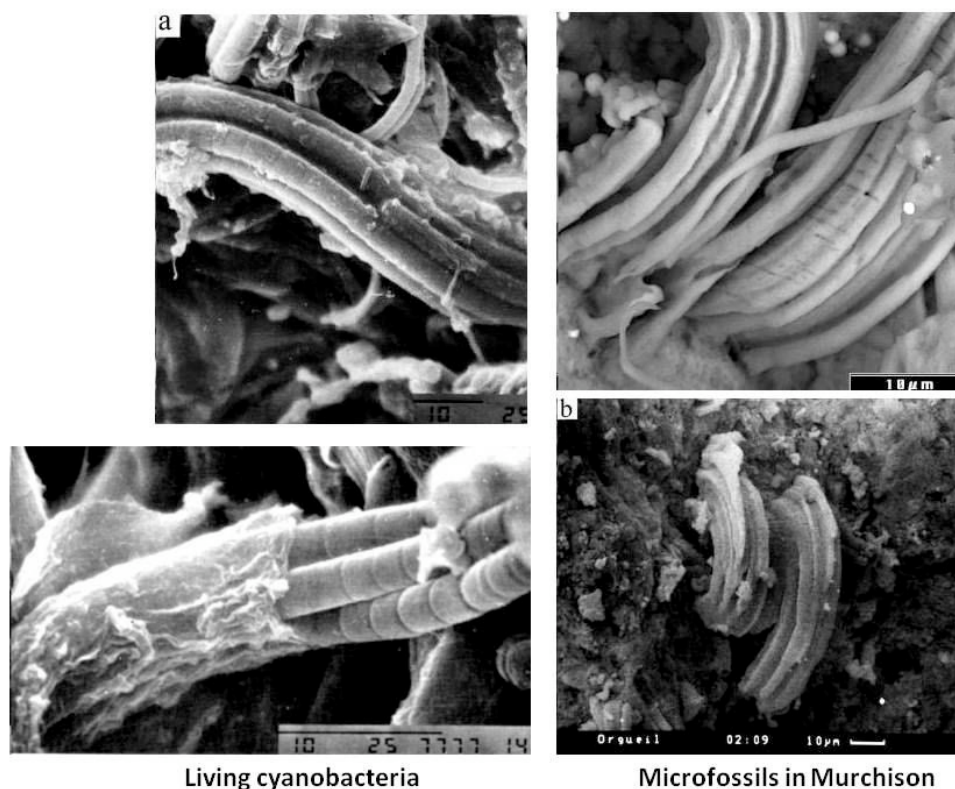Living cyanobacteria   Microfossils in Murchison

Fig. 4 Hoover's Murchison microfossils of cyanobacteria compared with modern cyanobacteria (Hoover, 2005)

It is against this backdrop that one should approach Richard B Hoover's recent re-examination of Murchison meteorite microfossils (Hoover, 2005, 2011).   (See for instance Fig.4). Using state of the art technology Hoover concludes that microbial fossils unambiguously exist in great profusion. The furore that greeted this new publication, with vocal condemnation from Science journals and from NASA chiefs, shows that earlier tactics of rejection by silence have now been replaced by strident ranting and even personal insults. Had we lived in the Middle Ages there is no doubt that Richard B Hoover, and possibly Fred Hoyle, Pflug, and I too, would have come to a bad end – suffering the fate of Giordano Bruno in 1600!

The handicap facing 21st century science is an excess of specialisation. Although some extent of specialisation is predicated by the huge quantity of information within each separate discipline, the disadvantage is that cross-disciplinary developments are discouraged. This, I believe, is one factor at least that has impeded the acceptance of the cosmic theories of life. To astronomers the association of bacteria with interstellar grains would appear understandably strange; and to biologists the intrusion of astronomy into their discipline

would be equally repugnant. But the Universe encompasses everything, and is no respecter of any man-made boundaries between disciplines.

In the year 2011 all the relevant facts appear to converge in favour of the cosmic origins of life. Resisting the facts and imposing censorship would in the long run turn out to be futile. The Universe will always have its last say.

(Note: The proceedings of the 1982 conference in Sri Lanka is published in Wickramasinghe, 1984 (ed) detailed in a reference below.)

References

A'Hearn, M.F., Belton, M.J.S., Delamare, W.A., et al, 2005. "Deep Impact: Excavating Comet Tempel 1", *Science*, 310, 258

Anders, E., 1962. "Meteoritic hydrocarbons and extraterrestrial life", *Ann. N. Y. Acad Sci.* 93, pp. 651-657

Anders, E. and Fitch, F., 1962. "Search for organized elements in carbonaceous chondrites", *Science* 138, 1392

Claus, G. and Nagy, B., 1961. "A microbiological examination of some carbonaceous chondrites", *Nature* 192, 594

Gibson, C.H. and Wickramasinghe, N.C., 2011. "Imperatives of cosmic biology, Journal of Cosmology, arXiv:1003.0091

Gibson, C. H., Schild, R. A., and Wickramasinghe 2010. "The origin of life from primordial planets", Int. J. of Astrobiol., doi:10.1017/S1473550410000352, 1-16, arXiv:1004.0504.

Gibson, C., Wickramasinghe, N. & Schild, R. 2011. "First life in the oceans of primordial-planets: the biological big bang", Journal of Cosmology 11, 3490-3499, arXiv:1009.1760.

Fitch, F.W., Schwarz, H.P. and Anders, E., 1962. "Organized elements in carbonaceous chondrites", *Nature,* 193, 1123

000279

Greene, V.W., Pederson, P.D., Lundgren, D.A., Hagberg, C.A. and Soffen, G.A., 1962-65, NASA Report, N65-23980

Hoover, R.B., 2005. In R.B. Hoover, A.Y. Rozanov and R.R. Paepe (eds) "Perspectives in Astrobiology", (IOS Press Amsterdam)

Hoover, R. B. 2011. "Fossils of Cyanobacteria in CI1 Carbonaceous Meteorites: Implications to Life on Comets, Europa, and Enceladus", Journal of Cosmology 13, xxx-xxx.

Hoover, R.B., Hoyle, F., Wickramasinghe, N.C., Hoover, M.J. and Al-Mufti, S., 1986. "Diatoms on Earth, Comets, Europa and in interstellar space", *Earth Moon and Planets*, 35, 19

Hoyle, F. and Wickramasinghe, N.C., 1976. "Primitive grain clumps and organic compounds in carbonaceous chondrites", *Nature*, 264, 45

Hoyle, F. and Wickramasinghe, N.C., 1977a. "Polysaccharides and the infrared spectra of galactic sources", *Nature*, 268, 610

Hoyle, F. and Wickramasinghe, N.C., 1977b. "Identification of the 2200A interstellar absorption feature", *Nature,* 270, 323

Hoyle, F. and Wickramasinghe, N.C., 1978. *Lifecloud* (J.M. Dent & Sons, London)

Hoyle, F., Wickramasinghe, N.C. and Olavesen, A.H., 1978. "Identification of interstellar polysaccharides and related hydrocarbons", *Nature*, 271, 229

Hoyle, F. and Wickramasinghe, N.C., 1981. "Comets - a vehicle for panspermia", in *Comets and the Origin of Life*, ed. C. Ponnamperuma, D. Reidel Publishing Co. Dordrecht

Hoyle, F. and Wickramasinghe, N.C., 1986a. "The case for life as a cosmic phenomenon", *Nature,* 322, 509

Hoyle, F. and Wickramasinghe, N. C. 1986b. "On Deliberate Misreferencing as a Tool in Science Policy", *Comments*, Cardiff Astrophysics and Relativity Preprint No. 125, arXiv:1009.1379

Hoyle, F. and Wickramasinghe, N.C., 2000. "Astronomical Origins of Life – Steps towards panspermia" (Kluwer Academic Publishers, Dordrecht)

Hoyle, F., Wickramasinghe, N.C., Al-Mufti,S., Olavesen, A.H. and Wickramasinghe, D.T. , 1982. "Infrared spectroscopy over the 2.9-3.9 micron waveband in biochemistry and astronomy", *Astrophys. Sp.Sci.,* 83, 405

Hoyle, F. and Wickramasinghe, N.C., 1982. "A model for interstellar extinction", *Astrophys.Sp.Sci.,* 86, 321

Hoyle, F., Wickramasinghe, N.C., and Al-Mufti, S., 1984. "The spectroscopic identification of interstellar grains", *Astrophys. Sp.Sci.*, 98, 343.

Hoyle, F., Wickramasinghe, N.C., and Pflug, H.D., 1985. "An object within a particle of extraterrestrial origin compared with an object of presumed terrestrial origin", *Astrophys. Sp.Sci.*, 113, 209

Kwok, S., 2009, "Organic matter in space: from stardust to the solar system", *Astrophys.Sp.Sci.,* 319, 5

Lisse, C.M., van Cleve, J., Adams, A.C. et al., 2006. "Spitzer Spectral Observations of the Deep Impact Ejecta", *Science*, 313, 635

Miller, S.L., 1953. "Production of Amino Acids Under Possible Primitive Earth Conditions", *Science*, 117, 528

Miller, S.L. and Urey, H.C., 1959. "Organic Compound Synthesis on the Primitive Earth," *Science,* 130, 245

Nagy, B., Claus, G. and Hennessy, D.J., 1962. "Organic particles embedded in minerals in the Orgueil and lvuna carbonaceous chondrites", *Nature,* 193, 1129-1133

Nagy, B., Frederickson, K., Urey, H.C., Kudynowski, J., Claus, G., Andersen, C.A., and Percy, J., 1963. "Electron probe microanalysis of organized elements in the Orgueil meteorite", *Nature* 198, 121

Narlikar, J.V., Wickramasinghe, N.C., Wainwright, M. And Rajaratnam, P., 2003. "Detection of Microorganisms at High Altitudes", *Current Science*, 85 (No.1), 29

Oparin, A.I., 1953. "The Origin of Life" (trans. S. Marguli) (Dover, NY)

Ponnamperuma, C.and Mark, R., 1965. "Formation of Dinucleoside Phosphates and Dinucleotides in the Study of Chemical Evolution", *Science,* 148, 1221

Sagan, C. and Khare, B.N., 1971. "Long-wavelength ultraviolet photoproduction of amino acids on the primitive Earth", *Science*, 173, 417

Smith, J.D.T., Draine, B.T., Dalie, D.A. et al, 2007. " Dust Masses, PAH Abundances, and Starlight Intensities...." *Astrophys.J.,* 656, 770

Wainwright, M., Wickramasinghe, N.C., Narlikar, J.V. and Rajaratnam, P., 2003. "Microorganisms cultured from stratospheric air samples obtained at 41km", *FEMS Microbiology Letters*, 218, 161

Wallis, M.K., Wickramasinghe, N.C., Hoyle, F. and Rabilizirov, R., 1989. "Biologic versus abiotic models of cometary dust", *Mon. Not. Roy.Astr.Soc*., 238, 1165

Wickramasinghe, N.C., 1974. "Formaldehyde polymers in interstellar space", *Nature*, 252, 462

Wickramasinghe, N.C., Hoyle, F., Brooks, J., and Shaw, G., 1977. "Prebiotic polymers and infrared spectra of galactic sources", *Nature*, 269, 674

Wickramasinghe, NC., Wickramasinghe, J.T. amd Mediavilla, E., 2004. "The interpretation of a 2175A absorption feature in the gravitational lens galaxy SBS0909+53f2 at z=0.83" *Astrophysics and Space Science*, 298, 453

Wickramasinghe, C. 1984 (ed) "Fundamaental Studies and the Future of Science" (University College, Cardiff Press, Cardiff)

Wickramasinghe, N.C. 1994. "Cosmic Grains", in "*Infrared Astronomy*" (eds. A. Mampsaso, M. Prieto & F. Sanchez) Proceedings of the 4th Canary Islands Winter School of Astrophysics (Cambridge University Press)(ISBN 0521 464625) pp 275-299

Wickramasinghe, J.T., Wickramasinghe, N.C.. and Napier, W.M. 2010. "Comets and the Origin of Life", (World Scientific Press, Singapore)

Wickramasinghe, C., 2005. "A Journey with Fred Hoyle", (World Scientific Press, Singapore)

Wickramasinghe, C., 2010. "The astrobiological case for our cosmic ancestry", *International Journal of Astrobiology* 9 (2) : 119–129

000299

Commentary on Hoover (2011) claim about extraterrestrial fossils, Gibson/Schild, March 30, 2011

Hydro-Gravitational-Dynamics Cosmology supports Hoyle/Wickramasinghe panspermia and an extraterrestrial origin of life at 2-8 million years

Carl H. Gibson [1,2]

[1] University of California San Diego, La Jolla, CA 92093-0411, USA
[2] cgibson@ucsd.edu, http://sdcc3.ucsd.edu/~ir118

and

Rudolph E. Schild [3,4]

[3] Center for Astrophysics, 60 Garden Street, Cambridge, MA 02138, USA
[4] rschild@cfa.harvard.edu

Commentary

Richard Hoover (2011) claims that three carbonaceous meteorites he and his astrobiology team have examined at NASA Marshall Space Flight Center show strong evidence of extraterrestrial cyanobacterial life. His claim is supported by a tediously careful Journal of Cosmology peer review process and the present set of commentaries reflecting a wide range of viewpoints. It is hereby also supported by the two founders of hydro-gravitational-dynamics cosmology (Gibson 1996, Schild 1996). Hoover's claim is, however, contradicted by the standard "concordance" ΛCDMHC cosmology. Whether or not Hoover's claim is true depends on which cosmology is correct, since HGD and NASA-CDM cosmologies reach opposite conclusions about the formation of life. Timelines for life formation by HGD versus ΛCDMHC are compared in Figure 1.
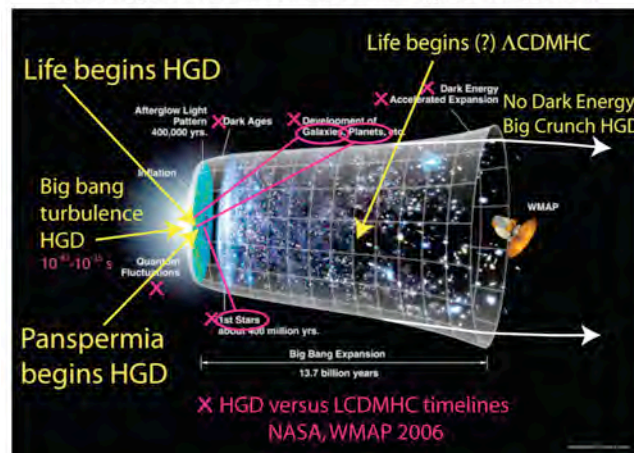

Fig. 1 NASA-CDM astrobiological and cosmological versus HGD timelines. Life according to NASA-CDM is virtually impossible because primordial hydrogen planets are not produced to make stars, chemicals, oceans and the first life at 2 Myr (the time when C,N,O-seeded oceans condense, at critical temperature 705 F), from HGD.

HGD (new) cosmology drastically modifies standard (old) cosmology in ways that make life formation statistically inevitable, early and widespread. Several fluid mechanics concepts (viscosity, turbulence, fossil turbulence, diffusivity of the non-baryonic dark matter) are recognized as critical by HGD but are neglected by NASA-CDM that relies on Jeans 1902 for its fluid mechanics. Without HGD, life anywhere or any time in the universe is statistically an isolated miracle. In old cosmology the first star cannot form until after 400 million years, when it is so cold that hydrogen freezes. A handful of planets per star appear later. Primordial H-^{4}He gas planets like the outer Jovians of the solar system are impossible to condense by the Jeans 1902 mechanism because the universe never gets cold enough; that is, < 2.7 K the present temperature. Galaxies form gradually, followed by galaxy clusters and superclusters. Whatever life might form would be too little and too late, and isolated. Life could not be communicated far beyond its star of origin and the few planets produced, with the star, by condensing gas and dust. Life must somehow appear independently on scattered planets, only a few of which have liquid oceans. Organic chemicals are widely observed in space, but cannot be explained without further miracles. In new cosmology life exists for 99.99% of the age of the universe on planets and comets that make the stars, and the chemicals that make life by exploding the stars (Gibson, Schild & Wickramasinghe 2010).

According to HGD, all of the hydrogen and ^{4}helium plasma formed by the big bang fragments into protosuperclusters, protoclusters and protogalaxies, in that order, under viscous-gravitational control starting at 30 kyr and turning to gas at 300 kyr (Gibson 1996). Planets in clumps are observed as the missing mass of galaxies (Schild 1996). The hot gas of the protogalaxies fragments into clumps of Earth-mass planets, a trillion planets per clump. The planets merge to larger planets and eventually stars that slow the merging rate by radiation pressures. Further merging causes supernovae and the production of life chemicals C, N, O etc. that seed the remaining planets in the clump. Oceans of water appear on iron-rock cores of the growing planets at 2 myr when the universe temperature cools to 705 F, the critical temperature of water. Organic chemistry begins in these communicating planets, and in their hydrogen saturated, chemically seeded oceans. The biological big bang (Gibson, Wickramasinghe, Schild 2011) proceeds in the 10^{80} or more hot water oceans under crushing hydrogen atmospheres till the oceans freeze at 32 F at 8 myr: a cosmological mass primordial soup. Intergalactic cometary panspermia is enhanced by the 10^8 increase in average spatial density of galaxies.

Evidence of planets as the source of stars is provided by the discovery of more than 400 extra-solar planets, including many "hot Jupiters" at 10^{10} m Mercury-orbit scale distances from stars. Such planets are clearly hydrogen gas planets, either in the process of accretion by the star or evaporation to expose the rocky-iron core expected from HGD.

Figure 2 compares the HGD based biological big bang with the concept of genetic gradualism discussed by Line (2010) in a Commentary on Sharov (2010).

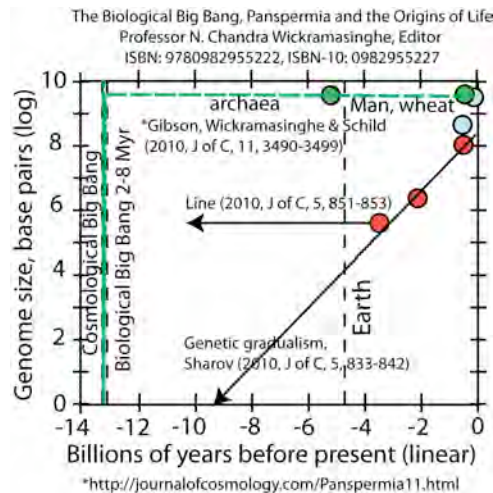Commentary on Hoover (2011) claim about extraterrestrial fossils, Gibson/Schild, March 30, 2011

Fig. 2 Genome size in log base pairs versus billions of years before present. Both the HGD
biological big bang at 2-8 myr and the genetic gradualism of Sharov (2010). In his
Commentary, Line (2010) suggests life originated long before it appeared on Earth
(horizontal arrow).

The difference between the biological big bang of HGD and the genetic gradualism time
scales shown in Fig. 2 is attributed to the apparent need for many billions of years of
evolution to produce advanced species such as man or wheat from nanometer sized
extremophiles like archea that are most appropriate for cometary panspermia.

Summary

Millions of known organic chemical reactions were and are in competition for the
powerful carbon bonds forming the backbone of DNA and RNA in the countless planets,
moons, comets and meteors formed in the cascade of merging hydrogen planets to stellar
mass, from HGD. Rather than ~10 planets per star, HGD predicts 30 million, with all
stars forming in protoglobularstarclusters of a trillion planets. Hoyle/Wickramasinghe
cometary panspermia is vindicated by HGD. The most efficient self replicating system to
emerge, one that has apparently taken over the entire cosmos, is apparently the CHON
organic chemistry of DNA and RNA. Hoover (2011) and the several others that have
inferred fossilized life from the CI1 meteorites are vindicated by HGD.

References

Gibson, C.H. 1996. Turbulence in the ocean, atmosphere, galaxy and universe, Appl.
Mech. Rev., 49, no. 5, 299–315.

Gibson, C. H., Schild, R. A., and Wickramasinghe 2010. The origin of life from
primordial planets, Int. J. of Astrobiol., doi:10.1017/S1473550410000352, 1-16,
arXiv:arXiv:1004.0504.

3

Gibson, C., Wickramasinghe, N. & Schild, R. 2011.   First life in the oceans of primordial-planets: the biological big bang, Journal of Cosmology 11, 3490-3499, arXiv:1009.1760.

Hoover, R. 2011.   Fossils of Cyanobacteria in CI1 Carbonaceous Meteorites: Implications to Life on Comets, Europa, and Enceladus, Journal of Cosmology 13, xxx-xxx.

Jeans, J. H. 1902. The stability of spherical nebula, Phil. Trans., 199A, 0-49.

Line, M. A. 2010. Extraterrestrial Origin of Life and Genetic Gradualism: Commentary, Journal of Cosmology, Vol 5, 851-853.

Schild, R. E. (1996). Microlensing variability of the gravitationally lensed quasar Q0957+561 A,B, ApJ 464, 125.

Sharov, A. A. 2009. Genetic Gradualism and the Extra-Terrestrial Origin of Life, Journal of Cosmology, Vol. 5, 833-842.

000248

Fossils of Cyanobacteria in CI1 Carbonaceous Meteorites: Implications to Life on Comets, Europa, and Enceladus

Richard B. Hoover

Space Science Office, Mail Code 62, NASA/Marshall Space Flight Center, Huntsville, AL 35812

ABSTRACT

Environmental (ESEM) and Field Emission Scanning Electron Microscopy (FESEM) investigations of the internal surfaces of the CI1 Carbonaceous Meteorites have yielded images of large complex filaments. The filaments have been observed to be embedded in freshly fractured internal surfaces of the stones. They exhibit features (e.g., the size and size ranges of the internal cells and their location and arrangement within sheaths) that are diagnostic of known genera and species of trichomic cyanobacteria and other trichomic prokaryotes such as the filamentous sulfur bacteria. ESEM and FESEM studies of living and fossil cyanobacteria show similar features in uniseriate and multiseriate, branched or unbranched, isodiametric or tapered, polarized or unpolarized filaments with trichomes encased within thin or thick external sheaths. Filaments found in the CI1 meteorites have also been detected that exhibit structures consistent with the specialized cells and structures used by cyanobacteria for reproduction (baeocytes, akinetes and hormogonia), nitrogen fixation (basal, intercalary or apical heterocysts) and attachment or motility (fimbriae).

Energy dispersive X-ray Spectroscopy (EDS) studies indicate that the meteorite filaments are typically carbon rich sheaths infilled with magnesium sulfate and other minerals characteristic of the CI1 carbonaceous meteorites. The size, structure, detailed morphological characteristics and chemical compositions of the meteorite filaments are not consistent with known species of minerals. The nitrogen content of the meteorite filaments are almost always below the detection limit of the EDS detector. EDS analysis of terrestrial minerals and biological materials (e.g., fibrous epsomite, filamentous cyanobacteria; mummy and mammoth hair/tissues, and fossils of cyanobacteria, trilobites, insects in amber) indicate that nitrogen remains detectable in biological materials for thousands of years but is undetectable in the ancient fossils. These studies have led to the conclusion that the filaments found in the CI1 carbonaceous meteorites are indigenous fossils rather than modern terrestrial biological contaminants that entered the meteorites after arrival on Earth. The $\delta^{13}C$ and D/H content of amino acids and other organics found in these stones are shown to be consistent with the interpretation that comets represent the parent bodies of the CI1 carbonaceous meteorites. The implications of the detection of fossils of cyanobacteria in the CI1 meteorites to the possibility of life on comets, Europa and Enceladus are discussed.

Keywords: CI1 meteorites, Orgueil, Alais Ivuna, microfossils, cyanobacteria, comets, Europa, Enceladus

1. INTRODUCTION

The CI1 carbonaceous chondrites are the most primitive of all known meteorites in terms of solar elemental abundances and the highest content of volatiles. Carbonaceous chondrites are a major clan of chondritic meteorites that contain water, several weight % Carbon, Mg/Si ratios at near solar values, and oxygen isotope compositions that plot below the terrestrial fractionation line. The CI1 classification indicates the meteorites belong to the CI (Ivuna Type) chemical group and are of petrologic Type 1. The CI1 meteorites are distinguished from other carbonaceous chondrites by a complete absence of chondrules and refractory inclusions (destroyed by aqueous alteration on the parent body) and by their high degree (~20%) of indigenous water of hydration. The aqueous alteration took place on the parent bodies of the CI1 meteorites at low temperature (<50 °C) and produced hydrated phyllosilicates similar to terrestrial clays, carbonates and

1

oxides magnetite Fe_3O_4 and limonite $Fe_2O_3 \cdot nH_2O$. Sparsely distributed throughout the black rock matrix are fragments and crystals of olivine, pyroxene and elemental iron, presolar diamonds and graphite and insoluble organic matter similar to kerogen.

The CI1 carbonaceous chondrites are extremely rare. Although over 35,000 meteorites have been recovered there are only nine CI1 meteorites known on Earth **(Table I)**. Five of them were observed falls: *Alais, Orgueil, Ivuna, Tonk* and *Revelstoke*) and the other four (*Y-86029, Y-86737, Y980115* and *Y-980134*) were collected in 1986 and 1998 from the blue ice fields of the Yamato Mountains by Antarctic Expeditions of the National Institute of Polar Research, Japan. The great rarity of the CI1 stones is undoubtedly due to the fact that they are friable micro-regolith breccias. All five CI1 meteorites known before 1986 were collected soon after they were observed to fall. The particulates of the CI1 meteorites are cemented together by water soluble evaporite minerals such as epsomite ($MgSO_4 \cdot 7H_2O$) and gypsum ($CaSO_4 \cdot 2H_2O$). The fact that these stones disintegrate immediately after they are exposed to liquid water was observed during the initial studies of the Alais meteorite (Thénard, 1806; Berzelius, 1834, 1836) and the Orgueil stones (Leymerie, M. 1864). These stones are destroyed and disaggregate into tiny particles as the water soluble salts that cement the insoluble mineral grains together in the rock matrix dissolve (Hoover, 2005).

TABLE I. CI1 Carbonaceous Meteorites

FALLS				
NAME	**DATE**	**LOCATION**	**MASS**	**INITIAL DESCRIPTION**
Alais	3/15/1806	Alais, Languedoc-Roussillon, France – (44° 7'N, $4\,^o$ 5'E)	6 kg	Berzelius, J. J., 1834
Orgueil	5/14/1864	Orgueil,Tarn-et-Garonne, France - (43° 53'N, 1° 23'E)	14 kg	Cloëz, S., 1864a,b; Daubrée, A.., 1864; Leymerie, M., 1864
Tonk	1/22/1911	Tonk, Rajasthan, India (24° 39'N, 76° 52'E)	7.7 g	V. Brief Notices, Geolog. Mag. (Decade. VI), 2, pp. 87-90, 1915
Ivuna	12/16/1938	Ivuna, Mbeya, Tanzania (8° 25'S, 32° 26'E)	705 g	
Revelstoke	3/31/1965	64 km NW of City of Revelstoke, British Columbia, Canada (51° 20'N, 118° 57'W)	1 g	Folinsbee, 1965; Folinsbee *et al.,* 1967
FINDS				
Y-86029	1986	Yamato Mountains, Antarctica (71° 30'S, 35° 40'E)	11.8 g	Tonui *et al.,* 2001
Y-86737	1986	Yamato Mountains, Antarctica (71° 30'S, 35° 40'E)	2.8 g	Tonui *et al.,* 2001
Y-980115	1998	Yamato Mountains, Antarctica	772 g	Kojima, H., Yamaguchi, A., 2008
Y-980134	1998	Yamato Mountains, Antarctica	12.2 g	Kojima, H., Yamaguchi, A., 2008

Although ejecta from the moon and Mars are associated with several known meteorites, the parent bodies for vast majority of all meteorites on Earth are the asteroids. The high water content, D/H ratios, and the evidence of extensive aqueous alteration of the CI1 carbonaceous meteorites indicate their parent bodies were either water-bearing asteroids or comets.

1.1. Chemical, Mineral and Morphological Biomarkers in CI1 Carbonaceous Meteorites. A number of biominerals and organic chemicals (that are interpreted as biomarkers when found in Earth rocks) have been detected in CI1 carbonaceous meteorite. These include weak biomarkers such as carbonate globules,

magnetites, PAH's, racemic amino acids, sugar alcohols, and short chain alkanes, alkenes and aliphatic and aromatic hydrocarbons that are produced in nature by biological processes but can also be formed by catalyzed chemical reactions such as Miller-Urey and Fisher-Tropsch synthesis. However, the CI1 meteorites also contain a host of strong biomarkers for which there are no known abiotic production mechanisms. These include magnetites in unusual configurations (framboids and linear chains of magnetosomes), protein amino acids with significant enantiomeric excess, nucleobases (purines and pyrimidines), and diagenetic breakdown products of photosynthetic pigments such as chlorophyll (pristine, phytane, and porphyrins), complex kerogen-like insoluble organic matter and morphological biomarkers with size, size range and recognizable features diagnostic of known orders of *Cyanobacteriaceae* and other prokaryotic microfossils. **Table II** provides a chronological summary of chemical, mineral and morphological biomarkers found by many independent researchers who have studied carbonaceous meteorites since 1806 when research began shortly after the fall of the Alais CI1 carbonaceous meteorite**.**

TABLE II. Biomarkers in CI1 Carbonaceous Meteorites

METEORITES	WEAK BIOMARKERS	REFERENCE
ALAIS	Carbon, Water, Clay Minerals, Organic Matter ~ humus and lignite with Odor of Bitumen	Thénard (1806); Berzelius (1834)
ALAIS	Sulph-Hydrocarbons	Smith (1876); Roscoe (1864)
ORGUEIL	Organic Matter ~ humus, peat and lignite coal & Clay Minerals,	Daubrée (1864); Cloez, (1864a,b) Pisani, (1864); Bass (1971)
ALAIS, ORGUEIL & IVUNA	Petroleum-like Hydrocarbons, Aliphatic and Aromatic Hydrocarbons and PAH's	Berthelot (1868); Commins & Harrington, (1966); Olson *et al.*(1967); Nooner&Oró (1967)
ORGUEIL	Amino Acids	Nagy, (1961)*;* Kaplan *et al.* (1963), Vallentyne (1965); Nagy & Bitz (1963)
ORGUEIL	Normal alkanes	Gelpi & Oró, (1970)
ORGUEIL	"Organized Elements", Microvessicles	Claus and Nagy (1961, 1962); Claus *et al.* (1963); Pflug (1984)
STRONG BIOMARKERS		REFERENCE
ORGUEIL	Long-Chain Fatty Acids, Isoprenoids, Kerogen	Nagy & Bitz, (1963); Bitz & Nagy, (1966)
ALAIS, ORGUEIL & IVUNA	Porphyrins, Pristane, Phytane and NorPristane	Kaplan (1963) Hodgson & Baker, (1964); (1969); Oró *et al.* (1966), Nooner & Oró, (1967); Kissin, (2003)
ORGUEIL & IVUNA	Protein Amino Acids with Enantiomeric Excess	Oró *et al.*,(1971); Engel *et al..* (1980, 2003) Cronin *et al..* (1997); Ehrenfreund *et al.,* (2001)
ALAIS , IVUNA & ORGUEIL	Nitrogen Heterocycles and Nucleobases - Purines and Pyrimidines	Hayatsu, *et al* .1964, 1968 ; Folsomme *et al.* 1973; Hua *et al.*,1986; Stoks & Schwartz**,**1981; Glavin & Bada, (2004); Martins *et al.,*(2008)
ALAIS , IVUNA & ORGUEIL	Filamentous Microfossils ~ Trichomic Prokaryotes and Cyanobacteria	Hoover (1997); Zhmur *et al.* (1997); Hoover *et al.* (1998, 2003a,b; 2004; 2005a,b; 2006a,b; 2007, 2008, 2009; 2008); 2009);

1.2. The Alais CI1 Carbonaceous Meteorite. Alais was the first carbonaceous meteorite known to science. Two thunderous detonations were heard across southern France at 5:30 P.M on March 15, 1806. Two soft, black stones that emitted a "strong odor of bitumen" were then observed to fall in small villages near Alais, Languedoc-Roussillon, France – (44° 07'N, 4° 05'E). One black stone of 2 kg mass landed in the small village of St. Eteinne de Lolm and a 4 kg stone landed near Valence, France and broke a branch from a fig tree as it fell. Louis Jacques Thénard (1806), the reknowned Professor of Chemistry at the College de France in Paris, conducted the first study of the Alais CI1 carbonaceous meteorite. He realized that these stones were different from all other meteorites since they had the appearance of solidified clay. Thénard reported that *"when the*

3

stones were placed in water they disintegrated immediately and gave off a strong clay-like odor." He found the Alais meteorite stones contained 2.5% carbon and oxides of iron, magnesium, and nickel.

The Alais stone was subsequently analyzed by Jöns Jacob Berzelius, the distinguished Swedish organic chemist and mineralogist. Berzelius discovered the elements silicon, selenium, thorium and cerium. He obtained a small fragment of the Alais meteorite from the French mineralogist Lucas. Berzelius (1834, 1836) was initially astonished to find this stone contained water and almost discarded it as being contaminated. In the English translation provided by Nagy, (1975, p. 45) he says: *"I was so suspicious, because this meteorite contained water that I was about ready to throw my sample away. However, fortunately before I discarded the sample, I reread the record and found certain data which completely agreed with the meteoritic origin of the stone. This intrigued me so that I then carried on the investigation with great interest. The question arose in my mind; does this carbonaceous earth contain humus or a trace of other organic substances? Could this give a hint to the presence of organic formations on other planets?"* Berzelius was the first scientist to recognize that the Alais meteorite consisted mostly of clay-type minerals and he confirmed Thénard's observation that the Alais stones were destroyed by liquid water: "*These stones are different from all other meteorites because they look like solidified clay and because when they are placed in water they disintegrate and give off a clay-like odor."* Berzelius concluded that the Alais meteorite contained a portion of metallic iron and nickel (12%) that was attracted to a magnet as well as indigenous extraterrestrial water and carbon, saying: *"some organic matter and 10 per cent of a salt which contained no iron, being a mixture of sulphates of nickel, magnesia, soda, potash and lime with a trace of sulphate of amnonia."* When he heated the sample it turned brown and *"gave off a tarry odor."* Berzelius reported "*in water it disintegrates instantaneously to a greyish-green powder which has an odor reminding one of fresh hay."* He also found it to contain carbon dioxide and a soluble salt containing ammonia.

1.3. The Orgueil CI1 Carbonaceous Meteorite. The Orgueil meteorite is one of the most extensively documented and thoroughly investigated of all known meteorites. At 8:08 P.M. on May 14, 1864 a brilliant fireball illuminated a large region of southern France and thunderous explosions were heard as the blue-white fireball streaked across the sky, turned a dull red color and produced a long thin white smoke trail (Jollois, 1864; d'Esparbés, 1864). The weather was nice on this spring evening in the south of France. Soon after the explosions were heard, a shower of stones fell within an 18 km east-west scatter ellipse between the villages of Orgueil, Campsas and Nohic (Tarn-et-Garonne). The main fall occurred near the village of Orgueil (43° 53' N; 01° 23' E) and villagers collected over 20 jet-black stones immediately after the fall. Many of the Orgueil stones had complete fusion crusts and a few were quite large (one with mass ~11 kg).

The Orgueil bolide was so spectacular that many villagers at St. Clar thought they were surrounded by flames. The Marquise de Puylaroque (1864) reported that her house looked like *"the interior of a furnace"* and she heard a rumbling noise that sounded like firearms and lasted for 2-3 minutes. The detonations were so violent that some villagers thought the event was an earthquake (Bergé, 1864). Eyewitness reports from all over the region were sent to M. Le Verrier, Director of the Imperial Observatory, and to the eminent geologist Academician G. A. Daubrée. These accounts were published immediately (Daubrée, 1864) and English translations have subsequently been made available (Nagy, 1975). The observations of the fireball and timing of the detonations made it possible to set the upper limit for the altitude at which the bolide exploded at 30 km and to conclude that the main part of the meteoritic mass continued to move in its orbit after the explosion leaving "only a few minor pieces of its pre-terrestrial body" (Daubrée and Le Verrier 1864).

M. Leymerie (1864) examined a 211g stone that fell in Campsas and reported that the interior of the Orgueil stones exhibited a "stunning difference" as compared with ordinary stony meteorites: *"The broken surface reveals a dark charcoal colored substance so soft that it can be easily cut with a knife. One can even write with the fragments on a piece of paper. The knife cut creates smooth and shiny surfaces which is an indication of*

fine, paste-like matter. Fragments placed in water disintegrate immediatel.y" This astonishing observation that the Orgueil stones immediately disintegrated into minute particulates when they came in contact with cold water was independently confirmed by Cloëz (1864a) and Pisani (1864) exhibiting a behavior similar to that of the Alais meteorite.

Cloëz (1864a) correctly recognized that the Orgueil meteorite was a breccia composed of microscopic particles cemented together by magnesium sulfate and other water soluble salts. When these salts dissolve in water, the tiny particulates that constitute the Orgueil meteorite are released from the matrix. He found that the Orgueil stones also disintegrate in alcohol, but that the dispersed particles released were not as finely divided and that the disintegration in alcohol takes place more slowly than in water. These very important observations were recently confirmed at the NASA Astrobiology Laboratory using video optical microscopy and Environmental Scanning Electron Microscopy (ESEM) methods. Small samples of Orgueil meteorite stones were placed on a sterile silicon wafer and exposed to a droplet of sterile de-ionized water at 20 ^{o}C. Immediate profuse effervescence was observed and within a few minutes the samples were completely disaggregated into an assemblage of micron-sized particulates. Immediately after the water had evaporated a white residue was found on the silicon wafer substrate around the meteorite mineral grains and particulates. Energy Dispersive X-Ray Spectroscopy (EDS) analyses established that the residue was composed primarily of magnesium, sulfur, and oxygen, which is consistent with magnesium sulfate (Hoover, 2005a; Hoover, 2006a).

The Orgueil silicate minerals are more properly designated as serpentine rather than peridotite. The dominant mineral (62.6 %) of the Orgueil meteorite is Chlorite $[(Fe, Mg, Al)_6(Si, Al)_4O_{10}(OH)_8]$ of the clay phyllosilicates mineral group. The other major minerals of Orgueil include: 6.7% Epsomite $(MgSO_4·7H_2O)$; 6% Magnetite (Fe_3O_4); 4.6% Troilite (FeS), 2.9% gypsum $(CaSO_4· nH_2O)$ and 2.8% Breunnerite $(Fe,Mg)CO_3$. Epsomite forms white veins in the meteorite and is a significant evaporite mineral that helps cement together the meteorite particulates into the stones.

In 1868, Pierre Marcellin Berthelot The famous French chemist who had shown in 1860 that all organic compounds contain C, H, O, and N experimented with hydrogenation to explore the organic chemistry of the Orgueil CI1 meteorite. He found complex hydrocarbons in Orgueil that were analogous to carbonaceous substance of organic origin on Earth (Berthelot, 1868).

It is now well established that the total organic content of carbonaceous meteorites consists of 90-95% polymer-type organic matter that is insoluble in common solvents. Nagy (1975) reported that this substance is *"structurally not unlike coal or the aromatic-type kerogen that is the insoluble organic matter encountered in terrestrial sedimentary rocks."* The complex polymer-like organic matter similar to kerogen in the carbonaceous meteorites is clearly indigenous and constitutes an important biomarker. In terrestrial rocks, Kerogen, isoprenoids, pristine, phytane and other biochemical fossils have long been considered valid biomarkers. Kaplan (1963) reported that the Ivuna CI1 meteorite contained significantly larger quantities of pristane and phytane (diagenetic breakdown components of chlorophyll) than the Orgueil and Alais meteorites. These types of geochemical biomarkers comprise a standard tool for petroleum exploration as they are stable of geologically significant time periods (~ billions of years). On Earth they are undeniably biological in origin. Diagenesis and catagenesis processes that alter the original biochemicals is usually minimal and the basic carbon skeleton remains intact. For this reason, although functional groups (e.g., -OH, =O, etc.) may be lost, the chemical structure derived from biological origins of these stable fossil biomolecules remains recognizable.

1.4. The Ivuna CI1 Carbonaceous Meteorite

The Ivuna CI1 carbonaceous meteorite fell near Ivuna, Mbeya, Tanzania (8° 25'S, 32° 26'E) in southeast Africa at 5:30 P.M on December 16, 1938. Approximately 705 gms were recovered shortly after the stones were

observed to fall. Clayton (1963) investigated carbon isotope abundances in the carbonates of both the Ivuna and Orgueil meteorites and found the Ivuna carbon isotopic values to be virtually identical to those of Orgueil. The $\delta^{13}C$ value for these meteorites was approximately +60 per mil, which is dramatically different from the abiotic or biotic terrestrial carbon. This provides conclusive evidence that the meteoritic carbon is extraterrestrial in origin and cannot be associated with terrestrial bio-contaminants. The Alais, Ivuna and Orgueil CI1 meteorites have also been found to contain chiral amino acids, nucleobases, pristine and phytane, spectacular magnetite framboids and platelets, and the well-preserved and mineralized remains of diverse filaments interpreted as the mineralized remains of cyanobacteria and other trichomic prokaryotes. Amino acid analyses using HPLC of pristine interior pieces of the Orgueil and Ivuna meteorites resulted in the detection of β-alanine, glycine, and γ-amino-*n*-butyric acid (GABA) at concentrations ranging from ≈600 to 2,000 parts per billion (ppb). Other α-amino acids such as alanine, α-ABA, α-aminoisobutyric acid (AIB), and isovaline are present in trace amounts (<200 ppb). Carbon isotopic measurements of β-alanine and glycine and the presence of racemic (D/L ≈ 1) alanine and β-ABA have established that these amino acids are extraterrestrial in origin. The amino acid composition of the CI1 meteorites is strikingly distinct from that of the Murchison and Murray CM2 carbonaceous meteorites. This indicates that the CI1 meteorites came from a different parent body than CM2 meteorites, possibly from an extinct comet.

Claus and Nagy (1961) studied the Ivuna and the Orgueil CI1 meteorites and found a large number of forms that they originally interpreted as indigenous microfossils. After intense criticism, they subsequently designated them as "organized elements" so as to not make any judgement as to their biogenicity. Since they used standard palynological methods to dissolve the rock matrix in acids for extracting the insoluble kerogen-like bodies, any unseen pollen contaminants on the exterior surfaces of the meteorite would remain intact and be concentrated in the acid-resistant residue they analyzed. They failed to recognize a pollen grain and erroneously included an image of it in their original paper. This resulted in their work being discredited and it is still widely believed that all of the the "organized elements" they described were either abiotic mineral grains or pollen. Subsequent work by Rossignol-Strick and Barghoorn (1971) revealed that the "organized elements" type microstructures were in fact not pollen grains and were indigenous to the meteorites, but their forms are too simple to make any decision regarding whether they are abiotic or biogenic in origin.

1.5. The Tonk and Revelstoke CI1 Carbonaceous Meteorites.

Although the mineralogy and petrology of the Tonk and Revelstoke CI1 meteorites have been carried out, no data has yet been published on the organic chemistry, amino acids and other possible chemical or morphological biomarkers that may be present on these meteorites has ever been published. This is undoubtedly due to the fact that only a tiny amount of the Tonk (7.7 g) and Revelstoke (1 g) meteorites was recovered. After the Tonk meteorite fell, it spent two years at an unknown location in India (Christie, 1913). The Revelstoke meteorite fell on a frozen lake in Canada. It remained on the ice for almost two weeks before the stone was recovered (Folinsbee *et al.,* 1967). Both the Tonk and Revelstoke meteorites have been found to contain hydrated magnesium and calcium sulfates (Christie, 1913; Endress *et al.,* 1994). Larson *et al.* (1974) performed thermomagnetic analysis of all five CI1 meteorites known at the time and found that the predominant phase of magnetite in the Revelstoke meteorite was essentially Nickel-free Fe_3O_4. This was in contrast to the other four CI1 meteorites known at the time, which all contained magnetite with nickel at <6%. Based on their studies of saturation moments, the weight percentage of magnetite for the CI1 meteorites was reported to be: Alais (5.3 ± 0.4%); Orgueil, (11.9 ± 0.8%); Ivuna, (12.2 ± 0.9%); Tonk, (9.4 ± 0.6%) and Revelstoke, (7.2 ± 0.5%).

000254

2. MATERIALS AND METHODS

Samples used in this study were:

Ivuna CI1 Carbonaceous Meteorite
DuPont Meteorite Collection, Planetary Studies Foundation, Chicago
1 stone: (0.1 gm). *Courtesy: Dr. Paul Sipiera*

Orgueil CI1 Carbonaceous Meteorite
Musée Nationale d'Histoire Naturelle, Paris
1 stone S219: (0.5 gm) *Courtesy: Dr. Claude Perron*
2 stones: (0.6 gm & 0.3 gm) *Courtesy: Dr. Martine Rossignol-Strick*

DuPont Meteorite Collection, Planetary Studies Foundation, Chicago
2 stones: (0.4 gm & 0.1 gm). *Courtesy: Dr. Paul Sipiera*

EDS elemental analysis of the Orgueil filaments indicated that many of them were carbonized sheaths that infilled with magnesium sulfate minerals. To evaluate the morphology, chemical composition and size and size range of abiotic mineral structures that might have similar compositions, samples of native fibrous epsomite were obtained and studied using the Hitachi FESEM and the FEI Quanta ESEM and FESEM.

The abiotic mineral samples investigated were:

Native Fibrous Epsomites

$$MgSO_4 \bullet 7H_2O$$

Hot Lake, Oroville, Washington - Fibrous Epsomite Evaporites (6 Stones- 2 kg).
Courtesy: Brent Cunderla, USDI-Bureau of Land Management, Washington

Zaragoza, Spain - Fibrous Epsomite - 1 stone: (21.5 gm)
Courtesy: Keck Museum, Reno, Nevada

Cryptohalite
$$(NH_4)_2[SiF_6]$$

Schoeller Mine, Kladno, Central Bohemia Region, Czech Republic -
1 stone with many Cryptohalite crystals (68.5 gm)
Courtesy: Mineralogical Research Co., San Jose, California

Several other terrestrial rocks have been investigated in collaboration with Academician Alexei Rozanov and Marina Astafieva of the Paleontological Institute of the Russian Academy of Sciences, Many of these were found to contain the permineralized and fossilized remains of acritarchs, bacteria, cyanobacteria and biofilms. These included samples of phosphorites from Khubsugul, Mongolia; Bauxites from Russia and Arkansas; Oil Shales, Shungites and Kukersites from Russia

000255

and Siberia; Ongeluk Lavas and carbon leader from Gold Mines of South Africa; and chimney stones from the Rainbow Deep Sea Hydrothermal Vent and Upper Archaean (Lopian) rocks from Northern Karelia.

Modern Cyanobacteria

Plectonema (Lyngbya) wollei–**Lake Guntersville, Al**
Richard B. Hoover - Collected in May, 2004 (Living Environmental Sample)
Lyngbya (Leptolyngbya) subtilis **– Lake Michigan,**
Courtesy: Ann St. Amand, Phycotech, Inc. (Fixed Environmental Sample)
Oscillatoria lud –**UTex Collection LB 1953**
F. T. Haxo - Deposited October, 1972 in UTex Collection as C-43 (Living Axenic Culture)
Arthrospira platensis **– Carolina Biological Supply** *(Living Axenic Culture)*
Calothrix sp.–**Little White River, Oregon,**
Courtesy: Ann St. Amand, Phycotech, Inc. (Fixed Environmental Sample)

Living Microbial Extremophiles

Carnobacterium pleistocenium **str. FTR-1**[T]; Fox Tunnel, Alaska
Richard B. Hoover-Coll. May, 2000 - Pleistocene ice (Living Axenic Culture; Type Strain)

Dried Herbarium Material

Bangia quadripunctata, Lyngbye–Collected 5/20/1816 Hoffman Bang, Hals Peninsula
Courtesy: Dr. Walter van den Bergh, Henri van Heurck Museum, Antwerp, (Dried Type)

Fossilized Cyanobacteria

Upper Archaean (Lopian) tufa-genic rocks (2.8 Ga) of Northern Karelia
Courtesy: Dr. Alexei Yu. Rozanov, Paleontological Institute, RAS, Moscow

Hair and Tissues of Egyptian Mummies (2 Kya & 5 Kya) and Mammoths (32 Kya & 40 Kya)
Lyuba Mammoth Tissue & Stomach Milk Samples Courtesy: Dr. Daniel Fisher, Univ. Michigan

Cambrian Trilobites

Perinopsis interstricta & Perinopsis pygidia – Cambrian **(505 Mya) Wheeler Shale, Utah**
Coll. Richard B. Hoover

Instruments used in this study were:

ElectroScan Environmental Scanning Electron Microscope (ESEM)
- Secondary Electron Detector (SED); Water vapor (10 Torr vacuum) 90-100,000X
- Noran EDS (Z> Boron)

Hitachi S-4100 Field Emission SEM (FESEM)
- Cold cathode field emission electron gun; 20 - 300,000X;
- Secondary Electron Detector (SED) and Backscattered Electron Detector (BSED);
- KEVEX EDS - Lithium Drifted Silicon detector (Z>Boron)

Hitachi S-3700N Variable Pressure Scanning Electron Microscope
- Tungsten emitter electron gun; 5 - 300,000X; SED & BSED;
- 4 Pi EDS - Silicon Drifted Silicon Detector (Z>Boron)

FEI Quanta 600 (FESEM and ESEM)
- Simultaneous SED and BSED images; 5 - 300,000X
- 4 Pi EDS - Lithium Drifted Silicon detector (Z>Boron)

In order to minimize the possibility of the detection of coating artifacts or recent contamination by terrestrial biological materials, the study was confined to investigations of uncoated, freshly fractured, interior surfaces of the meteorites. All tools, sample holders and stubs were flame sterilized. Lunar dust samples and silicon wafers were used as negative controls. The further protect the samples from biological contamination, the meteorites were stored in sealed vials at -80 ^{o}C and after preparation, electron microscopy stubs were kept in sealed containers in dessicator cabinets or in the freezer. The fusion crust and old cracks in the stones were carefully avoided. The meteorite samples were placed in the instrument chamber (with the fresh fracture surface up) a pumped down immediately after the stones were fractured. All solvents, acids or other liquids were strictly avoided. Acids and solvents were used in early studies by other workers h to extract "acid resistant microfossils" from the host rock. However, this method sometimes resulted in the inadvertent contamination of the sample with acid resistant modern pollen grains that could have been on the external surface or in old fissures within the stones. It should be noted that only one seriously Murchison sample was found to be contaminated with fungal filaments (in old cracks in the fusion crust) and not a single pollen grain has been encountered during extensive studies of carbonaceous meteorites carried out since 1996 at the NASA/Marshall Space Flight Center. While fingerprints, pollen grains, fungi, bacteria, laboratory oils and other contaminants could be encountered on the fusion crust or exposed old cracks and fractured surfaces of meteorites, the hypothesis that the interior surfaces carbonaceous meteorites are seriously contaminated by modern bacteria, fungi, or pollen is simply not consistent with the observational results. For this reason, it is extremely important that studies of biomarkers such as amino acids, nucleobases, complex organic chemicals and microfossils should be rigorously restricted to freshly fractured interior portions of the stones. .

## 3. OBSERVATIONAL RESULTS AND INTERPRETATIONS

Field Emission Scanning Electron Microscopy (FESEM) studies of the interior surfaces of freshly fractured CI1 carbonaceous meteorites carried out at NASA/MSFC resulted in the detection of a diverse suite of large and complex filamentous microstructures embedded in the matrix of carbonaceous meteorites. Energy dispersive x-ray analysis of these structures reveals that these filaments are permineralized with minerals rich in magnesium and sulfur. Most of the filaments are encases within a carbon-rich external envelope. Images and EDS elemental data for several selected filaments are presented. To increase readability, the interpretation for each set of images is presented immediately after the Observational Results section for each Figure.

3.1. Images and EDS Spectra of Filaments in the Ivuna CI1 Carbonaceous Meteorite. Figure 1 provides images and Energy Dispersive X-Ray Spectroscopy elemental data for filaments found embedded in the Ivuna CI1 carbonaceous meteorite. **Fig. 1.a** is a FESEM image of a thin uniseriate filament that is flattened at the terminal end. The filament is cylindrical in the lower portion embedded in the meteorite rock matrix. This small, undulatory filament (diameter 0.7 to 1.0 m) is rich in C, Mg, and S and depleted in N. The filament is only partially encased within a broken and very thin carbonaceous sheath. EDS elemental data is shown for **spot 1** on the thin sheath **(Fig. 1.b)** and for **spot 3** on the nearby mineral matrix **(Fig. 1.c)**. The sheath has higher carbon content and biogenic elements N and P are below the 0.5% detection limit of the instrument. **Fig. 1.d** is a FESEM image of 5 m diameter X 25 m long spiral filament Ivuna with white globules that are sulfur-rich as compared with the rest of the filament and the meteorite matrix. A tuft of fine fibrils is visible at the left terminus of the filament and the terminus at the lower right is rounded. **Fig. 1.e** is a FESEM Backscattered Electron image of an Ivuna filament with sulfur-rich globules S and rounded terminus R that is similar in size and morphology to the giant bacterium "*Titanospirillum velox*".
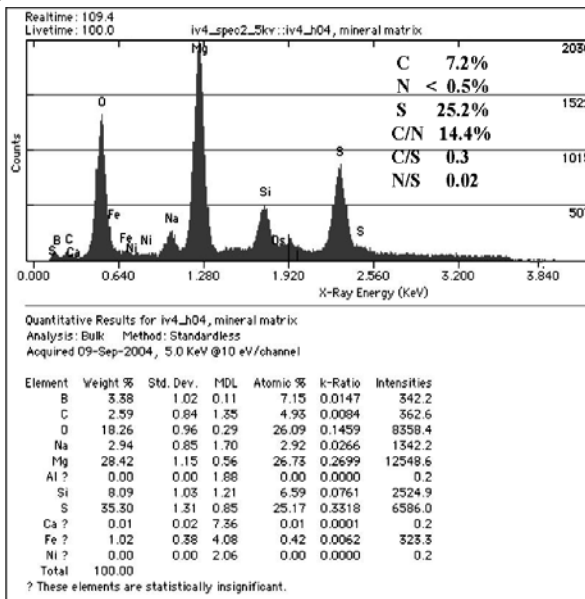
000257

a.

b.

c.

d.   **e.**
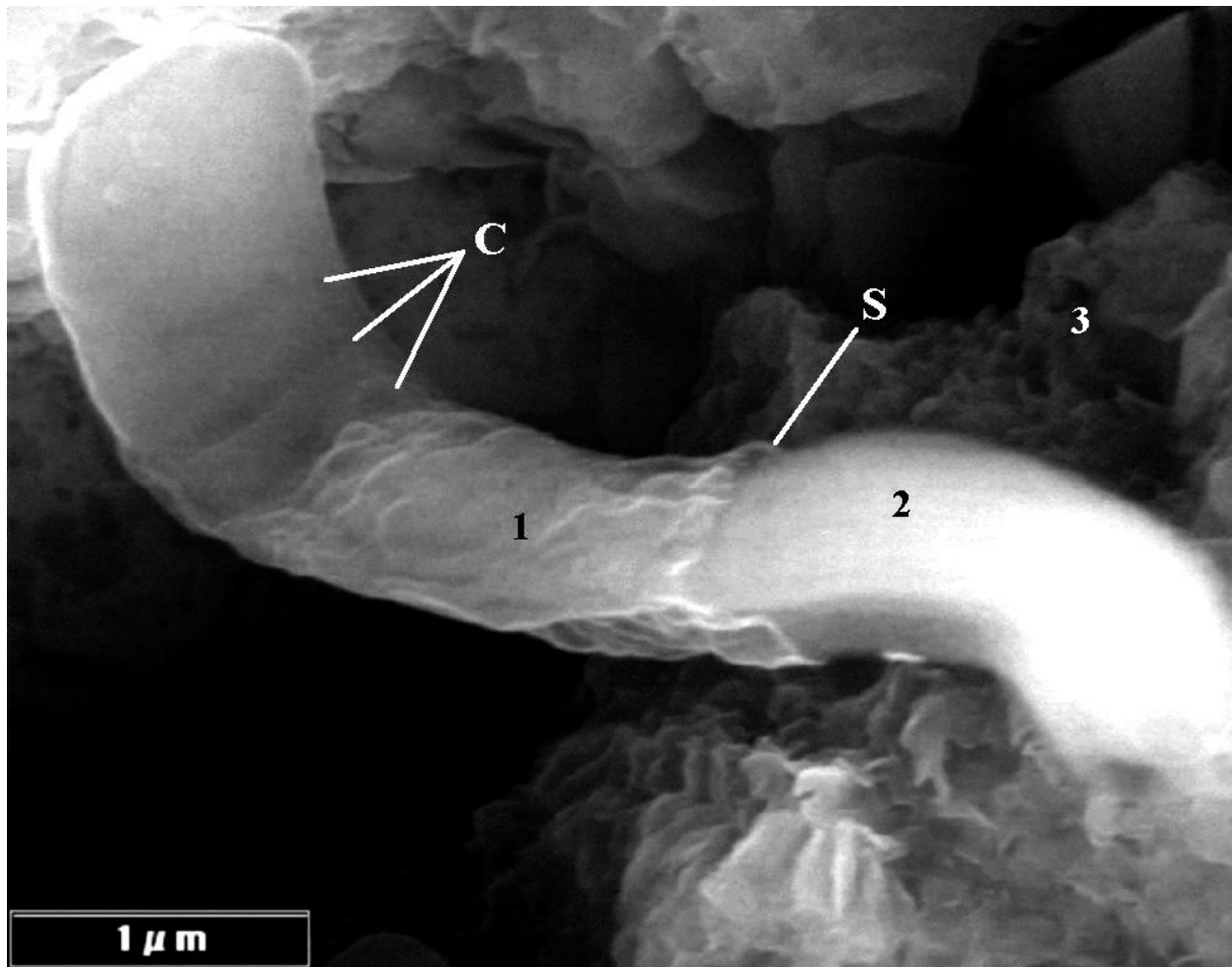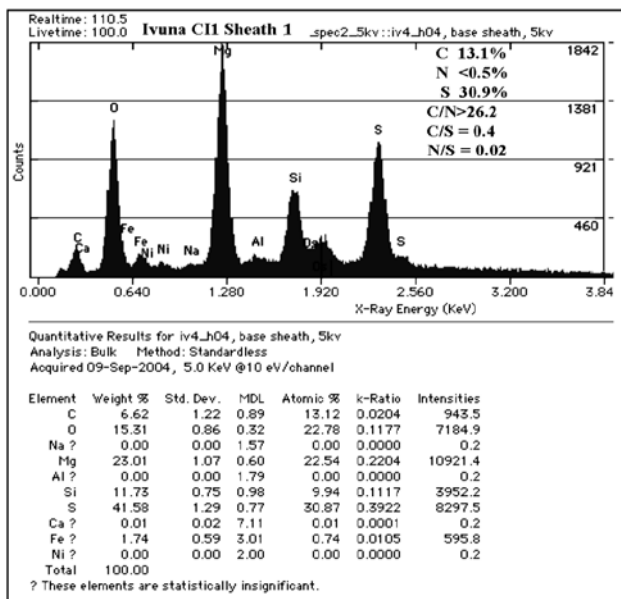
Fig. 1.a. Ivuna CI1 meteorite filament (0.8 μm diameter) with dark lines **C,** partially encased in thin carbon-rich sheath. **b**. EDS elemental data of the filament sheath at spot 1 shows typical biogenic elements Nitrogen and Phosphorus (<0.5%) and Carbon (13.1%) enriched as compared with nearby meteorite matrix (C 7.2%) at spot 3; **d.** FESEM Backscattered Electron image of an Ivuna filament with N<0.5% and sulfur-rich globules S and rounded terminus R that is similar in size, morphology and internal composition to **(e.)** giant bacterium *Titanospirillum velox"* with sulfur **(S)** globules collected from *Microcoleus* mat of Ebro Delta, Spain. (Scale bar = 5 μm)   Ivuna Meteorite Courtesy: Dupont Meteorite Collection, Planetary Studies Foundation; Image 1.e Courtesy: Dr. Riccardo Guerrero

3.1.1. Interpretation of Images and EDS Data of Ivuna Filaments. The flattened embedded filament shown in **Fig. 1.a** is interpreted as the permineralized remains of a partially uniseriate, undulatory, ensheathed trichomic prokaryote. The measured diameter (0.7 - 1.0 μm) as determined from the scale bar of this calibrated FESEM image and the detailed morphology of this Ivuna filament is consistent with some of the smaller filamentous cyanobacteria. The dark lines **C** near the terminus of the sheath are consistent with cross-wall constrictions that are often seen as faint transverse lines in FESEM images obtained with living cyanobacteria. In this image it is possible to see an extremely thin sheath **S** that is broken and covers only the upper portion of the trichome, which appears to have been completely replaced by infilling minerals. The size and morphology of this filament is consistent with filaments of the undulatory trichomic filamentous cyanobacteria *Spirulina subtilissima* (filaments 0.6 - 0.9 μm diameter) and *S. laxissima* (filaments 0.7 to 0.8 μm diameter). These cyanobacteria have not been reported as possessing a sheath, but the sheath seen in this FESEM image is extremely thin and would be very difficult to discern in by visible light microscopy techniques. There are also very small species of the genus *Limnothrix* that are undulatory on nature and possess facultative sheaths. However, it shoud be pointed out that there also exist groups of ensheathed filamentous anoxygenic phototrophic bacteria (photosynthetic flexibacteria) possess a thin sheath and are capable of gliding motility. There include filamentous representatives of the bacterial Phylum Chloroflexi. The thermophilic species *Chloroflexus aurantiacus* has a thin sheath and trichomes as narrow as 0.8 μm. There also other bacterial photoautotrophs that oxidize hydrogen sulfide and deposit it externally as sulfur (e.g., *Oscillochloris trichoides)* and these trichomic filaments have diameters in the 0.8 to 1.4 μm range.

The length, diameter and spiral configuration and apparent tuft of small filaments at one pole and rounded end at the other along with the internal sulfur globules distributed along the axis of filament **(Fig. 1.d)** found embedded in a freshly fractured surface of the Ivuna meteorite a complex suite of features.that are very similar to those observed in SEM images of the novel bipolar lophotrichous gram-negative bacterium *"Titanospirillum velox"* **(Fig. 1.e)** which was described by Guerrero *et al* (1999). *"Titanospirillum velox"* is a very large mat-forming bacterium with 3–5 μm diameter X 20–30 μm long filaments. It was collected from a

11

mud sample beneath a *Microcoleus chthonoplastes* mat in the Ebro Delta in Tarragona, Spain. "*T. velox*" swims very rapidly (10 body lengths/sec) with spiral motility, propelled by the lophotrichous tuft of flagella at the cell terminus. The intracellular elemental sulfur storage globules are seen as white spots in this Scanning Electron Microscope image. This extremophile was grown only in mixed culture with other bacteria, which would explain the fact that this genus and species has not yet been accepted as validly published. The Bacteriological Code rules of nomenclature requires that prokaryotic microorganisms must be isolated and grown in *pure culture* and the designated type stain must be deposited in two international culture collections in two different countries before the genus and species names can be validated (Tindall *et al.,* 2006). The absence of detectable nitrogen content the Ivuna filaments provides evidence that these embedded filaments are indigenous and cannot be dismissed as a modern biological contaminant.

3.2 Images and EDS Spectra of Filaments in the Orgueil CI1 Carbonaceous Meteorite. Figure 2.a. is a low magnification (1000X) Secondary Electron Detector (SED) FESEM image of freshly fractured fragment of the Orgueil CI1 meteorite that is densely populated with several different types of embedded filaments and electron transparent sheaths. Even though the field of view shown of this image is very small (~120 µm wide) a wide variety of diverse filamentous microstructures are present. To facilitate the description, the filaments and sheaths have been numbered, and all numbers are located on the filament at the site where the EDS elemental spot data were recorded. A 2D X-ray elemental map of this region of the Orgueil meteorite is shown in **Figure 2.b.** The large image in the upper left corner is a Backscatter Electron Detector (BSED) image. The bright spots in this image are high Z elements where clusters and crystallites of magnetite, iron and nickel are concentrated. Other images reveal where relative concentrations Oxygen, Silicon, Magnesium, Sulfur, Iron, Nitrogen; Calcium, and Aluminum are located. The major filaments and sheaths are clearly seen as bright features in the Carbon, Oxygen, Magnesium and Sulfur maps and they appear as dark features in Silicon, Iron, and Nickel due to the relatively higher content of these elements in the underlying Orgueil meteorite rock matrix. In general, the filament and sheath structures are not discernible in the Nitrogen, Phosphorus and Sodium maps, although Filament **1** can be seen in the Nitrogen map. Empty sheath **7** is wrinkled and electron transparent with a relatively high (47%) content of Carbon. This sheath is unusual in that it is one of the few filaments found in the Orgueil meteorite to have detectable levels of Nitrogen (1%) and Phosphorus (0.8%).

3.1.1 Interpretation and Discussion of Images and EDS Data of the Orgueil Filaments. Filaments **1** and **2** of **Fig. 1.a** are observed to have sheaths with longitudinal striations that run the length of the filaments. This is characteristic of multiseriate trichomic prokaryotic filaments in which multiple parallel oriented trichomes are enclosed within a common homogeneous sheath. These filaments are observed to be either attached to or physically embedded in the Orgueil meteorite matrix. The end of filament **1** becomes slightly wider (~10 µm) where it joins the rock matrix and it appears to contain four internal trichomes, each with a diameter ~2.5 µm. Filament **2** is considerable larger (~ 20 µm dia.) and the longitudinal striations suggest it contains ~5 trichomes, each with diameters ~4 µm/trichome. Faint transverse lines orthogonal to the long axis of filament **2** are marked **C.**
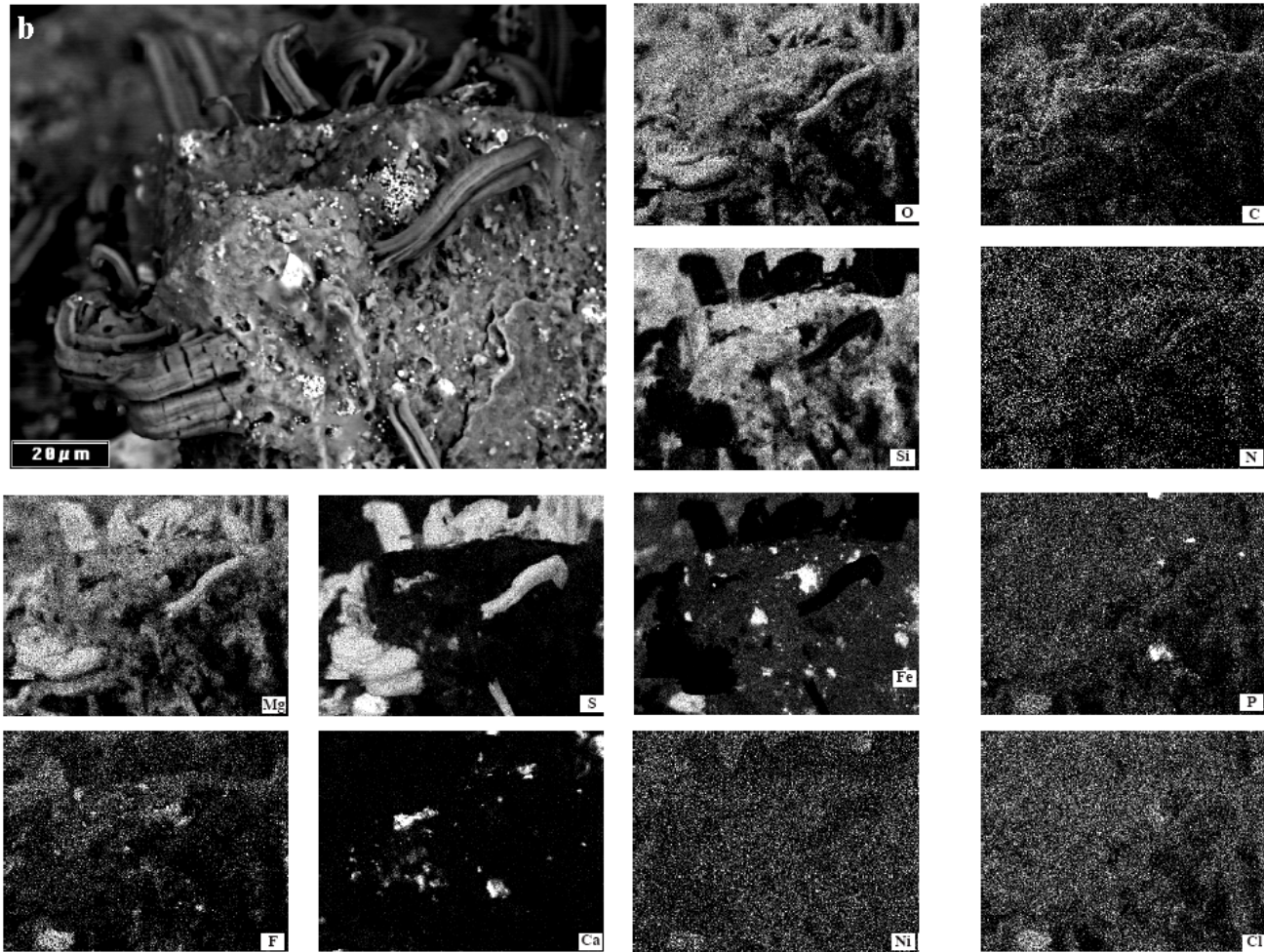
000260
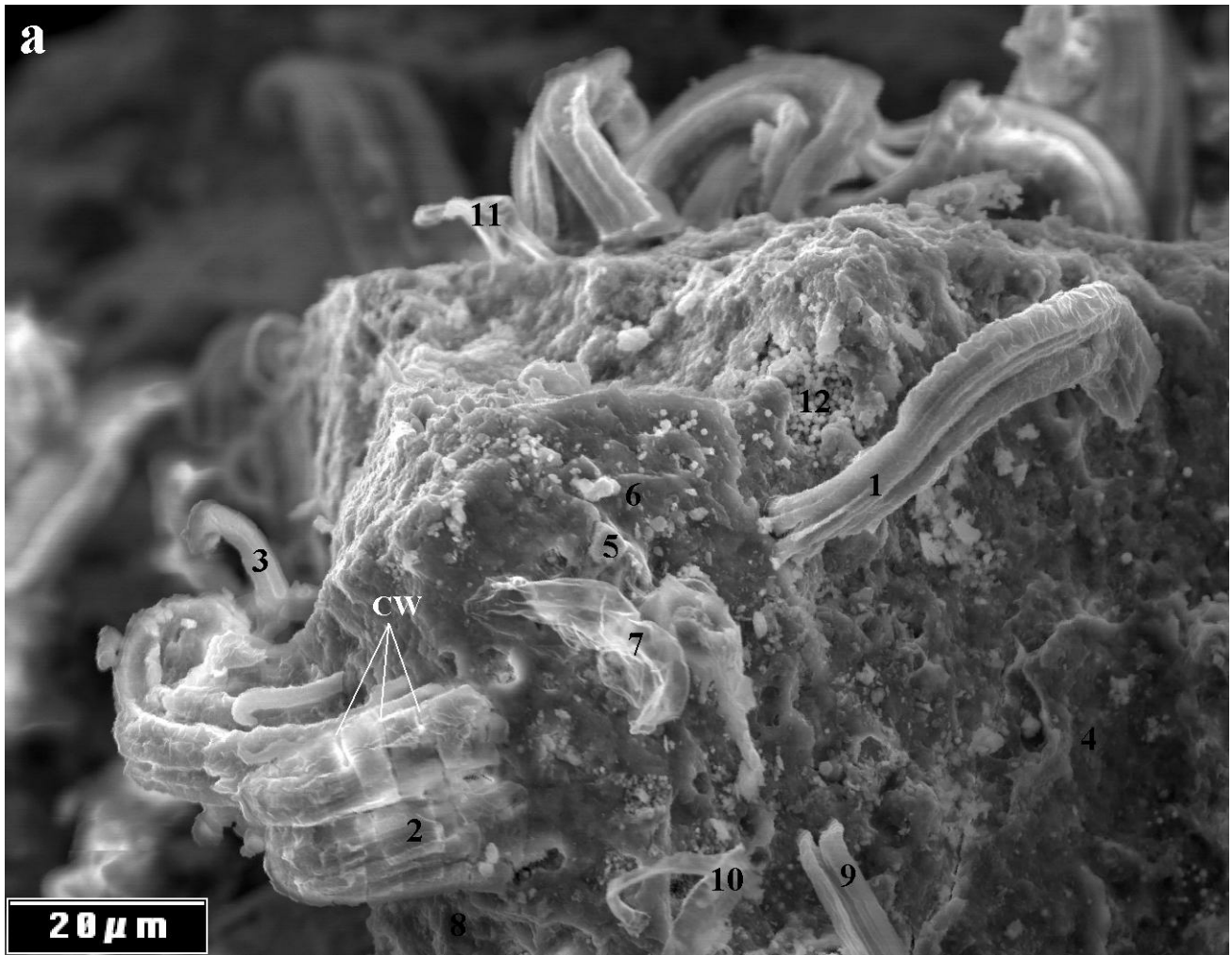
Figure 2.a. Hitachi FESEM Secondary Electron Detector image at 1000 X of multiple filaments and sheaths embedded in Orgueil meteorite matrix and **b.** Backscatter Electron Detector image along with 2-D x-ray maps showing distribution of elements O, C, Si, N, Mg, S, Fe, P, F, Ca, Ni and Cl in filaments for comparison with SED and BSED images.
Orgueil Sample Courtesy: Dr. Paul Sipiera, DuPont Meteorite Collection, Planetary Studies Foundation, Chicago

The longitudinal striations of the long filament **1** and the shorter, curved filament **2** are interpreted as indicating these are multiseriate filaments consisting of a bundle of multiple parallel trichomes encased within a common sheath. If the transverse striations **C** of filament **2** are interpreted as represent cross-wall constrictions, this would indicate that the internal cells within each trichome are ~ 4 μm in length and hence isodiametric. Consequently, the image of filament **2** is interpreted as composed of trichomes made up of spherical or cylindrical isodiametric cells of 4 μm diameter. This interpretation is consistent with morphotypes of undifferentiated filamentous cyanobacteria of the Order Oscilliatoriacea. There are many genera and species within this very common cyanobacterial order, including the genus *Microcoleus* Desmazières ex Gomont (*Form Genus VIII. Microcoleus* Desmazières 1823) (Castenholz, Rippka & Herdman, 2001; Boone *et al.,* 2001). Reproduction within this order occurs by trichome fragmentation and the production of undifferentiated short trichome segments (hormogonia) by binary fission of the cells in one plane at right angles to the long axis of the trichomes. The small solitary uniseriate filaments **3** and **4** may be interpreted as representing members of the genus *Trichocoleus* Anagnostidis, which was separated from the genus *Microcoleus* on the basis of cell size and morphology. Filament **4** is a 2 μm diameter hook-shape filament with a narrowed terminus. Several

species of the genus *Trichocoleus* have filaments typically in the 0.5 μm to 2.5 μm diameter range (Wehr and Sheath, 2003, pg. 136). Energy Dispersive X-Ray Spectroscopy (EDS) spot spectral data were obtained on the meteorite rock matrix as well as on all of the numbered filaments and sheaths at positions where the numbers are located in the FESEM image**.**
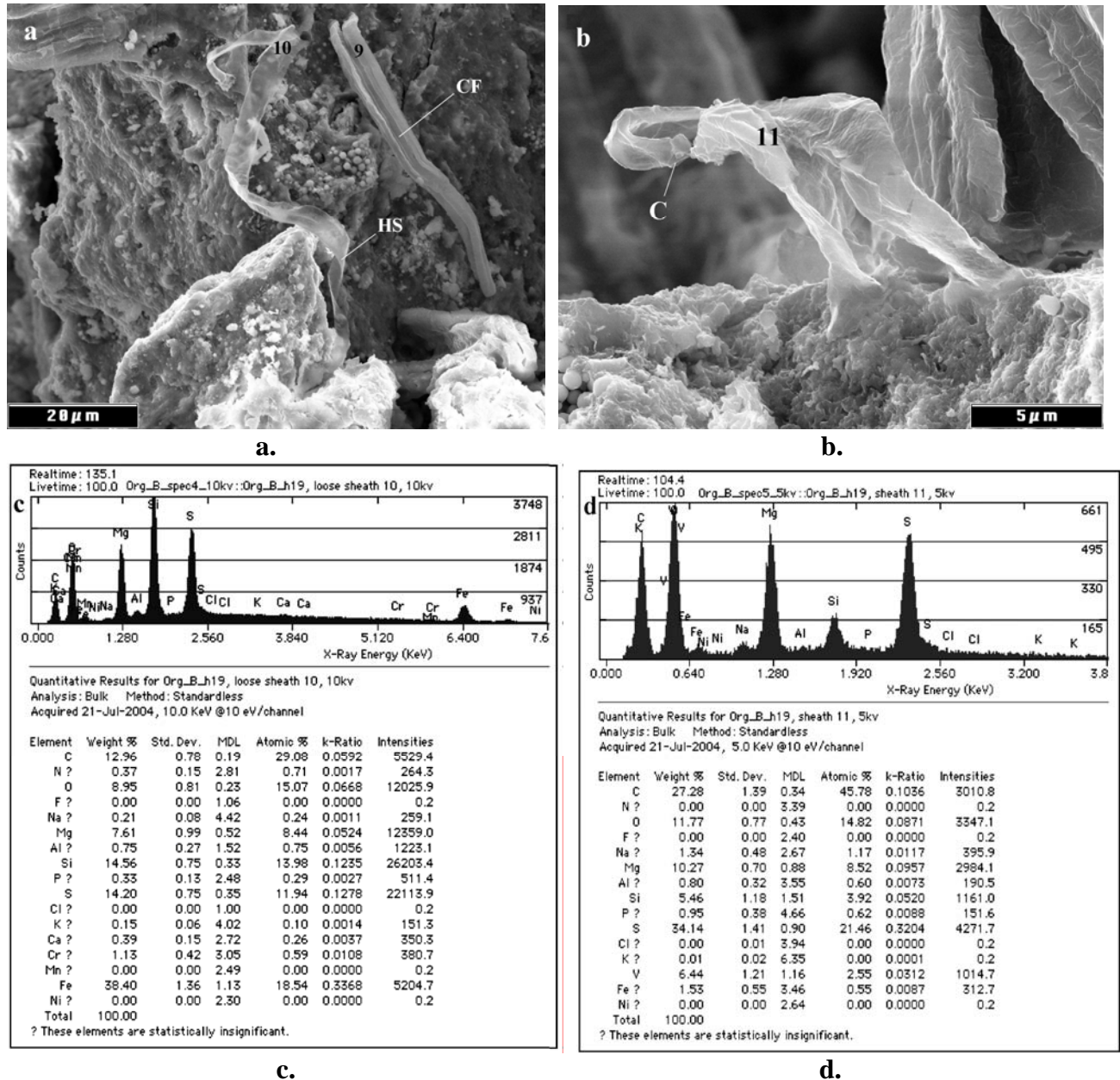

Figure 3. Hitachi FESEM images at 1500X of **a.** collapsed filament **9** and helical coiled empty sheath **10** and **b.** 6000X image of filament **11** showing hook and calyptra or conical apical cell. **c.** EDS spot spectra show elemental compositions **c.** of loose sheath **10 (C 29.1%; N=0.7%)** and **d.** sheath **11 (C 47.8%; N<0.5%).**

Figure 3.a is a1500X FESEM SED images of the collapsed Filament **9** and the hollow, flattened, twisted and folded sheath **10.** Sheath **10** is 4.6 μm in diameter and it is folded at the top where the EDS spectra were taken.

15

The flattened portion of Sheath **10** forms a spiral coil near the base where it is attached to the meteorite matrix. This is very similar to helical coiled sheath of *Phormidium stagninum* shown in the illustration at *http://www.cyanodb.cz//Phormidium/Phormidium.jpg* illustration. This type of flattened, coiled hollow sheath is often seen in other species of filamentous cyanobacteria and hence does not constitute a unique diagnostic feature. **Figure 3.b.** provides a higher magnification (6000X) image of Sheath **11,** which is visible at the top of **Fig. 2.a.** Sheath **11** is a tapered and hooked form with a conical terminal cell or calyptra at the apex. It is 8.5 µm wide where it emerges from the rock matrix and it tapers to 1.5 µm diameter just after the sharp hook. **Figure 3.c.** is a 10 keV EDS spectrum taken at spot **10** in the fold of Sheath **10** and shows detection of low, but measurable level of Nitrogen (0.7%) and Phosphorus (0.3%) and higher levels of Iron (19%) and Silicon (14%), which are probably from the meteorite matrix beneath the this, electron transparent carbon-rich sheath. The EDS spectrum at 5 keV for spot **11** on sheath **11** as shown in **(Fig. 3.d)** reveals this flattened sheath to be highly carbonized (48% C atomic), This small filament appears as a bright feature in the carbon map of **(Fig. 2.b)** and as a dark shadow in the Magnesium and Sulfur maps as it crosses in front of large filaments more heavily mineralized with magnesium sulfate. Filament **11** is also sulfur-rich (21% S), but has Nitrogen below the level of detectability ($< \sim 0.5\%$).

3.2 Orgueil Filaments with Differentiated Heterocysts. Several genera of the cyanobacterial orders *Nostocales* and *Stigonometales* use specialized cells known as "heterocysts" to fix atmospheric nitrogen. Nitrogen fixation is an unambiguously biological process that is absolutely crucial to all life on Earth. Although nitrogen comprises almost 78% of our atmosphere, it is completely useless to life in its relatively inert molecular form. The biological process of nitrogen fixation occurs by the reduction of gaseous nitrogen molecules (N_2) into ammonia, nitrates, or nitrogen dioxide. Many species of several genera of cyanobacteria (e.g., *Anabaena, Nostoc, Calothrix, Rivularia, Scytonema,* etc.) use highly specialized cells for nitrogen fixation by encapsulating the nitrogenase enzyme in thick-walled protective heterocysts.

Cyanobacteria play the key role in nitrogen fixation on Earth and many genera and species of are capable of diazotrophic growth and nitrogen metabolism. Nitrogen fixation occurs via the nitrogenase enzyme with some other proteins involved in this complex biological process. Since the activity of the nitrogenase enzyme is inhibited by oxygen the enzyme must be protected. In many species it is contained within the thick-walled specialized nitrogen-fixing cells called "heterocysts." The heterocysts have very distinctive, thick, hyaline, refractive walls that provide well-protected centers in which the nitrogenase enzyme, which is inactivated by oxygen, can carry out its required activity. Heterocysts of cyanobacteria produce three additional cell walls, including one with glycolipids that form a hydrophobic barrier to oxygen. This is crucial since cyanobacteria are aquatic photoautrophs that evolve oxygen during their photosynthesis. To provide additional protection, the cyanobacterial heterocysts lack photosystem II (Donze *et al.,* 1972). Therefore the heterocysts produce no oxygen and they also up-regulate glycolytic enzymes and produce proteins that scavenge any remaining oxygen. As early as 1949, Fogg recognized that heterocysts are formed from the vegetative cells of the cyanobacteria when the concentration of ammonia or its derivative falls below a critical level and by 1968 it was becoming clear that the heterocysts were the site of nitrogen fixation (Fogg, 1949; Fay *et al.,* 1968; Stewart *et al.,* 1969).

Heterocysts are found in cyanobacteria of the Order *Nostocales* and the Order *Stigonematale*s, but they are never found in any of the genera or species of the other three orders (*Chroococcales, Oscillatoriales,* or *Pleurocapsales*). Furthermore, heterocysts have not been observed in any the known filamentous sulfur bacteria of any other trichomic prokaryotes. Consequently, the detection of heterocysts provides clear and convincing evidence that the filaments are not only unambiguously biological but that they belong to one of these two orders of cyanobacteria rather than trichomic ensheathed sulfur bacteria or any other group of filamentous trichomic prokaryotes. The presence or absence, location and configuration of heterocysts is a critical diagnostic tool for the recognition and classification of cyanobacterial taxa.

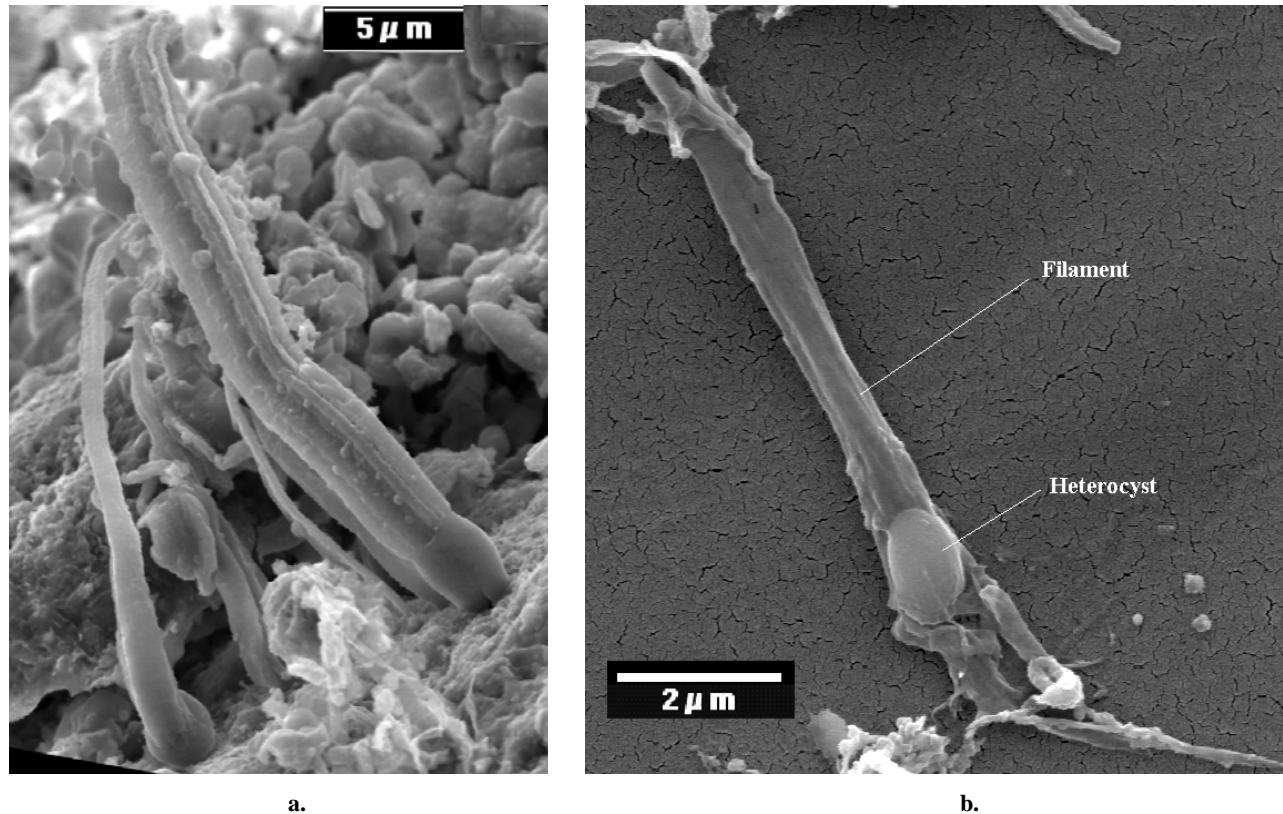**a.**   **b.**

Figure 4.a. FESEM image of permineralized remains in the Orgueil meteorite of polarized tapered filaments (diameter ~ 1 to 2.5 μm) with recognizable heterocysts interpreted as morphotypes of the cyanobacterium *Calothrix spp.* and. **b.** living filament of *Calothrix sp.* with a diameter ~ 0.8 μ and a basal heterocyst from the White River, Washington.

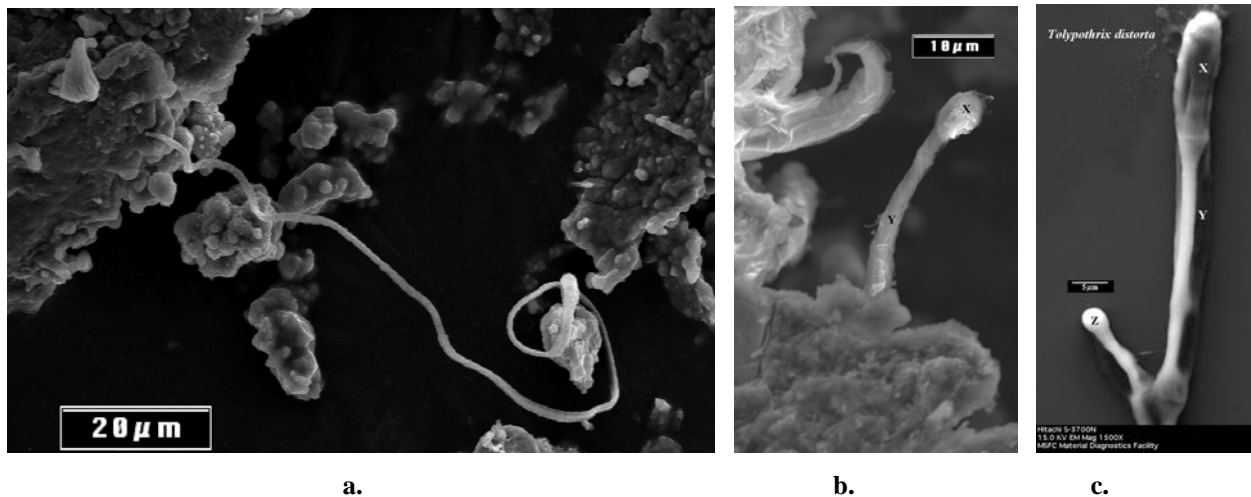**a.**   **b.**   **c.**

Figure 5. Long sinuous, helical coiled and polarized filament with conical apex (<1.3 μm) and terminal heterocyst similar to cyanobacterium *Cylindrospermopsis* sp. in the Orgueil meteorite and **b.** short embedded filament in Orgueil compared with **c.** living *Tolypothrix distorta* grown in pure culture at the NASA/NSSTC Astrobiology Laboratory. *Orgueil Meteorite Sample Courtesy: Dr. Martine Rossignol-Strick, Musée Nationale d'Histoire Naturelle, Paris*

The FESEM image of the mineralized remains of polarized filaments interpreted as morphotypes of the cyanobacterium *Calothrix spp.* found embedded in the Orgueil CI1 carbonaceous meteorite. Several tapering

17

filaments (diameter ~ 1 to 2.5 µm) and recognizable enlarged cells are seen in close proximity to each other with the smooth basal heterocyst attached to the meteorite matrix (Fig. 4.a). AFESEM image of a living *Calothrix sp.* (diameter ~ 0.8 µm and basal heterocyst from White River, Washington is shown in **Fig. 4.b**.

Figure 5.a is a Hitachi S4100 FESEM image of helical coiled polarized filament in Orgueil CI1 carbonaceous meteorite. The filament has a conical apex (<1.3 µm)at left end and a bulbous (2.3 µm diameter) heterocyst is seen at the other terminus. This filament has size and morphological characteristics of morphotypes of cyanobacteria of species of the genus *Cylindrospermopsis.*   **Fig. 5.b**. is an image of a 2.5 µm diameter filament embedded in Orgueil. This filament has a 4.7 µm diameter bulbous terminal heterocyst and is interpreted as a morphotype of cyanobacteria of the genus *Tolypothrix.* **Fig. 5.c** is an image of a morphotype of living Nostocalean cyanobacterium *Tolypothrix distorta* shown for comparison.

Although many modern cyanobacteria are resistant to desiccation, they do not carry out active growth and mat building when they are in a dried state. However, it has been known since 1864 that the Orgueil meteorite is a microregolith breccia, comprised of minute particulates cemented together by water-soluble salts that are readily destroyed by exposure to liquid water. Therefore, it is suggested that none of the Orgueil samples could have ever been submerged in pools of liquid water needed to sustain the growth of large photoautotrophic cyanobacteria and required for the formation of benthic cyanobacterial mats since the meteorite arrived on Earth. Many of the filaments shown in the figures are clearly embedded in the meteorite rock matrix. Consequently, it is concluded that the Orgueil filaments cannot logically be interpreted as representing filamentous cyanobacteria that invaded the meteorite after its arrival. They are therefore interpreted as the indigenous remains of microfossils that were present in the meteorite rock matrix when the meteorite entered the Earth's atmosphere. EDS elemental analyses carried out on the meteorite rock matrix and on living and fossil cyanobacteria and old and ancient biological materials have shown that the Orgueil filaments have elemental compositions that reflect the composition of the Orgueil meteorite matrix but that are very different from living and old microorganisms and biological filaments. Recently dead cyanobacteria and living cyanobacteria and other modern extremophiles are usually damaged by exposure to the focused FESEM electron beam during EDS analysis of small spots. This beam damage behavior was not observed in the Orgueil filaments or in Devonian, Cambrian, or Archaean fossils investigated. The C/N and C/S ratios of the Orgueil filaments are similar to fossilized materials and kerogens but very different from living biological matter, providing further evidence that the Orgueil filaments are not modern biological contaminants.

Figure 6.a is a compilation of the nitrogen level measured by EDS for a number of the filaments encountered in Ivuna and Orgueil CI1 carbonaceous meteorites compared with modern and ancient terrestrial life forms. The meteorite filaments are typically severely depleted in nitrogen (N < 0.5%) whereas life forms on Earth have nitrogen levels from 2% to 15%. Nitrogen is encountered at detectable levels even in the hair/tissue of mummies from Peru (2Kya) and Egypt (5Kya) and the hair and tissues of Pleistocene Mammoths (40-32 Kya). **Fig. 6.b** is a FESEM image the Guard Hair of a 32,000 year old Pleistocene mammoth collected by Hoover in the Kolyma Lowlands of NE Siberia. The square spot in the image is EDS beam damage (10 KeV electron beam) during spot analysis, which revealed a strong peak (11.94% atomic) at the nitrogen Kα line between the Carbon and Oxygen lines. Even though the biological material was 32,000 years old, the nitrogen of the proteins was still present. Similar results have been obtained for cyanobacterial filaments found in the stomach milk of the 40,000 year old baby mammoth "Lyuba" and for pre-dynastic (5,000 year old Egyptian mummies) However, truly ancient biological materials (e.g., Cambrian trilobites of Wheeler Shale of Utah (505 Mya) and 2.7 Gya filamentous cyanobacteria from Karelia) have nitrogen levels below the limit of detection with the FESEM EDS detector. These results provide definitive evidence that the filaments in the CI1 carbonaceous meteorites are indigenous to the stones and are not the result of microbiota that invaded the stones after they arrived on Earth in 1864 or 1938. Hoover (2007) has discussed the use of Nitrogen levels and biogenic element ratios for distinguishing between modern and fossil microorganisms as a mechanism for recognizing recent biological contaminants in terrestrial rocks and meteorites.
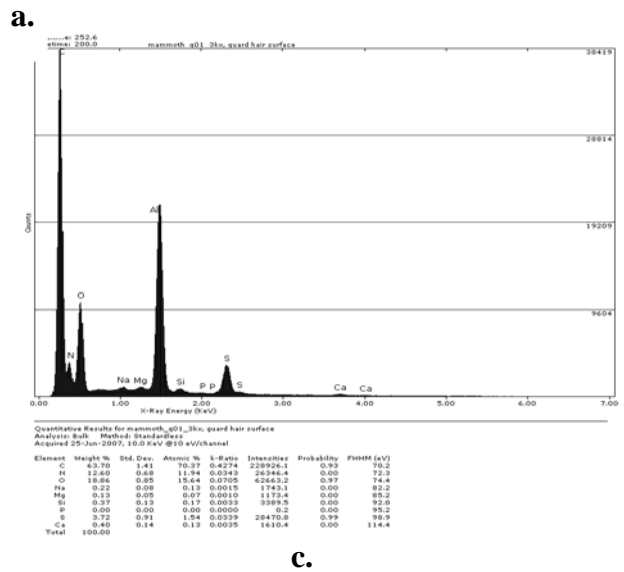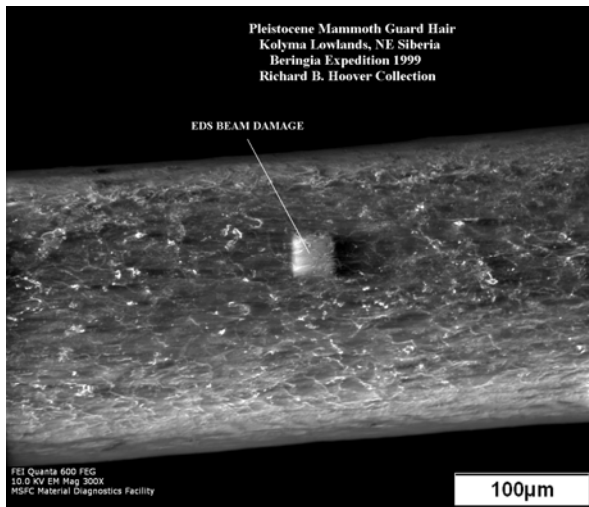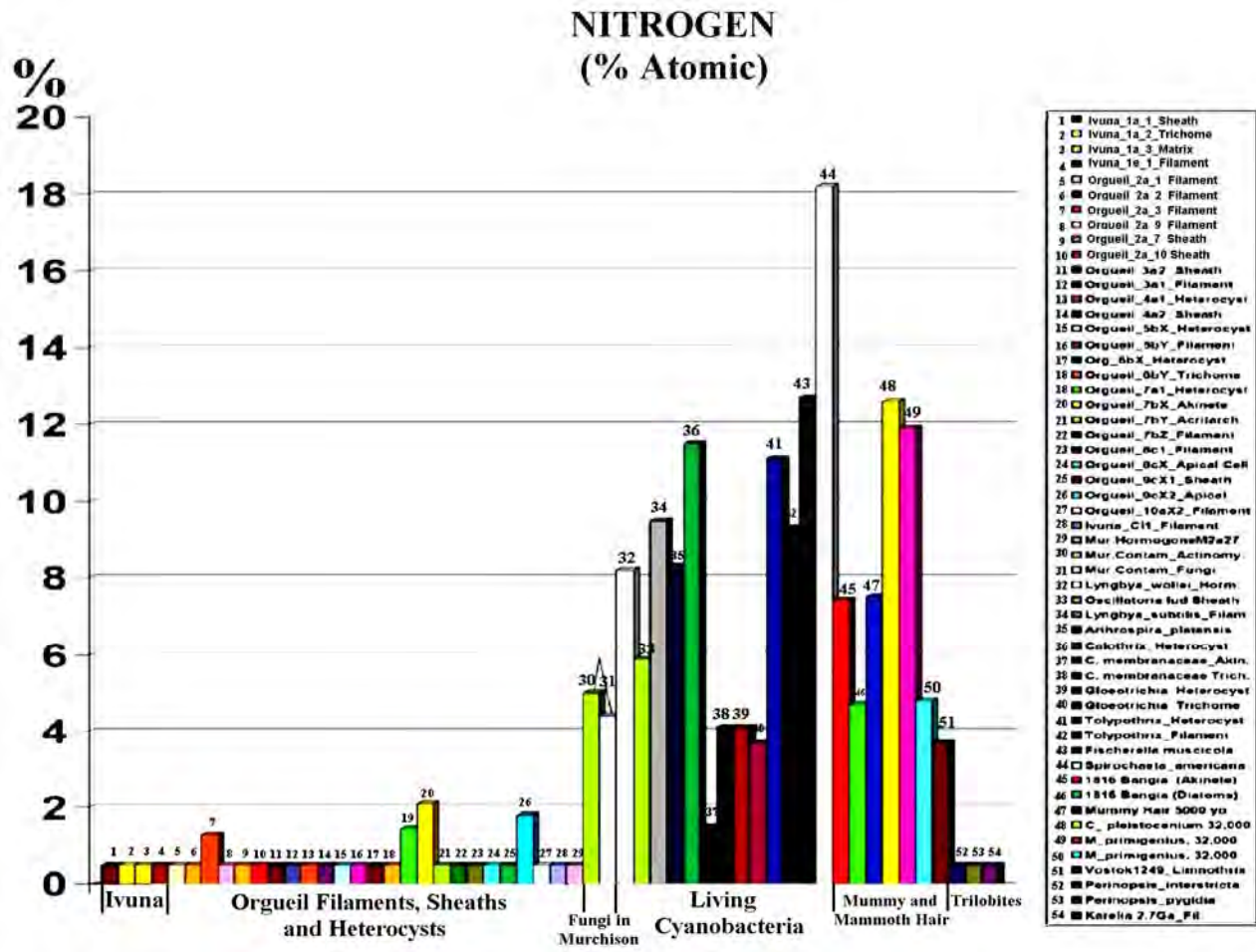
Figure 6.a. EDS data on Nitrogen content of filaments in Ivuna and Orgueil meteorites compared with modern fungal contaminant in Murchison and living, dead and fossil cyanobacteria, mummy/mammoth hair, trilobites & 2.7 Gya cyanobacteria; **b.** Mammoth Hair with beam damage at EDS spot & strong Nitrogen peak (N 11.9% atomic).

4. DISCUSSION

4.1 Classification of Carbonaceous Meteorites. The type meteorites for the different clans of carbonaceous chondrites are CI (Ivuna), CM (Mighei), CO (Ornans), CV (Vigarano), CR (Renazzo) and CK (Karoonda). Wiik (1956) and Van Schmus & Wood (1967) classified carbonaceous chondrites based upon their chemical composition and petrology. In the Wiik classification system, the Group I carbonaceous chondrites have ~7% C, 20% H_2O, and ~22% SiO_2; the Wiik Group 2 (e.g. Murchison, Mighei and Cold Bokkeveld) chondrites, have ~ 4% C, 13% H_2O, and 27.5% SiO_2 and the Group 3 (e.g. Mokoai & Felix) have <1% C. Carbonaceous chondrites are further subdivided into petrologic types (1-7). The petrologic type is an indicator of the degree of chemical equilibrium within the meteorite minerals. In this system, the type 3 chondrites have not been significantly altered by either water or thermal metamorphism. Unequilibrated chondrites from lack of thermal metamorphism are of petrologic types 1-3 and types 4 to 7 are increasingly equilibrated due to extended thermal processes. The petrologic types 2 and 1 are found only in the carbonaceous chondrite clan and they have been subjected to an increasing degree of aqueous alteration. Carbonaceous chondrites of petrologic type 1 have been so extensively altered by water that chondrules are entirely absent, even though they have chondritic composition and must have contained chondrules during their early history before the aqueous alteration occurred. The type 2 chondrites have few somewhat less aqueously altered chondrules. The chondrules of type 3 are numerous, unaltered and very distinct, whereas those of types 4 to 6 again become more indistinct due to thermal metamorphism and re-crystallization. By petrologic type 7 the chondrules are again absent due to thermal destruction.

4.2 Mineralogy, Petrology and Organic Chemistry of CI1 Carbonaceous Meteorites. Cloëz and Pisani conducted the first detailed chemical analysis and study of the mineralogy and the Orgueil meteorite. Pisani (1864) concluded that Orgueil silicate minerals are more properly designated as serpentine rather than peridotite. Cloëz (1864a,b) found the Orgueil meteorite to be comprised of a soft, black, friable material, with 5.92% carbon, humic substances, magnetite, silicic acid, hygroscopic water (5.2-6.9%) and 8-10% indigenous water of hydration that is liberated only at a temperature > 200 ^{o}C. He also reported the detection of a variety of evaporite minerals including magnesium, ammonium, calcium and sodium salts. Microscopic and chemical analysis led Cloëz to conclude that the dominant portion of the carbonaceous material within the Orgueil meteorite was in the form of complex polymeric carbon insoluble in water and similar to humic substances, peat, and coal but unlike living organic matter **(TABLE III).**

TABLE III. Elemental Composition of the Orgueil IOM, Peat, and Lignite Coal

SAMPLE	CARBON	HYDROGEN	OXYGEN	O/C
Orgueil Insoluble Organic Matter	63.45%	5.98%	30.57%	0.48
Peat from Long (Somme Valley)	60.06%	6.21%	33.73%	0.51
Lignite Coal from Ringkuhl	66.50%	5.33%	28.17%	0.42
Black Matter - Les Landes Sand	60.40%	5.65%	33.65%	0.56
Living Bacteria	6.4%	63%	26%	(~2-10)

Since these early studies a great deal of research has been dedicated to a detailed study of the mineralogy, petrology, and organic chemistry of the CI1 carbonaceous meteorites. This work has been summarized in detail by (Tomeoka and Buseck, 1988; Nagy, 1975; Kissin, 2003; Sephton, 2005). It is now established that the CI1 carbonaceous meteorites contain ~65 wt% fine scale phyllosilicate aggregates and intergrowths of serpentine and smectite/saponite, 10% magnetite, sulfides such as aqueously altered iron-nickel sulfides 7% pyrrhotite ($[Fe,Ni]_{1-x}S$), and 5% ferrihydrite ($5Fe_2O_3 \cdot 9H_2O$) and troilite (FeS) as well as 5% recomposed carbonates like Breunnerite $(Mg,Fe)CO_3$ and a small fraction (<1%) of olivine and pyroxene crystallites

20

(Endre and Bischoff, 1996, Bland *et al.,* 2004). The Orgueil meteorite also contains 4.56 Gy magnetites (as individual crystals, framboids, stacks of platelets) and presolar diamonds, silicon carbide and graphite (Huss and Lewis, 1994). Magnetite and pyrite framboids and platelets are present in the CI1 (Alais, Ivuna, and Orgueil) and C2 Ungrouped (Tagish Lake) carbonaceous meteorites that have been investigated in this research. Spectacular platelets and magnetite framboids with extremely well preserved uniform crystallites are common in the Tagish Lake meteorite. Studies carried out at the Paleontological Institute in Moscow by Academician Alexei Yu. Rozanov has revealed that framboids are present in the upper Permian black shales of the Berents Sea shelf which are similar in similar size distribution and characteristics as those found in the Alais and other carbonaceous meteorites. Independent studies confirmed the very early findings that the CI1 carbonaceous meteorites contained a complex insoluble organic matter very similar to kerogen as is typically encountered in coal. Boström and Frederickson (1966) described the Orgueil meteorite as a *"bituminous clay with a breccia structure and clastic texture."* They concluded there were three main stages of mineral formation on the meteorite parent body –

1. Early hot stage with minerals like troilite that are stable a several hundred degrees centigrade.
2. Middle stage with minerals like chlorite and limonite forming below 170 $^{\circ}$C
3. Late stage with carbonates and sulphates forming below 50 $^{\circ}$C.

Guo *et al.* (2007) used carbonate clumped isotope thermometry to determine the conditions of aqueous alteration sequence (of calcite to dolomite to bruennerite) as the carbonaceous meteorite parent bodies were cooling. They concluded the Orgueil dolomite formed at 26 $^{\circ}$C and the bruennerite formed at -6 $^{\circ}$C. The Orgueil and Ivuna CI1 meteorites appear to have experienced an extended period of aqueous alteration by acidic hydrothermal fluids that completely destroyed the pentlandite ($[Fe,Ni]_9S_8$) which is present in the Alais and Tonk meteorites, which probably experienced a shorter period of alteration (Bullock *et al.,* 2003, 2005). The dissolved nickel was eventually re-combined with sodium to form sodium nickel sulfate (Ni-bloedite) or iron to form ferrihydrite. These diverse mineral grains and particulates contained within the CI1 carbonaceous are typically cemented together by epsomite and other water soluble salts.

4.3 Heating of CI1 Carbonaceous Meteorites during Atmospheric Transit. Immediately after the fall of the Orgueil CI1 carbonaceous meteorite, the villagers collected more than 20 jet-black stones. Many of these stones had complete fusion crusts and a few were quite large (one with mass ~11 kg). Leymeri (1864a) related that one of the stones "fell into a farmer's attic, and this man burned his hand when he touched it." He also described using a knife to cut one of the Orgueil stones soon after the fall: *"The knife cut creates smooth and shiny surfaces which is an indication of a fine, paste-like matter"* (Leymeri, 1864b). These observations indicate that the interior of the Orgueil stones had the consistency of wet clay-like just after the fall. Even though a thin fusion crust was formed on the exterior of the stones by intense heating during the transit through the atmosphere, it is clear that the interior of the stones never became hot. (Some of the Orgueil stones (as well as those of the Murchison CM2 meteorite that landed in Australia in 1969) were found a few hours after the fall with a thin coating of frost on the outer surface. This finding indicates that the inner portions of the stones were below zero after transit though the atmosphere. The interior portions of these stones were apparently protected by ablative cooling during atmospheric transit in a manner analogous to that experienced during the re-entry of an Apollo Command Module. This is important with regard to the possible transport of bacteria remaining viable during atmospheric entry.

4.4 Amino Acids and Chiral Biomarkers Modern Bacteria and Carbonaceous Meteorites. A suite of 20 life-critical amino acids are present in the proteins of all life forms known on Earth. The protein amino acids exhibit homochirality in that they are exclusively the *L*-enantiomer. **Table IV** shows the protein *L*-amino acids in the exopolysaccharide (EPS) slime sheath of the cyanobacterium *Microcystis aeruginosa* K-3A; living cells of the bacteria *E. Coli* and *Salmonella* sp. and ancient terrestrial biology (e.g., a Fly in amber and teeth of a Cretaceous Duck-Billed Hadrosaur) for comparison with extraterrestrial amino acids detected in the Murchison, Murray, Orgueil and Ivuna meteorites (Ehrenfreund *et al.*, Engel *et al.* and Cronin and Pizarello).

21

000269

The amino acids of **Table IV** shown in *italics* or marked with "–" or "*n.d.*" were either not detected or present at only trace levels in the fossils in terrestrial rocks and carbonaceous meteorites. Even though there is no doubt that the amber encased fly and the Hadrosaur teeth are biological in origin, it is seen that these fossils are also missing several of the same amino acids that absent in the carbonaceous meteorites. Only 8 of the 20 life-critical protein amino acids are detectable in water/acid extracts of carbonaceous meteorites. The fact that several of the amino acids missing in meteorites and ancient terrestrial fossils are abundant in living bacteria provides strong evidence that the meteorites are not contaminated by modern biological materials. If modern bio-contaminants were present, all 20 protein amino acids should be detected.

TABLE IV: Amino Acids in Living Bacteria Terrestrial Fossils and Carbonaceous Meteorites

Protein Amino Acids	Living Bacteria				Fossils		Carbonaceous Meteorites				
	Microcystis	*E. coli*	*Salm. pull*	*Salm. senf*	*Fly/ Amber*	*Hadrosaur*	Murch. CM2	Murch. CM2	Murray CM2	Orgueil CI1	Ivuna CI1
	Wt %	Mol/ ALA	Mol/ ALA	Mol/ ALA	Mol/ GLY	Mol/ GLY	Nmol /g	ppb	ppb	ppb	Ppb
L-Alanine ALA	10.3	1.00	1.00	1.00	0.37	0.53	15.3	956	647	69	157
D-Alanine ALA	-	-	-	-			-	720	617	69	82
Arginine ARG	4.4	0.51	0.48	0.52	-	-	-	-	-	-	-
L-Aspartic Acid ASP	12.0	1.01	1.00	1.00	0.23	0.77	8.5	342	65	54	146
D-Aspartic Acid ASP	-	-	-	-			-	100	51	28	30
L-Glutamic acid GLU	12.3	1.14	1.11	1.14	0.57	0.67	18.2	801	261	61	372
D-Glutamic Acid GLU	-	-	-	-			-	537	135	15	8
Glycine GLY	8.7	0.93	1.02	0.96	1.00	1.00	45.8	2919	2110	707	617
Histidine HIS	1.0	0.18	0.21	0.19	-	-	-	-	-	-	-
Isoleucine ILEU	5.0	0.55	0.51	0.55	-	-	-	-	-	-	-
Leucine LEU	8.2	0.83	0.78	0.78	-	-	1.9	-	-	-	-
Lysine LYS	4.4	0.56	0.59	0.56	-	-	-	-	-	-	-
Methionine MET	1.9	0.31	0.37	0.23	-	-	-	-	-	-	-
Phenalyalanine PHE	3.8	0.34	0.33	0.33	-	-	-	-	-	-	-
Proline PRO	4.9	0.25	0.26	0.28	-	-	13.5	-	-	-	-
Serine SER	6.6	0.41	0.48	0.43	0.56	0.91	4.7	-	-	-	-
Threonine THR	6.6	0.48	0.50	0.48	-	0.41	-	-	-	-	-
Tryptophan TRY	-	0.05	0.05	0.04	-	-	-	-	-	-	-
Tyrosine TYR	3.4	0.12	0.15	0.08	-	-	-	-	-	-	-
Valine VAL	6.5	0.73	0.66	0.75	-	0.24	8.6	-	-	-	-
Non-Protein Amino Acids											
a-Aminoisobutyric AIB	-	-	-	-				2,901	1,968	39	46
D,L-Isovaline IVA	-	-	-	-							

22

The data of **Table IV** indicates that the most abundant (by weight%) amino acids in the cyanobacterium *Microcystis* sp. are GLU, ASP, ALA, GLY and LEU (all above 8%) followed closely by THR, SER, VAL, ILEU and PRO (all above ~5%). However, GLY is by far the most abundant protein amino acid in the Murchison (CM2), Murray (CM2), Orgueil (CI1) and Ivuna (CI1) carbonaceous meteorites and it is followed by ALA, GLU and ASP. However, in these carbonaceous meteorites, the protein amino acids LEU, THR, SER, VAL, ILEU and PRO, *which are abundant in all life on Earth, are either totally absent or detected only at trace levels.* As has been pointed out by Engel and Macko (2005) these missing protein amino acids provide clear and convincing evidence that the interior portions of the CI1 and CM2 carbonaceous meteorites are not contaminated by modern cyanobacteria, pollen, fingerprints or other microbial contaminants. Isovaline (IVA), α-aminoisobutyric acid (AIB) and γ -Aminobutyric Acid (GABA) are the most abundant non-protein amino acids in carbonaceous meteorites. While they are not protein amino acids it is wrong to conclude that they are not biological in nature. The amino acids IVA and AIB are formed on Earth by the diagenetic alteration of ancient biological materials and γ -Aminobutyric Acid is synthesized by organisms on Earth. However, most protein amino acids are absent in meteorites and terrestrial fossils and only 8 of the 20 life-critical protein amino acids have been found in carbonaceous meteorites using the most sensitive modern methodologies available.

4.5 Comets as Parent Bodies of CI1 Carbonaceous Meteorites. The CI1 carbonaceous meteorites are jet-black stones that contain indigenous extraterrestrial water. The albedo of the Orgueil meteorite is extremely low (~0.05) and comparable to that of the very dark C-type asteroids and the nuclei of comets. This is blacker than asphalt which has an albedo of ~ 0.07. The European Space Agency Halley Multicolor Camera aboard the Giotto Spacecraft obtained images at the closest approach (00:03:01.84 UT on March 14, 1986) at a distance of 596 km from the centre of the nucleus revealing detailed topographic features on the black (albedo 0.04) surface and jets Lamarre *et al.* (1986) reported that IKS-Vega data indicated the temperature of nucleus of comet Halley was 420 K +/- 60K at 0.8 A.U which was consistent with *"a thin layer of porous black material covering the comet nucleus."* The Deep Space 1 spacecraft found the 8 km long nucleus of Comet 19P/Borrelly to be very hot (~345 K) with prominent jets aligned with the orientation of the rotation axis of the nucleus and albedo of 0.01 to 0.03 (Soderbloom *et al.* 2002). Ices of water, carbon dioxide, methane and other volatiles in the cold nucleus in proximity to the hot crust would melt and then boil to produce high pressure beneath the crust if gas is released faster than it can escape through the porous crust. In regions where the pressure exceeds the strength of the crust, localized failure of portions of the crust could result in explosive release of the gas giving rise to the observed flaring of comets and the dramatic jets.

Once a comet enters the inner solar system, it becomes hot from solar radiation on the black nucleus and loses mass rapidly. The European Space Agency Infrared Space Observatory (ISO) showed that water was the primary volatile (75-80 %) of the 40-50 km diameter nucleus of Comet Hale-Bopp. Minor volatile fractions detected (CH_4, NH_3 and H_2CO) could have come from clathrates (H_2O ice with simple gasses like CO_2 and NH_3 in a stable lattice structure) or result from atmospheric chemistry. ISO found that Hale-Bopp released water vapor, carbon monoxide and carbon dioxide at a rate of 2×10^9 kg/sec and detected olivine in the dust. Olivine is commonly encountered in meteorites. As comets lose ices they develop an inert outer crust from the less volatile material. The nuclei of comets are extremely complex – they exhibit rugged terrain, smooth rolling plains, deep fractures and are composed of very dark material. This black crust becomes very hot while the comet is in the inner regions of the Solar System.

Figure 7.a. is a NASA Deep Space 1 spacecraft composite false color image showing geyser-like jets erupting from the long prolate nucleus (8 km) of comet 19P/Borrelly on Sept. 22, 2001. (The colors indicate three orders of magnitude in light level (red is 1/10, blue 1/100 and purple 1/1000 the intensity of the comet nucleus). The red bumps on the nucleus are real and show where the main jet resolves into three distinct

23

narrow jets coming from distinct sources on the comet nucleus. These narrow jets are entirely consistent with the hypothesis that internal pressures generated by steam produced by melting of internal ices which then boil into gases as they are vaporized as heat conducts through hot crust. The NASA Deep Impact probe obtained the valuable data about the nature of comets as it approached and when the impactor collided with the nucleus of comet 9/P Temple 1 on July 4, 2005. **Fig. 7.b** is a Deep Impact image of the nucleus of comet Temple 1. The regions shown in blue are where exposed deposits of water ice that were detected on the surface of the comet nucleus Sunshine *et al.* (2005). These water ice regions ere observed to be ~30% brighter than the surrounding areas and probably were exposed when portions of the black crust was blown off into space by the explosive eruptions such as were recorded in a video by the spacecraft. The Deep Impact measurements of the temperature profile of comet P/Temple 1 nucleus at 1.5 AU is shown in **Figure 7.c.** Even as far away from the Sun as Mars the jet-black comet nucleus reaches temperatures as high as 330 K (57 $^{\circ}$C). Furthermore, the lowest temperatures measured on the crust were ~ 280 K (7 $^{\circ}$C) which is slightly above the temperature at which water ice changes from solid to liquid phase. Prior to the impact, the ambient outgassing of Temple 1 was ~6x10^{27} molecules/s of water. However, the free sublimation of ice calculated above (~200 K) was only ~4.5 x 10^{21} molecules/m^2/s indicating that the ambient outgassing had significant subsurface sources. The Deep Impact spacecraft also observed numerous events of flaring of the nucleus and eruption of geyser-like jets as the comet was approached and before the collision of the impactor. On November 4, 2010, the NASA EPOXI extended mission of the Deep Impact Spacecraft passed within 435 miles of the 2.2 km long nucleus of comet Hartley 2 and revealed bright jets of carbon dioxide gas and dust.

These observations of comets are consistent with the hypothesis that the comet crust impedes the flow of gasses such that pressures develop as ices melt and vaporize in pockets and cavities beneath the crust. This provides the pressures needed to allow water to transition from the solid to the liquid state and then into the gaseous state. This would create micro-niches with pools of liquid water trapped within pockets in rock and ice, very much analogous to the cryoconite and ice bubble ecosystems contained psychrophilic microbial extremophiles such as those described from the glaciers and frozen Pleistocene thermokarst ponds of Alaska and Siberia and the glaciers and perennially ice covered lakes of the Schirmacher Oasis and Lake Untersee in East Antarctica (Hoover, 2008; Hoover and Pikuta, 2010; Pikuta *et al.* 2005). If gas is produced faster than it can escape through the porous crust, it could high pressures resulting in localized failure of weaker portions of the crust and the violent eruption into space of carbon dioxide, water vapor and chunks of crust and particles of ice and dust propelled into space and directed into the dust tail of the comet. These dust particulates could give rise to meteor showers as the comet passes through the tail. From time to time, larger chunks of the ejected may survive passage through the Earth's atmosphere and this could be the link between comets and the CI1 (and possibly the CM2) carbonaceous meteorites. The fact that the CI1 meteorites contain minerals that were extensively altered by liquid water on the parent body and that the stones have been found to contain a large amount of indigenous extraterrestrial water clearly establishes that their parent bodies were most likely comets or water-bearing asteroids. It is now well known that the black nuclei of comets get very hot (significantly above >273 K where water ice melts) as they approach the Sun.
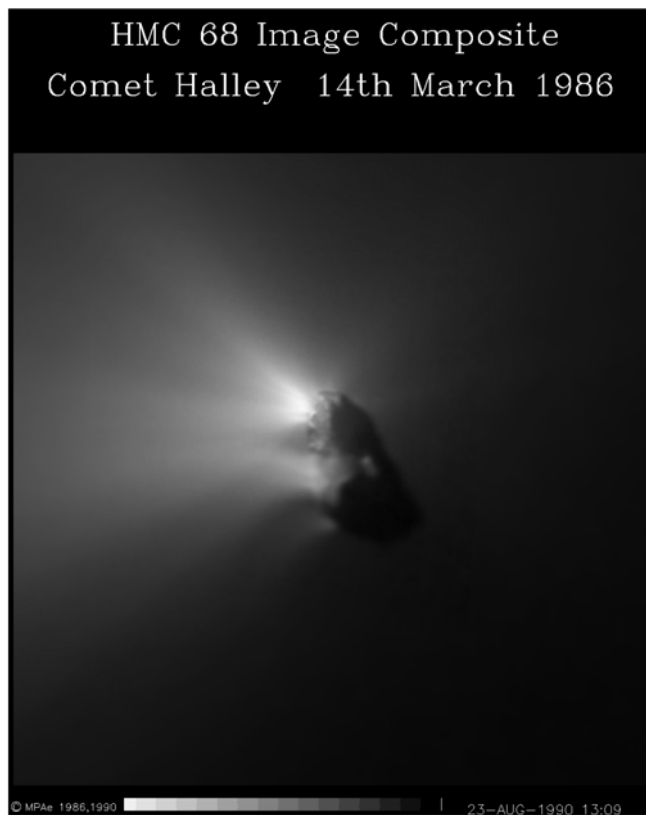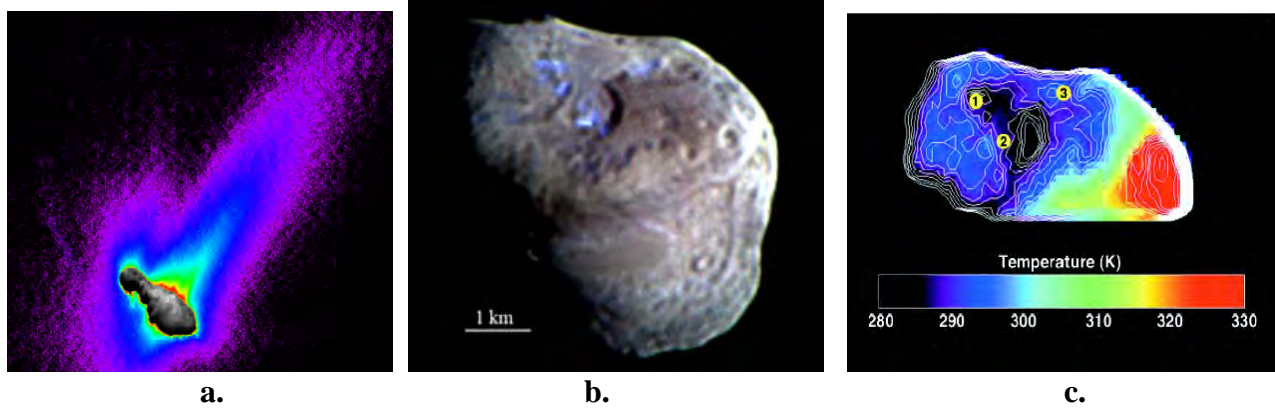
000272

a.   b.   c.

d.   e.

Figure 7.a. Deep Space 1 image of Comet P/Borrelly with jets of gas and dust; **b.** Deep Impact image of nucleus of Comet 9P/Temple 1 shows regions of exposed water ice and **c.** temperature map from Deep Impact IR spectra **d.** Giotto Halley Multicolor Camera (HMC) image showing jets emanating from of the 0.04 albedo nucleus of Comet P/Halley Image Courtesy: Max Plank Institute for Solar System Research http://www.mps.mpg.de/en/projekte/giotto/hmc/; **e.** Deep Impact spacecraft extended mission (EPOXI) image of the nucleus of comet Hartley 2 showing jets of dust and gas. Image Courtesy: NASA/JPL UMD).

Gounelle et al. (2006) used the eyewitness accounts to compute the atmospheric trajectory and orbit of the Orgueil meteoroid and concluded that the orbital plane was close to the ecliptic and that entry into the atmosphere took place at a height of approximately 70 km and an angle of ~20°. Their calculations indicated the meteoroid terminal height was ~20 km and the pre-atmospheric velocity was > 17.8 km/sec. They found

000273

the aphelion to be 5.2 AU (the semi-major axis of orbit of Jupiter) and perihelion ~0.87 AU, which is just inside the Earth's orbit as would be expected for an Earth-crossing meteorite. This calculated orbit suggests the Apollo Asteroids and the Jupiter-family of comets are likely candidates for the Orgueil parent body include (although Halley-type comets are not excluded).

The cosmochemistry data for a cometary parent body is entirely consistent with the composition and characteristics of the CI1 meteorites. This suggestion that the parent body of the CI1 carbonaceous meteorites were possibly comets is significant with regard to possible existence of indigenous microfossils in the Alais, Ivuna and Orgueil meteorites. From the extensive evidence of aqueous alteration on the Orgueil parent body and the presence of indigenous water in the Orgueil meteorite it is clear that the parent body was either a water-bearing asteroid or a comet. However the Giotto and Vega observations of Halley and the Deep Impact Observations of the nucleus of 9P/Temple-1 have clearly established that these bodies get very hot as they enter the inner regions of the Solar System. It is now clear that any water bearing asteroid with an albedo of the Orgueil meteorite would reach a temperature above 100 C at 1AU. At these temperatures, water ice and other volatiles would be converted to liquid water, steam, and produce an expanding cloud of gas and expelled particulates. Any planetessimal orbiting the Sun and possessing a gaseous envelope and dust tail is traditionally refered to as "comet" rather than an asteroid, and therefore it seems logical that comets represent the most probable parent bodies for these water rich, black meteorites that travel in trajectories that cross the orbit of planet Earth.

4.6 Role of Comets and Carbonaceous Meteorites in the Origin and Evolution of the Earth's Atmosphere, Hydrosphere, and Biosphere

The relationship of comets with carbonaceous meteorites and their role in the origin and evolution of the atmosphere, hydrosphere, and biosphere of Earth has become better understood during the past few decades. The cratered surface of the moon provides clear evidence of the intense Hadean bombardment of the inner planets and moons by comets, asteroids and meteorites during the early history of the Solar System. Watson and Harrison (2005) interpreted the crystallization temperatures of 4.4 Ga Zircons from Western Australia as providing evidence that liquid water oceans were present on the early Earth within 200 million years of the formation of the Solar System. It has recently become more widely recognized that comets played a crucial role in the formation of the atmosphere and oceans of early Earth during the Hadean bombardment (Delsemme, 1997; Steel, 1998; Owen, 1997).

In 1978, Sill and Wilkening proposed that comets may have delivered life-critical biogenic elements carbon and nitrogen trapped within clathrate hydrates in their icy nuclei. In the same year, Hoyle and Wickramasinghe (1978, 1981, 1982, 1985) have proposed that comets delivered not only water, biogenic elements and complex organic chemicals to the surface of planet Earth, but that they also delivered intact and viable microorganisms. The detection of microfossils of cyanobacteria and other filamentous trichomic prokaryotes in the CI1 carbonaceous meteorites (which are likely cometary crustal remnants) may be interpreted as direct observational data in support of the Hoyle/Wickramasinghe Hypothesis of the role of comets in the exogenous origin of terrestrial life.

Eberhardt *et al.* (1987) measured the deuterium/hydrogen ratios in the water of comet P/Halley. Delsemme (1998) found that that the D/H ratio of the water molecules of comets Halley, Hale–Bopp and Hyakutake were consistent with a cometary origin of the oceans. Dauphas *et al.,* (2000) interpreted the deuterium/hydrogen ratios indicate that the delivery of water and ice to the early Earth during the late Hadean heavy bombardment by comets, asteroids and meteorites helped to cool the Earth's crust and form the early oceans. **Table V** shows data extracted from the Robert *et al.* (2000) compilation of Deuterium/Hydrogen ratios of selected components of the Cosmos.

26

<div align="center">

**TABLE V.**
Deuterium/Hydrogen Ratios

</div>

OBJECT	Species	D/H x 10^{-6}	Reference
Proto-Solar Nebula	H_2	21 ± 5	Geiss and Gloeckler, 1998
Local Interstellar Medium	H	16 ± 1	Linsky *et al.,* 1993
PLANETS			
Venus (Atmosphere)	H_2O	16,000±200	Donahue *et al.,* 1982
Earth (Oceans)	H_2O	149 ± 3	Lecuyer *et al.,* 1998
Mars (Atmosphere)	H_2O	780±80	Owen *et al.,* 1988
Saturn	H_2	15-35	Griffin *et al.,* 1995
Jupiter	H_2	21 ± 8	Lellouch *et al.,* 1996
Neptune	H_2	65 ± 2.5	Feuchtgruber *et al.,* 1997
Uranus	H_2	55 ± 15	Feuchtgruber *et al.,* 1998
COMETS			
Comet P/Halley	H_2O	310±30	Eberhardt *et al.,* 1987, 1995
Comet Hyakutake	H_2O	290±100	Bockelee *et al.,* 1998
Comet Hale-Bopp	H_2O	330±80	Meier *et al.,* 1998
CARBONACEOUS METEORITE			
Orgueil CI1 Meteorite	Kerogen	370±6	Halbout *et al.,* 1990
Orgueil CI1 Meteorite	Amino Acids	315-545	Pizzarello *et al.,* 1991
Orgueil CI1 Meteorite	Carboxylic Acids	180-310	Pizzarello *et al.,* 1991
CM, CV & CR Meteorites	Kerogen	370±6	Halbout *et al.,* 1990
SNC AND STONY METEORITES			
LL 3 Meteorites (Clays)	-OH	780±120	Deloule and Robert, 1995
Mars - SNC Meteorites	H_2O	530±250	Watson *et al.,* 1994

When these bodies are grouped in accordance with their D/H ratio it is easily seen that the telluric inner planets and the LL3 (stony) and SNC (Mars) meteorites have high (~500-16,000) ratios and the gas giants, protosolar nebula, ISM and Galaxies are very low (~15-65). The D/H ratios of the comets (~290-330) and carbonaceous meteorites (~180-370) are much closer to that of Earth (~149) and support the hypothesis that they may have made significant contributions to the formation of the oceans of our planet. It is interesting that the D/H ratios of comets are very similar to the ratios measured in the kerogen, amino acids and carboxylic acids of the Orgueil (CI) and other (CM, CV, and CR) carbonaceous meteorites. This supports the view that although stony meteorites are most probably derived from rocky asteroids, the carbonaceous meteorites most probably are derived from water-bearing asteroids or the nuclei of comets. The 30 m diameter fast-spinning carbonaceous asteroid 1998 KY26 that was discovered on June 2, 1998 has been found to contain 10-20% water. However, the small carbonaceous, water-rich asteroid 1998 KY26 also has color and radar reflectivity similar to carbonaceous meteorites and it may be a spent comet. Near IR observations indicated the presence of crystalline water ice and ammonia hydrate on the large Kuiper Belt object (50000) Quaoar with resurfacing suggesting cryovolcanic outgassing. The Cassini/Huygens spacecraft has recently obtained data indicating that a vast liquid water ocean may also exist beneath the thick frozen crust of Titan. Cassini/Huygens has also detected evidence for cryovolcanic water-ice geysers on Titan and Saturn's moon Enceladus.

5. EVIDENCE OF MICROFOSSILS IN CI1 METEORITES AND LIFE IN ICE: IMPLICATIONS TO POSSIBLE LIFE ON COMETS, EUROPA, AND ENCELADUS

The detection of evidence of viable microbial life in ancient ice (Abyzov *et al.*, 1998, 2003; Hoover and Pikuta, 2010) and the presence of microfossils of filamentous cyanobacteria and other trichomic prokaryotes in the CI1 carbonaceous meteorites has direct implications to possible life on comets and icy moons with liquid water oceans of Jupiter (e.g. Europa, Ganymede or Callisto) and Enceladus **(Fig. 8.a)** Saturn's spectacular moon that is exhibiting cryovolcanism and spewing water, ice and organics into space from the region of the blue and white "tiger stripes."
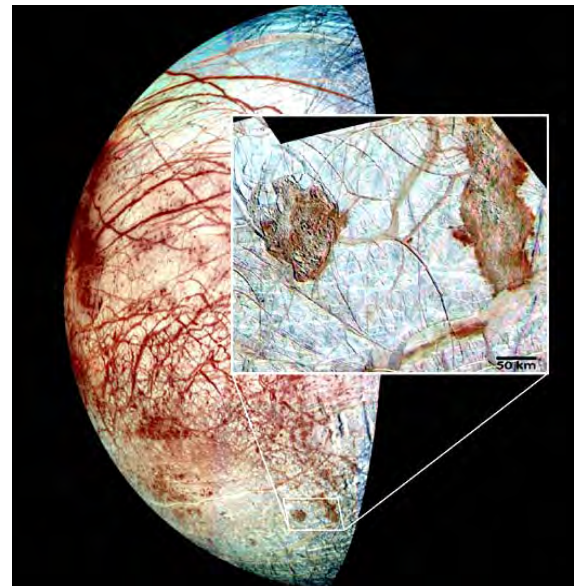

a.

b .

c.

d.

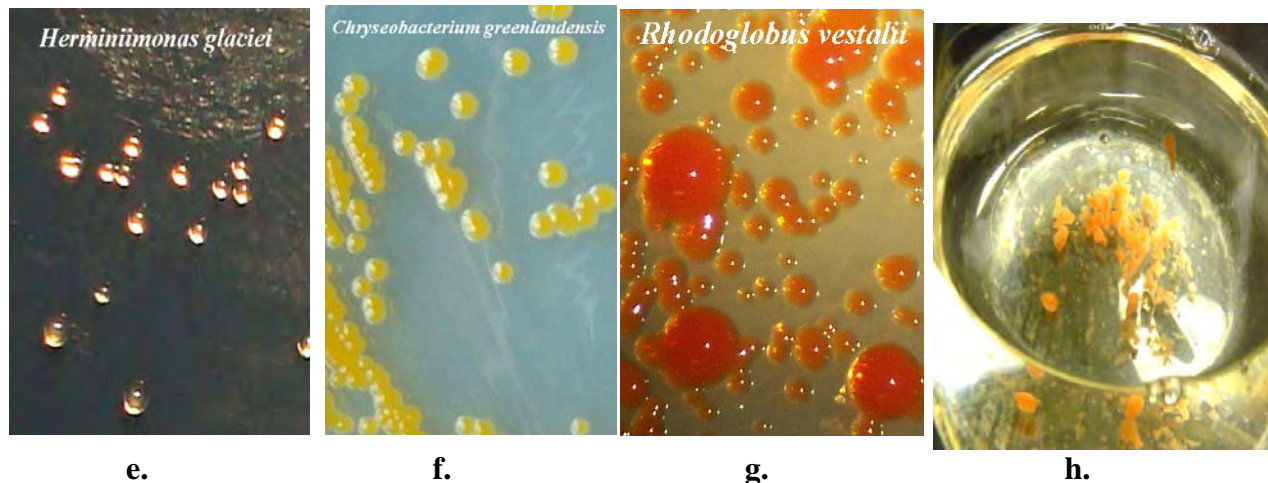|			
e.	**f.**	**g.**	**h.**
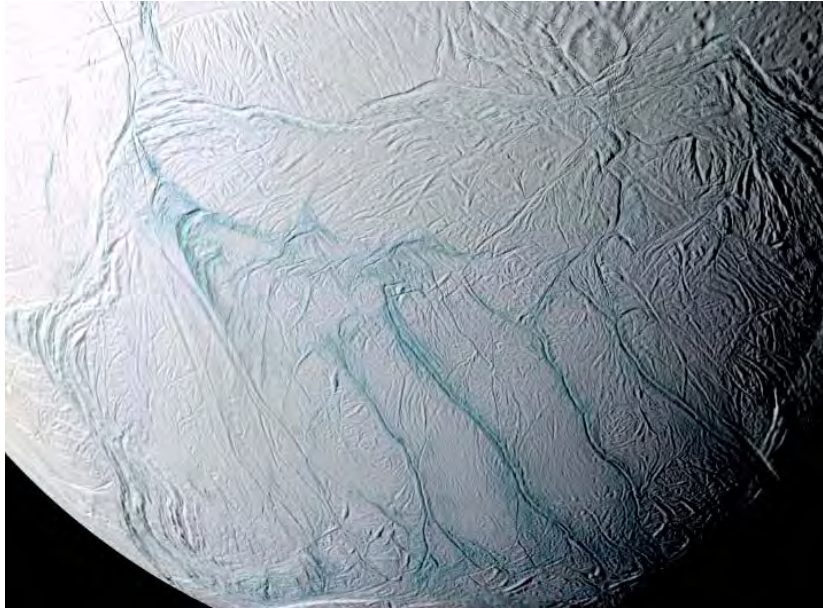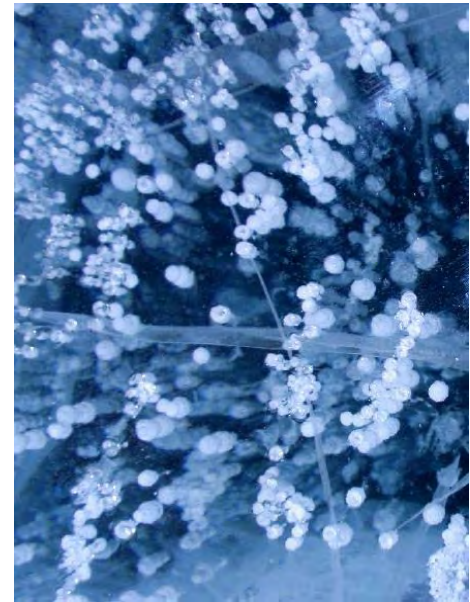
Figure 8.a. Blue and white snow and glacial ice tiger stripes on Saturn's moon Enceladus and **b.** ice bubbles from Lake Glubokoye, Antarctica. Color images from the Galileo spacecraft of **c**. the Conamara Chaos region and **d.** the Thrace region of Europa. Colonies of pigmented bacteria from the deep Greenland glacier ice core: **e.** red *Herminiimonas glacei* and **f.** yellow *Chryseobacterium greenlandensis.* From the McMurdo Valley ice sheet are colonies of **g.** red *Rhodoglobus vestalii*; and from the Schirmacher Oasis Ice Cave **h.** the red-ochre colony of *Hymenobacter* sp. strain IS118C-5s. *Photos Courtesy:* **a.,c., & d.** NASA/JPL/Arizona State University; **b.** R. B. Hoover; **e.,f.,&g.** Jennifer Loveland-Curtze/Penn State University and **h.** Asim K. Bej/UAB

Europa exhibits red, orange, yellow and ochre colors and fractured regions indicating the icy crust is floating on a liquid water ocean. The possibility of life on Europa has been discussed by Hoover *et al.* (1986): Chyba *et al.* (2001) and Dalton *et al.* (2003). Hoover *et al.* (1986) argued while deep blue and white colors in the Galileo images of the Jovian moon Europa were typical of glacial ice, ice bubbles and snow on Earth as seen in this image of ice bubbles from the Schirmacher Oasis of East Antarctica **(Fig, 8.b)**. The red, yellow, brown, golden brown, green and blue colors detected by the Galileo spacecraft in the Conamara Chaos region **(Fig. 8.c.)** and the deep red lines of the icy crust of Europa **(Fig. 8.d.)** are consistent with microbial pigments rather than evaporite minerals. The 1986 paper suggested that the colors seen in Europa images resulted from microbial life in the upper layers of the ice. A number of more recent studies have been published concerning the significance of ice microbiota to the possibility of life elsewhere in the Solar System.[76-80] Diatoms are golden brown and cyanobacteria exhibit a wide range of colors from blue-green to red, orange, brown and black. Bacteria recovered from ice are often pigmented. For example, the extremophiles isolated from the ancient Greenland ice cores produce pigmented colonies. *Herminiimonas glaciei* colonies are red **(Fig. 8.e)** and the colonies of *"Chryseobacterium greenlandensis"* exhibit yellow pigments **(Fig. 6.b.)**. **Figure 5.c.** shows the red pigmented colonies of the new genus of psychrophile, *Rhodoglobus vestali* isolated from a lake near the McMurdo Ice Shelf, Antarctica (Sheridan *et al.* 2003). Colonies of *Hymenobacter sp.* **(Fig. 6.d.)** isolated from the Schirmacher Oasis Ice Cave are red-ochre in color (Hoover and Pikuta, 2009, 2010). The possibility of life on Enceladus and the detection of biomarkers in the plumes of water, ice and organic chemicals ejected from the "Tiger Stripes" of Enceladus has been discussed by McKay *et al.,* (2008) and Hoover and Pikuta (2010).

6. CONCLUSIONS

It is concluded that the complex filaments found embedded in the CI1 carbonaceous meteorites represent the remains of indigenous microfossils of cyanobacteria and other prokaryotes associated with modern and fossil prokaryotic mats. Many of the Ivuna and Orgueil filaments are isodiametric and others tapered, polarized and exhibit clearly differentiated apical and basal cells. These filaments were found in freshly fractured stones and are observed to be attached to the meteorite rock matrix in the manner of terrestrial assemblages of aquatic benthic, epipelic, and epilithic cyanobacterial communities comprised of species that grow on or in mud or

clay sediments. Filamentous cyanobacteria similar in size and detailed morphology with basal heterocysts are well known in benthic cyanobacterial mats, where they attach the filament to the sediment at the interface between the liquid water and the substratum. The size, size range and complex morphological features and characteristics exhibited by these filaments render them recognizable as representatives of the filamentous *Cyanobacteriaceae* and associated trichomic prokaryotes commonly encountered in cyanobacterial mats. Therefore, the well-preserved mineralized trichomic filaments with carbonaceous sheaths found embedded in freshly fractured interior surfaces of the Alais, Ivuna, and Orgueil CI1 carbonaceous meteorites are interpreted as the fossilized remains of prokaryotic microorganisms that grew in liquid regimes on the parent body of the meteorites before they entered the Earth's atmosphere.

The Energy Dispersive X-ray spectroscopy data reveals that the filaments detected in the meteorites typically exhibit external sheaths enriched in carbon infilled with minerals enriched in magnesium and sulfur. These results are interpreted as indicating that the organisms died on the parent body while aqueous fluids were present and the internal cells were replaced by epsomite and other water soluble evaporite minerals dissolved in the liquids circulating through the parent body. The nitrogen level in the meteorite filaments was almost always below the detection limit of the EDS detector (0.5% atomic). However, nitrogen is essential for all amino acids, proteins, and purine and pyrimidine nitrogen bases of the nucleotides of all life on Earth.

Extensive EDS studies of living and dead cyanobacteria and other biological materials have shown that nitrogen is detectable at levels between 2% and 18% (atomic) in cyanobacterial filaments from Vostok Ice (82 Kya) and found in stomach milk the mammoth Lyuba (40 Kya); mammoth hair/ tissue (40-32 Kya); pre-dynastic Egyptian and Peruvian mummies (5-2 Kya) and herbarium filamentous diatom sheaths (1815). However, Nitrogen is not detected in ancient biological materials such as fossil insects in Miocene Amber (8 Mya); Cambrian Trilobites from the Wheeler Shale (505 Mya) or cyanobacterial filaments from Karelia (2.7 Gya). Consequently the absence of nitrogen in the cyanobacterial filaments detected in the CI1 carbonaceous meteorites indicates that the filaments represent the remains of extraterrestrial life forms that grew on the parent bodies of the meteorites when liquid water was present, long before the meteorites entered the Earth's atmosphere. This finding has direct implications to the distribution of life in the Cosmos and the possibility of microbial life on in liquid water regimes of cometary nuclei as the travel within the orbit of Mars and in icy moons with liquid water oceans such as Europa and Enceladus.

ACKNOWLEDGEMENTS

References

Abyzov, S.S., Mitskevich, I.N., Poglazova, M.N., Barkov, M.N., Lipenkov, V.Ya., Bobin, N.E., Koudryashov, B.B., Pashkevich, V.M., (1998). Antarctic ice sheet as a model in search of Life on other planets. Advances in Space Research, 22, 363-368.

Abyzov, S. S., Gerasimenko, L. M., Hoover, R. B., Mitskevich, I. N., Mulyukin, A. L., Poglazova, M. N., Rozanov, A. Yu., (2005). Microbial Methodology in Astrobiology. SPIE, 5906, 0A 1-17.

Berthelot M. P. (1868). Sur la métiere charbonneuse des météorites. Compt. Rend. Acad. Sci. Paris 67, 449.

Bass, M. N. (1971). Montmorillonite and serpentine in Orgueil meteorite. Geochim. Cosmochim. Acta, 35, 139-147.

Bergé, M. (1864). Lettre de M. Bergé. Compt. Rend. Acad. Sci., Paris, 58, 936-936.

Berthelot, M. (1868). Sur la Matiere charboneuse des meteorites. Compt. Rend. Acad. Sci., Paris 67, 849.

Berzelius,J. J. (1834). Über Meteorsteine, 4. Meteorstein von Alais. Ann. Phys. Chem. 33, 113-123.

Berzelius, Professor (1836). LXXX. On Meteoric Stones. The London and Edinburg Philosophical Magazine and Journal of Science, (Brewster, D., Taylor, R and Philips, Eds.) 9, 429-441.
(English Translation by M. Vallet of extract of Memoir in Poggendorf's Annalen der Physik und Chemie.

Bitz, M. C., Nagy, B. (1966). Ozonolysis of "polymer type" material in coal, kerogen, and in the Orgueil meteorite: a preliminary report. Proc. Nat. Acad. Sci. 56, pp. 1383-1390.

Boström, K. and Frederickson, K. (1966). Surface Conditions of the Orgueil Meteorite Parent Body as Indicated by Mineral Associations. Smithsonian Misc. Coll. 151, 1-39.

Bland, P. A., Cressey, G., Menzies, O. N. (2004). Modal mineralogy of carbonaceous chondrites by X-ray diffraction and Mössbauer spectroscopy. Meteoritics & Planetary Science, 39, 3-16.

Bockelée-Morvan D., Gautier D., Lis D. C., Young K., Keene J., Phillips T., Owen T., Crovisier J., Goldsmith P. F., Bergin E. A., Despois D., Wooten A. (1998) Deuterated water in comet C/1996 B2 (Hyakutake) and its implications for the origin of comets. Icarus, 193, 147–162.

Botta, O.; Ehrenfreund, P.; Glavin, D. P.; Cooper, G. W.; Kminek, G.; Bada, J. L. (2000). A Cometary Origin of the Amino Acids in the Orgueil Meteorite. Lunar and Planetary Science XXXI

Bullock, E. S., Gounelle, M,, Grady, M. M., Russell, S. S. (2003). Different Degrees of Aqueous Alteration in Sulphides within the CI1 Chondrites. Lunar & Planetary Science XXXIV, 1542.pdf
http://www.lpi.usra.edu/meetings/lpsc2003/pdf/1542.pdf

Bullock, E. S., Gounelle, M,, Lauretta, D. S., Grady, M. M., Russell, S. S. (2005). Mineralogy and texture of Fe-Ni sulfides in CI1 chondrites: Clues to the extent of aqueous alteration on the CI1 parent body. Geochim. Cosmochim. Acta, 69, 2687-2700.

Bunch, T. E., and Chang, S. (1980). Carbonaceous chondrites-II. Carbonaceous chondrite phyllosilicates and light element geochemistry as indicators of parent body processes and surface conditions, Geochim. Cosmochim. Acta 44, 1543-1577,

Christie, W. A. K. (1913). A carbonaceous aerolite from Rajputana. Records Geol. Survey India, 44, 41-51.

Chyba, C. F., Phillips, C.B. (2001). Possible ecosystems and the search for life on Europa. Proc. Natl. Acad. Sci. USA 98, 801-804.

Claus G., Nagy, B. (1961). A microbiological examination of some carbonaceous chondrites, Nature 192, 594-596.
Claus, G., Nagy, B. (1962). Considerations of Extraterrestrial Taxa, Taxon, 11, 160-161.

Claus, G., Nagy, B., Europa, D. L. (1963). Further observations on the properties of the "organized elements." Ann. N. Y. Acad. Sci. 108, 580-605.

Clayton, R. N. (1963). Carbon isotope abundances in meteoritic carbonates." Science, 140, 192-193.

Cloëz, S. (1864a). Note sur la composition chimique de la pierre météorique d'Orgueil. Compt. Rend. Acad. Sci., Paris 58, 986-988.

Cloëz, S. (1864b). Analyse chimique de la pierre météorique d'Orgueil. Note de M. S. Cloëz presentée par M. Daubrée. Compt. Rend. Acad. Sci. 59, 37-40.

Dalton, J.B., Mogul, R., Kagawa, H. K., Chan, S. L., Jamieson, C. S. (2003). Near-Infrared detection of potential evidence for microscopic organisms on Europa." Astrobiology 3, 505-529.

Daubrée, A. (1864).. Note sur les meteorites tombées le 14 Mai aux environs d'Orgueil (Tarn-et-Garonne). Compt. Rend. Acad. Sci., Paris 58, 984-986.
http://visualiseur.bnf.fr/ark:/12148/CadresFenetre?O=NUMM-3015&M=tdm

Daubrée, A.., LeVerrier, M. (1864). Communication. Compt. Rend. Acad. Sci. Paris 58, 932-934.
http://visualiseur.bnf.fr/ark:/12148/CadresFenetre?O=NUMM-3015&M=tdm\

Dauphas, N., Robert, F., Marty, B. (2000). The Late Asteroidal and Cometary Bombardment of Earth as Recorded in Water Deuterium to Protium Ratio. Icarus, 148, 508-512.

d'Esparbés. M. (1864). Written communication with M. LeVerrier. Compt. Rend. Acad. Sci., Paris 58, 934-935. http://visualiseur.bnf.fr/ark:/12148/CadresFenetre?O=NUMM-3015&M=tdm

de Puylaroque, M. 1864. Lettre du Juin 1 a M. Petit. Compt. Rend. Acad. Sci., Paris 58, 1070.
http://visualiseur.bnf.fr/ark:/12148/bpt6k3015d/CadresFenetre?O=NUMM-3015&M=tdm

Deloule E., Robert F. (1995) Interstellar water in meteorites? Geochim. Cosmochim. Acta, 59, 4695–4706.

Delsemme, A. (1997). The origin of the atmosphere and of the oceans. in: Comets and the Origin and Evolution of Life. (P. J. Thomas, C. F. Chyba, and C. P. McKay, Eds.) Springer-Verlag, New York. 29-67.

Delsemme, A. H. (1998). The deuterium enrichment observed in recent comets is consistent with the cometary origin of seawater. Planet. and Space Sci., 47, 125-131.

Donahue T. M., Hoffman J. H., Hodges R. R. Jr., Watson A. J. (1982) Venus was wet: A measurement of the ratio of deuterium to hydrogen. Science, 216, 630–633.

32

Donze, M., Haveman, J. and Schiereck, P. (1972). Absence of Photosystem 2 in heterocysts of the blue-green alga Anabaena. Biochim. Biophys. Acta. 256, 157-161.

Dufresne, E. P. and Anders, E. (1962). On the Chemical Evolution of carbonaceous chondrites", Geochim. Cosmochim. Acta 26, 1085-1114.

Eberhardt, P., Dolder, U., Schulte, W., Krankowsky, D., Lämmerzahl, P., Berthelier, J. J., Woweries, J., Stubbemann, U., Hodges, R. R., Hoffman, J. H., Illiano, J. M. (1987). The D/H ratio in water from comet P/Halley. Astron. Astrophys. 187, 435-437.

Eberhardt P., Reber M., Krankowsky D., Hodges R. R. (1995) The D/H and $^{18}O/^{16}O$ ratios in water from comet P/Halley. Astron. Astrophys., 302, 301–316.

Endre, M., Bischoff, A. (1996). Carbonates in CI chondrites: Clues to parent body evolution. Geochim. et Cosmochim. Acta, 60, 489-507.

Fay, P., Stewart, W. D. P., Walsby, A. E. and Fogg, G. E. (1968) "Is the heterocyst the site of nitrogen fixation in blue-green algae?" Nature, 220, 810-812.

Feuchtgruber H., Lellouch E., de Graauw T., Encrenaz Th., Griffin M. (1997). Detection of HD on Neptune and determinations of D/H ratio from ISO/SWS observations. Bull. Am. Astron. Soc., 29, 995.

Feuchtgruber H., Lellouch E., Encrenaz Th., Bezard B., de Graauw T., Davies G. R. (1998). Detection of HD in the atmosphères of Uranus and Neptune: A new determination of the D/H ratio. Astron. Astrophys., 341, L17–L21.

Fogg, G. E. (1949). Growth and heterocyst production in Anabaena cylindrica Lemm. II. In relation to carbon and nitrogen. metabolism. Ann Bot, N. S. 13, 241–259.

Folinsbee, R. E, (1965). Fall of Revelstoke Stony Meteorite, Canada, Letter July 26, 1965, The Meteoritical Bulletin, 34, Moscow, Russia.

Folinsbee, R. E., Douglas, D. A. V., Maxwell, J. A. (1967). Revelstoke, a new Type I carbonaceous chondrites. Geochem. Cosmochim. Acta, 31, 1625-1635.

Fredriksson, K., Kerridge, J. F. (1988). Carbonates and sulfates in CI Chondrites: Formation by aqueous activity on the parent body. Meteoritics, 23, 35-44.

Geiss J. and Gloecker G. (1998) Abundances of deuterium and helium in the protosolar cloud. Space Science Rev., 84, 239– 250.

33

Gelpi, E., Oró, J. 1970. Organic compounds in meteorites, 4. Gas chromatographic mass spectrometric studies on the isoprenoids and other isomeric alkanes in carbonaceous chondrites. Geochem. Cosmochim. Acta 34, 981-994.

Glavin, D. P. and Bada, J. L. (2004). Isolation of Purines and Pyrimidines from the Murchison Meteorite Using Sublimitaion", Lunar & Planet. Science XXXV, 1022.
www.lpi.usra.edu/meetings/lpsc2004/pdf/1022.pdf

Griffin M. J., Naylor D. A., Davis G. R., Ade P. A. R., Oldman P. G., Swinyard B. M., Gautier D., Lellouch E., Orton G. S., Encrenaz Th., de Graauw T., Furniss I., Smith I., Armand C., Burgdorf M., Del Giorgio A., Ewart D., Gry C., King K. J., Lim T., Molinari S., Price M., Sidher S., Smith A., Texier, D. N., Trams S. J., Unger S. J., and Salama A. (1996). First detection of the 56 mm rotational line of HD in Saturn's atmosphere. Astron. Astrophys., 315, L389–L392.

Guo, W., Perronnet, M., Zolensky, M. E., Eiler, J. M. (2007). Temperatures of Aqueous Alteration on Carbonaceous Chondrite Parent Bodies. 70th Annual Meteoritical Society Meeting.
http://www.lpi.usra.edu/meetings/metsoc2007/pdf/5276.pdf

Halbout J., Robert F., Javoy M. (1990). Hydrogen and oxygen isotope compositions in kerogens from the Orgueil meteorite: Clues to solar origin. Geochim. Cosmochim. Acta, 54, 1453– 1462.

Hoover, R. B., Hoyle, F. Wickramasinghe, N. C., Hoover, M. J. and Al-Mufti, S., "Diatoms on Earth, Comets, Europa, and in Interstellar Space," Earth, Moon, and Planets, 35, 19-45 (1986).

Hoover, R. B. (1997). Meteorites, microfossils and exobiology. in: Instruments, Methods, and Missions for the Investigation of Extraterrestrial Microorganisms, (R. B. Hoover, Ed.), SPIE, 3111, 115-136.

Hoover, R. B., Rozanov, A. Yu., Zhmur, S. I., Gorlenko, V. M., (1998). Further evidence of microfossils in carbonaceous chondrites. in Instruments, Methods and Missions for Astrobiology, SPIE, 3441, 203-216.

Hoover, R. B., Rozanov, A. Yu., (2003a). Microfossils, Biominerals, and Chemical Biomarkers in Meteorites. in: Instruments Methods and Missions for Astrobiology VI, (Hoover, R. B., Rozanov, A. Yu. and Lipps, J. H., Eds.), SPIE, 4939, 10-27.

Hoover, R. B., Jerman, G., Rozanov, A. Yu., Davies, P. C. W. (2003b). Biomarkers and Microfossils in the Murchison, Tagish Lake and Rainbow Meteorites. in Instruments Methods and Missions for Astrobiology V, (Hoover, R. B., Rozanov, A. Yu. and Paepe, R. R., Eds.), SPIE, 4859, 15-31.

Hoover, R. B., Rozanov, A. Yu., Jerman, G. A., Coston, J. (2004). Microfossils in CI and CO Carbonaceous Meteorites. Instruments Methods and Missions for Astrobiology VII, SPIE,5163, 7-23.

Hoover, R. B. (2005a). Microfossils, biominerals, and chemical biomarkers in meteorites. in: Perspectives in Astrobiology, Vol. 366, NATO Science Series: Life and Behavioural Sciences, (R. B. Hoover, R. R. Paepe, and A. Yu. Rozanov, Eds.), IOS Press, Amsterdam, Netherlands, 43-65.

Hoover, R. B. (2005b). Mineralized Remains of Morphotypes of Filamentous Cyanobacteria in Carbonaceous Meteorites. Astrobiology and Planetary Missions, SPIE, 5906, 0J 1-17.

Hoover, R. B. (2006a). Comets, asteroids, meteorites, and the origin of the Biosphere. in: Instruments, Methods and Missions for Astrobiology, IX (R. B. Hoover, A. Yu. Rozanov, and G. V. Levin, Eds.), SPIE, 6309, 0J1-12.

Hoover, R. B. (2006b). Fossils of prokaryotic microorganisms in the Orgueil meteorite. in: Instruments, Methods and Missions for Astrobiology, IX (R. B. Hoover, A. Yu. Rozanov, and G. V. Levin, Eds.), SPIE, 6309, 6309- 02, 1-17.

Hoover, R. B.   (2007). Ratios of Biogenic Elements for Distinguishing Recent from Fossil Microorganisms. Instruments, Methods, and Missions for Astrobiology X, Proc. SPIE 6694, 66940D.

Hoover, R. B. (2008). Comets, Carbonaceous Meteorites and the Origin of the Biosphere" in Biosphere Origin and Evolution (N. Dobretsov, N. Kolchanov, A. Rozanov and G. Zavarzin, Eds.) Springer US, New York, pp. 55-68. http://www.springerlink.com/content/u17384273280174l/

Hoover, R. B., Pikuta, Elena V., Townsend, A., Anthony, J., Guisler, M., McDaniel, J., Bej, A. K., Storrie-Lombardi, M. (2008). Microbial extremophiles from the 2008 Schirmacher Oasis Expedition: preliminary results. In Instruments, Methods, and Missions for Astrobiology XI, SPIE 7097, 70970L 1-9.

Hoover, R. B., Pikuta, E. V. (2009). Life in Ice: Implications to Astrobiology, SPIE, 7441, 1-14.
.
Hoyle, F. (1983). From Virus to Cosmology. Jour. Roy. Soc. Medicine, 76, 99-111.

Hoover, R. B. and Pikuta, E. V. (2010) Psychrophilic and Psychrotolerant Microbial Extremophiles. In: Polar Microbiology: The Ecology, Biodiversity and Bioremediation Potential of Microorganisms in Extremely Cold Environments. (Asim K Bej, Jackie Aislabie, and Ronald M Atlas, Eds.) pp. 115-151.

Hoyle, F. and Wickramasinghe, N.C. (1978). Lifecloud: the origin of life in the galaxy. London: J.M. Dent.

Hoyle, F. and Wickramasinghe, N.C., (1981). In: C. Ponnamperuma, Ed. Comets and the Origin of Life. Dordrecht: D. Reidel, pp. 1-227.

Hoyle, F. and Wickramasinghe, N.C., (1982). Proofs that Life is Cosmic. Colombo: Govt. Press, Sri Lanka http://www.astrobiology.cf.ac.uk/proofs...pdf

Hoyle, F. and Wickramasinghe, N.C., (1985). Living Comets. Cardiff: University College Press.

Hua, L. L, Kobayashi, K., Ochiai, E. I., Gerke, C. W., Gerhardt, K. O., Ponnamperuma, C., 1986. Identification and quantification of nucleic acid bases in carbonaceous chondrites, Origins of Life 6, 226–227.

Huss, G. R., Lewis, R. S. (1995). Presolar diamond, SiC, and graphite in primitive chondrites: Abundances as a function of meteorite class and petrologic type. Geochem. Cosmochim. Acta, 59, 115-160.

Jollois, M. (1864). Lettre de M. Jollois à M. LeVerrier, Blois, le 20 Mai 1864. Compt. Rend. Acad. Sci., Paris 58, 936-937. http://visualiseur.bnf.fr/ark:/12148/bpt6k3015d/CadresFenetre?O=NUMM-3015&M=tdm

Kissin, Y. V. (2003). Hydrocarbon components in carbonaceous meteorites. Geochim Cosmochim. Acta 67, 1723-1735.

Kojima, H., Yamaguchi, A. (Eds.), (2008). Meteorite Newsletter, Japanese Collection of Antarctic Meteorites, NIPR, Tokyo, pp. 1-24. http://yamato.nipr.ac.jp/AMRC/AMRC/MeteoriteNewsletter_16.pdf

Lamarre, J. M., Emerich, C., Moroz, V. I., Combes, M., Sanko, N., Rocard, F., Gispert, R., Nikolsky, Y., Coron, N., Bibring, J. P. (1986). Temperature of the Nucleus of Comet P/Halley Deduced from IKS-Vega Observations. Bulletin of the American Astronomical Society, 18, 794.

Larson, E. E., Watson, D. E., Herndon, J. M., Rowe, M. W. (1974). Thermomagnetic analysis of meteorites, 1. C1 chondrites. Earth and Planetary Science Letters, 21, 345-350.

Lécuyer C., Gillet Ph., Robert F. (1998) The hydrogen isotope composition of sea water and the global water cycle. Chem. Geol., 145, 249–261.

Lellouch E., Encrenaz Th., Graauw Th., Scheid S., Fëuchtgruber H., Benteima D. A., Bézard B., Drossart P., Griffin M., Heras A., Kesselr M., Leech K., Morris A., Roelfserna P. R., Roos-Serote M., Salama A., Vandenbussche B., Valentijn E. A., Davies G. R., Naylor D. A. (1996) Determinations of D/H ratio on Jupiter from ISO/SWS observations. Bull. Am. Astron. Soc., 28, 1148.

Leymerie, M. (1864a). Sur l'aérolithe d'Orgueil (Tarn-et-Garonne), tombé le 14 Mai, 1864, a huit heures de Soir, Lettre de M. Leymerie a M. Daubrée, Compt. Rend. Acad. Sci., Paris 58, 988-990.

Leymerie, M. (1864b). Lettre du 10 Juin a A. Daubrée, Compt. Rend. Acad. Sci., Paris 58, 1072.

Linsky J. L. (2003) Atomic deuterium/hydrogen in the galaxy. In Solar System History from Isotopic Signatures of Volatile Elements (R. Kallenbach et al., eds.) ISSI Space Science Series, Vol. 16. 49–60.

Martins, Z., Botta, O., Fogel, M. L., Sephton, M. A., Glavin, D. P., Watson, J. S. Dworkin, J. P. Schwartz, A. W. Ehrenfreund, P. "Extraterrestrial nucleobases in the Murchison meteorite," Earth and Planetary Science Letters, 270, 130-136, 2008.

McKay, C.P., Porco, C. C., Altheide, T., Davis, W. L., Kral T. A. (2008). The possible origin and persistence of life on Enceladus and detection of biomarkers in the plume. Astrobiology 8, 909-919.

Meier R., Owen T. C., Matthews H. E., Jewitt D. C., Bockelée-Morvan D., Biver N., Crovisier J., Gautier D. (1998). A determination of the HDO/H_2O ratio in Comet C/1995 O1 (Hale-Bopp). Science, 279, 842–898.

Nagy, B. (1975). Carbonaceous Meteorites, Elsevier Scientific Publishing Co., New York, pp. 1-747.

Nagy, B., Bitz, M. C. (1963). Long-chain fatty acids in the Orgueil meteorite. Arch. Biochem Biophys., 101, 240-248.

Nooner, D. W., Oró, J. (1967). Organic compounds in meteorites, 1. Aliphatic hydrocarbons. Geochim. Cosmochim. Acta 31, pp. 1359-1394.

Olson, R. J., Oró, J., Zlatkis, A. (1967). Organic compounds in meteorites, 2. Aromatic Hydrocarbons. Geochim Cosmochim. Acta 31, 1935-1948.

Owen, T. C. (1998). The origin of the atmosphere," in The Molecular Origins of Life: Assembling Pieces of the Puzzle, (A. Brack, ed.), Cambridge University Press, 13-34.

Owen T., Encrenaz T. (2003) Element abundances and isotope ratios in the giant planets and Titan. Space Sci. Rev., 106, 121–138.

Owen T., Maillard J. P., Debergh C., Lutz B. (1988) Deuterium on Mars: The abundance of HDO and the value of D/H. Science, 240, 1767–1770.

Pikuta, E. V., Hoover, R. B., Marsic, D., Bej, A., Tang, J., Krader, P. (2005). Carnobacterium pleistocenium sp. nov., a novel psychrotolerant, facultative anaerobe isolated from Fox Tunnel permafrost, Alaska. Int J Syst Evol Microbiol, 55, 473-478.

Pizzarello S., Krisnamurthy R. V., Epstein S., Cronin J. R. (1991. Isotopic analyses of amino acids from the Murchison meteorite. Geochim. Cosmochim. Acta, 55, 905–910.

Pflug, H.D. (1984). Microvesicles in meteorites, a model of pre-biotic evolution. Naturwissenschaften, 71, 531-533.

Pisani, F. (1864). Étude chimique et analyse de l'aerolithe d'Orgueil. Compt. Rend. Acad. Sci., Paris 59, 132-135.

Robert, F., Gautier, D. and Dubrulle, B. (2000). The Solar System D/H ratio: Observations and Theories. Space Sci. Rev., 92, 201-224.

Roscoe, P. (1864). On the existence of a crystallizable carbon compound and free sulphur in the Alais meteorite. Proc. Literary Soc. Manchester 13, 57-59.

Rossignol-Strick, M. and Barghoorn, E. S. (1971). Extraterrestrial abiogenic organization of organic matter: The hollow spheres of the Orgueil meteorite", Space Life Sci. 3, 89-107.

Sephton, M. A. (2005). Organic Matter in Carbonaceous Meteorites: Past Present & Future Research. Phil. Trans. Roy. Soc. A, 363, 2229-2742.

Sheridan, P. P., Loveland-Curtze, J., Miteva, V. I., Brenchley, J. E. (2003). Rhodoglobus vestalii gen. nov., sp. nov., a novel psychrophilic organism isolated from an Antarctic Dry Valley lake." Int. J. Syst. Evol. Microbiol., 53, 985-994.

Sill G. T. and Wilkening, L. (1978). Ice clathrate as a possible source of the atmosphere of the terrestrial planets. Icarus, 33, 13-27.

Smith, J. L. (1876) Researches on the solid carbon compounds in meteorites. Am. J. Sci. 11, 433-442.

Soderblom, L.A., Becker, T. L., Bennett, G., Boice, D. C., Britt, D. T., . Brown, R. H , Buratti, B. J., Isbell, C., Giese, B., Hare, T., Hicks, M. D., Howington-Kraus, E., . Kirk, R. L , Lee, M., Nelson, R. M., Oberst, J., Owen, T. C., Rayman, M. D., Sandel, B. R., Stern, S. A., Thomas, N., Yelle, R. V. (2002). Observations of Comet 19P/Borrelly by the Miniature Integrated Camera and Spectrometer aboard Deep Space 1. Science, 296, 1087-1091.

Steel, D. (1997). Cometary Impacts in the Biosphere. in Comets and the Origin and Evolution of Life. (Paul J. Thomas, Christopher F. Chyba, and Christopher P. McKay, Eds.) Springer-Verlag, New York. 216-230.

Stewart, W. D. P., Haystead, A., Pearson, H. W. (1969). Nitrogenase activity in heterocysts of blue-green algae. Nature, 224, 226-228.

Stoks, P. G., Schwartz, A. W. (1981). Nitrogen-heterocyclic compounds in meteorites: significance and mechanisms of formation, Geochim Cosmochim Acta 45, 563–569.

Tomeoka, K. and Buseck, P. R.. (1988). Matrix mineralogy of the Orgueil C1 carbonaceous chondrite. Geochim. Cosmochim. Acta 52, 1627-1640 (1988).

Thénard, L. J. (1806). Analyse d'un aérolithe tombée de l'arrondissement d'Alais, le 15 mars, 1806. Ann. Chim. Phys., 59, 103-110.

Tindall, B. J., Kämpfer, P., Euzéby, J. P., Oren, A. (2006). Valid publication of names of prokaryotes according to the rules of nomenclature: past history and current practice. Int. J. Syst. Evol. Microbiol. 56, 2715-2720.

Tonui, E., Zolensky, E. M.., Lipschutz, M. (2001). Petrography, mineralogy and trace element chemistry of Y-86029, Y-793321 and LEW 85332: Aqueous alteration and heating events. Antarctic Meteorites XXVI. Papers presented to the 26th Symposium on Antarctic Meteorites, NIPR, Tokyo, June 12-14, 2001, 148-150.

Tonui, E. K., Zolensky, M. E. (2001). Mineralogy and Petrology of Yamato 86029: A New Type of Carbonaceous Chondrite. 32nd Annual Lunar and Planetary Science Conference, March 12-16, 2001, Houston, Texas, abstract no.1248, http://www.lpi.usra.edu/meetings/lpsc2001/pdf/1248.pdf

V. Brief Notices (1915). Geological Magazine (Decade. VI), 2, 87-90.

Vallentyne, J. R. (1965). Two Aspects of the Geochemistry of Amino Acids. In: S. W. Fox (Ed.) The Origins of Prebiological Systems and of Their Molecular Matrices. Academic Press, New York, N. Y., 105-125.

Van Schmus, W. R., Wood, J. A. (1967). A chemical-petrologic classification for the chondritic meteorites. Geochem. Cosmochim. Acta, 31, 747-766.

Watson W. D. (1976). Interstellar molecule reactions. Rev. Mod. Phys., 48, 513–552.

Watson E. B. and Harrison, T. M. (2005). Zircon thermometer reveals minimum melting conditions on earliest Earth, Science.308, 841-844.

Wiik, H. B. (1956). The Chemical Composition of some stony meteorites. Geochem. Cosmochim. Acta, 9, 279-289.

Wirick, S., Flynn, G. J., Keller, L. P., Nakamura-Messenger, K., Peltzer, Jacobsen, C., Sandford, S., Zolensky, M., (2009). Organic matter from comet 81P/Wild 2, IDPs, and carbonaceous meteorites; similarities and differences. Meteoritics & Planetary Science, 44, 1611-1626.

Zhmur, S. I., Rozanov, A. Yu., Gorlenko, V. M. (1997). Lithified Remnants of Microorganisms in Carbonaceous Chondrites, Geochemistry International, 35, 58-60.

Journal of Cosmology, Vol 6, 2010   **R.E. Schild and D.J. Leiter**

BLACK HOLE OR MECO? DECIDED BY A THIN LUMINOUS RING STRUCTURE DEEP WITHIN QUASAR Q0957+561

Rudolph E. Schild, Center for Astrophysics, 60 Garden Street, Cambridge, MA 02138, USA, rschild@cfa.harvard.edu

Darryl J. Leiter, Visiting Scientist, National Radio Astronomy Observatory, Charlottesville, VA 22903, USA (dleiter@nrao.edu)

ABSTRACT

Optical, Infrared, X-ray, and radio wavelength studies of quasars are beginning to define the luminous quasar structure from techniques of reverberation and microlensing. An important result is that the inner quasar structure of the first identified gravitational lens, Q0957+561 A,B seems not to show the kind of structure expected for a super-massive black hole, but instead show a clean-swept interior region due to the action of an intrinsic magnetic propeller, just as expected for a MECO (Magnetic Eternally Collapsing Object) structure. Given the present state of the observations, the strongest model discriminator seems to be the existence of a thin luminous band around the inner edge of the accretion disc, at a distant radius ~70 Rg from the M ~ 4×10^9 Mo central object. Since the existence of a clean magnetic propeller swept inner region ~70 Rg surrounded by a sharp ~ 1 Rg disc edge are the low-hard state spectral properties associated with a highly red shifted central MECO object, we are led to the conclusion that these observations imply that the Q0957 quasar contains a central super-massive MECO instead of a black hole. In this report we review the details of the observations which have compelled us to reach this conclusion.

.

1.   Introduction

In this paper we present observational and theoretical arguments that black holes, as the active ingredient in quasars seen at large cosmological distances, may have outlived their usefulness. Black holes were first conceived as possible sites of extreme physics, but interest in them grew during the 1960's era when quasars were discovered and understood to be at such large cosmological distances that they could not be understood as stars. So black holes were invoked to explain how such a prodigious quantity of energy, equivalent to the combined light of a billion ordinary stars, could originate in such a small object.

As a long literature about quasar properties unfolded, problematic difficulties with the black hole objects were encountered because of the complexities associated with their event horizons. As the theory is presently understood, the event horizon in a black hole represents a surface inside of which nothing, even light, can escape the essentially infinite gravitational force which would be measured by a local observer. Hence observers inside of the event horizon cannot communicate with observers outside of the event horizon by the use of light signals. However this represents a violation of the Strong Principle of Equivalence, which states that Special Relativity must hold locally for all local observers at all spacetime points in the universe. Thus black holes have always been in violation of the Strong Principle of Equivalence in General Relativity, and for this reason a new understanding of the physics involved is required.

Rarely mentioned is another seeming contradiction; if black holes are the place where

– 4 –

light cannot escape to the rest of the universe, how does it happen that they are the most luminous objects in the universe? The currently accepted answer is that the luminosity originates in an accretion disc around the black hole. However this picture fails because a "standard black hole model" of quasars which can explain spectral states involving radio loud and radio quiet emission cannot be found. Instead, patchwork additions to the black hole theory need to be added in an ad hoc manner as surprising observations of radio, X-ray, and outer "dusty torus" structures accumulate. For this reason the standard black hole picture of quasars is very limited in its predictive power.

In spite of these difficulties, black holes were consistently invoked in all discussions of quasars since the discovery in 1964 (Schmidt, 1965). Today, practically any theoretician will say with certainty that the objects at the centers of galaxies are black holes, and will also say that black hole theory is reasonably well understood.

But this ignores the fact that two new key observations were not at all anticipated or predicted by this standard black hole theory.

The first unexpected observation by Robert Antonucci (1993) showed that the quasar objects must be surrounded by a "dusty torus" region whose elliptical contoured surface guides the Elvis outflow wind structure. The theory community responded by cobbling up an ad hoc theory for the dusty torus, which has not survived modern scrutiny. A recent study of UV-optical continuum reverberations by Lovegrove et al showed that all 55 of the radio quiet quasars studied show evidence of this structure, establishing that it is a universal property of quasars not predicted theoretically.

A second discovery will be the subject of this report. The standard black hole theory predicts that an accretion disc penetrates to the inner region at 6 gravitational radii, or perhaps a bit less. Since a black hole has no hair, meaning that no magnetic field can penetrate its event horizon, there cannot be a centrally anchored dipole magnetic field in

the innermost region. But direct observation of reverberation of the optical light from the center of quasar Q0957 shows that the inner region is surprisingly swept clear, as if by a strong rotating magnetic field from its central supermassive compact object. Furthermore, the inner accretion disc edge has the apparent structure of a hot ring, again suggesting that a strong centrally located magnetic field is abrading the inner accretion disc edge and strongly heating it. The existence of such a centrally located magnetic propeller effect inside of the accretion disc strongly contradicts the standard black hole theory.

The existence of such a hot ring where none was expected has already been reported by Schild et al (2006, hereafter SLR06). However that report brought in many reverberation and microlensing observations of many kinds that were most often collected to study the time delay measured for calculation of the Hubble constant, or the nature of the baryonic dark matter. So many key observations are presently scattered in an unfocused literature already published. To fortify the conclusion based on these results, we present in this report a summarized compendium of the results of published investigations in order to make a comparison of relevant observations to competing theoretical models.

Recall that the Q0957+561 A,B quasar lens system, the first discovered multiple image gravitational lens system (Walsh, Carswell, and Weymann, 1979), was heavily observed in the two decades since its discovery with the expectation that measurement of its time delay would allow determination of the Hubble constant by the Refsdal (1964) method, independent of the classical methods based upon Cepheids. With the discovery of the time delay by Schild and Cholfin (1986) an unexpected rapid microlensing was found (Schild 1996), and since the baryonic dark matter implications eclipsed the time delay and Hubble constant program, a long literature that followed (Schild 2004a, 2004b, 2007, Schild & Dekker, 2006) emphasized the rapid microlensing.

But the same measured brightness record had implications for the nature of the

luminous quasar structure as well. Already the first Q0957 rapid microlensing report by Schild (1996) concluded that the quasar must be larger than previously believed, and "dominated by rings or shells." A double-ring model simulation by Schild and Vakulik (2003) showed that the amplitudes and the durations of the observed microlensing brightness fluctuations on long and short time scales could be understood to be compatible with reverberation and autocorrelation measurements.

The structure of this paper is as follows. In sections 2-5 we discuss the basic statistics defining the accuracy of the data, followed by a detailed discussion about the reverberation data used to infer the location of the Elvis outer outflow wind structure, and the signature of a sharp ring at the inner edge of the accretion disc. Then in sections 6 and 7 we conclude by showing that, instead of a black hole driven structure, the observational results for Q0957 favor structure dominated by a central dipole field of a MECO object in a low-hard state. In an appendix we show how an additional contradiction of standard black hole physics related to space connectivity for the completeness of quantum fields, can be resolved if MECO instead of black holes are the central compact objects in quasars

2.   The Q0957 Brightness Monitoring Data Quality and Quantity

We begin with a discussion about the quality of brightness monitoring data. The analyzed data table, available online at http://www.cfa.harvard.edu/ rschild/fulldata2.txt reduces all data taken on an individual calendar night and averages the data together, and assigns an observation time from the mean for the individual observations. Data are almost always averages of 4 CCD image frames analyzed for brightness separately. This usually gives 4 nightly brightness estimates, which usually have a 1-sigma rms near .01 mag, or 1% brightness error for the nightly mean. Independent confirmation of this estimate was made by statistician David J. Thomson, who estimates nightly average errors of 0.006 and 0.008

– 7 –

mag for the A and B images, respectively (Schild and Thomson, 1995). A comprehensive analysis of the statistics of the data set focused on the time delay controversy is given in Thomson and Schild (1997).

Figure 1 is a plot showing the number of nights where there is data overlap between images A and B after correction for cosmological time delay. This includes interpolations of up to 2 days, meaning suppose one makes an observation on Jan 1 2000. Then does one have an observation for Jan 1 + 417 days in 2001, with the possibility that on Jan 1 + 417 days one actually made the observation on that date, or could interpolate to that date with at most a 2-day interpolation window? This makes sense, where our sampling rate is 1 day so the Nyquist frequency is 2 days. We can still expect that the data point compared to image A on Jan 1 2000 will have a magnitude estimate accurate at the 1% level for 417 days later, after the Q0957 brightness record structure function given by Colley and Schild (2000).

Thus Figure 1 shows how many dates for image A observation will have a 1 % accurate image B brightness estimate. When this plot was made in Jan 1993, for any date of observation of image A there would be several hundred 1% quality measurements for image B made 417 days later. We are interested in lags in this plot of less than 10 nights. The Fig. 1 plot shows that by 1993, at least 270 data points define brightness for lags up to 10 days from the cosmological 417 days lag.

This means that when one compares the measured brightness of image A with brightness of image B, 417 +/- 10 days later, that brightness is estimated with high accuracy. Over 200 points overlap. Therefore we may conclude that we know very well the brightness properties of the two images for lags near the cosmological lag, 417.1 days (Colley et al, 2003).

The quality of the data, usually expressed as a 1 σ error, has been commented upon

repeatedly. Thus Schild and Thomson (1995) reported a median error of 0.006 magnitudes for both images, and Schild and Thomson (1997) reported mean error estimates of (.00954, .01202) for images (A,B). And when Colley and Schild (2000) compared their refined magnitude estimates with the long Schild et al record, they found mean rms differences of only (.006, .008) magnitudes for images (A,B). Because the quasar shows nightly brightness fluctuations of approximately 1%, and larger trends on longer time scales, these trends are well measured with available photometry. The observed nightly brightness fluctuations for Q0957 have been expressed as a structure function by Colley and Schild (2000) and as a wavelet amplitude by Schild (1999). Hence on the basis of the above analysis it is safe to conclude that both the quality and the quantity of quasar brightness data are sufficient to allow meaningful analysis of the quasar's internal structure to be made.

3.   Outer Quasar Structure Seen in Autocorrelation and Simple Inspection

The Figure 2 auto-covariance (auto-correlation) plot is expected to show correlation on time scales related to the outer Elvis structures, around 100 proper days, and structure related to the inner edge of the accretion disc. In Fig. 2, which was originally shown at the 1993 Padua Symposium (Thomson and Schild, 1997) the auto-correlation for the A (dashed) and B (solid line) images are shown together. Multiple peaks for time lags near 100 proper days are presumed to result from a disturbance taking place at the inner region of the quasar, near the inner edge of the accretion disc, and then with reflections or fluoresces off the Elvis outflow structures which are expected near to but just within the light cylinder radius (Schild and Vakulik, 2003; SLR06, SLR08). Because microlensing is expected to cause complications in the detection of these outer reflections, the B image with its higher microlensing optical depth should show different autocorrelation than A. Thus we have included a schematic "bottom" or "continuum" level in figure 2 for the two quasar

– 9 –

images. This emphasizes how similar the peaks measured for the two lensed images are in amplitude and width. Since microlensing can locally amplify random parts of the quasar structure, we consider as significant only peaks found in the autocorrelation estimates of both images.

The images arising in the lowest-lag Elvis structure, at 129 and 190 days (observer's clock), have about the same width, about 50 days, and half again larger widths of 75 days, for 540 and 620 day lag peaks. The 620 day lag peak is not convincing, by itself, and call it unobserved if you like, but if somebody insists that it must be there, one could argue that it is.

A similar pattern of quasar optical reverberations are now recognized by direct inspection of the measured brightness curves in a second lensed quasar system, the Einstein Cross (Q2237), with excellent quality data (Wozniak et al 2000) available at:

http://www.astrouw.edu.pl/ ogle/ogle3/huchra.html

In examining the above website the reader is encouraged to scroll down to see the plot of optical brightness monitoring for the 4 lensed images. The pattern of brightness peaks to be seen are similar in amplitude and duration to similar peaks found in Q0957. The Einstein Cross peaks I refer to are best seen in the upper green plot for image A, and the peaks occurred at (HJD - 24400000) = 2500, 2950, and 3300, with possibly more, but microlensing makes interpretation insecure. The peaks have a brightness amplitude of approximately 0.2 magnitudes and durations of approximately 50 days. The peaks have been discussed in the context of quasar structure by SLR08. These peaks were used by Vakulik et al (2006) to determine the time delays of the quasar images.

Comparison of the Q2237 direct brightness curves shows that reverberation of a central quasar disturbance reflects off the outer quasar structure at lags and time durations about

as inferred from the Q0957 autocorrelation estimates. We find that for both quasars, outer structure gives reverberation estimates of size at observed scales near 200 days and observed widths near 75 days; with (1+z) cosmological time dilation correction, these become proper (intrinsic) reverberation delays near 100 days and widths near 25 days.

Of more interest is the question of whether structure is evident on scales comparable to the expected structure at the inner edge of the accretion disk, at $6R_G$. This size scale would correspond to elapsed times of less than a day on the observer's clock. Moreover, in typical autocorrelation estimates, any significant noise contribution should decrease calculated correlation away from 0 lag; detection noise and cosmic dispersion cause longer lags to give strongly decreasing correlation. But here, the curves are quite different; the Q0957 inner structure has the character of wide peaks of approximately 10 days, with additional sub-peaks at 15 days (A image) and 5 days (B image). This means that for these short lags the data are correlated, and insofar as the quasar is bright today it will probably also be bright for 10 days or so. In other words, an inner structure is in evidence, and insofar as the autocorrelation peak reflects internal structure limited by causality at light propagation speed, a structure size scale is implied. Since an inner scale of 1 light day for the inner accretion disc edge is expected but not observed, and since instead a broad inner plateau is found, we conclude that the inner Q0957 quasar structure is not at the location of the innermost stable orbit (or that quasar brightening effects propagate much slower than light speed). A further discussion of the nature of this reverberation plot allowed Schild (2005) to infer the quasar orientation with respect to the plane of the sky. Even more importantly, SLR06 showed how this data implied the existence of a bright narrow band at the inner edge of the accretion disc, which was required to explain the extremely rapid 5-hour brightness fluctuations that were seen in the microlensing data.

We present in Fig. 3 a more recent cross-correlation calculation with finer output

scaling that shows better the results for 10-day lags, which relate more to the central quasar structure. This calculation from 1995, with half again as much data, is for A image alone. The peaks from the outer Elvis structures at 129 days and 190 days are strong. Their widths are comparable, about 45 days, which is twice the width of the peak around 0 lag, suggesting that the widths are dominated by the light scattering or fluorescence from the Elvis structures, which have larger dimensions, as estimated in SLR06.

It is now extremely significant that the auto-correlation has strong structure between 0 and 25 day lags. Recall that for noise-dominated data the data point for 0 lag should be highest and the autocorrelation function should rapidly decline for lags of 1, 2, 3, ... 10 days. But the plot shows sub-peaks around 6, 11, and 20 days, within a broad general peak of about 25 days width. This probably is the result of the Q0957 quasar's innermost structure.

Figure 4 shows similar data for the B image. It gives similar results for the 129 and 190 day peaks, understood to be related to the outer Elvis structures. The heights and widths are similar for the Elvis peak lags at 129 and 190 days seen in image A (Fig. 3).

And the inner peak again has a width of about 25 days, with again substructure peaks at 5 and 20 days. The fact that these inner sub-peaks do not exactly agree probably has to do with microlensing, (which originates in the random star field in the lens galaxy), of this inner structure.

Combining results from Figures 3 and 4 showing autocorrelation estimates from 1995, we have the suggestion of structure on time scales of 6, 11, and 20 days and an overall size limit for the inner quasar structure of approximately 25 light days (observed).

4.   Results from Cross-correlation analysis

The above two plots have been about autocorrelation. Now we wish to discuss the previously published plots for CROSS-correlation.

First you must ask yourself, with many hundreds of data points of 1% quality and with observed nightly brightness fluctuations at least 1% between observations, isn't it obvious that for some cosmological time delay, say for example, 417 days, there will be a very large spike in the cross-correlation curve? With excellent data sampling, characterised by hundreds of data points at resolution of 1 day and with detection noise at or below the amplitude of quasar brightness fluctuations, this large spike should have a width of 1 or 2 days.

But this cross-correlation spike has never been found by any of the 10 research groups that have sought it.

Thus we immediately are confronted with the fact that probably the inner quasar structure is softening the expected cross-correlation peak. Fig. 5 is a cross-correlation plot to illustrate this. It was already published as Fig. 2 in Schild and Thomson (1997). Instead of a large spike with a 1-day half-width, we find a broad cross-correlation peak with a 50 day half width. The broad peak is punctuated by sub-peaks as already noticed by Schild and Thomson, who comment that the cross-correlation sub-peaks "... tend to have a uniform spacing of 16 days, which may correspond to an internal reflection within the inner quasar structure."

Everybody agrees that the central object must be illuminating the inner edge of the accretion disc, and that since we are dealing with high luminosity quasars one should use the Shakura-Sunyaev (1973) thin accretion disc model. For the case of a central black hole in Q0957, this would be at a radius less than or equal to $6R_G$, which is less than a light

day for either quasar system, even with cosmological (1+z) correction to the observer's clock. The fact that a luminosity associated with the inner edge of the accretion disc is not observed in cross-correlation, or autocorrelation, or microlensing for Q0957 means that there is nothing there. What is seen instead is the structure in the autocorrelation plot with sub-peaks around the 417-day peak of the overall autocorrelation curve, Fig. 5.

These sub-peaks are always around 10 days away from the cosmological time delay, 417 days, and so they are easily understood as the bright inner edge of the accretion disc that everybody agrees must exist. But this makes the inner quasar structure approximately 10 times larger than expected. With elaborate corrections for the inclination of the object, SLR06 found the luminous accretion disc inner edge to have a radius $\sim 70 R_G$ in Q0957, instead of the $\sim 6 R_G$ expected for a black hole. The sub-peaks in the Fig. 5 autocorrelation plot are around 379, 392, 408, 417, 420, and 425 days.

These cross-correlation experiments have long shown an interesting effect, namely that the cosmological time delay measured for this data has been changing with time. This was discovered in Thomson & Schild (1997) where contours of the cross-correlation time delay as a function of observation date are shown. It may be seen that the time delay peak was shortening with calendar date. This may be understood as a result of the magnification cusp of a microlensing star passing across the face of this quasar, and highlighting the internal structure progressively.

Thus from many points of view we infer that if there is any luminosity within $70 R_g$ we will have seen it selectively amplified at some time. Instead, we just seem to see those $70 R_g$ structures being selectively amplified at time scales near 10 days. Moreover, hypothetical structure at $6 R_G$ orbiting at the inner edge of the accretion disc, would be expected to create strongly periodic brightness fluctuations, not observed. On the basis of these observations it was concluded in SLR06 that an intrinsic magnetic propeller contained within the central

compact object of Q0957 had cleared out the inner region of the accretion disc. This was found to be consistent with the MECO model while being inconsistent with inner structure at $6R_G$ inferred for a standard black hole model. The existence of internal structure is probably part of the reason why seemingly reliable calculations do not consistently indicate the same time delay even for data sets considered reliable by Oscoz et al (2001).

The published SLR06 report contains an explanation for the cross-correlation peaks at the particular values around 392, 404, 424 days found, for the already determined inclination of the quasar and inner structure at a radius $\sim 70R_G$. The discussion in Section 2 of SLR06, which we do not repeat here, shows that inner luminous ring structure produces cross-correlation at a variety of lags as observed, since the nearest and farthest surfaces would both produce strong reflection.

Also discussed in SLR06 is the location of the radio emitting region. As demonstrated there, reverberation of the compact core radio emission has been found to be 30 days (observer's clock, UV-optical leading radio) and a series of microlensing events of the radio emission allow the size and fraction of the compact radio source emission to be determined from the duration and radio brightness amplitude of the events.

5.   The Implications of Rapid Quasar Microlensing

The preceding sections have detailed why we believe that evidence exists for quasar luminous continuum structure on size scales of the outer Elvis structure, 50 proper light days, and for an inner structure $\sim 70R_g$. But another observation shows an important characteristic of the inner structure.

In Fig. 6, which is a repeat of Colley and Schild (2003), we show a simple plot of the quasar brightness measured unusually carefully for the duration of the night, in 1995.9

and again 417 days later. In this plot, brightness measured for the first arriving A image is plotted as open circles, with a single data point and error bar plotted for the hourly averaged brightness. It may be seen that nightly brightness trends with typical amplitudes of .01 magnitude were found for the A image.

The brightness of the B image at the same quasar time, measured at Earth 417.1 days later and plotted as filled circles, shows evidence for the same pattern of brightness trends. Thus on JD-2449701.9 the A image underwent a 0.01 magnitude fading and the B image recorded 417 days later shows that the A fading was a continuation of a quasar fading trend that had begun several hours earlier. Similar trends observed on the 3 following nights provide simple evidence that the quasar has intrinsic brightness drifts with amplitude 0.02 magnitudes on time scales of 12 hours, that are being recorded with reasonable accuracy and seen at Earth with the 417.1 day cosmological time delay lag. And that the 417.1 day time delay found from a continuous monitoring campaign reported in Colley et al (2003) must be correct for this data sample.

Now we remark on the events recorded on JD - 2449706, where image A had a deep (2%) minimum and image B, observed 417 days later, had a shallow minimum. The difference between the two brightness trends must have been caused by microlensing. A more convincing plot of this observed event is shown as Fig. 2 in Colley and Schild (2003). This simple observation od a 1% microlensing brightness change in 5 hours proper time challenges theory on two points; it is not understood in the black hole model how the quasar can change brightness due to intrinsic quasar fluctuation processes for quoted accretion disc sizes, or how microlensing can change so quickly for the quoted quasar luminous accretion disc sizes. And for microlensing to occur on such short time scales, a fine structure in the microlensing caustic pattern due to a graininess of the mass distribution in the lens galaxy from planet mass microlenses must be present. Comparable fluctuations have been

simulated by Schild and Valukik (2003) with equal positive and negative sub-cusps on day time scales only if planet-mass microlenses dominate the mass of the lens galaxy.

We emphasize that the rapid microlensing event requires two physical effects not expected in astronomy; the quasar must have fine structure, and the mass distribution within the lens galaxy must be dominated by planetary mass bodies. Direct simulations of the Q2237 microlensing by Vakulik et al (2007) also conclude that the microlensing must be caused by Jupiter mass, $10^{-3}M_{\odot}$, compact objects.

Standard arguments of causality require that the existence of observed fluctuations intrinsic to the quasar imply structure on scales of 12 light hours, which after correction for cosmological (1+z) time dilation corresponds to a size scale of less than $1R_g$. With the spherical or cylindrical geometry assumed for the quasar central source, this implies the existence of a ring structure dimension of such size, and we have interpreted this as the radial thickness of the accretion disc inner edge, since that would be the smallest dimension associated with an accretion disc model. Thus the rapid fluctuations seen convincingly in Fig. 6 and found previously in the data and structure function, Figs. 3 and 5, of Colley & Schild (2000) probably imply the existence of quasar structure with significant luminosity on a small spatial scale of $1R_G$.

Further analysis in section 2 of SLR06 amplifies this result, with the additional conclusion that the linear increase in the wavelet amplitude with lag found by Schild (1999) is also compatible with a ring structure for the central emitting region.

6.   Summary and Model Comparison

The purpose of this section is to summarize the results from each preceding section, and to comment upon the relevance to the fundamental issue, which is whether these first

results of the direct detection of UV-optical and radio inner quasar structure favor a black hole or MECO interpretation.

In section 2, we considered the quantity and quality of data that contribute to the conclusion that Q0957 does not have accretion disc structure expected at approximately $6R_G$ (somewhat smaller for rapid rotation of the central object). We showed that hundreds of data points define the autocorrelation and cross-correlation estimates of structured quasar brightness trends, and their 1 % accuracy was emphasized.

In section 3 we emphasized that autocorrelation estimates for long lags, up to 2 years, showed structure that suggested that any disturbance seen first in the central region reverberates in outer structure that has size scales attributed previously to the Elvis outflow structures. Originally discovered in Thomson and Schild (1997) these structures now are interpreted to reveal the details of the quasar's central structure and orientation in space (Schild 2005).

We also found in section 3 that autocorrelation plots revealed the presence of UV-optical luminous inner structure not at the location of the innermost stable orbit (less than or on the order of $6R_G$) but rather at a much larger radius on the order of $70R_G$. This observation, consistent with the intrinsic magnetic propeller model associated with the MECO theory for quasar structure (SLR06), is not that which is expected from black hole quasar structure models. Figures 3 and 4 seem to indicate the existence of inner structure, and the width of the central autocorrelation peak (25 days, observed) is interpreted as a determination of the structure's central radius in light days.

In section 4 we recalled that many cross-correlation calculations have sought a sharp peak for the cosmological time delay, but it has not been found for any of the long brightness time-series records available. This is most easily understood as the result of the internal structure and its significant microlensing, and evidence for this interpretation

is probably seen in the fine structure of the cross-correlation estimates. The evident cross-correlation fine structure is arguably on the time scale of the inner structure evident in the auto-correlation plots, Figs 3 and 4, with evident structure at lags 10 - 20 days.

In section 5 we examined the evidence for a rapid microlensing that is seen to 99.9% significance in data obtained in two separate observing seasons. The generally good agreement of the data from the two seasons within the quoted error bars for overlapping data points provides confirmation that the brightness estimates and adopted time delay are correct. And the existence of such rapid microlensing requires the existence of sharp quasar structure that is incompatible with black hole physics and was not predicted before it was observationally discovered.

With these key observational results in mind, we discuss the comparison of standard black hole models to MECO model results. Although a general relativistic 3-dimensional simulation of a MECO object has not yet been undertaken, an analytical model has been created by Robertson and Leiter (2002, 2003, 2004, 2005) and is the basis for these conclusions.

Based on the analysis of the observational evidence presented in this paper it has been shown in SLR06 that Q0957+561 has the four intrinsic structural elements as follows:

- 1. Elliptical Elvis Structure located at distance Re from the central object and height He above the accretion disc plane: $Re = 2 \times 10^{17}$cm (320 R_G, 77 light days), He = 5×10^{16}cm (80 R_G, 19 light days).

- 2. Inner Radius of Accretion Disk: $R_{disk} = 4 \times 10^{16}$cm $= 64 R_G = 15$ light days.

- 3. Hot Inner Accretion Disk Annulus: delta(R) $= 5.4 \times 10^{14}$cm $= 1$ $R_G = 5$ light hours.

- 4. Base of Radio Jet: $R_{rad} = 2 \times 10^{16}$cm (8 light days), $H_{rad} = 9 \times 10^{16}$cm (35 light

days).

A cartoon illustrating a cross-section of this quasar structure model has been given as Fig. 1 in SLR06. Attempts to explain all four components of the observed inner structure of the quasar Q0957 in terms of standard central black hole models have failed for the following reasons:

a) Modeling them in terms of an intrinsic magnetic moment generated by a central spinning charged black hole fails because the necessary charge on the spinning black hole required would not be stable enough to account for the long lifetime of the inner quasar structure.

b) Modeling them in terms of a Kerr black hole ADAF accretion- disk-coronajet (Narayan & Quataert 2005; McKinney & Narayan 2007) in which the magnetic field is intrinsic to the accretion disk and not intrinsic to the central rotating black hole, fails because it cannot account for the very large opening angles for the coronal Elvis outflows, and in particular it cannot account for the hot thin inner disk annulus that is observed

c) Modeling them in terms of a Magnetically Arrested Disk (MAD) black hole (Igumenschev et al. 2003, Igmnenschev, 2008) fails since it cannot account for the hot thin inner disk annulus that is observed within the inner structure of Q0957. Instead the MAD simulations show a broad band of material starting at 74 Rg and extending inward to about 64 Rg from which a stochastic injection of "magnetic islands" of low density plasma would occur. These plasma blobs would not be visible to the observer since they would have a much lower optical luminosity compared to that of the accretion disc. Hence instead of the observed truncated disc with a very narrow annular band of material of radial thickness on the order or 1 Rg, the MAD model predicts a truncated disc with a broad irregular inner annular band of radial thickness on the order of 10 Rg. Thus it follows that the MAD black hole model can be ruled out as an explanation of the inner structure observed in Q0957+561

because if a MAD black hole accretion disc had been operating, the clean fluctuation signal associated with the hot ring structure would not have been seen.

However it has been shown that all the four components of the observed inner structure in the quasar Q0957+561 can be consistently described within the context of the Magnetospheric Eternally Collapsing Object (MECO) model described in SLR06, in which a very strong intrinsic magnetic field anchored to a highly redshifted rotating central compact MECO interacts in a magnetic propeller mode with the surrounding accretion disk and generates all the four components of the Q0957 structure. Such MECO models are characterized by highly redshifted, Eddington-limited, collapsing central compact objects containing strong intrinsic magnetic fields aligned with their MECO axis of rotation.

The MECO contains a central rotating magnetic object whose dynamo sweeps clean the central region of the quasar out to a distance at which the magnetic propeller acts on the inner edge of the accretion disk, and a radio-emitting region above the disk where magnetic field lines must twist and bunch up until they eventually break and reconnect at relativistic speeds. Such an object does not have an event horizon; instead, infalling material collects at an inner structure just beyond 2Rg that further collapses to higher redshift while remaining in causal connection for all time. Because of the small light cone angle for radiation escaping from this highly redshifted region to the distant observer, the resulting low luminosity in the far-infrared wavelengths makes this region difficult to detect.

In the MECO model for Q0957, the magnetic propeller interacts with the inner regions of the accretion disk and creates a very thin hot inner annular (band-like) structure and an outer coronal structure characterized by strong relativistic outflow with a wide opening angle to the z-axis of rotation as is observed. In addition the size and location of the radio-emitting region associated with the structure in the quasar Q0957+561 have been found to correspond to the region above the central compact object where the reconnection

of magnetic field lines at relativistic Alfven speeds, like that generated by a rotating central MECO containing an intrinsic magnetic field, should occur. The structures found to dominate the UV-optical and radio emission are shown correctly scaled in Figure 7.

It is important to note that the MECO model that best fits the inner structure observed in the quasar Q0957+561 differs significantly from most black hole models currently under consideration. In particular, the observed structure they generate seems to resemble the complex inflow-outflow pattern seen in magnetic propeller models for young stellar objects. The action of such magnetic propeller forces on young stellar objects has been discussed and simulated by Romanova et al. (2002, 2003a, 2003b) with non-relativistic models that produce observable structures whose spatial geometry is very similar to the inferred Schild-Vakulik (2003) structure.

On the basis of the above arguments we come to the conclusion that observation of the four components of the stable non-standard inner structure within the quasar Q0957+561, and especially the existence of the hot thin inner disk annulus that is observed, represents strong evidence for the existence of an observable intrinsic magnetic moment, generated by a supermassive $3 - 4 \times 10^9 M_\odot$ MECO acting as the central compact object in this active galaxy, which implies that this quasar does not have an event horizon.

7.   Concluding Remarks

We have shown that a comprehensive analysis of the gravitational lensing and microlensing observations of the quasar Q0957 indicates that the internal structure of this quasar appears to be dominated by a highly redshifted supermassive central compact object that contains an observable intrinsic magnetic moment and therefore cannot be described by a black hole. The implications of this startling discovery are so profound that it is

– 22 –

necessary to clarify and review the supporting observational evidence.

For the benefit of the astrophysics community, this paper has summarized within
a single document the full list of unique gravitational microlensing and reverberation
observations of quasar Q0957 which have permitted a detailed reconstruction of the intrinsic
structures emitting radiation from its interior regions. Surprisingly these observations failed
to reveal the expected accretion disk extending in close to the central object. Instead it
was found that the inner accretion disk contained a large empty region which ended at a
large radius where we found a thin hot inner ring. In addition, it was found that there was
a large hyperbolic Elvis outflow structure about ten times further out.

The four components associated with these internal structures were found to be similar
to the features revealed in simulated accretion flows into the central magnetic dipole
objects contained within Young Stellar Objects, which have been successfully simulated
by Romanova et al. Hence our main conclusion was that we were seeing a similar type of
central magnetic object in this quasar and if so, such an object cannot be a black hole
because black holes cannot possess an intrinsic anchored magnetic dipole field. Hence these
observations were found to represent strong evidence for the existence of a new kind of
central collapsed object in the quasar Q0957 called a "Magnetospheric Eternally Collapsing
Object" (MECO) which is permitted within the framework of general relativistic gravity
(SLR06).

MECO form by the same gravitational collapse process believed to result in black
holes, but due to internal Eddington limited radiation pressure, they are never observed to
collapse through an event horizon (Mitra, 2006). Due to the extreme surface redshift of a
MECO, its surface radiation is too faint to be easily detected at astronomical distances.
Hence MECO differ observationally from black holes primarily by the ability of the MECO
to exhibit observable manifestations of its intrinsic magnetic field on its surrounding

accretion disk and environment.

While many models of quasars based on black holes exist in the literature, none of them are able to account all four of the components of the internal structure observed within Q0957. This was especially true for the observed inner accretion disk structure, which contained a large empty region that was truncated at a large radius by a very thin hot inner ring (illustrated white in Figure 7) characteristic of an intrinsic magnetic propeller interaction with the accretion disc. Hence we conclude in response to the question asked in the title of this report, that the observational evidence for the existence of a very hot thin luminous ring deep within quasar Q0957 represents a strong observational argument in favor of the existence of a supermassive MECO in the center of this quasar, instead of a black hole.

8.   Acknowledgements

– 24 –

9.   Appendix I: Resolution of the Black Hole Information Paradox and the MECO Membrane Paradigm

Our main report was written specifically to show how direct observation, of a hot thin ring within the internal structure of the quasar Q0957, favors the existence of an intrinsically magnetic MECO object residing at the center of this quasar rather than a black hole. In this appendix we briefly discuss two additional properties of MECO which are more esoteric, but are nonetheless further capable of distinguishing them from Black Holes. The first property is associated with the manner in which the MECO resolves well-known the Black Hole Information Paradox, while the second is associated with what is known as the MECO Membrane Paradigm.

9.1.   The MECO Resolution of the Black Hole Information Paradox

The Black Hole Information Paradox(1) results from the application of quantum field theory near the event horizon of a black hole which by necessity contains an internal singularity which can ultimately destroy all information about the physical objects which penetrate through the event horizon. Because of this, the black hole has the capability to perform non-unitary, information destroying measurement processes on the states of entangled quantum systems located outside of the black hole event horizon. This leads to the Black Hole Information paradox because this type of black hole information destroying measurement process violates the Principle of Unitarity associated with the conservation of probability in quantum field theory.

This type of quantum information paradox does not occur for the MECO. This is because its highly red shifted physical surface dynamically prevents the formation an event horizon containing internal information destroying singularities. Since there is no internal

information destroying singularity inside of the MECO, the surface of the MECO has the potential to perform an irreversible non-unitary measurement process, on the state of an entangled quantum system initially located outside of the event horizon, without violating the Principle of Unitarity associated with the conservation of probability in quantum field theory. In summary no quantum information paradox results for the MECO because: a) it satisfies the Strong Principle of Equivalence which implies that the inside and the outside of the MECO are capable of being connected by light signals, and; b) there are no singularities inside of the MECO surface which can destroy information.

9.2.   The MECO Membrane Paradigm

The best way to understand the MECO Membrane Paradigm is by comparing it to the well-known Black Hole Membrane Paradigm (Price et al, (1988)). Since black holes have event horizons which are not physical surfaces, the Black Hole Membrane Paradigm is actually only an approximation used for visualizing and calculating the effects predicted by quantum field theory applied to the exterior physics of black holes. It models the black hole as having a thin classically-radiating surface vanishingly close to the black hole's event horizon. In this picture the black hole is described by an array of exterior, stationary, non-inertial observers whose coordinate system ends at $r = 2R_g = 2GM/c^2$, since such observers cannot hover at or below the black hole event horizon under the rules of standard general relativity. These fiducial observers describe the "Hawking Radiation" (Hawking, (1975) produced by black holes as being emitted by an arbitrarily-thin shell of "hot" material at or just above the critical radius $r = 2R_g$ where this coordinate system fails. Hence while the physical effects of Hawking Radiation appear to be occurring all the way down to the event horizon of the black hole at $r = 2R_g$, they do not actually come from the event horizon because it is not a physical surface. However by associating this radiation

with a hypothetical thin radiating membrane located near the horizon, this allows models to be constructed which do not explicitly contradict general relativity's prediction that the boundary associated with the event horizon at $2R_g$ is inescapable.

In contradistinction to the case of black holes, MECO have highly red shifted physical surfaces which are not event horizons. Hence a MECO Membrane Paradigm can be constructed which is an exact result that can be used for calculating the effects predicted by quantum field theory exterior to the MECO surface. The highly red shifted Eddington limited radiating physical surface of the MECO is dynamically balanced by radiation pressure just outside of the radius $R = 2R_g$. In this context the MECO Membrane Paradigm states that this highly red shifted physical surface can be described by an array of exterior, stationary, non-inertial observers whose coordinate system can be continued up to and thru this physical surface of the MECO. This is allowed in the absence of an event horizon, since under the rules of standard general relativity such observers can dynamically hover at or below the physical surface of the MECO.

Since the red shift of the MECO surface has a large but finite value, Hawking Radiation plays no significant role in its dynamics. Instead the fiducial observers describe the source of the thermal radiation, produced by the highly red shifted MECO surface just outside of $R = 2R_g$, as being due to synchrotron radiation generated by a "hot" internal electron-positron plasma in the presence of the very strong intrinsic magnetic field of the MECO. Since there is no event horizon the physical effects of this surface radiation appear to be occurring all the way down as well, coming through the highly red shifted surface of the MECO.

Because of the very high red shift associated with the surface of the MECO, a distant fiducial observer would view the highly red shifted surface of MECO Membrane as containing information about the entire history of the MECO and its environment.

– 27 –

Hence the MECO Membrane Paradigm implies that the highly red shifted surfaces of the MECO have properties which allow them to act like cosmological memory storage devices within which the entire history of the Universe may be stored. This physical phenomenon associated with the MECO Membrane Paradigm may play a fundamental role in cosmological models of consciousness in the universe (Schild, 2010).

REFERENCES

Antonucci, R. 1993. Unified Models for Active Galactic Nuclei and Quasars. Annual
     Reviews of Astronomy and Astrophysics, 31, 473-521.

Colley, W. & Schild, R. 2000, "Hourly Variability in Q0957+561," ApJ, 540, p. 104-112

Colley, W. & Schild, R. 2003. A Rapid Microlensing Event in the Q0957+561A, B
     Gravitational Lens System. ApJ, 594, 97-100 (CS03).

Colley, W. et al, 2003. Around-the-Clock Observations of the Q0957+561A,B Gravitationally
     Lensed Quasar. II. Results for the Second Observing Season. ApJ, 587, p 71-79.

Hawking, S. 1997. Black Holes and the Information Paradox, Scientific American, April
     1997 (cover story)

Igumenshchev, I. Narayan, R. and Abramowicz, M. 2003. Three-dimensional Magneto-
     hydrodynamic Simulations of Radiatively Inefficient Accretion Flows. ApJ, 592, p
     1042-1059.

Igumenshchev, I. V. 2008, Magnetically Arrested Disks and the Origin of Poynting Jets: A
     Numerical Study. ApJ 677, p317-326.

McKinney, J. & Narayan, R. 2007. Disc-jet coupling in black hole accretion systems - II.
     Force-free electrodynamical models. MNRAS, 375, p 513-547.

Mitra, A., 2006. Sources of stellar energy, Einstein Eddington timescale of gravitational
     contraction and eternally collapsing objects. New Astronomy, 12, p146-160.

Narayan, R. & Quataert, E. 2005. Black Hole Accretion. Science, 307, p 77-80.

Oscoz, A. et al, 2001, Time Delay in QSO 0957+561 from 1984-1999 Optical Data. ApJ,
     552, p81-90.

Price, R. and Thorne, K. 1988. The Membrane Paradigm for Black Holes. Scientific
        American, vol 258, No. 4(April 1988), p69-77.

Refsdal, S. 1966. On the possibility of determining Hubble's parameter and the masses of
        galaxies from the gravitational lens effect. M.N.R.A.S. 128, p307.

Robertson, S. and Leiter, D. 2002. Evidence for Intrinsic Magnetic Moments in Black Hole
        Candidates. ApJ, 565, p447-454

Robertson, S. and Leiter, D. 2003. On Intrinsic Magnetic Moments in Black Hole
        Candidates. ApJ, 596, L203-206.

Robertson, S., and Leiter, D. 2004. On the origin of the universal radio-X-ray luminosity
        correlation in black hole candidates. MNRAS, 350, p1391-1396.

Robertson, S., and Leiter, D. 2005, " The Magnetospheric Eternally Collapsing (MECO)
        Model of Galactic Black Hole Candidates and Active galactic Nuclei. In "New
        Directions in Black Hole Research," ed. P.V.Kreitler, Nova Science Publishers, Inc,
        ISBN 1-59454-460-3, novapublishers.com, p1-45.

Romanova, M. et al, 2002. Magnetohydrodynamic Simulations of Disk-Magnetized Star
        Interactions in the Quiescent Regime: Funnel Flows and Angular Momentum
        Transport. ApJ, 578, p420-438.

Romanova, M. et al, 2003a. Magnetohydrodynamic Simulations of Accretion onto a Star in
        the "Propeller" Regime. ApJ, 588, p400-407.

Romanova, M. et al, 2003b. Three-dimensional Simulations of Disk Accretion to an Inclined
        Dipole. I. Magnetospheric Flows at Different Theta. ApJ, 595, 1009-1031.

Romanova, M. et al, 2004. The Propeller Regime of Disk Accretion to a Rapidly Rotating
        Magnetized Star. ApJ, 616, L151-155.

Schild, R., 1990. The time delay in the twin QSO Q0957 + 561. AJ, 100, p1771-1776.

Schild, R. E. 1996. Microlensing Variability of the Gravitationally Lensed Quasar Q0957+561 A,B. ApJ, 464, p125-130.

Schild, R. E. 1999. A Wavelet Exploration of the Q0957+561A,B Brightness Record. ApJ, 514, p 598-606.

Schild, R. E. 2004a. Some Consequences of the Baryonic Dark Matter Population. astro-ph/0409549.

Schild, R. E. 2004b. The Detection and Nature of the Baryonic Dark Matter. astro-ph/0406491.

Schild, R. E. 2005. Accretion Disk Structure and Orientation in the Lensed and Microlensed Q0957+561 Quasar. AJ, 129, p1225-1230.

Schild, R. E. 2007, The Evolution of the Chemical Elements of the Universe. astro-ph/07082917.

Schild, R. E. 2010. A Computer Model of Consciousness. in Anthropology of Consciousness, in preparation

Schild, R. E., & Cholfin, B. 1986. CCD camera brightness monitoring of Q0957 + 561 A, B. ApJ, 300, p 209-215.

Schild, R. E., & Thomson, D.J. 1995. Twin QSO Q0957+561 Time Delay Dataset. AJ, 109, p1970.

Schild, R. E. & Thomson, D.J. 1997. The Q0957+561 Time Delay From Optical Data. AJ, 113, p130.

Schild, R. E. & Vakulik,V. 2003. Microlensing of a Ring Model for Quasar Structure. AJ,
     126, p 689-695.

Schild, R. E. & Dekker, M. 2007. The Transparency of the Universe limited by Ly-alpha
     Clouds. A.N. 327, p729.

Schild, R. Leiter, D. & Robertson, S. 2006. Observations Supporting the Existence of an
     Intrinsic Magnetic Moment inside the Central Compact Object within the Quasar
     Q0957+561. AJ, 132, p420-432 (SLR06).

Schild, R. Leiter, D. & Robertson, S. 2007. Direct Microlensing-Reverberation Observations
     of the Intrinsic Magnetic Structure of Active Galactic Nuclei in Different Spectral
     States: A Tale of Two Quasars. AJ, 135, p 947-956.

Schmidt, M. 1965, Optical Spectra and Redshifts of 31 Radio Galaxies. ApJ, 141, 1.

Shakura, N. & Sunyaev, R. 1973. Black holes in binary systems: Observational appearance.
     A&A, 24, p 337-355.

Suskind. L. 1997, Black Holes and the Information Paradox, Scientific American, April 1997
     (cover story).

Susskind, L. (2008), The Black Hole War: My Battle with Stephen Hawking to Make the
     World Safe for Quantum Mechanics, Little, Brown, ISBN 0-316-01640-3.

Thomson, D. J. & Schild, R. 1997, in Applications of Time Series Analysis in Astronomy
     and Meteorology, ed. T. Subba Rao, M. Priestly, & O. Lessi [Chapman and Hall:
     New York], p187.

Vakulik, V. et al, 2006. Observational determination of the time delays in gravitational lens
     system Q2237+0305. A&A, 447, p905-913.

– 32 –

Vakulik, V. et al, 2007. Q2237+0305 source structure and dimensions from light-curve simulation. MNRAS, 382, p819-832.

Walsh, D. Carswell, R. and Weymann, R. 1979. 0957 + 561 A,B - Twin quasistellar objects or gravitational lens. Nature, 279, p381-384.

Wozniak, H. et al, 2000. The Optical Gravitational Lensing Experiment Monitoring of QSO 2237+0305. ApJ, 529, p88-92.

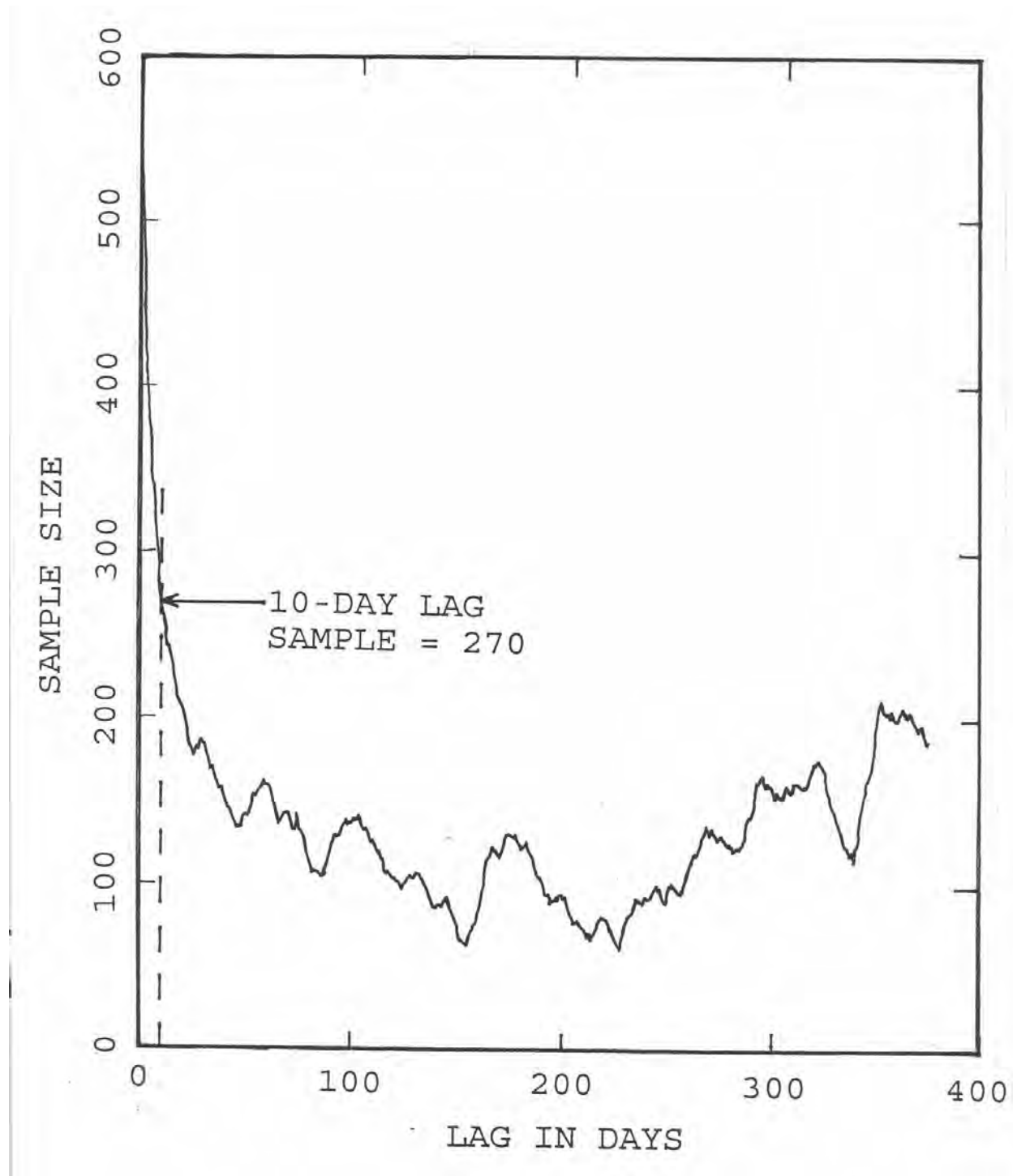This manuscript was prepared with the AAS LATEX macros v5.2.

Fig. 1.— The data sample size emphasizing the number of nights contributing to correlation estimates of quasar brightness. As described in the text, interpolations of up to 2 days were included to describe the quantity of data contributing to correlation calculations. For the present example, data measured first in image A and compared to the later arriving B image, measure in the hundreds, for lags relevant to quasar structure, as well as to microlensing.
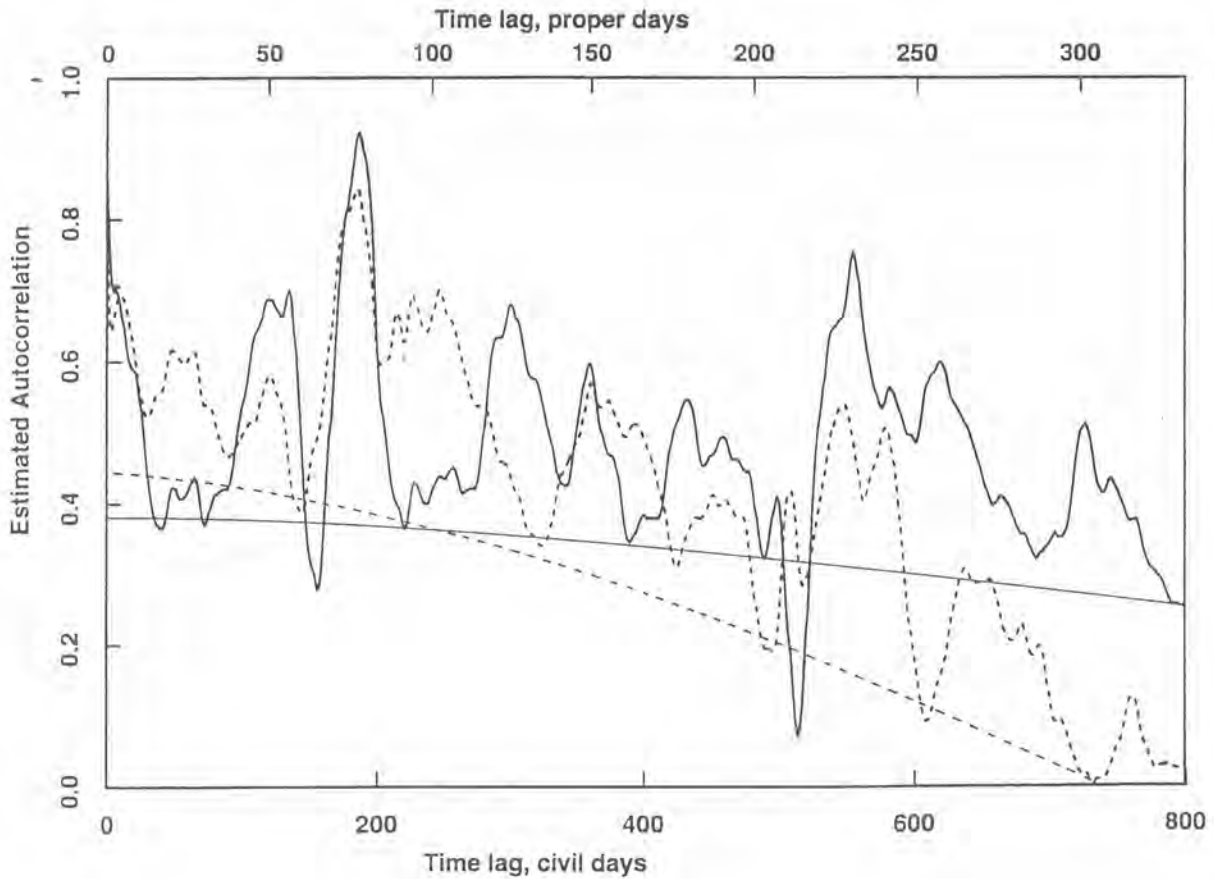
Fig. 2.— An autocorrelation plot for the A (dashed curve) and B(solid curve) quasar images. While previously this data analysis was used to infer the quasar outer structure, we now emphasize the evidence for inner structure, for lags less than 20 days (civil days). The central peak, near 0 lag, does not have the rapid falloff with a time scale near the sampling time expected for noise-dominated data. Instead it shows structure on time scales near 20 days, understood as indicative of inner quasar structure.
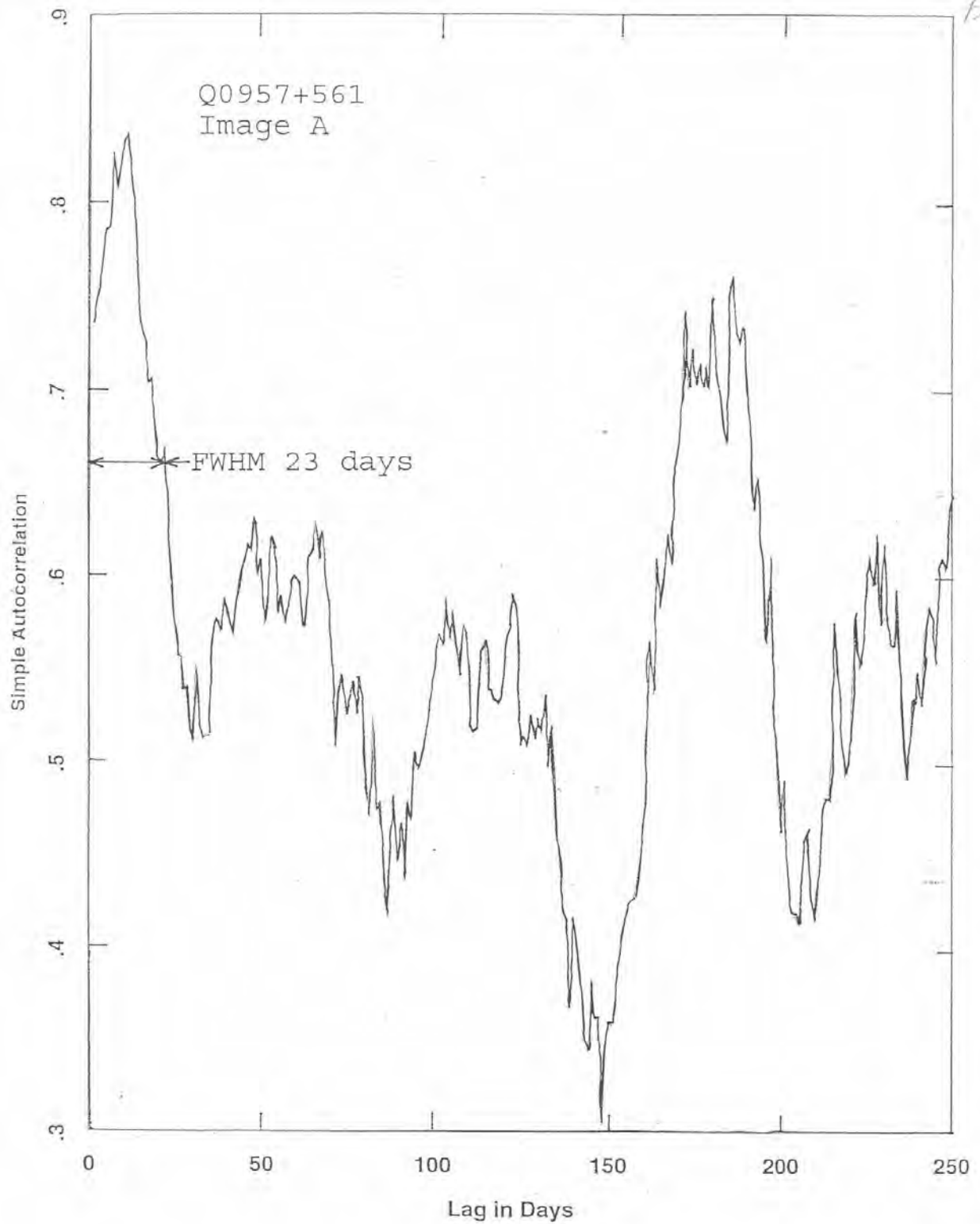
Fig. 3.— An autocorrelation plot of the image A data with finer resolution for smaller lags. Prominently seen are the lags for outer Elvis structures, as well as structure from the central peak with an overall half-width of 23 days and finer sub-structure at 6, 11, and 20 days.
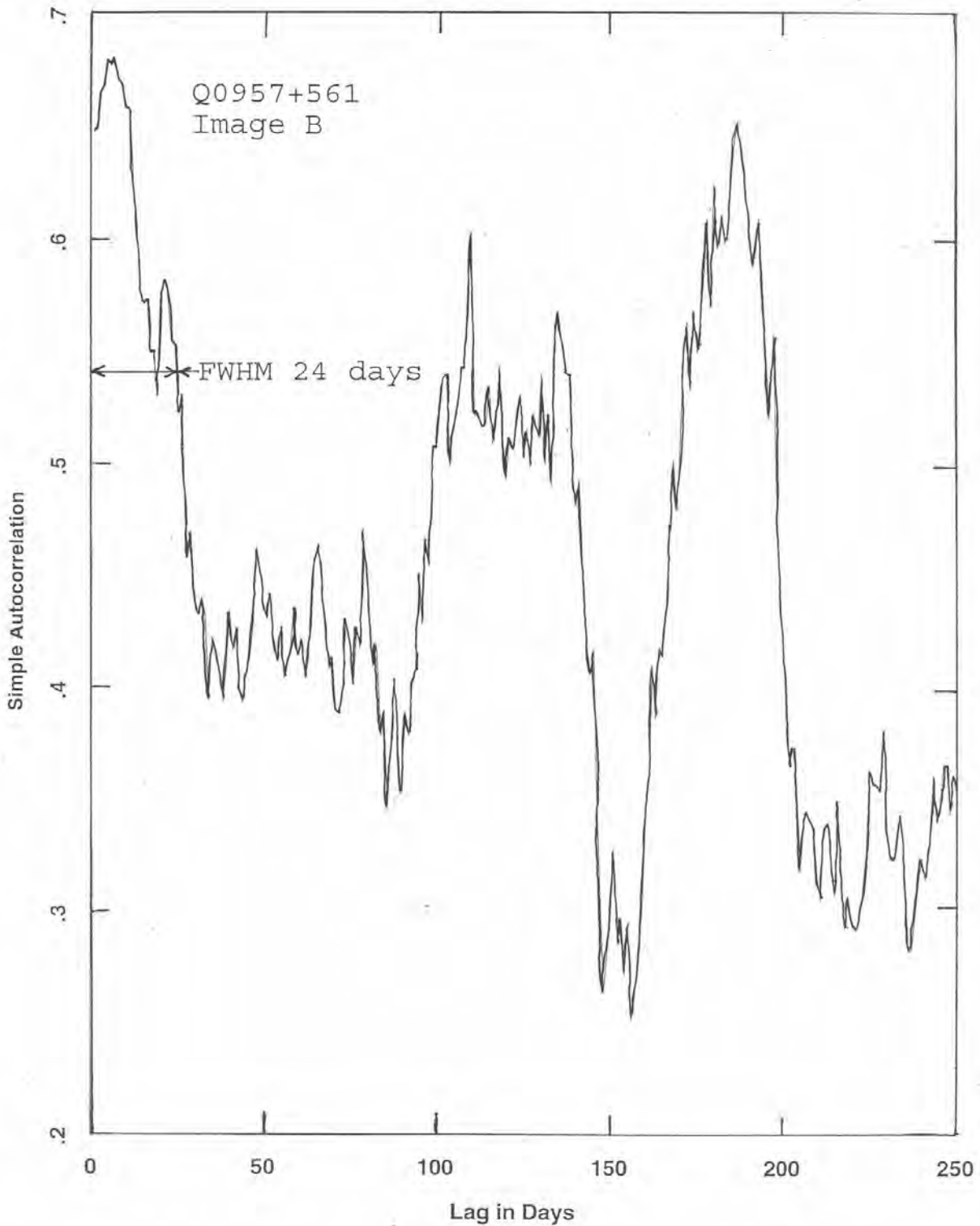
Fig. 4.— A fine structure autocorrelation plot for the B quasar image. Strong autocorrelation peaks at 129 and 192 days from the outer Elvis structures are evident. Also well seen is the structure surrounding the central peak and evidencing central quasar structure. The overall width is approximately 24 days, and substructure peaks are found at 5 and 20 days.
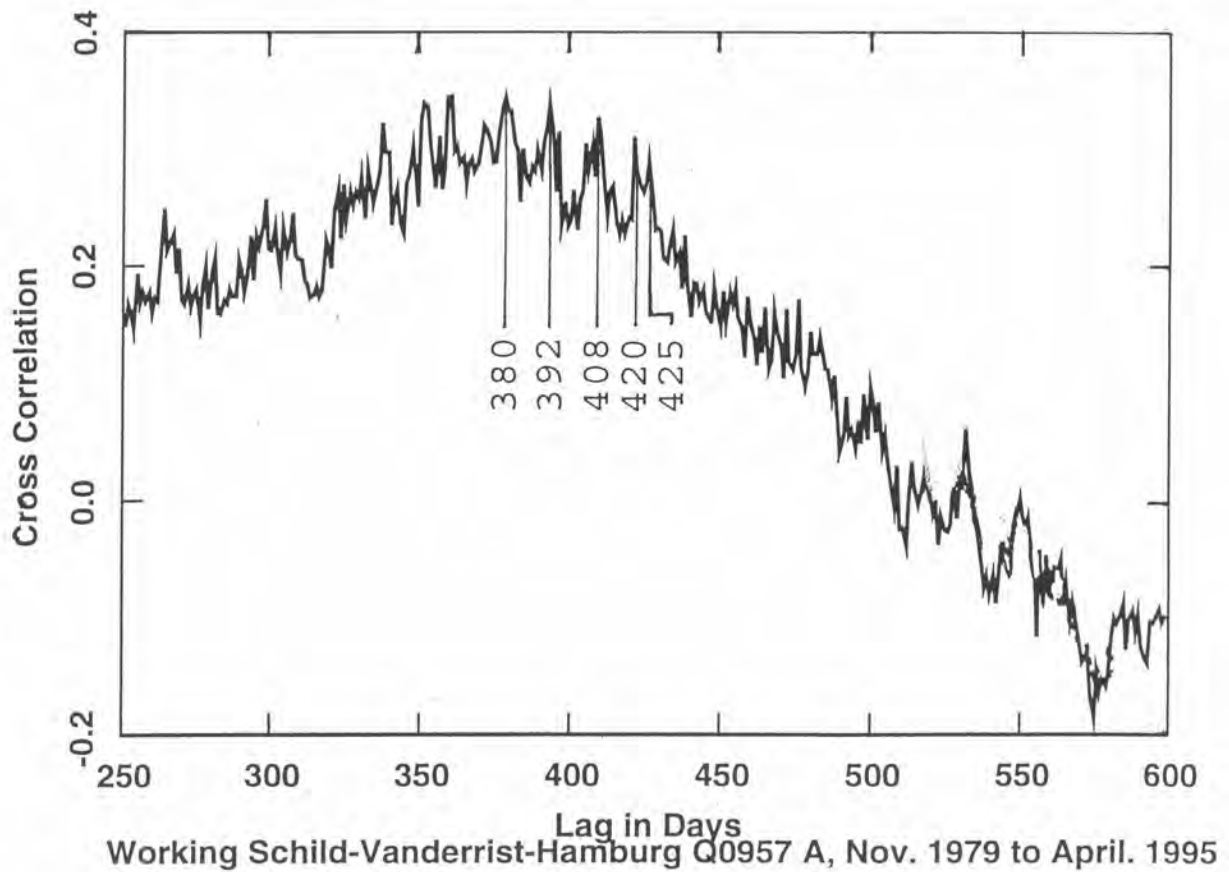
Fig. 5.— A cross-correlation plot centered on the value of the cosmological time delay, but showing the complications from quasar structure. In a simplistic view with no influence of quasar structure, the cross-correlation should be a strong peak at the cosmological value, 417 days. Because of quasar structure, a broad peak with FWHM near 100 days is found instead. Fine structure within this broad peak is evidently indicative of the quasar's inner structure.
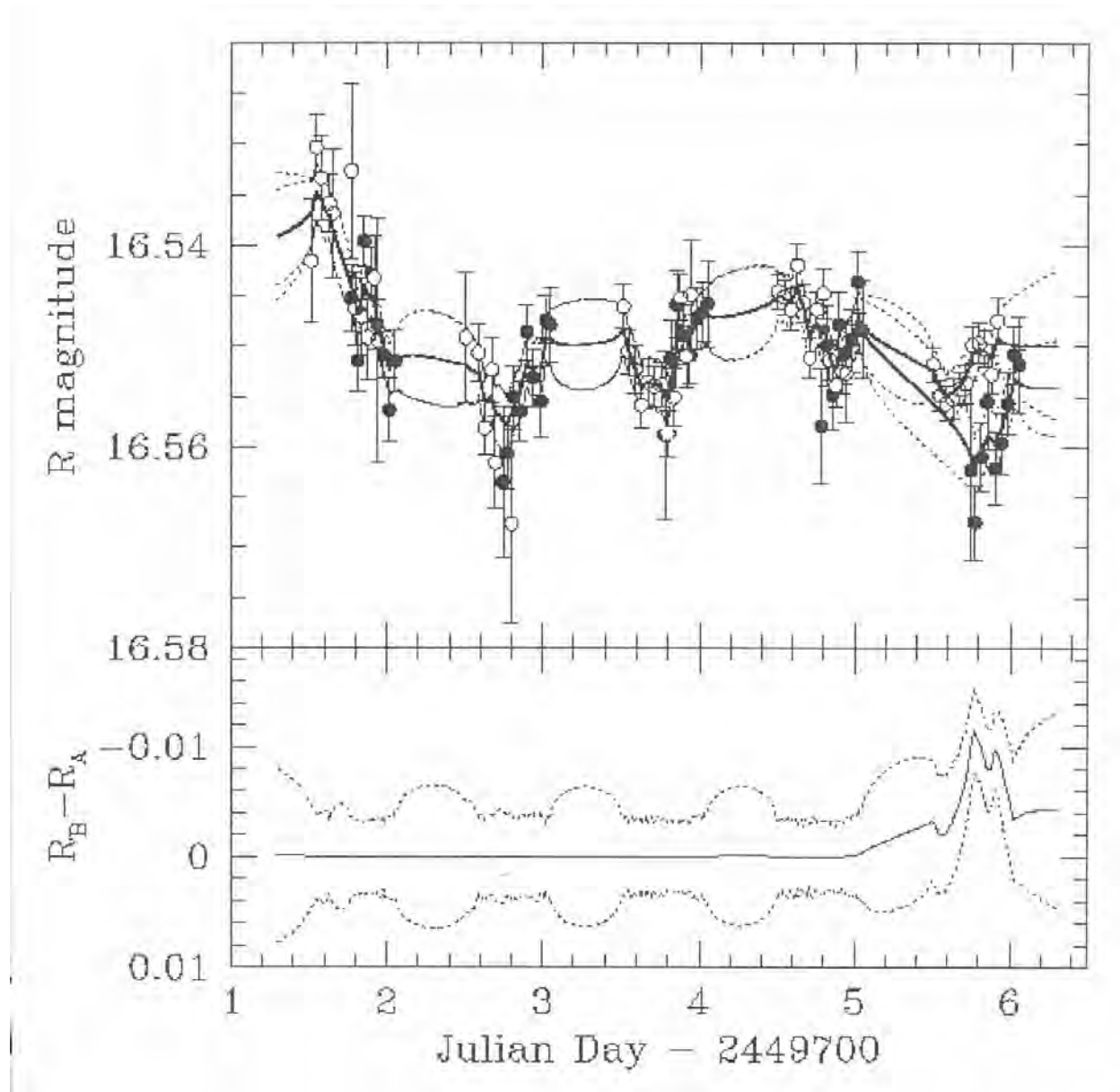
Fig. 6.— A simple plot of R magnitude measured for image A (open circles) in 1995.9 and in 1997.1 for image B (filled circles). A pattern of well-defined quasar brightness variations seems indicated for the first four nights. But on the fifth night, the brightness records significantly diverge, meaning that microlensing by a planet mass compact object in the microlensing galaxy made image B fainter on a time scale of hours. In the lower panel, the smoothed time-delay-corrected A-B magnitude is plotted with linear interpolation, and with 1 σ outer limits per hourly data point shown as a dotted line. We see that the rapid microlensing event at JD 2449706 was securely observed as probably an event where the quasar faded and the microlensing also diminished.
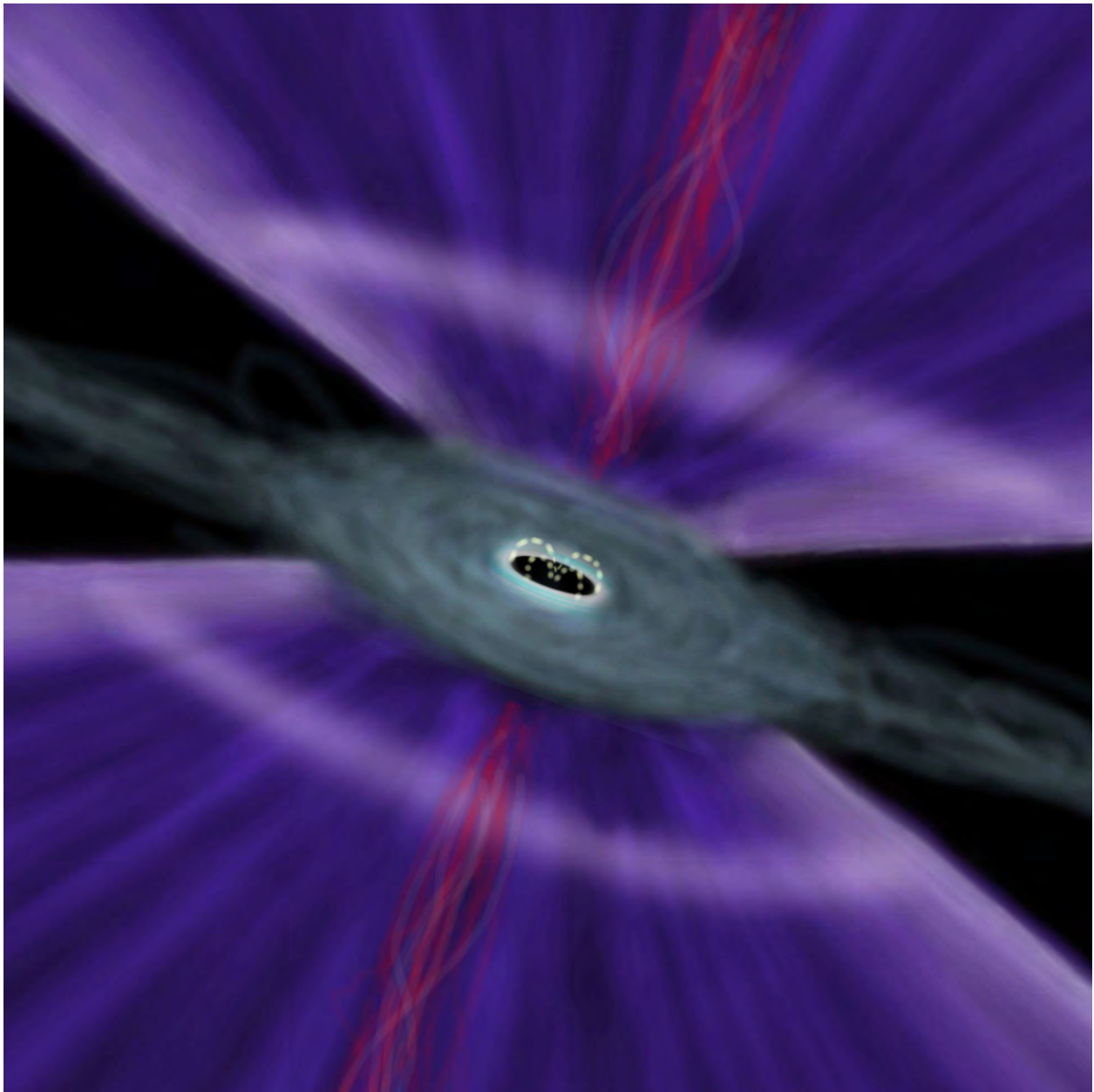
Fig. 7.— A schematic figure demonstrating the principal luminous quasar structures as determined by our reverberation-microlensing analysis. The dark compact central object is surrounded by dipole field lines (dotted yellow) and the sharp luminous ring at the inner edge of the accretion disc is white. A dark accretion disc intersects the outflow wind structures (Elvis surfaces) whose fluoresence above and below the plane (blue) contributes to the UV-optical continuum observed. The compact radio core (red) is shown in size and distance scaled to the overall structure.

Round Table Discussion at the Workshop "New Directions in Modern Cosmology"

Theo M. Nieuwenhuizen[1,2], Peter D. Keefe[3] and Vaclav Špička[4]

[1] *Center for Cosmology and Particle Physics, New York University, 4 Washington Place, New York, NY 10003, USA*

[2] *On leave of: Institute for Theoretical Physics, Science Park 904, P.O. Box 94485, 1090 GL Amsterdam, The Netherlands*

[3] *University of Detroit Mercy, 24405 Gratiot Avenue, Eastpointe, MI 48021,USA*

[4] *Institute of Physics, Academy of Sciences of the Czech Republic, Na Slovance 2, 182 21 Praha 8, Czech Republic*

The workshop "New directions in modern cosmology", organized by Theo Nieuwenhuizen, Rudy Schild, Francesco Sylos Labini and Ruth Durrer, was held from September 27 until October 1, 2010, in the Lorentz Center in Leiden, the Netherlands. A transcript of the final round table discussion, chaired by Theo Nieuwenhuizen and Rudy Schild, is presented. The subjects are: 0) spread in data; 1) back reaction; 2) N-body simulations; 3) neutrinos as the dark matter; 4) gravitational hydrodynamics, 5) missing baryons and lensing in an inhomogeneous universe, and 6) final points.

INTRODUCTION

Theo Nieuwenhuizen: There are a couple of subjects that I would like to bring in for this discussion. Point 0 is the spread in the data themselves. Point 1 will be about dark energy or back reaction or inhomogeneity, we have heard 3 talks about that. Point 2 will be about N-body simulations and dwarf galaxies and, as it was announced yesterday, no ΛCDM. In point 3, I will break in for 2 or 3 minutes saying something about neutrinos as dark matter candidate, and then discuss that scenario. And for point 4, we go back to the first talk of this morning, gravitational hydrodynamics or hydro gravitational dynamics or baryonic dark matter, whatever you want to call it. If we have time left over, we will get to point 5 and 6.

SUBJECT 0: SPREAD IN THE DATA

Theo Nieuwenhuizen: Point 0 is of course obvious. We have the data and that is what we should describe. In particular, there is noise in data. Of course some part is statistical. You don't want to care about that. But let us keep in mind that some part can be non-statistical and can be part of our physics. We have seen this in the CMB plot this morning where you had enormous spread of individual data points of the temperature fluctuations and it can be well that there's a lot of physics. That you do not only describe the average which is one property, but there's also a variance and higher moments and so on.

Let us keep that in mind that there can be important physics both in this CMB spread of individual data points and what we saw later for the supernovas. There was also an enormous spread. Of course, the more data points we have, the better average we get. We should describe not only the average. In the end, we should describe the whole data set and it could be more physics than we are now aware of.

Francesco Sylos Labini: One of the main things I have learned here is that we have to take care of systematics much more. Knowing the error bars that we see in this plot, may be completely meaningless if the systematics have not been taken into account. So to do that is a hard job. If there is somebody that is willing to invest some time in understanding the data then that is something very useful.

Theo Nieuwenhuizen: Thank you, Francesco. Yes we have seen one person, Richard Lieu, who had spent a lot of time on WMAP data. Thank you for your point.

Alexander Unzicker: I am advocating that the source code of data processing should be as public as possible. That everybody should try, at least try to be as reproductive as possible. I think were doing this in the wrong way because everybody works in these codes and it's not really transparent. This is a big problem and everybody should think about it.

Theo Nieuwenhuizen: Indeed, it may save us from being on the wrong track for decades.

SUBJECT 1: BACKREACTION

David Wiltshire: (short intro) There are various approaches to dealing with models of the universe. Traditionally we use exact solutions and CM homogeneity and get the Friedman model and the ΛCDM model which is really a Friedman model plus tiny perturbations, so this is the standard cosmology. We've also heard about you can give up

the assumption of homogeneity but have isotropy and you're led to these large void models so, I'm not sure whether one of the questions is how it needs to be treated. Chris Clarkson said they're crazy even according to many people who use them, so what do they tell us. Independently of that, there is a test of the Friedman equation which is of course put forward, so this homogeneity assumption is actually testable but to actually do it is going to require measurements of $H(z)$ and that might require something like the Sandage load test of the red shift drift which we maybe deal with the next generation of extremely large telescopes.

So, we can certainly test that standard paradigm with enough technology. So we go to inhomogeneous, things which are not exact, but of course first we have a Friedman model with Newtonian perturbation, this is a standard cosmology so one question is how much does this agree or disagree with observations. That was the question that Ruth posed in the first round table discussion of this workshop.

Ruth Durrer: I have a question: what happens on small scales ?

David Wiltshire: Correct. So, these perturbations ... what I was thinking here mainly was in terms of the N-body simulations. N-body simulations pose results. Certainly, general perturbations you can treat by many different means at the surface of last scattering; here I'm particularly thinking of structure, large scale structure and what's currently used. In this sort of framework there are discussions about back reactions in the perturbative regime. This is the arguments that went on a few years ago between Robbie Kolb and others. We haven't had a lot of discussion about that at this meeting. So that's one route you can take. Here, what Alexander Wiegand and I both decided to look at was under-average evolution and e.g. the Buchert approach and then you've got a question: is it just the average or is the fitting problem also important and this is where I diverge from Thomas Buchert in that I think the fitting problem is also important in trying to address that and make a testable and falsifiable model. I don't know what people see as the biggest questions here ... I wasn't asked to pose a question, but this is the scheme of things we've been discussing so ...

Theo Nieuwenhuizen: So let's take questions.

Jan Smit: In the Buchert scheme you have a hyper surface chosen only one time for the hyper surface. Now, you're saying somehow that's wrong. Why is it not just a gauge choice?

David Wiltshire: Well, what I'm saying in my approach is that indeed it is a gauge choice and you shouldn't restrict yourself to having a single gauge choice. I'm looking at different gauges and trying to mesh them together somehow. So I'm saying that even though in the Buchert schemes, things are expanding at different rates. That there is a choice of slicing in which the expansion is locally uniform and its actually general relativity anything which is related to first derivatives of the metric ... that's the connection. Connections are, in a sense, a gauge choice and the Hubble parameter is, in a sense, a gauge choice. We should be able to do our averaging and think about these problems in ways in which we understand when we make a gauge choice and what things should be independent of gauge choices. The way that I'm looking at it is that those gauge choices are important in the fitting problem.

Jan Smit: But then the connection to how you want to use it to connect these observations comes into play. Isn't that the essential issue?

David Wiltshire: Yes. So, my approach to this essential issue, because I do it by Ansatz, which I think is well motivated, so one would say that the difference between any other homogeneous model of this sort and the Friedman model is that in the Friedman model we have a uniform expansion then everything has a velocity perturbation on top of it, whereas here, what you think of as a peculiar velocity is in some sense actually most of it is due to variations in expansion because of regions of different density. So, the velocity perturbations around any scale are going to be small. Then there's a gauge choice about how you relate these different things. I know the weak point of my approach, as far as mathematical relativist are concerned, is that I haven't solved that problem to the level of satisfaction that people would like.

Francesco Sylos Labini: My question is not a question, just a comment in general. In this approach when I see the papers ... ... people trying to include different matter distribution then just the uniform density field. But then, for example, especially from Thomas Buchert models, I can see an effort to go into the data and see whether the actual distribution of galaxies fit with the theoretical prediction of your models. In your case, basically, what you are interested in is the size of the voids. How much matter, how big are the voids. The parameter you want to get from the observations and use for the theoretical predictions. While in the Lemaitre Bondi model, I don't see something equivalent to that. For example, I was trying to develop a test to see the effect of the void but on scales which may not be relevant for what you do. If we are in the center of the void, then we look far away, we have to see a change in the density according to the density outside the void itself.

Chris Clarkson: It's just a function of scale. Its going toward 100 mega parsecs. The density profile in the very large void models just doesn't change much.

Francesco Sylos Labini: What about the fluctuations. Which level of fluctuations do you expect or can be compatible on some scales?

Chris Clarkson: So it's an open question where perturbations are involved, but along the central world line one can assume that they evolve as in a curved Friedman model. The trouble is, you don't have an amplitude to compare it to with your primordial power spectrum from the CMB because you don't know the initial amplitude. You don't have another observation for that. So your σ_8 is just a measurement of your primordial density power along the central world line. So a priority it's difficult to know what that could tell you as a constraint on the models rather than just an observation of a particular part.

Theo Nieuwenhuizen: Do I collect more questions? Yes.

Giovanni Marozzi: When you say a gauge choice, do you mean the dependence on the observer?

David Wiltshire: If spatial curvature isn't the same everywhere, (in the Friedman model we had that thin ...) The question is: If I've got large variations in spatial curvature, how do I calibrate rods and clocks of some average statistical quantity with those of any particular observer. So when you have genuine inhomogeneity, there is variance in the geometry. So, not every observer is the same observer. That's what I think is the problem with this approach in that we just forget the fitting problem. Here we just pretend the universe is a smooth fluid which is homogeneous isotropic. When we pretend it's a smooth fluid that has got spherical symmetry, but it's still a smooth fluid. We don't ask: what are the fluctuations and what is the result of having big fluctuations on a particular scale. For me, the fitting problem is very important and the universe gives a natural observer selection effect.

Giovanni Marozzi: Did that correspond in a formal way with the observer. Did it not connect different observers like with a mathematical function. Cannot you define away with the observer?

David Wiltshire: If you've got an exact solution or, even a Swiss cheese model (in a Swiss cheese model you punch holes in the cheese; the evolution so, in a sense, it's still Friedman at some level) then everything is well defined because you just write down your matrix and you've got a single matrix and everythings hunky-dory. The problem comes when we're observers and super nova and distant galaxies are effectively things that are being observed. So, in between, there is nothing in the void. So, we may have a messed biased view of the universe. So, the question is: If I've got some average quantity ... if I'm doing something like a spatial average on some big cube, we can always define statistical things. How do those statistical things relate to the observations of the particular observers in the galaxy? So, what I'm suggesting with the fitting problem is that the way those statistical quantities relate to the actual observations of observers in galaxies, don't have to be the same as the way that they might relate to some hypothetical observer who probably doesn't exist in actual reality and who would be not bound to any structure but in a void.

SUBJECT 2: N-BODY SIMULATIONS

Theo Nieuwenhuizen: So, it will be about the exciting talk that we heard yesterday. I could hear and see a big silence in the audience yesterday afternoon which, of course, if you give a talk and there's a big silence, you always have to watch the audience to see whats going on. We had such an occasion here yesterday, not due to the boring talk, flabbergasting was what was going on and let us recall shortly what was the issue and then discuss it.

Pavel Kroupa: Basically, I was asked to put up 2 slides maximum. I have put 6 together into 1 slide and just yesterday, I tried the argument with the conclusion essentially and that is that, if this is true in whatever framework, even if you believe in the planets or if these are tidal dwarfs in an expanding tidal tail, then one is forced to essentially conclude that we are in this sort of situation the real universe where purely baryonic galaxies merge and produce dwarf galaxies surrounding the larger galaxies and given that then, this is the statement which is correct.

Francesco Sylos Labini: There is a question that I wanted to ask you yesterday. Basically, your conclusion is that the simulations don't fit the observations. You can say that ΛCDM doesn't work because you are comparing the result of the simulation with the result of the observations. This is again a question of systematic effects. The problem is up to which scale that was the problem addressed yesterday in the first lecture, in the talk before yours, Michael, so up to which extent you can think that the simulations are really reproducing the models because, in the simulations there are a lot of parameters which are not in the model. How much they influence the numerical evolution of the particles is not really clear and it's an open question because, again, what is missing is a systematic studies of effect of these discretizations of dynamical evolution of the real system. I mean, it is not like their predictions of the model ... but mixed with a grain of salt.

Alexander Unziger: If you do that then you are left without the testable theory and then it's metaphysics. For me science is, you have a theoretical framework, you make predictions, then work all that out. This is what this is. I'm from the numerical sector myself so, I can also estimate whether the predictions are reliable following the advance in code technology, as well as the computer architecture and just generally the advancing in computer capabilities over the last 15 years. The situation is very robust. It's not so that you can change some parameters in the ΛCDM

framework and get completely different results concerning the dark matter substructure this is completely ruled out but if you claim that is the case, then one would have show it in a refereed publication and, until that is the case, I think one has to simply look at the fact that this is the situation.

Francesco Sylos Labini: I don't object that this is the situation, the problem is more conceptual. The problem is to understand in which limit the simulation of particles is approaching the theoretical model.

Ruth Durrer: I fully agreed with your situation of the observations but, Im not sure that this is really ruling out ΛCDM for the following reason: Clearly the N-body simulations of the ΛCDM show much too much small scale structure. On the other hand, we know that on small scales (small, let's say out to roughly one mega parsec maybe even more but roughly the size of a cluster) I would not be surprised if other pieces of physics, which are not in N-body simulations, become relevant. Be that hydrodynamics, turbulence, magnetic fields and all these things are not in the N-body simulations, and if they become relevant, then on these small scales the N-body simulations are not the relevant thing. That's why I think it is very difficult to rule out ΛCDM by looking at small scales.

Theo Nieuwenhuizen: I think one can never really ever rule anything out, but one can just bring more arguments in favor or against.

Pavel Kroupa: Well, personally I think one can rule out. I think that stage is already achieved.

Alexander Unzicker: I would agree with Francesco but, this is not a counter argument to Pavel Kroupa, I think it's the business of the people who do the dark matter simulations to comment that right. I mean, the fear could be that extra simulations with extra parameters, one day could fit even the anomalies you are pointing out. But, I would be careful to encourage you people to introduce more parameters to just fit. Even if it's called a physical process like magnetic fields because at the very end we know very little and the more parameters you put in, the easier it would fit. By the way, I think he showed, in a very general way that the very basic concept of halos is in contradiction. That's, I think, quite model independent of how you do the simulations. He showed that the very idea of a dark halo is in contradiction with many observations and that will be hard to fix.

Carl Gibson: I think you really did rule out halos. I agreed with your conclusion.

Luciano Pietronero: I'm a little embarrassed to hear that this ΛCDM cannot be ruled out or can be ruled out. It looks to me that we are not in presence of a theory. We are in presence of a filthy scheme in which we have a large number of parameters and a large number of assumptions and at any moment we are allowed to pick new effects, scale corrections bias and so on. And out of this incredible soup, then we say nothing is excluded but, if this is so, Ruth, this means nothing. This contains zero information so the information exists only if you get into something very clearly. Otherwise, if it doesn't fit, you add bias. You add this, you add that and you define bias as the difference between experiment and theory. As dark matter is also the difference between experiment and theory. So, I would like to push the discussion into something which is absolutely outside the prediction of whatever this blob is. Otherwise, it's useless.

Ruth Durrer: Just a quick answer to why I think on small scales, the physics is too complicated. There are too many effects that you cannot really use to rule out ΛCDM. So go to someplace where the physics is more simple.

Luciano Pietronero: Yes, but you do not answer my question. What do you exclude, Ruth?

Ruth Durrer: For example ... If you would measure the deflection of light around the sun, would be twice the solar potential. You would have ruled out general relativity. This measurement has been done. It's a simple thing. It could be calculated. One knew what one has to get ... etc. The ΛCDM, I think we also have some pieces of simple physics, and the simplest, I think, is the CMB. And if we could rule it out there then that would be clear cut. But on small scales, it's difficult. Maybe with large scale structures we can also do it with the 100 mega parsec, 200 mega parsec.

Rudy Schild: I think that astronomers like to take refuge in the CMB which we can analyze and reanalyze forever. I think that Dr. Kroupa's point, that we do not see these objects which are a fundamental, is a profound prediction, yes, prediction, now of the cold dark matter theory. It is the death now of cold dark matter theory. I am extremely impatient of the idea of adding an epicycle to that theory. That was discarded hundreds of years ago. In other words, going back now and saying we add a new parameter to our theory to have these sub-halos disappear in the local universe is adding an epicycle. That's a posteriori calculation. I think that science should get away from that.

Richard Lieu: I should add that Simon White did email me two or three years ago, pointing out that this is in his opinion the single biggest blow to ΛCDM.

Pavel Kroupa: Considering small scale, I hear this a lot. It's always said whenever all of this is brought up it is always said yes, we don't understand the small scale physics. Now, maybe the reason why I'm so completely convinced of the essential of this statement is because I come from the small scale physics. I started my research career by looking at the nearest star, Proxima Centauri, and then advanced to understand star clusters and stellar dynamics and how stars form out of gas. I'm very well acquainted with that and I know what that are and I know what dynamics is about concerning galaxies. My conclusion is that the uncertainties ... there are uncertainties but they're by far not

of that magnitude to impact on that argument. And that's why I'm making the argument because I've convinced myself that that is the situation otherwise I would not be standing here making this statement which goes against 99.999% of the astronomical community.

Theo Nieuwenhuizen: Not that much of thís community.

David Wiltshire: So, strong and weak gravitational lensing is a very powerful argument for the standard picture. Quite apart from the cosmic micro background radiation, I think that gravitational lensing is something that is very hard to get right in some other model. Something with epicycles like TeVeS if you want to do it and in model scenario for example.

Pavel Kroupa: Why would that be an epicycle?

David Wiltshire: Well, you're trying to get a whole theory of gravitation.

Pavel Kroupa: That's not an epicycle.

David Wiltshire: Speaking as someone who comes from a background of theory. I did continents and many other things and I'm a theorist who's used to adding what I think are theoretical epicycles which are not particularly well motivated. It's very easy to add a field that you've never observed just for the purpose of fitting rotation curves. I think that if you're doing that with TeVeS then effectively your adding epicycles in a way that you add epicycles in other places. The MOND phenomenology is really interesting but it's saying something which is much deeper I think than simply adding a field to the action.

Pavel Kroupa: If I might just add, consistency of the theory ... how much you love the theory ... as much as you might love the theory, is not a proof of the theory. That's how we exclude, actually, models, by looking at the disagreements and that what has been done here so you might find agreement in certain range of parameter space from large substructure but it doesn't prove the theories.

David Wiltshire: Certainly but, there are so many theories because its very easy to cook up certain theories and the theory has to be falsifiable. But amongst all the theories that you can choose to examine because, there is an infinite number of them, you do so on esthetic grounds. Inflation, there are a few hundred models of inflation so, I think inflation is something more like phenomological thing that's easy to get though we don't really understand it at a fundamental level. So, I agree with you that you can have parameters and it should be falsifiable. Many of these modified gravity theories have problems at the solar system level. So, the first thing is, can you rule it out for other reasons. So, it's a judgment in saying that it's epicycles. I think the phenomenology is interesting, in saying something that we probably missed some deep point.

Ruth Durrer: I would like to add something about extra's which you need to make flat rotation curves. If you want to compute the CMB with something extra, you have to have a realistic version of it and there's not a realistic version of MOND, the only one I know is TeVeS and if you want to get the CMB correct with TeVeS you have to introduce massive neutrinos, which is ok, it's not so bad, right. So you have dark matter but you also need Λ. You cannot get the CMB correct without Λ. You introduce a cosmology, you fix your parameter which you have to get the solar system correct to get the flat rotation curves and to get the MOND like dynamics on galactic scales and I think you need ... you also must make careful not to get the problems which you can't do with usual MOND. And then, if you want to get the CMB also right, you have to introduce Λ.

Pavel Kroupa: I'm not arguing for MOND. I'm saying ΛCDM doesn't work. I mean what are the physicists and now, look at your research budgets. 99% of it goes into ΛCDM research. There are maybe 3 people in the looking at MOND in a cosmological context. So, you can't say MOND fails. You don't have the large quantity of theoretical as well as observational results to do testing. You can't do it.

Ruth Durrer: If you had looked at the TeVeS model, maybe you would say, ok, that's epicycles.

Pavel Kroupa: Im not arguing for TeVeS, I'm saying ΛCDM doesn't work. Now the conclusion is, we have to do a lot of work to find an alternative. Is general relativity wrong or right, I do not know. It might be right; It might be wrong. Maybe there are additional effects in the field equations, which we haven't dealt with. We discovered a new effect which was unknown 5 years ago. Possibly the back reaction ... Write your first paper, but that's a very new effect.

Pierre Astier: I just wanted to say that the points of failure are linked with bound states of a gravitationally bound system, which is something complicated. We have another example which is QCD. We never threw away QCD because we not able to compute bound states. And, that is you can do a theoretical QCD, something which is calculable can be checked. And it works. Bound states are extremely difficult and I'm not surprised that in a theory like ΛCDM we had a hard time in computing bound states.

Pavel Kroupa: You lost me there. That's Newtonian dynamics what you're talking about. I thought that that is understood pretty well.

Pierre Astier: In Newtonian dynamics, no one is able to solve anything rigorously. It is an N-body problem. I'm not surprised that we don't get the right solution.

Theo Nieuwenhuizen: Well this is a very hopeful position. Ahhh ... Francesco, you go first.

Francesco Sylos Labini: I think the point is that we don't know, nobody knows, is how to have some analytical solutions in the non-linear regime in gravity. So this is a problem which goes beyond ΛCDM. And if you take any initial condition and any cosmology (which is funny because cosmology doesn't change very much in these simulations) you'll always form the same kind of new linear structures which are ... these structures which are called halos. Now the problem is I would say given that what you observed is different from these halos. Or there are other ingredients, as Ruth was saying, that are missing in the gravitational simulation or maybe there is a problem with the standard way in which gravitational simulations have been done. And this is something that we are studying. We think that probably there can be a problem in the numerical simulations.

Pavel Kroupa: Sure, I would fully accept it if what you are saying showed that there is an effect which one has to fully understand in the nonlinear regime at which effects what galaxies look like in a very, very significant manner and of course, that would be a tremendous break though, of course.

Francesco Sylos Labini: On the other hand, the predictions of ΛCDM in the linear achievement (so at 100 mega parsecs) then there are no problems in linear regime, there we understand a lot of things, more or less everything. So, for example: If the baryon peak is not there, then it's a big problem for ΛCDM.

Ruth Durrer: I think this is an important point which now Francesco has brought. Probably this lots of substructures which is in the numerical simulation has nothing to do with Λ but more with CDM of course, its just Newtonian clustering of particles with all others.

Pavel Kroupa: So will we be challenging the cold dark matter aspect of the theory or the Λ aspect of the theory? I mean if you are challenging ... So which of those aspects would you be questioning?

Tom Shanks: It seems to me that I don't mind the argument that if you push away from CDM you have to want the flat rotation curves. I just don't think that applies. If you have a surface density that falls off as $1/r$ in a spiral galaxy that gives you a flat rotation curve and H_1 neutral-hydrogen falls off as $1/r$ exactly where you want, by a factor 7 too low, then if you fill up with molecular hydrogen (which is very difficult to observe) you have to hide it from UV surveys; it has to be in a special fractal. Francoise Combes showed us this a few years ago ... then you use the CO when you see orbservational curves of the galaxy. That is an H_2 tracer and it did seem to be in that fractal distribution that she wanted. So, I don't think you can jump from abandoning CDM to having to have MOND just because of flat rotation curves.

Ruth Durrer: Do you think one could do it without baryons?

Tom Shanks: Yes, yes because the argument also used to be that you were prone to baryon stabilities and suppose you didn't have anything like that standing spherical halo. But these days the bars of observation are smaller anyway, and that problem, to some extent, has gone away. So, flat rotation curves ... I mean its my opinion ... can be extremely boring and say there are errors in the observations or things we know anyway, but in this case, I think its true. Flat rotation curves I don't think equate to satisfaction. We could also talk. It's always good to stir up the conference with the bullet cluster, which nobody has mentioned; I'm amazed at this point. That's a very interesting point too. Fight usually break out when the bullet cluster is mentioned. I think that's sort of a swindle of an argument but we could get into that as well.

Carl Gibson: I know you can rule things out observationally but, can't you rule out some ideas theoretically. To me from a fluid mechanical point of view, the concept of cold dark matter is absurd. It's completely inconsistent with the concept of fluid mechanics. That something with a very low collision cross section could condense. Alright ... if you make it absolutely cold dark matter, then I will agree. If it's absolute zero, you start off with an initial chunk of cold dark matter somehow given to you initially, then it will condense. But then it will defuse away and the idea that you could have a permanent halo of it is absurd.

Jan Smit: The interactions are just very weak.

Pavel Kroupa: Let me just say something. So, if you say it's natural, then how does that now agree with that. With what you've been saying. Because you're saying that maybe the substructures are not there. But you just said it's natural, so ...

Theo Nieuwenhuizen: Well, what Carl is pointing is the fluid mechanics of the cold dark matter itself which I have never seen any discussion of it. We as humans ... ... Carl is saying, if you look at the fluidity of this stuff, you must convince yourself that it will cluster and stay clustered.

Carl Gibson: Suppose you had some of that. What would you put it in? It would diffuse away. It's like having a bottle of neutrinos. What would happen, it would diffuse through the walls.

Francesco Sylos Labini: It depends on gravitation. If you have gravitation of a collisionless system, that way it works perfectly it won't diffuse away. If you do the simulations ...

Carl Gibson: If these are point particles with a very low cross section for collision, they will diffuse away.

Ruth Durrer: Without gravity, yes.

Carl Gibson: With gravity, they will diffuse to the center ...

Ruth Durrer: No, not necessarily ... ... some of them go out into infinity and some of them go into the center.

Theo Nieuwenhuizen: Let us agree that there is a point here. And then that's the matter and also ... yes

Francesco Sylos Labini: The problem is that, how certain particles relax to a kind of stationary state. OK, that's the question. So, what's the physical mechanism? In certain systems there are mechanisms which are not based on particle collision. They have a coherent effect on those systems what is called violent relaxation this is the way in which ... otherwise we would not be here without violent relaxation.

Theo Nieuwenhuizen: So we must check for violent relaxation of the cold dark matter.

Pavel Kroupa: No, because haven't you just sort of argued against yourself? Because if you said there's violent relaxation, which I understand pretty well I think, (that's why this is here) then you form these substructures. I mean, there's no way out of that. So either you say the simulations are not convincing but then you can't say violent relaxation forms the halos or you say that the simulations are convincing and then you can say that you've got violent relaxation and it formed the halos. So what is the status?

Francesco Sylos Labini: What happens in the simulations is something very difficult to understand. So, it's not violent relaxation, which is something that has been understood in an isolated system. The relaxation occurs in an infinite system in which you have contribution to the force from many different scales. So, it's a process which in unknown actually. It's something like violent relaxation but it's not the violent relaxation we know for an isolated system because it's not isolated.

Theo Nieuwenhuizen: Rudy ... you have a remark?

Rudy Schild: This really was a question. Ruth brought up MOND and I think some of you may know some things about MOND and frankly, it was my understanding that when you make the MOND modification which is then the relativistic version which then is applicable and tuned to the WMAP to the SZ effect of weak lensing that then you don't get the correct calculation of strong lensing of quasars. In other words, the double imaging of a distant quasar or by the foreground galaxy. Does anybody know the status of that now? Maybe Ruth? Maybe another of you? Thank you, that was just a question.

SUBJECT 3: NEUTRINOS AS THE DARK MATTER

Theo Nieuwenhuizen: (short intro) OK, given the time schedule of the discussion, we are doing fairly well. We are slightly ahead and slightly halfway through the series of topics. I now give Rudy the chairmanship and I will now become a member of the discussion team. A short, short story about neutrino dark matter because I have brought it up a few times in this conference. I look at a galaxy cluster, Abel 1689 is well known, and the idea is just to solve the Poisson equations so there's Newtonian physics and the mass density is of course dark matter next to Hydrogen gas and galaxies. So, there are 3 ingredients to the matter. I take an isothermal model, we know this very well, but I apply it for isothermal fermions. So they give a Fermi Dirac distribution of free particles in the gravitational well of all this stuff together. Then there is X-ray gas and this I take from observations. Then I get the electron density and proton density and temperature, and so on. And galaxies I simply model as isotherma;l this is not completely correct but, that's what I did and there was some data. These are lensing data. This is weak and strong lensing and some data are based on a mixture of weak and strong lensing. From the figure I show, you see that the fit works. What comes out is a mass of the putative dark matter particle and an 1.5 electron volt mass would fit the best to neutrinos. The active neutrinos, the normal ones, would yield 10% dark matter in the cosmic budget. So your active ones would be 10% and the right-handed ones or sterile ones could also have 1.5 electron volt and in principal they can also be 10% or maybe even more, but probably depending on the Majorana coupling in the mass matrix. This would then go together with baryonic dark matter. So, there would be a 4.5% baryonic dark matter as we understand it today and there could be 20% from these neutrinos and at least what this shows is that the cosmology that you get from this is not too bad. But we could not go to the CMB predictions because it was just started and it would be an important task to do still and also difficult. That's the situation for today. Rudy, I see a question.

Rudy Schild: Yes, the question in back please and your name?

Pierre Astier: What is the temperature of the neutrinos?

Theo Nieuwenhuizen: 0.04 Kelvin. It is below the 1.9 K because the 1.9 is the momentum temperature $T_p = \langle |p| \rangle c$, but, what you have to think of here is the kinetic temperature and that's $T_K = \langle p^2 \rangle / 2m$ and this is well below this 1.95 K. And the value I find is above this kinetic temperature. If they would not be clustered on the galaxy cluster which would still be homogenous they would have a few times 10^{-4} K and this 0.04 K is above that.

Carl Gibson: Just a comment. As I understand, this is about 20 times the mass of anybody elses estimate of the massive and electron neutrinos. Is that right?

Theo Nieuwenhuizen: Yes. It's completely ruled out by the WMAP analysis. They have 1% of the neutrinos but they do assume cold dark matter there. But this is replacing the cold dark matter. It would be warm dark matter. But if you assume we have cold dark matter you don't have much space for the neutrinos anymore.

Carl Gibson: And there's going to be an experimental test you had mentioned?

Theo Nieuwenhuizen: Oh yes. It will be tested in 2015 I hope. It will be the KATRIN experiment and they tell me it will start in 2015. It's tritium decay in Karlsruhe, perhaps they start in 2012.

Francesco Sylos Labini: Thank you. Im not a fan of CDM at all. Something that I've learned just by doing simulations and studying cosmology is that you need the matter to be cold in order to form structures. If you're going to match hot dark matter how can you have some reasonable predictions on structure formation?

Theo Nieuwenhuizen: This we get the next item but it was Carl Gibson's talk in the morning. Baryons don't need neutrinos or anything, they will do it by themselves. It's not even clustering but fragmentation what goes on.

Rudy Schild: Other discussion of the neutrino and the particle?...OK, thank you.

SUBJECT 4: GRAVITATIONAL HYDRODYNAMICS

Theo Nieuwenhuizen: (Short intro) Great. We move on the next item which is Hydrogravitational Dynamics. I have problems pronouncing that so I pronounce it as Gravitational Hydrodynamics, GHD. And so, this stuff, what Carl gave his talk about, it goes in 3 steps. The whole point is viscosity, ν, the viscosity, first in the plasma. There you get the void formation. You do viscosity and if you look a bit, the red shift at which the viscous length scale enters the horizon happens to be $z = 5,100$, well before the 1,100 of the decoupling. So at the moment of decoupling the density is not homogeneous. But, we have observed that the temperature is extremely homogeneous 10^{-5} variations. So there's something to explain there. This void formation is a prediction. This is step 1. Step 2; we know all it's the Jeans mechanism which creates Jeans gas clumps of say 600,000 solar masses. This we know since Jeans 1902. The idea is that all we have passed the decoupling ... so we have gas now and all the gas in the whole universe does what Mr. Jeans told us, it will break up in these clumps. And then in each of these clumps ... there is again viscosity but now, not the viscosity of the plasma, this is 10^{26} m^2/s, but of the gas and this is 10^{13} m^2/s. So this is much smaller, 13 orders of magnitude so you again get clumps but much, much less than what you had there and these clumps, they have earth mass and these have been discussed already a few times. Which means that each of these Jeans clusters have something like 10^{11} of them. These earth mass H-He gas clouds are sometimes called micro brown dwarfs, today they were also called planets or small Jupiters. Of these Jeans clusters in the Galaxy you have a million, 10^6, in the Galaxy. And in the Galaxy they are just the halo, so here you have your disk and they are everywhere. They form an ideal gas in which they act as point particles. These Jeans clusters act as point particles which traverse along the disk and along the milky way. If they are point particles and if they are isothermal you have the flat rotation curves that come from the isothermal model. You can find this in Binney and Tremaine. So you get the flattening of the rotation curves. We have heard this item several times today. And this is the end of my introduction. So, are there any questions/remarks to this.

Alexander Unziger: How do you form a halo?

Carl Gibson: They can interact and things like to accrete to a central mass on a accretion disk. I don't know how better to say it. I mean if you just throw particles up into the air ... It's like Saturn. It's more comfortable to come in on the plane of rotating massive object. I'm sure there are people in this room that know how accretion disks are formed. Stickiness helps.

Rudy Schild: Carl? Would the clump that was to become a galaxy have a net rotation which would enable the accretion disk I suppose?

Carl Gibson: It doesn't need it. All it needs to do is have a mechanism to collide a little bit and you can actually see the orbits of these things. Somebody mentioned star streams around dim globular clusters. The PAL, the Palomar Observatory. Very dim globular ...

Rudy Schild: PAL 15.

Carl Gibson: Yes. This is a ... I mean all these PAL ... you know, very dim globular. This is why we're talking about this proto globular star clusters are just loaded with these planets. Stars form at the edges because they get agitated from the planets and then you can actually see more stars in the wakes of these orbiting ... As Theo says, they orbit around the center of the galaxy and leave streams of stars to show they are there. But they have this tendency ... they are trying to get into the center. Some of them will diffuse far out and then they will go out to complex orbits and wind up in the plane of the galaxy. The question comes: where does the disk of a spiral galaxy come from? Well, it's from these diffusing proto globular star clusters finding their way to this accretion disk.

000333

Theo Nieuwenhuizen: You are now in a different paradigm. As a paradigm you have two colliding galaxies, they merge and then half of the material ends up in the spiral disk. This is now gone because we have big halos. And we have to start thinking from the halos. Kroupa put up this picture. We saw things that are explained in terms of halo behavior.

Jan Smit: I don't understand this viscosity. You would expect because the mean free path in the gas phase to be bigger that viscosity is bigger but, it's much smaller.

Carl Gibson: Its much smaller because the mean free bath is much smaller. You have to understand the mechanism of viscosity in the plasma. It's photon viscosity. It's a photon colliding with an electron. So, you have Thompson scattering, you know the cross section precisely and you know the density of electrons. So you know precisely the mean free path but we also know the speed of the particle, the product is the viscosity.

Jan Smit: But I thought the mean free path came with a denominator.

Carl Gibson: Well, look at the dimensions. It's the length times the speed, it is meter squared per second. That's the kinematic viscosity. You're transporting momentum.

Jan Smit: What is the role played in making these predictions?

Theo Nieuwenhuizen: Ah ... that's the viscous length. Carl gave the formula for that. If it is within your physical reach, within the sound horizon, you can get structures on that scale.

David Wiltshire: Whenever you put something up, it's always important to think about what will falsify it and the questions that I would have would relate specifically to anisotropy spectrum in the CMB data because were used to thinking of various features for example in terms of the ratio of baryonic matter to non-baryonic cold dark matter. We usually think about the cold dark matter is clustered with some density contrast maybe 10^{-4} or something like this. Its more clumped than the baryons. You'd be saying that the baryons are more clumped at some scale which has perhaps something to do with the planet size scale and zoning at the very high multiples. Another issue ... Im not quite sure what part vorticity plays in this because vorticity perturbations are damped as long as we are expanding so the vorticity wouldn't have any effect on the large angles it would only at the very tiny angles. Have you computed the CMB anisotropy spectrum or do you have some qualititative way of saying what features should be there? Because, this calculation would surely be able to give you something that's predictable and could falsify it.

Theo Nieuwenhuizen: What we have is the position of the first peak and this is related to the size of the clumps you make here. You will have voids and clumps.

David Wiltshire: Surely the position of the first peak is just geometry and surface of last scattering. It's got nothing to do with the small details..

Carl Gibson: It has to do with the speed of sound in the plasma.

David Wiltshire: Correct.

Carl Gibson: The speed of sound in the plasma determines the speed of the rarefaction wave at the boundary of the proto super cluster voids. See, you have a rarefaction wave ...

David Wiltshire: Well, my understanding is that the first peak is a compression peak and there are two things involved; one is the speed of sound of the plasma and the distance of the surface of last scattering cause there's a degeneracy as people have been talking about. So, just having the speed of sound by itself is not enough.

Carl Gibson: This produces a length scale at the surface of last scattering (as you put it) because, you know, your proto super cluster void fragments at 10^{12} seconds and then you have this sudden empty space formed that then everything surrounding this empty space falls away from the empty space. So the void expands. How fast does it expand? You know this from gas dynamics or plasma dynamics it can go no faster than the speed of sound. Mach 1 from thermodynamics.

Theo Nieuwenhuizen: What Carl is saying is there is a candidate physical mechanism, but the precise calculation has to be done. We are not at that level and we would kindly invite everybody interested.

David Wiltshire: See I think , well at least I know that people, in Sydney actually, some people that are looking at back reaction who do these perturbative things have put in viscosity and things like that and these thing are always very small.

Carl Gibson: What number did they put in?

David Wiltshire: Ahhh ... I don't know.

Theo Nieuwenhuizen: There is the problem with viscosity. Namely ... you can have nonlinear effects and that's a problem. If you don't put that in you don't get it out.

David Wiltshire: But we're talking about any part where the universe was very close to homogeneity.

Theo Nieuwenhuizen: But there was fossil of turbulence and linear regions and they will trigger your stuff and those are never in models.

David Wiltshire: On very tiny scales ... I can imagine something but, I can't imagine big effects.

9

000334

Carl Gibson: You have to understand that in this model you have a turbulent big bang, you know, a fully Kolmogorov turbulence big bang at length scales between 10^{-35} meters, and increasing up to 10^{-27} meters. So you have a spinning turbulent cylinder of gas pulled out of the vacuum against gravity by negative stresses. Think of it that way, with a gas of Planck particles and antiparticles. Stretch out the vortex lines ... it does turbulent mixing of the temperature and it is fossilized as soon as you get inflation from gluon viscosity. You're beyond the scale of causal connections so it can't move.

Theo Nieuwenhuizen: Thank you. Francesco.

Francesco Sylos Labini: So maybe I've surely missed a lot of steps in these ideas but, so basically the thought is that you are including viscosity terms in a gravitational system. But I don't understand exactly; what's the meaning with your isothermal model to explain reflecting of the rotation curves?

Theo Nieuwenhuizen: Well, given the fact that you have these planets, what will they do? Well they will ... you have somehow a Jeans cluster of these objects and what happens when these things inside the Jeans cluster? Well, that will be the violent relaxation that you have already mentioned and therefore they go to the isothermal model. So, inside the Jeans cluster you will have some rotation curves which are flattened but then you will have a million of these Jeans clusters in the galaxy and also these things among each other will thermalize according to violent relaxation and therefore explain flattening of rotation curves of the galaxy.

Francesco Sylos Labini: No! With violent relaxation never would you form an isotropic sphere, never. I mean, why would you say that. And then, something I do not understand. You are talking about arguing no linear process of structural formation. The description is not so ...

Theo Nieuwenhuizen: There, we make two statements. To let these things be there, you say they don't make the isothermal model.

Francesco Sylos Labini: Violent relaxation doesn't give you an isotropic sphere.

Theo Nieuwenhuizen: Then what does give it to you.

Francesco Sylos Labini: It's another profile. It depends on many things. Whether the system is isolated or whether the system is not. This is well known also the arrows that people get in the simulations and they are not ... ... clearly because they are not isolated and never told that ... ... It's many things. It's a complex story.

Carl Gibson: You forgot to tell Francesco, that these initially gaseous hydrogen clumps, primordial gas planets, were gas planets. Real gas planets, hot gas planets. They gradually freeze and then they become collisionless and then what Theo says is right. They first start off with the same density as the initial fragmentation at 10^{-17} kg/m^3, very dense, 10^4 times more dense than the Galaxy. But then they cool down with the universe and every one of these fluffy gas clouds gets colder and colder and finally it freezes. It gets to the freezing point of hydrogen which is 13.8 K.

Rudy Schild: That 13.8 degrees crosses the photon temperature when the universe is at redshift $z = 5 - 6$.

Theo Nieuwenhuizen: OK, but still, Francesco, your point is taken. You say it does not go into the isothermal sphere.

Francesco Sylos Labini: Violent relaxation is for a collisionless system. They provide a density that falls of as $1/r^4$. For an isothermal sphere you need $1/r^2$.

Theo Nieuwenhuizen: Well come back to that. Other points, other statements? Ah, Richard, are you up.

SUBJECT 5: MISSING BARYONS, LENSING IN AN INHOMOGENEOUS UNIVERSE

Richard Lieu: It's to do with the point made by Tom Shanks this morning about the baryons. The Coma cluster, this is actually a topic that by now, it's not a new topic, but by now it has about 200 citations. For instance ... this particular paper is 2003 already and if you look at the Coma cluster in the normal weak field, which is what Tom is talking about, the normal spatial extent is 1 degree in radius and that already harbors an awful lot of baryons. If you look at it in soft X rays it goes out to 3 degrees. That's sometimes the most extreme soft of excess. More commonly known as the soft excess and if you look at an image of it, you see that the cluster extends to some enormous distance, about several mega parsecs. This halo is actually a lot bigger than the normal X-ray halo. In fact I think that the low level SZ in fact Planck detected in the form of that finger you saw the other day connecting three clusters may well be, in fact looking at another system of a manifestation of the same thing and that is that at the outskirts there are still baryons falling in. Large amounts of them are not yet virialized and therefore at a lower temperature of about 1 million degrees, consistent with what Ostriker, in that paper I showed you the other day, predicted in 1998 that missing baryons, 50% of them in the near universe, still in the form of this million degree temperature gas. That's very, very difficult to observe. So we still have to keep a close eye on the baryons when trying to solve cosmological problems.

The other point we may need to be making is connecting with the question of the back reaction and so on. This paper appeared in 2005 in which concerning the averaging to recover the FRW universe that is. In the context of gravitational lensing we heard from Anthony Lewis yesterday. There are issues even on lensing, not to mention the back reaction problem ... to do in an inhomogeneous universe. When a universe has clumps and voids, how do you recover an average lensing magnification that equals the FRW universe of the same mean density? It turns out, among many different ways doing the average magnification, only a particular rather esoteric way would give you back that consistency and its known as the average reciprocal magnification. Which basically means you take the 1 over the average of 1 over something and you call that the average of something. And you do that ... then the next thing is whether there's any means to performing such an average and if it in particular corresponds to the magnification that's relevant to WMAP data. So that's why I do strongly believe now that the question is not just simply the data pipeline of WMAP, that's part of the interpretation force but also, the model itself. How do you implement the model? Because you know that there are self consistency, very big problems, concerning what's the model predicting homogeneities at low red shift. Then how do you propagate the inhomogeneities back in terms of the construction of a mean Friedman universe. You can't do it. Then you just have to admit, even if you can, is your averaging process corresponding to reality in terms of whether it resonates with the observational matter. Thats all I wanted to say. Thank you.

Theo Nieuwenhuizen: Thank you. Are there some remarks on this point? Everybody agrees? Richard, you have been very convincing.

Richard Lieu: Well, everybody is very, very tired.

Theo Nieuwenhuizen: No, no, no ... they would throw tomatoes if they could. Well, thank you Richard. It is obvious we have a problem here and we don't know how to solve it.

THE FINAL

Theo Nieuwenhuizen: Are there other things we would like to discuss?

Alexander Unzicker: I would just like to draw the attention to a historic perspective. We all know about the epicycles and we realize that nobody really likes the up to date model. But what about in 20 or 50 years, how will science evolve. I think there could be a good chance all people doubting today and having their serious problems with the model, just dying out and the dark matter and dark energy ... all this stuff will be very accepted and the community will be ready to digest new parameters. How can we avoid this ...

Theo Nieuwenhuizen: We have an item here and that is the sociology of the community. Of course, you being here and still at the last moment are not directly the people ... the people I need to explain it. We have already heard several people have had troubles getting their stuff published. Although probably the main scientific approach was more or less correct. It need not be completely correct. What we can at least do is when we meet other people, try to open up their minds for a more fluent attitude concerning new ideas. Because there are some problems we have seen them, but right or wrong, that is another issue. But there are problems. There are at least 20 problems with ΛCDM, so there maybe something out in any case and hopefully we get, maybe in 10 years well have it done, we'll have a better model. Still including or not including an ΛCDM, but a better theory and ΛCDM won't do this alone. So new ingredients are needed but of course you are the wrong parish to preach for it, those that come in to church are supposed to believe as opposed to not believe, but if we can spread out the news to others they'll be a bit more open minded to accept papers and fund proposals in this direction and in such a way that the student is not immediately killed off after his papers but he/she can continue his approach because what he did was sound physics whether or not the ballpark was correct in the end. I think that's the right approach. Yes, Luciano.

Luciano Pietronero: Maybe I can make a little comment in the respect of statistical physics which is what dragged me in this business. So if we take a fresh look at the situation of clustering, essentially what we observe is a fractal structure basically. Whether there is homogeneity or not is not clear but for sure there is fractal structure for at least 2 decades. As Michael Joyce pointed out, this is very interesting conceptually. It's not power load one with respect to an explanation but there's a deep meaning in sense of self organized criticality and so on. So in my opinion the simple issue, one which I believe can be resolved, is like, are these simulations good enough to produce a fractal structure, yes or no? Do they produce it when you do them well? I mean, basically, the approach of Michael Joyce was very clean. This is ... just this one piece ... you know, whether clustering is fractal or not is important in view of self organized criticality. The other thing that ... I mean, many things I had, I would comment, but I don't. The other thing that really surprises me a little bit is the little attention on the fact that after all the very large structures out there and there and they are very large, now, as I understand, the structure formation even with tons of dark matter and whatever people put, these structures so large and so are impossible to build from the point of decoupling

from $z = 1000$ to now with gravity. So, I wonder, I mean, such a big structure of 300 to 400 mega parsecs with large amplitude, which is now being clear that it has a large amplitude, where does it come from? Can we think of other mechanisms to build structures than gravity? For example, a combination, some other dynamics. So this should be considered. So I would say, there is a simple part which is, I mean, well understanding gravity from other simulations but also a very open ended story of the very large structures.

Carl Gibson: The answer is no. You need gravity. But, gravity will do it. By making super cluster voids at the speed of sound in the plasma. This will make you a void that is 10^{25} meters 10% of the size of our horizon.

Luciano Pietronero: In how long of a time?

Carl Gibson: From then till now, 10^{12} seconds.

Luciano Pietronero: From the decoupling?

Carl Gibson: From the big bang, 30,000 years. So, it starts early, at the speed of light.

Theo Nieuwenhuizen: OK, thank you. The point has been made.

David Wiltshire: I would like to ask a question. If people ... ... these very large structures in numerical simulations may be ... ... if general relativistic effects are put into the simulations? So, if these very large structures that seem to very difficult at finding N-body simulations are actually a result of general relativistic effects that aren't being included?

Alexander Unziger: So what do you mean?

Carl Gibson: Well, hundreds of mega parsecs.

David Wiltshire: Well, it's impossible to answer that question without having done the simulations. The only person I know who claims they have done anything like this in his spare time is Voychek Ludman, I mean, he's never published anything so I don't know what he's done. He just says he gets things happening a lot faster so ...

Theo Nieuwenhuizen: Alexander ... would you like to answer to this point?

Alexander Unzicker: Yes ... there are hints. I mean, usually you can have really optimistic corrections here in the strong field. Usually if you talk about evolution, because the weak fields are slower accelerations. There is no hint that this could change things.

Ruth Durrer: There are two places, the strong field and the large scale, this is large scale? Yes ... I thought so.

Carl Gibson: Well, even Peebles has said that the size of the biggest hole or void or whatever you want to call it is the way that Λ cold dark matter hierarchical clustering can be falsified. If the voids get bigger than about 10^{23} to 10^{24} meters he will give it up and now they're 10^{25}. So ten times bigger.

Theo Nieuwenhuizen: He will not give up.

Carl Gibson: Well, all we can do is argue with the data.

Theo Nieuwenhuizen: OK, we got your point. Richard.

Richard Lieu: First is does not depend on Λ and even on cluster scales, a cluster mass of 10^{15} solar mass. Then beyond the distance about 20 mega parsecs actually Λ shields the gravitational force. And in fact 2 clusters in other words, or a cluster and a galaxy satellite, their separated by 20 mega parsecs they will feel each others mutual attraction. That's actually a neutral zone. Beyond which it become repulsion in fact, and that's why there is this anti-correlation turning over that requires Λ. That's something that you do need GR to produce. That's almost like a barrier penetration.

Theo Nieuwenhuizen: This reminds me of a remark I have made before. If these neutrinos are true then they will be free streaming for a long time and homogenous so the voids you then have are only baryonic voids which are still filled with a lot of neutrinos. There is much more dark matter than baryons. So basically you'll have a uniform universe still then but later at redshift of 5 or 10 maybe, these neutrinos will condense on the baryons and then the voids will be really empty. And then you should have strong back reaction effects because voids are empty and matter is clumped.

Carl Gibson: They're totally empty of everything. They should be.

Rudy Schild: So you would say that is a prediction, actually?

Carl Gibson: Well, exactly. This is the difference between the Λ cold dark matter hierarchical clustering model and this ... I like to call it HGD, is that the last thing that happens to the baryons, you know, when you make super clusters by hierarchical clustering, in between those is the voids, but it's not empty. It's still full of the neutrinos. However, when you start from fragmentation.

Theo Nieuwenhuizen: Thank you Carl. Anna, we have not heard you. Is there anything you would like to say or ask?

Anna Achúcarro: One thing that I would have like to have asked this morning was, ... what observations would disprove your theory?

Carl Gibson: Well if you ... I mean, what I was saying was that for every star in the galaxy there are 30 million earth mass Jupiter-like planets, not 8 or 9. So, this is a rather strong prediction that is easily verifiable. If one looks

where I say they are and you don't find them then ... I mean, I think I have shown you pictures of them in the planetary nebula. If those turn out not to be planets, if somebody manages to get there, and show that this is a Rayleigh Taylor instability in the gas then I will give it up.

Theo Nieuwenhuizen: Thank you Carl. Rudy, you want to make a statement?

Rudy Schild: So, to answer your question, an important prediction of this idea as Carl is saying is the existence of all of these planets. In Europe you've had two experiments looking for these but, I don't think they did a very good job. They were basically biased to look for stellar mass objects and that comes in the cadence of making one observation per night. And so, in that way, you would find stellar mass objects for which a micro lensing macho profile would take 10 or 20 days and this is seen in the Macho program in America, Eros and Ogle here in Europe. There have been some attempts to repeat the experiment with a more rapid cadence but only with a small telescope and so they look at bright stars in the Magellanic clouds and therefore they were looking at super giants and there was no hope of seeing the micro lensing objects on large sources. You have to have a point source and a point lens and so there were 2 assumptions in the attempts to preclude them. Micro lensing of quasars gives a very different result. Micro lensing of quasars where we look at a distant quasar through a foreground galaxy and the graininess in the foreground galaxy produces micro lensing with its character 6 signature the event duration telling the size. This occurs at optical depth 1 in each gravitational lens, meaning, there would be continuous micro lensing by the baryonic dark matter or the galaxy dark matter. It has shown, first by me actually in Q0957 and then 4 other observatories found the same signature in 5 or 6 different gravitational lenses, found that yes, they always show a highly probable optical depth $\tau = 1$ approximately signal indicating that, yes there is a $\tau = 1$ distribution of rogue planet mass not necessarily 10^6, sometimes 10^5, sometimes 10^4 objects. We have now, a new experiment to repeat this. We now have a sense of where to look in the Magellanic clouds because we believe that we have now seen the thermal signature of the baryonic dark matter. Now Tom, listen ... I didnt get a chance to describe this to you.

Theo Nieuwenhuizen: Carry on ... Tom is on board.

Rudy Schild: If Carl is right, the planets would have been made everywhere in the halo of the galaxy in these clumps. These clumps have now been seen in these very low temperature maps like Dirbe at 200 microns and the longest WMAP and in some other experiments and these have given a spectral signature by showing a peak at a temperature always prone to be about 15 degrees Kelvin . That's seen in the halo of our galaxy in these globs that they see and also halos of other galaxies. So, why is there a spectral signature at 13.7 K? It is because the triple point of hydrogen at near vacuum conditions is at 13.8 K. So these objects are cooling but they get stuck at the triple point because of the heat of fusion and so we see them everywhere and we call them infrared cirrus. By looking at the infrared cirrus clumps seen in the maps of the Magellanic clouds and doing the micro lensing experiment, the same Macho, Ogle, Eros, experiment through the Magellanic clouds through these 13.8 degree clumps which should then be the hydrogen spheres, we would then be to detect whether, in fact, that prediction of the theory was correct. Those should be the hydrogen spheres.

Theo Nieuwenhuizen: And if they are not there ... then the game is over.

Rudy Schild: If they're not there ... then I shut up.

Anna Achúcarro: I guess what I was asking, from what I understood, the micro lensing ... you can detect these things obviously. In your history, it would seem to me that your combination was more or less ... I should expect to see a micro cosmic background ... your peaks are coming from somewhere else.

Theo Nieuwenhuizen: OK, let me take it from Carl. This is a weak point because we didn't work it out and we are not in that field. We would invite people to do it for us. The idea is that the plasma breaks up into clumps and the size of the clumps is more or less the position of the first peak. Now the higher peaks, they will come from inside these clumps and this is, I think, more or less what it is now. It will be gas dynamics more or less as it is done now but there will not be dark matter for us so, theres a good chance that it will fail because we don't have dark matter, as these neutrinos do nothing. They are just homogenous, they do not help and baryons must do it alone.

Anna Achúcarro: OK, so you will be in a position to make a prediction that you can compare?

Theo Nieuwenhuizen: If this works out, it should be compared to the CMB, now, listen ... if you have a real theory you must describe everything. Including all observations that are well established.

Anna Achúcarro: I also had a question about the Bullet cluster but I don't know whether you have discussed it or not.

Tom Shanks: The Bullet cluster is often used ... ... for a cold dark matter model. At least the first paper, I thought, was a swindle. You know what I'm talking about? I looks like Bullet 2 clusters and that the gas in the galaxies is separated out and then you ask the question: where the gas is. Is it in the galaxies? If it's something gas, then it could be a baryonic model or MOND model. If it's in the galaxies, that's where you would expect the cold dark matter to be, as collisionless particles, associated with the galaxies around the gas. And so, the gravitational lensing results seem to favor the idea that the mass was with the galaxies, and therefore the cold dark matter rather

than the gas. But, we actually took very nice pictures that looks like the gas is very separate, separated out in this cluster by the event of the one cluster passing through another. We actually get numbers, the gas is where they say the gas is quite spread, ... as is the mass from lensing so the only way they got the result was by subtracting off a slender circally symmetric profile set it on the galaxy position which then means that you see no mass near the gas. But if they had done it the other way around they would have gotten the completely opposite result. So that's why I say it's somewhat of a swindle. It depends on you thinking that this structure, the gas is separated out from the galaxies when actually it hasn't been separated out long enough to do the experiment. So I don't think that is a very good argument for cold dark matter down to the masses for cold dark matter cluster. When you begin to look at the details ...

Theo Nieuwenhuizen: Well now, I think we have almost set up everything that we knew before we came here. We have put it upside down. Some things have been said back again. Other things are still ... in the air. Alexander, you had a nice quote, can you read it?

Alexander Unzicker: I will not talk, I will just quote and shut up and not comment. It's Richard Feynman, and he said "Correct theories of physics are perfect things, and the replacement theory must be a new perfect thing, not an imperfection added on to an old perfect thing." This is the essence of revolution the replacement of the old with the new. Not the adding of more crap on to the old.

Theo Nieuwenhuizen: Well, for me this is the end. We have already thanked the Lorentz Center, I would still like to thank my co-organizers. First of all Ruth; Ruth, you came in late, we were very happy you were willing to do that, thank you. (applause) Rudy, you are our "Nestor". You know the best. You have all the experience, thank you very much. (applause) But I think you all know who was the real organizer of this meeting, Francesco, thank you. (applause)
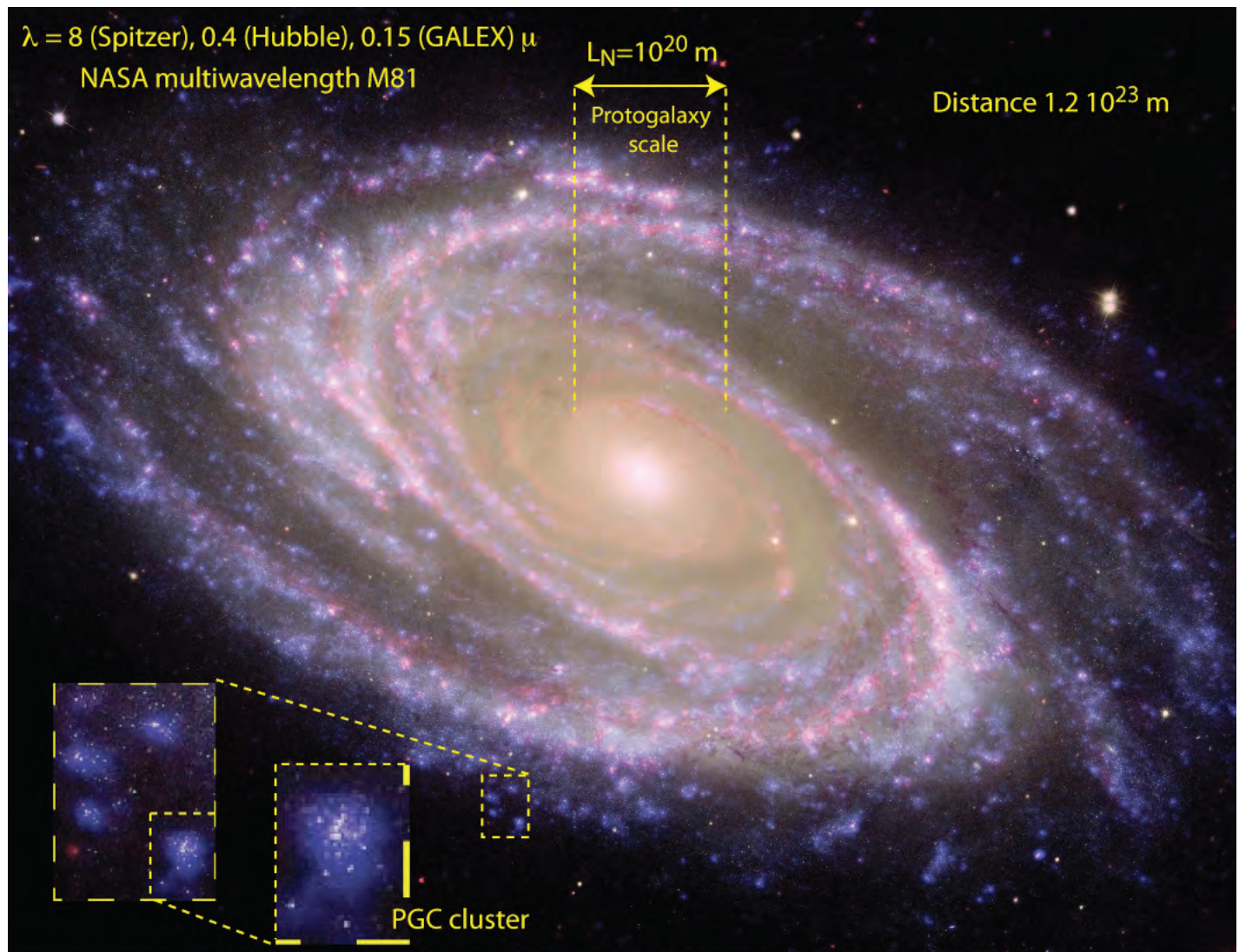
Rudy Schild: And someone has to thank you Theo. (applause)

Theo Nieuwenhuizen: OK, it's done.

14

000339

λ = 8 (Spitzer), 0.4 (Hubble), 0.15 (GALEX) μ
NASA multiwavelength M81

$L_N = 10^{20}$ m

Protogalaxy scale

Distance 1.2×10^{23} m

PGC cluster

http://www.spitzer.caltech.edu/images/2126-sig07-009-Multiwavelength-M81

According to hydrogravitational dynamics cosmology HGD, all galaxies fragmented at a plasma viscous-gravitational scale L_N at 10^{13} seconds, 300,000 years after the big bang when the plasma turned to gas. These gas protogalaxies then fragmented into proto-globular-star-cluster PGC clumps of Earth-mass primordial gas planets: the missing mass of galaxies such as M81. Stars form from mergers of these planets.